Oxidative Medicine and Cellular Longevity

Molecular Aspects of Cellular Ageing

Lead Guest Editor: Milena Georgieva
Guest Editors: Natalia Krasteva and ChangHui Shen

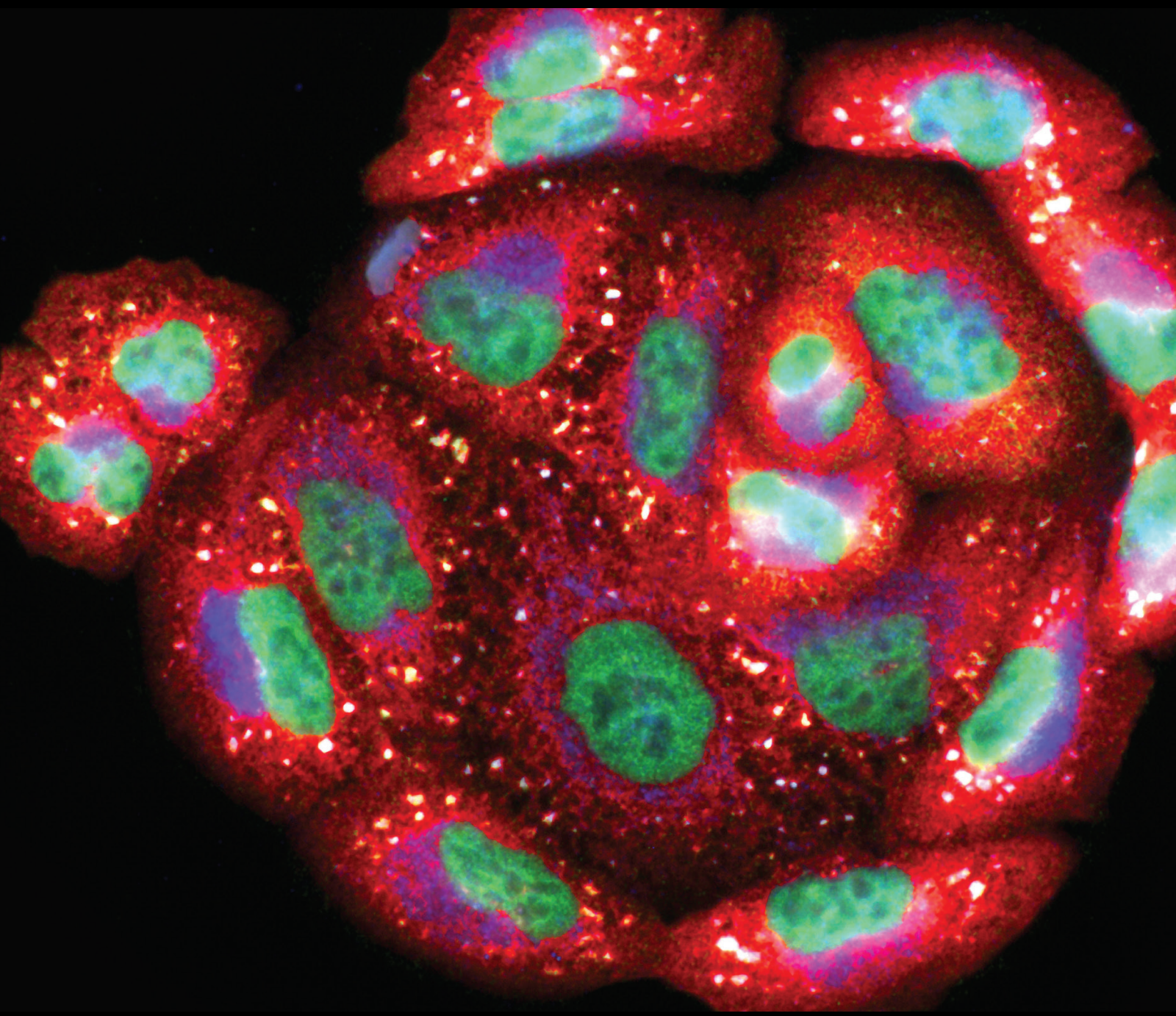

Molecular Aspects of Cellular Ageing

Oxidative Medicine and Cellular Longevity

Molecular Aspects of Cellular Ageing

Lead Guest Editor: Milena Georgieva
Guest Editors: Natalia Krasteva and ChangHui Shen

Contents

Contents

Hindawi
Oxidative Medicine and Cellular Longevity
Volume 2022, Article ID 6009787, 19 pages
https://doi.org/10.1155/2022/6009787

Research Article

Dissecting Regulators of Aging and Age-Related Macular Degeneration in the Retinal Pigment Epithelium

Pabalu P. Karunadharma,[1,2] **Rebecca J. Kapphahn**,[1] **Madilyn R. Stahl**,[1] **Timothy W. Olsen**,[1] **and Deborah A. Ferrington**[1,2]

[1]*Department of Ophthalmology and Visual Neurosciences, University of Minnesota Twin Cities, MN 55455, USA*
[2]*Graduate Program in Biochemistry, Molecular Biology, And Biophysics, University of Minnesota Twin Cities, Minneapolis, MN 55455, USA*

Correspondence should be addressed to Deborah A. Ferrington; dferrington@doheny.org

Received 25 March 2022; Accepted 16 September 2022; Published 16 November 2022

Academic Editor: Deepak Chhangani

Age-related macular degeneration (AMD), the leading cause of blindness in elderly populations, involves the loss of central vision due to progressive dysfunction of the retinal pigment epithelium (RPE) and subsequent loss of light-sensing photoreceptors. While age is a key risk factor, not every aged individual develops AMD. Thus, the critical question is what specific cellular changes tip the balance from healthy aging to disease. To distinguish between changes associated with aging and AMD, we compared the RPE proteome in human eye bank tissue from nondiseased donors during aging ($n = 50$, 29-91 years) and in donors with AMD ($n = 36$) compared to age-matched donors without disease ($n = 28$). Proteins from RPE cells were separated on two-dimensional gels, analyzed for content, and identified using mass spectrometry. A total of 58 proteins displayed significantly altered content with either aging or AMD. Proteins involved in metabolism, protein turnover, stress response, and cell death were altered with both aging and AMD. However, the direction of change was predominantly opposite. With aging, we detected an overall decrease in metabolism and reductions in stress-associated proteins, proteases, and chaperones. With AMD, we observed upregulation of metabolic proteins involved in glycolysis, TCA, and fatty acid metabolism, with a concurrent decline in oxidative phosphorylation, suggesting a reprogramming of energy utilization. Additionally, we detected upregulation of proteins involved in the stress response and protein turnover. Predicted upstream regulators also showed divergent results, with inhibition of inflammation and immune response with aging and activation of these processes with AMD. Our results support the idea that AMD is not simply advanced aging but rather the culmination of perturbed protein homeostasis, defective bioenergetics, and increased oxidative stress within the aging RPE, exacerbated by environmental factors and the genetic background of an individual.

1. Introduction

Age-related macular degeneration (AMD) is the leading cause of blindness in individuals over the age of 65 in developed countries and globally the third leading cause of vision loss [1, 2]. This disease manifests as a loss of central, high-acuity vision, caused by the death of the retinal pigment epithelium (RPE) and photoreceptors in the macular region of the retina. Patients with advanced AMD have difficulties performing essential daily functions, such as reading, writing, and driving, thereby significantly impacting their quality of life [2]. While the exact cause of AMD is still not completely resolved, most of the experimental evidence points to the dysfunction and death of the RPE as a critical pathogenic event. Located between the retinal photoreceptors and the outer retinal blood supply of the choroid, the RPE performs many key functions that helps maintain vision. These functions include daily phagocytosis of the oldest portion of photoreceptor outer segments, transport of nutrients and oxygen from the choroid to the outer retina, and secretion of molecules that are crucial for the health and integrity of the retina and choroid [3].

Multiple environmental (e.g., high-fat diet and smoking) and genetic risk factors (e.g., single nucleotide polymorphisms in complement genes) have been linked to an increased likelihood for developing AMD. However, age remains the strongest risk factor as approximately 30% of individuals over 75 years develop AMD [4]. Since not every aged individual develops AMD, the critical question is what specific cellular changes tip the balance from healthy aging to disease. Distinguishing molecular changes that occur during aging from changes with AMD onset and progression will provide important new insight into how the RPE responds to the challenges of aging and disease.

Currently, there are no reliable animal models that fully replicate the key characteristics of AMD due to the involvement of the macula, which is unique to primate eyes, and the age-dependent onset of the disease. Our laboratory investigates the biochemical changes occurring in the retina using human donor eyes that have been characterized for the presence and severity of AMD by the Minnesota Grading System (MGS) [5]. The MGS incorporates clinical phenotypes defined by the Age-Related Eye Disease Study (AREDS), considered to be a standard in clinical trials, to classify human donor eyes [6]. Thus, the biochemical phenotypes observed at each stage in donor retinas are directly relevant to a patient's clinical phenotype.

In two prior studies, we employed a proteomics approach to begin defining how retinal proteins are altered with AMD progression. A global proteome analysis of the RPE found content of 12 proteins localized to the mitochondria were altered with AMD [7]. This initial study provided the first indication that defects in RPE mitochondria may play a role in AMD pathology. Subsequent studies of the RPE mitochondria from AMD donor tissue have shown mtDNA damage and dysfunction of the energetics [8, 9]. The current study extends our previous work by including an analysis of RPE protein changes during aging ($n = 50$, 29-91 years) performed in parallel with a comparison of donors at progressive stages of AMD ($n = 36$) compared with their age-matched nondiseased controls ($n = 28$). Based on a review of studies applying proteomics to analyze RPE [10], the current study provides the most comprehensive examination of human RPE proteome since it spans a significant range in ages and stages of AMD to distinguish how aging and disease affect the RPE.

2. Materials and Methods

2.1. Human Tissue Procurement. Donor eyes were obtained from the Lions Gift of Sight (formerly Minnesota Lions Eye Bank, St. Paul, MN, USA) with written consent either from the donor or the donor's family for use in medical research in accordance with the principles outlined in the Declaration of Helsinki. Criteria established by the Minnesota Grading System (MGS) were used to determine the donor's disease stage from high resolution photomicrographs [5]. MGS 1 represents the control group with no AMD. MGS 2, 3, and 4 are early, intermediate, and advanced stages of AMD, respectively. Donor demographics included time and cause of death, a limited medical history and ocular history (Table S1). RPE was dissected fresh and frozen at -80°C until analysis. Exclusion criteria for the present study include a history of diabetes or glaucoma, clinical symptoms of diabetic retinopathy, advanced glaucoma, and myopic degeneration or atypical debris in the eyes.

2.2. Protein Isolation. RPE cells used in this study were dissected fresh by gently separating from the Bruch's membrane in a balanced saline solution. It was pelleted at 1100 × g and frozen at −80°C until processing. Cells from the peripheral RPE were processed as described [11]. Briefly, pelleted RPE cells from a pair of globes were homogenized in a buffer containing 20 mM HEPES, 10 mM KCl, 1.5 mM $MgCl_2$, 250 mM sucrose, 1 mM EDTA, 1 mM EGTA, 1 mM phenylmethylsulfonyl fluoride, and 0.5% NP40. The cells were subjected to two freeze-thaw cycles and gently passed six times through a 26-gauge needle. The lysate was cleared of nuclei, intact cells, and plasma membrane fragments by centrifugation at 600 × g for 15 minutes at 4°C. The supernatant was retained, and the pellet was subjected to a second mechanical homogenization and centrifugation as described above. The second supernatant was combined with the first and centrifuged at 13,000 × g for 15 minutes at 4°C to pellet the mitochondria. The resultant supernatant enriched for cytoplasmic proteins was used in this study. Protein concentrations were determined using the bicinchoninic acid protein assay (Pierce Biotechnology, Rockford, IL, USA), with bovine serum albumin as the protein standard.

2.3. 2D Gel Electrophoresis. The conditions for strip rehydration, focusing, equilibration, and 2D gel electrophoresis were performed as outlined [11]. RPE protein (125 μg) were dissolved in a rehydration solution (9 M urea, 3 M thiourea, 6% CHAPS, 1% ASB-14, 1% Biolytes pH 3–10 (Bio-Rad), and 50 mM dithiothreitol) and incubated with 11 cm IPG strips (pH 5 to 8 linear gradient) (Bio-Rad, Hercules, CA, USA). Proteins separated in the first dimension were resolved on 12% polyacrylamide gels. The 2D gels were stained with Flamingo™ Fluorescent Gel Stain according to the manufacturer's protocol. Gels for mass spectrometry were stained with silver using a mass spectrometry-compatible kit (Silver Stain Plus Kit; Bio-Rad).

2.4. Two-Dimensional (2D) Gel Spot Quantification and Analysis. Flamingo-stained gels were imaged using a Dark Reader Transilluminator (Clare Chemical Research, Dolores, CO, USA) and a ChemiDoc XRS (Bio-Rad) imager system. Gel images chosen for analysis were based on the saturation of a standard protein run in a separate lane in the gel. Spot alignment and density quantification were performed using a 2D gel analysis software (PDQuest 7.1.1; Bio-Rad). Prior to spot matching, artefactual noise was removed from each 2D gel using the filter options in PDQuest. Automatic spot detection and matching were followed by manual inspection and editing. Spot intensities of each gel were normalized to the total intensity of valid spots of that gel. Natural log transformed spot density values were used for statistical analysis.

2.5. In-Gel Digestion and MS Analysis. Spots were manually excised from 2D silver-stained gels and in-gel digestion

performed with trypsin as described [11]. After trypsin digestion, extracted peptides were purified using "stage tips" containing a plug of "Empore" disk (3M, Minneapolis, MN, USA) [12]. LC-MS/MS analysis of trypsin digested 2D PAGE protein spots was carried out using an LTQ Orbitrap mass spectrometer (Thermo Fisher Scientific, San Jose, CA) equipped with a Flex nano-ESI source (Thermo Fisher Scientific, San Jose, CA). Data dependent scanning was performed using Xcalibur v 2.1.0 software, a survey mass scan at 60,000 resolution in the Orbitrap analyzer scanning mass/charge (m/z) 360-1800, followed by collision-induced dissociation (CID) tandem mass spectrometry (MS/MS) of the 5 most intense ions in the linear ion trap analyzer [13]. Precursor ions were selected by the monoisotopic precursor selection (MIPS) setting with selection or rejection of ions held to a ±10 ppm window. Dynamic exclusion was set to place any selected m/z on an exclusion list for 20 seconds after a single MS/MS. Tandem mass spectra were searched against a human FASTA protein database downloaded from UniprotKB on March 09, 2017, which at that time contained 20121 protein entries. All MS/MS spectra were searched using Thermo Proteome Discoverer 1.4 (Thermo Fisher Scientific) considering fully tryptic peptides with up to 2 missed cleavage sites. SEQUEST (embedded with Proteome Discoverer) was searched with a fragment ion mass tolerance of 0.80 Da and a parent ion tolerance of 10.0 PPM. Carbamidomethyl of cysteine (57.021 Da) was specified in SEQUEST as a fixed modification. Deamidation (0.984 Da) of asparagine and glutamine and oxidation (15.995 Da) of methionine were specified in SEQUEST as variable modifications. Protein and peptide identification results were visualized with Scaffold v 4.11 (Proteome Software Inc., Portland OR), a program that relies on various search engine results (*i.e.*: SEQUEST, X!Tandem, MASCOT) and which uses Bayesian statistics to reliably identify more spectra [14]. Accepted proteins passed a minimum of 3 peptides identified at a 95% protein and peptide confidence by the Peptide and Protein Prophet algorithm, within Scaffold [15].

2.6. Statistical Analysis. To recognize significant linear changes in protein spot density with aging, we performed regression analysis using GraphPad Prism (version 9). Significant spot quantity changes in the diseased donors (AMD) compared to age-matched controls were examined using two models. Linear density changes across disease stages were tested with linear regression and stage-specific changes using one-way ANOVA and Dunnett's post hoc test for means comparison. The results are expressed as mean ± SEM (AMD data). Statistical significance was set at $p \leq 0.05$ for both aging and AMD comparisons.

2.7. Bioinformatic Analysis. Categorization of proteins into class, molecular function, and biological process was done according to Gene Ontology notation using the PANTHER (version 16.0) classification system [16]. The Kyoto Encyclopedia of Genes and Genomes (KEGG) mapper tool was utilized to categorize the proteins into functional categories [17]. Pathway analysis was performed using the Ingenuity Pathway Analysis (IPA, Qiagen Inc.). Significantly changing proteins from 2D spots that had 3 or fewer protein identifications were utilized for pathway and gene ontology analysis. For the aging IPA analysis, the spot densities were converted to a ratio for comparing pathway changes across different age groups. Donors were separated into 4 age groups: group 1 (29-48 yrs), group 2 (53-63 yrs), group 3 (65-76 yrs), and group 4 (79-91 yrs). The spot densities for each age group were averaged and normalized to group 1. This ratio was input into IPA with p values for expression analysis. AMD protein changes were submitted as an expression ratio by normalizing averaged protein density values at each stage to MGS 1 (control) along with p values.

3. Results

3.1. Donor Characteristics. A summary of the donor demographics and clinical information (provided from Eye Bank records) is presented in Figure 1 and Table S1. All donor eyes were evaluated for the presence and severity of AMD using the Minnesota Grading System [5]. Control donors without AMD (MGS 1) ranging in age from 29 to 91 years old ($n = 50$) were used to determine protein changes that occur with normal aging (Figure 1(a), solid box). Twenty-eight of the MGS1 donors (ages 61-91) were the age-matched controls for determining protein changes that occur at early (MGS 2, $n = 11$), intermediate (MGS 3, $n = 13$), and late (MGS 4, $n = 12$) stages of AMD (Figure 1(a), hatched box). Donors in the MGS 1 group consisted of 20 females and 30 males (Figure 1(b)). There was a relatively balanced distribution of each sex in the AMD analysis except for MGS4, consisting of 9 females and 3 males.

3.2. Proteomic Analysis of RPE with Aging and AMD. Average protein yield for the isolated RPE protein fractions was 534 ± 36 μg (mean ± SEM). There was no significant difference in protein yield among MGS stages ($p = 0.2$, $n = 64$). Proteins were separated by 2D gel electrophoresis and stained with Flamingo Fluorescent Gel Stain prior to analysis of spot density (representative Flamingo-stained gels are shown in Figure 2). For the aging comparison (MGS 1 only), 465 spots were resolved and analyzed (Figure 2(a)). A total of 519 spots were analyzed in AMD age-matched donors (Figure 2(b)). For clarity, we are using "A" for gel spots from the aging analysis and "D" for gel spots from the AMD disease analysis. In the aging comparison, twenty-four spots showed significant linear density changes (Figures 2(a) and 3(a) show a subset, Table 1, and Table S2). Five spots increased in spot density with age, while 19 spots demonstrated a decrease (Table 1 and Table S2).

For the comparison between MGS stages, 23 spots changed with disease progression (Table 2, Table S3). Three distinct patterns of spot density change were observed, including (1) at disease onset (starting at MGS 2), (2) linear changes with disease progression, and (3) at later stages (MGS3 or MGS4, Figure 3(b)). Sixteen spots changed significantly at disease onset (MGS 2), 4 exhibited a linear response, and 4 others were altered at later stages of AMD (Figure 3(b)).

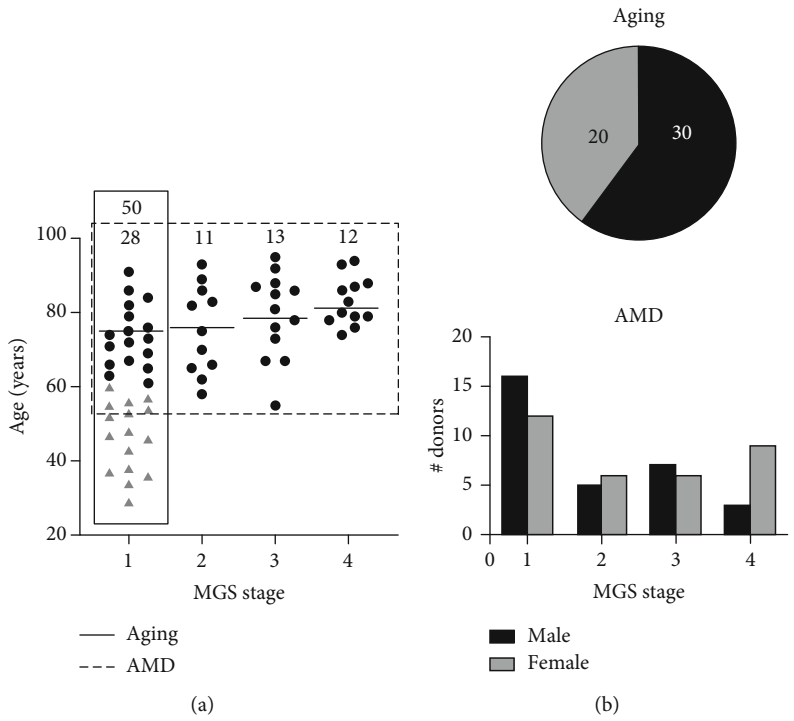

Figure 1: Donor ages and gender distribution in the aging and AMD comparison. (a) Age of donors used in this study. Solid line (—) outlines the control donors used in the aging comparison ($n = 50$). Triangles are donors aged 29–60 ($n = 22$). Circles are donors aged 61–91 ($n = 28$). These donors are also the age-matched controls for AMD comparison. Dashed line (—) outlines the age-matched donors used in the AMD comparison ($n = 64$). Number of donors for each MGS stage is shown at top. Mean age of each age-matched MGS group indicated by line. There was a significant increase in age in MGS 4 compared to controls (one-way ANOVA, $p = 0.0502$). (b) Pie chart showing gender distribution in aging study. Bar graph showing gender distribution per MGS stage.

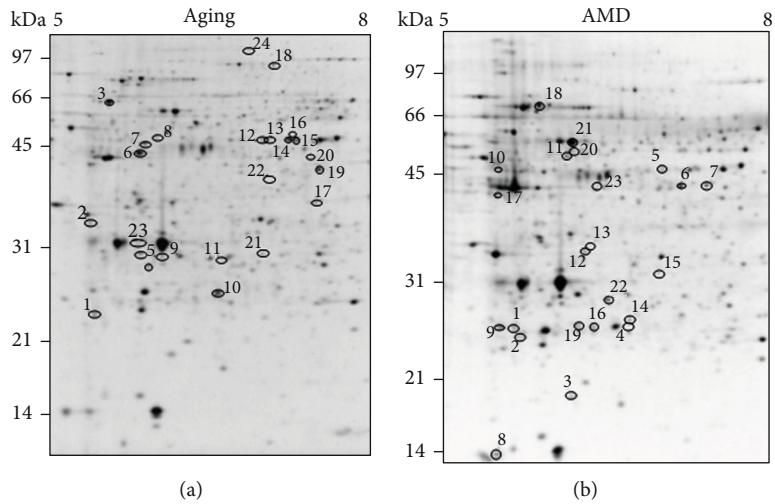

Figure 2: RPE proteins resolved by 2D gel electrophoresis. Representative flamingo-stained gels (125 μg) from the (a) aging and the (b) AMD comparison. Spots indicated showed altered content with each process. A linear range of pI 5 to 8 is indicated at the top and molecular weights of the standard are marked on the left.

3.3. Protein Identification. Proteins were identified by LTQ-Orbitrap mass spectrometry. A high confidence match to a specific protein was based on the criteria of at least 3 unique peptides matching with greater than 95% protein and peptide probability [15]. Seventy-eight unique proteins were identified from all the significantly altered gel spots from both analyses (Tables 1, 2, S2 and S3). Approximately 50% of the significantly changing spots in the aging and AMD comparisons matched a single protein. On average, 26% of the spots in both analyses matched 2 unique proteins and 8% matched 3 proteins. Tables 1 and 2 (also Tables S2 and S3) provide a list of proteins identified in each spot, along

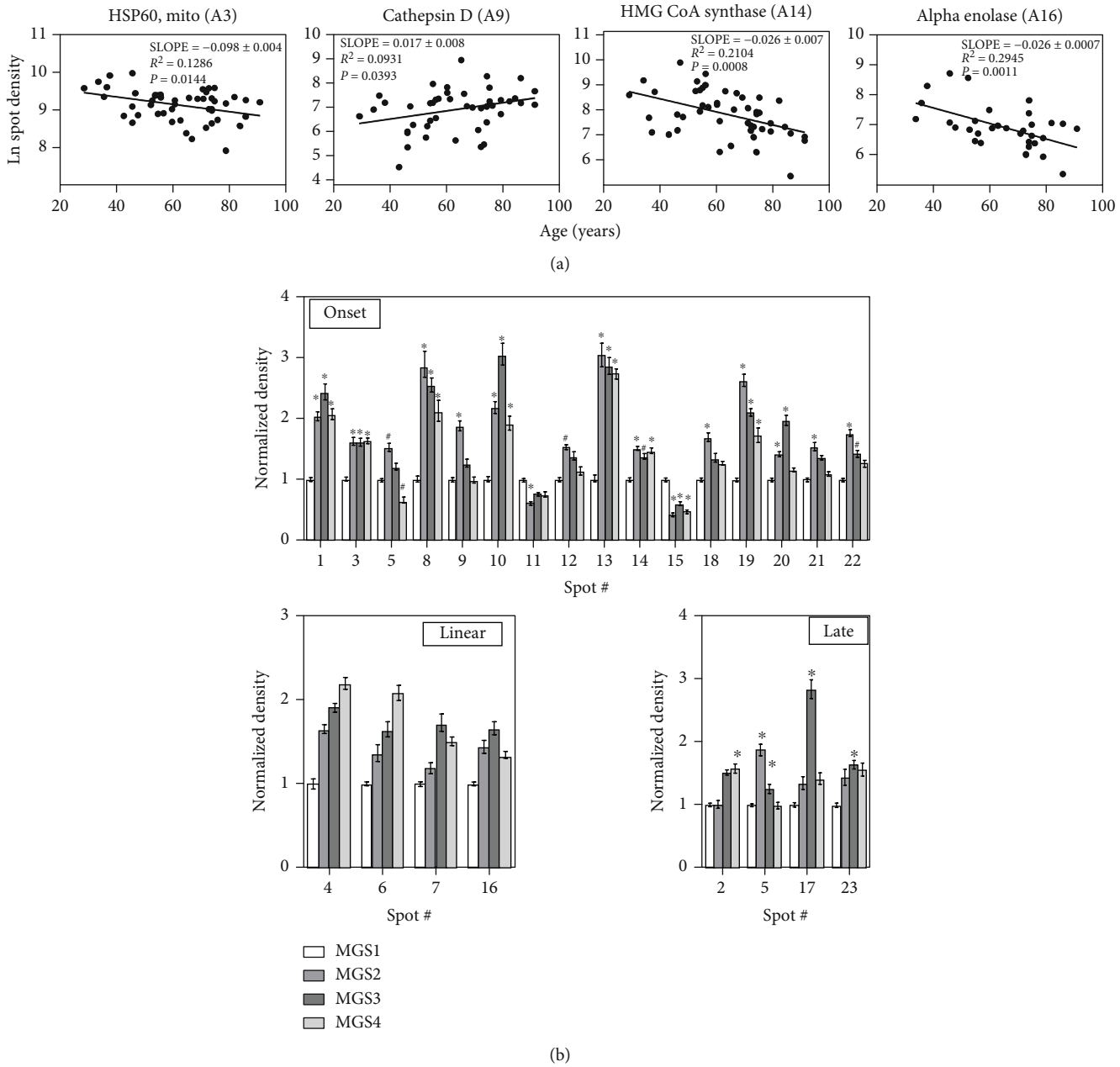

Figure 3: Spots altered with aging and AMD. (a) Four representative spots significantly changing with age. Age in years in the x-axis and Log_e transformed spot densities are on the y-axis. Slope, coefficient of correlation, and regression p value are shown for each spot. Additional spots from the aging analysis are listed in Table 1 and Table S2. (b) Average densities at each MGS stage for spots demonstrating significant changes at disease onset, linear over disease progression, and at late stage are shown. Data are the means (±SEM) normalized to MGS 1. Asymmetric error bars: back transformed density values from Log_e. One-way AOVA with Dunnett's post hoc test was used to determine if different than MGS1. $^*p < 0.05$. $n = 6$ or more per group. All proteins identified from the AMD analysis are listed in Table 2 and Table S3.

with information about significance, molecular weight, sequence coverage, and number of unique peptides identified for each protein. Approximately 20% of the 2D gel spots identified 4 or more proteins (Table S2, S3). These proteins were not considered in subsequent pathway analysis.

The comigration of multiple proteins in a single 2D gel spot or a single protein migrating at different isoelectric points (pI) reflects challenges associated with 2D gels when resolving a highly complex mixture of proteins. Posttranslational modifications (PTM), such as phosphorylation, acetylation, or oxidation, can alter the intrinsic charge of a portion of the protein population by introducing a charge or quenching an existing one, thereby making single proteins migrate at different pIs. An example among the proteins in the aging comparison is HMG CoA Synthase (HMGCS2, 52 kDa, pI 8.16) and alpha Enolase (ENO1, 47 kDa, pI 7.39), which were identified comigrating in four spots (A12-15) at ~48 kDa with an isoelectric point (pI) of 7.1 to 7.4. HMGCS2 was previously observed to show an

Table 1: Proteins identified from spots changing with Aging (3 or less protein ID spots).

Spot no.†	p value	R^2	Direction‡	Protein ID	Accession UniProt	Gene	Experimental MW/pI§	Theoretical MW/pI ¥	MSMS scaffold Sequence coverage	MSMS scaffold Unique peptides	MSMS scaffold Total spectra
A1	0.0319	0.09428	D	ATP synthase subunit d, mitochondrial	O75947	ATP5PD	21/5.6	18/5.30	30	4	6
				Ras-related protein Rab-18	Q9NP72	RAB18		23/5.11	17	3	3
A2	0.0148	0.1364	D	Transducin β-1	P62873	GNB1	33/5.5	37/6.00	45	9	17
				Retinaldehyde-binding protein 1	P12271	RLBP1		36/5.05	25	7	15
				Cathepsin D	P07339	CTSD		37.9/5.6 €	11	3	3
A3	0.0144	0.1286	D	HSP 60, mitochondrial	P10809	HSPD1	62/5.7	61/5.87	65	34	101
A4	0.0003	0.2497	D	NADH dehydrogenase iron sulfur protein 3, mitochondrial	O75489	NDUFS3	25.5/6.0	30/7.5	19	4	10
				Cathepsin D	P07339	CTSD		26.7/5.56 ₡	11	3	3
A5	0.0075	0.1933	D	Prohibitin	P35232	PHB	27/5.9	30/5.76	46	10	19
A6	0.0057	0.01576	D	Creatine kinase B	P12277	CKB	44/5.9	43/5.89	20	5	6
				Tripeptidyl-peptidase 1	O14773	TPP1		39.8/5.75 Δ	8	3	7
A9	0.0393	0.0931	I	Cathepsin D	P07339	CTSD	27.2/6.2	26.7/5.56 ₡	26	6	19
A12	0.0004	0.2391	D	Alpha enolase	P06733	ENO1	47.5/7.1	47.2/7.01	51	16	60
				HMG CoA synthase, mitochondrial	P54868	HMGCS2		52/8.16 δ	18	7	10
A14	0.0008	0.2104	D	HMG CoA synthase, mitochondrial	P54868	HMGCS2	47.5/7.2	52/8.16 δ	35	15	26
A15	0.0002	0.2558	D	Alpha enolase	P06733	ENO1	47/7.4	47/7.39	44	15	47
				HMG CoA synthase, mitochondrial	P54868	HMGCS2		52/8.16 δ	17	6	7
A16	0.0011	0.2945	D	Alpha enolase	P06733	ENO1	52/7.3	47/7.39	44	15	47
A17	0.0027	0.2233	D	Aldose reductase	P15121	AKR1B1	35/7.5	36/6.98	38	9	16
				Malate dehydrogenase, cytoplasmic	P40925	MDH1		36/7.39	21	5	5
				GAPDH	P04406	GAPDH		36/8.46	18	4	4
A18	0.0274	0.1082	I	Serotransferrin	P02787	TF	86/7.1	77/7.12	60	36	107
A19	0.0346	0.0955	D	Fructose-bisphosphate aldolase C	P09972	ALDOC	43/7.5	39/6.87	67	17	89
A20	0.0229	0.1228	D	Glutamine synthetase	P15104	GLUL	44.5/7.4	42/6.89	26	9	14
				Isocitrate dehydrogenase [NADP] cytoplasmic	O75874	IDH1		47/7.01	25	9	14
				Elongation factor Tu, mitochondrial	P49411	TUFM		50/7.61	13	4	4
A21	0.0314	0.3558	D	Phosphoglycerate mutase 1	P18669	PGAM1	29.6/7.1	29/7.18	19	5	11

Table 1: Continued.

Spot no.†	p value	R^2	Direction‡	Protein ID	Accession UniProt	Gene	Experimental MW/pI§	Theoretical MW/pI ¥	MSMS scaffold Sequence coverage	MSMS scaffold Unique peptides	MSMS scaffold Total spectra
A22	0.02	0.149	D	Transaldolase	P37837	TALDO1	42.5/7.1	38/6.81	19	6	6
A23	0.061 **	0.2286	I	Prohibitin	P35232	PHB	30.5/5.9	30/5.76	58	12	23
A24	0.0079	0.2124	I	Programmed cell death 6-interacting protein	Q8WUM4	PDCD6IP	97/6.9	96/6.52	13	9	10

† Spot number indicated on gel picture in Figure 2 left panel. Only spots with ≤3 proteins identifications are listed in this table. The remaining spots are listed in Table S2. ‡ Direction increasing (I) or decreasing (D) with age. § Experimental molecular weight (MW) of each spot was calculated based on the relative mobility of the MW markers and distance traveled on the 2D gel. Isoelectric point (pI) estimated from gel image. ¥ Theoretical MW and pI from Expasy MW/pI calculator (http://www.expasy.ch/tools). € Cathepsin D Active form (aa 65-412). ₡ Cathepsin D Heavy chain (aa169-412). Δ TPP1 (aa 196-563). ł 3,2-trans-enoyl-CoA isomerase (aa 42-302). ** trend. δ without mitochondrial signal sequence.

Table 2: Proteins identified from spots changing with AMD (3 or less protein ID spots).

Spot no.†	*p* value	Diff. From MGS 1	Multiple comparisons	Direction/ model ‡	Protein ID	Accession UniProt	Gene	Experimental MW/pI §	Theoretical MW/pI ¥	Sequence coverage	MSMS Unique peptides	Total spectra
D1	0.0002	2,3,4	0.0130, 0.0004, 0.0044	I, O	Apolipoprotein A-I	P02647	APOA1	22.8/5.6	28.1/5.27	43	12	23
					GST π	P09211	GSTP1		23.3/5.64	35	5	9
D2	0.0185	3 **, 4	0.0614, 0.0294	I, A	Ras-related protein Rab-6A	P20340	RAB6A	22/5.7	23.6/5.54	23	3	3
					GST π	P09211	GSTP1		23.3/5.64	26	3	3
D3	0.0068	2,3,4	0.0287, 0.0306, 0.0206	I, O	Superoxide dismutase 1	P00441	SOD1	17.8/6.3	15.8/5.7	29	3	5
D4	<0.0001	Linear		I, L	Peroxiredoxin-3	P30048	PRDX3	22.5/6.7	27.7/7.0	21	3	4
D5	0.0019	2**,4**	0.0638, 0.0602	I, A	Alpha enolase	P06733	ENO1	47.5/7.1	47.1/7.39	51	16	60
					HMG CoA synthase, mitochondrial	P54868	HMGCS2		52/6.64 ǂ	18	7	10
D6	0.0014	Linear		I, L	Phosphoglycerate kinase 1	P00558		44.5/7.2	44.6/8.1	30	7	10
D7	0.0168	Linear		I, L	Glutamine synthetase	P15104	GLUL	44.5/7.4	41.9/6.89	26	9	14
					Isocitrate dehydrogenase [NADP] cytoplasmic	O75874	IDH1		46.5/6.53	25	9	14
					Elongation factor Tu, mitochondrial	P49411	TUFM		45.0/6.31 ǂ	13	4	4
D8	0.0011	2, 3,4	0.0028, 0.0044, 0.0339	I, O	Retinol-binding protein 1	P09455	RBP1	14/5.4	15.8/5.11	54	7	10
D11	0.0171	2	0.0088	D, O	Aldehyde dehydrogenase 9A1	P49189	ALDH9A1	52.8/6.3	53.7/5.69	9	3	3
D12	0.0849**	2**	0.0655	I, O	Inactive C-alpha-formylglycine-generating enzyme 2	Q8NBJ7	SUMF2	36/6.3	31.2/6.52	20	4	4
					Geranylgeranyl pyrophosphate synthase	O95749	GGPS1		34.9/5.78	13	3	3
D13	0.0048	2,3,4	0.0150, 0.0128, 0.0577	I, O	Inorganic pyrophosphatase 2, mitochondrial	Q9H2U2	PPA2	38.2/6.4	37.9/7.01 Δ	31	7	12
					Retinaldehyde-binding protein 1	P12271	RLBP1		36.3/4.98	19	4	4
D14	0.0061	2,3**,4	0.0157, 0.0680, 0.0202	I, O	Peroxiredoxin-3	P30048	PRDX3	23.5/6.8	27.7/7.68	24	4	6
D16	0.0318	Linear		I,L	NADH-ubiquinone oxidoreductase, mitochondrial	P19404	NDUFV2	22.8/6.4	23.8/5.71	44	8	13
					Ras-related protein Rab-7a	P51149	RAB7A		23.4/6.32	29	4	5

Table 2: Continued.

Spot no.†	*p* value	Diff. From MGS 1	Multiple comparisons	Direction/ model ‡	Protein ID	Accession UniProt	Gene	Experimental MW/pI §	Theoretical MW/pI ¥	Sequence coverage	MSMS Unique peptides	Total spectra
D17	0.0009	3	0.0002	I, A	Beta actin	P60709	ACTB	41.3/5.6	41.7/5.29	20	5	9
D18	0.0106	2	0.005	I, O	HSP70, mitochondrial	P38646	HSPA9	66/6.0	68.8/5.44	35	17	35
D19	<0.0001	2,3,4	<0.0001, 0.0018, 0.0016	I, O	Transforming RhoA	P61586	RHOA	24.5/6.3	21.4/5.83	28	4	4
D20	0.0098	2,3	0.0491, 0.0096	I, O	Aldehyde dehydrogenase, mitochondrial	P05091	ALDH2	56.5/6.3	56.4/6.63 Δ	11	4	4
D21	0.0146	2	0.0096	I, O	Protein disulfide-isomerase A3	P30101	PDIA3	59.1/6.3	56.8/5.98 Δ	25	11	20
D22	0.0078	2,3**	0.0037, 0.0948	I, O	Enoyl-CoA hydratase, mitochondrial	P30084	ECHS1	29.4/6.6	28.3/5.88	48	14	30
					Phosphoglycerate mutase 1	P18669	PGAM1		28.7/6.75	17	3	3
D23	0.0305	3,4**	0.0266, 0.0887	I, A	Aminoacylase 1	Q03154	ACY1	44.5/6.4	45.9/5.77	13	4	4

† Spot number indicated on gel picture in Figure 2 right panel. ≤ 3 proteins identifications are listed in this table. The remaining spots are listed in Table S2. ‡ Direction increasing (I) or decreasing (D); models include onset (O), linear (L), and advanced stage (A). § Experimental molecular weight (MW) of each spot was calculated based on the relative mobility of the MW markers and distance traveled on the 2D gel. Isoelectric point (pI) estimated from gel image. ¥ Theoretical MW and pI from Expasy MW/pI calculator (http://www.expasy.ch/tools). ** trend. € Cathepsin B Active form (aa 80-333). Δ precursor. ǂ processed.

acidic shift in the pI and attributed to oxidatively modified thiols [18]. ENO1 was observed to migrate in a "charge train" previously, and multiple PTMs were identified including phosphorylated Serine, acetylation at Lys, and methylation at several sites [19]. Importantly, all comigrating spots exhibited a decrease with aging, thereby providing greater confidence in our conclusions for these proteins.

Proteolytic processing from the inactive to active form or removal of a signal sequence can also result in identification of an individual protein in multiple spots that are migrating at different apparent molecular masses. Cathepsin D provides an example where it is synthesized as a single chain polypeptide (pre-pro-enzyme 48 kDa) in the endoplasmic reticulum and transported to the lysosomal compartment via the trans-Golgi network for maturation [20]. The pro-Cathepsin D undergoes proteolytic processing that ultimately produces the mature 37 kDa protein, which exists as both a single polypeptide or can be further processed to form a two-chain polypeptide consisting of the 27 kDa heavy and 10 kDa light chain [21]. We identified Cathepsin D in multiple spots in the aging analysis, migrating at 33 kDa (A2) and ~27 kDa (A4, A9) that demonstrated divergent changes with aging. This result suggests age-related changes in the proteolytic processing of Cathepsin D.

3.4. Summary of Functional Categories. To provide a more comprehensive analysis of how aging or AMD affects the RPE proteome, we utilized multiple pathway analysis software to assist in summarizing our findings. We included proteins from gel spots that had 3 or fewer proteins identified by mass spectrometry. For the AMD analysis, we also included results from our previous studies that investigated global protein changes in RPE homogenates and in an enriched RPE mitochondrial fraction (Table S4) [7, 8, 22]. Our rationale for including these data was based on the similarity of protocols in each study, including tissue handling and processing by the Lions Gift of Sight Eye Bank and using the Minnesota Grading System for evaluating AMD severity for individual donors. Using results from all our studies would also increase our ability to map changes associated with AMD to specific biological pathways. Of the 25 proteins identified previously [7, 8, 22], three mitochondrial-localized proteins (Elongation factor Tu, GST-π, and HSPA9) were also identified in the current study. The overlap of altered proteins in different donor populations provides greater confidence in the relevance of these findings to AMD.

Eight identified proteins were common to both aging and AMD, while 15 and 35 proteins were unique to aging and AMD, respectively (Figure 4(a) Venn). ENO1 (glycolysis), HMGCS2 (mitochondrial ketogenesis), and HSP60 (mitochondrial chaperone) were three proteins that decreased in both aging and AMD. The remaining five proteins, which decreased with aging and increased with AMD, were from metabolic pathways (PGAM11, GLUL, and IDH1), mitochondrial protein synthesis (TUFM), and from the visual cycle (RLBP1). The preponderance of metabolic proteins changing with both aging and AMD provides an early indication that altered energy production and utilization may be one of the key processes affected under both conditions.

Protein identifications were mapped to biological process, protein class, and molecular function, using the Panther classification system (Figure 4(b)) [16]. In considering each classification, proteins from AMD donors showed a more diverse distribution involving a greater number of categories. These results suggest that AMD has a more complex and broad effect on the proteome. For both aging and AMD, the predominant protein class was metabolic enzyme, which is consistent with major changes in energy utilization for both aging and AMD.

To further distinguish the protein changes in top functional categories, we analyzed our data using the KEGG mapper classification system [17]. The number of proteins associated with each KEGG pathway was plotted with their direction of change (Figure 4(c)). Major categories involving metabolism, protein turnover, stress response, and cell death were impacted heavily with both aging and AMD, but notably, the direction of change was predominantly opposite between the two processes. For example, proteins in the metabolism, degradative pathways, and stress response were decreased with aging and increased with AMD. Specific to AMD was the upregulation of three proteins involved in cell junctions and adhesion (INSR, RHOA, and ACTB), potentially reflecting the disease-induced disruption in RPE tight junctions and connection with Bruch's membrane. These results show divergence between pathways associated with retinal aging that is free of AMD and pathways changing with AMD progression.

To gain additional insight into the top altered pathways, downstream effects, and upstream regulators, the differentially expressed proteins were analyzed by the Ingenuity Pathway Analysis (IPA, Qiagen Inc.). The top pathways in the aging and AMD analyses that significantly changed (Fisher's exact test ≤ 0.05) with an absolute Z-score between $-2.23 \geq z < 1.5$ are shown in Figure 4(d). Glycolysis was significantly altered in both groups, although opposing patterns of activation or inhibition was observed (Figure 4(c)). With aging, glycolysis and gluconeogenesis were predicted to be significantly inhibited (Z-score ≥ -2), while AMD showed activation from MGS2 (Figure 4(d)). This suggests a strong impact in this quintessential pathway with both aging and disease in the RPE. HIF1 alpha signaling pathway showing activation with AMD suggests a significant response to oxidative stress with disease. Other pathways that were inhibited with AMD include oxidative phosphorylation (OXPHOS), PPARa/RXRa activation, estrogen receptor signaling, and xenobiotic metabolism. The inhibition of these critical signaling pathways suggest disruption to the nutrient and damage sensing network with AMD.

The IPA upstream regulator analysis provides insight into the biologically significant changes upstream of the observed protein changes and can identify transcription factors or any other molecules that have been experimentally observed to affect gene/protein expression (Figures 5 and 6). For aging, IPA identified 5 potential regulators (Figure 5). Three of the regulators (TCR, PLA2R1, and IL15) predicted to be inhibitory (Figure 6(a)) are associated with inflammation and

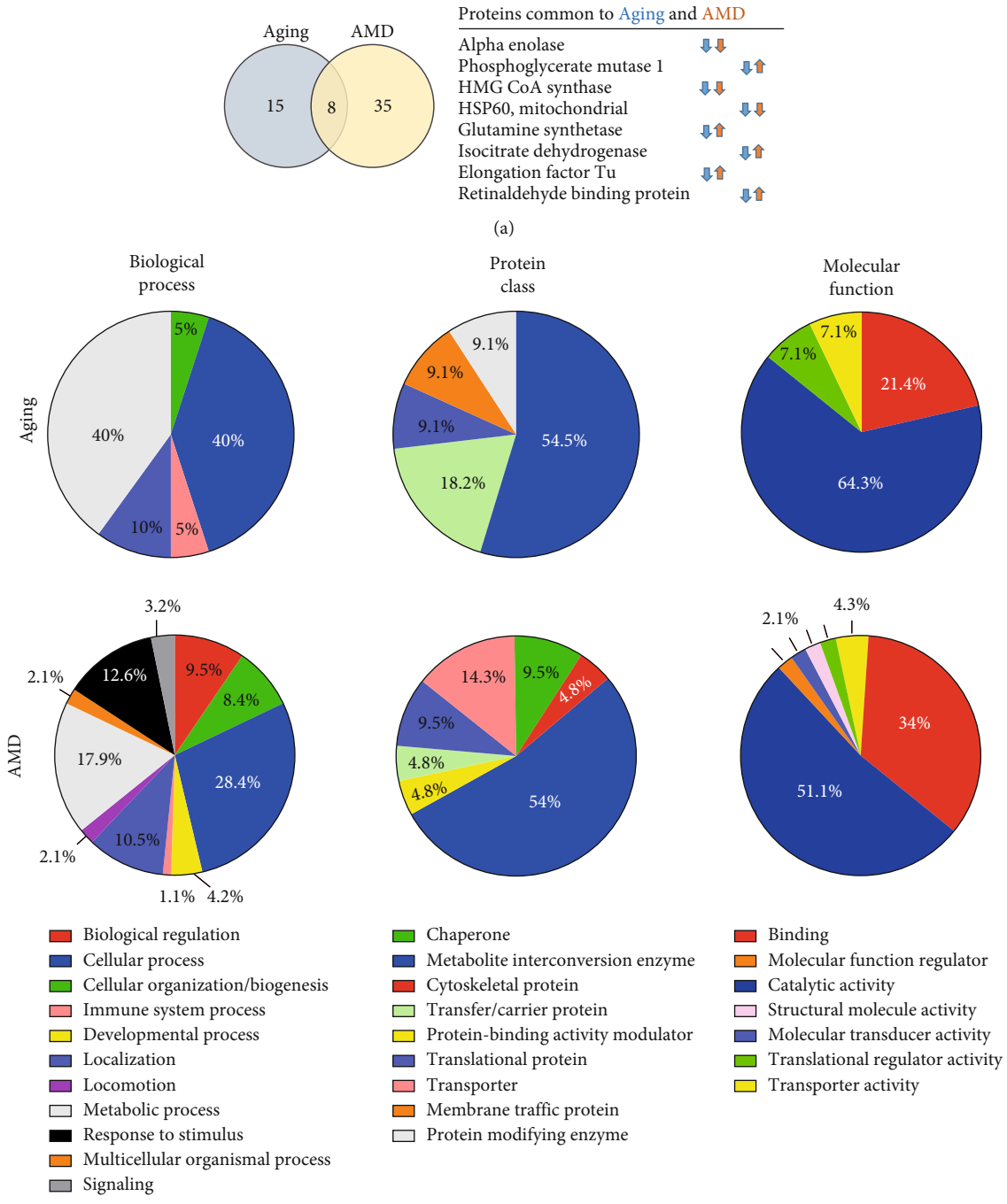

Figure 4: Continued.

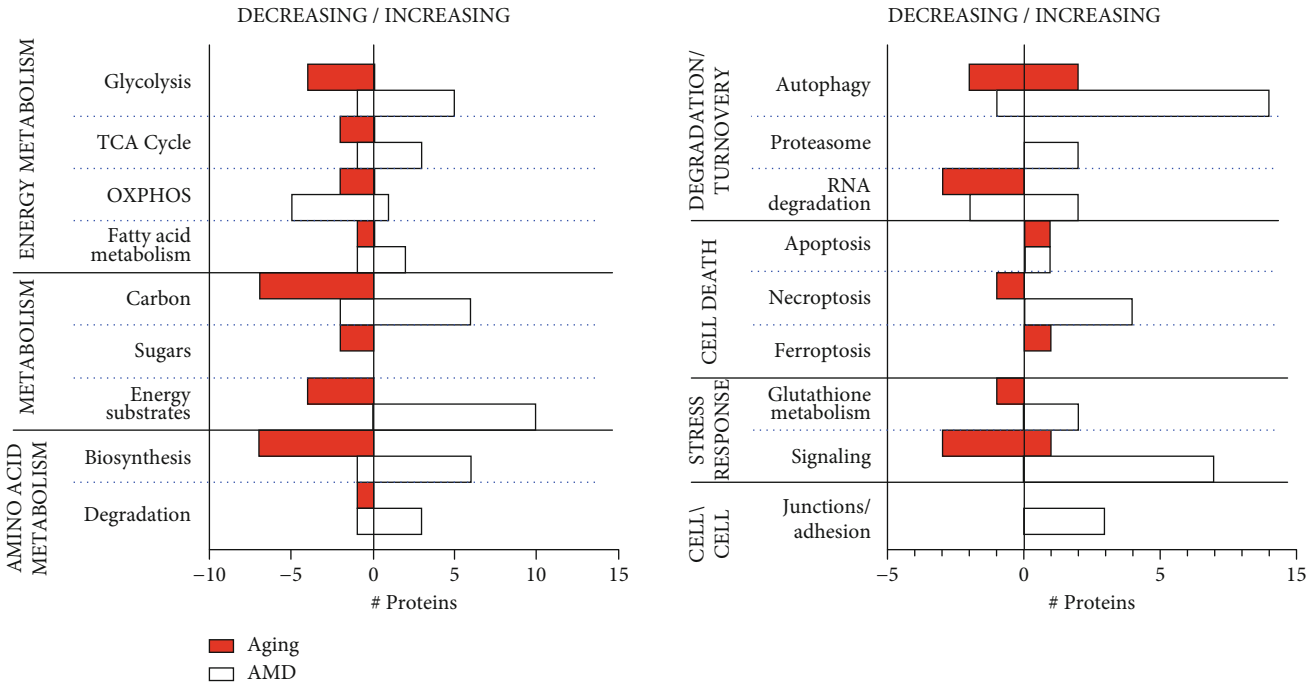

(c)

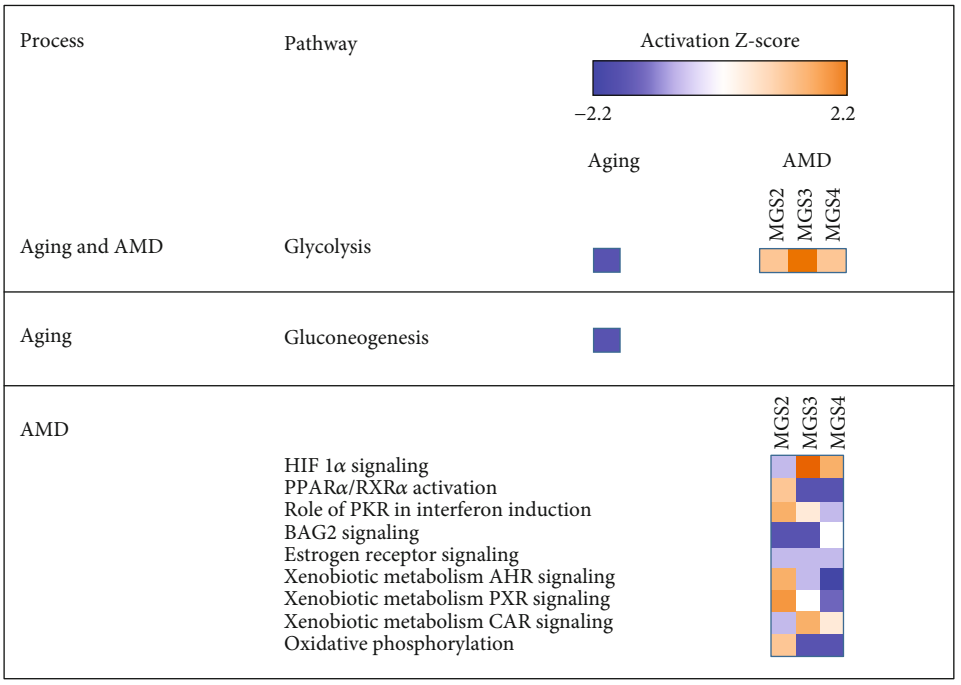

(d)

Figure 4: Comparison of functional categories represented in the aging and AMD proteomic analyses. (a) Venn diagram comparing proteins associated with altered 2D spot quantities in the aging and AMD analyses. A total of 15 proteins were identified from the aging analysis and 35 proteins from the AMD comparison. Only 8 proteins were common to both processes. (b) Functional classification of differentially expressed proteins in aging and AMD. Pie charts demonstrate the distribution of proteins according to their protein class, molecular function, and biological function based on Gene Ontology notation and PANTHER online tool for categorization. (c) Comparison of proteins identified from the aging and AMD analyses graphed based on direction of change. Proteins categorized to functional groups based on KEGG mapper were plotted based on whether they increased or decreased with aging or AMD. y-axis shows the functional categories, and x-axis the number of proteins increasing or decreasing. (d) Canonical pathways with significant activation Z-scores ($-2.23 \geq Z < 1.5$) are shown for aging and AMD after Ingenuity pathway analysis. Blue color depicts inhibition and orange activation.

Aging

Upstream regulator	Molecule type	Function	*p* value
TCR	Complex	Immune response	8.28E -11
PLA2R1	Transmembrane receptor	Cytokine production ROS metabolic process	2.13E -08
ESRRG	Ligand-dependent nuclear receptor	Transcriptional regulation	9.87E -08
PCGEM1	Non -protein coding transcript	Negative regulator of apoptosis	1.34E -07
IL15	Cytokine	Immune response	6.81E -06

AMD

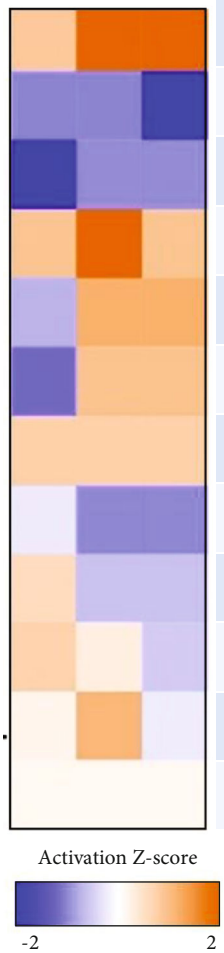

Upstream regulator	Molecule type	Function	*p* value
NFE2L2	Transcriptional regulator		8.96 E -06
CUL4B	Enzyme	E3 Ubiquitin Ligase	4.76E -08
IFNG	Cytokine	Immune response	9.98E -03
IL15	Cytokine	Immune response	1.52E -04
MYC	Transcriptional regulator		7.58E -05
TNF	Cytokine	Immune response	2.59E -02
TCR	Complex	Immune response	8.91E -07
HSF1	Transcriptional regulator		7.27E -06
HIF1A	Transcriptional regulator		2.09E -03
LONP1	Peptidase		2.06E -19
PCGEM1	Non-protein coding transcript	Negative regulator of apoptosis	2.80E -06
TRAP1	Enzyme		1.49E -06

Figure 5: Upstream regulator analysis for aging and AMD. Upstream transcriptional regulators (TRs) predicted by IPA to be significantly altered given the protein changes detected with aging (top) and AMD (bottom). Significance reported using Fisher's exact test *p* values calculated based on the overlap between protein changes and genes regulated by the TR. Activation Z-scores comparing MGS 2, 3, and 4 show inhibition (blue) or activation (orange) when compared with MGS1.

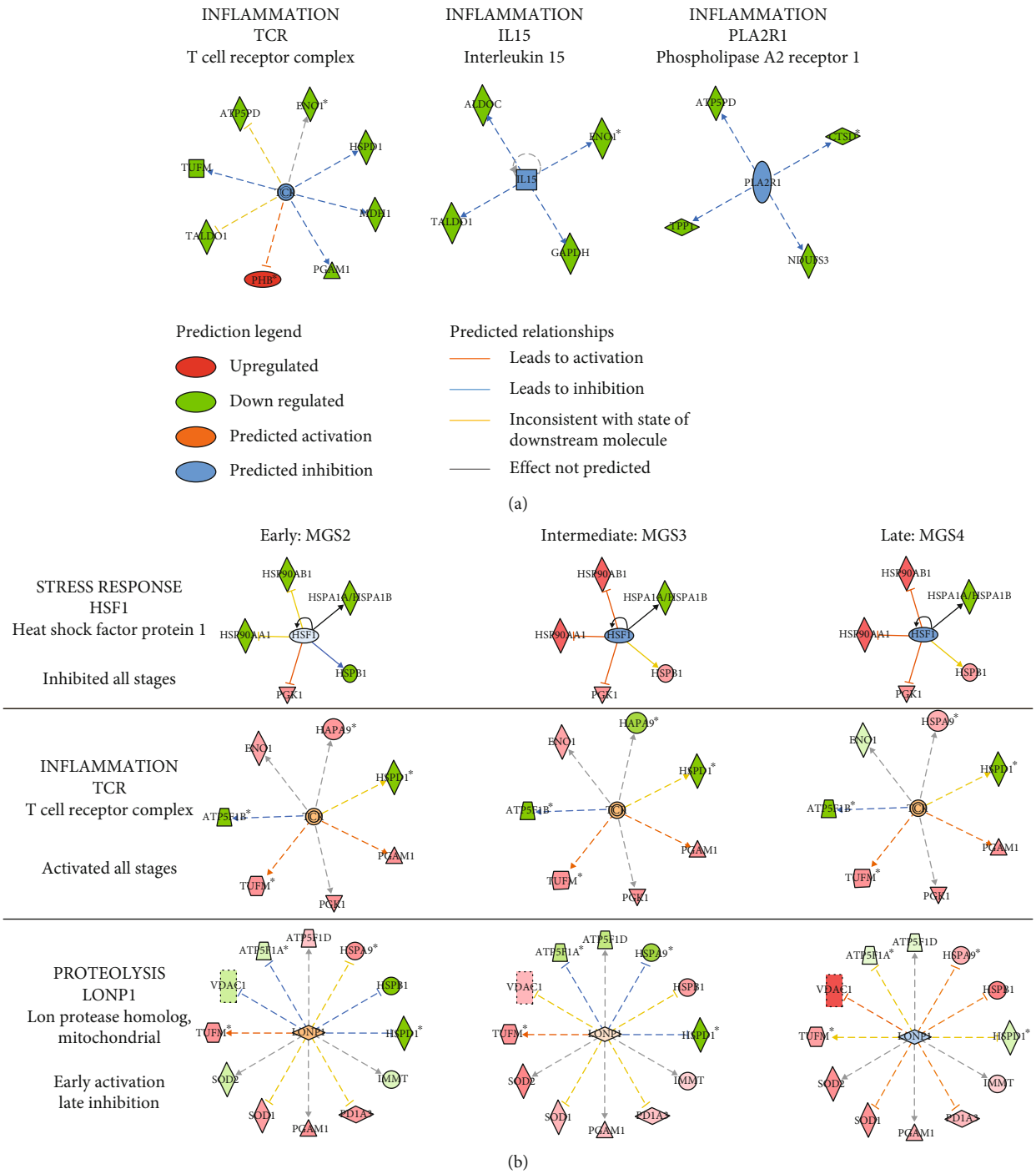

Figure 6: Upstream regulator analysis from IPA. Representative networks showing upstream regulators and target molecules from the data set for the aging (a) and AMD (b) analysis. Upstream regulators and differentially expressed proteins are displayed as nodes and edges (biological relationship between nodes). The color intensity of each node represents expression: red (upregulated), and green (down regulated). The edges connecting the proteins to the proposed upstream regulator represent the predicted relationships: blue inhibition, orange activation, and gray no effect predicted based on the IPA activation Z-score. Additional networks are in Supplemental Figure S1.

immune response. Prostate-specific transcript 1, also known as PCGEM1, is a long noncoding RNA that is hypoxia-responsive and a negative regulator of apoptosis. Estrogen-related receptor gamma (ESRRG), a nuclear receptor, regulates transcription of genes involved in mt biogenesis, OXPHOS, TCA cycle, glycolysis, and fatty-acid oxidation [23]. Both regulators were predicted to be inhibited based on the protein changes associated with aging (Figures 5 and S1A).

AMD upstream analysis revealed 12 regulator molecules predicted to be significantly affected (Figures 5 and 6(b), Figure S1B). Similar to aging, several immune regulators were affected with AMD including TCR (Figure 6(b)),

TNF, IL-15, and IFNG (Figure 5, Figure S1B). Notably, all immune regulators were activated with disease progression except IFNG. This agrees with previous findings of increased inflammation and immune response with AMD progression [24]. Additionally, several transcription factors involved in oxidative stress and hypoxia were affected with AMD. MYC and NFE2L2 were predicted to be activated (Figures 5 and S1B). MYC is a master regulator of transcription that control many genes involved in cell division, chromatin modification, ribosome, and mt biogenesis [25]. NFE2L2 is also a major transcription factor that upregulates expression of antioxidant proteins and protects against ROS-induced oxidative damage [26]. Two other transcriptional regulators of the oxidative stress response, HSF1 (Figure 6(b)) and HIF1A (Figure S1B), showed inhibition at later stages of AMD but activation at MGS2 (Figure 5, Z-score heat map). This suggests an early response to oxidative stress and the increased response to hypoxia due to thickening Bruch's membrane and drusen accumulation that starts early in AMD [27–31]. Two other regulators showed a similar pattern of early activation followed by inhibition at later disease. They include PCGEM1, a negative regulator of apoptosis, and LONP1, a mitochondrial protease that functions as a chaperone and assists with mt OXPHOS subunit assembly and mt protein biogenesis [32]. One additional mitochondrial protein tumor necrosis factor receptor-associated protein 1 (TRAP1), also known as heat shock protein 75 (Hsp75), is a mitochondrial member of the Hsp90 family of molecular chaperones [33]. It acts as a key regulator of mitochondrial bioenergetics by downregulating OXPHOS and promoting glycolysis to reduce reactive oxygen species and increase mt tolerance to oxidative stress [34]. Thus, TRAP1 activation predicted with AMD (Figure 5) could be an indication of the metabolic reprograming with AMD and attenuation of mt energetics.

4. Discussion

In the current work, a parallel proteomic comparison of aging and AMD was performed using RPE proteins extracted from human donor eyes categorized for the presence and severity of AMD. The use of donor eyes in conjunction with the MGS provided a platform to identify altered retinal proteins and pathways to distinguish normal aging from pathology. Our results show that while there is overlap between aging and AMD, the majority of protein changes were unique to each process (Figure 4(a)). Importantly, the expression profile for most major categories was divergent comparing the two processes; the content of most proteins was decreased with aging and increased with AMD (Figure 4(c)) suggesting that normal aging and AMD are distinct processes.

The process with the most dramatically contrasting proteome when comparing biological aging versus pathology was the proteome changes in metabolic pathways (Figures 4(c) and 4(d)). Proteins from the glycolytic pathway (ALDOC, GAPDH, PGM1, and ENO1), TCA cycle (Transaldolase 1 and MDH1), electron-transport chain (ATP5PD and NDUFS3), and ketogenesis (HMG CoA synthase 2) were decreased with aging (Table 1). IPA pathway analysis suggested a significant decline in both glycolysis and gluconeogenesis, including predicted inhibition of ERR gamma signaling (ESRRG, Figure S1 Aging) that regulate the above-mentioned metabolic pathways. These results, as well as another study [35], are consistent with a general decline in metabolic activity in the aging RPE.

In contrast to aging, increased glycolytic proteins (ENO1, PGM1, PGK1, PKM, and ALDH2) and decreased content of OXPHOS proteins (NDUFV2, PPA2, COX6B1, ATP5F1A, ATPF1B, and ATPF1C) were observed with AMD progression (Figures 4(c) and 4(d), Table S4). These results are consistent with measurements of ATP production in primary RPE cultures from AMD donors where the majority of the ATP was generated via glycolysis and not from OXPHOS [36]. Notably, the significant loss in RPE mitochondrial function in cultures from AMD donors was corroborated in another study [37]. Results from proteomic analysis as well as functional analysis in primary RPE is consistent with the idea that AMD has a significant negative impact on RPE mitochondria. Other data using different experimental approaches also strongly implicate mitochondrial dysfunction as a pathologic feature of AMD. Supportive data from human donor tissue include ultrastructural defects in RPE mitochondria [38], altered protein content in RPE mitochondria and choroid/Bruch's membrane [39], increased mtDNA damage in macular RPE from AMD donors [9, 40], and decline in mt ETC proteins and function observed in a recent large-scale proteomic study on differentiated RPE cells from AMD patients [41]. For example, depletion of mtDNA in the RPE cell line, ARPE-19, using ethidium bromide, resulted in induction of genes indicating a switch in metabolism from oxidative phosphorylation to glycolysis and fatty acid metabolism as a mechanism for maintaining energy production [42]. Results from the current study, including upregulation of proteins in glycolysis, TCA, and fatty acid metabolism, suggest a reprogramming of energy utilization and provide further support for the hypothesis that mitochondrial dysfunction is a pathologic feature of AMD.

While our results suggest significant metabolic restructuring has occurred with AMD in RPE, it is important to note that we cannot directly infer causality as the protein changes simply correlate with disease. However, important insight about how alterations in the RPE mitochondrial function could initiate AMD has been developed using transgenic mice, which show the existence of a highly coordinated "metabolic ecosystem" between photoreceptors and RPE [43–45]. In this model, RPE transports glucose from choroidal blood to the photoreceptors where it is utilized for aerobic glycolysis. The by-product lactate is transported from photoreceptors back to the RPE and used for ATP production via OXPHOS. Data show that under normal conditions, glycolysis is suppressed in the RPE due to the high levels of lactate received from the retina [45]. However, with AMD, the loss in RPE mitochondrial function and subsequent decrease in ATP production would trigger a greater reliance on glycolysis to supply RPE energy demands. The

change in energy source to glucose could ultimately starve the underlying photoreceptors of glucose that is required for their energy needs. Decreased photoreceptor glycolysis could eventually lead to degeneration and cell death, a hallmark of AMD.

Another major class of proteins affected with both aging and AMD include chaperones and proteases that participate in the stress response. With aging, proteins involved in degradation (TPP1 and Cathepsin D) and refolding (HSP60, prohibitin, and ERP29) were significantly altered (Figure 4(c)) with most proteins decreasing in content. In our AMD analysis, GRP75 (mtHSP70, #D18), a mitochondrial matrix chaperone, and PDIA3 (#D21) an endoplasmic reticulum (ER) chaperone, were increased at onset (Figure 3(b)). IPA upstream regulator analysis showed activation of TRAP1 (Figure S1B) and activation of LONP1 at MGS2 with decline at later stages (Figure 6(b)). Since these proteins function as mt chaperones that assist with OXPHOS assembly and reduce oxidative stress, these patterns of activation agree with an early increase in oxidative stress in RPE that affect mt protein folding and homeostasis. Previous work from our lab suggest damage to mtDNA and altered content of ETC and mt heat shock proteins (mtHSP70, mtHSP60) from the earliest stage of AMD [7, 8, 22]. Damage to mtDNA and chaperones can consequently lead to production of damaged mtDNA-encoded proteins and improper folding and transport of nuclear-encoded proteins. Proteolysis is also affected, based on the increase in the 20S proteasome observed in RPE with disease progression [22]. The processes of protein refolding and degradation are essential for maintaining proteostasis. Deficiency in proteostasis could be especially detrimental to postmitotic RPE that is involved in many functions to maintain retinal health throughout life. Also, the contrast in the protein alterations between aging and pathology indicate distinct differences between the two processes, suggesting significant effects on AMD pathogenesis by disrupting protein homeostasis.

Several key proteins involved in oxidative stress response were upregulated at AMD onset (GST π, SOD1, Peroxiredoxin-3, Aldh2, glutamine synthetase). The observed upregulation of these redox-sensitive proteins may represent a compensatory response to increased oxidative stress in the RPE, which is consistent with a growing body of evidence implicating cumulative oxidative damage in AMD pathogenesis [46]. For example, the aged SOD1-deficient mouse demonstrated drusen-like deposits, choroidal neovascularization, and RPE abnormalities similar to AMD suggesting that oxidative stress is a major event in AMD pathogenesis [47]. We observed a significant increase in SOD1 content from MGS2 onwards (Figure 3(c), spot #D3). GST π is an inhibitor of proapoptotic signaling and stabilizes reactive electrophiles in response to increased oxidative stress [48–50]. For mitochondrion-specific Peroxiredoxin-3, considered a first line of defense against superoxide-derivative hydrogen-peroxide in the mitochondria, we observed a steady increase in Peroxiredoxin-3 (>2-fold) with progression of AMD (Figure 3(c), spot #D4) [51]. Mitochondrial ALDH2 (Figure 3(c), spot #D20) is essential for the removal of toxic aldehydes that are by-products of lipid peroxidation in the RPE [52]. In a recent study, overexpression of ALDH2 restored retinal function by reducing apoptosis and enhancing chaperone activity in mice [53]. Glutamine synthetase is an enzyme that generates glutamine via the condensation of glutamate and ammonia. Glutamine is one of the three amino acids that make up the important cellular redox regulator, glutathione [54]. Thus, upregulation of glutamine synthetase with AMD could indicate a requirement for more glutathione in response to increase oxidative stress. Previously enhanced utilization of glutathione was observed in primary RPE cultures when subjected to an oxidative stress [55]. Brown and colleagues showed that elevated oxidative stress is sufficient for RPE loss of function including mt disruptions, photoreceptor structural alterations, and a metabolic shift in the RPE to glycolysis in a RPE-specific SOD2-deficient mouse model [43]. Therefore, results from the current study and our previous studies showing increased content of multiple redox-sensitive proteins with AMD is consistent with increased oxidative stress as a major contributor AMD pathology [22].

In our aging analysis, IPA pathway and upstream regulator analysis predicted a decline in TCR, PLA2R1, and IL15 (Figure 6(a)), and this agrees with reduced T-cell receptor repertoire, lower production of naïve T-cells and interleukin's, and an inhibition of adaptive immunity that is observed with normal aging [56]. But with AMD, predicted activation of the inflammatory markers TCR, TNF, and IL15 (Figure 6(b), S1B) along with the apparent increase in oxidative stress (as discussed above) that is highly intertwined with inflammation agrees with prior reports that associate an inflammatory imbalance with AMD. Also supporting this idea are genetic association studies that linked the complement pathway (CFH, CFB, CFHR1/CFHR3, C3, and C5) to AMD, as well as the presence of complement proteins identified in significant quantity in retinal drusen [57, 58]. AMD inflammatory processes include complement activation, microglia activation, and macrophage infiltration [59]. Therefore, the immune system is a major player in AMD where immune dysregulation in the aging retina could be exacerbated by increased complement activation, increased proinflammatory cytokines, and activation of microglia in response to oxidative stress and soft-drusen accumulation.

In this study, we resolved and quantified ~500 protein spots from a complex mixture of RPE proteins. While this represents only a portion of the total RPE proteome, we identified 58 proteins that exhibited a significant change with either aging or AMD. There are several caveats associated with our experimental design and analysis, including that the proteins identified herein represent a conservative estimate of the total proteins changing due to the limitations inherent in 2D gels. With our sample size, a 50% change in spot density was the lower limit of change required for statistically significance. However, much smaller, physiologically relevant differences may have gone undetected. In the analysis of protein density changes with aging, linear regression analysis was used to identify age-dependent changes and would miss nonlinear changes that are biologically meaningful. In the first dimension of separation, a pH range

of 5 to 8 was utilized because it provided the greatest resolution for the majority of spots; however, protein changes outside this range would not be detected. While we were able to identify several plasma membrane proteins (i.e., prohibitin, apolipoprotein A-1, and transforming RhoA) from spots that showed differential content, membrane proteins resolve poorly in the first dimension and may be underrepresented. Given these caveats, we are currently employing proteomics techniques with more sensitivity and quantitative accuracy using state-of-the-art mass spectrometry and label-free proteomic quantification to extend and validate findings from the current study,

5. Conclusion

In summary, we used a proteomic approach to compare protein changes associated with normal aging and AMD in human donor RPE. While our results show some overlap in the biological processes affected, such as metabolism, energy utilization, and inflammation, a divergent direction of change was observed. Changes unique to aging include an overall decline in metabolic proteins and a decrease in chaperones and proteases, which refold and degrade damaged proteins to maintain cellular proteostasis. There was also inhibition of inflammation and immune response. The overall suppression of processes that protect against invading pathogens and cellular damage could establish an environment that promotes disease, especially in the presence of environmental or genetic risk factors.

The proteomic profile of AMD was distinct from that observed with aging. For example, in contrast to the decrease in glycolysis observed with aging, glycolytic enzymes were increased with AMD. This metabolic switch that favors glycolysis is likely due to defects in mitochondrial function, as shown by multiple studies [36, 42] and reflected in the observed decreased content of OXPHOS proteins. There was also multiple indicators of elevated oxidative stress and activation of inflammation and the immune response. The important contribution of an overactive inflammatory response in AMD development was recently proposed by two different groups who promoted the idea that the cumulative damage induced by aging, accompanied by the chronic inflammation, sets the stage for AMD pathogenesis [57, 60]. What "tips the balance" to disease is how the host responds to these challenges, which depends on the individual's genetic background. In general, our results are consistent with this idea.

Data Availability

All data generated or analyzed during this study are included in the published article.

Disclosure

Pabalu P. Karunadharma, Novozymes Inc., 1445 Drew Ave, Davis, CA 95618, USA; Timothy W. Olsen, Department of Ophthalmology, Mayo Clinic, 200 First Ave SW, Rochester, MN 55902, USA; Deborah A. Ferrington, Doheny Eye Institute, 150 N Orange Grove Blvd., Pasadena, CA 91103, USA. Dr. Olsen is owner of iMacular Regeneration, LLC and receives industry grant funding through Mayo Clinic from Novartis (no conflict with information from this manuscript).

Conflicts of Interest

The authors declare no conflict of interest for information presented in this study.

Authors' Contributions

Pabalu P. Karunadharma and Rebecca J. Kapphahn contributed equally to this work.

Acknowledgments

The authors wish to extend their sincere thanks to the personnel at the Lions Gift of Sight Eye Bank for their assistance in procuring eyes and processing tissue, Dr. George Tsaprailis (Scripps Research Institute, Scientific Director, Proteomics Core) for his expertise in mass spectrometry and helpful comments, and the Mass Spectrometry Consortium for the Life Sciences at the University Minnesota. We gratefully acknowledge the important contribution from the donors and their families. This work was supported in part with funds from the National Institutes of Health/National Institute of Aging (R01 AG025392 to TO), the Elaine and Robert Larson Endowed Vision Research Chair (DAF), the Lindsay Family Foundation (DAF), and an Anonymous Benefactor for AMD Research (DAF).

Supplementary Materials

All supplementary materials are provided in the supplementary file. Table S1: Donor demographics and clinical information. Table S2: Proteins identified from spots changing with Aging (spots with >3 protein identifications were not included in downstream pathway analysis). Table S3: Proteins identified from spots changing with AMD (spots with >3 protein identifications were not included in downstream pathway analysis). Table S4: Proteins identified from significantly altered spots from our previous studies and included in the IPA analysis. *(Supplementary Materials)*

References

[1] W. L. Wong, X. Su, X. Li et al., "Global prevalence of age-related macular degeneration and disease burden projection for 2020 and 2040: a systematic review and meta-analysis," *The Lancet Global Health*, vol. 2, no. 2, pp. e106–e116, 2014.

[2] Vision Loss Expert Group of the Global Burden of Disease Study, "Causes of blindness and vision impairment in 2021 and trends over 30 years: evaluating the prevalence of avoidable blindness in relation to "VISION 2020: the Right to Sight"," *The Lancet Global Health*, vol. 9, no. 2, pp. e144–e160, 2021.

[3] S. Somasundaran, I. J. Constable, C. B. Mellough, and L. S. Carvalho, "Retinal pigment epithelium and age-related macular degeneration: a review of major disease mechanisms,"

Clinical & Experimental Ophthalmology, vol. 48, no. 8, pp. 1043–1056, 2020.

[4] *Sources for Macular Degeneration: Facts & Figures*August 2022, http://www.brightfocus.org/sources-macular-degeneration-facts-figures.

[5] T. W. Olsen and X. Feng, "The Minnesota grading system of eye bank eyes for age-related macular degeneration," *Investigative Ophthalmology & Visual Science*, vol. 45, no. 12, pp. 4484–4490, 2004.

[6] Group A-REDSR, "The Age-Related Eye Disease Study system for classifying age-related macular degeneration from stereoscopic color fundus photographs: the Age-Related Eye Disease Study Report Number 6," *American Journal of Ophthalmology*, vol. 132, no. 5, pp. 668–681, 2001.

[7] C. L. Nordgaard, K. M. Berg, R. J. Kapphahn et al., "Proteomics of the retinal pigment epithelium reveals altered protein expression at progressive stages of age-related macular degeneration," *Investigative Ophthalmology & Visual Science*, vol. 47, no. 3, pp. 815–822, 2006.

[8] C. L. Nordgaard, P. P. Karunadharma, X. Feng, T. W. Olsen, and D. A. Ferrington, "Mitochondrial proteomics of the retinal pigment epithelium at progressive stages of age-related macular degeneration," *Investigative Ophthalmology & Visual Science*, vol. 49, no. 7, pp. 2848–2855, 2008.

[9] P. P. Karunadharma, C. L. Nordgaard, T. W. Olsen, and D. A. Ferrington, "Mitochondrial DNA damage as a potential mechanism for age-related macular degeneration," *Investigative Ophthalmology & Visual Science*, vol. 51, no. 11, pp. 5470–5479, 2010.

[10] S. Beranova-Giorgianni and F. Giorgianni, "Proteomics of human retinal pigment epithelium (RPE) cells," *Proteomes*, vol. 6, no. 2, p. 22, 2018.

[11] A. Decanini, P. R. Karunadharma, C. L. Nordgaard, X. Feng, T. W. Olsen, and D. A. Ferrington, "Human retinal pigment epithelium proteome changes in early diabetes," *Diabetologia*, vol. 51, no. 6, pp. 1051–1061, 2008.

[12] J. Rappsilber, Y. Ishihama, and M. Mann, "Stop and go extraction tips for matrix-assisted laser desorption/ionization, nanoelectrospray, and LC/MS sample pretreatment in proteomics," *Analytical Chemistry*, vol. 75, no. 3, pp. 663–670, 2003.

[13] N. L. Andon, S. Hollingworth, A. Koller, A. J. Greenland, J. R. Yates, and P. A. Haynes, "Proteomic characterization of wheat amyloplasts using identification of proteins by tandem mass spectrometry," *Proteomics*, vol. 2, no. 9, pp. 1156–1168, 2002.

[14] A. Keller, A. I. Nesvizhskii, E. Kolker, and R. Aebersold, "Empirical statistical model to estimate the accuracy of peptide identifications made by MS/MS and database search," *Analytical Chemistry*, vol. 74, no. 20, pp. 5383–5392, 2002.

[15] A. I. Nesvizhskii, A. Keller, E. Kolker, and R. Aebersold, "A statistical model for identifying proteins by tandem mass spectrometry," *Analytical Chemistry*, vol. 75, no. 17, pp. 4646–4658, 2003.

[16] H. Mi, D. Ebert, A. Muruganujan et al., "PANTHER version 16: a revised family classification, tree-based classification tool, enhancer regions and extensive API," *Nucleic Acids Research*, vol. 49, no. D1, pp. D394–D403, 2021.

[17] M. Kanehisa and S. Goto, "KEGG: kyoto encyclopedia of genes and genomes," *Nucleic Acids Research*, vol. 28, no. 1, pp. 27–30, 2000.

[18] K. K. Andringa, M. L. Bajt, H. Jaeschke, and S. M. Bailey, "Mitochondrial protein thiol modifications in acetaminophen hepatotoxicity: effect on HMG-CoA synthase," *Toxicology Letters*, vol. 177, no. 3, pp. 188–197, 2008.

[19] W. Zhou, M. Capello, C. Fredolini et al., "Mass spectrometry analysis of the post-translational modifications of alpha-enolase from pancreatic ductal adenocarcinoma cells," *Journal of Proteome Research*, vol. 9, no. 6, pp. 2929–2936, 2010.

[20] A. H. Erickson, G. E. Conner, and G. Blobel, "Biosynthesis of a lysosomal enzyme. Partial structure of two transient and functionally distinct NH2-terminal sequences in cathepsin D," *The Journal of Biological Chemistry*, vol. 256, no. 21, pp. 11224–11231, 1981.

[21] V. Stoka, V. Turk, and B. Turk, "Lysosomal cathepsins and their regulation in aging and neurodegeneration," *Ageing Research Reviews*, vol. 32, pp. 22–37, 2016.

[22] A. Decanini, C. L. Nordgaard, X. Feng, D. A. Ferrington, and T. W. Olsen, "Changes in select redox proteins of the retinal pigment epithelium in age- related macular degeneration," *American Journal of Ophthalmology*, vol. 143, no. 4, pp. 607–615.e2, 2007.

[23] É. Audet-Walsh, T. Yee, S. McGuirk et al., "Androgen-dependent repression of ERRγ reprograms metabolism in prostate cancer," *Cancer Research*, vol. 77, no. 2, pp. 378–389, 2017.

[24] J. Ambati, J. P. Atkinson, and B. D. Gelfand, "Immunology of age-related macular degeneration," *Nature Reviews Immunology*, vol. 13, no. 6, pp. 438–451, 2013.

[25] Y. Li, X. X. Sun, D. Z. Qian, and M. S. Dai, "Molecular crosstalk between MYC and HIF in cancer," *Frontiers in cell and developmental biology*, vol. 8, article 590576, 2020.

[26] J. Strom, B. Xu, X. Tian, and Q. M. Chen, "Nrf2 protects mitochondrial decay by oxidative stress," *The FASEB Journal*, vol. 30, no. 1, pp. 66–80, 2016.

[27] D. A. Ferrington, D. Sinha, and K. Kaarniranta, "Defects in retinal pigment epithelial cell proteolysis and the pathology associated with age-related macular degeneration," *Progress in Retinal and Eye Research*, vol. 51, pp. 69–89, 2016.

[28] O. Arjamaa, M. Nikinmaa, A. Salminen, and K. Kaarniranta, "Regulatory role of HIF-1α in the pathogenesis of age-related macular degeneration (AMD)," *Ageing Research Reviews*, vol. 8, no. 4, pp. 349–358, 2009.

[29] O. Arjamaa, V. Aaltonen, N. Piippo et al., "Hypoxia and inflammation in the release of VEGF and interleukins from human retinal pigment epithelial cells," *Graefe's Archive for Clinical and Experimental Ophthalmology*, vol. 255, no. 9, pp. 1757–1762, 2017.

[30] P. Mammadzada, P. M. Corredoira, and H. André, "The role of hypoxia-inducible factors in neovascular age-related macular degeneration: a gene therapy perspective," *Cellular and Molecular Life Sciences*, vol. 77, no. 5, pp. 819–833, 2020.

[31] A. García-Layana, F. Cabrera-López, J. García-Arumí, L. Arias-Barquet, and J. M. Ruiz-Moreno, "Early and intermediate age-related macular degeneration: update and clinical review," *Clinical Interventions in Aging*, vol. 12, pp. 1579–1587, 2017.

[32] C. S. Shin, S. Meng, S. D. Garbis et al., "LONP1 and mtHSP70 cooperate to promote mitochondrial protein folding," *Nature Communications*, vol. 12, no. 1, p. 265, 2021.

[33] A. Hoter, M. E. El-Sabban, and H. Y. Naim, "The HSP90 family: structure, regulation, function, and implications in health and disease," *International Journal of Molecular Sciences*, vol. 19, no. 9, p. 2560, 2018.

[34] I. Masgras, C. Sanchez-Martin, G. Colombo, and A. Rasola, "The chaperone TRAP1 as a modulator of the mitochondrial adaptations in cancer cells," *Frontiers in Oncology*, vol. 7, no. 7, p. 58, 2017.

[35] B. Rohrer, M. Bandyopadhyay, and C. Beeson, "Reduced metabolic capacity in aged primary retinal pigment epithelium (RPE) is correlated with increased susceptibility to oxidative stress," *Advances in Experimental Medicine and Biology*, vol. 854, pp. 793–798, 2016, PMID: 26427491.

[36] N. Golestaneh, Y. Chu, Y. Y. Xiao, G. L. Stoleru, and A. C. Theos, "Dysfunctional autophagy in RPE, a contributing factor in age-related macular degeneration," *Cell Death & Disease*, vol. 8, no. 1, article e2537, 2018.

[37] D. A. Ferrington, M. C. Ebeling, R. J. Kapphahn et al., "Altered bioenergetics and enhanced resistance to oxidative stress in human retinal pigment epithelial cells from donors with age-related macular degeneration," *Redox Biology*, vol. 13, pp. 255–265, 2017.

[38] J. Feher, I. Kovacs, M. Artico, C. Cavallotti, A. Papale, and G. C. Balacco, "Mitochondrial alterations of retinal pigment epithelium in age-related macular degeneration," *Neurobiology of Aging*, vol. 27, no. 7, pp. 983–993, 2006.

[39] X. Yuan, X. Gu, J. S. Crabb et al., "Quantitative proteomics: comparison of the macular bruch membrane/choroid complex from age-related macular degeneration and normal eyes," *Molecular & Cellular Proteomics*, vol. 9, no. 6, pp. 1031–1046, 2010.

[40] M. R. Terluk, R. J. Kapphahn, L. M. Soukup et al., "Investigating mitochondria as a target for treating age-related macular degeneration," *Journal of Neuroscience*, vol. 35, no. 18, pp. 7304–7311, 2015.

[41] A. Senabouth, M. Daniszewski, G. E. Lidgerwood et al., "Transcriptomic and proteomic retinal pigment epithelium signatures of age-related macular degeneration," *Nature Communications*, vol. 13, no. 1, p. 4233, 2022.

[42] M. V. Miceli and S. M. Jazwinski, "Nuclear gene expression changes due to mitochondrial dysfunction in ARPE-19 cells: implications for age-related macular degeneration," *Investigative Ophthalmology & Visual Science*, vol. 46, no. 5, pp. 1765–1773, 2005.

[43] E. E. Brown, A. J. DeWeerd, C. J. Ildefonso, A. S. Lewin, and J. D. Ash, "Mitochondrial oxidative stress in the retinal pigment epithelium (RPE) led to metabolic dysfunction in both the RPE and retinal photoreceptors," *Redox Biology*, vol. 24, article 101201, 2019.

[44] W. Wang, A. Kini, Y. Wang et al., "Metabolic deregulation of the blood-outer retinal barrier in Retinitis pigmentosa," *Cell Reports*, vol. 28, no. 5, pp. 1323–1334.e4, 2019.

[45] M. A. Kanow, M. M. Giarmarco, C. S. Jankowski et al., "Biochemical adaptations of the retina and retinal pigment epithelium support a metabolic ecosystem in the vertebrate eye," *eLife*, vol. 6, article e28899, 2017.

[46] H. Mao, S. J. Seo, M. R. Biswal et al., "Mitochondrial oxidative stress in the retinal pigment epithelium leads to localized retinal degeneration," *Investigative ophthalmology & visual science*, vol. 55, no. 7, pp. 4613–4627, 2014.

[47] Y. Imamura, S. Noda, K. Hashizume et al., "Drusen, choroidal neovascularization, and retinal pigment epithelium dysfunction in SOD1-deficient mice: a model of age-related macular degeneration," *Proceedings of the National Academy of Sciences of the United States of America*, vol. 103, no. 30, pp. 11282–11287, 2006.

[48] H. M. Beere, ""The stress of dying": the role of heat shock proteins in the regulation of apoptosis," *Journal of Cell Science*, vol. 117, no. 13, pp. 2641–2651, 2004.

[49] T. Wang, P. Arifoglu, Z. Ronai, and K. D. Tew, "Glutathione *S*-transferase P1-1 (GSTP1-1) inhibits c-Jun N-terminal kinase (JNK1) signaling through interaction with the C terminus," *The Journal of Biological Chemistry*, vol. 276, no. 24, pp. 20999–21003, 2001.

[50] L. A. Ralat and R. F. Colman, "Glutathione *S*-transferase Pi has at least three distinguishable xenobiotic substrate sites close to its glutathione-binding site," *The Journal of Biological Chemistry*, vol. 279, no. 48, pp. 50204–50213, 2004.

[51] L. Li and A. Q. Yu, "The functional role of peroxiredoxin 3 in reactive oxygen species, apoptosis, and chemoresistance of cancer cells," *Journal of Cancer Research and Clinical Oncology*, vol. 141, no. 12, pp. 2071–2077, 2015.

[52] S.-Y. Li, Z.-J. Fu, H. Ma et al., "Effect of lutein on retinal neurons and oxidative stress in a model of acute retinal ischemia/reperfusion," *Investigative Ophthalmology & Visual Science*, vol. 50, no. 2, pp. 836–843, 2009.

[53] L. Pan, W. Ding, J. Li et al., "Aldehyde dehydrogenase 2 alleviates monosodium iodoacetate-induced oxidative stress, inflammation and apoptosis in chondrocytes via inhibiting aquaporin 4 expression," *Biomedical Engineering Online*, vol. 20, no. 1, pp. 1–15, 2021.

[54] R. Curi, P. Newsholme, J. Procopio, C. Lagranha, R. Gorjao, and T. C. Pithon-Curi, "Glutamine, gene expression, and cell function," *Frontiers in Bioscience*, vol. 12, no. 1, pp. 344–357, 2007.

[55] M. R. Terluk, M. C. Ebeling, C. R. Fisher et al., "N-acetyl-L-cysteine protects human retinal pigment epithelial cells from oxidative damage: implications for age-related macular degeneration," *Oxidative Medicine and Cellular Longevity*, vol. 2019, Article ID 5174957, 14 pages, 2019.

[56] N. Salam, S. Rane, R. das et al., "T cell ageing: effects of age on development, survival & function," *The Indian Journal of Medical Research*, vol. 138, no. 5, pp. 595–608, 2013.

[57] D. Ardeljan and C. C. Chan, "Aging is not a disease: distinguishing age-related macular degeneration from aging," *Progress in Retinal and Eye Research*, vol. 37, pp. 68–89, 2013.

[58] J. W. Crabb, M. Miyagi, X. Gu et al., "Drusen proteome analysis: an approach to the etiology of age-related macular degeneration," *Proceedings of the National Academy of Sciences*, vol. 99, no. 23, pp. 14682–14687, 2002.

[59] M. Patel and C.-C. Chan, "Immunopathological aspects of age-related macular degeneration," *Seminars in Immunopathology*, vol. 30, no. 2, p. 97, 2008.

[60] M. P. Rozing, J. A. Durhuus, M. Krogh Nielsen et al., "Age-related macular degeneration: a two-level model hypothesis," *Progress in Retinal and Eye Research*, vol. 76, article 100825, 2020.

Hindawi
Oxidative Medicine and Cellular Longevity
Volume 2022, Article ID 7985596, 13 pages
https://doi.org/10.1155/2022/7985596

Research Article

Immunophenotypic Analysis of T Lymphocytes and Cytokine Production in Elderly Practicing Physical Activities and Its Relationship with Quality of Life and Depression

Tamires Marielem de Carvalho-Costa,[1] José Rodrigues do Carmo Neto,[2] Anna Glória Fonseca Teodoro,[1] Flávia Zero Soares,[1] Luiza Pimenta Rochael,[1] Thaís Farnesi Soares de Assunção,[1] Beatriz Coutinho de Souza,[1] Beatriz Sodré Matos,[1] Paula Degani Ferreira dos Santos,[1] Djalma Alexandre Alves Silva,[1] Juliana Reis Machado,[3] Paulo Roberto da Silva,[4] Monique Gomes Salles Tiburcio-Costa,[5] Carlo José Freire de Oliveira,[1] Virmondes Rodrigues Júnior,[1] Denise Bertulucci Rocha Rodrigues,[4,6] and Marcos Vinícius da Silva[1]

[1]*Department of Microbiology, Immunology and Parasitology, Institute of Biological and Natural Sciences, Federal University of Triângulo Mineiro, Uberaba, MG, Brazil*
[2]*Department of Bioscience and Technology, Institute of Tropical Pathology and Public Health, Federal University of Goias, Goiania, GO, Brazil*
[3]*Department of Pathology, Genetics and Evolution, Institute of Biological and Natural Sciences, Federal University of Triângulo Mineiro, Uberaba, MG, Brazil*
[4]*Cefores, Federal University of Triângulo Mineiro, Uberaba, MG, Brazil*
[5]*Federal University of Lavras, Lavras, MG, Brazil*
[6]*Laboratory of Biopathology and Molecular Biology, University of Uberaba, Uberaba, MG, Brazil*

Correspondence should be addressed to Marcos Vinícius da Silva; marcos.silva@uftm.edu.br

Received 28 March 2022; Accepted 12 September 2022; Published 22 September 2022

Academic Editor: Milena Georgieva

Aging is a complex process often associated with a chronic inflammatory profile that alters several biological functions, including the immune system and cognitive and physical capacity. The practice of physical activity is increasingly gaining popularity as a method of preventing infections, depression, and other disorders that affect the quality of life of the elderly. Thus, this work analyzes the profile of cytokines and molecular markers expressed in immune cells of elderly people who practice physical activities or not, evaluating their impacts on the immune system and quality of life. For this, 48 individuals were recruited, and peripheral blood samples were collected for hemogram analysis, cytokine determination, and immunophenotyping. Elderly people were separated into two groups: practitioners with low-intensity physical activity and non-practitioners. Quality of life was assessed using the Whoqol-Old instrument, and depression was assessed using the Beck II Depression Inventory. When comparing the scores of the Whoqol-Old and Beck questionnaires, we observed a significant negative correlation between these two factors. The perception of a higher quality of life was present in the elderly who exercised and was related to greater autonomy and sensory abilities, whereas the presence of depression was lower. In the hemogram, we observed higher basophil and segmented counts in the sedentary elderly, whereas lymphocytes and monocytes had lower counts. Elderly practitioners of physical activities had higher levels of IFN-γ, IL-4, and IL-10; increased expression of CD69, PD1, and TIM-3 in CD4+ T lymphocytes and increased CD14+CD80+ and CD14+CD86+ monocytes. Elderly people with an increased perception of quality of life had higher levels of IFN-γ, higher expression of CD14+CD80+CD86+, and decreased levels of TRAIL. An increase in TRAIL was observed in individuals with depression, in addition to an increased expression of CD14+CD86+. These results show a clear correlation between the quality of life, level of depression, physical activity, and immune system function. Although some cytokines with a typical proinflammatory profile (IFN-γ) were observed, the results point to a protective state with benefits reflected in the general well-being of the elderly who exercise.

1. Introduction

In general, aging is associated with complex changes in the body, including the immune system. These changes result from interactions with the external environment resulting in exposure to pathogenic microorganisms, poor quality of life, and genetic alterations [1]. In addition, early disability induced by loss of function and muscle mass in the elderly may be associated with chronic inflammatory processes commonly present during aging, known as the subclinical inflammatory state [2].

Another problem that affects many elderly people and contributes to reduced quality of life and disability is depression [3], a multifactorial disease that has grown worldwide. The elderly have many characteristics that favor their development [4], including the presence of chronic diseases [5] that lead them to lose their routine and independence. In addition, the symptoms of depression are strongly associated with the risk of morbidity during aging.

Drug treatments provide temporary relief and cannot be applied for prolonged periods owing to their side effects [6]. Thus, regular physical activity has been an explored alternative, bringing benefits related to the physiological improvement of the systems and the maintenance of the physical condition, preventing situations that generate disability in the elderly [6, 7]. The practice of physical activity can also help in the alternative treatment for depression [8], reducing symptoms, and improving the quality of life of the elderly [9].

In this context, this study analyzed the profile of cytokines and molecular markers expressed in the immune cells of elderly people who practice physical activities.

2. Materials and Methods

2.1. Participants. Forty-eight individuals aged 60 years or older (median 63.5, Min/Max 60/86), including 27 men and 21 women, were recruited during care at the Elderly Care Unit (UAI) in Uberaba, state of Minas Gerais, Brazil. UAI is a free municipal public space focused on the psychosocial well-being of the elderly, where they can perform different recreational physical and mental activities. Two groups were formed: elderly practitioners of physical and/or mental health ($n = 15$) and elderly individuals considered sedentary ($n = 33$). The type, intensity, and duration of physical and mental activity were assessed using the International Physical Activity Questionnaire-Short Form and patient self-reports. All elderly practitioners of regular physical and/or mental health performed low-to moderate-intensity activities, with an average duration of 55 minutes per day, three times a week. The physical or mental activities performed were hydrogymnastics ($n = 9$), gymnastics ($n = 5$), dancing ($n = 4$), weight training ($n = 3$), swimming ($n = 3$), snookering ($n = 3$), volleyball ($n = 2$), basketball ($n = 1$), capoeira ($n = 1$), and board games ($n = 1$). The comorbidities included systemic arterial hypertension ($n = 8$), dyslipidemia ($n = 4$), diabetes mellitus ($n = 2$), Chagas disease ($n = 2$), hypothyroidism ($n = 2$), arthrosis ($n = 1$), stroke ($n = 1$), back pain ($n = 1$), glaucoma ($n = 1$), insomnia ($n = 1$), and labyrinthitis ($n = 1$). This study was approved by the ethics committee for research with human beings of the Federal University of Triângulo Mineiro, and all participants signed the free consent form after clarification. This study was approved by the Research Ethics Committee of the Federal University of Triângulo Mineiro (CEP/UFTM/2390/2012).

2.2. Assessment of Individual Perception of Quality of Life and Assessment of the Depression Scale. The Whoqol-Old instrument was used to assess individual perceptions of the quality of life [10]. This questionnaire has 24 questions, grouped into six facets: sensory functioning; autonomy; past, present, and future activities; social participation; death and dying; and intimacy. The answers followed a Likert scale (from 1 to 5), and, according to the scores assigned to each question, a score ranging from 4 to 20 was obtained for each facet, which was later corrected to result in percentages. Higher scores represent a higher quality of life. The scores of these six facets combined provided an overall score separating the quality of life of the elderly into three categories: good (80–100), fair (60–80), and need for improvement (0–60).

The assessment of the depression scale was performed using the Beck II Depression Inventory (BDI) [11, 12]. Through 21 items, this questionnaire sought to measure the severity of depressive symptoms in two scenarios common to the elderly: cognitive-affective and physical-somatic scenarios. The assessment of the intensity of depressive symptoms is reflected in the score (BDI score) obtained by each of the elderly and classified as no depression (0–13), mild depression (14–19), moderate depression (20–28), and severe depression (29–63).

2.3. Blood Count and Determination of Serum Cytokine Levels. Two peripheral blood samples were collected for blood count assessment and serum cytokine quantification. For this, a sample was collected in a tube containing EDTA (for the blood count) and another in a tube without anticoagulant (for cytokine quantification).

The blood count was performed using an automated method and the serum levels of cytokines IL-1β, IL-4, IL-6, IL-10, IFN-γ, TNF-α, TGF-β, and TRAIL were quantified by ELISA (BD Pharmingen-USA). The concentration of cytokines was determined by linear regression with the absorbance obtained from the recombinant cytokines and expressed in pg/mL, always respecting the detection limit of each assay.

2.4. Evaluation of the Expression of Surface Molecules of $CD4^+$ and T $CD8^+$ Lymphocytes by Flow Cytometry. For immunophenotyping, a third sample was collected in a tube containing heparin. The circulating lymphocytes of the patients were characterized by their subpopulation between auxiliary and cytolytic (CD4+ or CD8+, respectively), concerning the expression of the activation marker (CD69), in addition to coinhibitory molecules (TIM-3 and PD-1). The monocytes were evaluated for the expression of CD14, CD80, and CD86.

Briefly, whole blood samples collected in heparinized tubes were blocked with phosphate-buffered saline containing 10% inactivated AB+ human serum. Specific monoclonal antibodies

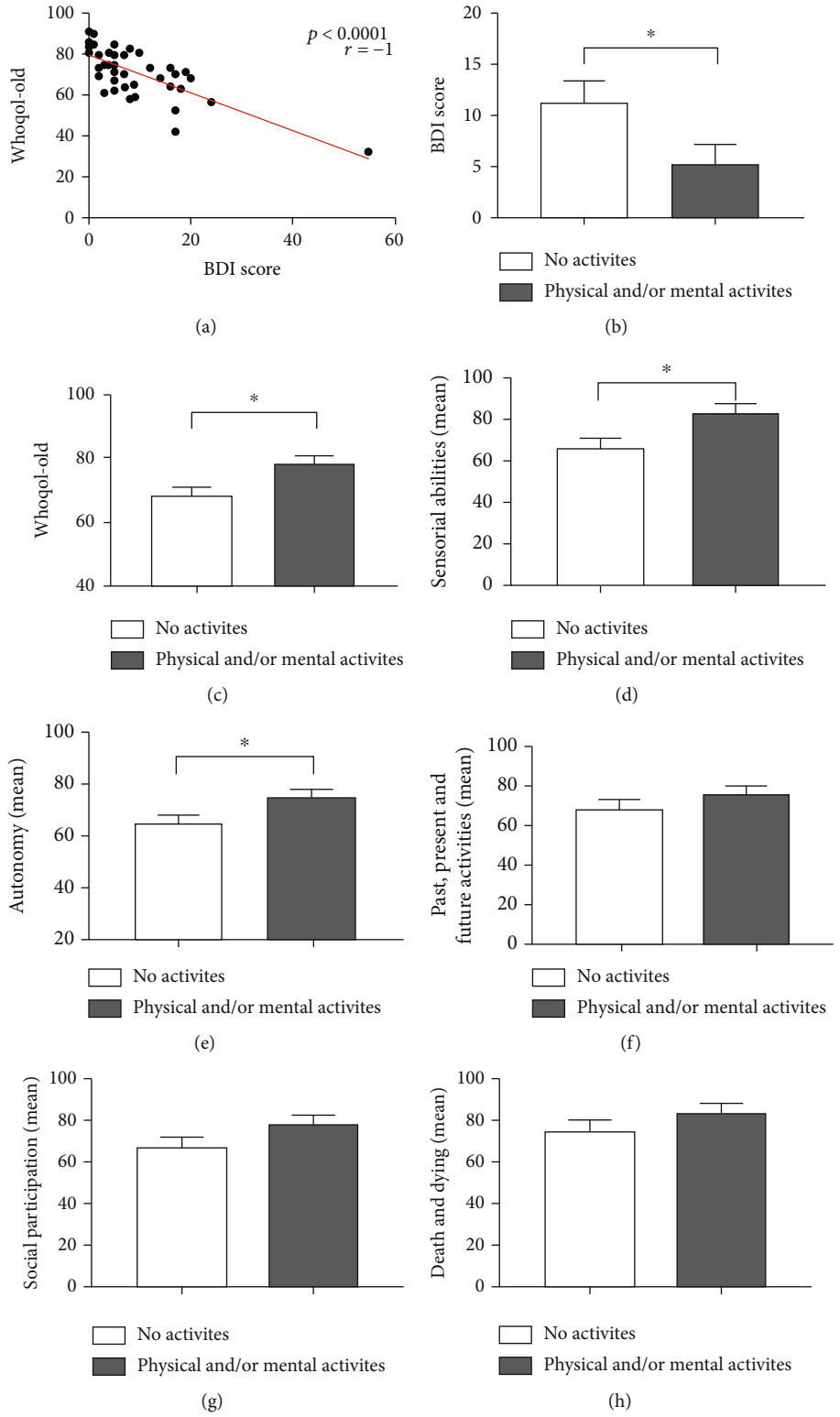

Figure 1: Continued.

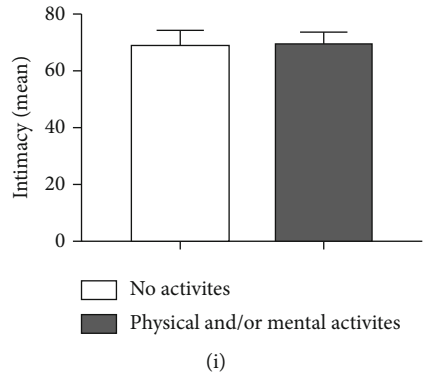

Figure 1: Assessment of individual perception of quality of life, depression scale, and impact of physical and/or mental activity in the elderly. (a) Correlation between the values obtained in the Whoqol-Old questionnaire and the Beck Depression Inventory II. (b) Impact of physical and/or mental activity on individual perception of quality of life (Whoqol-Old). (c) Impact of physical and/or mental activity on assessing the depression scale (BDI score). (D-I) Impact of physical and/or mental activity on the following assessment facets of individual perception of quality of life: sensory functioning; autonomy; past, present, and future activities; social participation; death and dying; and intimacy, respectively. Differences are considered statistically significant when $p < 0.05$.

directed to the surface molecules of lymphocytes were then added (anti-CD4, anti-CD8, anti-CD69, anti-TIM-3, anti-PD-1, anti-CD14, anti-CD80, and anti-CD86) conjugated to different fluorophores (FITC, PE, and PE-Cy5) and combined according to the convenience of the assay. When reading the assay, lysis of red blood cells was performed, and the cells were acquired using a FACS-CALIBUR cytometer (Becton & Dickinson, USA). The analysis of the acquired cells was performed using the Cell Quest program (Becton & Dickinson, USA), from the individualization of the leukocyte population through gates established according to the size (FSC) and granularity (SSC) standards and analyzed using FlowJo 10 software (Becton, Dickinson & Company).

2.5. Statistical Analysis. The database was created using the EXCEL 2016 program, and statistical analyses were performed using GRAPHPAD PRISM 8.0.1 (GRAPHPAD SOFTWARE, USA). The verification of the normal distribution of quantitative variables was evaluated using the D'Agostino and Pearson tests. For comparison between the two groups, the unpaired t-test was used for data with a normal distribution and the Mann–Whitney test for data with a nonnormal distribution. Correlations were determined using Spearman's test with a 95% confidence interval. The results were considered statistically significant at $p < 0.05$.

3. Results

3.1. Assessment of Individual Perception of Quality of Life and Depression Scale. Of the total number of elderly people evaluated, 34 (70.8%) answered questionnaires to assess their quality of life and depression. According to the Whoqol-Old questionnaire, 14 individuals had a quality of life classified as "good," 18 as "regular," and two as "need to improve." Of the 34 elderly people who responded to the Beck Depression Inventory, 23 had no depression, 10 had mild/moderate depression, and one had severe depression. When comparing the scores of the quality of life (Whoqol-Old) and depression (Beck) questionnaires, it was possible to report a significant, strong, and negative correlation ($p < 0.0001$ and $r = -1$) (Figure 1(a)). Thus, the better the quality of life, the lower the signs of depression.

When comparing the practice of physical activity with the answers obtained in the questionnaires, it was observed that elderly practitioners of physical activity had lower scores on the Beck Depression Inventory ($p = 0.0280$) (Figure 1(b)) and higher values on the Whoqol-Old ($p = 0.0276$) (Figure 1(c)). Interestingly, it was possible to observe that this same group, the physically active elderly, demonstrated greater sensory ($p = 0.0291$) (Figure 1(d)) and autonomy ($p = 0.0472$) skills (Figure 1(e)). Regarding the other facets of the Whoqol-Old test, such as past, present, and future activities ($p = 0.2623$) (Figure 1(f)); social participation ($p = 0.0779$) (Figure 1(g)); death and dying ($p = 0.3346$) (Figure 1(h)); and intimacy ($p = 0.7289$) (Figure 1(i)), there were no statistical differences between the groups.

3.2. Hematological Parameters and Determination of Serum Cytokine Levels. After analyzing the impact of physical activity on the parameters of individual perception of quality of life and on the BDI, the next step was to assess the effects on hematological parameters (Figure 2). Regarding total leukocyte count, there was no statistically significant difference between the groups ($p = 0.2344$) (Figure 2(a)). Interestingly, when the relative percentage of the main circulating leukocyte subpopulations was evaluated, it was observed that physical and/or mental activity induced an increase in basophils ($p = 0.0005$) (Figure 2(b)) and segmented ($p < 0.0001$) (Figure 2(c)). Furthermore, in the same group, monocytes ($p = 0.0001$) (Figure 2(d)) and lymphocytes ($p < 0.0001$) (Figure 2(e)) had lower counts than the group that did not practice physical activity. Finally, eosinophil counts were not significantly different between the groups ($p = 0.5293$) (Figure 2(f)).

Regarding serum cytokines (Figure 3), elderly people who exercised had higher levels of IFN-γ ($p = 0.0002$) (Figure 3(a)), IL-4 ($p = 0.0027$) (Figures 3(a) and 3(b)), and

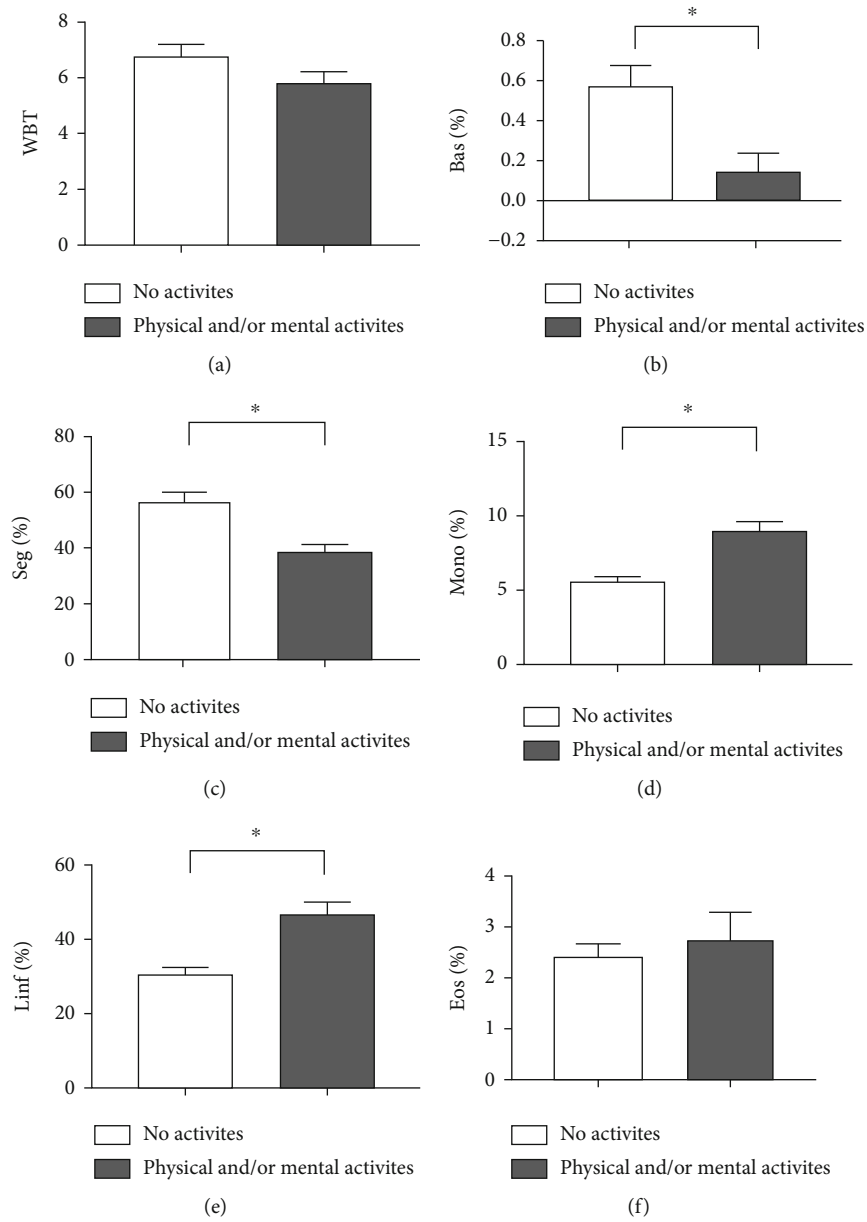

Figure 2: Impact of physical and/or mental activity on hematological parameters in the elderly. (a) total leukocytes (WBT), (b) basophils (bas), (c) segmented (sec), (d) monocytes (mono), (e) lymphocytes (lymph), and (f) eosinophils (eos). Differences are considered statistically significant when $p < 0.05$.

IL-10 ($p = 0.0007$) (Figure 3(c)) compared to sedentary individuals. No statistical differences were observed between the groups for IL-1β ($p = 0.5546$) (Figure 3(d)), IL-6 ($p = 0.8882$) (Figure 3(e)), TNF-α ($p = 0.5430$) (Figure 3(f)), TGF-β ($p = 0.9272$) (Figure 3(g)), and TRAIL ($p = 0.3851$) (Figure 3(h)).

Elderly people with an increased perception of quality of life (Figure 4) showed a tendency to have increased IFN-γ ($p = 0.0567$) (Figure 3(a)) and lower serum levels of TRAIL compared to the poor/fair group ($p = 0.0011$) (Figure 4(h)). For the remaining cytokines evaluated, no statistically significant differences were observed: IL-4 ($p = 0.4078$) (Figure 3(b)), IL-10 ($p = 0.1511$) (Figure 3(c)), IL-1β ($p = 0.4099$) (Figure 4(d)), IL-6 ($p = 0.1090$) (Figure 4(e)), TNF-α ($p = 0.6212$) (Figure 4(f)), and TGF-β ($p = 0.4562$) (Figure 4(g)) (Figure 4(h)).

Elderly people with a worse quality of life showed an inversely proportional correlation with TRAIL rates ($p = 0.027$ and $r = -0.48$) (Figure 5(a)). Higher values for TRAIL were also those that presented with more depression according to the BDI ($p = 0.04$ and $r = 0.44$) (Figure 5(b)).

3.3. Evaluation of the Expression of Surface Molecules of CD4 + and T CD8+ Lymphocytes by Flow Cytometry. When evaluating markers on the surface of T lymphocytes (Figure 6), it was observed that individuals who practiced physical activity showed a greater number of CD69+ ($p = 0.0062$)

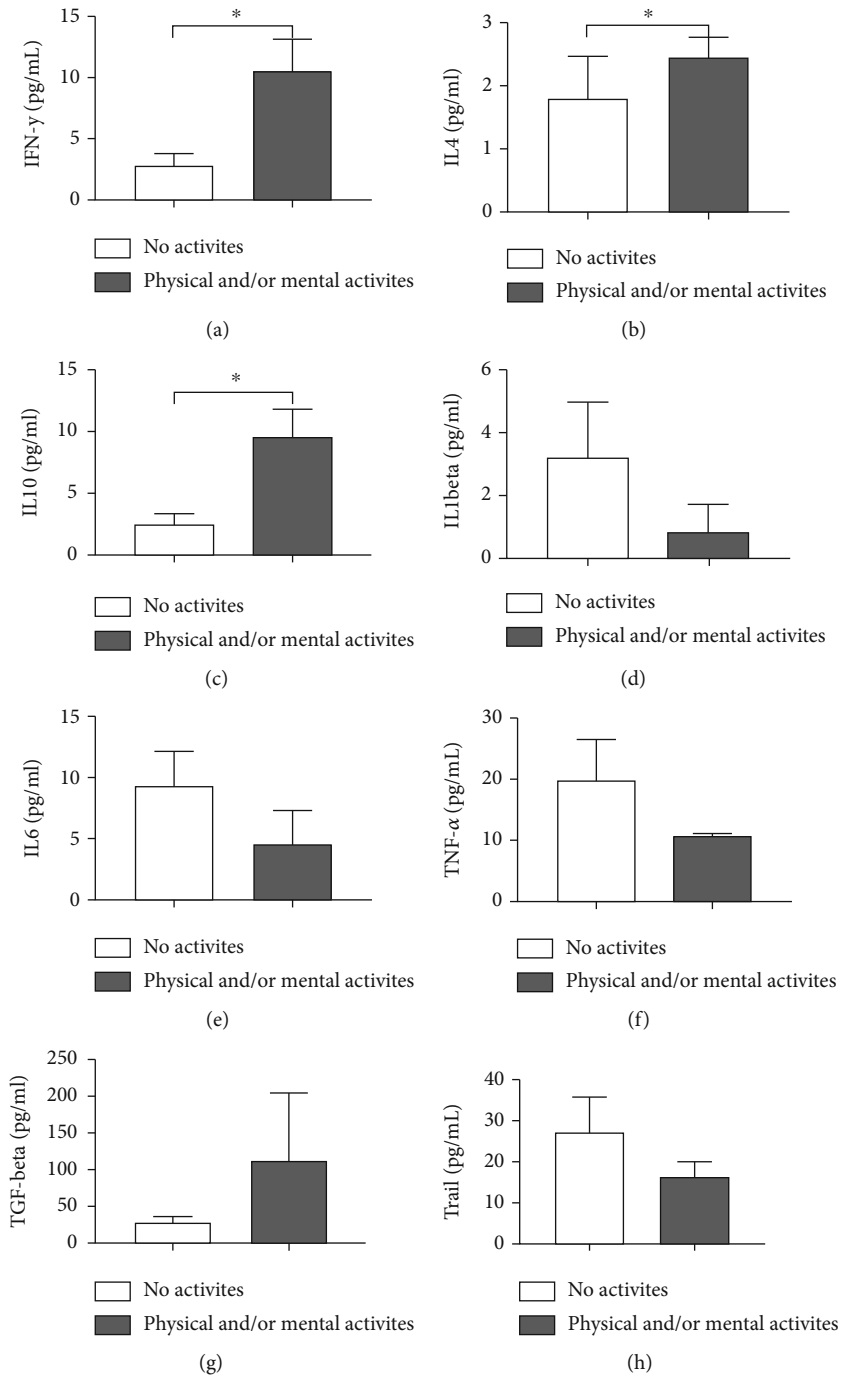

Figure 3: Impact of physical activity on the serum cytokine profile of the elderly. (a) IFN-γ, (B) IL-4, (c) IL-10, (d) IL-1β, (E) IL-6, (f) TNF-α, (g) TGF-β, and (h) TRAIL. Differences are considered statistically significant when $p < 0.05$.

(Figure 6(a)) and PD1 + (Figure 6(b)) cells ($p = 0.0008$) CD4 + cells but not CD8+ cells ($p = 0.3435$ and $p = 0.2672$, respectively) (Figures 6(d) and 6(e)). Furthermore, there was no statistical difference in TIM-3 expression in both CD4+ ($p = 0.1042$) (Figure 6(c)) and CD8+ ($p = 0.2167$) (Figure 6(f)) lymphocytes between the two groups.

CD14+ cells doubly positive for CD80 and CD86 were found in significantly higher amounts in physically active practitioners ($p < 0.0001$) (Figure 7(a)). When analyzing these two markers separately, we observed that CD86+ showed reduced expression in these individuals ($p = 0.0002$) (Figure 7(b)), whereas CD80+ showed no significant difference between the groups ($p = 0.1986$) (Figure 7(c)).

Regarding the perception of quality of life (Figure 8), elderly people who were classified as having a good quality of life had a higher number of CD14+CD80+CD86+ cells

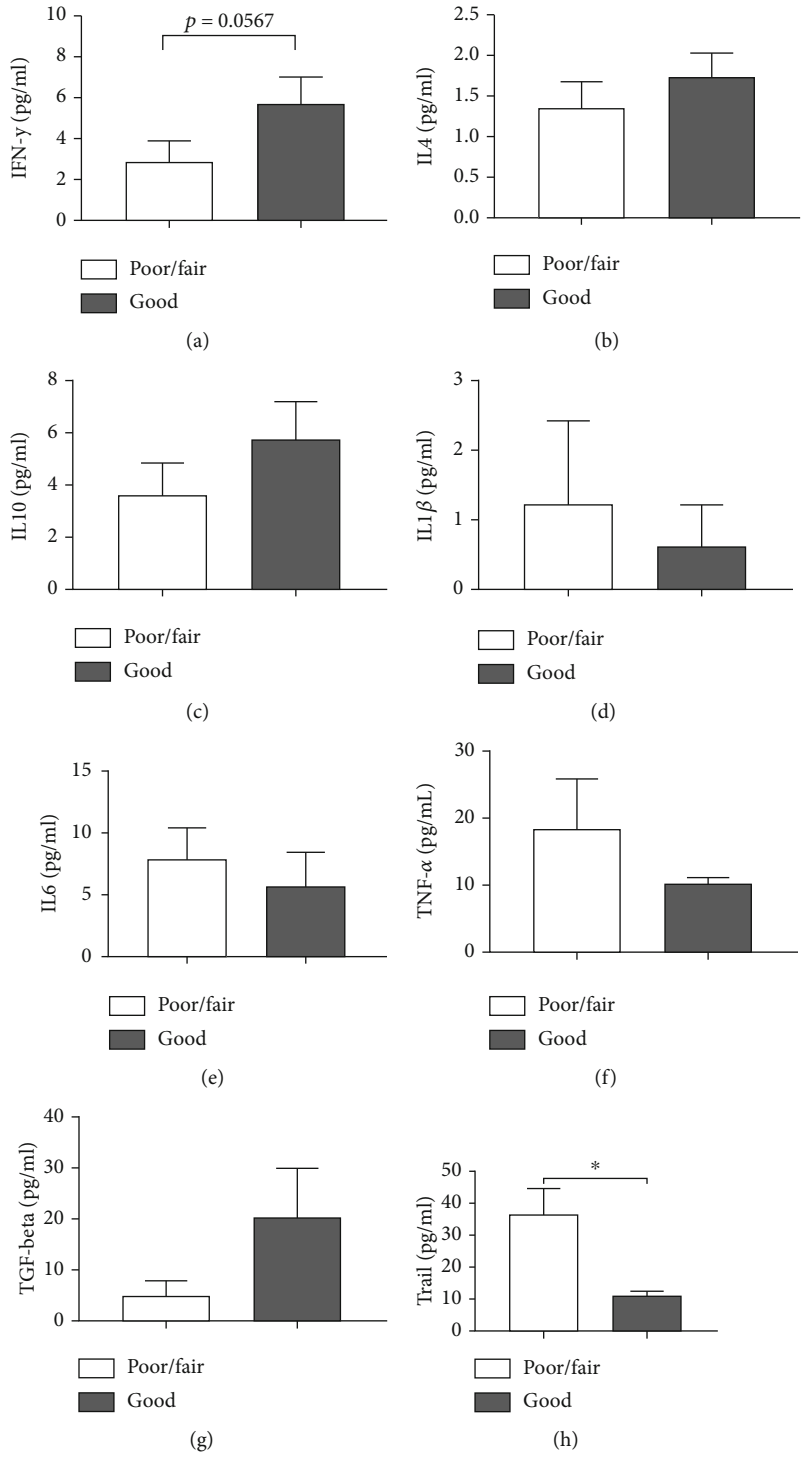

Figure 4: Impact of perceived quality of life on the serum cytokine profile of the elderly. (a) IFN-γ, (b) IL-4, (c) IL-10, (d) IL-1β, (e) IL-6, (f) TNF-α, (g) TGF-β and (h) TRAIL. Differences are considered statistically significant when $p < 0.05$.

($p = 0.0128$) (Figure 8(a)) than those classified as poor/fair. There was no significant difference between the groups in the CD14+CD80+ subpopulations ($p = 0.3638$) (Figure 8(b)). However, sedentary elderly individuals showed a higher level of CD14+CD86+ cells ($p = 0.0007$) (Figure 8(c)).

For the elderly with some level of depression (Figure 9), triple-positive cells for CD14+CD80+CD86+ showed a decreasing trend ($p = 0.0611$) (Figure 9(a)). Only those marked by CD14+CD86+ were increased in this group ($p = 0.0061$) (Figure 9(c)). In addition, there was no change in those marked CD14+CD80+ ($p = 0.8470$) (Figure 9(b)) between the groups.

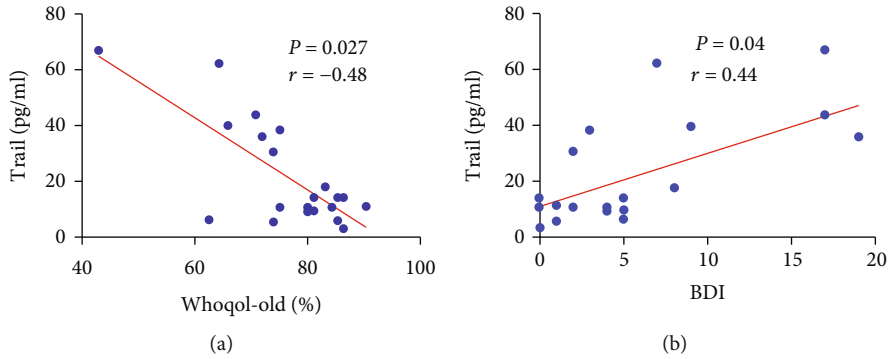

Figure 5: Correlation of TRAIL with (a) individual perception of quality of life (Whoqol-Old score) and with (b) depression scale (BDI). A Spearman correlation test was performed. Differences are considered statistically significant when $p < 0.05$.

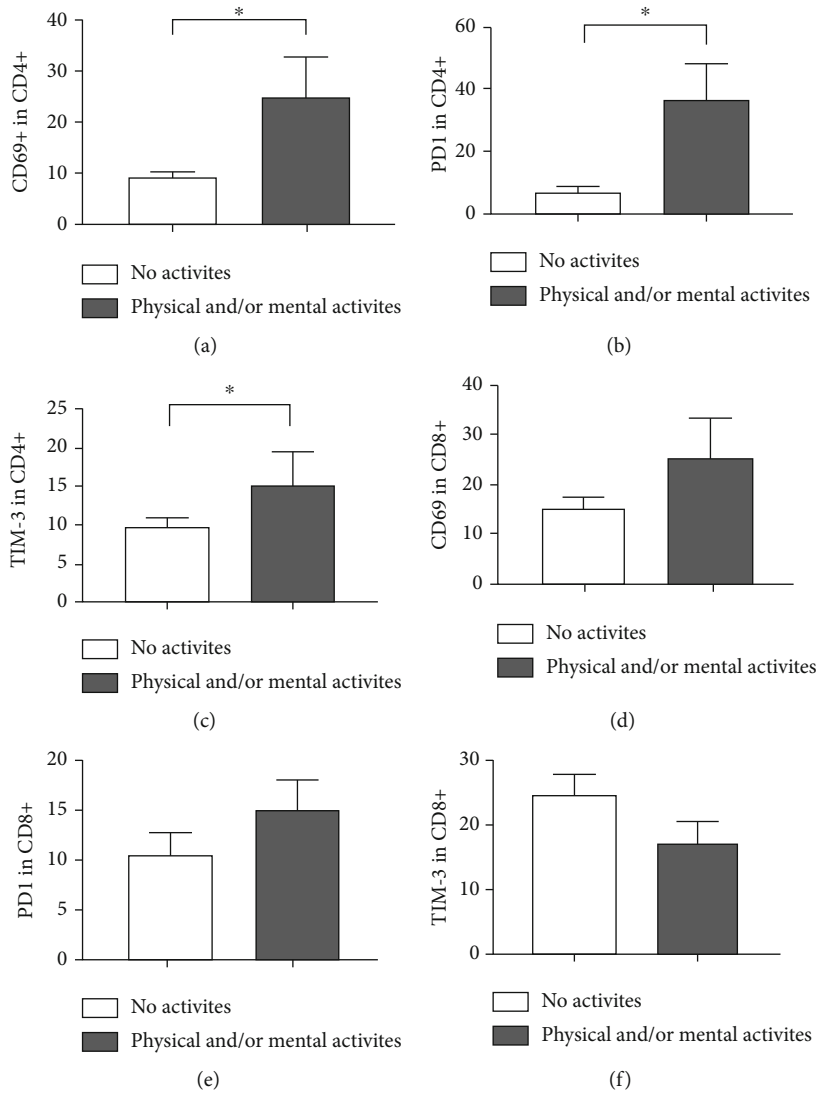

Figure 6: Impact of physical activity on the expression profile of surface markers in CD4+ and CD8+ T lymphocytes obtained from the blood of elderly people. Expressions of (a) CD69, (b) PD1, and (c) TIM-3 on CD4+ T lymphocytes. Expressions of (d) CD69, (e) PD1, and (f) TIM-3 on CD8+ T lymphocytes. Differences are considered statistically significant when $p < 0.05$.

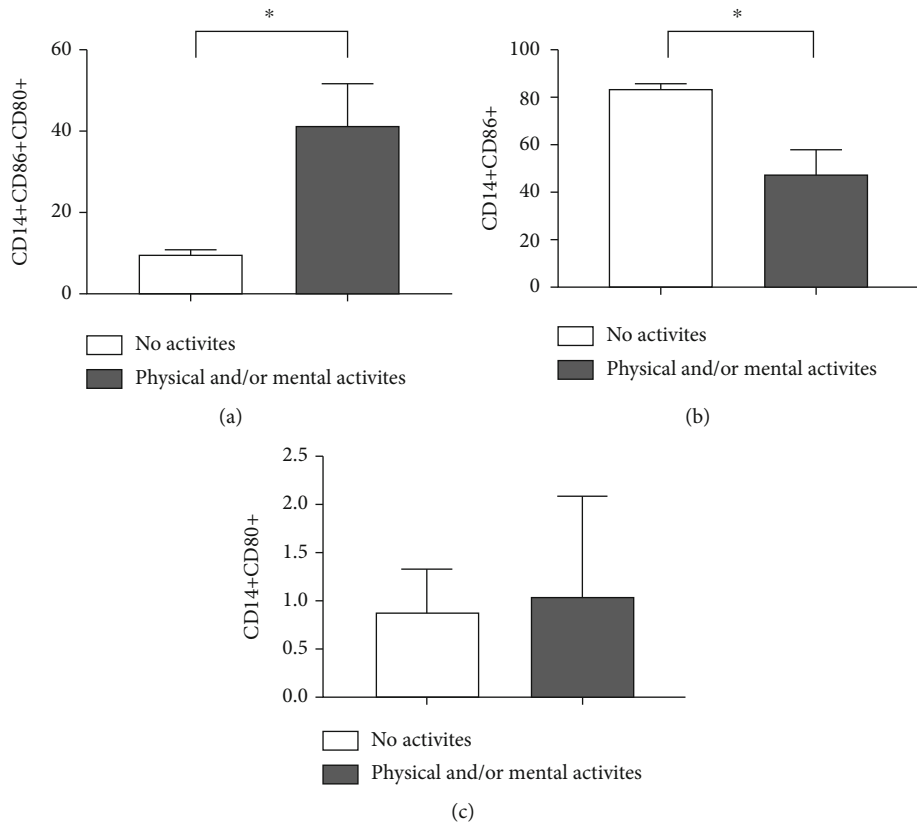

Figure 7: Impact of physical activity on the expression profile of surface markers on CD14+ cells obtained from the blood of the elderly. Expressions of (a) CD14+CD86+CD80+, (b) CD14+CD86+, and (c) CD14+CD80+ on CD14+ cells. Differences are considered statistically significant when $p < 0.05$.

4. Discussion

The inflammatory pathway is a potential target for reducing disability resulting from a persistent subclinical inflammatory state, commonly observed in the elderly [13]. Studies have shown that in this population, proinflammatory cytokines are naturally higher compared to the levels seen in middle-aged or young people [14]. Thus, one of the ways to improve this situation is the practice of regular physical activity because there is a good relationship between regular exercise and the serum reduction of proinflammatory cytokines [15]. However, little is known regarding the mechanisms involved in this process.

Among the hypotheses raised, (1) it has been reported that during physical training, the muscles undergo biochemical changes that result in the reduction of the local gene expression of proinflammatory cytokines, such as IL-6, TNF-α, and IL- 1β [16, 17]. (2) The increase in muscle strength has also been related to lower serum levels of cytokines such as IL-6 and TNF-α [18]. (3) Along with the two hypotheses highlighted above, physical activity may induce lower production of proinflammatory cytokines by immune cells [19]. However, immunomodulation seems to depend on the type of exercise, intensity, frequency, and the individual's health condition because there are reports in which physical activity does not influence the serum levels of cytokines [20]. In our study, IL-6, TNF-α, and IL-1β levels did not differ between the groups, which may be related to the difference in the type of exercise, intensity, and frequency performed among the participants and the time of blood collection for cytokine measurement (before, during, or after physical activity). Despite this, we observed an increase in IL-4 and IL-10 cytokines in the elderly who exercised, suggesting that exercise has a protective anti-inflammatory role [21] and possibly an immune balance (IFN-γ and IL-4/IL-10).

The increase in cells, such as lymphocytes and monocytes, in the blood count of the elderly that exercise corroborates the increased production of the cytokine profile. IFN-γ, a proinflammatory cytokine, is mainly synthesized by T lymphocytes. This cytokine generally activates macrophages and other immune cells to produce chemokines that recruit more cells to the inflamed site [22]. Although this cytokine is considered a stimulator of inflammation, proinflammatory cytokines can also play immunoregulatory roles, depending on the moment, the amount, and the disease model evaluated [23]. A fact that occurs, for example, during acute exercise, where there is an increase in the production of IL-6 to regulate the output of TNF-α and IL-1β and increase the production of IL-10, which helps in cellular homeostasis [21, 24]. In addition, it favors lipolysis and glucose homeostasis, consequently stimulating lean mass gain instead of fat [25]. Studies assessing the presence of exercise

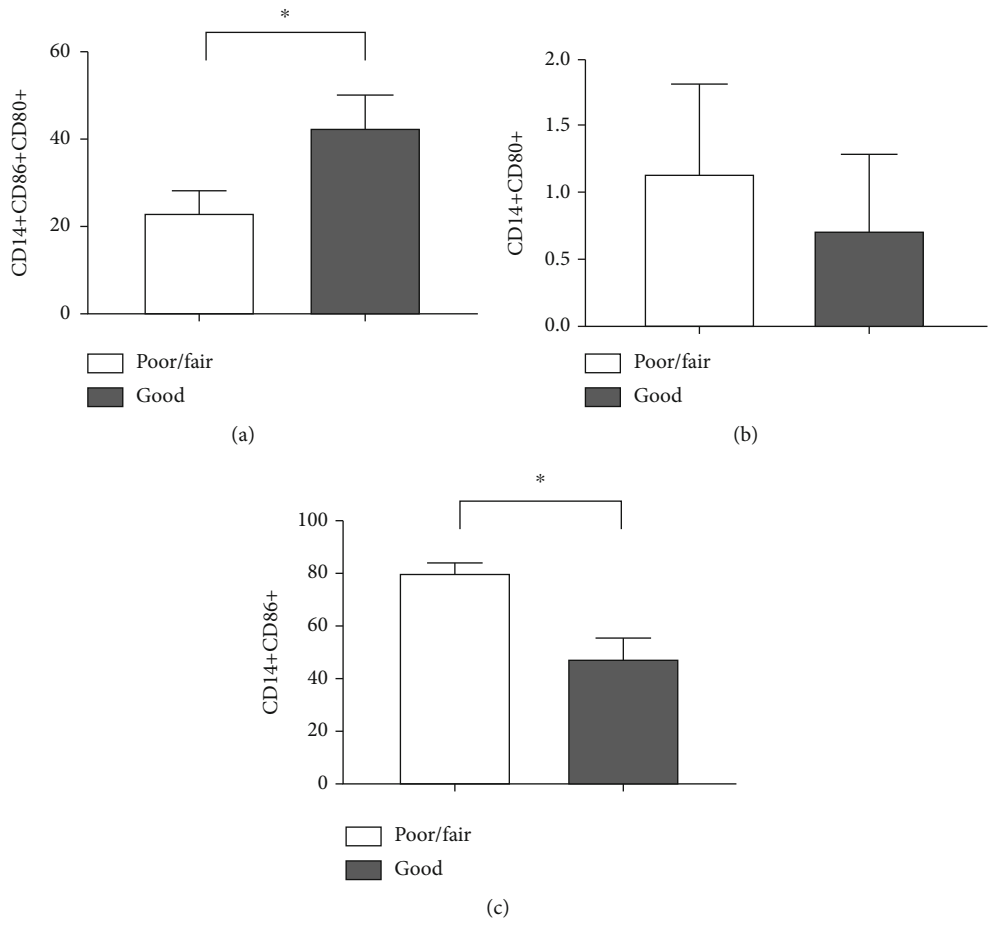

Figure 8: Impact of quality of life perception on the expression profile of surface markers in CD14+ cells obtained from the blood of the elderly. Expression of (a) CD14+CD86+CD80+, (b) CD14+CD80+, and (c) CD14+CD86+. Differences are considered statistically significant when $p < 0.05$.

throughout life show the various benefits involved in the balance of pro- and anti-inflammatory cytokines resulting from muscle activity [26], which may also be reflected in the quality of life of people who practice physical activity [27].

TIM-3+, a surface marker of immunosenescence, especially T lymphocytes, was found to have a higher expression of CD4+ lymphocytes in physically active elderly individuals. This increase may be related to the good results obtained for autonomy and sensory parameters because studies have shown that high levels of CD4+ and CD8+ TIM3+ T cells are inversely associated with the evolution of rheumatoid arthritis [28, 29]. This is a disease that affects many elderly individuals and is responsible for motor impairment in these individuals [30]. Low levels of TNF-α may also have contributed to this result [23].

Another interesting point was that the sedentary elderly had a worse perception of quality of life and developed some depression. This may be related to the fact that in elderly people, the subclinical chronic inflammatory state, common during the aging process, is associated with changes in the enzymatic pathways of monoamine metabolism. These molecules directly interfere with the production of serotonin, a substance that gives feelings of well-being [31, 32]. Tryptophan, for example, is a monoamine whose degradation is increased during inflammatory processes caused by stimulation by IFN-γ. Thus, an association between inflammatory processes and depressive symptoms is common [31]. In contrast, our findings point to an increase in IFN-γ in the elderly who exercise, a fact also found in the work of [33]. In this case, the authors argue that the types of exercise practiced by the evaluated individuals are responsible for these divergent levels. The good mood, perception of increased quality of life, and absence of depressive symptoms observed here are probably caused by the increase in neurotransmitter synthesis or other monoamines that may not bind to tryptophan under the conditions studied.

In our study, TRAIL was inversely correlated with quality of life and directly correlated with depression. Although the role of this cytokine in inflammation is not yet clearly defined [34, 35], studies have reported that this molecule can induce proinflammatory cytokines, such as IL-1β, IL-6, and TNF-α, in macrophages in vitro [36]. Furthermore, serum TRAIL levels are associated with TNF-α and decreased lung function in patients with chronic obstructive pulmonary disease [37]. Both studies support a proinflammatory function. Thus, the negative correlation between

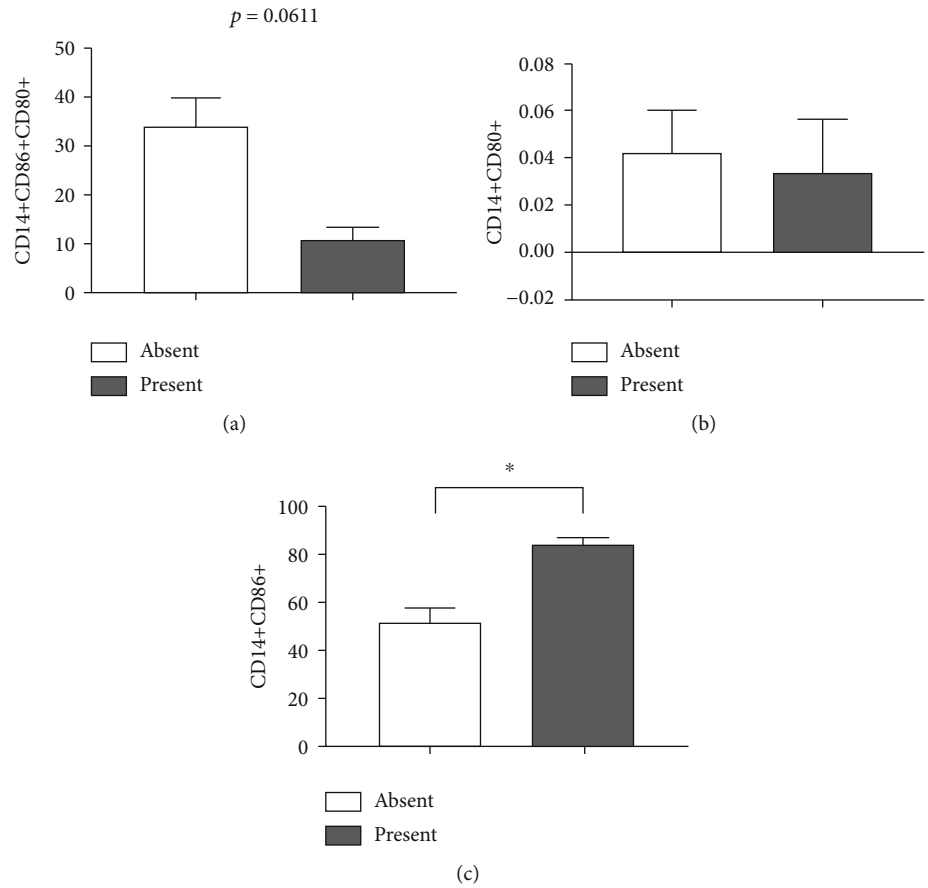

Figure 9: Impact of depression on the expression profile of surface markers on CD14+ cells obtained from the blood of elderly people. Expressions of (a) CD14 +CD86 + CD80+, (b) CD14+CD80+, and (c) CD14+CD86+. Differences are considered statistically significant when $p < 0.05$.

TRAIL and quality of life may be associated with the maintenance of an inflammatory profile in sedentary elderly individuals because an increase in anti/regulatory cytokines was not observed in this group. However, an increase in inflammatory cells was observed.

There was no relationship between this cytokine and physical activity. Although the impact of exercise on TRAIL levels is not known, there was no change in this molecule in individuals with atherosclerosis undergoing physical training [38]. More studies related to this topic are needed to elucidate the role of TRAIL better.

Physical activity increased CD69+CD4+ cells and CD80+ and CD86+ cells in our study. In addition, physically active individuals with a good perception of quality of life also showed higher levels of CD14+, CD80+, and CD86+ cells. These markers represent phenotypes of activated T cells [39] and macrophages [40, 41]. It has already been demonstrated that different types of physical exercise induce proliferation, increase, and activate lymphocytes and macrophages [1], including the same molecules evaluated in our work. In addition to activating these cells, physical activity increases in other cell types, such as monocytes, neutrophils, and natural killer cells, especially during and after acute exercise.

Although the study encompasses a small number of participants, which is a limitation in the study that needs to be expanded to cover an individual's larger number, this study showed a clear correlation between the quality of life, level of depression, physical activity, and immune system. Although some cytokines with a typical proinflammatory profile (IFN-γ) were observed, the results point to a protective state with evident benefits reflected in the general well-being of the elderly who exercise.

Data Availability

The original contributions of this study are included in this article. Further inquiries can be directed to the corresponding author.

Ethical Approval

The study was approved by the Research Ethics Committee of the Federal University of Triângulo Mineiro (CEP/UFTM/2390/2012).

Conflicts of Interest

The authors declare that they have no conflicts of interest.

Authors' Contributions

Tamires Marielem de Carvalho-Costa and José Rodrigues do Carmo Neto equally contributed to the manuscript.

Acknowledgments

The authors appreciate the financial support of the Conselho Nacional de Desenvolvimento Científico e Tecnológico (CNPq) and Coordenação de Aperfeiçoamento de Pessoal de Nível Superior (CAPES).

References

[1] M. Sellami, M. Gasmi, J. Denham et al., "Effects of acute and chronic exercise on immunological parameters in the elderly aged: can physical activity counteract the effects of aging?," *Frontiers in Immunology*, vol. 9, p. 2187, 2018.

[2] B. W. Penninx, S. B. Kritchevsky, A. B. Newman et al., "Inflammatory markers and incident mobility limitation in the elderly," *Journal of the American Geriatrics Society*, vol. 52, no. 7, pp. 1105–1113, 2004.

[3] E. F. Teston, L. Carreira, and S. S. Marcon, "Depressive symptoms in the elderly: comparison of residents in condominium specific for elderly and in the community," *Revista Brasileira de Enfermagem*, vol. 67, no. 3, pp. 450–456, 2014.

[4] I. R. A. P. Nóbrega, M. C. C. Leal, A. P. O. Marques, and J. C. M. Vieira, "Fatores associados à depressão em idosos institucionalizados: revisão integrativa," *Debate*, vol. 39, no. 105, pp. 536–550, 2015.

[5] A. F. Boing, G. R. Melo, A. C. Boing, R. O. Moretti-Pires, K. G. Peres, and M. A. Peres, "Associação entre depressão e doenças crônicas: um estudo populacional," *Revista de Saúde Pública*, vol. 46, no. 4, pp. 617–623, 2012.

[6] B. J. Nicklas and T. E. Brinkley, "Exercise training as a treatment for chronic inflammation in the elderly," *Exercise and Sport Sciences Reviews*, vol. 37, no. 4, pp. 165–170, 2009.

[7] W. J. Chodzko-Zajko, D. N. Proctor, M. A. Fiatarone Singh et al., "American College of Sports Medicine position stand. Exercise and physical activity for older adults," *Medicine and Science in Sports and Exercise*, vol. 41, no. 7, pp. 1510–1530, 2009.

[8] C. J. Frazer, H. Christensen, and K. M. Griffiths, "Effectiveness of treatments for depression in older people," *The Medical journal of Australia*, vol. 182, no. 12, pp. 627–632, 2005.

[9] I. G. S. Moraes, R. T. Pinheiro, R. A. Silva, B. L. Horta, P. L. R. Sousa, and A. D. Faria, "Prevalência da depressão pós-parto e fatores associados," *Revista de Saúde Pública*, vol. 40, no. 1, pp. 65–70, 2006.

[10] M. Power, K. Quinn, S. Schmidt, and Group WO, "Development of the WHOQOL-old module," *Quality of life research*, vol. 14, no. 10, pp. 2197–2214, 2005.

[11] A. T. Beck, R. A. Steer, and G. K. Brown, *Manual for the Beck Depression Inventory-II*, Psychological Corporation, San Antonio, TX, 1996.

[12] C. Gorenstein, W. Y. Pang, I. L. Argimon, and B. S. G. Werlang, *Inventário Beck de Depressão-II*, Casa do Psicólogo, São Paulo, 2011.

[13] C. Franceschi, M. Bonafè, S. Valensin et al., "Inflamm-aging: an evolutionary perspective on immunosenescence," *Annals of the New York Academy of Sciences*, vol. 908, no. 1, pp. 244–254, 2000.

[14] H. Cao Dinh, I. Beyer, T. Mets et al., "Effects of physical exercise on markers of cellular immunosenescence: a systematic review," *Calcified tissue international*, vol. 100, no. 2, pp. 193–215, 2017.

[15] D. B. Reuben, L. Judd-Hamilton, T. B. Harris, and T. E. Seeman, "The associations between physical activity and inflammatory markers in high-functioning older persons: MacArthur Studies of Successful aging," *Journal of the American Geriatrics Society*, vol. 51, no. 8, pp. 1125–1130, 2003.

[16] S. Gielen, V. Adams, S. Möbius-Winkler et al., "Anti-inflammatory effects of exercise training in the skeletal muscle of patients with chronic heart failure," *Journal of the American College of Cardiology*, vol. 42, no. 5, pp. 861–868, 2003.

[17] C. P. Lambert, N. R. Wright, B. N. Finck, and D. T. Villareal, "Exercise but not diet-induced weight loss decreases skeletal muscle inflammatory gene expression in frail obese elderly persons," *Journal of Applied Physiology*, vol. 105, no. 2, pp. 473–478, 2008.

[18] D. R. Taaffe, T. B. Harris, L. Ferrucci, J. Rowe, and T. E. Seeman, "Cross-sectional and prospective relationships of interleukin-6 and C-reactive protein with physical performance in elderly persons: MacArthur studies of successful aging," *The journals of gerontology Series A, Biological sciences and medical sciences*, vol. 55, no. 12, pp. M709–M715, 2000.

[19] K. L. Timmerman, M. G. Flynn, P. M. Coen, M. M. Markofski, and B. D. Pence, "Exercise training-induced lowering of inflammatory (CD14+CD16+) monocytes: a role in the anti-inflammatory influence of exercise?," *Journal of leukocyte biology*, vol. 84, no. 5, pp. 1271–1278, 2008.

[20] W. Y. So, M. Song, Y. H. Park et al., "Body composition, fitness level, anabolic hormones, and inflammatory cytokines in the elderly: a randomized controlled trial," *Aging clinical and experimental research*, vol. 25, no. 2, pp. 167–174, 2013, Epub 2013 Apr 9. Erratum in: Aging Clin Exp Res. 2013 Jun;25(3):355.

[21] B. K. Pedersen, "IL-6 signalling in exercise and disease," *Biochemical Society transactions*, vol. 35, no. 5, pp. 1295–1297, 2007.

[22] H. A. Young and J. H. Bream, "IFN-gamma: recent advances in understanding regulation of expression, biological functions, and clinical applications," *Current topics in microbiology and immunology*, vol. 316, pp. 97–117, 2007.

[23] E. Y. Kim and K. D. Moudgil, "Immunomodulation of autoimmune arthritis by pro-inflammatory cytokines," *Cytokine*, vol. 98, pp. 87–96, 2017.

[24] L. Â. Macêdo Santiago, L. G. Neto, G. Borges Pereira et al., "Effects of resistance training on Immunoinflammatory response, TNF-alpha gene expression, and body composition in elderly women," *Journal of aging research*, vol. 2018, Article ID 1467025, 10 pages, 2018.

[25] L. R. Silveira, C. H. J. Pinheiro, C. C. Zoppi et al., "Regulação do metabolismo de glicose e ácido graxo no músculo esquelético durante exercício físico," *Arquivos Brasileiros de Endocrinologia & Metabologia*, vol. 55, no. 5, pp. 303–313, 2011.

[26] L. G. Minuzzi, M. U. Chupel, L. Rama et al., "Lifelong exercise practice and immunosenescence: master athletes cytokine response to acute exercise," *Cytokine*, vol. 115, pp. 1–7, 2019.

[27] H. Eyre and B. T. Baune, "Neuroimmunological effects of physical exercise in depression," *Brain, behavior, and immunity*, vol. 26, no. 2, pp. 251–266, 2012.

[28] S. Li, D. Peng, Y. He et al., "Expression of TIM-3 on CD4+ and CD8+ T cells in the peripheral blood and synovial fluid of rheumatoid arthritis," *APMIS*, vol. 122, no. 10, pp. 899–904, 2014.

[29] Z. Koohini, H. Hossein-Nataj, M. Mobini, A. Hosseinian-Amiri, A. Rafiei, and H. Asgarian-Omran, "Analysis of PD-1 and Tim-3 expression on CD4(+) T cells of patients with rheumatoid arthritis; negative association with DAS28," *Clinical rheumatology*, vol. 37, no. 8, pp. 2063–2071, 2018.

[30] L. E. Petersen, R. Grassi-Oliveira, T. Siara et al., "Premature immunosenescence is associated with memory dysfunction in rheumatoid arthritis," *Neuroimmunomodulation*, vol. 22, no. 3, pp. 130–137, 2015.

[31] B. Strasser, B. Sperner-Unterweger, D. Fuchs, and J. M. Gostner, "Mechanisms of inflammation-associated depression: immune influences on tryptophan and phenylalanine metabolisms," *Current topics in behavioral neurosciences*, vol. 31, pp. 95–115, 2017.

[32] S. Geisler, B. Sperner-Unterweger, D. Fuchs, and J. M. Gostner, "Immunometabolism in the pathogenesis of depressive disorders - therapeutic considerations," *Current topics in medicinal chemistry*, vol. 18, no. 16, pp. 1408–1415, 2018.

[33] B. Strasser, D. Geiger, M. Schauer, H. Gatterer, M. Burtscher, and D. Fuchs, "Effects of exhaustive aerobic exercise on tryptophan-kynurenine metabolism in trained athletes," *PLoS One*, vol. 11, no. 4, article e0153617, 2016.

[34] S. Brost, R. Koschny, J. Sykora et al., "Differential expression of the TRAIL/TRAIL-receptor system in patients with inflammatory bowel disease," *Pathology, research and practice*, vol. 206, no. 1, pp. 43–50, 2010.

[35] C. Auffray, M. H. Sieweke, and F. Geissmann, "Blood monocytes: development, heterogeneity, and relationship with dendritic cells," *Annual review of immunology*, vol. 27, no. 1, pp. 669–692, 2009.

[36] J. Gao, D. Wang, D. Liu et al., "Tumor necrosis factor-related apoptosis-inducing ligand induces the expression of proinflammatory cytokines in macrophages and re-educates tumor-associated macrophages to an antitumor phenotype," *Molecular biology of the cell*, vol. 26, no. 18, pp. 3178–3189, 2015.

[37] Y. Wu, Y. Shen, J. Zhang et al., "Increased serum TRAIL and DR5 levels correlated with lung function and inflammation in stable COPD patients," *International Journal of Chronic Obstructive Pulmonary Disease*, vol. 6, no. 10, pp. 2405–2412, 2015.

[38] C. Davenport, H. Kenny, D. T. Ashley, E. P. O'Sullivan, D. Smith, and D. J. O'Gorman, "The effect of exercise on osteoprotegerin and TNF-related apoptosis-inducing ligand in obese patients," *European journal of clinical investigation*, vol. 42, no. 11, pp. 1173–1179, 2012.

[39] S. F. Ziegler, F. Ramsdell, and M. R. Alderson, "The activation antigen CD69," *Stem Cells*, vol. 12, no. 5, pp. 456–465, 1994.

[40] J. Henry, M. M. Miller, and P. Pontarotti, "Structure and evolution of the extended B7 family," *Immunology today*, vol. 20, no. 6, pp. 285–288, 1999.

[41] V. A. Boussiotis, G. J. Freeman, J. G. Gribben, and L. M. Nadler, "The role of B7-1/B7-2:CD28/CLTA-4 pathways in the prevention of anergy, induction of productive immunity and down-regulation of the immune response," *Immunological Reviews*, vol. 153, no. 1, pp. 5–26, 1996.

Hindawi
Oxidative Medicine and Cellular Longevity
Volume 2022, Article ID 1061274, 13 pages
https://doi.org/10.1155/2022/1061274

Review Article

Antidepressant Effect of Ketamine on Inflammation-Mediated Cytokine Dysregulation in Adults with Treatment-Resistant Depression: Rapid Systematic Review

Shiryn D. Sukhram, Grozdena Yilmaz, and Jianying Gu

Department of Biology, City University of New York-College of Staten Island, Staten Island, NY 10314, USA

Correspondence should be addressed to Shiryn D. Sukhram; shiryn.sukhram@csi.cuny.edu

Received 25 March 2022; Revised 25 July 2022; Accepted 23 August 2022; Published 16 September 2022

Academic Editor: Ajinkya Sase

Background. Major depressive disorder (MDD) and treatment-resistant depression (TRD) represent a global source of societal and health burden. To advise proper management of inflammation-related depression among TRD patients, it is important to identify therapeutic clinical treatments. A key factor is related to proinflammatory cytokines such as interleukin- (IL-) 1β, IL-6, and tumor necrosis factor- (TNF-) α which have been implicated in the pathogenesis of depressive symptoms in MDD patients. Ketamine may provide an anti-inflammatory therapeutic strategy by targeting proinflammatory pathways associated with depressive disorders, which may be exacerbated in the ageing population with TRD. *Objective*. Despite a burgeoning body of literature demonstrating that inflammation is linked to TRD, there is still a lack of comprehensive research on the relationship between proinflammatory biomarkers and ketamine's antidepressant effect on TRD patients. *Method*. The Cochrane Library and PubMed/MEDLINE databases were systematically searched from inception up to February 1, 2022, adopting broad inclusion criteria to assess clinical topics related to the impact of ketamine on inflammatory cytokines in TRD patients. The present work is in compliance with the World Health Organization Rapid Review Guide. *Results*. Five out of the seven studies examined in this review show that ketamine infusion may reduce depressive symptoms with a quick start of effect on TRD patients. Based on the Montgomery-Åsberg Depression Rating Scale (MADRS) and Hamilton Depression Rating Scale (HAM-D) scores, the overall response rate for ketamine was 56%; that is, 56% of those treated with ketamine had MADRS/HAM-D scores decreased by at least 50%. *Conclusions*. While the anti-inflammatory effects of ketamine modulate specific proinflammatory cytokines, its rapid antidepressant effect on TRD patients remains inconsistent. However, our study findings can provide a reliable basis for future research on how to improve systemic inflammatory immune disorders and mental health. We suggest that ketamine infusion may be part of a comprehensive treatment approach in TRD patients with elevated levels of depression-specific inflammatory biomarkers.

1. Introduction

Depression has been recognized as a pandemic [1], and its etiology remains largely unknown. Major depressive disorder (MDD) is a mental health disorder that clinically presents itself through changes in mood and perception as well as a loss of pleasure lasting at least two weeks [2]. Moreover, MDD is set to become the leading cause of disability worldwide by the year 2030 [3], and approximately one-third of patients with MDD have treatment-resistant depression (TRD) [4]. Patients with TRD are typically identified as a failure to achieve remission after two or more trials of appropriate pharmaceutical treatment for MDD of a suitable dose and duration. However, a universally recognized classification of TRD is lacking in the scientific literature. In a recent publication, Zhdanava et al. [5] evaluated the prevalence and national burden of TRD and MDD in the United States. The authors reported that the estimated 12-month prevalence of medication-treated MDD in the U.S. was 8.9 million adults, and 2.8 million (30.9%) had TRD. There is a significant prevalence of TRD patients with elevated inflammatory markers, and this could be helpful in

intervention strategies that can decrease their effects. The COVID-19 Mental Disorders Collaborators [6] recently published a systematic review on the mental health effects of the COVID-19 pandemic on the prevalence of depressive and anxiety disorders. The authors reported that the COVID-19 pandemic led to an additional 10.7 million (7.21–14.9) disability-adjusted life years (DALYs) for MDD globally, of which 7.07 million (4.80–9.80) were among women and 3.62 million (2.40–5.09) were among men. Furthermore, a recent World Health Organization (WHO) [7] brief indicated that the pandemic particularly affected the mental health of young people, consequently putting them at a disproportionate risk of suicidal and self-harming actions. The WHO brief further states that individuals with preexisting physical health conditions were more likely to develop symptoms of mental disorders.

The role of proinflammatory cytokines in depression has been investigated over the past decades [8], and recently, ketamine has been identified for therapeutic interventions. Previous animal studies have indicated ketamine's strong anti-inflammatory effect and propose cytokines as effective molecular biomarkers to examine ketamine's antidepressant effect [9]. According to clinical studies, ketamine's antidepressant effect may play a role in peripheral and central immune regulations [10, 11]. Ketamine may potentially lower cytokine levels associated with inflammatory processes, related to mood problems, or improve communication within certain brain regions [12]. It is hypothesized that the antidepressant treatment effect of ketamine may be associated with the ability of anti-inflammatory mediators to suppress proinflammatory mediators, such as IL-1β, IL-6, and TNF-α [13]. Figure 1 illustrates the putative targets of ketamine and its antidepressant effect on systemic regulators of the adaptive immune system. Disruptions of the Th1/Th2 immune ratio are associated with the pathophysiology of MDD [10]. Norepinephrine (NE) and 5-hydroxytryptamine (5-HT) present differential and distinct effects on inflammation and facilitate a Th1 shift and a Th2 shift, respectively, resulting in depressive symptoms. Hashimoto [10] indicates that NE inhibits the production of Th1 proinflammatory cytokines, such as TNF-α, whereas 5-HT inhibits the production of Th2 cytokines, such as IL-6. Also, a Th2 shift causes inflammation and an increase in proinflammatory cytokines consequently triggering depression. Ketamine may induce a Th1 and Th2 shift, respectively. A systemic protective anti-inflammatory effect is typically initiated when an individual faces a localized inflammatory reaction, specifically a predominance of the Th2 (anti-inflammatory) upon the Th1 (proinflammatory) pathway [14]. De Kock et al. [14] indicate that ketamine performs as a distinctive homeostatic regulator of the acute inflammatory response and associated stress-induced conditions. The administration of a single IV dose of ketamine (0.5 mg/kg) significantly interferes with this immune ratio and increases the Th1/Th2 ratio which may be advantageous to an individual's global immune function and overall health [14, 15]. Therefore, the regulation of the "immune balance" between Th1-mediated cellular immunity and Th2-mediated humoral immunity is essential for therapy and management of TRD.

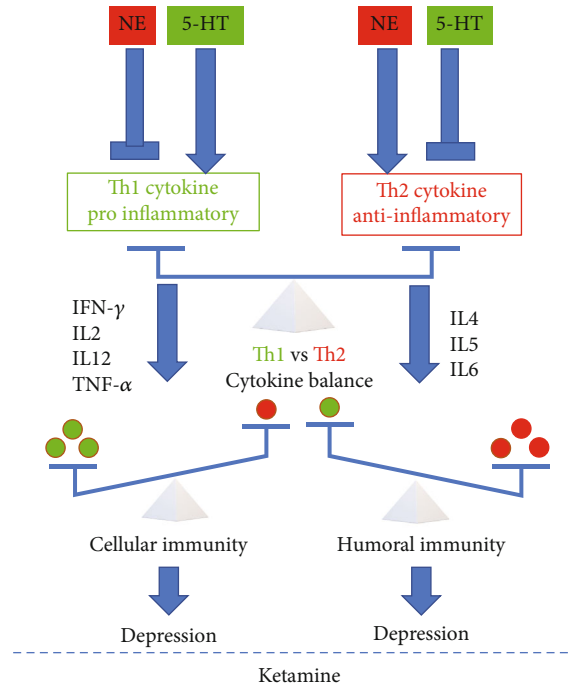

Figure 1: Schematic figure illustrating the putative targets of ketamine and its antidepressant effect on systemic regulators of the adaptive immune system. Adapted from [10]. Copyright by the Multidisciplinary Digital Publishing Institute.

Ketamine can suppress proinflammatory cytokine levels, and decreases in serum levels strongly correspond with the relief of depressive symptoms [13]. Emerging data suggest that ketamine delivers its positive antidepressant effect in a dose-dependent way through IL-6 blockage [16]. However, the use of various proinflammatory cytokines in ketamine intervention strategies warrants further investigation. The field of psychoneuroimmunology has established a significant relationship between immunological processes and mental disorders [17]. Increasing evidence proposes a reciprocal relationship between low-grade systemic inflammation and MDD, suggesting that depression is an inflammatory disease. Upregulation of inflammatory markers has been linked to MDD involving induction of a proinflammatory state. As described by Dinarello [18], proinflammatory cytokines act to make the disease worse while anti-inflammatory cytokines work to reduce inflammation and stimulate healing. A compelling body of evidence has emerged in recent years suggesting the role of inflammatory cytokines in the pathophysiology of MDD [19]. A distinct pattern of inflammatory cytokine concentrations in patients with MDD might explain their manifestation or prognosis mediated by IL-1 or IL-6 [20]. Additionally, several studies have shown that proinflammatory cytokine levels are increased in patients with inflammatory- and age-related processes. A significant cytokine associated with depression in the elderly is related to IL-1β. For instance, IL-1β levels were elevated in depressed elderly subjects older than 60 years, directly relative to the severity of disease [21]. A thorough understanding regarding the impact of ketamine treatment

on IL-1β may lead to novel treatment strategies for the ageing population [22].

Early and appropriate clinical treatment directed at proinflammatory cytokines may reduce the occurrence of depression-like symptoms commonly observed in TRD patients. Recent research findings indicate that intravenous (IV) ketamine infusion may potentially lower serum inflammatory cytokine levels associated with TRD. However, the limited studies available are inconsistent when reporting the antidepressant effect of ketamine on proinflammatory cytokines. The goal of the present report is to explore the available evidence and the existing gaps concerning the implications of ketamine treatment among dysregulated cytokine mediators in TRD.

While clinical researchers have yet to agree on a coherent explanation, individuals with dysregulated immune responses should be cautious of the prospective influence their condition could have on their mental health. According to the WHO [7], the COVID-19 pandemic has had negative effects on the mental health of the global population, including higher rates of suicidal ideation and suicide attempts. Inflammation induced by COVID-19 may contribute to the increased risk for depression. Furthermore, as the population ages, it is important to identify therapeutic strategies for depressive symptoms associated with inflammatory processes. Late-life depression may present high pathogenic complexity caused by chronic illness and psychosocial/physiological problems compared to depression at a younger age [1, 22]. Statistical data from the United Nations [23] indicate that by 2050, one in six people in the world will be older than 65 (16%).

As the world's ageing population is expected to increase, there is a need to investigate whether anti-inflammatory therapeutic strategies targeting proinflammatory pathways could reduce mental morbidity in the future. A population, intervention, comparison, and outcome- (PICO-) related question was used to guide the systematic review: "What are the effects of ketamine infusion of 0.5mg/kg (I) on adult patients diagnosed with treatment-resistant depression (P) on depression scale scores and serum proinflammatory cytokine levels (O) compared to healthy controls, or placebo (C)?" The aim of this rapid systematic review is to evaluate (a) the relationship between the antidepressant effect of ketamine and proinflammatory IL-1β, IL-6, and TNF-α cytokine response, (b) the impact of ketamine treatment in the management of inflammation-related TRD, and (c) knowledge gaps in these contexts. This manuscript is not intended to be a systematic review of the existing literature regarding the effectivity and/or management strategies of ketamine and instead is intended to provide relevant guidance to public health and policy-makers on strategies and interventions to improve TRD among individuals with inflammation-related depressive conditions. Systematic reviews providing a comprehensive overview of (1) the efficacy/tolerability/safety profile of ketamine as an equally effective treatment alternative to electroconvulsive therapy in TRD patients and (2) the effect of ketamine on the relationship between inflammation and glutamate signaling in depressive disorders are available elsewhere [11, 24–27]. However, there is still a lack of comprehensive research on the relationship between proinflammatory biomarkers and ketamine's antidepressant effect. This minisystematic review is aimed at presenting ketamine-induced effects on proinflammatory IL-1β, IL-6, and TNF-α cytokines. The guidance provided herein is based on clinical studies relevant to the antidepressant effect of ketamine on inflammation-mediated cytokines in adult TRD patients.

2. Methods

This rapid review was completed in accordance with the World Health Organization Rapid Review Guide [28]. Compliance with the WHO guidelines indicates methodological reliability and application of research findings across rapid reviews. Comprehensive systematic searches were conducted in the Cochrane Library and PubMed/MEDLINE databases from inception up to February 1st, 2022. The query was conducted with the following terms (in all fields): ("ketamine" AND "depression" AND "cytokine"). We also scanned the reference lists of all included articles for studies to be included in our work. The Preferred Reporting Items for Systematic Reviews and Meta-Analyses (PRISMA) 2020 flow diagram was used to illustrate the extraction of studies through the different phases of this review [29]. Please refer to Figure 2 for details about the adopted search strategy.

Two investigators (SS and GY) screened the retrieved references for eligibility both at the title/abstract and full-text levels. Disagreements were resolved by discussion or by the judgement of the third reviewer (JG). During the review process, studies were only included in the next phase of analysis upon the agreement of at least two reviewers. One reviewer obtained the data, and the findings of these extractions were thoroughly reviewed by the coauthors.

Key elements extracted from the literature included (1) first author, (2) year of publication, (3) country of origin, (4) study population and sample size, (5) methodology, (6) gender ratio, (7) average age, (8) intervention type and comparator (if applicable), (9) duration of the intervention (if applicable), (10) diagnostic test or criteria, and (11) key findings that relate to the review question.

We excluded non-English articles, unavailable full-text articles, animal studies, case reports, case studies, opinions, editorials, commentaries, letters, conference abstracts, preclinical studies, and reviews. Criteria for depression had to be established by a coded diagnosis according to the Diagnostic and Statistical Manual of Mental Disorders (DSM) criteria. After exclusion of duplicates, we screened the title/abstract or full-text reports and decided whether these met the inclusion criteria.

We included experimental studies (randomized—individually or cluster—and nonrandomized controlled trials) and observational studies with an internal comparison group (cohort—prospective and retrospective—and case-control) studies. Articles were included based on the following criteria: (a) written in English; (b) included any measure assessing ketamine, depression, and cytokine levels; and (c) qualitatively examined and presented results of the relationship between ketamine and cytokine-related outcomes (e.g.,

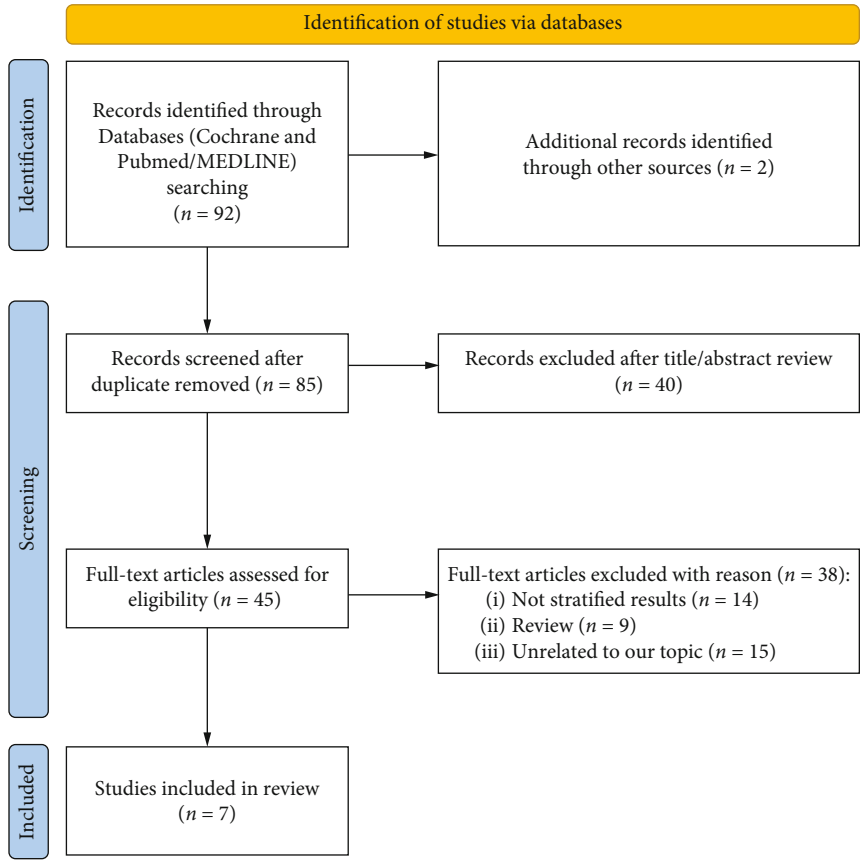

Figure 2: Study flow based on the 2020 flow diagram for new systematic review which included search of databases and registers only. Adapted from [29]. Copyright by the British Medical Association.

correlations). Notably, to be included in this systematic approach, it was not required for studies to test the association between TRD and proinflammatory cytokine levels; for instance, if a serum cytokine level and mental-related outcome variables were both included in a correlation matrix, the study was included.

3. Results

3.1. General Characteristics. Seven studies which reported on the association of the antidepressant effect of ketamine infusion on serum inflammatory cytokine levels in TRD patients were included in this systematic review. The overall age distributions for the six studies which included demographic data [30–35] were calculated as combined means and standard deviation of age to get a weighted mean and pooled standard deviation, which results in age distribution of 41.298 ± 11.74
(95%Confidence Interval (CI) = [18.29279, 64.30407]); thus, approximately 50% of the subjects are more than likely >40 years. The overall gender distribution was calculated by adding mean percentages which resulted in 58% female (Figure 3). Yang et al. [36] lack any demographic data; therefore, we only included studies that reported age and gender frequencies to calculate the overall age and gender distribution for this review. These relative estimates along with the key findings of their associated studies are summarized in Table 1.

According to six out of seven studies, this review examined 200 females and 159 males with TRD. Kruse et al.'s study [32] indicate that inflammatory profiles, depressive symptoms, and depression treatment response differ between females and males. Statistical analyses stratified by gender revealed that increasing IL-8 was associated with a decreasing Hamilton Depression Rating Scale (HAM-D) score in females ($p = 0.08$), while the inverse was found in males ($p = 0.02$). Gender-specific processes trigger the neural and/or behavioral effects of IL-8; however, further statistical analysis stratified by gender did not illustrate a differential change between ketamine treatment outcome and CRP, IL-6, IL-10, and TNF-α levels [32]. Our findings indicate no statistically significant relationship between gender and ketamine response rates or mean age and ketamine response rate, i.e., no associations were found between the number of females and how many responded positively.

3.2. Treatment-Resistant Depression (Population). In each of the studies reviewed, recurrent MDD was diagnosed according to the DSM criteria. The DSM criteria published by the American Psychiatric Association have been widely used by clinicians to diagnose mental health disorders. However, various versions of the DSM were utilized in the studies. The DSM has been revised seven times since it was first

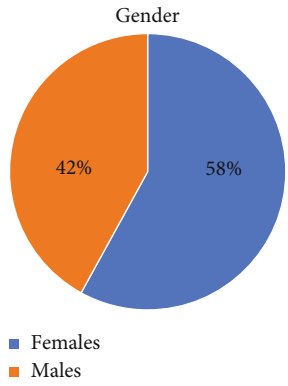

Figure 3: Gender distribution for articles reporting on the antidepressant effect of ketamine on inflammatory cytokines in adult patients with treatment-resistant depression.

published in 1952 [37]. Kruse et al. [32] was the only study that did not report which DSM version was used for MDD diagnosis. Kiraly et al. [31] and Yang et al. [36] utilized the DSM-IV criteria. The DSM-IV-TR was published in 2000 and used in the studies done by Chen et al. [30] and Park et al. [33]. The revised DSM-IV-TR version classified disorders using a multiaxial or multidimensional approach to ensure that biological, environmental, and psychological factors were considered when making a comprehensive mental health diagnosis. The DSM-V [38], published in 2013, was used in the studies examined by Zhan et al. [34] and Zhou et al. [35].

Reliability and consistency of clinical assessment for MDD based on the DSM criteria should remain consistent when diagnosing recurring MDD and accordingly TRD. There is no universally recognized classification of TRD, and consequently, it has been treated as a homogenous entity [39, 40]. In each of the studies reviewed, TRD was defined as MDD patients who had failed response to at least two different adequate antidepressant treatment trials. Additionally, treatment resistance occurs generally in approximately 30% of treated MDD patients [41]; therefore, improved TRD management is warranted that includes the effect of specific targeted treatment strategies encompassing psychological therapies. Kiraly et al. [31] and Park et al. [33] determined TRD by using the Antidepressant Treatment History Form (ATHF). The ATHF has been the most widely used instrument to systematically evaluate antidepressant treatment trials and identify treatment resistance [42].

3.3. Ketamine Infusion (Intervention). Ketamine hydrochloride (PubChem CID: 15851) is typically administered via IV infusion therapy. Each of the studies [30–36] reviewed utilized a constant IV ketamine dose of 0.5 mg/kg. There was variability in the frequency of IV ketamine infusions. Overall, five studies reported a single-dose ketamine infusion of 40 minutes, and all five publications reported elevations in at least cytokine inflammatory markers which were concomitant with depressive symptoms [30–33, 36]. Chen et al. [30] is the only study that compared different dosages of ketamine infusions. The patients were assigned randomly in a 3 : 1 ratio and received either a ketamine infusion of 0.5 mg/kg or a ketamine infusion of 0.2 mg/kg or a saline placebo infusion. Patients with higher baseline IL-6 (OR: 8.93, 95% CI: 1.16–68.86) levels were significantly associated with treatment response in the 0.5 mg/kg ketamine group. These findings suggest that a higher dose (0.5 mg/kg) of ketamine exerts an anti-inflammatory effect, and a lower dose (0.2 mg/kg) of ketamine may be associated with causal factors other than inflammation.

Zhan et al. [34] and Zhou et al. [35] were the only studies that examined longer ketamine treatment duration. Zhan et al. [34] administered six IV ketamine infusions in a 12-day period (days 1, 3, 5, 8, 10, and 12) and examined cytokine levels at baseline and 24 hours and 14 days after the sixth infusion (days 0, 13, and 26). Approximately 58.3% patients met the treatment response criteria after six ketamine infusions (day 13), and 25 (41.7%) attained remission. Zhou et al. [35] presented a post hoc analysis of the antidepressant effect of six adjunctive ketamine infusions on TRD patients with and without the presence of painful symptoms. TRD patients received ketamine infusions three times weekly for 2 weeks, and inflammatory cytokine levels were examined at baseline, day 13, and day 26. In both the pain and nonpain groups, significant reductions in Montgomery-Åsberg Depression Rating Scale (MADRS) scores were found at 24 hours postinfusion compared to baseline scores, and these reductions were maintained over the subsequent infusion period as well as on day 26 ($p < 0.05$ for both groups).

3.4. Healthy Controls and/or Placebo (Comparison). Kiraly et al. [31], Yang et al. [36], and Zhou et al. [35] were the only studies to include control subjects. It is normally assumed that a "healthy" control in a clinical study is defined as an individual who does not have the condition being investigated. However, a "healthy" control may have other underlying disorders that are not examined in the particular area of research. This leads to the question: how healthy are "healthy volunteers"? [43]. Twenty-six healthy volunteers in the study done by Kiraly et al. [31] were free of lifetime psychiatric conditions or major medical illnesses including active or systemic infections. Twenty-four matched healthy volunteers with no present or past history of any DSM-IV Axis I or Axis II diagnosis were examined by Yang et al. [36]. Inflammation plays a vital role in multiple disorders including depression, inflammaging, and pain, and the inclusion of reliable "healthy" controls with stricter criteria should be considered to prevent the risk of overestimating differences and possibly affecting the outcome of clinical studies. Zhou et al. [35] examined sixty healthy controls matched by age and gender.

Volunteer participation in clinical trials usually does not provide direct health benefits; however, participants are typically compensated with compensation dependent upon the duration of the study and clinical measures performed. Therefore, as discussed by Marchesini et al. [43], the terms "volunteer" and "normal range" also present difficulties in evidence-based medicine. Nevertheless, the inclusion of

Table 1: Study characteristics for articles reporting on the antidepressant effect of ketamine on inflammatory cytokines in adult patients with treatment-resistant depression.

References (year), country	Study design	Study population and sample size	Age, mean (SD) (y)	Gender differences (female/male)	Dosages, duration, and frequency of IV ketamine	Key findings
Chen MH, et al. [30], Taiwan	Double-blind randomized controlled trial	71 TRD Group 1: 0.5 mg/kg ($n = 25$) Group 2: 0.2 mg/kg ($n = 23$) Group 3: Placebo ($n = 24$)	Group 1: 48.46 ± 11.01 Group 2: 44.96 ± 12.31 Group 3: 48.63 ± 8.12	Group 1: $F = 21$ $M = 4$ Group 2: $F = 17$ $M = 6$ Group 3: $F = 15$ $M = 9$	Dose: 0.5 mg/kg vs. 0.2 mg/kg vs. saline placebo IV duration: 40 min Frequency: Single dose	Biomarkers analyzed: CRP, IL-6, and TNF-α Depression scale: (i) A significant dose-dependent decrease in MADRS scores was noted between the three groups across each time point, especially at 40, 80, 120, and 240 min and days 2 and 5 postinfusion (ii) A decrease in TNF-α between baseline and 40 min postinfusion was positively associated with changes in MADRS scores on day 4 and day 5 ($p < 0.05$) but not for other days ($p > 0.05$) for the 0.5 mg/kg infusion group Antidepressant: yes, for CRP, IL-6, and TNF-α Anti-inflammatory: yes (i) Higher IL-6 (OR: 8.93, 95% CI: 1.16–68.86) level at baseline was significantly associated with a likelihood of treatment response in the 0.5 mg/kg infusion group
Kiraly DD, et al. [31], USA	Open label, repeated measures (ClinicalTrials.gov IDs: NCT01880593, NCT00768430, and NCT00548964)	33 TRD; 26 HC	44.8 ± 13.6 (TRD) 39.0 ± 11.1 (HC)	TRD: $F = 14$ $M = 21$ HC: $F = 14$ $M = 14$	Dose: 0.5 mg/kg IV duration: Not specified Frequency: Single dose	Biomarkers analyzed: broad panel of inflammatory mediators, including IL-1β, IL-6, and TNF-α Depression scale: MADRS was examined in all patients by treatment response (≥50% reduction in MADRS at 24 h) versus nonresponse Antidepressant: no Anti-inflammatory: yes; however, this modulation is not directly linked to clinical antidepressant effects (i) Levels of all inflammatory cytokines were no longer significantly different from baseline levels ($p < 0.05$) at 24 h postinfusion
Kruse JL, et al. [32], USA	Open-label, clinical trial (ClinicalTrials.gov ID; NCT02165449)	46 TRD	42.3 (11.6)	TRD: $F = 17$ $M = 29$	Dose: 0.5 mg/kg IV duration: 40 min Frequency: Single dose	Biomarkers analyzed: CRP, IL-6, IL-8, IL-10, and TNF-α Depression scale: HAM-D scores were collected at baseline and 24 h postinfusion. Response was defined as 50% reduction in HAM-D score from baseline to posttreatment (i) Increasing IL-8 was associated with decreasing HAM-D score in females ($\beta = -0.45$, $p = 0.08$, effect size $(sr^2) = 0.20$), while the inverse

Table 1: Continued.

References (year), country	Study design	Study population and sample size	Age, mean (SD) (y)	Gender differences (female/male)	Dosages, duration, and frequency of IV ketamine	Key findings
						was found in males ($\beta = 0.43$, $p = 0.02$, effect size $(sr^2) = 0.18$) Antidepressant: (i) No, for CRP, IL-6, IL-10, and TNF-α (ii) Yes, for IL-8 in females only Anti-inflammatory: yes, depending upon gender (i) Lower baseline IL-8 was associated with more favorable antidepressant response according to gender, although the association was not significant (responder status × gender interaction: $\beta = -0.36$, $p = 0.096$), with evidence of an association in females ($\beta = -0.41$, $p = 0.095$, effect size $(sr^2) = 0.16$), but not males ($\beta = -0.01$, $p = 0.96$, effect size $(sr^2) < 0.01$)
Park M, et al. [33], USA	Double-blind placebo-controlled studies (post hoc analysis) (ClinicalTrials.gov ID: NCT0008699)	49 MDD-TRD; 31 BD-TRD	43.1 ± 12.8 (MDD-TRD) 44.3 ± 12.1 (BD-TRD)	MDD-TRD: $F = 21$ $M = 28$ BD-TRD: $F = 20$ $M = 11$	Dose: 0.5 mg/kg or saline placebo IV duration: 40 min Frequency: Single dose	Biomarkers analyzed: IFN-γ, IL-2, IL-5, IL-6, IL-8, IL-10, TNF-α, and sTNFR1 Depression scale: MADRS (i) Baseline cytokine levels at 230 min postinfusion were not associated with changes in depression rating scale scores at 230 min (measured as percent change in MADRS score, raw change in MADRS score, or antidepressant response (≥50% MADRS improvement)) Antidepressant: no Anti-inflammatory = yes (i) Levels changed significantly for IL-6 ($F_{3,209} = 25.51$, $p < 0.001$) and TNF-α ($F_{3,205} = 4.18$, $p = 0.007$) (ii) BD patients had significantly higher levels of IL-6 and TNF-α from baseline through day 3 postinfusion
Yang C, et al. [36], China/Japan	Open label, repeated measures	16 TRD + 24 HV	Not reported	Not reported	Dose: 0.5 mg/kg IV duration: 40 min Frequency: Single dose	Biomarkers analyzed: IL-1β, IL-6, KYN, TNF-α, and tryptophan Depression scale: HAM-D and MADRS were used to evaluate depressive symptoms at 60 min (baseline) preinfusion and then at 110 and 230 min and days 1, 3, and 7 postinfusion (i) Patients exhibiting ≥50% reduction in MADRS were classified as ketamine responders

Table 1: Continued.

References (year), country	Study design	Study population and sample size	Age, mean (SD) (y)	Gender differences (female/male)	Dosages, duration, and frequency of IV ketamine	Key findings
						($n = 12$), while nonresponders ($n = 4$) were defined as having <50% improvement Antidepressant: yes, for IL-6 Anti-inflammatory: yes (i) IL-1β significantly decreased at 230 min and 1 day postinfusion in the responder group ($p = 0.013$) but not in the nonresponder group ($p > 0.05$) (ii) IL-6 significantly decreased at 230 min to 3 days postinfusion in the responder group ($p < 0.001$) but not in the nonresponder group ($p > 0.05$) (iii) TNF-α remained the same postinfusion
Zhan Y., et al. [34], China	Open-label, clinical trial (secondary analysis)	60 TRD	34.45 (11.92)	TRD: $F = 38$ $M = 22$	Dose: 0.5 mg/kg IV duration: 40 min Frequency: Six times in a 12-day period (days 1, 3, 5, 8, 10, and 12)	Biomarkers analyzed: GM-CSF, fractalkine, ITAC, IFN-γ, IL-1β, IL-2, IL-4, IL-5, IL-6, IL-7, IL-8, IL-10, IL-12p70, IL-13, IL-17A, IL-23, MIP-1β, MIP-3α, and TNF-α Depression scale: MADRS was administered at the same time points, and treatment response was defined as ≥50% reduction in MADRS score at 24 h after the final infusion (day 13) compared to baseline MADRS score (i) Remission was indicated by MADRS total score ≤ 10 Antidepressant: yes, for IL-6 and IL-17A Anti-inflammatory: yes (i) 14 inflammatory cytokines, including IL-1β, IL-6, and TNF-α, differed significantly at 2 weeks postinfusion (day 26) than at baseline
Zhou Y., et al. [35], China	Open-label clinical trial (post hoc analysis)	66 TRD + 60 HC	35.8 ± 11.6	TRD: $F = 37$ $M = 29$	Dose: 0.5 mg/kg IV duration: 40 min Frequency: Three times in a 14-day period	Biomarkers analyzed: GM-CSF, fractalkine, ITAC, IFN-γ, IL-1β, IL-2, IL-4, IL-5, IL-6, IL-7, IL-8, IL-10, IL-12p70, IL-13, IL-17A, IL-23, MIP-1β, MIP-3α, and TNF-α Depression scale: MADRS was measured at pretreatment baseline, 24 h after each infusion, and again 14 days after the 6th infusion (day 26) (i) Changes in IL-6 levels were associated with reductions in MADRS ($\beta = 0.478$, $p = 0.005$) scores on day 13 in the pain group Antidepressant: yes, for IL-6 in

Table 1: Continued.

References (year), country	Study design	Study population and sample size	Age, mean (SD) (y)	Gender differences (female/male)	Dosages, duration, and frequency of IV ketamine	Key findings
						patients with comorbid pain only Anti-inflammatory: yes (i) 11 inflammatory cytokines, including IL-6, differed significantly among the pain, nonpain, and HC groups ($p < 0.05$)

Abbreviations: BD-TRD: bipolar disorder with treatment-resistant depression; CRP: C-reactive protein; GM-CSF: granulocyte-macrophage colony-stimulating factor; HAM-D: Hamilton Depression Rating Scale; HC: healthy controls; HV: healthy volunteers; IFN-γ: interferon-gamma; IL: interleukin; ITAC: interferon-inducible T cell alpha chemoattractant; IV: intravenous; KYN: kynurenine; MADRS: Montgomery-Åsberg Depression Rating Scale; MDD-TRD: major depressive disorder with treatment-resistant depression; MIP: macrophage inflammatory protein; sTNFR1: soluble tumor necrosis factor receptor-1; TNF: tumor necrosis factor; TRD: treatment-resistant depression.

healthy controls is significant to ketamine research, as it provides comparison data when investigating the effects of treatments on individuals with specific disorders, especially related to inflammatory conditions.

3.5. Depression Scale Scores and/or Proinflammatory Cytokine Levels (Outcome). After a basic statistical analysis of the studies included in the review, six papers reported response rates, defined as a ≥50% decrease in MADRS and HAM-D scores. The MADRS and HAM-D scales are commonly used in clinical studies to measure indicators of depression. Leucht et al. [44] compared the HAM-D and MADRS scores in a large sample of patients with MDD and proposed that the linking of the absolute change in HAM-D total scores with the MADRS total scores could be used in metastudies.

In this review, the findings of the HAM-D scores in Kruse et al.'s study [32] were pooled with the MADRS scores of other studies [31, 33–36]. The overall response rate for ketamine was 56% ± 8.41% (95%CI = [39.48635%, 72.45394%]); that is, 56% of those treated with ketamine had MADRS/HAM-D scores decrease by at least 50%. The response rates were reported 24 hours after treatment, except for Zhan et al. [34], which was only reported at 13 days after treatment. Note that for this analysis, patients who were healthy controls or placebos were excluded where relevant, i.e., did not receive ketamine. Response rates were available in Kiraly et al. [31], Kruse et al. [32], Zhan et al. [34], Zhou et al. [35], and Yang [36].

"Proinflammatory cytokines" was used as a comprehensive term that included at least one of the following proinflammatory mediators in the studies reviewed: IL-1β, IL-6, and TNF-α. It is noteworthy that IL-6 was the most characterized type of proinflammatory cytokine associated with TRD and consequent ketamine treatment efficacy. Regardless of increasing evidence in the literature, and as illustrated in this review (Table 1), the targeted regulation of cytokine IL-1β and TNF-α response for ketamine's antidepressant effect requires further investigation, especially with gender and characteristic age distribution.

The randomized controlled trial by Chen et al. [30] demonstrated that changes in TNF-α between 40 minutes and baseline, but not at 240 minutes, were positively correlated with changes in the MADRS across time; however, the significant relationship between TNF-α change and changes in MADRS scores was only noted for day 4 and day 5 ($p < 0.05$) but not for other days ($p > 0.05$). Furthermore, the findings indicated no significant changes in CRP levels between baseline and postinfusion ($p = 0.472$). The clinical trial by Kiraly et al. [31] reported that IL-6 and IL-1α levels, 4 hour postinfusion with ketamine, showed modest but statistically significant decreases from baseline ($p < 0.05$, $t = 2.369$ and $p < 0.05$, $t = 2.149$, respectively); however, the levels of all inflammatory cytokines investigated IL-6, IL-1α, IL-1β, and TNF-α were no longer significantly different from baseline to 24 hours postinfusion. Kruse et al. [32] found that an increase in IL-8 from baseline to 24 hours postinfusion was associated with a favorable depression treatment response in females and an unfavorable treatment response in males (females: $p = 0.095$, effect size $(sr^2) = 0.16$; males: $p = 0.96$, effect size $(sr^2) < 0.01$).

Park et al. [33] investigated eight cytokine levels and found that levels of IL-6 significantly increased ($p < 0.001$) and sTNFR1 significantly decreased ($p = 0.006$) at 230 minutes postinfusion. Levels changed significantly for IL-5 ($p = 0.001$) and TNF-α ($p = 0.007$), but no significant changes were observed from baseline to the later time points. No significant differences were noted for INF-γ ($p = 0.018$), IL-10 ($p = 0.03$), IL-2 ($p = 0.21$), or IL-8 ($p = 0.50$). Yang et al. [36] found that serum levels of IL-1β showed a significant decrease at 230 minutes and 1 day postinfusion, as did IL-6 at 230 minutes to 3 days postinfusion in the ketamine responder group ($F = 4.495$, $p = 0.013$ for IL-1β; $F = 9.450$, $p < 0.001$ for IL-6) but not in the nonresponder (defined as having less than 50% improvement) group ($p > 0.05$). Of the 19 cytokines that were examined in Zhan et al.'s study [34], 14 inflammatory cytokines that differed significantly at 2 week postinfusion (day 26) included GM-CSF, fractalkine, IFN-γ, IL-10, IL-12p70, IL-17A, IL-1β, IL-2, IL-4, IL-23, IL-5, IL-6, IL-7, and TNF-α. These inflammatory cytokines seemed to be downregulated and were significantly lower on day 26 postinfusion than at baseline. Furthermore, the levels of IL-17A and IL-6 were associated with depression symptom improvement on day 13.

4. Discussion

Emerging research shows that ketamine efficiently cures both typical and atypical depression symptoms, while the molecular basis underpinning its effectiveness is unknown [20]. Ketamine's likely target in the brain is N-methyl-D-aspartate (NMDA) receptors; by binding to such receptors, it seems to maximize the amount of glutamate in the spaces between neurons [45]. This synaptogenesis influences mood, cognitive habits, and comprehension. Ketamine appears to inhibit glutamate at large dosages, making it an efficient sedative. However, at low levels, glutamate synthesis is increased [46], which could potentially aid in the formation of new interconnections or neurotransmitters between neurons. Whenever individuals are stressed for an extended period, they may lose linkages. Some of these symptoms seem to revert once ketamine is delivered. Therefore, it is proposed to aid in the regeneration of neural synapses [47]. It has been hypothesized that the physiological and pharmacological properties of ketamine may play a therapeutic role in TRD with immediate effects and a decrease in suicidal ideation [48]. Additionally, ketamine treatment could provide a therapeutic option for patients with TRD in managing inflammation-mediated immune cell dysregulation, specifically by suppressing proinflammatory cytokines associated with depression relief [13].

The association between cytokines and their antidepressant effect is multidimensional. Five out of the seven studies examined in this review showed that ketamine may reduce depressive symptoms in patients with TRD with a quick start of effect [30, 32, 34–36]. However, other studies [31, 33] suggest cytokines to be unreliable biomarkers of ketamine's antidepressant effect. These varying findings could be due to differences in the study samples examined: patients with TRD and comorbid pain in Zhou et al.'s study [35] vs. patients with bipolar disorders in Park et al.'s study [33] vs. patients with only TRD in other studies [30–32, 34]. Reports showed that IL-6 levels correlated significantly with clinical response [30, 34, 35]; however, findings of other studies did find an association between the anti-inflammatory and antidepressant effects of ketamine [31–33]. Additionally, Chen et al.'s study [30] showed that patients with TRD in a higher inflammatory state respond to ketamine and other anti-inflammatory agents, while others in a lower inflammatory state did not. Zhou et al.'s study [35] indicated that ketamine had greater effects on modulating inflammation in TRD patients with pain as opposed to patients without pain. Although the anti-inflammatory effects of ketamine seem to modulate proinflammatory cytokines in TRD, its rapid antidepressant effect remains inconsistent. Inflammatory profiles may differ between depressed males and females. Kruse et al. [32] reported that lower baseline IL-8 levels and subsequent IL-8 increase are associated with depression improvement in females, and IL-8 decrease is associated with depression improvement in males. Additionally, Park et al. [33] reported higher IL-8 levels in patients with bipolar disorders ($p = 0.007$) as compared to patients with MDD. However, other studies noted no differences for IL-8 [33–35].

Ketamine seems to aid in the formation of new brain connections, which may aid in the development of resilience and guard against the recurrence of MDD symptoms. Every medicine has adverse effects. Misuse and diversion of these medications are becoming more widespread as their availability increases, and this public health risk undermines their therapeutic benefits. Sanacora et al. [49] indicated that ketamine can quickly relieve depression in people who do not respond well to other treatments. Despite these positive results, we recommend that clinicians consider the risk of ketamine before prescribing it. Zhang et al. [50] reported that the incorrect use of ketamine is a global health problem due to its hallucinogenic effects. The various clinical manifestations and outcomes of inflammation-related depression may be exacerbated in individuals with cytokine dysregulation.

New perspectives have emerged regarding the inflammatory pathways associated with MDD and associated comorbid disorders. Inflammation-related depression caused by cytokine dysregulation may lead to increased pain of varying severity and thus negatively affect depressive symptoms. Comorbid pain disorders are typically linked with depression, and research on ketamine treatment in TRD patients and pain syndromes is scarce. However, the post hoc analysis performed by Zhou et al. [35] suggests that improvements in depressive symptom severity were partly dependent on the improvements in pain symptoms. The authors report the direct ($\beta = 2.995$, $p = 0.028$) and indirect ($\beta = 0.867$, $p = 0.042$) effects of the changes of IL-6 levels on reduction in MADRS scores; both were statistically significant. Pain is an independent prognostic factor of depression, and it is therefore suggested that individuals with TRD be screened for inflammatory biomarkers predictive of acute and systemic pain. Because of common neurobiological and molecular pathways, pain and depression are inextricably linked. The pain route uses the same brain structures as the mood control pathway, including the anterior cingulate, thalamus, and prefrontal cortex. Depression and comorbid pain may develop from a shared underlying inflammation mechanism generated by the cytokine storm in individuals with TRD. As a result, early and suitable therapy aimed at proinflammatory cytokines activated by a dysregulated immune system may lower the incidence of inflammation-related pain and depression. Ketamine may aid in treating inflammation-related depression, as well as comorbid pain, which may be exacerbated in the ageing population.

This review identifies the need to examine anti-inflammatory therapeutic strategies targeting various proinflammatory mediators involved in the pathophysiological effect of the ageing process and TRD. While distinct risk variables have yet been identified, it is clear that the ageing population is at a greater risk of immune dysregulation and consequently associated MDD complications. The higher the likelihood of age-related inflammatory disorders, the greater the probability of psychological discomfort and pain. Immunosenescence, a term used to describe the ageing of the immune system, concerns us all. However, depression is not considered a normal part of the ageing process [51]. Age-related changes in immune cells are associated with dysregulation and decline of the immune response. Several dysregulated inflammatory mediators have been observed during immunosenescence and the development of chronic low-grade systemic inflammation, characterized as "inflammaging." Age-

associated immune alterations are characterized as a decrease in the number of peripheral blood naïve cells and increase in the number of memory cells. These alterations, along with inflammaging, are the hallmarks of immunosenescence [52]. There is no cure for immunosenescence and inflammaging; however, they may be managed in many circumstances. Scientific evidence supporting the association between immunological dysregulation and MDD has added to our understanding of inflammaging commonly observed in the ageing population. Aiello et al. [52] proposed that immunosenescence leads to a decline in immune ability causing increased vulnerability to infection and a predisposition to age-related inflammatory diseases. Low-grade inflammatory response, defined as an elevation in serum interleukins and CRP, could have a role in depression etiology and may be an effective indicator of active treatment. For instance, elevated levels of IL-6, TNF-α, and their receptors are associated with age-related pathogenesis [53]. According to Singh and Newman [54], older individuals have increased levels of proinflammatory cytokine levels, such as IL-6 and TNF-α, compared to younger individuals. Cytokine dysregulation between proinflammatory and anti-inflammatory pathways is a characteristic feature of age-related illnesses and may play an important role in the pathophysiology of inflammation-related MDD.

As indicated in this review, ketamine may have significant antidepressant effects; however, future studies are needed to fully explore its therapeutic benefit. If an individual suffers from TRD, especially with suicidal intent, the potential benefits of ketamine may exceed the potential hazards. Furthermore, ketamine may result in perceptual abnormalities, abdominal discomfort, high blood pressure, and detachment. In clinical practice, any alterations in awareness or detachment are most obvious during the initial ketamine infusion and disappear rapidly afterwards. Ketamine may have additional adverse effects if used regularly or over an extended period of time. Some individuals who have taken a high dosage of ketamine run into the danger of falling into a "K-hole," which is marked by vivid visual and aural delusions as well as disconnection from reality [55]. Administration of ketamine requires practitioner expertise with treatment-emergent adverse events (TEAEs) and/or related safety concerns. Short-term ketamine treatment in TRD patients may be associated with neuropsychiatric (dissociative, psychotomimetic, psychiatric, and neurologic), cardiovascular, gastrointestinal, genitourinary, and hepatic adverse events [56]. However, the discontinuation rate of ketamine due to TEAEs is moderately low in TRD patients. Ceban et al. [56] suggest that supportive interventions and effective monitoring are sufficient for most TEAEs associated with ketamine treatment.

5. Limitations

Systematic reviews provide an objective assessment of the scientific evidence and attempt to minimize bias by utilizing a methodological approach. However, this review is subject to various limitations. Our search strategy was limited to articles written in English, and it is therefore probable that our findings may not represent non-English-speaking settings. However, the studies represented in this review included countries from China, Japan, Taiwan, and USA. To ensure increased reliability in the validity of the methodologies and results, we only included studies that were published in peer-reviewed journals. Thus, unpublished data may be available through other sources that were not included in this review. Also, as in any rapid review, our findings may have been influenced by publication bias. Another methodological weakness of this review is the small sample size which could increase the risk of false-negative results, resulting from studies with conflicting results. Further original studies are needed to adequately advise the clinical practice about ketamine therapy in the management of inflammation-related depression among various age groups—young adults, middle-aged adults, and older adults—with cytokine dysregulation.

6. Conclusion

This rapid review identifies the compelling need to investigate several important clinical and public health concerns related to ketamine treatment and inflammatory cytokine markers in TRD patients, preferably by well-designed longitudinal prospective studies and randomized clinical trials. It is well known that depression is a multidimensional disorder, and there is an increasing need to address the biomedical root causes of inflammation-related depression and the immunological response induced by cytokine mediators. These should be looked at as etiological causes of MDD and TRD patients with inflammatory illnesses. Additionally, the pathogenesis of COVID-19 is associated with elevated cytokines such as IL-1β, IL-6, and TNF-α [57]. With the continuous danger of our ongoing pandemic and adverse mental health effects, clinical comprehension of these biochemical indicators (inflammatory cytokines) and symptomatic results (MADRS/HAM-D) in patients with TRD will aid in the treatment (IV ketamine) approach for this vulnerable cohort (inflammation-related depression). In the meantime, this report contributes to a growing body of information and provides essential guidance to researchers, clinicians, mental health practitioners, and policy-makers.

Data Availability

The raw data supporting the conclusions of this article will be made available by the authors, without undue reservation.

Conflicts of Interest

The authors declare that the research was conducted in the absence of any commercial or financial relationships that could be construed as a potential conflict of interest.

Acknowledgments

This study was supported by grant-funded release time from the City University of New York (CUNY)—Faculty Fellowship Publication Program 2022. The authors would like to thank Dr. William Carr (Medgar Evers College), Dr. Jorge Matias Caviglia (Brooklyn College), Dr. Margrethe

Horlyck-Romanovsky (Brooklyn College), and Dr. Jihyun Kim (Guttman Community College) for taking the time and effort necessary to review the manuscript. We sincerely appreciate all valuable comments and suggestions, which helped us to improve the quality of the manuscript. The authors would like to thank Dr. Avinash Rai Sukhram at the Kymera Hospitalist Group for his helpful medical advice on various topics examined in this manuscript. His willingness to give his time so generously has been very much appreciated. We would also like to express great appreciation to John Orellana-Li (CUNY—Graduate Center) for his constructive suggestions during the development of this research work.

References

[1] C. Y. Kuo, C. H. Lin, and H. Y. Lane, "Molecular basis of late-life depression," *International Journal of Molecular Sciences*, vol. 22, no. 14, p. 7421, 2021.

[2] World Health Organization, "The ICD-10 classification of mental and behavioural disorders: clinical descriptions and diagnostic guidelines," NLM Classification: WM 15, 2022, https://www.who.int/news/item/02-03-2022-covid-19-pandemic-triggers-25-increase-in-prevalence-of-anxiety-and-depression-worldwide.

[3] C. D. Mathers and D. Loncar, "Projections of global mortality and burden of disease from 2002 to 2030," *PLOS Medicine*, vol. 3, no. 11, p. e442, 2006.

[4] B. Soares, G. Kanevsky, C. T. Teng et al., "Prevalence and impact of treatment-resistant depression in Latin America: a prospective, observational study," *Psychiatric Quarterly*, vol. 92, no. 4, pp. 1797–1815, 2021.

[5] M. Zhdanava, D. Pilon, I. Ghelerter et al., "The prevalence and national burden of treatment-resistant depression and major depressive disorder in the United States," *Journal of Clinical Psychiatry*, vol. 82, no. 2, 2021.

[6] D. F. Santomauro, A. M. Herrera, J. Shadid et al., "Global prevalence and burden of depressive and anxiety disorders in 204 countries and territories in 2020 due to the COVID-19 pandemic," *Lancet*, vol. 398, no. 10312, pp. 1700–1712, 2021.

[7] World Health Organization, "COVID-19 pandemic triggers 25% increase in prevalence of anxiety and depression worldwide," News Release, 2 March, 2022. View at: https://www.who.int/news/item/02-03-2022-covid-19-pandemic-triggers-25-increase-in-prevalence-of-anxiety-and-depression-worldwide.

[8] K. Brebner, S. Hayley, R. Zacharko, Z. Merali, and H. Anisman, "Synergistic effects of interleukin-1β, interleukin-6, and tumor necrosis factor-α: central monoamine, corticosterone, and behavioral variations," *Neuropsychopharmacology*, vol. 22, pp. 566–580, 2000.

[9] Z. M. Xie, X. M. Wang, N. Xu et al., "Alterations in the inflammatory cytokines and brain-derived neurotrophic factor contribute to depression-like phenotype after spared nerve injury: improvement by ketamine," *Scientific Reports*, vol. 7, no. 1, article 3124, 2017.

[10] K. Hashimoto, "Inflammatory biomarkers as differential predictors of antidepressant response," *International Journal of Molecular Sciences*, vol. 16, no. 4, pp. 7796–7801, 2015.

[11] W. Cui, Y. Ning, W. Hong, J. Wang, Z. Liu, and M. D. Li, "Crosstalk between inflammation and glutamate system in depression: signaling pathway and molecular biomarkers for ketamine's antidepressant effect," *Molecular Neurobiology*, vol. 56, no. 5, pp. 3484–3500, 2019.

[12] S. M. Green and B. Krauss, "The semantics of ketamine," *Annals of Emergency Medicine*, vol. 36, no. 5, pp. 480–482, 2000.

[13] S. A. Syed, E. Beurel, D. A. Loewenstein et al., "Defective inflammatory pathways in never-treated depressed patients are associated with poor treatment response," *Neuron*, vol. 99, no. 5, pp. 914–924.e3, 2018.

[14] M. De Kock, S. Loix, and P. Lavand'homme, "Ketamine and peripheral inflammation," *CNS Neuroscience & Therapeutics*, vol. 19, no. 6, pp. 403–410, 2013.

[15] M. Gao, W. Jin, Y. Qian, L. Ji, G. Feng, and J. Sun, "Effect of *N*-methyl-D-aspartate receptor antagonist on T helper cell differentiation induced by phorbol-myristate-acetate and ionomycin," *Cytokine*, vol. 56, no. 2, pp. 458–465, 2011.

[16] D. Matveychuk, R. K. Thomas, J. Swainson et al., "Ketamine as an antidepressant: overview of its mechanisms of action and potential predictive biomarkers," *Therapeutic Advances in Psychopharmacology*, vol. 10, 2020.

[17] V. Soria, J. Uribe, N. Salvat-Pujol, D. Palao, J. M. Menchón, and J. Labad, "Psychoneuroimmunology of mental disorders," *Revista de Psiquiatría y Salud Mental (English Edition)*, vol. 11, no. 2, pp. 115–124, 2018.

[18] C. A. Dinarello, "Proinflammatory cytokines," *Chest*, vol. 118, no. 2, pp. 503–508, 2000.

[19] W. Nowak, L. N. Grendas, L. M. Sanmarco et al., "Pro-inflammatory monocyte profile in patients with major depressive disorder and suicide behaviour and how ketamine induces anti-inflammatory M2 macrophages by NMDAR and mTOR," *EBioMedicine*, vol. 50, pp. 290–305, 2019.

[20] S. Kakeda, K. Watanabe, A. Katsuki et al., "Relationship between interleukin (IL)-6 and brain morphology in drug-naive, first-episode major depressive disorder using surface-based morphometry," *Scientific Reports*, vol. 8, no. 1, article 10054, 2018.

[21] A. J. Thomas, S. Davis, C. Morris, E. Jackson, R. Harrison, and J. T. O'Brien, "Increase in interleukin-1β in late-life depression," *American Journal of Psychiatry*, vol. 162, no. 1, pp. 175–177, 2005.

[22] R. K. Farooq, K. Asghar, S. Kanwal, and A. Zulqernain, "Role of inflammatory cytokines in depression: focus on interleukin-1β," *Biomedical Reports*, vol. 6, no. 1, pp. 15–20, 2017.

[23] United Nations, "Growing at a slower pace, world population is expected to reach 9.7 billion in 2050 and could peak at nearly 11 billion around 2100," News Release, 17 June 2019. View at: https://www.un.org/development/desa/en/news/population/world-population-prospects-2019.html.

[24] C. Yang, K. J. Wardenaar, F. J. Bosker, J. Li, and R. A. Schoevers, "Inflammatory markers and treatment outcome in treatment resistant depression: a systematic review," *Journal of Affective Disorders*, vol. 257, pp. 640–649, 2019.

[25] Z. Yuan, Z. Chen, M. Xue, J. Zhang, and L. Leng, "Application of antidepressants in depression: a systematic review and meta-analysis," *Journal of Clinical Neuroscience*, vol. 94, no. 1, pp. 54–62, 2022.

[26] J. K. E. Veraart, S. Y. Smith-Apeldoorn, H. P. Spaans, J. Kamphuis, and R. A. Schoevers, "Is ketamine an appropriate alternative to ECT for patients with treatment resistant depression? A systematic review," *Journal of Affective Disorders*, vol. 281, pp. 82–89, 2021.

[27] E. Kopra, V. Mondelli, C. Pariante, and N. Nikkheslat, "Ketamine's effect on inflammation and kynurenine pathway in depression: a systematic review," *Journal of Psychopharmacology*, vol. 35, no. 8, pp. 934–945, 2021.

[28] A. C. Tricco, E. V. Langlois, and S. E. Straus, *Rapid reviews to strengthen health policy and systems: a practical guide*, World Health Organization, Geneva, 2017.

[29] M. J. Page, J. E. McKenzie, P. M. Bossuyt et al., "The PRISMA 2020 statement: an updated guideline for reporting systematic reviews," *The BMJ*, vol. 372, 2021.

[30] M. H. Chen, C. T. Li, W. C. Lin et al., "Rapid inflammation modulation and antidepressant efficacy of a low-dose ketamine infusion in treatment-resistant depression: a randomized, double- blind control study," *Psychiatry Research*, vol. 269, pp. 207–211, 2018.

[31] D. D. Kiraly, S. R. Horn, N. T. Van Dam et al., "Altered peripheral immune profiles in treatment-resistant depression: response to ketamine and prediction of treatment outcome," *Translational Psychiatry*, vol. 7, no. 3, article e1065, 2017.

[32] J. L. Kruse, M. M. Vasavada, R. Olmstead et al., "Depression treatment response to ketamine: sex-specific role of interleukin-8, but not other inflammatory markers," *Translational Psychiatry*, vol. 11, no. 1, article 167, 2021.

[33] M. Park, L. E. Newman, P. W. Gold et al., "Change in cytokine levels is not associated with rapid antidepressant response to ketamine in treatment-resistant depression," *Journal of Psychiatric Research*, vol. 84, pp. 113–118, 2017.

[34] Y. Zhan, Y. Zhou, W. Zheng et al., "Alterations of multiple peripheral inflammatory cytokine levels after repeated ketamine infusions in major depressive disorder," *Translational Psychiatry*, vol. 10, no. 1, article 246, 2020.

[35] Y. Zhou, C. Wang, X. Lan, H. Li, Z. Chao, and Y. Ning, "Plasma inflammatory cytokines and treatment-resistant depression with comorbid pain: improvement by ketamine," *Journal of Neuroinflammation*, vol. 18, no. 1, article 200, 2021.

[36] J. J. Yang, N. Wang, C. Yang, J. Y. Shi, H. Y. Yu, and K. Hashimoto, "Serum interleukin-6 is a predictive biomarker for ketamine's antidepressant effect in treatment-resistant patients with major depression," *Biological Psychiatry*, vol. 77, no. 3, pp. e19–e20, 2015.

[37] S. Kawa and J. Giordano, "A brief historicity of the Diagnostic and Statistical Manual of Mental Disorders: issues and implications for the future of psychiatric canon and practice," *Philosophy, Ethics, and Humanities in Medicine*, vol. 7, no. 2, 2012.

[38] American Psychiatric Association, *Diagnostic and Statistical Manual of Mental Disorders*, American Psychiatric Association, Washington, DC, 5th ed edition, 2013.

[39] G. S. Malhi, P. Das, Z. Mannie, and L. Irwin, "Treatment-resistant depression: problematic illness or a problem in our approach?," *British Journal of Psychiatry*, vol. 214, no. 1, pp. 1–3, 2019.

[40] K. Wilhelm, "Judging a book by its cover: changing 'treatment resistant' to 'difficult-to-treat' depression," *Australian and New Zealand Journal of Psychiatry*, vol. 53, no. 2, pp. 101–103, 2019.

[41] K. S. Al-Harbi, "Treatment-resistant depression: therapeutic trends, challenges, and future directions," *Patient Preference and Adherence*, vol. 6, pp. 369–388, 2012.

[42] H. A. Sackeim, "The definition and meaning of treatment-resistant depression," *Journal of Clinical Psychiatry*, vol. 62, no. 16, pp. 10–17, 2001.

[43] G. Marchesini, F. Marchignoli, and S. Petta, "Evidence-based medicine and the problem of healthy volunteers," *Annals of Hepatology*, vol. 16, no. 6, pp. 832–834, 2017.

[44] S. Leucht, H. Fennema, R. R. Engel, M. Kaspers-Janssen, and A. Szegedi, "Translating the HAM-D into the MADRS and vice versa with equipercentile linking," *Journal of Affective Disorders*, vol. 226, pp. 326–331, 2018.

[45] N. D. Iadarola, M. J. Niciu, E. M. Richards et al., "Ketamine and other N-methyl-D-aspartate receptor antagonists in the treatment of depression: a perspective review," *Therapeutic Advances in Chronic Disease*, vol. 6, no. 3, pp. 97–114, 2015.

[46] M. Clarke, S. Razmjou, N. Prowse et al., "Ketamine modulates hippocampal neurogenesis and pro-inflammatory cytokines but not stressor induced neurochemical changes," *Neuropharmacology*, vol. 112, no. Part A, pp. 210–220, 2017.

[47] S. Y. Kwon, J. H. Yeom, and J. D. Joo, "Ketamine reduces the induced spinal p38 MAPK and pro-inflammatory cytokines in a neuropathic rats," *Korean Journal of Anesthesiology*, vol. 66, no. 1, pp. 52–58, 2014.

[48] M. Kowalczyk, E. Kowalczyk, P. Kwiatkowski, Ł. Łopusiewicz, M. Sienkiewicz, and M. Talarowska, "Ketamine-new possibilities in the treatment of depression: a narrative review," *Life (Basel)*, vol. 11, no. 11, 2021.

[49] G. Sanacora, M. A. Frye, W. McDonald et al., "A consensus statement on the use of ketamine in the treatment of mood disorders," *JAMA Psychiatry*, vol. 74, no. 4, pp. 399–405, 2017.

[50] M. W. Zhang, K. M. Harris, and R. C. Ho, "Is off-label repeat prescription of ketamine as a rapid antidepressant safe? Controversies, ethical concerns, and legal implications," *BMC Medical Ethics*, vol. 17, 2016.

[51] G. S. Alexopoulos, I. R. Katz, C. F. Reynolds, D. Carpenter, J. P. Docherty, and R. W. Ross, "Pharmacotherapy of depression in older patients: a summary of the expert consensus guidelines," *Journal of Psychiatric Practice*, vol. 7, no. 6, pp. 361–376, 2001.

[52] A. Aiello, F. Farzaneh, G. Candore et al., "Immunosenescence and its hallmarks: how to oppose aging strategically? A review of potential options for therapeutic intervention," *Frontiers in Immunology*, vol. 10, article 2247, 2019.

[53] W. B. Ershler and E. T. Keller, "Age-associated increased interleukin-6 gene expression, late-life diseases, and frailty," *Annual Review of Medicine*, vol. 51, no. 1, pp. 245–270, 2000.

[54] T. Singh and A. B. Newman, "Inflammatory markers in population studies of aging," *Ageing Research Reviews*, vol. 10, no. 3, pp. 319–329, 2011.

[55] E. E. Acevedo-Diaz, G. W. Cavanaugh, D. Greenstein et al., "Comprehensive assessment of side effects associated with a single dose of ketamine in treatment-resistant depression," *Journal of Affective Disorders*, vol. 263, pp. 568–575, 2020.

[56] F. Ceban, J. D. Rosenblat, K. Kratiuk et al., "Prevention and management of common adverse effects of ketamine and esketamine in patients with mood disorders," *CNS Drugs*, vol. 35, no. 9, pp. 925–934, 2021.

[57] Y. Alnefeesi, A. Siegel, L. M. Lui et al., "Impact of SARS-CoV-2 infection on cognitive function: a systematic review," *Frontiers in Psychiatry*, vol. 11, article 621773, 2020.

Hindawi
Oxidative Medicine and Cellular Longevity
Volume 2022, Article ID 1655502, 15 pages
https://doi.org/10.1155/2022/1655502

Research Article

COMMD3 Expression Affects Angiogenesis through the HIF1α/VEGF/NF-κB Signaling Pathway in Hepatocellular Carcinoma *In Vitro* and *In Vivo*

Tingting Zhu, Xiaolin Peng, Ziwei Cheng, Xiuru Gong, Dongwei Xing, Wei Cheng, and Minguang Zhang

Shanghai Municipal Hospital of Traditional Chinese Medicine, Shanghai University of Traditional Chinese Medicine, Shanghai, China 200071

Correspondence should be addressed to Wei Cheng; chengwei2834740@163.com and Minguang Zhang; mgzhang09@163.com

Received 27 February 2022; Revised 9 August 2022; Accepted 10 August 2022; Published 2 September 2022

Academic Editor: Chan-Yen Kuo

Background. High expression of copper metabolizing MURR1 domain (COMMD3) is significantly correlated with poor prognosis in hepatocellular carcinoma (HCC) patients. Here, we explored the mechanism by which COMMD3 affects HCC angiogenesis through the HIF1α/VEGF/NF-κB signaling pathway. *Methods*. SK-Hep1 and Hep-3B cell lines were transfected by *COMMD3* overexpression and RNA interference lentivirus and verified using RT-qPCR and western blotting techniques. Using RNA sequencing, we analyzed differentially expressed genes in *COMMD3*-overexpressed and *COMMD3*-knockdown HCC cells. Altogether, colony formation assay, wound healing assay, transwell cell invasion assay, flow cytometry apoptosis experiments, HUVEC tube formation detection, phalloidin staining assay, western blotting, immunohistochemical staining, and a nude mouse xenograft model were used for experimental verification. *Results*. Lentivirus *COMMD3* overexpression and knockdown were successfully established in HCC cells. *COMMD3* overexpression significantly promoted the proliferation, angiogenesis, migration, and invasion capacities of HCC cells with no obvious effect on apoptosis versus controls while *COMMD3* knockdown showed the opposite trend. The expression and protein levels of COMMD3 as well as HIF1α, VEGF, and NF-κB were increased in *COMMD3*-overexpressing HCC cells versus control cells, while they were reduced after *COMMD3* knockdown. In addition, RNA-seq indicated that *COMMD3* is an indispensable gene for HCC angiogenesis through HIF1α and NF-κB signaling pathways. *Conclusion*. This study showed that low expression of COMMD3 can inhibit HCC angiogenesis by suppressing the HIF1α/VEGF/NF-κB pathway. This implicates COMMD3 as a potential biomarker for improving the therapeutic outcome of HCC.

1. Introduction

According to epidemiological studies, hepatocellular carcinoma (HCC) is the seventh most prevalent malignancy and the second leading cause of cancer-related deaths around the world [1, 2]. As a solid tumor, HCC is highly vascularized requiring angiogenesis for invasion and metastasis [3]. Without angiogenesis, HCC does not grow more than 1–2 mm [4]. Tumor formation creates a hypoxic microenvironment that activates hypoxia-inducible factor 1α (HIF1α) and nuclear transcription factor-κB [5, 6], ultimately triggering vascular endothelial growth factor A (VEGF-A) secretion and the subsequent angiogenesis [7]. In recent years, antiangiogenesis therapy for HCC has made significant progress in clinical practice. Drugs targeting angiogenesis, such as sorafenib, have been investigated for mechanism in clinical practice, but their adverse reactions seriously affect the quality of life of patients [8]. The rapid advances in gene technology have deepened our understanding of angiogenesis, with research focused on finding new gene targets and better treatment options for HCC therapy.

There are ten members of the copper metabolizing MURR1 domain (COMMD) family of proteins, i.e., COMMD1–10 [9]. COMM domain is the main feature of

COMMD protein that contains a conserved sequence of 70-85 amino acids. This domain is located at the carboxyl-terminal of the last protein and provides a platform for protein-protein interaction [10, 11]. COMMD family members are involved in many physiological activities of cells such as copper (Cu) homeostasis, sodium (Na) homeostasis, hypoxia responses, and endosomal adaptation, as well as inflammatory activities [11, 12]. Specifically, current studies have found that COMMD3 can promote the proliferation of HCC and be used as an independent prognosticator in HCC patients [13].

Angiogenesis is a complex process in tumor progression. Targeted angiogenesis is regulated by multiple signaling pathways, among which hypoxia is indispensable. Rius et al. [14] demonstrated that the nuclear factor of transcription kappa B (NF-κB) is an essential mediator of HIF1α transcription. Under hypoxia, the NF-κB pathway is activated and HIF1α expression is upregulated. It has been found that COMMD1, another member of the COMMD3 family, can inhibit downstream gene expression mediated by the NF-κB pathway via blocking the HIF1α and HIF1β isodimer formation pathway, in turn inhibiting the malignant progression of tumor cells [15]. However, the relationship between COMMD3 and tumor angiogenesis has rarely been studied. Therefore, we used lentivirus transfection technology and transcriptome sequencing technology to evaluate the angiogenesis mechanisms of COMMD3 and HCC angiogenesis.

2. Methods

2.1. Cell Culture. Two HCC cell lines (SK-Hep1 and Hep 3B) and human umbilical vein endothelial cells (HUVECs) were acquired from the Chinese Academy of Sciences cell bank (Shanghai, China). The three cell lines were cultured as monolayers at 37°C in a humidified atmosphere with 5% CO_2 pressure as previously described [16].

2.2. Cell Transfections. The slow virus vector was constructed by Genechem (Shanghai, China). SK-Hep1 and Hep-3B cells were seeded in 6-well plates to achieve 30~40% confluency on the next day. Then, following the manufacturer's instruction, sh*COMMD3*, ov*COMMD3*, or negative control (shCtrl) lentiviruses were transfected into the cells and cultured for 8–12 h with fresh complete media. The cells were monitored using a fluorescence microscope three days post-infection. Finally, stably transfected cell lines were screened with a puromycin-containing medium (2 g/mL). The short hairpin RNA (shRNA) sequences for targeting *COMMD3* included 5′-ACTCCAACGCCTTCACGCTTC-3′ and 5′-GGATGATCTAACACGGCCTCGTC-3′.

2.3. RNA-seq Analysis. Fully transfected *COMMD3* SK-HEP1 cells with overexpression and knockdown and wild-type SK-HEP1 cells were sent to Oebiotech (Shanghai, China) for total RNA extraction and total transcriptome sequencing. We used Gene Ontology (GO) enrichment analysis and gene set enrichment analysis (GSEA) to analyze the function and signaling pathway of the differentially expressed genes (DEGs). GSEA was specifically used to examine the relationships between stress responses in multiple cancer-related pathways, metabolic pathways, transcriptional processes, and biological processes.

2.4. Colony Formation Assay. After two weeks of culturing, 800 cells/well in 6-well plates were fixed using 4% paraformaldehyde. Then, the cell staining was performed using 0.2% crystal violet (Beyotime, Shanghai, China) for visualization, and individual colonies (>50 cells/colonies) were counted.

2.5. Wound Healing Assay. Briefly, when the cells in the 6-well plates reached 80–90% confluency, the cell monolayer was scratched with a 200 μL plastic pipette tip, then washed. Subsequently, cells were cultured in a complete medium for 24 h. The healed wound area was measured at the beginning, and 24 h later, we used an inverted microscope to assess cell migratory abilities.

2.6. Transwell Invasion Assay. Transwell cell invasion was evaluated as described before [16]. Briefly, a 24-well transwell plate and an 8 μm filter (Corning, NY, USA) were used. 50 μL Matrigel was added to the upper cavity before cells, and 500 μL containing 20% FBS medium was added to the lower lumen. Then, the invading cells were counted after 48 h.

2.7. HUVEC Tube Formation Detection. HUVEC tube formation was detected as described before [16]. Briefly, cells were incubated in 96-well plates with Matrigel at 37°C for 30 min. Subsequently, 100 μL/well HUVEC cell suspension was added. The cell suspension contained 2.5×10^4 HUVECs and the cell culture supernatant for each group. Then, cells were incubated for a further 4-6 h in a 37°C and the lumen formation was observed under a microscope. Finally, for fluorescent staining, calcein (Invitrogen, Carlsbad, CA, USA) was added to cells and incubated for another 30 min; then, cells were imaged and analyzed using a fluorescence microscope.

2.8. Phalloidin Staining Assay. A phalloidin staining kit (YEASEN, Shanghai, China) was used to stain the actin stress fibers following the manufacturer's instructions. Briefly, cells were grown on coverslips and fixed with 4% paraformaldehyde; then, 50-100 μL cyclopeptide working solution and DAPI solution were added. Finally, the micrographs were photographed.

2.9. Apoptosis Assay. Cells were cultured at a density of 5×10^5 per well in a 6-well plate and incubated overnight. On the next day, they were collected using EDTA-free trypsin and counted. Then, the apoptosis rate was evaluated using a PE Annexin V Apoptosis Detection Kit with a 7-AAD kit following the manufacturer's instructions (Tonbo Biosciences, San Diego, CA, USA). First, 5 μL 7-AAD was added to each group. Then, 95 μL 1 × 7-AAD binding solution was added before mixing, and finally, 5 μL propidium iodide was added before incubating at 25°C in the dark for 15 min. Finally, flow cytometry (Cytomics FC 500; Beckman

Coulter, Brea, CA, USA) was used for measuring the apoptosis rate.

2.10. Western Blotting (WB) Assay and qPCR Detection. WB and qPCR were performed referring to our previous articles [16]. Total RNA extraction was performed by the TRIzol™ reagent method. Per sample, 0.5 μg total RNA was used as a template in an RT-qPCR kit (Takara, Shiga, Japan). Primer synthesis and purification were performed by Sangon Biotech (Shanghai, China) according to the following sequences: *COMMD3* forward (5′-ACTCCAACGCCTTCACGCTTC-3′), *COMMD3* reverse (5′-GGATGATCTAACACGGCCT CGTC-3′), GAPDH forward (5′-CAGGAGGCATTGCTGA TGAT-3′), and GAPDH reverse (5′-GAAGGCTGGGG CTCATTT-3′). For WB, the 1 : 1,000 dilutions of primary antibodies were used, and then, the membrane was incubated overnight at 4°C. HIF1α, VEGF, NF-κB, p65, β-Catenin, p-VEGFR2, VEGFR2, and actin antibodies were provided from CST (Danvers, MA, USA). COMMD3 antibody was provided from Abcam (Cambridge, UK).

2.11. Animal Studies. In total, 24 4-week-old male BALB/c nude mice were provided by Shanghai Slack Laboratory Animal (China) and divided into four groups ($n = 6$ per group). Each group received either normal SK-Hep1 cells, transfected SK-Hep1 cells with no load, stably infected Ov*CommD3* SK-Hep1 cells, and Sh*CommD3* SK-Hep1 cells subcutaneously injected into the right axilla (5×10^6 cells treated with 100 μL PBS). We evaluated tumor diameter 10 days after administration and every 3 days until the 27th day following the injection. Then, the tumor volume V (mm^3) was calculated using the following formula: $V = L \times W^2/2$, where the L and W parameters represent the largest diameter (mm) and the smallest diameter (mm), respectively. On the 27^{th} day after implantation, the mice were sacrificed, and the tumor weight was measured. Then, tumors were subjected to immunohistochemical (IHC) staining and WB ex vivo as previously described [16]. This study was performed under the ethical approval of the Animal Ethics Committee of Shanghai Municipal Hospital of Traditional Chinese Medicine, Shanghai University of Traditional Chinese Medicine (Approval Number: SYXK, Shanghai, China 2020-0014).

2.12. Statistical Analyses. All experiments were performed in triplicate at least. Data are expressed as the mean ± SEM. For comparing the results, the means of multiple groups were compared by one-way analyses of variance (one-way ANOVA) in Prism v8.0 (GraphPad Software, San Diego, CA, USA). A P value < 0.05 was considered statistically significant.

3. Results

3.1. COMMD3 Overexpression and RNA Interference Lentivirus Stable Strains Were Successfully Constructed. HCC cells were infected and subcultured. The stably transfected cell lines were screened by puromycin. The expression of *COMMD3*-mRNA in lentivirus-infected stable strains was measured by RT-qPCR. The outcomes indicated the significantly elevated expression levels of *COMMD3*-mRNA in *COMMD3* overexpressed cells compared to the negative control group. *COMMD3*-mRNA expression level after *COMMD3*-RNA interference was significantly lowered compared to the negative control group (Figures 1(a) and 1(b)).

We used WB to explore the protein levels of COMMD3 in stable strains infected with lentivirus. The results indicated that *COMMD3* overexpression increased the COMMD3 protein levels compared to the negative control group. However, the COMMD3 protein levels after *COMMD3*-RNA interference were significantly decreased compared to in the negative control group (Figures 1(c)–1(h)). Meanwhile, the *shCOMMD3*-30 sequence showed the highest knockdown efficiency among the three knockdown sequences of 30, 31, and 32. Therefore, we chose *shCOMMD3*-30 for the follow-up study (Figures 1(c)–1(h)).

These results indicate that *COMMD3* overexpression and RNA interference lentivirus stable strains were successfully constructed and used for the mechanism studies.

3.2. COMMD3 Modulates the DEGs among OvCOMMD3, Control, and ShCOMMD3 SK-HEP1 Cells. Ov*COMMD3*, control, and Sh*COMMD3* SK-HEP1 cells were detected by RNA-seq analysis. First, according to gene expression in each sample, 193 DEGs (68 upregulated DEGs and 125 downregulated DEGs) were found between Ov*COMMD3* and control SK-HEP1 cells (Figure 2(a)). Among the DEGs of Sh*COMMD3* and control SK-HEP1 cells, a total of 2,447 DEGs were affected (1,254 upregulated DEGs and 1,193 downregulated DEGs) (Figure 2(b)). In addition, there were a total of 1,951 DEGs between Ov*COMMD3* and Sh*COMMD3* (949 up- and 1,002 downregulated) (Figure 2(c)). The logarithmic fold-change ($\log_2 FC \geq 1.5$) and q – value ≤ 0.05 were used as the screening conditions. Also, a Venn diagram was used for showing 101 common DEGs among the three groups (Figure 2(d)). In addition, using the GO functional enrichment analyses, we showed that *COMMD3*-enriched genes were mainly involved in angiogenesis processes ($P < 0.05$; Figure 2(e)). GSEA displayed that differentially expressed Ov*COMMD3* and control genes were enriched in the HIF1α (Figure 2(f)) and NF-κB signaling pathways (Figure 2(g)) ($P < 0.05$, FDR < 0.25).

3.3. COMMD3 Expression Affects the Formation of Clonal Plaques of Human HCC Cells. The colony formation assay after *COMMD3* overexpression showed an enhanced clone formation capacity in HCC cells. This finding evidenced the stronger proliferation ability of these cells compared to the control ones ($P < 0.001$ for both cell lines). However, after *COMMD3* knockdown, the plate clonal plaque formation ability showed a significant reduction compared to the control cells ($P < 0.001$ for both cell lines) (Figure 3(a)). These results show that *COMMD3* overexpression enhances the proliferation capacity of HCC cell lines, whereas *COMMD3* knockdown reduces their proliferation potential.

3.4. COMMD3 Expression Affects the Migration of HCC Cells. In both HCC cell lines with *COMMD3*-RNA interference, the number of migrating cells to the opposite side was

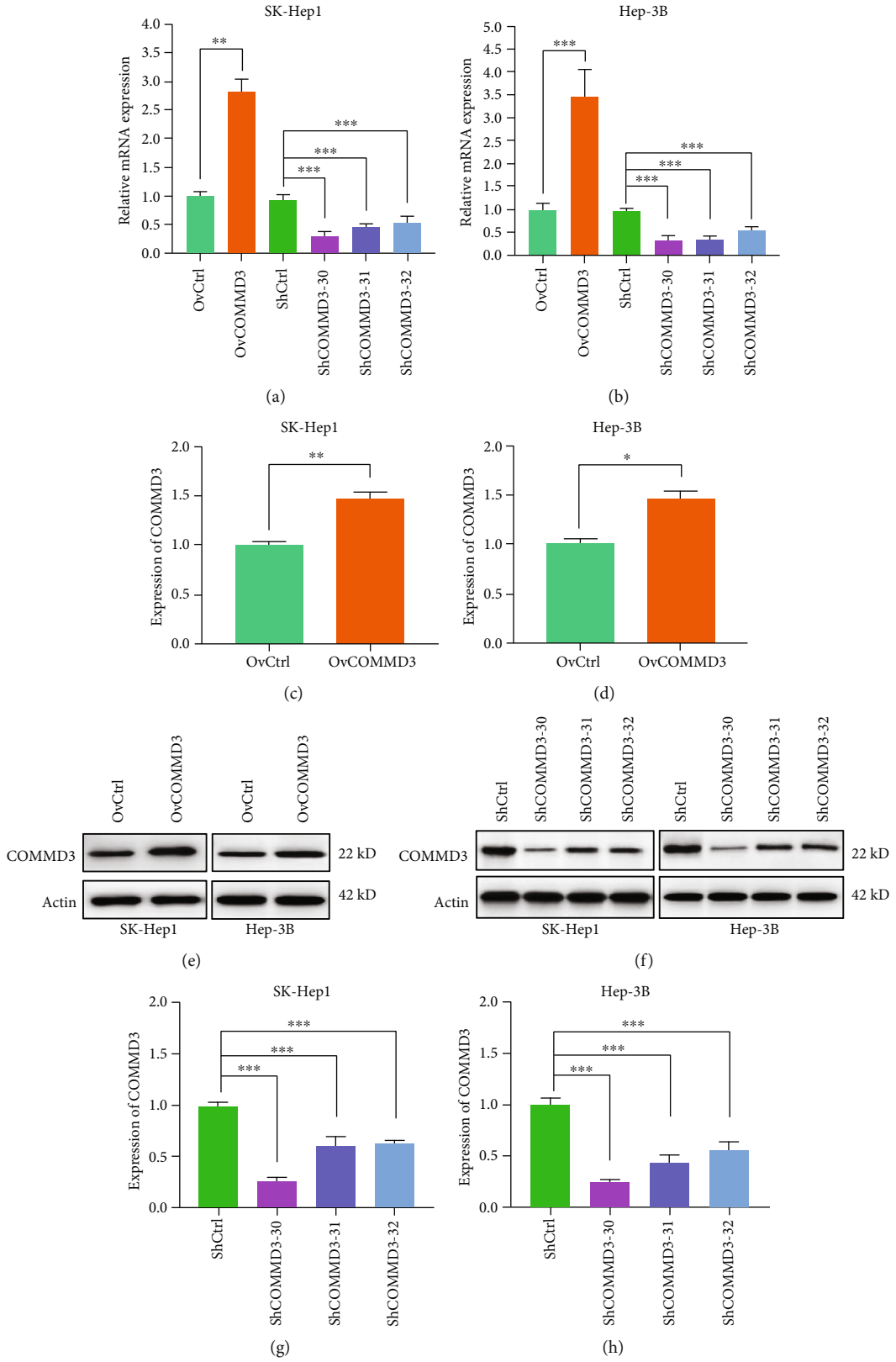

Figure 1: *COMMD3* expression and protein level after *COMMD3*-overexpression or *COMMD3*-knockdown in HCC cell lines. (a–b) Relative quantity of *COMMD3* mRNA level in SK-Hep1 and Hep-3B cell lines measured by RT-qPCR after *COMMD3* overexpression or knockdown. (c–d) COMMD3 protein levels increased after *COMMD3*-overexpressed transfection. (h–g) COMMD3 protein levels decreased after *COMMD3*-knockdown transfection. (e–f) Western blot of COMMD3 levels. Actin was used as the loading control. $^{*}P < 0.05$, $^{**}P < 0.01$, and $^{***}P < 0.001$.

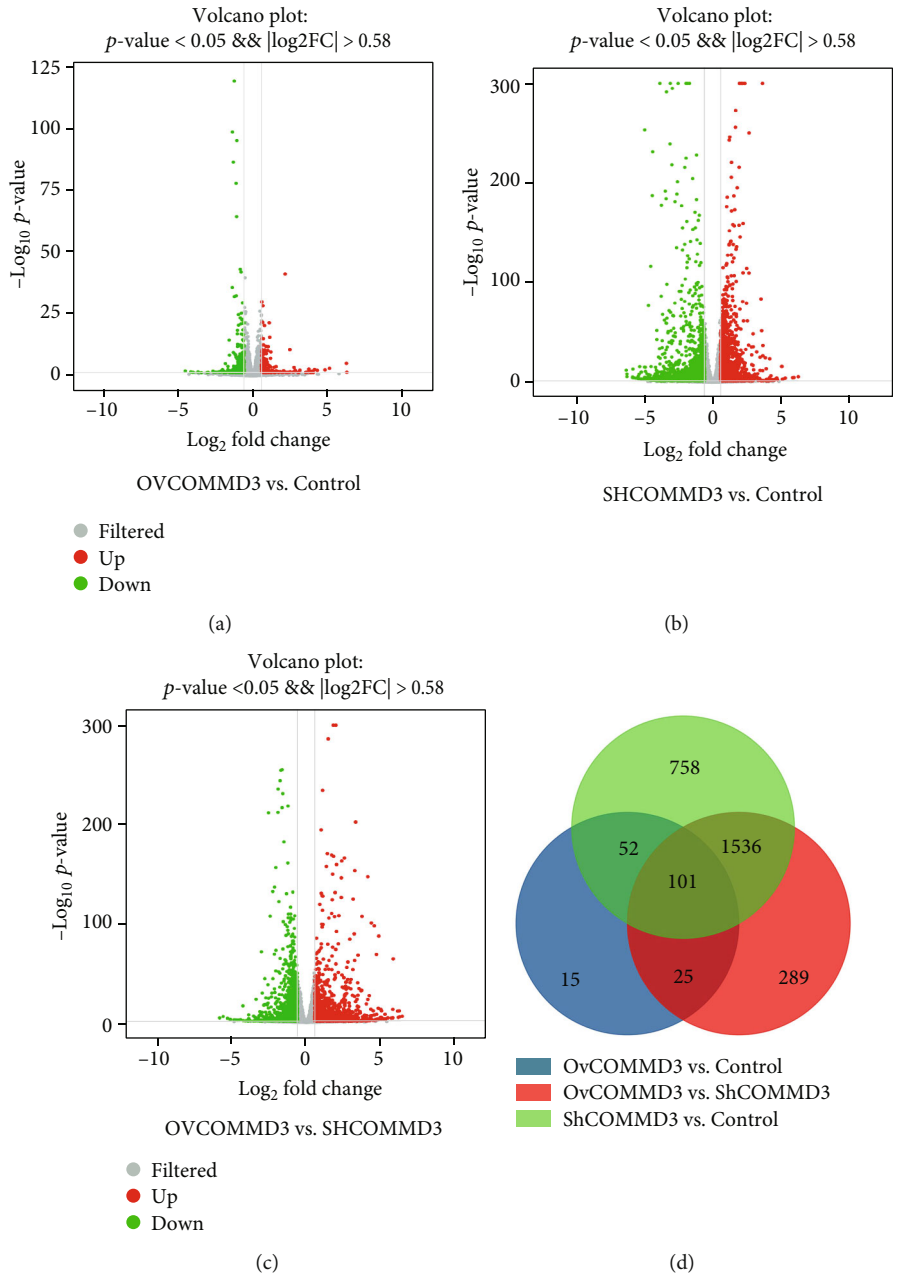

Figure 2: Continued.

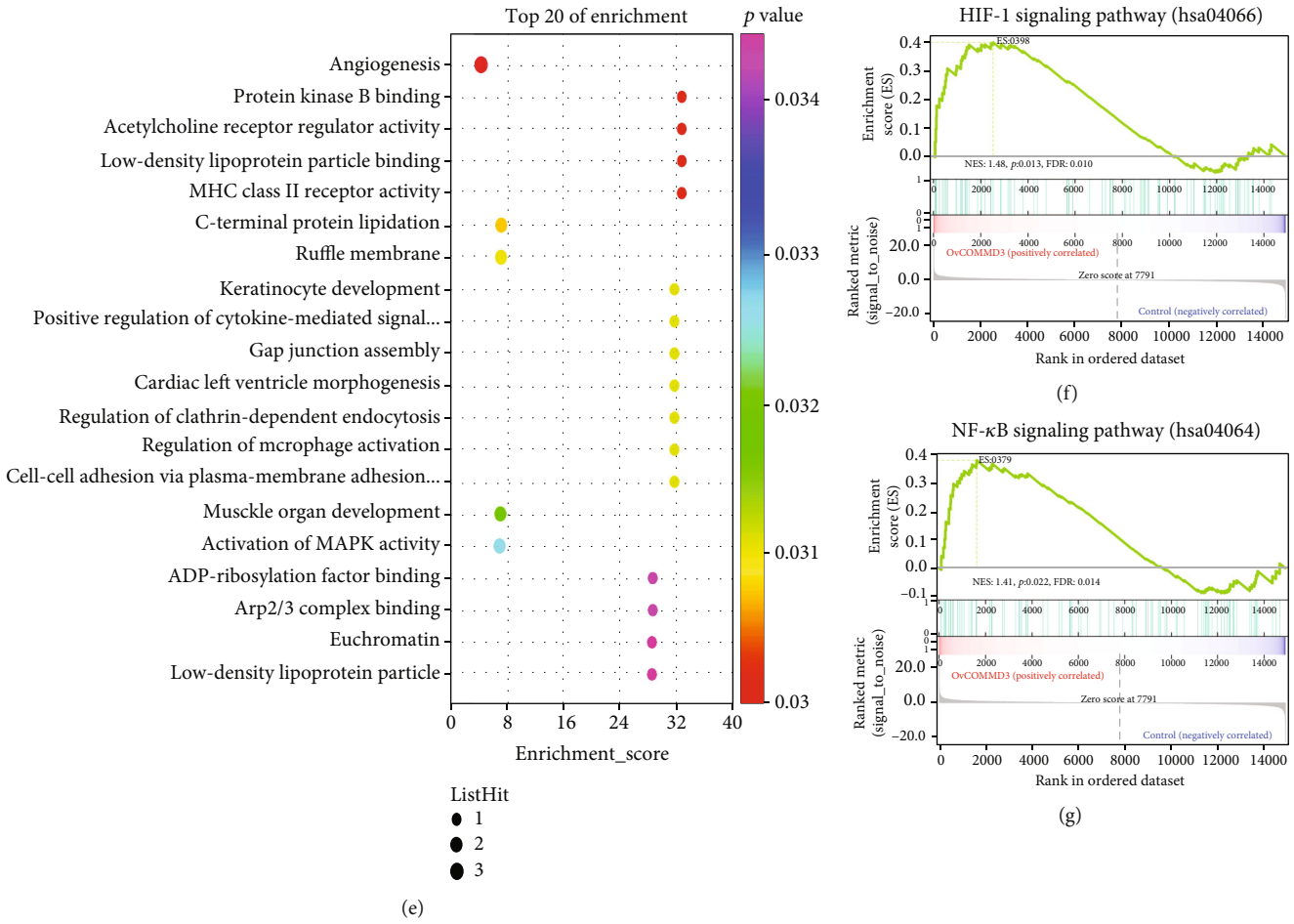

Figure 2: *COMMD3* modulates the DEGs among Ov*COMMD3*, control, and Sh*COMMD3* in SK-Hep1 cells. (a–c) The volcanic maps indicated the DEGs among the three comparative groups. The red color represents upregulated DEGs, the blue color represents downregulated DEGs, and the gray color represents the non-DEGs; $\log_2$FC ≥ 1.5 and $P < 0.001$. (d) Venn diagram of DEGs in control vs. Ov*COMMD3*, control vs. Sh*COMMD3*, and Sh*COMMD3* vs. Ov*COMMD3*; $\log_2$FC ≥ 1.5 and $P \leq 0.01$. (e) Bubble diagram showed GO functional enrichment analysis. The *Q*-value is the calibration value for the *P* value. (f–g) GSEA for the HIF1*α* and NF-*κ*B pathway. A nominal $P < 0.05$ and false discovery rate (FDR) < 0.25 were set as statistically significant thresholds.

less than that of the control cells 24 h after the scratch. In other words, the scratch area of both HCC cell lines was larger than that of the control group ($P < 0.001$ for both cell lines). However, in the two HCC cell lines with *COMMD3* overexpression, the area of the scratch remained smaller compared to the control group ($P < 0.001$ for both cell lines) (Figures 3(b) and 3(c)).

3.5. COMMD3 Expression Affects the Invasion Capacity of HCC Cells. Based on the transwell cell invasion experiment, the *COMMD3*-overexpressed HCC cells showed stronger invasive ability than control cells after 48 h ($P < 0.001$ for both cell lines). On the contrary, after *COMMD3*-knockdown, the invasion ability was significantly attenuated compared to the control cells ($P < 0.001$ for both cell lines) (Figure 4(a)).

3.6. COMMD3 Expression Affects the Angiogenesis of HCC Cells. According to Figure 4(b), the angiogenesis capacity of the *COMMD3*-overexpressing SK-Hep1 and Hep-3B cell lines was significantly higher than that of the control ones ($P < 0.001$ for both cell lines). However, RNA interference inhibited the angiogenesis capacity in both cell lines ($P < 0.001$ for both cell lines).

3.7. COMMD3 Expression Affects Actin Microfilament Morphology of HCC Cells. Phalloidin staining is used to mark the F-scaffolding protein actin in cells. The F-actin distribution is extensive when the angiogenesis ability of cells is weakened. In contrast, when angiogenesis is enhanced, F-actin distribution is dispersible. As shown in Figure 4(c), the cytoskeleton of the control groups formed a linear pattern assembly in parallel throughout ($P < 0.001$ for both cell lines). However, cells with *COMMD3* overexpression had densely distributed F-actin in the cytoskeleton, while *COMMD3*-RNA interference resulted in the dispersion of disordered or disappearing stress fibers, indicating that *COMMD3*-RNA interference induced F-actin depolymerization and weakened angiogenesis ability ($P < 0.001$ for both cell lines).

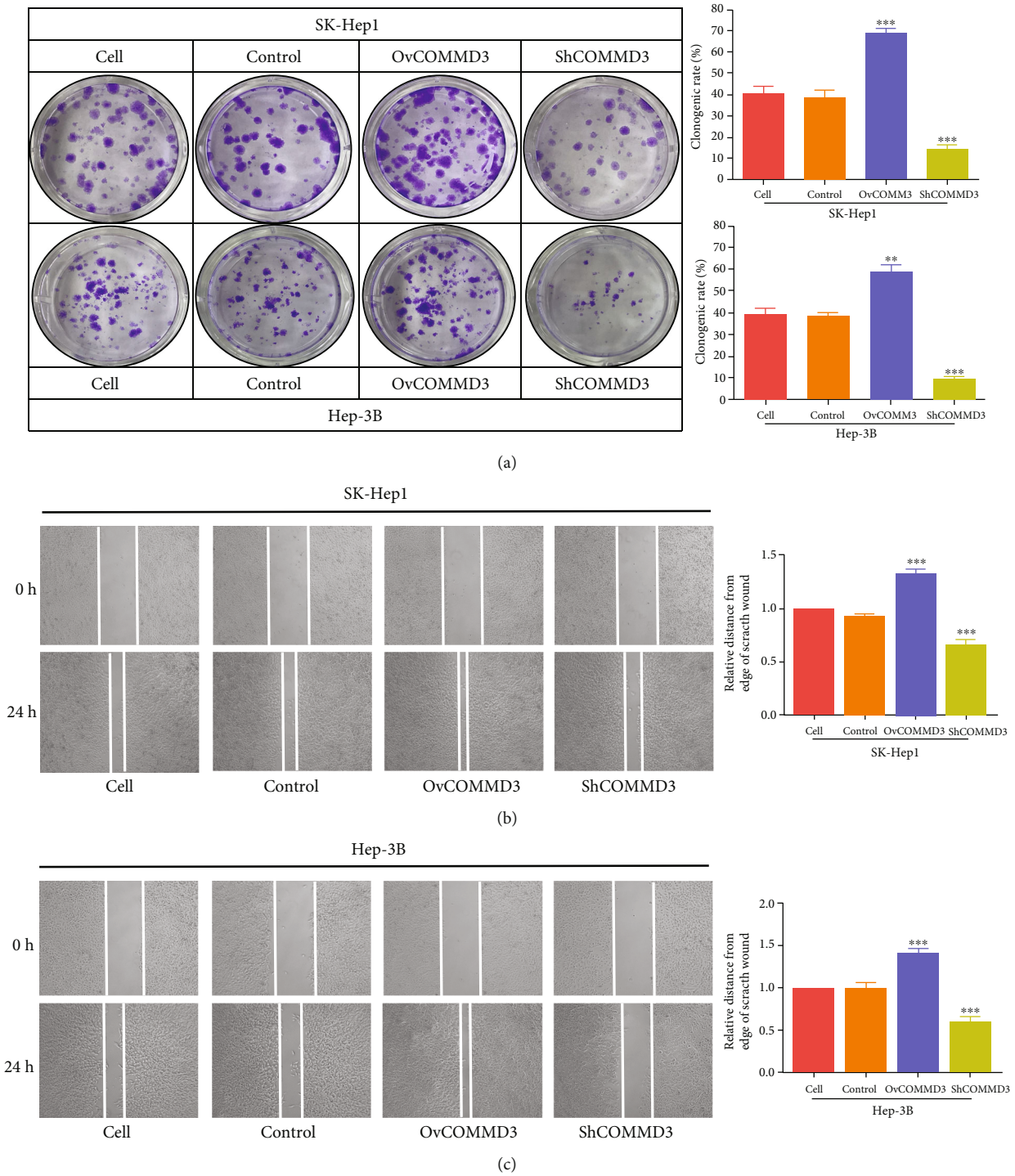

Figure 3: *COMMD3* regulates the proliferation and migration of HCC cell lines. (a) Clone formation assay showing the proliferation capacity of both HCC cell lines after *COMMD3* overexpression or knockdown. (b) Wound healing assessment displaying the migration capacity of SK-Hep1 and Hep-3B cell lines after *COMMD3* overexpression or knockdown. $^{**}P < 0.01$; $^{***}P < 0.001$.

3.8. COMMD3 Expression Affects the Apoptosis Capacity of Human HCC Cell Lines. In the apoptosis experiment using flow cytometry (Figures 5(a)–5(d)), after *COMMD3* overexpression and *COMMD3* knockdown, the apoptotic behavior of HCC cell lines did not significantly change compared to the control cells ($P > 0.05$ for both cell lines). Therefore, *COMMD3* expression showed no statistically significant effect on the apoptotic behavior of HCC cell lines.

3.9. COMMD3 Expression on β-Catenin and p-VEGFR2/VEGFR2 Protein Levels in HCC Cells. To explore the key factors involved in COMMD3 promoting angiogenesis in

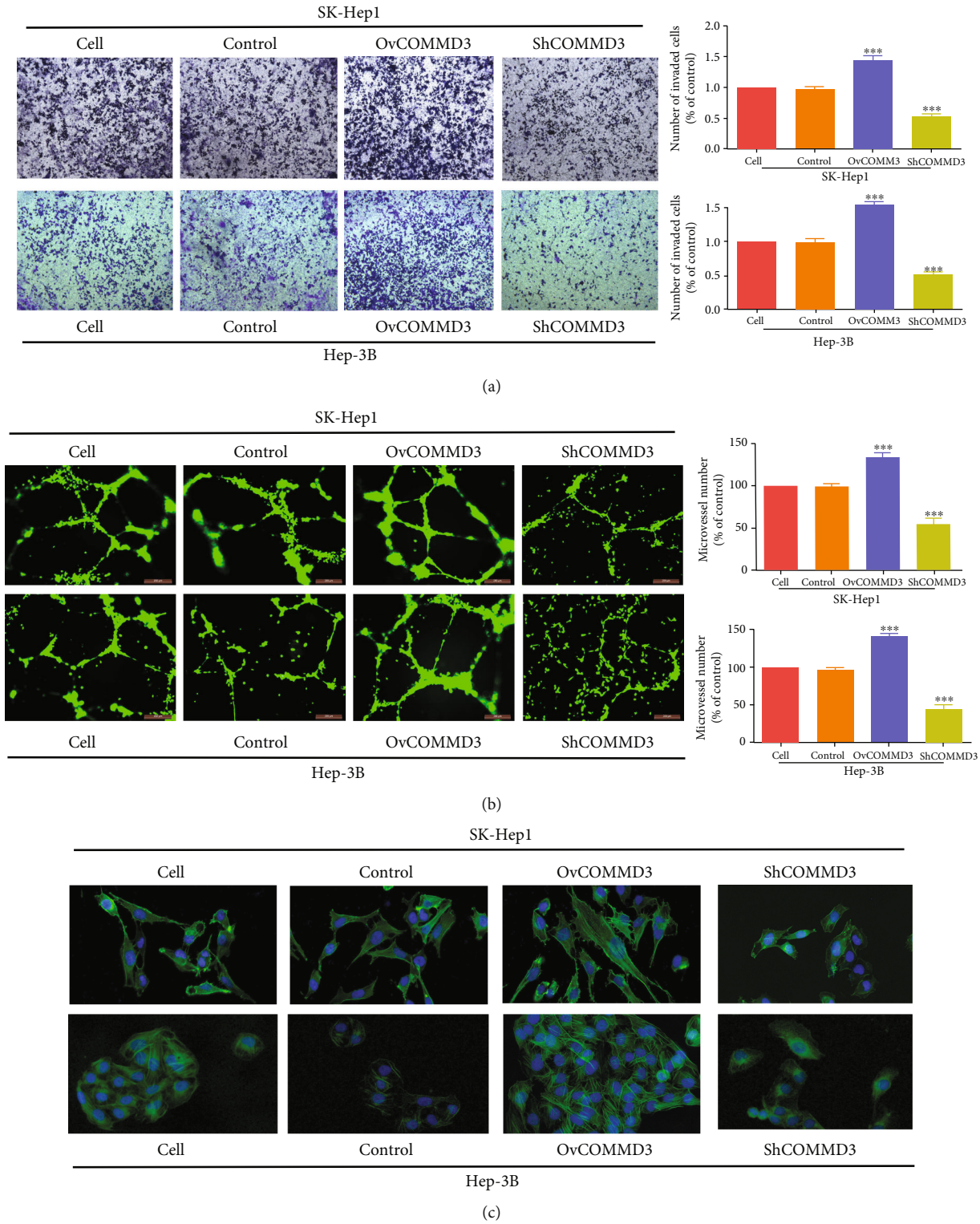

Figure 4: *COMMD3* regulates invasion and angiogenesis of HCC cell lines. (a) Transwell assay showing the invasion capacity of HCC cell lines after *COMMD3* overexpression or knockdown. (b) HUVEC tube formation detection of the angiogenesis capacity of HCC cell lines after *COMMD3* overexpression or knockdown. (c) Phalloidin staining assay of the F-scaffolding protein actin of HCC cell lines after *COMMD3* overexpression or knockdown. $^{***}P < 0.001$.

SK-Hep1 and Hep-3B cell lines, we used WB to explore the protein levels of β-Catenin and *p*-VEGFR2/VEGFR2 in *COMMD3*-overexpressed and *COMMD3*-RNA interference cells. According to the results (Figure 5(e)), *COMMD3* overexpression increased β-Catenin and *p*-VEGFR2/VEGFR2 protein levels compared with the controls, while *COMMD3*-

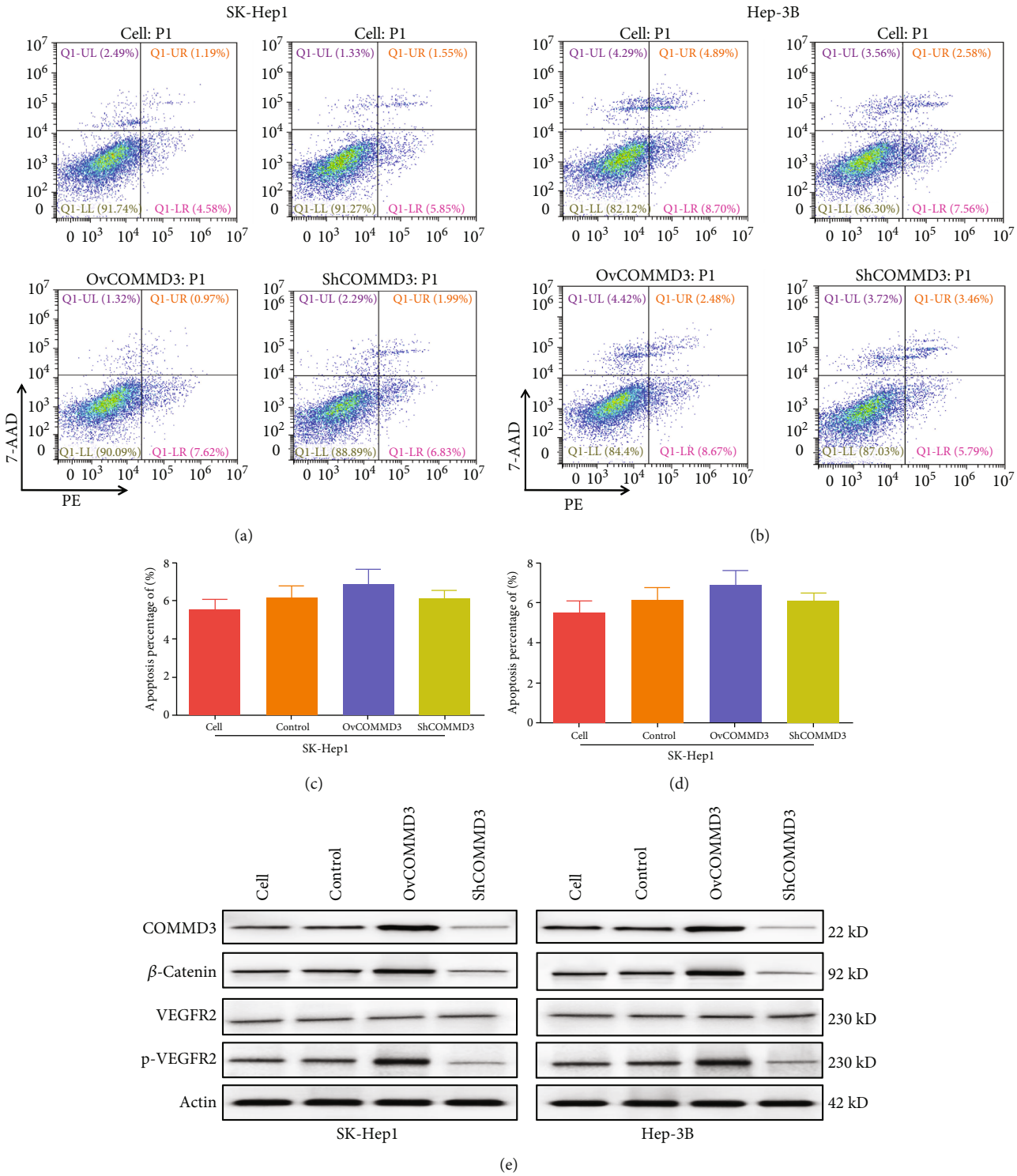

Figure 5: Continued.

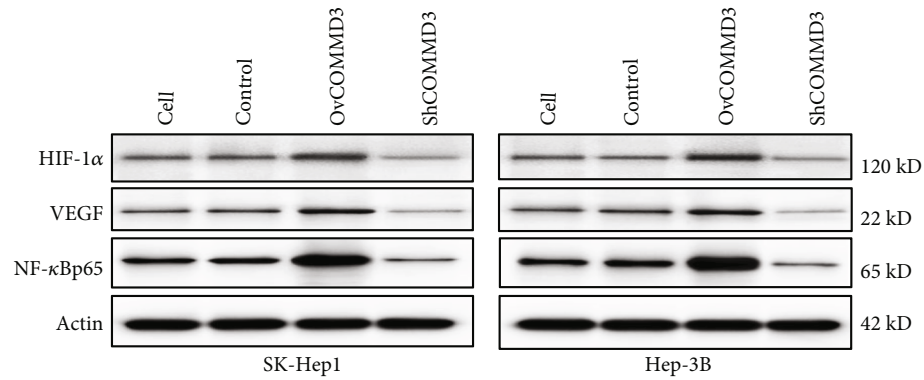

(f)

Figure 5: *COMMD3* regulated the protein expression levels of β-Catenin, *p*-VEGFR2, VEGFR2, HIF1α, VEGF, and NF-κB, without affecting apoptosis in HCC cell lines. (a–d) *COMMD3* expression had no significant effect on apoptosis of HCC cell lines. (e–f) Western blot for β-Catenin, *p*-VEGFR2, VEGFR2, HIF1α, VEGF, and NF-κB levels.

RNA interference suppressed these protein levels. These findings evidence that COMMD3 can enhance angiogenesis in HCC cell lines through activating β-Catenin and promoting the phosphorylation of VEGFR2.

3.10. COMMD3 Expression on the Levels of HIF-1α, VEGF, and NF-κB in HCC Cell Lines. The signaling pathways involved in COMMD3 promoting migratory, invasiveness, and angiogenic properties of HCC cell lines were explored along with the GSEA results. For this purpose, we used WB to evaluate the protein levels of HIF1α, VEGF, and NF-κB in the HCC cell lines of *COMMD3* overexpression and *COMMD3*-RNA interference. The *COMMD3*-overexpressed cells produced higher protein levels of HIF1α, VEGF, and NF-κB compared with the control cells. However, the expression of these proteins was inhibited in the *COMMD3*-RNA interference group compared to the control cells (Figure 5(f)).

The present findings indicate that *COMMD3* can promote HIF1α, VEGF, and NF-κB protein levels in HCC cell lines. Considering our results, the expression of *HIF1α*, *VEGF*, and *NF-κB* is upregulated in HCC, which promotes cancer cell migration and induces angiogenesis. Therefore, we postulate that *COMMD3* can promote the migratory, invasiveness, and angiogenic properties of HCC cell lines regulating the HIF1α/VEGF/NF-κB signaling pathway.

3.11. COMMD3 Regulates Tumor Growth in a Xenograft Mouse Model. To verify the role of *COMMD3* in the angiogenesis of HCC, we conducted experiments on transplanted tumors in nude mice. For this purpose, SK-Hep1 (as control), *COMMD3*-overexpressing cells, and *COMMD3*-knockdown cells were administrated into the nude mice subcutaneously (Figure 6(a)) to form a subcutaneous xenograft tumor model. Figures 6(b)–6(d) represent the nude mouse models subcutaneously transplanted with SK-Hep1 control cells, exhibiting a considerable tumor growth rate. The tumor growth rate and tumor weight in mice administered with the *COMMD3*-overexpressing cells showed a significant increase compared to the control group ($P < 0.001$). Conversely, the *COMMD3*-knockdown group represented with decreased tumor growth rate and tumor weight ($P < 0.001$).

3.12. COMMD3 Modulates Angiogenesis in Subcutaneous HCC Xenograft Mice. For detailing the function mechanism of *COMMD3* in regulating the growth of subcutaneous HCC xenograft tumors in nude mice, tumors were studied histologically. For this purpose, the tumors were collected after the nude mice were sacrificed, and the phalloidin staining was used to explore the F-actin of the tumor cells. As shown in Figure 7(a), F-actin was densely distributed in the *COMMD3*-overexpressing cytoskeleton, while F-actin was scattered in the *COMMD3*-RNA interference cytoskeleton. The results suggested that *COMMD3*-overexpression promoted F-actin aggregation and enhances angiogenesis, while *COMMD3*-RNA interference induced F-actin depolymerization and weakened angiogenesis.

The tumor was also tested by IHC staining to explore the protein expression levels of angiogenesis-related β-Catenin and CD34, and WB was used to detect the expression levels of β-Catenin and *p*-VEGFR2/VEGFR2 proteins. As shown in Figure 6(e), the WB results evidenced a significant increase in the protein levels of β-Catenin and *p*-VEGFR2/VEGFR2 in the *COMMD3*-overexpressed group compared to the controls, while they were suppressed in the *COMMD3*-RNA interference group. The outcomes of IHC staining also illustrated that the tumor staining intensity of β-Catenin and CD34 in the *COMMD3*-overexpressed group was higher than that of the control group, while the *COMMD3*-RNA interference group had lower intensity. Both *in vitro* and *in vivo* results verified cancer- and angiogenesis-promoting effects of *COMMD3* (Figure 7(b)).

3.13. COMMD3 Modulates Angiogenesis by Regulating HIF1α/VEGF/NF-κB Signaling Pathways In Vivo. WB and IHC staining were used to determine the protein expression levels of HIF-1α, VEGF, and NF-κB to further verify the mechanism of *COMMD3* regulation of angiogenesis of *COMMD3* in HCC subcutaneously transplanted nude mice. The results showed that for both WB (Figure 6(e)) and IHC staining (Figure 7(b)), *COMMD3* overexpression promoted

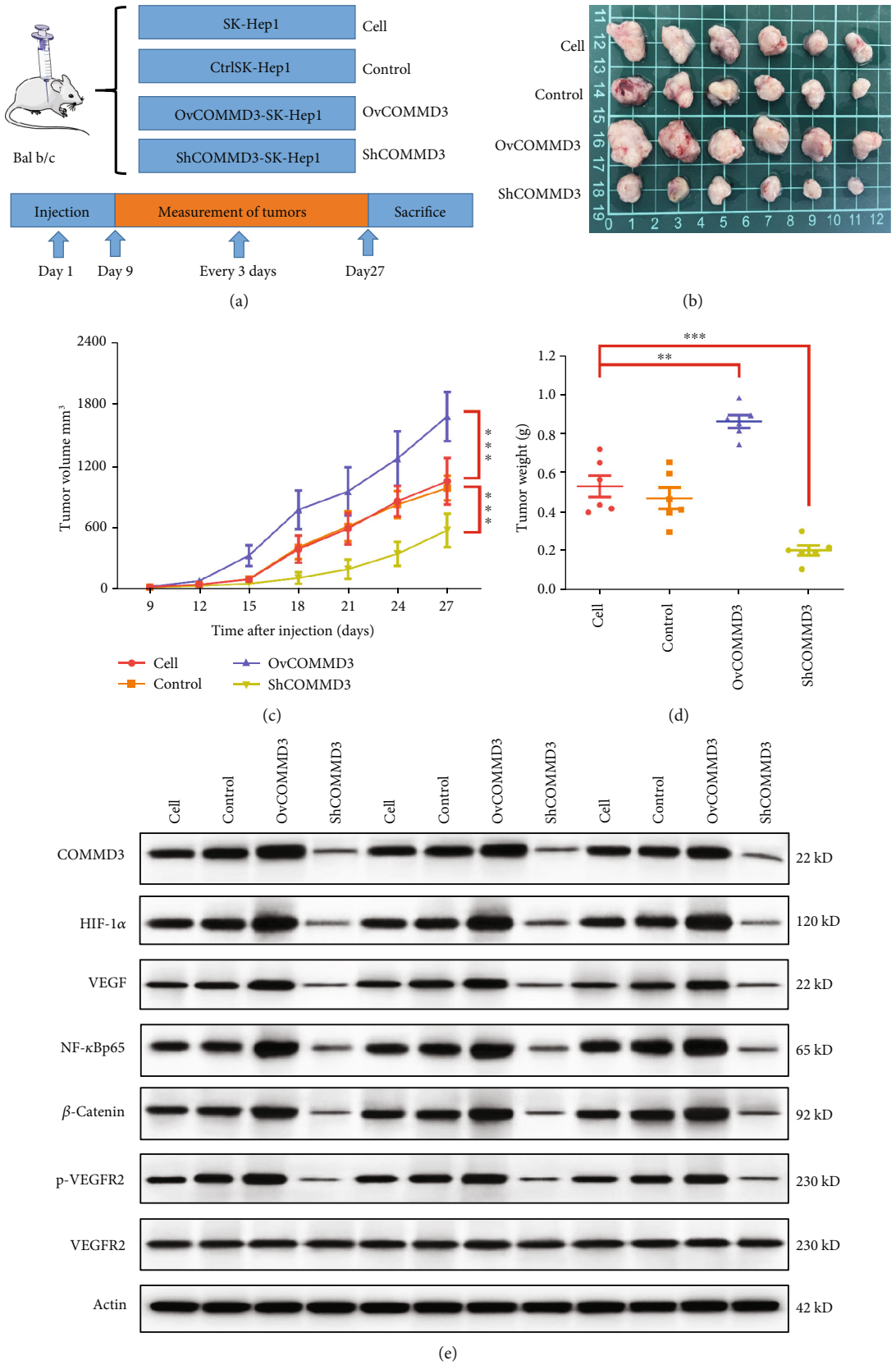

Figure 6: Effects of *COMMD3* on subcutaneous tumor growth and angiogenesis in nude mice. (a) Schematic diagram of animal experimental groups and time points. (b–d) Effects of COMMD3 on tumor progression. (e–f) Western blot for β-Catenin, *p*-VEGFR2, VEGFR2, HIF1α, VEGF, and NF-κB levels. Actin was applied as the loading control. $^{**}P < 0.01$; $^{***}P < 0.001$.

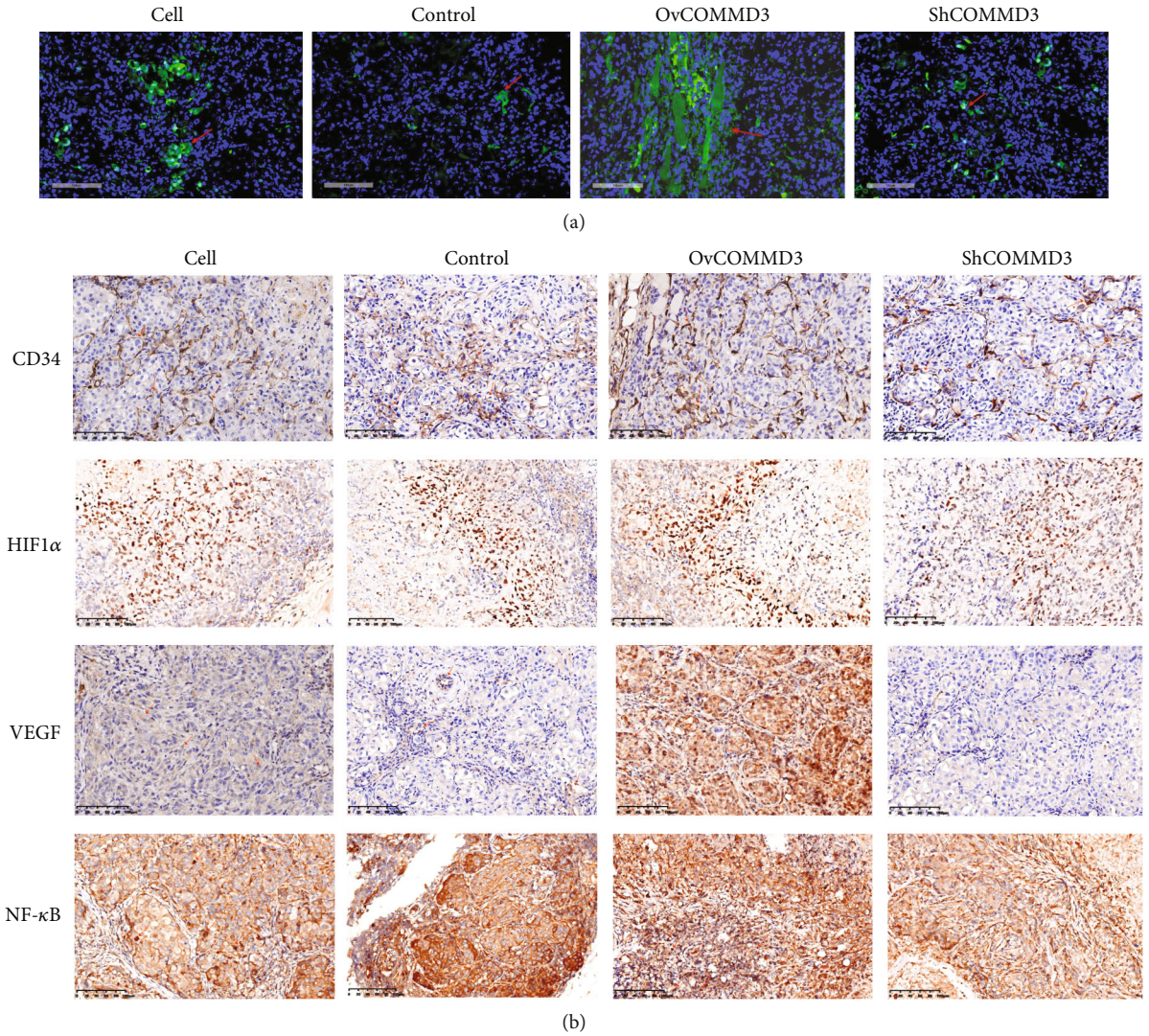

Figure 7: *COMMD3* modulates the F-scaffolding protein actin and the levels of CD34, HIF1α, VEGF, and NF-κB in nude mice. (a) Phalloidin staining assay of the F-scaffolding protein actin in nude mice. (b) Immunohistochemical staining for CD34, HIF1α, VEGF, and NF-κB levels.

the protein expression levels of HIF1α, VEGF, and NF-κB *in vivo* compared to the controls, while *COMMD3*-RNA interference had the opposite effect. These findings indicated that *COMMD3* plays a positive regulatory role in the growth and angiogenesis of subcutaneous HCC xenografts, and its effects may be achieved by regulating the HIF1α/VEGF/NF-κB signaling pathway.

4. Discussion

In this study, we successfully constructed two stable transgenic HCC cell lines (SK-Hep1 and Hep-3B) with *COMMD3* overexpression and *COMMD3* knockdown, respectively. We sequenced and compared the *COMMD3*-overexpressed SK-Hep1 cells, *COMMD3*-knockdown SK-Hep1 cells, and control SK-Hep1 cells, to show that changes in *COMMD3* expression were significantly related to angiogenesis. We also found that *COMMD3* overexpression induced the angiogenesis of HCC cells, while *COMMD3* knockdown inhibited HCC angiogenesis. Simultaneously, GSEA based on the sequencing results indicated that the NF-κB and HIF1α pathways were most related to the differential expression of *COMMD3*. Therefore, our *in vitro* and *in vivo* analyses indicated the activating effect of *COMMD3* on the HIF1α/VEGF/NF-κB pathway leading to the promotion of the angiogenesis and progression of HCC.

Recent studies have shown that the COMMD protein family is expected to become a potential therapeutic target for several cancers [13, 17, 18]. COMMD1 was the first member to be discovered and the most representative family member [19]. COMMD1 is a regulatory protein with several functions such as copper stabilization, iron transportation and secretion, oxidative stress response, DNA damage response, protein aggregation, NF-κB- and hypoxia-mediated transcription, and carcinogenesis [12, 15, 20, 21]. Furthermore, COMMD3, COMMD4, and COMMD6 are

suggested to be interacting with different NF-κB subunits and participating in the inhibition of transcription processes mediated by NF-κB. However, they all show relatively weaker effects compared to COMMD1 [22]. COMMD5, which is also known as HCaRG, is a hypertension-related calcium regulatory gene that inhibits the expansion of tumor cells [23–25]. COMMD7 is reported to have a suppressing effect on the expansion, migratory, and invasiveness capacities of hepatocarcinoma by regulating the chemokine CXCL10 [17, 26, 27]. Concurrently, it was found that COMMD7 regulates CXCL10 mainly through NF-κB and reactive oxygen species (ROS) [28]. COMMD9 is also reported to have an inhibitory effect on the expansion and migration of non-small-cell lung cancer cells, blocking cells in the G1/S phase and inducing autophagy [18]. COMMD10 is a common member of the COMMD family which suppresses the invasiveness and metastatic properties of colorectal cancer cells through NF-κB [29]. In contrast, COMMD2 and COMMD8 currently lack relevant reports on their functions, and limited research is available for COMMD3. Nevertheless, according to the literature, COMMD3 is expressed at a high level in prostate cancer, enhances migratory and invasiveness properties of tumor cells, and is also associated with tumor recurrence and low survival rate [30]. In recent years, research interest in the role of COMMD3 in HCC has steadily increased. By mining public information databases, Wang et al. [13] confirmed that COMMD3 is highly expressed in tissues of HCC patients and predicts poorer clinical outcomes. However, the experimental evidence on COMMD3 role in HCC, especially its mechanism, has remained uncertain.

Previous studies have shown that NF-κB seems to be inextricably linked with members of the COMMD family: it can positively or negatively regulate the NF-κB signaling pathway in a variety of ways. NF-κB is an essential factor in the process of inflammation and liver cell regeneration, and NF-κB is usually overactivated in HCC. In patients with HCC and high NF-κB activity, inflammation is difficult to control, pathological features are dangerous, and treatment effects are poor. Blocking the NF-κB signaling pathway can inhibit tumor proliferation, indicating the importance of inhibiting NF-κB activity in preventing the progression of HCC disease. In this study, we performed transcriptome sequencing and comparison of *COMMD3* overexpression and *COMMD3*-knockdown SK-Hep1 cell line with wild-type SK-Hep1 cell line. The findings indicate the involvement of *COMMD3* in the regulation of the NF-κB signaling pathway. On the other hand, the survival and progression of solid tumors cause local hypoxia. Under hypoxic conditions, the NF-κB pathway is activated and HIF-1α is accumulated. NF-κB is a key transcription factor regulating HIF1α. This experimental study showed that *COMMD3* overexpression elevated the protein levels of β-Catenin, *p*-VEGFR2/VEGFR2, HIF1α, VEGF, and NF-κB, whereas, after *COMMD3*-RNA interference, the expression levels of all these proteins were downregulated. Thus, we speculate that *COMMD3* interacts with NF-κB in the local hypoxic microenvironment, where HIF1α enters the nucleus and accumulates and is activated by NF-κB, β-Catenin expression is upregulated, VEGF secretion is induced, and VEGFR2 is phosphorylated. These processes ultimately promote angiogenesis in HCC, which assists with HCC invasion and metastasis, thereby causing more severe local tissue hypoxia and promoting tumor progression (Figure 8). Therefore, COMMD3 is expected to become a potential prognostic biomarker for HCC.

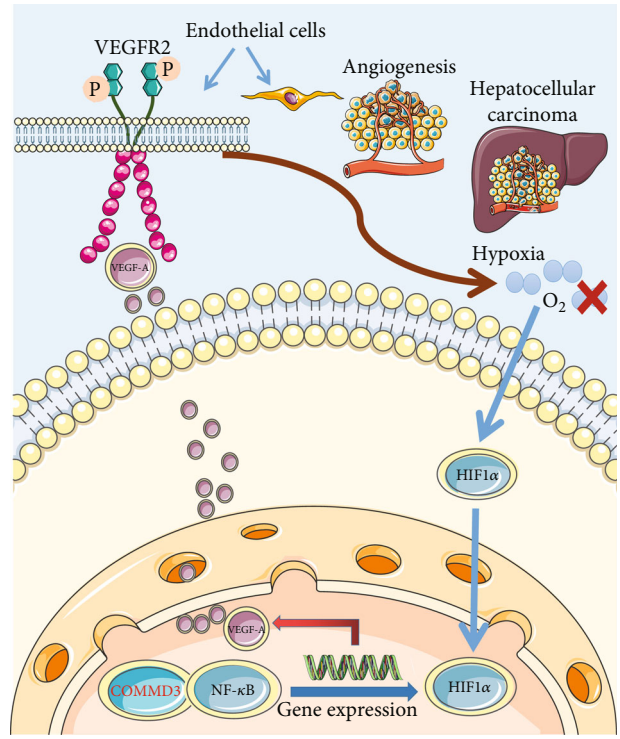

Figure 8: The schematic diagram of COMMD3 involved in HCC angiogenesis by regulating the HIF1α/VEGF/NF-κB signaling pathway.

5. Conclusions

Our results demonstrate that the HIF1α/VEGF/NF-κB signaling pathway participates in the effects of COMMD3 on HCC angiogenesis and progression both *in vitro* and *in vivo*. Further research in the future can be conducted to illustrate the potential of using COMMD3 as a therapeutic target in HCC.

Data Availability

All data obtained or analyzed during this study are included within the article.

Additional Points

Reporting Checklist. The authors have completed the ARRIVE reporting checklist.

Ethical Approval

Animal care and all animal experiments were approved by the Animal Ethics Committee of Shanghai Municipal Hospital of Traditional Chinese Medicine, Shanghai University of

Traditional Chinese Medicine (SYXK, Shanghai, China 2020-0014), and adhered to local animal care guidelines.

Conflicts of Interest

All authors declare no conflicts of interest.

Authors' Contributions

Dongwei Xing, Wei Cheng, and Minguang Zhang conceived and supervised the study; Tingting Zhu, Xiaolin Peng, and Ziwei Cheng were involved in the acquisition of data. Tingting Zhu, Xiaolin Peng, and Xiuru Gong analyzed the data; Tingting Zhu, Xiaolin Peng, Wei Cheng, and Minguang Zhang wrote the manuscript. All authors have read and approved the final version of the manuscript. All authors had full access to all data. Tingting Zhu and Xiaolin Peng contributed equally to this work.

Acknowledgments

This work was supported by the Natural Science Foundation of Shanghai (Research Grant no. 19ZR1452400) and the National Natural Science Foundation of China (Research Grant no. 81673743).

References

[1] F. Bray, J. Ferlay, I. Soerjomataram, R. L. Siegel, L. A. Torre, and A. Jemal, "Global cancer statistics 2018: GLOBOCAN estimates of incidence and mortality worldwide for 36 cancers in 185 countries," *CA: a Cancer Journal for Clinicians*, vol. 68, no. 6, pp. 394–424, 2018.

[2] J. M. Llovet, F. Castet, M. Heikenwalder et al., "Immunotherapies for hepatocellular carcinoma," *Nature Reviews. Clinical Oncology*, vol. 19, no. 3, pp. 151–172, 2021.

[3] A. X. Zhu, D. G. Duda, D. V. Sahani, and R. K. Jain, "HCC and angiogenesis: possible targets and future directions," *Nature Reviews. Clinical Oncology*, vol. 8, no. 5, pp. 292–301, 2011.

[4] W. J. Burdette, "Carcinoma of the colon and antecedent epithelium," *Cancer Research*, vol. 30, no. 1, pp. 253–256, 1970.

[5] J. Korbecki, D. Simińska, M. Gąssowska-Dobrowolska et al., "Chronic and cycling hypoxia: drivers of cancer chronic inflammation through HIF-1 and NF-κB activation: a review of the molecular mechanisms," *International Journal of Molecular Sciences*, vol. 22, no. 19, p. 10701, 2021.

[6] L. D'Ignazio, M. Batie, and S. Rocha, "Hypoxia and inflammation in cancer, focus on HIF and NF-κB," *Biomedicine*, vol. 5, no. 2, p. 21, 2017.

[7] N. Azoitei, A. Becher, K. Steinestel et al., "PKM2 promotes tumor angiogenesis by regulating HIF-1α through NF-κB activation," *Molecular Cancer*, vol. 6, no. 15, p. 3, 2016.

[8] S. Qin, A. Li, M. Yi, S. Yu, M. Zhang, and K. Wu, "Recent advances on anti-angiogenesis receptor tyrosine kinase inhibitors in cancer therapy," *Journal of Hematology & Oncology*, vol. 12, no. 1, p. 27, 2019.

[9] G. N. Maine and E. Burstein, "COMMD proteins: COMMing to the scene," *Cellular and Molecular Life Sciences*, vol. 64, no. 15, pp. 1997–2005, 2007.

[10] M. D. Healy, M. K. Hospenthal, R. J. Hall et al., "Structural insights into the architecture and membrane interactions of the conserved COMMD proteins," *eLife*, vol. 7, no. 7, p. e35898, 2018.

[11] S. Narindrasorasak, P. Kulkarni, P. Deschamps, Y. M. She, and B. Sarkar, "Characterization and copper binding properties of human COMMD1 (MURR1)," *Biochemistry*, vol. 46, no. 11, pp. 3116–3128, 2007.

[12] M. Riera-Romo, "COMMD1: a multifunctional regulatory protein," *Journal of Cellular Biochemistry*, vol. 119, no. 1, pp. 34–51, 2018.

[13] X. Wang, S. He, X. Zheng et al., "Transcriptional analysis of the expression, prognostic value and immune infiltration activities of the COMMD protein family in hepatocellular carcinoma," *BMC Cancer*, vol. 21, no. 1, p. 1001, 2021.

[14] J. Rius, M. Guma, C. Schachtrup et al., "NF-κB links innate immunity to the hypoxic response through transcriptional regulation of HIF-1α," *Nature*, vol. 453, no. 7196, pp. 807–811, 2008.

[15] B. van de Sluis, X. Mao, Y. Zhai et al., "COMMD1 disrupts HIF-1alpha/beta dimerization and inhibits human tumor cell invasion," *Journal of Clinical Investigation*, vol. 120, no. 6, pp. 2119–2130, 2010.

[16] T. Zhu, Z. Cheng, X. Peng, D. Xing, and M. Zhang, "HIF-1α RNAi combined with asparagus polysaccharide exerts an anti-angiogenesis effect on hepatocellular carcinoma in vitro and in vivo," *Evidence-based Complementary and Alternative Medicine*, vol. 2021, Article ID 9987383, 13 pages, 2021.

[17] L. Zheng, C. L. Deng, L. Wang et al., "COMMD7 is correlated with a novel NF-κB positive feedback loop in hepatocellular carcinoma," *Oncotarget*, vol. 7, no. 22, pp. 32774–32784, 2016.

[18] W. Zhan, W. Wang, T. Han et al., "COMMD9 promotes TFDP1/E2F1 transcriptional activity via interaction with TFDP1 in non-small cell lung cancer," *Cellular Signalling*, vol. 30, pp. 59–66, 2017.

[19] E. Burstein, J. E. Hoberg, A. S. Wilkinson et al., "COMMD proteins, a novel family of structural and functional homologs of MURR1," *Journal of Biological Chemistry*, vol. 280, no. 23, pp. 22222–22232, 2005.

[20] A. Zoubeidi, S. Ettinger, E. Beraldi et al., "Clusterin facilitates COMMD1 and I-kappaB degradation to enhance NF-kappaB activity in prostate cancer cells," *Molecular Cancer Research*, vol. 8, no. 1, pp. 119–130, 2010.

[21] M. Taskinen, R. Louhimo, S. Koivula et al., "Deregulation of COMMD1 is associated with poor prognosis in diffuse large B-cell lymphoma," *PLoS One*, vol. 9, no. 3, p. e91031, 2014.

[22] Y. F. Liu, M. Swart, Y. Ke, K. Ly, and F. J. McDonald, "Functional interaction of COMMD3 and COMMD9 with the epithelial sodium channel," *American Journal of Physiology. Renal Physiology*, vol. 305, no. 1, pp. F80–F89, 2013.

[23] N. Solban, H. P. Jia, S. Richard et al., "HCaRG , a novel calcium-regulated gene coding for a nuclear protein, is potentially involved in the regulation of cell proliferation," *The Journal of Biological Chemistry*, vol. 275, no. 41, pp. 32234–32243, 2000.

[24] B. L. Chen, J. Yu, Z. R. Zeng et al., "Rosiglitazone suppresses gastric carcinogenesis by up-regulating HCaRG expression," *Oncology Reports*, vol. 20, no. 5, pp. 1093–1097, 2008.

[25] H. Matsuda, C. G. Campion, K. Fujiwara et al., "HCaRG/COMMD5 inhibits ErbB receptor-driven renal cell carcinoma," *Oncotarget*, vol. 8, no. 41, pp. 69559–69576, 2017.

[26] L. Zheng, P. Liang, J. Li et al., "ShRNA-targeted COMMD7 suppresses hepatocellular carcinoma growth," *PLoS One*, vol. 7, no. 9, p. e45412, 2012.

[27] N. You, J. Li, X. Huang et al., "COMMD7 promotes hepatocellular carcinoma through regulating CXCL10," *Biomedicine & Pharmacotherapy*, vol. 88, pp. 653–657, 2017.

[28] N. You, J. Li, X. Huang et al., "COMMD7 activates CXCL10 production by regulating NF-κB and the production of reactive oxygen species," *Molecular Medicine Reports*, vol. 17, no. 5, pp. 6784–6788, 2018.

[29] S. S. Yang, X. M. Li, M. Yang et al., "FMNL2 destabilises COMMD10 to activate NF- κ B pathway in invasion and metastasis of colorectal cancer," *British Journal of Cancer*, vol. 117, no. 8, pp. 1164–1175, 2017.

[30] S. Umbreen, M. M. Banday, A. Jamroze et al., "COMMD3: BMI1 fusion and COMMD3 protein regulate C-MYC transcription: novel therapeutic target for metastatic prostate cancer," *Molecular Cancer Therapeutics*, vol. 18, no. 11, pp. 2111–2123, 2019.

Hindawi
Oxidative Medicine and Cellular Longevity
Volume 2022, Article ID 8368717, 19 pages
https://doi.org/10.1155/2022/8368717

Research Article

Natural Deep Eutectic Extracts of Propolis, *Sideritis scardica*, and *Plantago major* Reveal Potential Antiageing Activity during Yeast Chronological Lifespan

Bela Vasileva,[1] **Dessislava Staneva**,[1] **Tsvetinka Grozdanova**,[2] **Hristo Petkov**,[2] **Boryana Trusheva**,[2] **Kalina Alipieva**,[2] **Milena Popova**,[2] **George Miloshev**,[1] **Vassya Bankova**,[2] **and Milena Georgieva**[1]

[1]*Laboratory of Molecular Genetics, Institute of Molecular Biology "Roumen Tsanev", Bulgarian Academy of Sciences, Sofia, Bulgaria*
[2]*Institute of Organic Chemistry with Centre of Phytochemistry, Bulgarian Academy of Sciences, Sofia, Bulgaria*

Correspondence should be addressed to Milena Georgieva; milenageorgy@gmail.com

Received 18 June 2022; Accepted 5 August 2022; Published 30 August 2022

Academic Editor: Dragan Hrnčić

Nowadays, the environmentally friendly approach to everyday life routines including body supplementation with pharma-, nutraceuticals and dietary supplements gains popularity. This trend is implemented in pharmaceutical as well as cosmetic and antiageing industries by adopting a newly developed green chemistry approach. Following this trend, a new type of solvents has been created, called Natural Deep Eutectic Solvents (NADES), which are produced by plant primary metabolites. These solvents are becoming a much better alternative to the already established organic solvents like ethanol and ionic liquids by being nontoxic, biodegradable, and easy to make. An interesting fact about NADES is that they enhance the biological activities of the extracted biological compounds. Here, we present our results that investigate the potential antiageing effect of CiAPD14 as a NADES solvent and three plant extracts with it. The tested NADES extracts are from propolis and two well-known medicinal plants—*Sideritis scardica* and *Plantago major*. Together with the solvent, their antiageing properties have been tested during the chronological lifespan of four *Saccharomyces cerevisiae* yeast strains—a wild type and three chromatin mutants. The chromatin mutants have been previously proven to exhibit characteristics of premature ageing. Our results demonstrate the potential antiageing activity of these NADES extracts, which was exhibited through their ability to confer the premature ageing phenotypes in the mutant cells by ameliorating their cellular growth and cell cycle, as well as by influencing the activity of some stress-responsive genes. Moreover, we have classified their antiageing activity concerning the strength of the observed bioactivities.

1. Introduction

The World Health Organization (WHO) reports state that by 2050 the population of people over the age of 60 would double [1]. Though the real healthspan does not change a lot, yet older people are suffering from age-related diseases like cardiovascular, metabolic, and neurodegenerative, and many of them die because of them [2]. Ageing is defined by a decline in functional ability, dependent on time [3]. Many factors can contribute to the process like environmental and genetic influences and lifestyle. Many theories for ageing have been proposed, which are trying to describe the process [4]. For example, one of the most famous ones is the free radical theory, linking the accumulation of cellular damage with an increase of free radicals in the cells with age [5]. Lately, the epigenetics-focused "Information Theory of Ageing (ITA)" has been introduced [6–9], linking epigenetic changes with sequential switching on and off of certain genes that in turn lead to chromatin structure alterations, gene expression disbalance, and decreased DNA stability, all of which proven to speed up the ageing process. There have been numerous efforts to increase the maximum lifespan, and as the years have passed, with the modernization of healthcare and scientific advances, the human lifespan has

tremendously improved. Therefore, the emphasis is on how to postpone or prevent ageing most healthily. And here, natural nutraceuticals are gaining attention [10].

The modern area in the organic chemistry extraction field is the new type of solvents called Natural Deep Eutectic Solvents (NADES), designated also as green solvents [11, 12]. What distinguishes them from the already known and massively used solvents is their production origin. NADES are made by mixing natural ingredients, mainly plant primary metabolites like organic acids, sugars, and amino acids. Interestingly, NADES exhibit a lower melting point, compared to one of the separate ingredients used to make them, and they are liquid at room temperature [13]. NADES are an important part of the so-called green chemistry branch because they are eco-friendly, easy to make and inexpensive, biodegradable, and nontoxic, compared to the currently used solvents like ionic liquids, ethanol, and methanol [13–15]. In addition to these beneficial properties, NADES have also been shown to increase the biological properties of the extracted compounds [16]. Recently, it has been shown that NADES solvents extract different natural compounds with potential antiviral and antimicrobial properties that could be used in medicinal practice [17, 18]. Moreover, recent papers reported on NADES extraction of polyphenols as a much safer and more efficient extraction approach [19, 20]. Polyphenols are well-known and profoundly studied antiageing factors with strong antioxidant and antimicrobial properties [21–24].

It is known that ageing is triggered and accompanied by dynamic changes in chromatin structure [25–27]. Moreover, chromatin plays a key role in the ageing process and the maintenance of its proper structure is crucial for the fate of the organism [28]. To provide access to DNA, chromatin undergoes remodelling through various types of mechanisms [29]. In addition, the state of chromatin can be altered by environmental stimuli, which subsequently affect the expression of genes associated with ageing and longevity [30, 31]. Much of the data we know nowadays about ageing comes from different model organisms like yeast, roundworms, fruit flies, and mice [32–34]. The reasons why these models are preferred are shorter lifespans, the ability for close follow-up, large-scale genetic screening, and functional genomics [35–37]. One of the most widely used models for ageing research is the yeast *Saccharomyces cerevisiae* [38, 39]. *S. cerevisiae* is considered the golden model for ageing due to its high similarity with other organisms, including humans [38, 40]. For example, cellular homeostasis, metabolism regulating signalling pathways, organelle functioning, cell growth and division, stress response, cell death, and ageing are highly conserved among eukaryotes and many are studied in the yeast cells as a pioneer model organism [39, 41]. Moreover, *S. cerevisiae* yeast is unique as it allows separate studying of the replicative (RLS) and chronological (CLS) lifespans [33]. The last is impossible in the other eukaryotes, especially humans. The RLS is defined by the number of the produced daughter cells during the period of the lifespan [33], referred to as the ageing of actively dividing cells. In contrast, the CLS is the ageing of nondividing cells that have entered the stationary phase [42]. These two models of ageing, RLS and CLS, are used to study how mitotically active and postmitotic cells age.

In this study, we are showing the perspective of using NADES extracted biocompounds in prospective antiageing therapies. We have tested the effect of two well-known Bulgarian medicinal plants—*Sideritis scardica* Griseb. (*S. scardica*) and *Plantago major* L. (*P. major*), as well as propolis (a compound produced by bees). Propolis is an established ingredient, particularly in the cosmetics industry for its antiageing properties [43, 44]. It has a high content of phenolic compounds and flavonoids and has been shown to influence the proliferation of fibroblasts [43]. *S. scardica* is a popularly used remedy in natural medicine due to its anti-inflammatory properties [45]. It is endemic to the Balkan peninsula mountain region [46]. There also have been reports on its antioxidant activity [23]. The third examined plant—*P. major*—is also rich in polyphenol content. It is also a well-known herbal medicine drug with established anti-inflammatory properties [47]. We have followed the CLS of four *S. cerevisiae* strains: the WT control and its isogenic chromatin mutants: *hho1delta* (without the gene for the linker histone), *arp4* (with a point mutation in the *ARP4* gene), and the double mutant *arp4 hho1delta* (which harbours the two mutations) [30, 48]. The four strains have been previously reported as a model for studying the role of chromatin organization in ageing [30, 31]. We have proved that the abrogated healthy interaction among the linker histone Hho1p and Arp4p leads to premature ageing phenotypes [30], which we now study in the presence of the tested NADES plant and propolis extracts. Our results demonstrate a potential antiageing activity of these NADES extracts proved by their ability to confer the premature ageing phenotypes in the mutant cells.

2. Materials and Methods

2.1. Preparation of NADES CiAPD14 Solvent. The citric acid (Chem-Lab NV, Zedelgem, Belgium) and 1,2-propanediol (Valerus, Sofia, Bulgaria) in a 1 : 4 molar ratio were mixed and stirred in a water bath (300 rpm) at 50°C until a homogeneous liquid was formed [19].

2.2. Extraction of Plant and Propolis Bioactive Compounds with NADES CiAPD14 Solvent. Row propolis was ground by a coffee mill after freezing. Plant materials (air-dried) were ground in a coffee mill. 50 mg of ground material (propolis/plant material) was extracted with 1.5 mL CiAPD14 in a 2 mL Eppendorf tube in an ultrasound bath (Elmasonic S 30 H), without heating for 1 h. The extracts were then centrifuged (13,000 rpm, 40 min) and filtered through cotton.

In the text, the NADES solvent CiAPD14 in its pure form will be referred to as CiAPD14, and the extracts made with it are as follows: CiAPD14 propolis, CiAPD14 *S. scardica*, and CiAPD14 *P. major*.

2.3. Quantitative Determination of Total Phenolics and Total Flavonoids. Total phenolics and total flavonoids were measured using previously reported methods (details in [19]).

For blank: a solution of CiAPD14 instead of the test sample (CiAPD14 extract) was used in analogous procedures. For propolis, total phenolic content was estimated using a calibration curve of standard mixture pinocembrin–galangin 2 : 1 (*w*/*w*), and total flavonoid content was estimated using a calibration curve of galangin for the medicinal plants, calibration for total phenolics was performed using caffeic acid, and for total flavonoids with routine as the standard. Assays were carried out in triplicate.

2.4. Saccharomyces cerevisiae Strains

(i) Wild type (DY2864, WT): MATa *his4-912δ-ADE2 his4-912δ lys2-128δ can1 trp1 ura3 ACT3* [49]

(ii) *hho1Δ* (*HHO1* KO derivative of DY2864, in the text appears as *hho1delta*): MATa *his4-912δ-ADE2 his4-912δ lys2-128δ can1 trp1 ura3 ACT3 ypl127C::K.L.URA3* [50]

(iii) *arp4ts26* (DY4285, *arp4* mutant designated in the text as *arp4*): *MATa his4-912δ-ADE2 lys2-128δ can1 leu2 trp1 ura3 act3-ts26* [49]

(iv) *arp4ts26hho1Δ* (double mutant derivative of DY4285, denoted as *arp4 hho1delta*): *MATa his4-912δ-ADE2 lys2-128δ can1 leu2 trp1 ura3 act3-ts26 ypl127C::K.L.URA3* [51]

2.5. Culture Media

(i) Yeast Extract–Peptone–Dextrose (YPD) liquid medium: 1% yeast extract, 2% dextrose, and 2% peptone (*w*/*v*)

(ii) YPD-solid: 1% yeast extract, 2% dextrose, 2% peptone, and 1.5% agar (*w*/*v*)

(iii) Synthetic complete medium (SC): 2% dextrose; 1.7% yeast nitrogen base and supplements (lysine, adenine, histidine, tryptophan, uracil, and leucine) according to the auxotrophic requirements of the strains

2.6. Yeast Cell Culture Growth Spectrophotometrical Measurements. The four yeast strains (1×10^7 cells/mL) were cultivated in SC medium in a water bath shaker at 30°C for a CLS of nine consecutive days. Aliquots of yeast cell cultures were taken at four different time points—4th, 24th, and 72nd hour and 9th day of cultivation. For each, the optical density (OD_{600}) was measured, and the obtained data were used for growth curve analysis.

2.7. Chronological Survival after Treatment with NADES Solvent CiAPD14 and NADES CiAPD14 Extracts with Propolis, S. scardica, and P. major. Control yeast cells and cells supplemented with CiAPD14 at a concentration of 0.089 (%*v*/*v*, *μ*L) and with propolis, *S. scardica*, and *P. major* CiAPD14 extracts at concentrations of 0.027, 0.046, and 0.045 (%*v*/*v*, *μ*L), respectively, were cultivated for nine days in SC medium. Aliquots were taken at three time points of the CLS (24th and 72nd hour and 9th day), and 10^2 cells were plated on YPD agar plates in triplicates and incubated for three days at 30°C. The number of plated cells was calculated by LUNA-II™ Automated Cell Counter (Logos Biosystems, USA) as well as following previously developed protocols for cell number assessment for these cultures based on their OD_{600}. The percentage of viable cells in each group was determined by comparison of the number of colony-forming units (CFU) at the 72nd hour and 9th day time points with the number of CFUs at the 24th hour of cultivation, which was perceived as 100%. The results are represented in graphs showing the cell survival percentage as MEAN ± SD.

2.8. Cell Cycle Analysis. Cell cycle analysis using fluorescence-activated cell sorting (FACS) was performed according to [50]. Briefly, aliquots were taken on the 4th, 24th, and 72nd hour and 9th day of cultivation and fixed in 96% ethanol at -20°C overnight. Following the next day, cells were centrifuged, resuspended in 50 mM sodium citrate, pH 7, and sonicated at 50% power for 20 seconds, after which they were incubated at 37°C for 30 minutes with 0.25 mg/mL RNAse A. Cells were stained with propidium iodide (50 *μ*g/mL) and acquired by a BD FACSCanto apparatus. Data analyses were performed using FlowJo V10 software.

2.9. Gene Expression Analysis. Total RNA was extracted from untreated cells as well as treated with NADES solvent CiAPD14 and NADES CiAPD14 extract-supplemented cells of the four strains at the four time points (4th, 24th, and 72nd hour and 9th day of cultivation) using the phenol-chloroform extraction protocol, according to [30]. 280 ng of total RNA, treated with DNase I, was then reverse transcribed into cDNA, using NG dART RT-PCR kit (EURx). The expression of three genes was examined in the cells, both in and without the presence of the tested bioactive NADES CiAPD14 extracts. The two genes of interest were *CDC28* and *RAD9*. *ACT1* was used as a reference gene. Primer sequences are shown in Table 1. Results were analyzed using Rotor-Gene 6000 software (Corbett Life Science) and calculated by the $^{\Delta\Delta}C_T$ method [52].

2.10. Statistical Analysis. All experiments were performed in triplicates. The statistical analysis for comparison of control (untreated) cells and treated with the extracts was performed in Excel, using the paired-samples *T*-test, two-tailed distribution. Results are represented as MEAN ± SD. Statistically significant results are denoted with ∗, where $p < 0.05$.

3. Results and Discussion

The potential antiageing effect of the NADES solvent CiAPD14 (citric acid : 1.2-propanediol in a ratio of 1 : 4) and the bioactive extracts CiAPD14 propolis, CiAPD14 *S. scardica*, and CiAPD14 *P. major* was studied during the chronological ageing of four *S. cerevisiae* strains: WT, *hho1-delta*, *arp4*, and *arp4 hho1delta*, controls (nonsupplemented) and supplemented with the solvent and its three extracts. For each of the three mutant strains, we have previous data that evidenced their impaired chromatin organization and premature ageing phenotypes [30, 31, 48]. Briefly, the *arp4*

Table 1: RT-qPCR primer pairs.

Oligomer name	Sequence 5′–3′	Amplicon length (bp)
Sc*ACT1*_For	CGGTAACATCGTTATGTCCGGTG	93
Sc*ACT1*_Rev	ATGGAAGATGGAGCCAAAGCG	
Sc*CDC28*_For	AGGAAACCAATCTTCAGTGGCGA	91
Sc*CDC28*_Rev	CTGGCCATATAGCTTCATTCGGC	
Sc*RAD9*_For	GCATGTTTGAGCGCAGGTAG	102
Sc*RAD9*_Rev	TCTGGGTACTAAAGAATCTAAGGCA	

mutant bears a point mutation in the gene coding for Arp4p—a subunit of INO80, NuA4, and SWR1 chromatin remodelling complexes, crucial for the proper chromatin organization and function [49]. The *hho1delta* mutant cells lack the gene *HHO1*, coding for the linker histone, which is responsible for chromatin higher-order structure organization [50]. The third mutant is *arp4 hho1delta*. It combines the two above-discussed mutations: the gene for the linker histone is knocked out and there is a point mutation in the *ARP4* gene [48]. We have previously studied these strains and proved that they work as a perfect model for studying ageing phenotypes [30, 31, 48, 54, 53].

The concentrations of the solvent CiAPD14 and the extracts CiAPD14 propolis, CiAPD14 *S. scardica*, and CiAPD14 *P. major* for yeast cell culture supplementation during the CLS were considered in our previous work and are listed in Table 2 [19].

3.1. Cell Growth Analysis of WT, hho1delta, arp4, and arp4 hho1delta Yeast Strains. The studied yeast cells were cultivated in SC media for nine days. The control group of each yeast strain was not supplemented with the NADES solvent CiAPD14 or with any of the extracts. The supplemented yeast cell cultures were grown from day 1 of their CLS in SC media supplemented with CiAPD14, CiAPD14 propolis, CiAPD14 *S. scardica*, and CiAPD14 *P. major* at concentrations, which we have already designated as the half-maximal inhibitory concentrations (IC_{50}). These IC_{50} data came from recent tests for cyto- and genotoxicity of the studied NADES solvent and extracts [19]. Table 2 summarizes these data as well as the data for the total phenolic concentration in the extracts. The cellular growth of the studied control and supplemented yeast cells was first explored by spectrophotometric measurements of the optical density of the cell cultures at a wavelength of $\lambda = 600$ nm (OD_{600}). Cell culture aliquots of each of the four yeast strains were taken on the 4th, 24th, and 72nd hour and 9th day of cultivation in SC media for both control cells and treated with the solvent CiAPD14 and its three extracts: CiAPD14 propolis, CiAPD14 *S. scardica*, and CiAPD14 *P. major*. The results are presented as growth curves in Figure 1 (nontreated and cells supplemented with CiAPD14 or CiAPD14 propolis, CiAPD14 *S. scardica*, and CiAPD14 *P. major*). It is generally accepted that the chronological ageing of the yeast cells starts around the 24th hour of cultivation [33]. Considering the chosen time points, our previous results from the investigation of the CLS of the three chromatin mutant strains have shown that up to the 9th day of cultivation different premature ageing traits were detectable, which allowed us to test whether the NADES solvent CiAPD14 and its extracts CiAPD14 propolis, CiAPD14 *S. scardica*, and CiAPD14 *P. major* would exert antiageing properties [30, 31, 53].

First, to prove these yeast strains as a good model system for our studies, we compared the CLS cell culture growth of the control (untreated) yeast cells from the four strains. This analysis showed that WT yeast cells had the fastest cell growth during the fermentation period, i.e., between the 4th hour time point and the 24th hour (Figure 1(a)), whereas for the double mutant the growth was reduced by 20% (5.5-fold) (Figure 1(d)). During the stationary phase (from the 24th hour to the 9th day), we observed that for this period the WT cells increased furthermore their growth by 17% (Figure 1(a)), followed by the two single mutant cell cultures—*hho1delta* and *arp4*, respectively, with 21% and 10% (Figures 1(b) and 1(c)). The double mutant though did not show any increase in its growth for the observed period (Figure 1(d)). Compared to the other three yeast strains, the double mutant cell growth remained unchanged after the 24th-hour time point. These results indicated that at the 24th hour the double mutant *arp4 hho1delta* was already in the stationary phase. A possible explanation was the premature ageing of these cells as these standard growth curves coincided with our previously published results [30, 31].

We further tested the solvent CiAPD14 and its extracts CiAPD14 propolis, CiAPD14 *S. scardica*, and CiAPD14 *P. major* on the cell culture growth of these cells (Figure 1, dotted lines). Interestingly, in all supplementations of the cells, we did not observe a statistically significant increase in the optical density when compared to the nontreated cells. On the contrary, the cell growth was slightly slower in comparison to the untreated cells. The only statistically significant difference in the slower growth of supplemented cells was detected in the growth of the WT, supplemented CiAPD14 *P. major* at the 24th hour (Figure 1(a), $^{*}p < 0.05$), for *hho1delta* and *arp4* cells supplemented with CiAPD14 propolis on the 9th day (Figures 1(b) and 1(c), $^{*}p < 0.05$), while for the double mutant (Figure 1(d), $^{*}p < 0.05$) statistically significant appeared the detected slower growth of these cells with the solvent only.

In summary, we did not observe any notable changes in the cell culture growth of the studied yeast cells, supplemented with CiAPD14 and the three extracts. We consider this a positive result, especially in the light of the CLS of these cells as cell culture growth measured spectrophotometrically

Table 2: Concentrations at which the studied NADES solvent CiAPD14 and the respective propolis and plant extracts were used for culture media supplementation of the yeast cells during their CLS. The concentrations were chosen, based on the data collected in our previously published research [19].

Solvent/ extract	Final concentrations (f.c.) (%v/v, μL in 100 μL)	Total phenolic content in the used concentrations (μg/mL)
CiAPD14	0.089	—
CiAPD14 propolis	0.027	3.3048
CiAPD14 *S. scardica*	0.046	0.8878
CiAPD14 *P. major*	0.045	0.459

does not directly reflect the ageing of the yeast cells. Moreover, it is a sign of biocompatibility of the NADES solvent and its extracts and is a good prerequisite for the following experiments that target the in-depth study of the CLS of these cells in the presence of the studied NADES compounds.

3.2. Chronological Lifespan of Four Yeast Strains in the Presence of NADES Solvent and Extracts. Standard protocols for the study of chronological ageing in *S. cerevisiae* include observing the survival of cells at different time points from their growth in SC media. The presumption is that the preserved viability of cells, in particular, the ability to divide after being plated on a solid rich culture medium, is evidence for the progression of their chronological age [32, 48]. To monitor and analyze the cell survival of the four studied yeast strains, the cells were cultured in SC media for 9 days. The nonsupplemented cells of each strain served as controls. Three time intervals were analyzed: 24th and 72nd hour and 9th day. The analysis of the chronological lifespan was determined by counting the colony-forming units (CFUs) and calculating the cell survival of each strain at the given time point as a percentage of viable cells (CFUs) at the 24th hour of cultivation, taken as 100%. The 24th-hour time point is the period when the yeast cells enter the stage of the so-called diauxic shift (the time when fermentation stops as a result of depletion of glucose in the medium) and respiration begins [54, 55]. This is the moment when the yeast chronological ageing commences [48, 53].

First, we analyzed how the four strains survived without being supplemented (Figure 2(a)). The results showed that the wild type maintained a stable CLS until the last monitored time point with 87% and 94% viable cells on the 72nd hour and 9th day, respectively. The *arp4* mutant had the highest percentage of viable cells throughout its CLS, which on the last point dropped to only 15% (85% viable cells in comparison to the 24th h time point). The survival rate of the *hho1delta* gradually decreased in the course of CLS showing a reduction of 21% and 44% at 72nd h and 9th d, respectively ($^*p < 0.05$). As for *arp4 hho1delta*, its cells were short-lived and had a strong decrease with an almost 98% drop in their survival rate from the 24th h time point till the 9th day ($^*p < 0.05$). The abrogated survival rate detected for the double mutant *arp4 hho1delta* cells was proven by our previous results [30].

Figure 2(b) shows the CLS cell survival rates obtained for the control WT cells after treatment with CiAPD14 and with the three extracts. The graph clearly shows that after treatment with CiAPD14 or with CiAPD14 *P. major*, the viability at the 72nd hour increased by 10% compared to the initial time point and by 20% compared to the nonsupplemented cells ($^*p < 0.05$), with a subsequent decrease by 39% and 58%, respectively, on the 9th day. In the cells treated with CiAPD14 propolis, there was a significant increase in the percentage of colonies obtained on the 9th day, in comparison to the percentage of colonies in the untreated cells ($^*p < 0.05$). An increased cell survival during chronological ageing was also observed in the WT yeast cells treated with CiAPD14 *P. major*. There was an increase of 23% in the percentage of colonies formed at the 72nd hour for CiAPD14 solvent (nonsignificant) and CiAPD14 *P. major* ($^*p < 0.05$) supplemented WT cells when compared to the percentage of viable cells obtained in the nonsupplemented ones.

The results obtained for the *hho1delta* mutant (Figure 2(c)) differed from the data reported for the wild type, as on the last time point certain antiageing effects were observed for the CiAPD14 solvent and its extract with *S. scardica*, which was the most pronounced. In the *hho1delta* cells, treated with the CiAPD14 S. *scardica* extract, the cell survival at all-time points was around 100% ($^*p < 0.05$ for the 9th day). The CiAPD14 propolis and CiAPD14 *P. major* supplementation had a beneficial effect, i.e., increased survival percentage only at the 72nd hour representing the early stage of chronological ageing ($^*p < 0.05$).

The data reported for the *arp4* mutant (Figure 2(d)) showed no statistically significant differences in the cell survival of these cells among supplementations with different extracts, whereas the results obtained for the *arp4 hho1delta* strain (Figure 2(e)) showed that the highest percentage of cell survival appeared at the 72nd hour after supplementation of these cells with CiAPD14 S. *scardica* (34% increase in comparison to the same strain but nonsupplemented, compare Figures 2(a) and 2(e), 72nd h, where $^*p < 0.05$). Only 2% of cells of the double mutant survived on the 9th day if they are untreated; however, the supplementation with CiAPD14 propolis and CiAPD14 S. *scardica* increased insignificantly the viability of these cells on the 9th day to 18% and 12.8%, correspondingly (Figure 2(e)). We understand that these differences in the CLS of the double mutant are not so explicit on day 9th with CiAPD14 propolis and CiAPD14 *S. scardica*, but we discuss them here as they highlight their potential antiageing properties. Consider that these cells did not preserve their ability to divide at day 9th unsupplemented, then even 16% and 10% induction of it means potential for stimulating the division of these cells and deserves our attention.

Therefore, we conclude that CiAPD14 pure (for the *hho1delta* mutant, Figure 2(c), $^*p < 0.05$), CiAPD14 propolis, and CiAPD14 *S. scardica* (especially for the double mutant cells at the 72nd h and 9-day time points, Figure 2(e), $^*p < 0.05$) showed the most pronounced

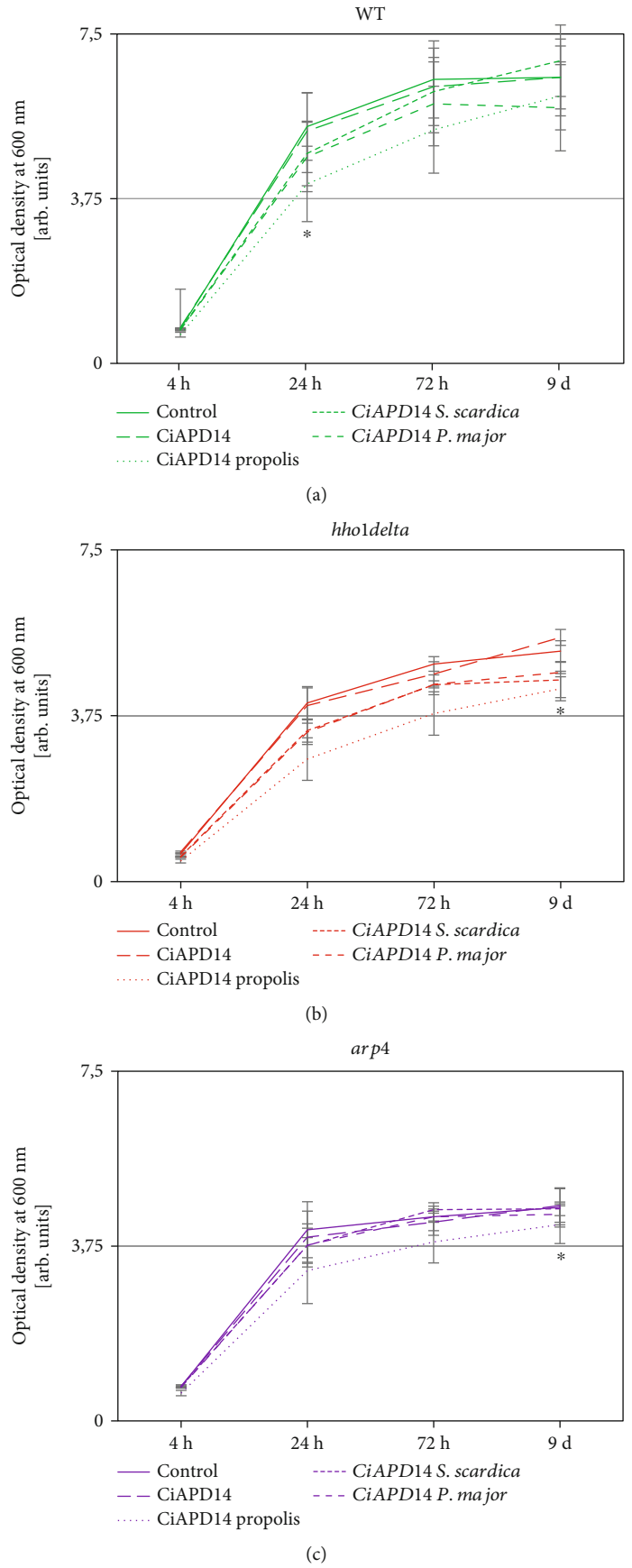

Figure 1: Continued.

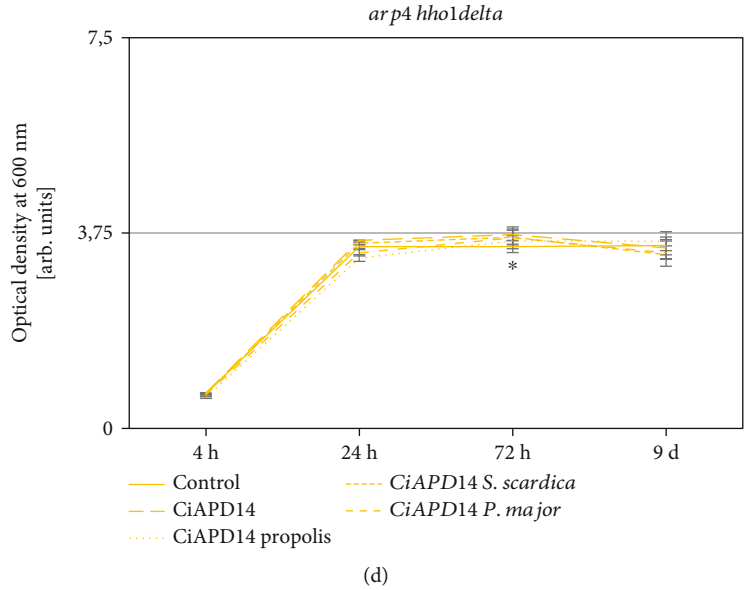

Figure 1: Cell culture growth of *WT*, *hho1delta*, *arp4*, and *arp4 hho1delta* without and with the presence of CiAPD14 NADES solvent and the three extracts. Cells were cultivated for the period of 9 days in SC media, supplemented with the studied NADES solvent and extracts. The control cells were not supplemented. At four time points: 4 h, 24 h, 72 h, and 9 d, aliquots were taken from the cell cultures and were analyzed spectrophotometrically. The optical density was measured in arb. units. Data are MEAN ± SD. Statistically significant differences between the growth of supplemented yeast cells compared to nonsupplemented are given with asterisk (∗); (a) WT, where ∗ means $p < 0.05$ for CiAPD14 *P. major*; (b) *hho1delta*, where ∗ means $p < 0.05$ for CiAPD14 propolis; (c) *arp4*, where ∗ means $p < 0.05$ for CiAPD14 propolis; (d) *arp4 hho1delta*, where ∗ means $p < 0.05$ for CiAPD14.

antiageing effect on the yeast cells. These results support the idea that the tested CiAPD14 extracts had antiageing activity on the prematurely aged mutant cells as well as in the single mutants that lack the linker histone and merit further investigations [50]. The results obtained for the supplemented with the three extracts cells roughly followed the measured total phenolic content in these extracts, where the CiAPD14 propolis extract has the highest phenolic content, followed by the CiAPD14 *S. scardica* and CiAPD14 *P. major* extracts (Table 2).

3.3. Analysis of Yeast Cell Cycle after Supplementation with NADES Extracts. An important measure of yeast chronological ageing is cell progression through the cell cycle phases. Typically, after entering the stationary phase, which generally happens at the 24th hour of cultivation, the majority of cells become quiescent [56]. Having this in mind, we tested whether CiAPD14 or the extracts would affect the cell cycle of the studied strains. We cultivated the four *S. cerevisiae* strains WT, *hho1delta*, *arp4*, and *arp4 hho1delta* in SC media for 9 days. Cells were supplemented with CiAPD14 and the NADES extracts of CiAPD14 propolis, CiAPD14 *P. major*, and CiAPD14 S. *scardica* at the studied concentrations (see Materials and Methods) from the 1st day of their cultivation in SC media. Aliquots were taken on the 4th, 24th, and 72nd hour and 9th day of cultivation. Cells were washed and stained with propidium iodide and subsequently analyzed by FACS. FACS results are represented as both percentages of cells in the cell cycle phases and descriptive histograms (Figure 3).

We first analyzed the way the untreated cells of the four strains chronologically aged by assessing the percentage of cells in the cell cycle phases (Figure 3, see the control in bar charts of each panel). We confirmed a similar trend found in our previous results. This trend resulted in the distribution of logarithmically growing yeast cells from the WT and *arp4* mutant (4th h) predominantly found in the G2/M phase of the cell cycle (Figures 3(a) and 3(c), histograms, control cells), which is considered the normal way the yeast cell cycle goes at this time point [30, 31, 57, 58]. In our case, the two chromatin mutants that lack the *HHO1* gene encoding the linker histone demonstrated a visible shift of the cells from G2/M to G0/G1 cell cycle phase (4th h) (Figures 3(b) and 3(d), representative histograms, controls). Following the rest of the time points, the control cells showed that the chronologically aged nonsupplemented cells from the four strains were mainly in the G0/G1 phase of the cell cycle, which was especially prominent on the last day of cultivation, the 9th day [26, 58–60]. Moreover, according to previous reports [59, 60], after the diauxic shift, two distinguishable cell populations are presented in the G1 phase of stationary phase yeast *S. cerevisiae* cultures, quiescent (Q) population, in which daughter cells are predominant and are the longest-lived, and non-Q population, in which mother cells are predominant and are the shorter-lived. On day 9, the largest percentage of cells was in G1, which was most distinctive for the *hho1delta* and *arp4* h*ho1-delta* strains and less pronounced for the WT. We could speculate that although stationary cultures of these mutants have a high percentage of G1 phase cells, they are rather

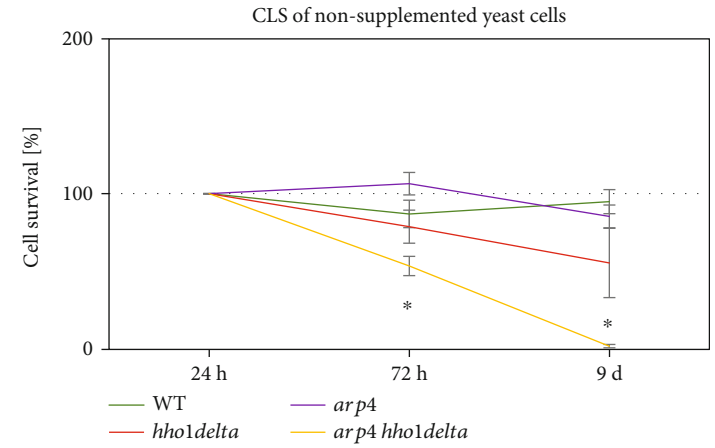

(a)

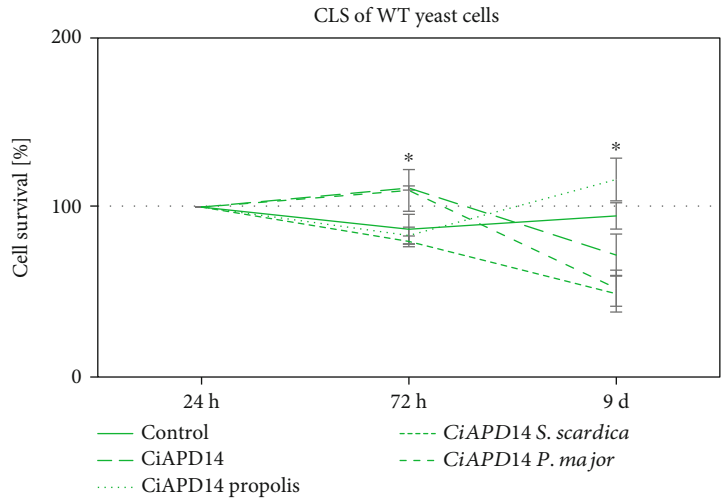

(b)

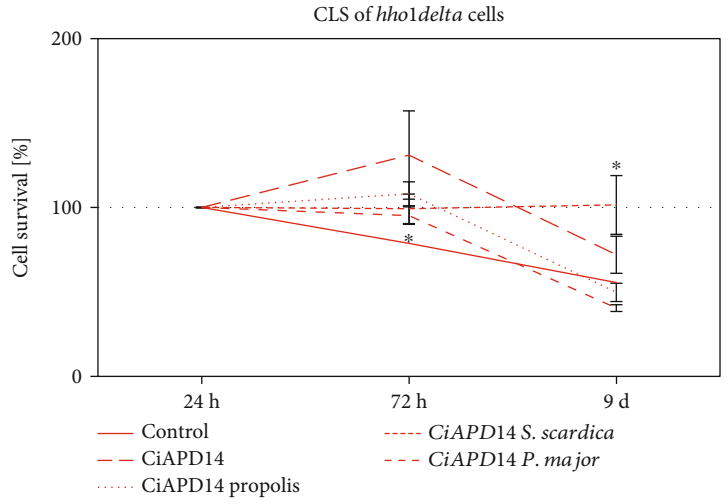

(c)

Figure 2: Continued.

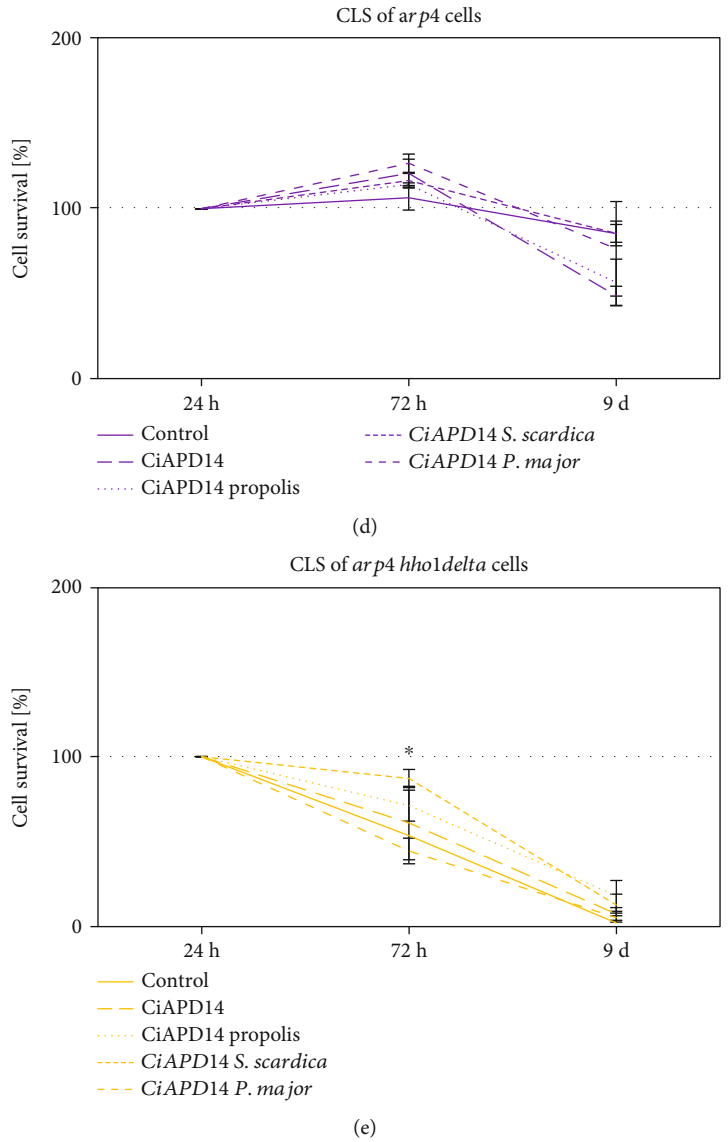

Figure 2: CLS of WT, *hho1delta*, *arp4*, and *arp4 hho1delta* in the presence of CiAPD14 and the three extracts. Cells were cultivated for the period of 9 days in SC media supplemented with the studied NADES solvent and extracts. At three time points: 24 h, 72 h, and 9 d 100, cells were taken from the cell cultures and were seeded on rich solid YPD media. Cells were allowed to recover under optimal conditions (30°C). The cell survival at the 24th-time point was assumed as 100%, and the survival of cells at all other time points were calculated as a percentage of it. (a) CLS of the four studied strains without any treatment; (b) CLS of the WT cells, control and supplemented with CiAPD14 and extracts; (c) CLS of *hho1delta* mutant cells, control and supplemented with CiAPD14 and extracts; (d) CLS of *arp4* mutants; (e) CLS of the double *arp4 hho1delta* control cells and in the presence of CiAPD14 and extracts. Data are MEAN ± SD. Statistically significant differences are marked with ∗ where $p < 0.05$.

non-Q, non-long-lived cells and therefore poor survivors. This in turn raises the question of the relationship between the ability of chromatin mutants to form a proper quiescent cell population and the chronological lifespan, thus highlighting the need for further research to elucidate it.

The yeast cells supplemented with CiAPD14 or CiAPD14 propolis, CiAPD14 *P. major*, and CiAPD14 *S. scardica* were also analyzed by FACS, and the results are demonstrated in Figure 3 (see supplemented cells).

For the WT cells (Figure 3(a)) there were different tendencies of transition of supplemented with the NADES extracts cells from G0/G1 into the G2/M and *vice versa* in the cell cycle phase from the 4th to 72nd hour of CLS, compared to the untreated control, which corresponded with the cell survival experiments (Figure 2(b)). CiAPD14 propolis-supplemented WT cells by the 9th day of cultivation experienced the highest survival (Figure 2(b)) and the highest percentage of cells transiting through the cell cycle phases (Figure 3(a)). There was a tendency for predominant accumulation of cells in the G0/G1 phase of the cell cycle for the logarithmically growing mutants *hho1delta* and *arp4 hho1delta* that lack the linker histone gene *HHO1*, which did not change after treatment with the solvent, nor with any of the three plant extracts (Figures 3(b) and 3(d)). G0/

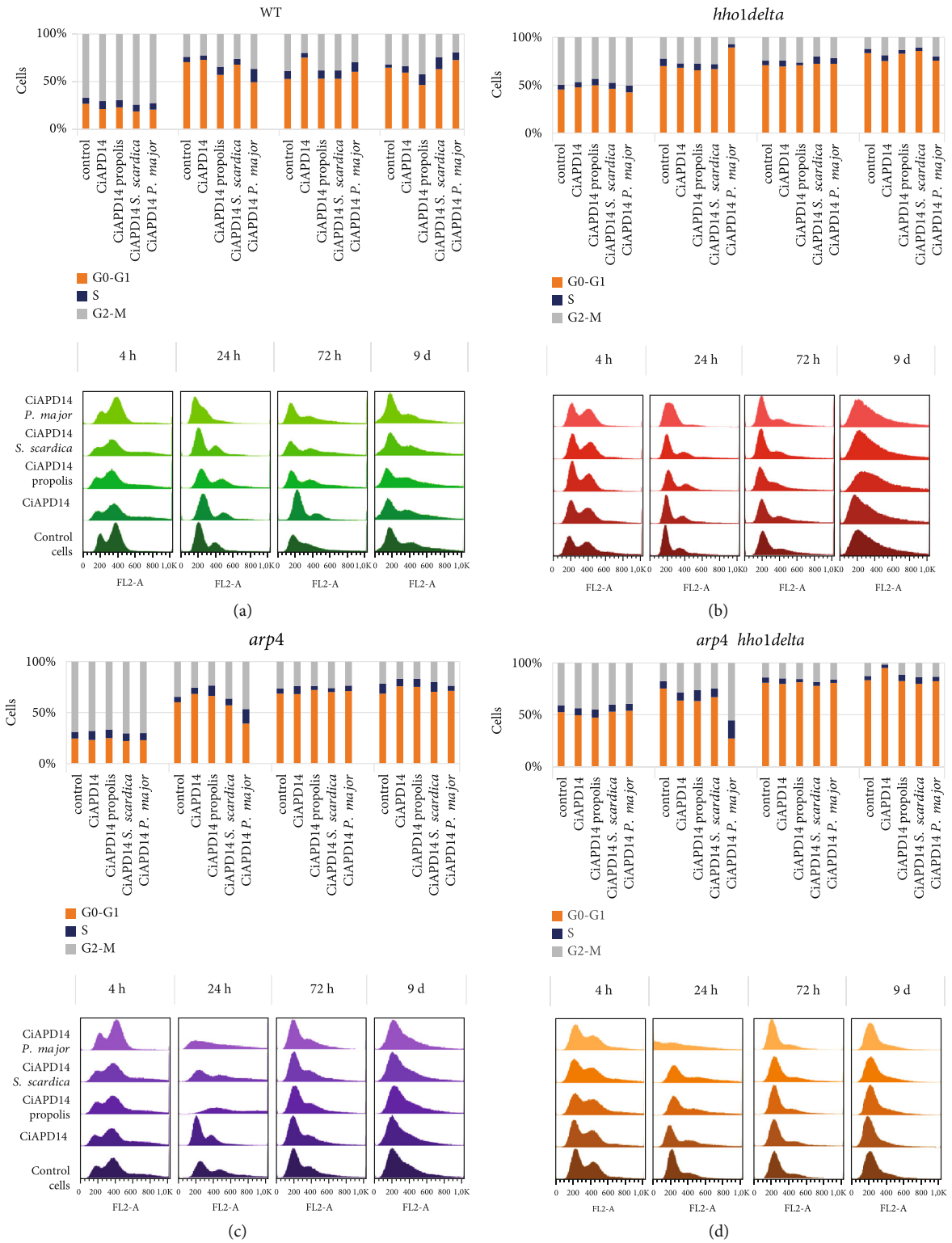

Figure 3: Cell cycle analysis of the four studied strains WT, *hho1delta*, *arp4*, and *arp4 hho1delta* in the presence of CiAPD14 and the three extracts during their CLS. Cells were cultivated during the CLS for nine days. At four time points: 4 h, 24 h, 72 h, and 9 d, aliquot cells were taken from the cell cultures and were analyzed by FACS after propidium iodide staining. (a) WT strain FACS data quantitation (bar chart) and representative histograms (below) for each time point; (b) *hho1delta* strain FACS data quantitation (up) and representative histograms for each time point; (c) *arp4* FACS data quantitation (up, bar chart) and representative histograms for each time point; (d) *arp4 hho1delta* FACS data quantitation (up) and representative histograms for each time point. Data are represented as % of cells in each phase of the cell cycle.

G1 accumulation of cells is important for the longevity of cells though could be accepted as a positive and negative trait. On day 9, for all cultures studied, the largest percentages of cells were in phase G1. Moreover, we detected a correlation of the effect of CiAPD14 propolis extract which increased both the cellular viability and the percentage of G2/M cell fraction. We find these results intriguing and deserve our attention. In general, there was no bold cytostatic, nor proproliferative effect of the solvent and its extracts on any of these two mutant strains. Slight exceptions showing an increased % of cells in G0/G1 after treatment with CiAPD14 *P. major* were detected for the *hho1delta* cells at the 24th h time point (Figure 3(b)). The results with *hho1delta* and the double mutant *arp4 hho1delta* confirmed that the lack of the linker histone highly influenced the CLS of the mutant cells and its absence was an obstacle for cells to cope with the ageing process, most probably due to their strongly abrogated chromatin structure [30, 48, 50, 53]. The above-discussed tendencies in cell cycle progression of the studied cells, non- and supplemented with the studied CiAPD14 solvent and extracts, are depicted with representative histograms for ease of comparison (Figure 3, in-built histograms, green—WT, red—*hho1delta*, purple—*arp4*, and orange—*arp4hho1delta*). This yet again verified how important were the linker histone and the proper chromatin organization for the ageing process.

3.4. RT-qPCR Analysis of the Expression of DNA-Damage Response Genes during CLS of the Yeast Cells with and without CiAPD14 and Extract Supplementation. During the experimental monitoring of the growth potential, cell survival, and cell cycle of yeast *S. cerevisiae* cells of the four strains, aliquots were also taken to track the gene expression of two key genes, *CDC28* and *RAD9*. Untreated yeast cells of each strain were used as a control group. To examine the gene expression of the selected genes, total RNA was isolated from aliquots of the yeast cultures and converted to cDNA. This cDNA was used as a template in experiments to analyze the expression of the two genes of interest with *ACT1* as a reference gene. The results were calculated by the $^{\Delta\Delta}$CT method using specialized Rotor-Gene 6000 software. Primer pairs used in the RT-qPCR are shown in Table 1. We examined the expression of *CDC28* and *RAD9* genes in the course of the chronological ageing of the studied four yeast strains with and without supplementation with the CiAPD14 and with the three biological NADES extracts (Figures 4 and 5). The main role of the *CDC28* gene product is to regulate the mitotic and meiotic cell cycle. Cdc28p is also involved in the regulation of cellular metabolism, the maintenance of chromosome dynamics, cell growth, and morphogenesis. The gene is associated with a cell cycle block in the G2/M checkpoint [61]. Studies show that this gene is active during the G2/M cell cycle phase, compared to its relative inactivity in the G0/G1 phase, due to low cyclin expression and abundance in CDK inhibitors Sic1 and Far1 [61].

In our experiments, an insignificant decrease of *CDC28* gene expression (less than 2-fold) was observed in the four yeast strains when they entered the stationary phase at the 24th hour of cultivation (see Figure 1) and had their cells predominantly in the G0/G1 cell cycle phase in all types of NADES supplementations (see Figure 3). These results were in agreement with the role of Cdc28p in the cell cycle regulation as discussed above. The studied WT yeast cells supplemented with CiAPD14 and extracts did not show any statistically significant changes in *CDC28* expression during all time points (Figure 4(a)). This was an indication that in the normally ageing cells the NADES extracts did not influence the expression of this gene as cells were able to moderate their ageing process. In the course of the chronological ageing, the *hho1delta* mutant showed the highest increment in *CDC28* expression of 12-fold, after treatment with CiAPD14 at the 72nd hour, as well as an increase of 9-fold and 2.4-fold in *CDC28* expression after treatment with CiAPD14 propolis on day 9th ($^{*}p < 0.05$). On the 9th day, these cells supplemented with CiAPD14 *S. scardica* and CiAPD14 *P. major* also demonstrated a statistically significant increase (2-fold change, $^{*}p < 0.05$) (Figure 4(b)). It is worth mentioning that the Cdc28 kinase is an important part of the homologous recombination process [62–64], for which the linker histone is an inhibitor [65]; therefore, the lack of Hho1p in the *hho1delta* mutant cells increased *CDC28* expression, especially on the last day of CLS and specifically after supplementation with CiAPD14 propolis, CiAPD14 *S. scardica*, and CiAPD14 *P. major*. Interestingly, the comparison of the results for the expression of this gene after supplementation with CiAPD14 propolis in WT and *hho1delta* cells at the 9th day showed unchanged expression of *CDC28* for WT and increased by 9.4-fold for *hho1delta* mutant, which coincided with the high phenolic content of this extract (Table 2, propolis—3.3048 μg/mL), but did not correlate with the CLS survival of these *hho1delta* mutant cells on day 9th after CiAPD14 propolis supplementation (Figure 2(b)). We observed that indeed the CiAPD14 propolis extract led to the unchanged survival rate of the WT cells at the last time point for the *hho1delta* (compare Figures 2(b) and 2(c)). The last was an indication that *hho1delta* cells experienced stress on the 9th day, which led to increased expression of *CDC28* and a slight recovery in the G0/G1 blockage of these cells after CiAPD14 propolis supplementation (Figure 3(b), see representative histograms for this strain). We speculate that the highest phenolic content in the CiAPD14 propolis probably led to the induction of oxidative stress, to which these mutant cells were intolerant [30]. This hypothesis is strengthened to an extent by the results with the supplementation of *hho1delta* cells with the CiAPD14 solvent only on the 72nd h time point, where we detected a correlation between the *CDC28* elevated expression and the CLS survival rates of these cells at that particular time point probably due to lack of phenols in the solvent. We find these results interesting and a good groundwork for our future experiments for studying the underlying mechanisms of the potential antiageing properties of the tested NADES solvent and extracts.

Arp4 cells experienced an increase in the relative amount of *CDC28* mRNA at the 4th h and on the 9th d after supplementation with CiAPD14 *P. major* and CiAPD14 *S. scardica* with a 3.5-fold and 2-fold change, respectively ($^{*}p < 0.05$) (Figure 4(c)). On the 9th day of cultivation, there was an

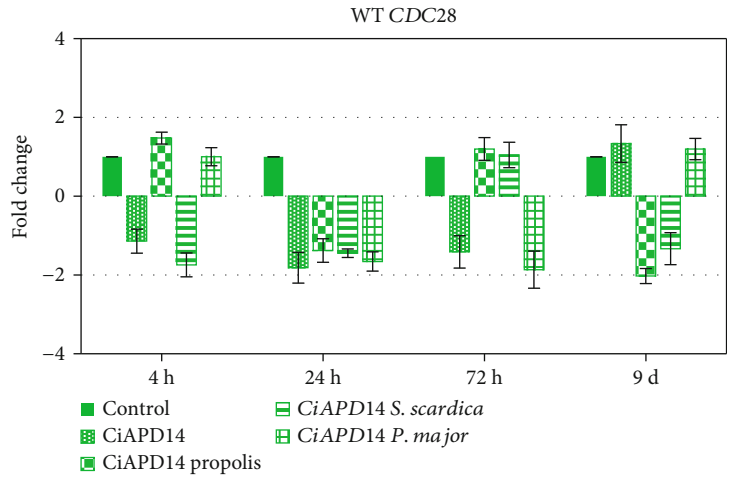

(a)

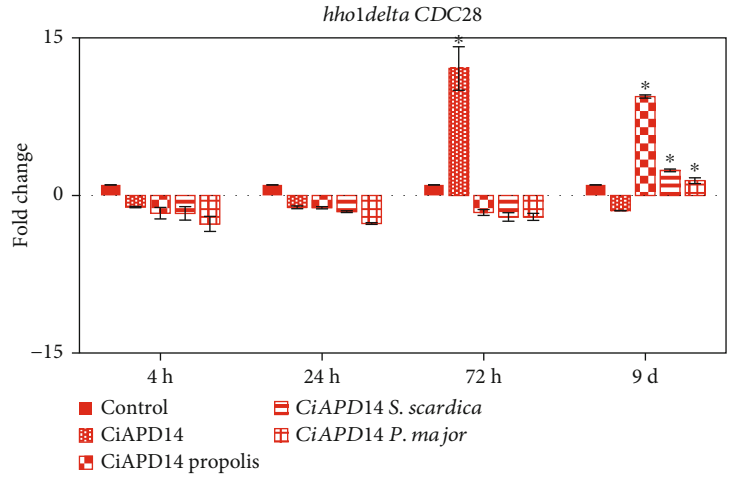

(b)

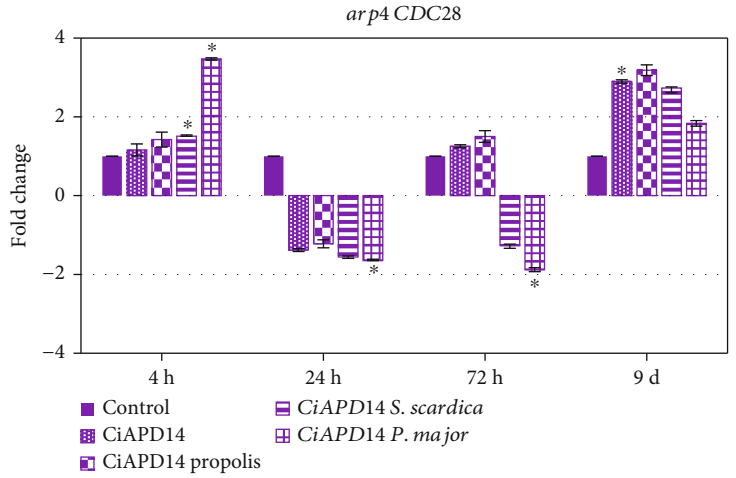

(c)

Figure 4: Continued.

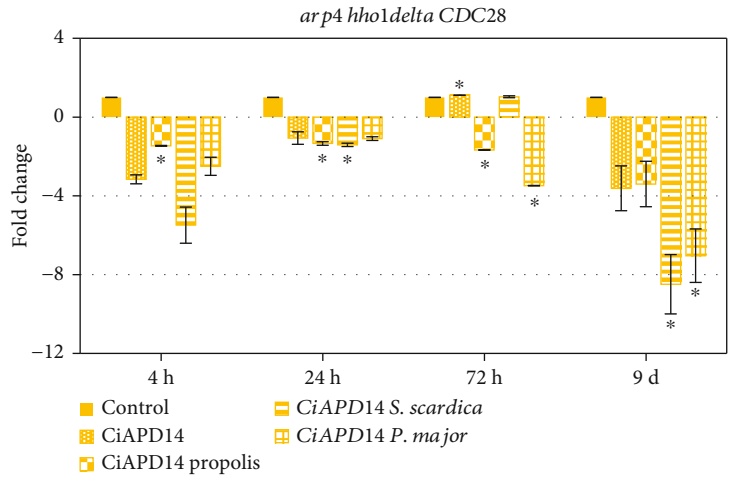

(d)

Figure 4: Gene expression analysis of the *CDC28* gene of treated with CiAPD14, CiAPD14 propolis, CiAPD14 *S. scardica*, and CiAPD14 *P. major* extract yeast cells. Total RNA was isolated from aliquots of the yeast cultures and converted to cDNA. cDNA was used as a template in RT-qPCR experiments to analyze the expression of *CDC28*. *ACT1* was expression the reference gene. (a) WT, (b) *hho1delta*, (c) *arp4*, and (d) *arp4 hho1delta*. The results were calculated by the $^{\Delta\Delta}$CT method using specialized Rotor-Gene 6000 software. Data are MEAN ± SD. Statistically significant differences are marked with ∗ where $p < 0.05$.

increment in the *CDC28* expression levels after treatment with CiAPD14 propolis, CiAPD14 *S. scardica*, and CiAPD14 *P. major* extracts with a 3.2-, 2.7-, and 1.8-fold change increase ($^*p < 0.05$) (Figure 4(c)). These results though statistically significant did not correlate with the CLS survival results of these cells (Figure 2(d)) as we did not detect any statistically significant differences among the CLS survival in the supplemented with the NADES solvent and its extracts cells and the nonsupplemented ones. We, therefore, find these results as a good basis for future experiments that aim at elucidation of the underlying mechanisms of the potential antiageing effect of the studied NADES solvent and its extracts. An interesting observation was that the double mutant had a general reduction in the expression of the *CDC28* gene in the cells supplemented either with the solvent or with an extract during all measured time points (Figure 4(d)), with the most pronounced decrease of 3.4- and 8.5-fold at the 9th day ($^*p < 0.05$). The results of *CDC28* expression in the double mutant were in a good agreement with the results from the CLS and cell cycle experiments. It can be seen that the lower expression of *CDC28* in this mutant coincided with shorter CLS (Figures 1 and 2) and the detection of the fewest cells in the S and G2/M phase of the cell cycle at later points of CLS (Figure 4(d); 9th day) compared to all other strains.

Next, we examined the expression of *RAD9* during the ageing of the studied yeast cells (Figure 5). *RAD9* is responsible for early DNA damage response and cell cycle checkpoint regulation [66, 67]. For the WT (Figure 5(a)), we did not observe any significant changes in the expression of the *RAD9* gene on the 4th h for the control WT cells except after supplementation with CiAPD14 *S. scardica*, which led to a statistically significant slight increase in its expression ($^*p < 0.05$). On the 24th hour, we did not detect any significant differences, while at the 72nd hour, we noticed a 5-fold decrease ($^*p < 0.05$) of *RAD9* expression in the WT cells supplemented with CiAPD14 propolis and a twofold increase ($^*p < 0.05$) after CiAPD14 *S. scardica* supplementation. On the last 9th day, none of the detected differences was statistically significant. *RAD9* expression in the *hho1delta* mutant (Figure 5(b)) on the 24th hour had an increase in the cells supplemented with CiAPD14 *P. major* around 2-fold ($^*p < 0.05$). *RAD9* expression was increased, particularly after treatment with CiAPD14 solvent only for the 72nd hour with 10-fold ($^*p < 0.05$). We detected a 6.3- and 2.2-fold increase after CiAPD14 propolis and CiAPD14 *S. scardica* treatment on the 9th day, though the last two differences were statistically insignificant. Thus, as for *CDC28*, *RAD9* transcription was upregulated upon supplementation with CiAPD14 on the 3rd day and upon supplementation with propolis and *S. scardica* extracts on day 9 of the CLS. Quite similar was the trend of *CDC28* and *RAD9* gene expression in the *arp4* cells supplemented with CiAPD14 or the CiAPD14 biological extracts in all examined time points. We did not detect any correlation between the CLS survival of these cells and the detected changes in the expression of *RAD9*. We assume that in some of our mutants the detected changes in the expression of the studied genes could require more time to be visualized as a change in the ageing process as the mutants are different and express different features of ageing. The double mutant had a general decrease in *RAD9* expression (Figure 5(d)) for cells supplemented with CiAPD14 propolis at the 4th h time point ($^*p < 0.05$) and an increase of 3.5-fold for cells supplemented with CiAPD14 *P. major* ($^*p < 0.05$). On the 24th hour, this tendency for CiAPD14 propolis-supplemented cells was preserved. A similar decrease in *RAD9* was observed for the cells supplemented with CiAPD14 *P. major* too ($^*p < 0.05$). Statistically significant differences were not detected in the expression changes of *RAD9* at the 72nd hour in these cells. The most

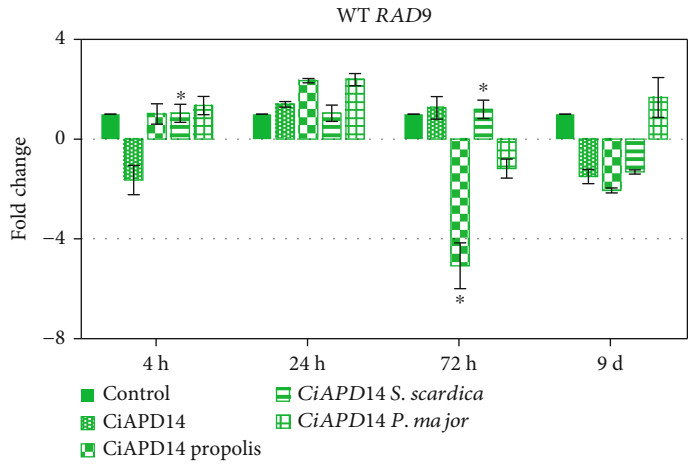

(a)

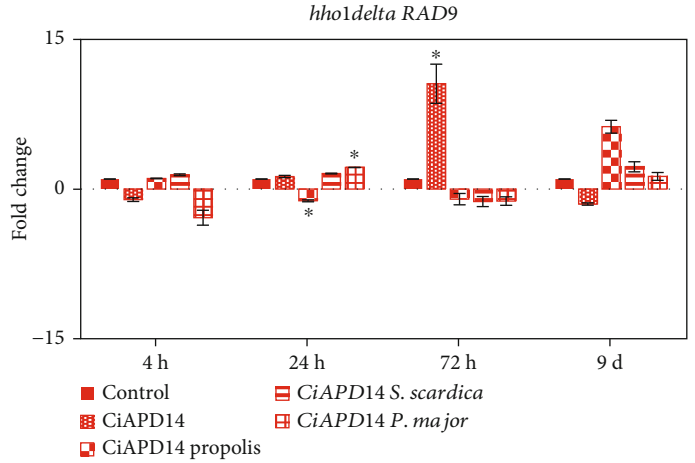

(b)

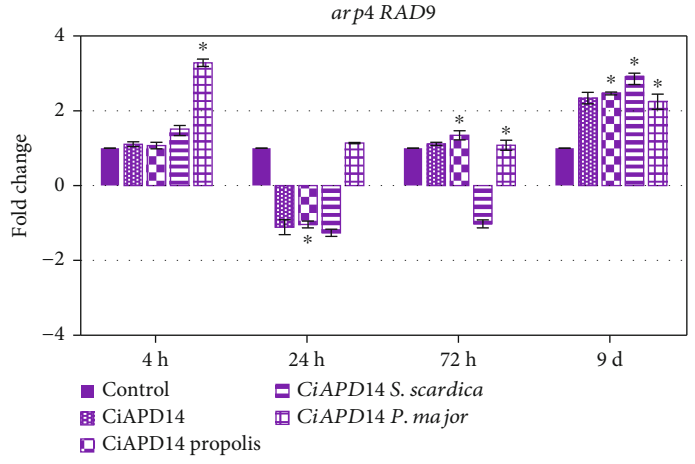

(c)

Figure 5: Continued.

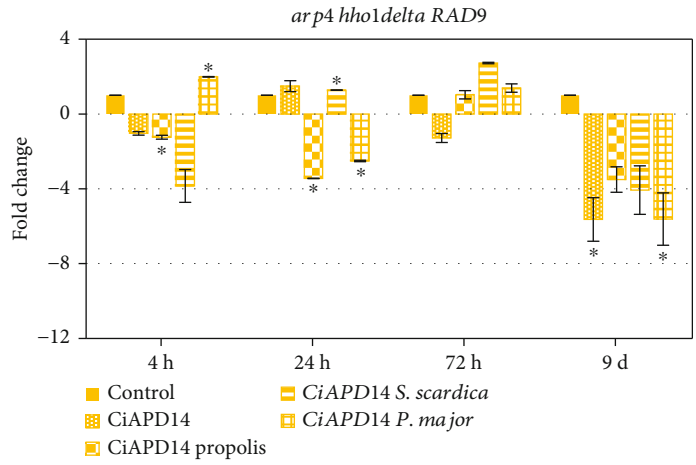

Figure 5: Gene expression analysis of the RAD9 gene of supplemented with CiAPD14, CiAPD14 propolis, CiAPD14 *S. scardica*, and CiAPD14 *P. major* extract yeast cells during their CLS. Total RNA was isolated from aliquots of the yeast cultures and converted to cDNA. cDNA was used as a template in RT-qPCR experiments to analyze the expression of *RAD9*. *ACT1* was the reference gene. (a) WT control cells, (b) hho1delta mutant yeast cells, (c) arp4 mutants, and (d) arp4 hho1delta double mutant cells. The results were calculated by the $^{\Delta\Delta}$CT method using the specialized Rotor-Gene 6000 software. Data are MEAN ± SD. Statistically significant differences are marked with ∗ where $p < 0.05$.

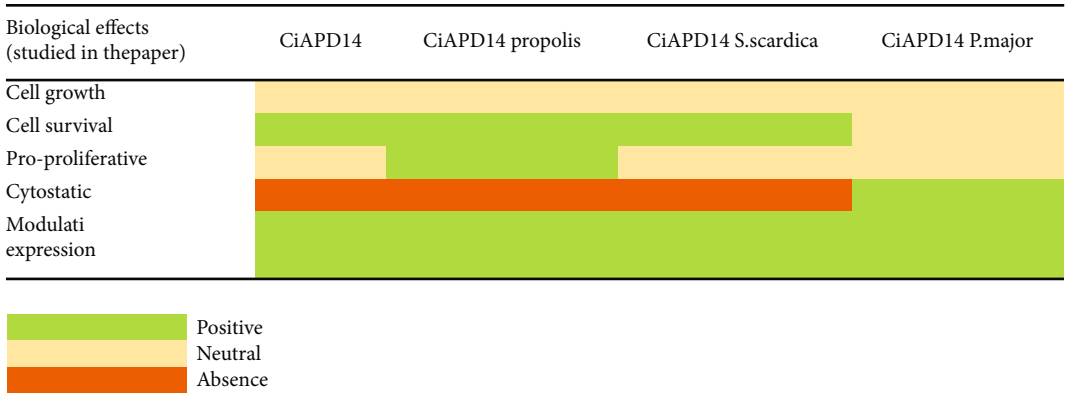

Figure 6: Combined general antiageing effects of CiAPD14 and its extracts for all the studied *S. cerevisiae* strains during their CLS.

prominent decline was detected on day 9th, where all the treatments resulted in significantly lower *RAD9* expression levels. The statistically significant differences were detected for the supplementation of these double mutant cells with CiAPD14 solvent and CiAPD14 *P. major* ($^*p < 0.05$).

We have summarized the obtained results of the potential antiageing properties of the tested NADES solvent and plant extracts in Figure 6. The effects are combined and evaluated for all yeast strains. The biological activities of the NADES solvent and extracts are combining data from the cell growth and survival assays, FACS analyses, and gene expression studies for all studied strains. This is done for the ease of classification of their antiageing properties.

What we observed was that the solvent itself (CiAPD14) exhibited slight antiageing properties (follow the green coloured boxes for CiAPD14 in Figure 6). This result was further acceptable given the fact that the solvent alone should not change the way cells age, though the combination of citric acid and 1,2-propanediol could induce certain biological effects as recent studies showed [68]. These data discussed that the citric acid exerted certain biological effects on the studied HaCaT cells by inhibiting their proliferation via the induction of cell cycle arrest and apoptosis. Treatment of cells with citric acid or malic acid led to apoptotic features, DNA damage, and an increase of sub-G1 cells, which was connected with cell regeneration.

The comparison among the overall antiageing activities of the studied CiAPD14 extracts showed that CiAPD14 propolis was the most potent one (follow the green boxes in Figure 6 for CiAPD14 propolis), followed by CiAPD14 *S. scardica* and CiAPD14 *P. major*. This classification based on the combined antiageing properties of the tested NADES extracts was in full compliance with the total phenolic content, presented in Table 2, and further confirmed the antiageing potential of these extracts. We believe that these results are another important indicator of the increasing

need for a detailed evaluation of the mechanism of action of natural compounds and metabolites in biological processes.

4. Conclusions

NADES origin is completely natural as NADES solvents are made typically of plant primary metabolites, and one of their most important characteristics, apart from being nontoxic, is the fact that they have been proven to increase the beneficial properties of the extracted biological compounds, which gives them a new ground for future development of different therapies [18, 19]. In this study, we tested the potential antiageing effects of a novel NADES solvent—CiAPD14, as well as three biological extracts with it from propolis, *S. scardica*, and *P. major*. The advantages of our work come from the fact that this is the first report on the potential antiageing properties of a NADES solvent (CiAPD14) and its extracts with propolis, *S. scardica*, and *P. major*. We tested their antiageing properties on yeast *S. cerevisiae* cells, commonly accepted as a golden model organism for studying ageing. The chronological ageing of three chromatin mutants was studied with and without supplementation with the NADES extracts, which further enriched our studies as the chromatin mutants have disorganized chromatin structures resulting in premature ageing phenotypes [30, 31, 50, 53]. The results confirmed the potential of NADES for extraction of biologically active secondary metabolites from propolis and the studied medicinal plants and further suggested that NADES CiAPD14 could improve the effects of bioactive constituents of the extracts. This finding is important, because the recovery of the extracted compounds from the NADES, which are nonvolatile, is challenging. Further studies are needed to elucidate the role of the studied NADES on the bioactivity of dissolved substances and the possibility to use such extracts in the food industry and pharmacy. Our results showed that the solvent CiAPD14 did exert a slight antiageing effect, which was something that would not be typically expected, considering the solvent was in its pure form. When the three NADES extracts were tested, however, we noted articulate antiageing effects (Figure 6). The antiageing properties are reflected in the slowed course of their CLS, especially for the double mutant, in the transition of their cells in the cell cycle phases and the change in expression of genes involved in DNA repair pathways. We further detected changes in the cell proliferation of these cells supplemented with the NADES solvent and extracts. On the last time point tested for all cultures, the largest number of cells was in phase G1, which was most distinctive for the *hho1-delta* and *arp4 hho1delta* strains and less pronounced for the WT. We hypothesized that although stationary cultures of these mutants have a high percentage of G1 phase cells, they are rather poor survivors. This in turn raises the question of the relationship between the ability of chromatin mutants to form a proper quiescent population and the chronological lifespan and the need for further research to elucidate it. Moreover, we detected a correlation of the effect of CiAPD14 propolis extract which increased both, the cellular viability and the percentage of G2/M cell fraction. Our unpublished data show that the yeast mutants that lack the gene for the linker histone have aberrant and decreased percentage of quiescent cells during the CLS, which results in their premature ageing phenotypes and this is further confirmed by the results in this study. This premature ageing trait was ameliorated to an extent with some of the NADES extracts (CiAPD14 propolis) and further provided us with confidence to study the underlying mechanisms in detail. These antiageing effects varied in the different combinations studied and in the different mutant cells, for some of which like the single *hho1delta* mutant we did not observe a correlation between the CLS survival on the last time point and the expression of *CDC28*. In contrast, supplementation of these cells with the pure solvent at the 72^{nd}-hour time point led to a correlation with *CDC28* expression levels, thus suggesting that the phenol compounds in the CiAPD14 extracts, especially propolis, exerted oxidative stress [69]. In general, the NADES CiAPD14 propolis and CiAPD14 *S. scardica* extracts had a stronger antiageing effect compared to the CiAPD14 *P. major* extract. We associated these results with the phenolic content (Table 2) where the CiAPD14 propolis extract had the highest content, followed by the CiAPD14 *S. scardica* and CiAPD14 *P. major* ones. We, therefore, assume that future developments and applications of NADES plant extracts in antiageing interventions need extensive research in the light of their phenolic content and their biological underlying mechanisms, some of which even induction oxidative stress.

Our future perspectives lie in the anticipation of a more detailed study of the effects of these NADES solvents and extracts on higher eukaryotic model systems. This will shed light on the molecular mechanisms triggered by these NADES solvents and extracts and will allow systematic studies among species on their antiageing features.

Data Availability

All data supporting this study are freely available.

Conflicts of Interest

The authors declare no conflict of interest.

Authors' Contributions

M.G. and V.B. were responsible for conceptualization; B.V., M.G., V.B., K.A., and M.P. were responsible for methodology; B.V. and M.G. were responsible for software; M.G., B.V., G.M., D.S., M.P., K.A., and V.B. were responsible for validation; B.V. and M.G. were responsible for formal analysis; B.V., M.G., T.G., K.A., H.P., B.T., and M.P. were responsible for investigation; B.V., V.B., and M.G. were responsible for resources; B.V. and M.G. were responsible for original draft preparation; M.G., D.S., V.B., and G.M. were responsible for writing—review and editing; M.G. and B.V. were responsible for visualization; M.G. and V.B. were responsible for supervision; V.B. and M.G. were responsible for project administration; V.B. and M.G. were responsible for funding acquisition. All authors have read and agreed to the published version of the manuscript.

Acknowledgments

This research was funded by the Bulgarian National Science Fund (grant number DN-19/4).

References

[1] M. S. Shon, Y. Lee, J. H. Song et al., "Anti-aging potential of extracts prepared from fruits and medicinal herbs cultivated in the Gyeongnam area of Korea," *Preventive Nutrition and Food Science*, vol. 19, no. 3, pp. 178–186, 2014.

[2] R. Hodgson, B. K. Kennedy, E. Masliah et al., "Aging: therapeutics for a healthy future," *Neuroscience and Biobehavioral Reviews*, vol. 108, pp. 453–458, 2020.

[3] B. R. Troen, "The biology of aging," *Mount Sinai Journal of Medicine*, vol. 70, no. 1, pp. 3–22, 2003.

[4] S. I. Liochev, "Which is the most significant cause of aging?," *Antioxidants*, vol. 4, no. 4, pp. 793–810, 2015.

[5] K. Jin, "Modern biological theories of aging," *Aging and Disease*, vol. 1, no. 2, pp. 72–74, 2010.

[6] S. Sahabi, D. Jafari-Gharabaghlou, and N. Zarghami, "A new insight into cell biological and biochemical changes through aging," *Acta Histochemica*, vol. 124, no. 1, article 151841, 2022.

[7] A. Vujin and K. Dick, "The information theory of aging," *Health Science Inquiry*, vol. 11, no. 1, pp. 148–154, 2020.

[8] M. Hayano, J.-H. Yang, M. Bonkowski et al., "DNA break-induced epigenetic drift as a cause of mammalian aging," *SSRN Electronic Journal*, 2019.

[9] D. A. Sinclair, M. D. LaPlante, and C. L. Delphia, *Lifespan: Why We Age - and Why We Don't Have to*, Atria Books, New York, 2019.

[10] A. S. Chopra, R. Lordan, O. K. Horbańczuk et al., "The current use and evolving landscape of nutraceuticals," *Pharmacological Research*, vol. 175, article 106001, 2022.

[11] A. Paiva, R. Craveiro, I. Aroso, M. Martins, R. L. Reis, and A. R. C. Duarte, "Natural deep eutectic solvents–solvents for the 21st century," *ACS Sustainable Chemistry & Engineering*, vol. 2, pp. 1063–1071, 2014.

[12] M. Ivanović, M. Islamčević Razboršek, and M. Kolar, "Innovative extraction techniques using deep eutectic solvents and analytical methods for the isolation and characterization of natural bioactive compounds from plant material," *Plants*, vol. 9, no. 11, article 1428, 2020.

[13] Y. Liu, J. B. Friesen, J. B. McAlpine, D. C. Lankin, S. N. Chen, and G. F. Pauli, "Natural deep eutectic solvents: properties, applications, and perspectives," *Journal of Natural Products*, vol. 81, no. 3, pp. 679–690, 2018.

[14] Y. H. Choi, J. van Spronsen, Y. Dai et al., "Are natural deep eutectic solvents the missing link in understanding cellular metabolism and physiology?," *Plant Physiology*, vol. 156, no. 4, pp. 1701–1705, 2011.

[15] W. W. Oomen, P. Begines, N. R. Mustafa, E. G. Wilson, R. Verpoorte, and Y. H. Choi, "Natural deep eutectic solvent extraction of flavonoids of Scutellaria baicalensis as a replacement for conventional organic solvents," *Molecules*, vol. 25, no. 3, p. 617, 2020.

[16] M. Ruesgas-Ramon, M. C. Figueroa-Espinoza, and E. Durand, "Application of deep eutectic solvents (DES) for phenolic compounds extraction: overview, challenges, and opportunities," *Journal of Agricultural and Food Chemistry*, vol. 65, no. 18, pp. 3591–3601, 2017.

[17] A. E. Ünlü, "Green and non-conventional extraction of bioactive compounds from olive leaves: screening of novel natural deep eutectic solvents and investigation of process parameters," *Waste and Biomass Valorization*, vol. 12, no. 10, pp. 5329–5346, 2021.

[18] D. T. da Silva, R. F. Rodrigues, N. M. Machado et al., "Natural deep eutectic solvent (NADES)-based blueberry extracts protect against ethanol-induced gastric ulcer in rats," *Food Research International*, vol. 138, article 109718, 2020.

[19] T. Grozdanova, B. Trusheva, K. Alipieva et al., "Extracts of medicinal plants with natural deep eutectic solvents: enhanced antimicrobial activity and low genotoxicity," *BMC Chemistry*, vol. 14, no. 1, pp. 1–9, 2020.

[20] J. Torres-Vega, S. Gómez-Alonso, J. Pérez-Navarro, J. Alarcón-Enos, and E. Pastene-Navarrete, "Polyphenolic compounds extracted and purified from Buddleja globosa Hope (Buddlejaceae) leaves using natural deep eutectic solvents and centrifugal partition chromatography," *Molecules*, vol. 26, no. 8, article 2192, 2021.

[21] I. Rukavina, M. J. Rodrigues, C. G. Pereira et al., "Greener is better: first approach for the use of natural deep eutectic solvents (NADES) to extract antioxidants from the medicinal halophyte Polygonum maritimum L," *Molecules*, vol. 26, no. 20, article 6136, 2021.

[22] T. Bhattacharya, P. S. Dey, R. Akter, M. T. Kabir, M. H. Rahman, and A. Rauf, "Effect of natural leaf extracts as phytomedicine in curing geriatrics," *Experimental Gerontology*, vol. 150, article 111352, 2021.

[23] M. Kratchanova, P. Denev, M. Ciz, A. Lojek, and A. Mihailov, "Evaluation of antioxidant activity of medicinal plants containing polyphenol compounds. Comparison of two extraction systems," *Acta Biochimica Polonica*, vol. 57, no. 2, pp. 229–234, 2010.

[24] M. M. Rahman, M. S. Rahaman, M. R. Islam et al., "Role of phenolic compounds in human disease: current knowledge and future prospects," *Molecules*, vol. 27, no. 1, article 233, 2022.

[25] Á. Dos Santos and C. P. Toseland, "Regulation of nuclear mechanics and the impact on DNA damage," *International Journal of Molecular Sciences*, vol. 22, no. 6, p. 3178, 2021.

[26] L. Roger, F. Tomas, and V. Gire, "Mechanisms and regulation of cellular senescence," *International Journal of Molecular Sciences*, vol. 22, no. 23, article 13173, 2021.

[27] R. U. Pathak, M. Soujanya, and R. K. Mishra, "Deterioration of nuclear morphology and architecture: a hallmark of senescence and aging," *Ageing Research Reviews*, vol. 67, article 101264, 2021.

[28] G. Pegoraro and T. Misteli, "The central role of chromatin maintenance in aging," *Aging (Albany NY)*, vol. 1, no. 12, pp. 1017–1022, 2009.

[29] B. Liu, R. Yip, and Z. Zhou, "Chromatin remodeling, DNA damage repair and aging," *Current Genomics*, vol. 13, no. 7, pp. 533–547, 2012.

[30] G. Miloshev, D. Staneva, K. Uzunova et al., "Linker histones and chromatin remodelling complexes maintain genome stability and control cellular ageing," *Mechanisms of Ageing and Development*, vol. 177, pp. 55–65, 2019.

[31] B. Vasileva, D. Staneva, N. Krasteva, G. Miloshev, and M. Georgieva, "Changes in chromatin organization eradicate cellular stress resilience to UVA/B light and induce premature aging," *Cell*, vol. 10, no. 7, article 1755, 2021.

[32] P. Fabrizio and V. D. Longo, "The chronological life span of Saccharomyces cerevisiae," *Aging Cell*, vol. 2, no. 2, pp. 73–81, 2003.

[33] V. D. Longo, G. S. Shadel, M. Kaeberlein, and B. Kennedy, "Replicative and chronological aging in _Saccharomyces cerevisiae_," *Cell Metabolism*, vol. 16, no. 1, pp. 18–31, 2012.

[34] L. Fontana, L. Partridge, and V. D. Longo, "Extending healthy life span–from yeast to humans," *Science*, vol. 328, no. 5976, pp. 321–326, 2010.

[35] C. Fatouros, G. J. Pir, J. Biernat et al., "Inhibition of tau aggregation in a novel Caenorhabditis elegans model of tauopathy mitigates proteotoxicity," *Human Molecular Genetics*, vol. 21, no. 16, pp. 3587–3603, 2012.

[36] Z. Huang, K. Chen, J. Zhang et al., "A functional variomics tool for discovering drug-resistance genes and drug targets," *Cell Reports*, vol. 3, no. 2, pp. 577–585, 2013.

[37] X. Zhang, D. L. Smith, A. B. Meriin et al., "A potent small molecule inhibits polyglutamine aggregation in Huntington's disease neurons and suppresses neurodegenerationin vivo," *Proceedings of the National Academy of Sciences of the United States of America*, vol. 102, no. 3, pp. 892–897, 2005.

[38] M. Kaeberlein, "Lessons on longevity from budding yeast," *Nature*, vol. 464, no. 7288, pp. 513–519, 2010.

[39] F. Sherman, "Getting started with yeast," *Methods in Enzymology*, vol. 350, pp. 3–41, 2002.

[40] S. Tenreiro, M. C. Munder, S. Alberti, and T. F. Outeiro, "Harnessing the power of yeast to unravel the molecular basis of neurodegeneration," *Journal of Neurochemistry*, vol. 127, no. 4, pp. 438–452, 2013.

[41] C. Boone, H. Bussey, and B. J. Andrews, "Exploring genetic interactions and networks with yeast," *Nature Reviews. Genetics*, vol. 8, no. 6, pp. 437–449, 2007.

[42] I. Muller, M. Zimmermann, D. Becker, and M. Flomer, "Calendar life span _versus_ budding lifespan of _Saccharomyces cerevisiae_," *Mechanisms of Ageing and Development*, vol. 12, no. 1, pp. 47–52, 1980.

[43] J. Y. An, C. Kim, N. R. Park et al., "Clinical anti-aging efficacy of propolis polymeric nanoparticles prepared by a temperature-induced phase transition method," *Journal of Cosmetic Dermatology*, pp. 1–12, 2022.

[44] S. I. Anjum, A. Ullah, K. A. Khan et al., "Composition and functional properties of propolis (bee glue): a review," *Saudi Journal of Biological Sciences*, vol. 26, no. 7, pp. 1695–1703, 2019.

[45] V. M. Tadic, I. Jeremic, S. Dobric et al., "Anti-inflammatory, gastroprotective, and cytotoxic effects ofSideritis scardicaextracts," *Planta Medica*, vol. 78, no. 5, pp. 415–427, 2012.

[46] M. Todorova and A. Trendafilova, "_Sideritis scardica_ Griseb., an endemic species of Balkan peninsula: traditional uses, cultivation, chemical composition, biological activity," *Journal of Ethnopharmacology*, vol. 152, no. 2, pp. 256–265, 2014.

[47] A. D. Farcas, A. C. Mot, A. E. Parvu et al., "In vivo pharmacological and anti-inflammatory evaluation of xerophyte Plantago sempervirens Crantz," *Oxidative Medicine and Cellular Longevity*, vol. 2019, Article ID 5049643, 13 pages, 2019.

[48] M. Georgieva, D. Staneva, K. Uzunova et al., "The linker histone in _Saccharomyces cerevisiae_ interacts with actin-related protein 4 and both regulate chromatin structure and cellular morphology," *The International Journal of Biochemistry & Cell Biology*, vol. 59, pp. 182–192, 2015.

[49] M. Harata, Y. Zhang, D. J. Stillman et al., "Correlation between chromatin association and transcriptional regulation for the Act3p/Arp4 nuclear actin-related protein of Saccharomyces cerevisiae," *Nucleic Acids Research*, vol. 30, no. 8, pp. 1743–1750, 2002.

[50] M. Georgieva, A. Roguev, K. Balashev, J. Zlatanova, and G. Miloshev, "Hho1p, the linker histone of _Saccharomyces cerevisiae_ , is important for the proper chromatin organization _in vivo_," *Biochimica et Biophysica Acta*, vol. 1819, no. 5, pp. 366–374, 2012.

[51] M. Georgieva, D. Staneva, K. Uzunova, and G. Miloshev, "The deletion of the gene for the linker histone inARP 4mutant yeast cells is not deleterious," *Biotechnology & Biotechnological Equipment*, vol. 26, no. sup1, pp. 134–139, 2012.

[52] K. J. Livak and T. D. Schmittgen, "Analysis of relative gene expression data using real-time quantitative PCR and the $2^{-\Delta\Delta\_C\_}{}_T$ method," *Methods*, vol. 25, no. 4, pp. 402–408, 2001.

[53] K. Uzunova, M. Georgieva, and G. Miloshev, "Saccharomyces cerevisiae linker histone—Hho1p maintains chromatin loop organization during ageing," *Oxidative Medicine and Cellular Longevity*, vol. 2013, Article ID 437146, 9 pages, 2013.

[54] V. D. Longo and P. Fabrizio, "Chronological aging in Saccharomyces cerevisiae," *Sub-Cellular Biochemistry*, vol. 57, pp. 101–121, 2012.

[55] L. Galdieri, S. Mehrotra, S. Yu, and A. Vancura, "Transcriptional regulation in yeast during diauxic shift and stationary phase," *OMICS*, vol. 14, no. 6, pp. 629–638, 2010.

[56] K. Mohammad and V. I. Titorenko, "Yeast chronological aging is linked to cell cycle regulation," *Cell Cycle*, vol. 17, no. 9, pp. 1035-1036, 2018.

[57] H. Zhang and W. Siede, "Analysis of the budding yeast Saccharomyces cerevisiae cell cycle by morphological criteria and flow cytometry," *Methods in Molecular Biology*, vol. 241, pp. 77–91, 2004.

[58] V. Gire and V. Dulic, "Senescence from G2 arrest, revisited," *Cell Cycle*, vol. 14, no. 3, pp. 297–304, 2015.

[59] C. Allen, S. Büttner, A. D. Aragon et al., "Isolation of quiescent and nonquiescent cells from yeast stationary-phase cultures," *The Journal of Cell Biology*, vol. 174, no. 1, pp. 89–100, 2006.

[60] L. Li, S. Miles, Z. Melville, A. Prasad, G. Bradley, and L. L. Breeden, "Key events during the transition from rapid growth to quiescence in budding yeast require posttranscriptional regulators," *Molecular Biology of the Cell*, vol. 24, no. 23, pp. 3697–3709, 2013.

[61] C. Zimmermann, P. Chymkowitch, V. Eldholm et al., "A chemical-genetic screen to unravel the genetic network of < em> CDC28/CDK1 links ubiquitin and Rad6–Bre1 to cell cycle progression," *Proceedings of the National Academy of Sciences*, vol. 108, no. 46, pp. 18748–18753, 2011.

[62] K. A. Henderson, K. Kee, S. Maleki, P. A. Santini, and S. Keeney, "Cyclin-dependent kinase directly regulates initiation of meiotic recombination," *Cell*, vol. 125, no. 7, pp. 1321–1332, 2006.

[63] G. Ira, A. Pellicioli, A. Balijja et al., "DNA end resection, homologous recombination and DNA damage checkpoint activation require CDK1," *Nature*, vol. 431, no. 7011, pp. 1011–1017, 2004.

[64] Y. Aylon, B. Liefshitz, and M. Kupiec, "The CDK regulates repair of double-strand breaks by homologous recombination

during the cell cycle," *The EMBO Journal*, vol. 23, no. 24, pp. 4868–4875, 2004.

[65] J. A. Downs, E. Kosmidou, A. Morgan, and S. P. Jackson, "Suppression of homologous recombination by the _Saccharomyces cerevisiae_ linker histone," *Molecular Cell*, vol. 11, no. 6, pp. 1685–1692, 2003.

[66] H. B. Lieberman, "Rad9, an evolutionarily conserved gene with multiple functions for preserving genomic integrity," *Journal of Cellular Biochemistry*, vol. 97, no. 4, pp. 690–697, 2006.

[67] A. Ciccia and S. J. Elledge, "The DNA damage response: making it safe to play with knives," *Molecular Cell*, vol. 40, no. 2, pp. 179–204, 2010.

[68] S. C. Tang and J. H. Yang, "Dual effects of alpha-hydroxy acids on the skin," *Molecules*, vol. 23, no. 4, article 863, 2018.

[69] Y. C. Tsai, Y. H. Wang, C. C. Liou, Y. C. Lin, H. Huang, and Y. C. Liu, "Induction of oxidative DNA damage by flavonoids of propolis: its mechanism and implication about antioxidant capacity," *Chemical Research in Toxicology*, vol. 25, no. 1, pp. 191–196, 2012.

Hindawi
Oxidative Medicine and Cellular Longevity
Volume 2022, Article ID 7175027, 13 pages
https://doi.org/10.1155/2022/7175027

Research Article

Transmissible Endoplasmic Reticulum Stress Mediated by Extracellular Vesicles from Adipocyte Promoting the Senescence of Adipose-Derived Mesenchymal Stem Cells in Hypertrophic Obesity

Jia Fang,[1] **Li Li**,[1] **Xingguo Cao**,[1] **Han Yue**,[2] **Wanying Fu**,[3] **Yi Chen**,[1] **Zhiwei Xu**,[1] **Qiongrui Zhao**,[1] **Jingge Zhao**,[1] **Yuebo Wang**,[1] **and Wulong Liang**[4]

[1]*Clinical Research Service Center, Henan Provincial People's Hospital, Zhengzhou University People's Hospital, Henan University People's Hospital, Zhengzhou, Henan 450000, China*
[2]*Stem Cell Research Center, Henan Key Laboratory of Stem Cell Differentiation and Modification, Henan Provincial People's Hospital; Zhengzhou University People's Hospital; Henan University People's Hospital, Zhengzhou, Henan 450000, China*
[3]*School of Basic Medicine, Xinxiang Medical University, Xinxiang, Henan 453003, China*
[4]*Department of Neurosurgery, The Fifth Affiliated Hospital of Zhengzhou University, Zhengzhou, Henan 450000, China*

Correspondence should be addressed to Jia Fang; fangjiatg@163.com and Wulong Liang; liang_wulong@163.com

Received 7 February 2022; Revised 5 July 2022; Accepted 13 July 2022; Published 5 August 2022

Academic Editor: Franco J. L.

Hypertrophic obesity, characterized by an excessive expansion of subcutaneous adipocytes, causes chronic inflammation and insulin resistance. It is the primary feature of obesity in middle-aged and elderly individuals. In the adipose microenvironment, a high level of endoplasmic reticulum (ER) stress and changes in the extracellular vesicle (EV) composition of adipocytes may cause the senescence and restrained differentiation of progenitor cells of adipose, including adipose-derived mesenchymal stem cells (ASCs). In this study, a hypertrophic obesity mouse model was established, and the effects of adipocytes on the ER stress and senescence of ASCs were observed in a coculture of control ASCs and hypertrophic obesity mouse adipocytes or their derived EVs. The adipocytes of hypertrophic obesity mice were treated with GW4869 or an iron chelation agent to observe the effects of EVs secreted by adipocytes and their iron contents on the ER stress and senescence of ASCs. Results showed higher ER stress level and senescence phenotypes in the ASCs from the hypertrophic obesity mice than in those from the control mice. The ER stress, senescence phenotypes, and ferritin level of ASCs can be aggravated by the coculture of ASCs with adipocytes or EVs released by them from the hypertrophic obesity mice. GW4869 or iron chelator treatment improved the ER stress and senescence of the ASCs cocultured with EVs released by the adipocytes of the hypertrophic obesity mice. Our findings suggest that EV-mediated transmissible ER stress is responsible for the senescence of ASCs in hypertrophic obesity mice.

1. Background

Metabolic diseases caused by obesity are important public health problems in modern society. Subcutaneous adipose tissue (SAT) is the largest lipid depot of the body [1]. Adipose tissues expand through the recruitment of adipogenic progenitors and hypertrophic expansion of differentiated adipocytes that contribute to hypertrophic obesity [2]. However, the ability of adipocytes to expand and store excess calories is limited, causing obesity-associated metabolic complications [1]. Hypertrophic adipocytes result in an altered secretion profile characterized by increased levels of leptin and inflammatory cytokines and reduced level of adiponectin, which lead to chronic inflammation, increased oxidative stress, and endoplasmic reticulum (ER) stress [3]. Adipose tissues regulate metabolism, insulin resistance (IR), and the development of type 2 diabetes (T2D) through the secretion of extracellular vesicles (EVs) [4]. EVs are

spherical vesicles with outer lipid bilayers and internal contents including RNA, proteins, and lipids [5]. In T2Ds, EVs released from adipocytes play an important role in intercellular communications between adipocytes and macrophages [6] and may affect the function of mesenchymal stem cells in adipose tissues.

Adipose-derived mesenchymal stem cells (ASCs) are adult stem cells, with self-renewal and multipotential differentiation capacities [7]. ASCs can be differentiated into adipocytes and are components of the lineage hierarchy of adipocyte progenitors [8, 9]. The senescence and differentiation inhibition of ASCs are more serious in individuals with obesity or metabolic diseases than in normal individuals [9], but the underlying mechanisms are unclear.

Growing evidence has shown that ER stress activation is a central feature involved in the pathogenesis of different diseases, including obesity-associated IR and diabetes [10]. ER stress is the consequence of a lack of control in the amount of poorly folded proteins inside the ER, resulting in a reduction in the protein synthesis and expression of various transcription factors. Cells upon ER stress can induce ER stress to other cells. This concept is defined as transmissible ER stress (TERS) [11]. EVs can be a contributory factor in transmitting ER stress in the tissue microenvironment [12].

The present study is aimed at elucidating the mechanisms by which ER stress transmitted from expanded adipocytes promotes senescence and inhibits the differentiation of ASCs in a mouse model with hypertrophic obesity. Results show that EVs accomplish these changes in part by trafficking iron, a regulator that causes senescence through its accumulation.

2. Results

2.1. High ER Stress Levels in Adipocytes and ASCs of Hypertrophic Obesity Mice. The hypertrophic obesity murine model was fed a high-fat diet for 16 weeks to induce obesity. The mean subcutaneous adipocyte diameter was significantly larger in the hypertrophic obesity mice than in the control mice (Figures 1(a) and 1(c)). The body weights of the hypertrophic obesity mice were significantly higher than those of the control mice (Figure 1(b)). Analysis of subcutaneous adipose tissue samples revealed that the mRNA expression levels of ER stress markers (*Xbp1*, *sXbp1*, *Atf6*, *Atf4*, and *Grp78*) were significantly higher in the hypertrophic obesity mice than in the control mice (Figure 1(d)). To further investigate the contribution of each cell type to ER stress, we examined the mRNA expression and protein levels of ER stress markers of adipocytes and ASCs. Before this procedure, we isolated the ASCs and identified their differentiation ability. Isolated ASCs can differentiate into adipocyte (Figure 2(a)), chondrocyte (Figure 2(b)), and osteoblast (Figure 2(c)) in corresponding differentiation induction culture medium. The surface markers of ASCs were positive for CD73, CD90, and negative for CD34 and CD45 (Figure 2(d)). The expression levels of ER stress-related genes and GRP78 protein were significantly higher in the adipocytes than in the ASCs derived from the subcutaneous adipocytes of the hypertrophic obesity mice (Figures 1(e) and 1(f)).

2.2. Increased Senescent Phenotype in ASCs in Hypertrophic Obesity Mice. We previously reported that chronic ER stress increases with aging [13]. The aging phenotype of adipogenic precursor cells was detected in the hypertrophic obesity individual at high risk of T2D [9]. Therefore, we measured the senescence phenotype of the ASCs in the hypertrophic obesity mice. The positive rate of SA-β-gal staining was significantly higher in the ASCs from the hypertrophic obesity mice than in those from the control mice (Figure 3(a)). The results of Oil red O staining (Figure 3(b)) and adipocyte-specific genes (*Pparg*, *Plin1*, and *Insr*) expression detection (Figure 3(f)) indicated that the adipogenic differentiation potential of ASCs decreased in the hypertrophic obesity mice. The population doubling time (Figure 3(c)) increased, and the relative telomerase length T/S ratio (Figure 3(d)) decreased in the ASCs from the hypertrophic obesity mice. Senescent markers (*P16* and *P53*) and senescence-associated secretory phenotype (SASP) markers (*IL6* and *Ccl2*) also increased in the ASCs from the hypertrophic obesity mice (Figures 3(e) and 3(h)).

2.3. Adipocyte Induces ER Stress and Senescence in ASCs In Vitro. Considering that the ER stress levels in the adipocytes are higher than those in the ASCs from the hypertrophic obesity mice, we suspected that adipocytes transmit ER stress to ASCs. We cocultured normal ASCs with subcutaneous adipocytes from the hypertrophic obesity and normal control mice, respectively. ASCs were collected 48 h after coculture, and results showed that the mRNA expression and protein levels of senescent (*P16* and *P21*) and SASP (*IL6* and *Ccl2*) markers and ER stress-related genes (*sXbp1* and *Grp78*) (Figures 3(g) and 3(j)) were significantly higher in the ASCs cocultured with adipocytes from the hypertrophic obesity mice than in the ASCs cocultured with adipocytes from the control mice. The positive rate of SA-β-gal staining was significantly higher in the ASCs cocultured with adipocytes from the hypertrophic obesity mice than in the ASCs cocultured with adipocytes from the control mice (Figure 3(i)).

2.4. EVs from Obesity Adipocytes Promote TERS and Senescence in ASCs. Cells can transmit ER stress to other cells in the microenvironment through EVs [12]. EVs in the supernatant culture of adipocytes from hypertrophic obesity and control mice were isolated and cocultured with control ASCs to explore the effects of EVs on the ER stress and senescence of ASCs. The morphology of the EVs was detected using transmission electron microscopy (Figure 4(a)). The protein markers for EVs (CD63 and CD81) were identified through western blot (Figure 4(b)). The EVs isolated from the adipocytes in the obese group had a higher protein content than the EVs from the adipocytes in the control group. EVs were stained with DIO before coculture with ASCs. By fluorescence microscope observation, EVs secreted by adipocytes could enter ASCs and locate in the region near the ER (Figure 4(c)). The mRNA

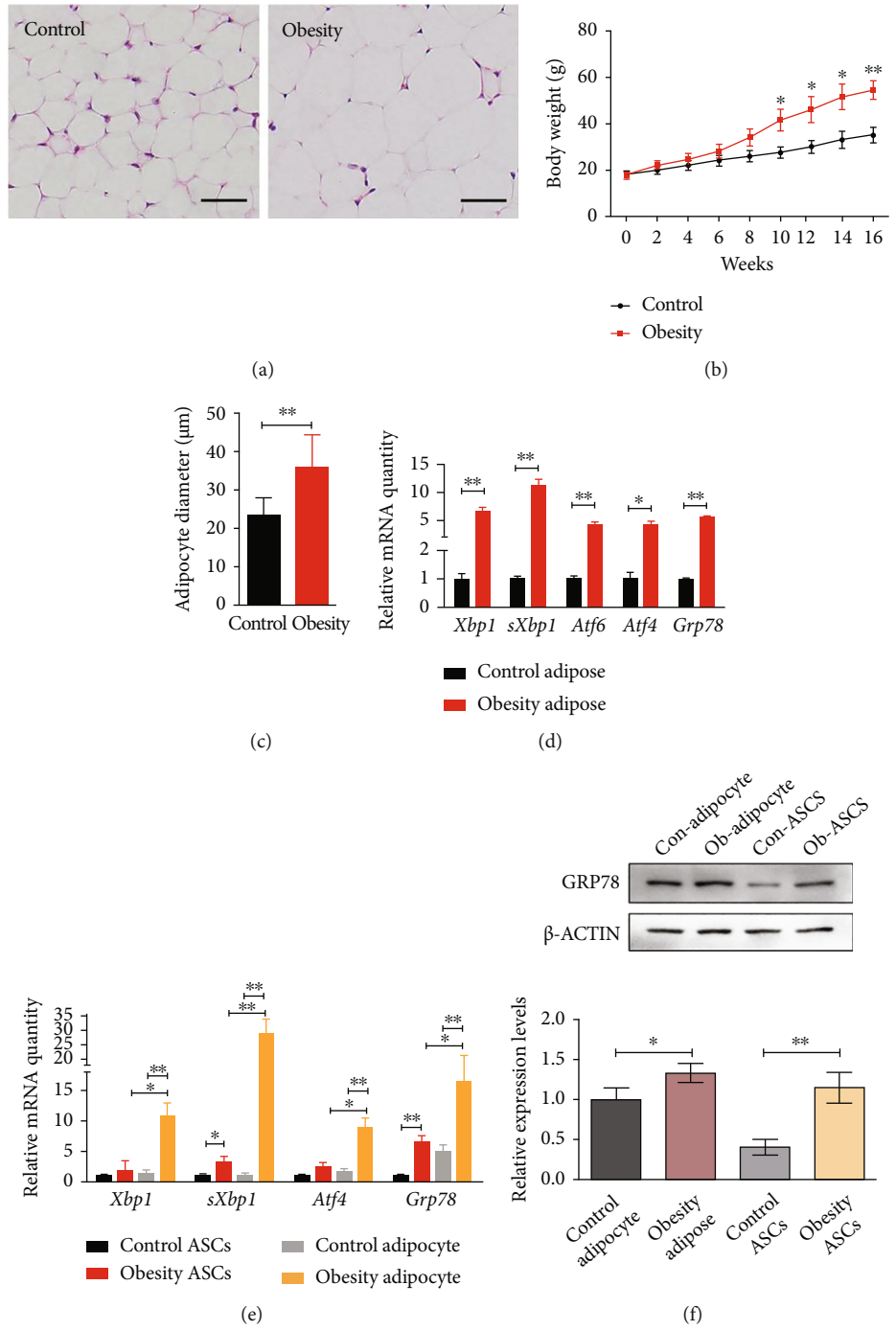

Figure 1: Higher ER stress levels in the adipocytes and ASCs of hypertrophic obesity mice. (a) HE staining of subcutaneous adipose tissue section of control and hypertrophic obesity mice. Bar = 50 μm. (b) Mean subcutaneous adipocyte diameter of control and hypertrophic obesity mice. (c) Body weight of mice after control and hypertrophic obesity diet. (d) QRT-PCR analysis of the relative mRNA expression of ER stress-related genes in adipose of control and hypertrophic obesity mice. (e) QRT-PCR analysis of the relative mRNA expression of ER stress-related genes in adipocytes and ASCs. (f) Western blot and multiple quantifications of ER stress-related protein in adipocytes and ASCs of control and hypertrophic obesity mice.

expression levels of ER stress markers (*Xbp1*, *sXbp1*, *Atf4*, *Atf6*, and *Grp78*) were significantly higher in the ASCs treated with hypertrophic obesity adipocyte-derived EVs than in the ASCs treated with control adipocyte-derived EVs (Figure 4(d)). After 2 days of EV treatment, ASCs were placed in an adipocyte induction solution for 14 days. Oil red O staining showed that the adipogenic potential of the ASCs pretreated with EVs from the hypertrophic obesity adipocytes was lower than that of the ASCs pretreated with EVs from the control obesity adipocytes (Figure 4(g)).

To investigate the effect of adipocyte EVs on ASCs, adipocytes from the obesity mice were treated with 20 μM

GW4869, which can inhibit EV secretion, or DMSO for 12 h. Then, adipocytes were switched to normal serum-free medium for 12 h. EVs from the GW4869-pretreated adipocytes or control adipocytes were added to ASCs culture medium for 12 h. The mRNA and protein levels of ER stress (*Xbp1*, *sXbp1*, *Atf4*, and *Grp78*) (Figures 4(e) and 4(i)), senescent (*P16* and *P21*), and SASP (*IL6* and *Ccl2*) markers (Figures 4(f) and 4(i)) and the positive rate of SA-β-gal staining (Figure 4(h)) were lower in the ASCs cocultured with EVs derived from the GW4869-pretreated obesity adipocytes than in the ASCs cocultured with EVs derived from obesity adipocytes.

2.5. EVs Carrying Iron Promotes Iron Storage and Senescence in ASCs. Iron accumulation is closely related to cell senescence [14]. The iron contents in the adipose tissues of obese individuals are significantly higher than those in the adipose tissues of individuals with normal weights [15]. Therefore, we examined the expression levels of iron metabolism-related genes in adipocytes and ASCs, respectively. The iron metabolism gene (*Ftl*, *Fth*, *Fpn1*, and *Tfrc*) and protein (FTH) levels were higher in the adipocytes and ASCs of the hypertrophic obesity mice than in those of the normal control mice (Figures 5(a), 5(b), and 5(g)).

Transport by EVs is an important route for iron metabolism. Coculture of adipocyte-derived EVs from the obese mice with EVs from the control mice could also improve the expression of iron metabolism-related genes and proteins in ASCs (Figures 5(c) and 5(h)). Adipocytes from the hypertrophic obesity mice were cultured in medium containing 50 μM desferioxamine (DFO) or DMSO for 12 h to verify whether or not these cells can transmit ions through EVs and cause ASCs senescence. Then, the adipocytes were switched to the normal serum-free medium for 12 h. EVs from the DFO-pretreated adipocytes or control adipocytes were placed on ASCs culture medium for 12 h. ASCs were collected, and the expression levels of senescence and ER stress-related genes were measured. The expression levels of ER stress, iron metabolism, and senescence-related genes (Figure 5(d)) and proteins (Figure 5(i)) were significantly lower in the DFO-treatment group than in the control group. Oil red O staining and SA-β-gal staining showed that the adipogenic potential and senescence were lower in the ASCs cocultured with EVs derived from the obesity adipocytes pretreated with DFO than in the ASCs cocultured with EVs derived from the obesity adipocytes (Figures 5(e) and 5(f)).

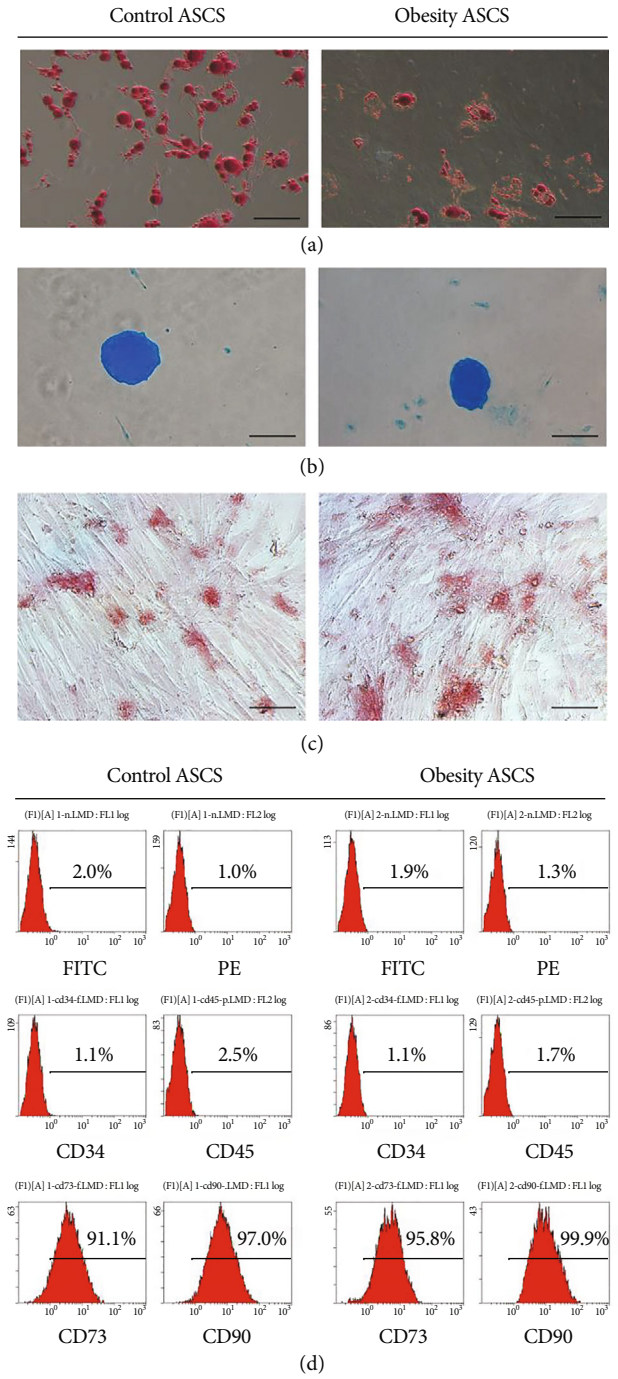

Figure 2: Identification of ASCs. (a) Oil red O staining for adipocyte differentiation of ASCs. Bar = 100 μm. (b) Alcian blue staining for chondrocyte differentiation of ASCs. Bar = 200 μm. (c) Alizarin red staining for osteoblast differentiation of ASCs. Bar = 50 μm. (d) Characterization of ASC surface markers by flow cytometry.

3. Discussion

Adipose tissue expands its ability to store lipids through adipocyte proliferation and hypertrophy. Approximately 10% of adipocytes renew every year, and hypertrophic adipocytes renew more slowly. Furthermore, the number of subcutaneous adipocytes is unlikely to change after puberty [1]. Thus, hypertrophic obesity tends to occur in adults. Adipocyte hypertrophy leads to morbid obesity and increases the incidence of metabolic diseases, such as IR and T2Ds, which are prevalent age-related pathologies. Transplanting adipose precursors or ASCs improves metabolic status [16]. Thus, the proliferation or differentiation of adipose precursors or ASCs is important to maintain the metabolic function of adipose tissue. In hypertrophic obesity, SAT adipogenesis is impaired by the poor differentiation rather than the reduced number of mesenchymal progenitor/precursor

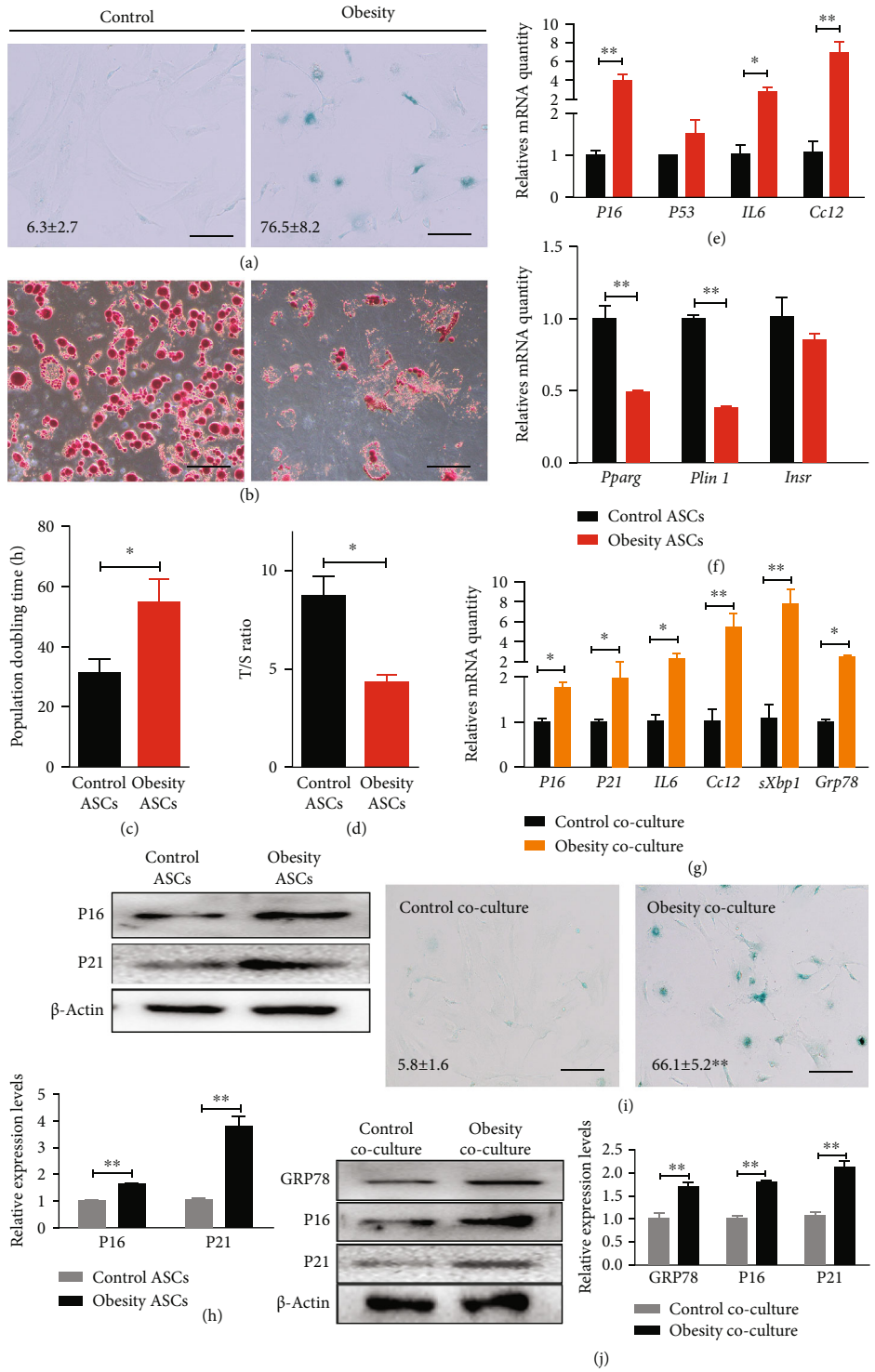

Figure 3: Increased senescent phenotype in ASCs in hypertrophic obesity mice. (a) SA-β-gal staining of control and hypertrophic obesity ASCs. Bar = 100 μm. (b) Oil red O staining of adipogenic-induced control and hypertrophic obesity ASCs. Bar = 100 μm. (c) Population doubling time of control and hypertrophic obesity ASCs. (d) Relative telomere length of control and hypertrophic obesity ASCs. (e) QRT-PCR analysis of the relative mRNA expression of senescent markers (*P16* and *P53*) and SASP-related markers (*IL6* and *Ccl2*) in control and hypertrophic obesity ASCs. (f) QRT-PCR analysis of the relative mRNA expression of adipogenic differentiation-related genes in adipogenic induced of control and hypertrophic obesity ASCs. (g) QRT-PCR analysis of the relative mRNA expression of senescence and ER stress-related genes in control and hypertrophic obesity adipocytes cocultured ASCs. (h) Western blot and multiple quantifications of senescent markers (P16 and P21) of control and hypertrophic obesity ASCs. (i) SA-β-gal staining of control and hypertrophic obesity adipocytes cocultured ASCs. Bar = 100 μm. (j) Western blot and multiple quantifications of senescence and ER stress-related proteins in control and hypertrophic obesity adipocytes cocultured ASCs.

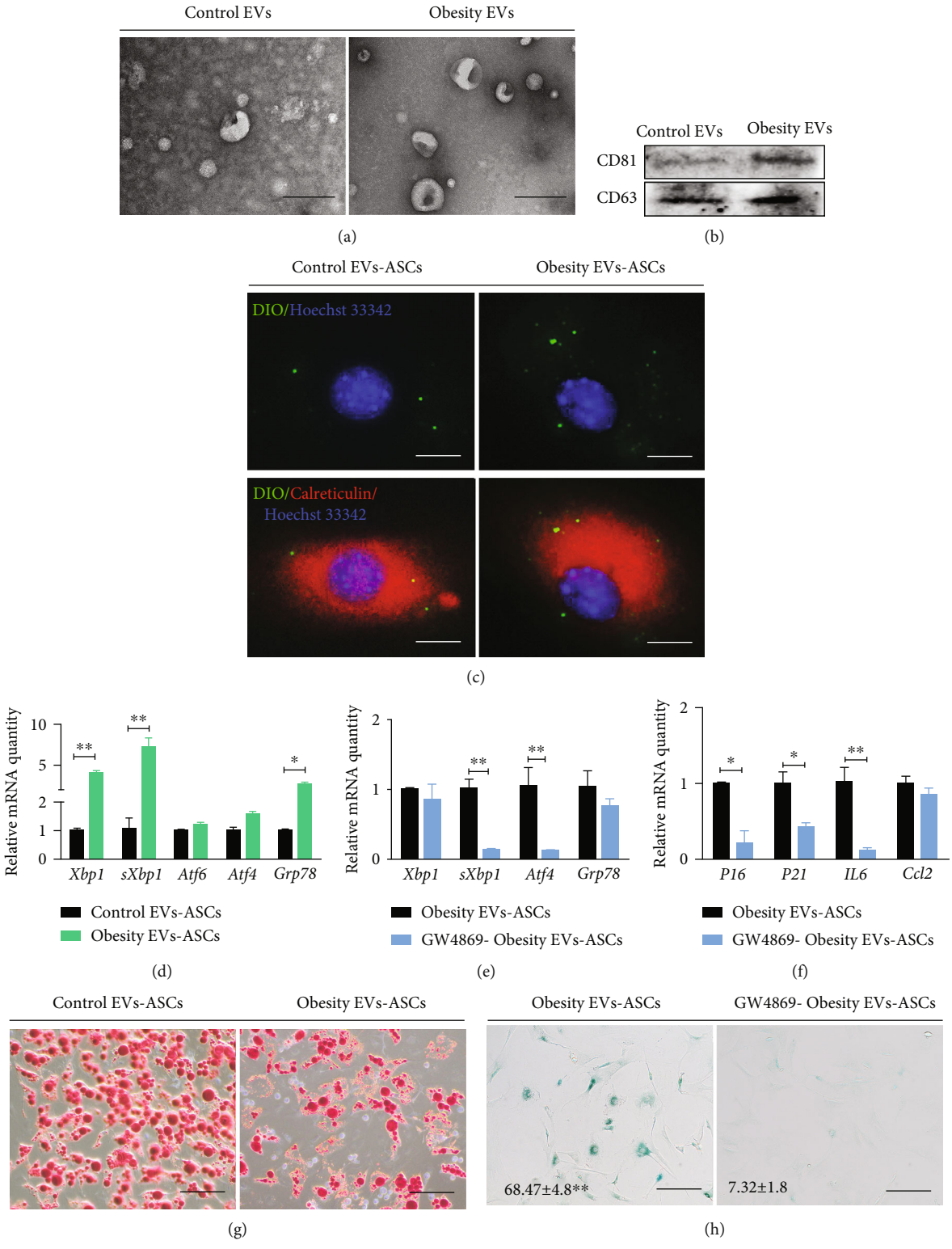

Figure 4: Continued.

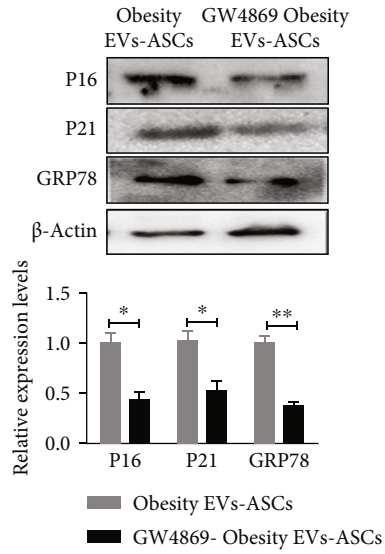

Figure 4: Effects of adipocyte-secreted EVs on ASCs senescence and ER stress. (a) Transmission electron microscopy showed that the EVs of control and hypertrophic obesity adipocytes presented with the typical morphology. Bar = 200 nm. (b) Western blot on EV markers for control and hypertrophic obesity adipocyte-secreted EVs. (c) Immunofluorescence staining of ER marker Calreticulin in ASCs pretreated with DiO-labeled EVs from control and hypertrophic obesity adipocytes. Bar = 50 μm. (d) QRT-PCR analysis of the relative mRNA expression of ER stress-related genes in ASCs pretreated with EVs secreted by control and hypertrophic obesity adipocytes. (e, f) QRT-PCR analysis of the relative mRNA expression of ER stress and senescence markers in hypertrophic obesity adipocyte-derived EVs cocultured ASCs and GW4869 pretreated hypertrophic obesity adipocyte-derived EVs cocultured ASCs. (g) Oil red O staining of adipogenic-induced ASCs pretreated with EVs secreted by control and hypertrophic obesity adipocytes. Bar = 100 μm. (h) SA-β-gal staining of hypertrophic obesity adipocyte-derived EVs cocultured ASCs and GW4869 pretreated hypertrophic obesity adipocyte-derived EVs cocultured ASCs. Bar = 100 μm. (i) Western blot and multiple quantifications of P16, P21, and GRP78 in hypertrophic obesity adipocyte-derived EVs cocultured ASCs and GW4869 pretreated hypertrophic obesity adipocyte-derived EVs cocultured ASCs.

cells [17]. The senescence of mesenchymal progenitor/precursor cells may be the cause of adipose differentiation failure and responsible for adipocyte hypertrophy in adult individuals [18]. To demonstrate the prevalence of this view on diet-induced adult obesity, we fed adult mice a high-fat diet to create hypertrophy obesity mouse model. Similar results were observed in the senescence and differentiation inhibition of ASCs in the obesity mouse model.

In line with the prolongevity effect of ER stress inhibitors, ER stress has been described as a typical feature of molecular aging and that it accelerates aging across species [19]. Evidence suggests that ER stress-induced unfolded protein response (UPR) is not only an outcome but also an inducer of cellular senescence [20]. The IRE1 and ATF6 branch of the UPR control SASP through NF-κB signaling and regulate the flat morphology of replicative senescence cells [20, 21]. The uncontrollable aggregation of unfolded or misfolded proteins is induced by electron leakage and reactive oxygen species (ROS) accumulation increases with age and activates ER stress, which induces many age-related and metabolic diseases, such as T2D.

Given that ER is the main site for the assembly and secretion of adipokines, ER stress plays an important role in adipocytes [22, 23]. Metabolic stress caused by excessive fatty acids and toxic lipids, including ceramides and palmitates, exerts cytotoxic effects on the ER [24]. Free fatty acids directly affect the ordering of the ER membrane and blockage of the ER-specific Ca^{2+}–ATPase pump and increase adipocyte ROS production, a pathogenic event that can inhibit ER–Ca^{2+} channels and induce ER stress [25]. ER stress is higher in the adipose tissues of mice and humans with obesity, and reducing ER stress improves IR in obesity models [26, 27]. The results of the present study confirm that ER stress increases not only in the adipocytes of obese mice but also in ASCs. We also observed that ER stress can be transferred from adipocytes to ASCs, similar to previously reported ER stress transfer in tumor microenvironment [11, 12, 28]. However, most published studies have suggested that cells acquire ER stress by soluble factors released from cancer cells, such as BMP2. We suggest that EVs from adipocytes are also mediators that cause ER stress transmission. Studies have reported that EVs can enter cells through the filopodia, and that endocytic vesicles with high efficiency are targeted for ER scanning and probably release cargoes [29]. EV-treated cells display a dilated ER and an increased ER stress level [12, 30], consistent with our observations.

In the present study, iron transfer through EVs from adipose cells triggered ER stress and senescence in ASCs. Iron has prooxidant properties owing to its redox activity. Therefore, iron plays vital roles in oxygen transport, electron transfer, and cell growth and differentiation. Iron accumulation can increase the aggregation of toxic proteins and induce oxidative stress and inflammation through the Fenton reaction, which lead to cellular damage and accelerate

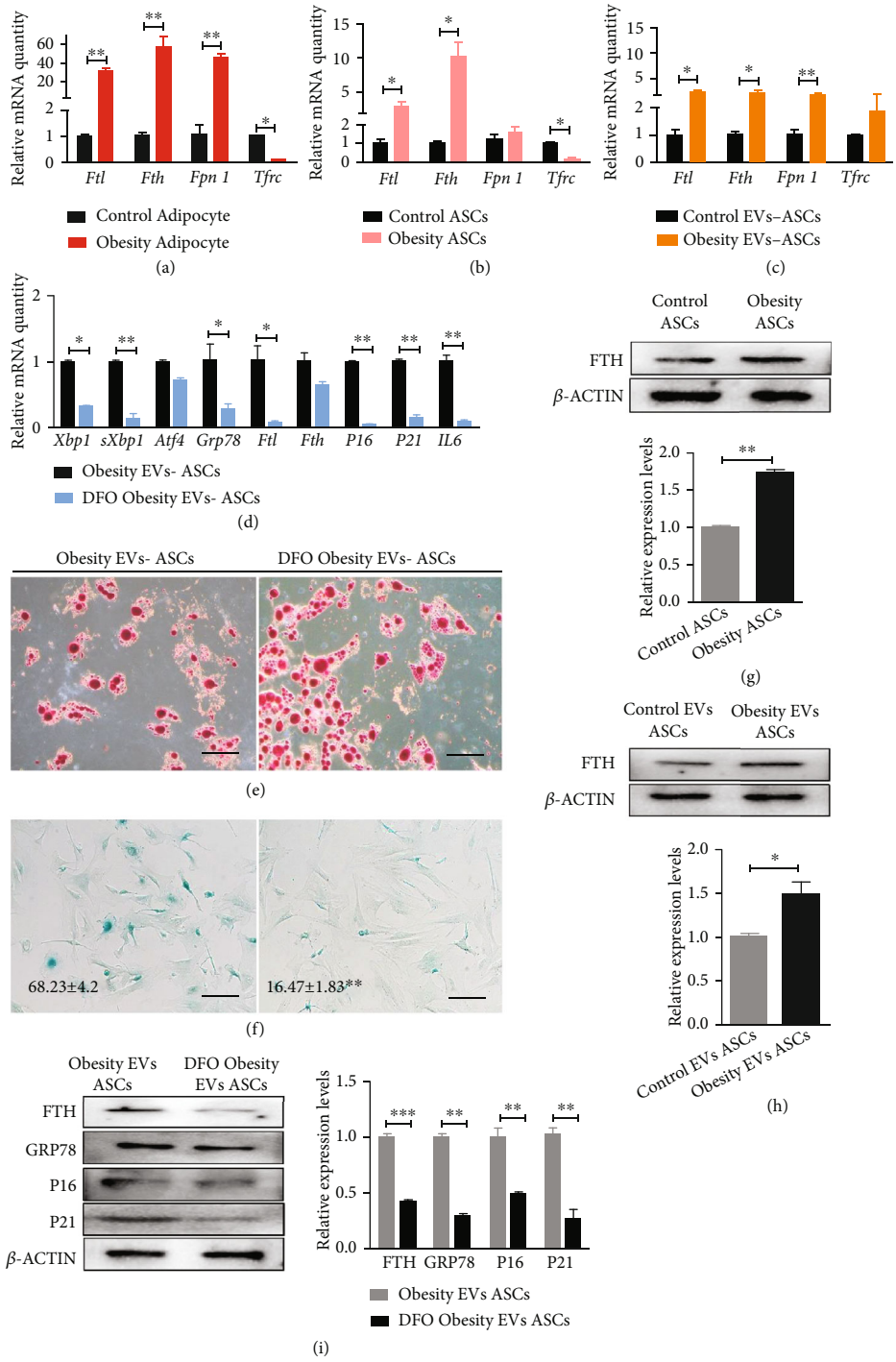

Figure 5: Effects of iron in adipocyte-derived EVs on ASC senescence and ER stress. (a) QRT-PCR analysis of the relative mRNA expression of iron-related genes in control and hypertrophic obesity adipocytes. (b) QRT-PCR analysis of the relative mRNA expression of iron-related genes in control and hypertrophic obesity ASCs. (c) QRT-PCR analysis of the relative mRNA expression of iron-related genes in control and hypertrophic obesity adipocyte-derived EVs cocultured ASCs. (d) QRT-PCR analysis of the relative mRNA expression of ER stress-related genes, senescence, and SASP-related genes in hypertrophic obesity adipocytes and DFO pretreated hypertrophic obesity adipocyte-derived EVs cocultured ASCs. (e) Oil red O staining of adipogenic-induced ASCs cocultured with EVs secreted by hypertrophic obesity adipocytes and DFO pretreated hypertrophic obesity adipocytes. Bar = 100 μm. (f) SA-β-gal staining of ASCs cocultured with EVs secreted by hypertrophic obesity adipocytes and DFO pretreated hypertrophic obesity adipocytes. Bar = 100 μm. (g) Western blot and multiple quantifications of iron-related protein in control and hypertrophic obesity ASCs. (h) Western blot and multiple quantifications of iron-related protein in control and hypertrophic obesity adipocyte-derived EVs cocultured ASCs. (i) Western blot and multiple quantifications of ER stress, senescence, and iron-related proteins in ASCs treated with EVs secreted by hypertrophic obesity adipocytes and DFO pretreated hypertrophic obesity adipocytes.

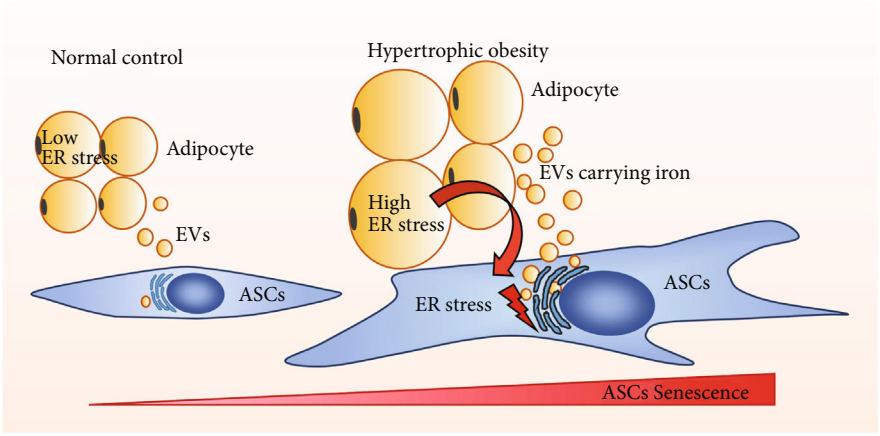

Figure 6: Mode of transmissible ER stress promoting ASC senescence. High level of ER stress in hypertrophic obesity adipocytes can be transferred to ASCs through iron carried by EVs. Senescence phenotype intensifies with increasing ER stress level in ASCs.

Table 1: Primers used in quantitative real-time PCR analysis.

Gene	Forward primer (5′-3′)	Reverse primer (5′-3′)
18S	GGTCTGTGATGCCCTTAGATGTC	GAATGGGGTTCAACGGGTTAC
Grp78	TCATCGGACGCACTTGGAA	AACCACCTTGAATGGCAAGAA
Xbp1	AGCAGCAAGTGGTGGATTTG	GAGTTTTCTCCCGTAAAAGCTGA
sXbp1	GGTCTGCTGAGTCCGCAGCAGG	AGGCTTGGTGTATACATGG
Atf4	CTCAGACAGTGAACCCAATTGG	GGCAACCTGGTCGACTTTTATT
Atf6	CCCAAGCTCTCCGCATAGTC	TAAAATGCCCCATAACTGACCAA
P16	TTGCCCATCATCATCACCT	GGGTTTTCTTGGTGAAGTTCG
P21	CACAGCTCAGTGGACTGGAA	CCACCACCACACACCATAGA
P53	GGAAATTTGTATCCCGAGTATCTG	GTCTTCCACAGTGTGATGATGGTAA
Il6	AGTTGCCTTCTTGGGACTGATG	AACTCTTTTCTCATTTCCACGATTT
Ccl2	AGGTCCCTGTCATGCTTCTGG	AGGTGAGTGGGGCGTTAACTG
Pparg	GCCCTTTGGTGACTTTATGGAG	GCAGCAGGTTGTCTTGGATG
Plin1	GCAGAGGACCCAGAAGGCTC	GCCCATGCTGTGGTTTGC
Insr	CCACCAADAACTCGTGAAAGG	TGCACGCAGGAAAGAACCT
Fth	TGCCTCCTACGTCTATCTGTCTATG	CAGTCATCACGGTCTGGTTTCTT
Ftl	TCGTCAGAATTATTCCACCGAG	CCGATCAAAAAAGAAGCCCA
Fpn1	GCTGGTATTGATTTCAGTCTCCTT	GACCACAAACAAAAATCTGGTTG
Trfc	GAGCAGGGGAAATTACTTTTGC	CTGATGACTGAGATGGCGGA

telomere shortening and senescence [31, 32]. The precise mechanisms by which ER stress is affected by changes in iron levels remains unclear. Previous studies have shown that iron chelators lower ER stress by blocking the phosphorylation of PERK and its downstream [33].

Iron is mainly found in the hemoglobin and myoglobin and present in trace amounts in enzymes, such as cytochrome, cytochrome oxidase, peroxidase, and catalase. Iron overload can activate an abnormal oxidative phosphorylation pathway in the mitochondria. Large amounts of ROS are produced during ATP production. ROS can oxidize unsaturated fatty acids on cell and organelle membranes and promote the formation of lipid peroxides, which directly or indirectly damage cell structure and function and ultimately lead to cell damage or ferroptosis [34]. Iron also regulates ferroptosis by forming enzymes involved in lipid peroxidation, such as lipoxygenase. Thus, iron input, storage, and circulation are closely related to ferroptosis. During ferroptosis, a large amount of accumulated lipid peroxides and lipid ROS are dispersed in the membrane and organelle membranes, such as mitochondrial, lysosome, and ER membranes, and destroy membrane structures [35]. The excessive accumulation of iron also occurs in senescent cells. The decrease in antioxidant capacity of senescent cells accelerates lipid peroxidation and aging of the body. This process is defined as ferrosenescence [36]. In the mitochondria, iron-mediated p53 inactivation can stimulate the iron–sulfur cluster assembly enzyme and promote iron accumulation.

Mitochondrial p53 inactivation may lead to mitochondrial DNA damage. This vicious cycle destroys mitochondrial function and accelerates aging [37].

Iron overload is associated with high risk of neurodegenerative, metabolic, and other age-related diseases. Iron in excessive amounts leads to the impaired differentiation of adipose progenitor cells [38], weight gain, adipocyte hypertrophy, adipose tissue macrophage infiltration, and IR, all of which are phenotypes of diabetogenic adipocyte [38, 39]. However, iron reduction reverses these phenotypes [40, 41]. In the present study, senescence phenotypes, ER stress, and the adipogenic differentiation potential of ASCs can be alleviated by iron chelation agents in adipocytes. Thus, the iron content of adipocytes may affect the senescence and differentiation potential for ASCs in microenvironment.

The main transport mode of iron is dependent on transferrin and its receptor system. A recent study has reported that ferritin carrying iron can be transmitted via EVs. Exosome-mediated iron secretion is a protective mechanism against ferroptotic cell death [42]. In hypertrophic adipocytes with elevated stress levels, the amount of EVs released increases [43]. This iron output may be a self-protection mechanism. This study showed that increased iron content in the adipocytes indirectly increased stress in surrounding ASCs. Therefore, iron may also play a mediating role in individual energy metabolism through intercellular transmission. However, we only carried out in vitro experiments on this phenomenon. Thus, the transmission of EVs carrying iron in the microenvironment in vivo and the resulting ER stress transmission remain unknown. In addition, iron may not be the only factor that transfers ER stress. Other EV contents, such as miRNA, may be also transmit ER stress, which needs further experimental verification in the future.

4. Conclusion

Hypertrophic adipocytes cause the aging and differentiation retardation of ASCs through transportable ER stress (Figure 6). The targeted reduction of EV secretion or iron output with hypertrophic adipocytes may contribute to the treatment of hypertrophic obesity and IR.

5. Methods and Materials

5.1. Cell Isolation and Culture. ASCs and adipocytes were isolated from the subcutaneous inguinal white adipose tissues of mice with collagenase type I solution (Roche Diagnostics, Switzerland). Adipocytes were obtained in the upper layer of the tissue digests. ASCs isolated from the stromal vascular fraction (SVF) in the bottom layer. ASCs and adipocytes were cultured in α-MEM or DM/F12 (Invitrogen, Carlsbad, CA) supplemented with 10% FBS (HyClone, USA), 2 mM L-glutamine, and 1% nonessential amino acids (Invitrogen) in a humid atmosphere with 5% CO_2 at 37°C. Cells were dissociated every 2 days with trypsin- EDTA (Invitrogen, USA). ASCs were identified by flow cytometry for positive markers CD73, CD90, and negative markers CD34 and CD45.

5.2. Adipogenic Differentiation of ASCs In Vitro. For inducing adipogenic differentiation, 2×10^4 cells were seeded into 12-well plates and induced by solution A and B alternate every three days for 14 days. Solution A was α-MEM consisting of 10% FBS, 1 μM dexamethasone, 1 μg/mL insulin, and 0.1 mM indomethacin. Solution B was α-MEM consisting of 10% FBS, 1 μM dexamethasone, 1 μg/mL insulin, 2 μM rosiglitazone, and 0.1 mM indomethacin (Sigma-Aldrich, St. Louis, MO, USA). Adipogenic differentiation was identified by Oil red O staining.

5.3. Chondrogenic Differentiation of ASCs In Vitro. 2×10^5 ASCs were seeded into 35 mm suspension culture plates with 1 ml chondrogenesis differentiation medium. Chondrogenesis differentiation medium consists of α-MEM, 10% FBS, 40 ng/mL dexamethasone, 50 μg/mL ascorbic acid, 50 μg/mL L-proline, 1 mmol/L sodium pyruvate (all Sigma-Aldrich), insulin-transferrin-selenium X (Gibco, Carlsbad, California, USA), and 10 ng/mL transforming growth factor-β3 (PeproTech, Rocky Hill, NJ, USA) for 7 days. The chondrogenesis differentiation medium was changed every 2 days. Chondrogenic differentiation was identified by Alcian blue staining.

5.4. Osteogenic Differentiation of ASCs In Vitro. To induce osteogenic differentiation, 2×10^4 cells were seeded into 12-well plates induced by α-MEM consisting of 10% FBS, 100 nmol/L dexamethasone, 30 μg/mL ascorbic acid, and 10 mmol/L β-glycerophosphate (Sigma-Aldrich, St. Louis, MO, USA) for 7 days. Osteogenic differentiation was identified by Alizarin red staining.

5.5. Senescence-Associated β-Galactosidase Staining. ASCs were stained with a senescence-associated β-galactosidase (SA-β-gal) staining kit (Beyotime, China) according to the manufacturer's instructions. Fix ASCs for 15 min and wash with PBS for three times. Staining with the solution A, B, C, and X-gel mixed liquor for 10 h at 37°C. The positive rate of the SA-β-gal staining was the ratio of positive cells to the total number of cells in three different visual fields in each group.

5.6. Population Doubling Time (PDT) Determination. The population doubling time (PDT) of ASCs was estimated according to the formula $PDT = [\log 2/(\log Nt - \log N0)] \times t$. N0 indicates the number of seeded cells, Nt means the number of cells after t hours of culturing, and t stands for cell culturing time.

5.7. Telomere Length Assays. The genomic DNA of ASCs was extracted by using DNA Isolation Kit (Tiangen, China). The ratio of the telomere repeats copy number to single gene copy number (T/S) was determined using QRT-PCR in the CFX96 Real-Time PCR system. The QRT-PCR procedures were described as follows: predenaturation at 94°C for 10 min, followed by 39 cycles for 15 s at 94°C, and annealing for 1 min at 56°C. The telomere reaction mixture consisted of 2× Quantitect Sybr Green Master Mix, 100 nmol/L of Tel-F primer (CGGTTTGTTTGGGTTTGGGTTTGGGT TTGGGTTTGGGTT), and 900 nmol/L of Tel-R primer

(GGCTTGCCTTACCCTTACCCTTACCCTTACCCTTAC CCT). 36B4 was used as the loading control, with 36B4 primer (F: ACTGGTCTAGGACCCGAGAAG, R: TCAA TGGTGCCTCTGGAGATT). Comparative CT values from QRT-PCR were used to draw the standard curve of control DNA samples of different concentrations. DNA quantitation of each gene can be calculated by using standard curve. The T/S ratio of each sample was calculated by dividing the average telomere ngDNA by the average 36B4 ngDNA value.

5.8. Quantitative Real-Time PCR Analysis. Trizol reagent (Takara, Japan) was used to extract the total RNA of ASCs according to the manufacturer's instructions. RNA was reverse transcripted into cDNA by using Reverse Transcriptase Reagent kit (Takara, Japan) according to the manufacturer's instructions. The quantitative real-time PCR (QRT-PCR) was carried on in the CFX96 Real-Time PCR system, and the QRT-PCR procedures were described as follows: predenaturation at 94°C for 5 min, followed by 39 cycles for 30 s at 94°C, and annealing for 30 s at 58°C and 30 s at 72°C for extending. 18S ribosomal RNA gene was used as the loading control. Comparative CT values from QRT-PCR were to measure relative gene expression. Primers are listed in Table 1.

5.9. EV Isolation and Uptake of DiO-Labeled EVs by ASCs. Conditioned medium from 2×10^6 ASCs was collected and passed through a 0.8 μm vacuum filter (Millipore, USA). According to the manufacturer's instruction, the EVs were collected with exoEasy Maxi Kit (Qiagen, Germany) to a final volume of 100 μl and stored at -80°C for further analysis. EVs were identified by detecting tetraspanin protein CD81 and CD63 by western blots. The morphology of EVs was detected using transmission electron microscopy (Hitachi H7500 TEM, Japan).

EVs were incubated with DiO solution (Thermo, USA) for 20 min at 37°C. Excessive DiO was removed from Exosome Spin Columns (Thermo, USA). For immunocytochemistry, DiO-labeled EVs were added to the 1×10^5 ASC culture media and incubated for 3 h at 37°C.

5.10. Immunofluorescence Staining. Cells were fixed in 4% paraformaldehyde at room temperature for 10 min. After washing with phosphate-buffered saline (PBS) for three times, cells were permeabilized for 15 min with 0.1% Triton-X 100 (Sigma, USA) at RT. Cells were blocked with 5% bovine serum albumin for 30 min and incubated with primary antibodies against Calreticulin (1 : 200; Abcam, UK), at 4°C for 16 h, washed three times with PBS. Cells were incubated with secondary antibodies for 1 h at 37°C in the dark. Nucleus counterstaining was performed with 1 μg/mL Hoechst 33342 (Sigma-Aldrich), after three washing steps in PBS. Fluorescence images were obtained by IX73 fluorescence microscope (Olympus, Japan).

5.11. Western Blot Analysis. Total cell extracts were extracted with sodium dodecyl sulfate-polyacrylamide gel electrophoresis (SDS-PAGE) sample loading buffer. Cell proteins were resolved by SDS-PAGE, transferred to a polyvinylidene difluoride membrane, and probed for β-Actin (1 : 1000, Proteintech, USA), GRP78 CD63, CD81, and FTH (1 : 200; Bosterbio, USA), and P16 and P21 (1 : 200, Santa Cruz, USA). Horseradish peroxidase-conjugated anti-rabbit, anti-mouse (1 : 1000, Proteintech, USA) was used as a secondary antibody. Detection was performed using a Thermo Scientific Pierce enhanced chemiluminescence western blotting substrate (Thermo, USA). Results were analyzed by Bio-RAD ChemiDoc XRS gel imaging system (Bio-RAD, USA). The band density was determined by the Image J software (National Institutes of Health, Bethesda, USA).

5.12. Animals and Model. All procedures were performed in accordance with *Regulations for the Administration of Affairs Concerning Experimental Animals* in China and were approved by Life Science Ethics Review Committee of Zhengzhou University. Two-month-old male C57BL/6 mice were used according to Chinese Laboratory Animal Guidelines. There were 6 mice in each group. All mice were maintained under controlled light-dark cycle (12 h : 12 h lights cycle), temperature of 25 ± 1°C, and relative humidity 53 ± 2% and granted free access to standard dry chow and water. They were randomly assigned to two groups: control (low-fat diet contains 75.9% carbohydrate, 14.7% protein, and 9.4% fat) and hypertrophic obese (high-fat diet contains 20.8% carbohydrate, 18.3% protein, and 60.9% fat, in % kcal). All mice were fed in isolation cages for 16 weeks.

5.13. Statistical Analysis. One-way analysis of variance (one-way ANOVA) was used, and posttests were conducted using Newman–Keuls multiple range tests if p values were significant. Student's t-test was used in comparing only two pairs of data. All data were represented as mean ± SD, and statistical significance was expressed as follows: $^{*}p < 0.05$; $^{**}p < 0.01$; $^{***}p < 0.001$. Each group had three independent samples. All data were analyzed using the GraphPad Prism software (CA, USA) and were representative of a minimum of three different experiments.

Abbreviations

ER stress: Endoplasmic reticulum stress
EVs: Extracellular vesicles
ASCs: Adipose-derived mesenchymal stem cells
SAT: Subcutaneous adipose tissue
IR: Insulin resistance
T2D: Type 2 diabetes
TERS: Transmissible ER stress
SVF: Stromal vascular fraction
SA-β-gal: Senescence-associated β-galactosidase
PDT: Population doubling time
QRT-PCR: Quantitative real-time PCR
DFO: Desferioxamine
UPR: Unfolded protein response
ROS: Reactive oxygen species.

Data Availability

No data were used to support this study.

Ethical Approval

Animal experiments were approved by the Life Science Ethics Committee of Zhengzhou University and were performed according to the guidelines and standards of *Regulations for the Administration of Affairs Concerning Experimental Animals* in China.

Conflicts of Interest

The authors declare that they have no conflict of interest.

Acknowledgments

This work was funded by the National Natural Science Foundation of China (Grant No. 32000511), the Medical Science and Technology Joint Construction Program of Henan Province (No. LHGJ20200032), and the Scientific Startup Foundation for Doctors of Henan Provincial People's Hospital.

References

[1] A. Hammarstedt, S. Gogg, S. Hedjazifar, A. Nerstedt, and U. Smith, "Impaired adipogenesis and dysfunctional adipose tissue in human hypertrophic obesity," *Physiological Reviews*, vol. 98, no. 4, pp. 1911–1941, 2018.

[2] Q. Qiao, F. G. Bouwman, J. Renes, and E. C. M. Mariman, "An in vitro model for hypertrophic adipocytes: time-dependent adipocyte proteome and secretome changes under high glucose and high insulin conditions. Journal of cellular and molecular medicine," *Journal of Cellular and Molecular Medicine*, vol. 24, pp. 1–12, 2020.

[3] C. Graf and N. Ferrari, "Metabolic health- the role of adipo—myokines," *International Journal of Molecular Sciences*, vol. 20, no. 24, p. 6159, 2019.

[4] G. Xuan, S. Carlos, and D. J. Freeman, "Extracellular vesicles from adipose tissue—a potential role in obesity and type 2 diabetes?," *Frontiers in Endocrinology*, vol. 8, p. 202, 2017.

[5] R. Isaac, F. C. G. Reis, W. Ying, and J. M. Olefsky, "Exosomes as mediators of intercellular crosstalk in metabolism," *Cell Metabolism*, vol. 33, no. 9, pp. 1744–1762, 2021.

[6] N. Akbar, V. Azzimato, R. P. Choudhury, and M. Aouadi, "Extracellular vesicles in metabolic disease," *Diabetologia*, vol. 62, no. 12, pp. 2179–2187, 2019.

[7] P. Samadi, S. Saki, H. Manoochehri, and M. Sheykhhasan, "Therapeutic applications of mesenchymal stem cells: a comprehensive review," *Current Stem Cell Research & Therapy*, vol. 16, no. 3, pp. 323–353, 2021.

[8] D. Merrick, A. Sakers, Z. Irgebay et al., "Identification of a mesenchymal progenitor cell hierarchy in adipose tissue," *Science*, vol. 364, no. 6438, article eaav2501, 2019.

[9] K. Eckel-Mahan, A. Ribas Latre, and M. G. Kolonin, "Adipose stromal cell expansion and exhaustion: mechanisms and consequences," *Cell*, vol. 9, no. 4, p. 863, 2020.

[10] Y. Nakatani, H. Kaneto, D. Kawamori et al., "Involvement of endoplasmic reticulum stress in insulin resistance and diabetes," *The Journal of Biological Chemistry*, vol. 280, no. 1, pp. 847–851, 2005.

[11] J. J. Rodvold, N. R. Mahadevan, and M. Zanetti, "Immune modulation by ER stress and inflammation in the tumor microenvironment," *Cancer Letters*, vol. 380, no. 1, pp. 227–236, 2016.

[12] B. Doron, S. Abdelhamed, J. T. Butler, S. K. Hashmi, T. M. Horton, and P. Kurre, "Transmissible ER stress reconfigures the AML bone marrow compartment," *Leukemia*, vol. 33, no. 4, pp. 918–930, 2019.

[13] J. Fang, Y. Yan, X. Teng et al., "Melatonin prevents senescence of canine adipose-derived mesenchymal stem cells through activating NRF2 and inhibiting ER stress," *Aging (Albany NY)*, vol. 10, no. 10, pp. 2954–2972, 2018.

[14] S. Masaldan, S. A. S. Clatworthy, C. Gamell et al., "Iron accumulation in senescent cells is coupled with impaired ferritinophagy and inhibition of ferroptosis," *Redox Biology*, vol. 14, pp. 100–115, 2018.

[15] M. K. Ameka and A. H. Hasty, "Fat and Iron Don't Mix," *Immunometabolism*, vol. 2, no. 4, p. e200034, 2020.

[16] N. Liao, Y. Zheng, H. Xie et al., "Adipose tissue-derived stem cells ameliorate hyperglycemia, insulin resistance and liver fibrosis in the type 2 diabetic rats," *Stem Cell Research & Therapy*, vol. 8, no. 1, p. 286, 2017.

[17] B. Gustafson, A. Nerstedt, and U. Smith, "Reduced subcutaneous adipogenesis in human hypertrophic obesity is linked to senescent precursor cells," *Nature Communications*, vol. 10, no. 1, p. 757, 2019.

[18] M. Alicka, P. Major, M. Wysocki, and K. Marycz, "Adipose-derived mesenchymal stem cells isolated from patients with type 2 diabetes show reduced "stemness" through an altered secretome profile, impaired anti-oxidative protection, and mitochondrial dynamics deterioration," *Journal of Clinical Medicine*, vol. 8, no. 6, p. 765, 2019.

[19] H. L. Kang, S. Benzer, and K. T. Min, "Life extension in drosophila by feeding a drug," *Proceedings. National Academy of Sciences. United States of America*, vol. 99, no. 2, pp. 838–843, 2002.

[20] O. Pluquet, A. Pourtier, and C. Abbadie, "The unfolded protein response and cellular senescence. A review in the theme: cellular mechanisms of endoplasmic reticulum stress signaling in health and disease," *American Journal of Physiology. Cell Physiology*, vol. 308, no. 6, pp. C415–C425, 2015.

[21] M. Oubaha, K. Miloudi, A. Dejda et al., "Senescence-associated secretory phenotype contributes to pathological angiogenesis in retinopathy," *Science Translational Medicine*, vol. 8, no. 362, p. 362ra144, 2016.

[22] I. Hapala, E. Marza, and T. Ferreira, "Is fat so bad? Modulation of endoplasmic reticulum stress by lipid droplet formation," *Biology of the Cell*, vol. 103, no. 6, pp. 271–285, 2011.

[23] I. Torre-Villalvazo, A. E. Bunt, G. Alemán et al., "Adiponectin synthesis and secretion by subcutaneous adipose tissue is impaired during obesity by endoplasmic reticulum stress," *Journal of Cellular Biochemistry*, vol. 119, no. 7, pp. 5970–5984, 2018.

[24] E. Kakazu, A. S. Mauer, M. Yin, and H. Malhi, "Hepatocytes release ceramide-enriched pro-inflammatory extracellular vesicles in an IRE1α-dependent manner," *Journal of Lipid Research*, vol. 57, no. 2, pp. 233–245, 2016.

[25] T. Plötz, A. von Hanstein, B. Krümmel, A. Laporte, I. Mehmeti, and S. Lenzen, "Structure-toxicity relationships of saturated and unsaturated free fatty acids for elucidating the lipotoxic effects in human EndoC-βH1 beta-cells," *Biochimica et Biophysica Acta - Molecular Basis of Disease*, vol. 1865, no. 11, p. 165525, 2019.

[26] N. Kawasaki, R. Asada, A. Saito, S. Kanemoto, and K. Imaizumi, "Obesity-induced endoplasmic reticulum stress causes chronic inflammation in adipose tissue," *Scientific Reports*, vol. 2, no. 1, p. 799, 2012.

[27] Y. Chen, Z. Wu, S. Zhao, and R. Xiang, "Chemical chaperones reduce ER stress and adipose tissue inflammation in high fat diet-induced mouse model of obesity," *Scientific Reports*, vol. 6, no. 1, p. 27486, 2016.

[28] J. J. Rodvold, K. T. Chiu, N. Hiramatsu et al., "Intercellular transmission of the unfolded protein response promotes survival and drug resistance in cancer cells," *Science Signaling*, vol. 10, no. 482, p. eaah7177, 2017.

[29] W. Heusermann, J. Hean, D. Trojer et al., "Exosomes surf on filopodia to enter cells at endocytic hot spots, traffic within endosomes, and are targeted to the ER," *The Journal of Cell Biology*, vol. 213, no. 2, pp. 173–184, 2016.

[30] C. H. Wu, J. Li, L. Li et al., "Extracellular vesicles derived from natural killer cells use multiple cytotoxic proteins and killing mechanisms to target cancer cells," *Journal of Extracellular Vesicles*, vol. 8, no. 1, p. 1588538, 2019.

[31] N. Nanthatanti, A. Tantiworawit, P. Piriyakhuntorn, T. Rattanathammethee, and N. Chattipakorn, "Leukocyte telomere length in patients with transfusion-dependent thalassemia," *BMC Medical Genomics*, vol. 13, no. 1, p. 73, 2020.

[32] C. E. Hughes, T. K. Coody, M.-Y. Jeong, J. A. Berg, D. R. Winge, and A. L. Hughes, "Cysteine toxicity drives age-related mitochondrial decline by altering iron homeostasis," *Cell*, vol. 180, no. 2, pp. 296–310.e18, 2020.

[33] A. M. Merlot, G. M. Porter, S. Sahni, E. G. Lim, P. Peres, and D. R. Richardson, "The metastasis suppressor, NDRG1, differentially modulates the endoplasmic reticulum stress response," *Biochimica et Biophysica Acta - Molecular Basis of Disease*, vol. 1865, no. 9, pp. 2094–2110, 2019.

[34] X. Chen, C. Yu, R. Kang, G. Kroemer, and D. Tang, "Cellular degradation systems in ferroptosis," *Cell Death and Differentiation*, vol. 28, no. 4, pp. 1135–1148, 2021.

[35] B. R. Stockwell, J. P. Friedmann Angeli, H. Bayir et al., "Ferroptosis: a regulated cell death nexus linking metabolism, redox biology, and disease," *Cell*, vol. 171, no. 2, pp. 273–285, 2017.

[36] A. Sfera, K. Bullock, A. Price, L. Inderias, and C. Osorio, "Ferrosenescence: the iron age of neurodegeneration?," *Mechanisms of Ageing and Development*, vol. 174, pp. 63–75, 2018.

[37] B. Do Van, F. Gouel, A. Jonneaux et al., "Ferroptosis, a newly characterized form of cell death in Parkinson's disease that is regulated by PKC," *Neurobiology of Disease*, vol. 94, pp. 169–178, 2016.

[38] J. M. Moreno-Navarrete, F. Ortega, M. Moreno, W. Ricart, and J. M. Fernández-Real, "Fine-tuned iron availability is essential to achieve optimal adipocyte differentiation and mitochondrial biogenesis," *Diabetologia*, vol. 57, no. 9, pp. 1957–1967, 2014.

[39] A. A. Tinkov, V. S. Polyakova, and A. A. Nikonorov, "Chronic administration of iron and copper potentiates adipogenic effect of high fat diet in Wistar rats," *Biometals*, vol. 26, no. 3, pp. 447–463, 2013.

[40] H. F. Yan, Z. Y. Liu, Z. A. Guan, and C. Guo, "Deferoxamine ameliorates adipocyte dysfunction by modulating iron metabolism in ob/ob mice," *Endocrine Connections*, vol. 7, no. 4, pp. 604–616, 2018.

[41] S. Tajima, Y. Ikeda, K. Sawada et al., "Iron reduction by deferoxamine leads to amelioration of adiposity via the regulation of oxidative stress and inflammation in obese and type 2 diabetes KKAy mice," *American Journal of Physiology. Endocrinology and Metabolism*, vol. 302, no. 1, pp. E77–E86, 2012.

[42] C. W. Brown, J. J. Amante, P. Chhoy et al., "Prominin2 drives ferroptosis resistance by stimulating iron export," *Developmental Cell*, vol. 51, no. 5, pp. 575–586.e4, 2019.

[43] S. E. Flaherty, A. Grijalva, X. Xu, E. Ables, A. Nomani, and A. W. Ferrante, "A lipase-independent pathway of lipid release and immune modulation by adipocytes," *Science*, vol. 363, no. 6430, pp. 989–993, 2019.

Hindawi
Oxidative Medicine and Cellular Longevity
Volume 2022, Article ID 3087916, 12 pages
https://doi.org/10.1155/2022/3087916

Review Article

HDAC4 Inhibitors as Antivascular Senescence Therapeutics

Chuoji Huang,[1,2] **Zhongxiao Lin**,[1,2] **Xiaoyan Liu**,[1,2] **Qian Ding**,[1,2] **Jianghong Cai**,[1,2] **Zhongyi Zhang**,[1,2] **Peter Rose**,[3] **and Yi Zhun Zhu**[1,2]

[1]*State Key Laboratory of Quality Research in Chinese Medicine and School of Pharmacy, Macau University of Science and Technology, Macau 999078, China*
[2]*Shanghai Key Laboratory of Bioactive Small Molecules, Department of Pharmacology, School of Pharmacy, Fudan University, Shanghai 201203, China*
[3]*School of Biosciences, University of Nottingham, Loughborough, Leicestershire, UK*

Correspondence should be addressed to Yi Zhun Zhu; yzzhu@must.edu.mo

Received 19 March 2022; Revised 3 June 2022; Accepted 8 June 2022; Published 29 June 2022

Academic Editor: Milena Georgieva

Aging is an inevitable consequence of life, and during this process, the epigenetic landscape changes and reactive oxygen species (ROS) accumulation increases. Inevitably, these changes are common in many age-related diseases, including neurodegeneration, hypertension, and cardiovascular diseases. In the current research, histone deacetylation 4 (HDAC4) was studied as a potential therapeutic target in vascular senescence. HDAC4 is a specific class II histone deacetylation protein that participates in epigenetic modifications and deacetylation of heat shock proteins and various transcription factors. There is increasing evidence to support that HDAC4 is a potential therapeutic target, and developments in the synthesis and testing of HDAC4 inhibitors are now gaining interest from academia and the pharmaceutical industry.

1. Introduction

Despite gains in average life expectancy, the aging process poses many challenges in the management of age-related diseases such as neurodegeneration and cardiovascular diseases (CVDs). Neurodegenerative diseases have become the most debilitating maladies in older people with risk increasing with advancing age [1]. Neurodegeneration has both hereditary and biochemical traits resulting in progressive degeneration of neurons [2]. Similarly, CVDs are responsible for approximately 4 million deaths each year in China and 17.9 million worldwide [3]. CVDs are caused by multiple factors including epigenetic modification and reactive oxygen species (ROS) [4–6]. Elevations in ROS are widely associated with aging and diseases being produced by four systems including NOX xanthine oxidases, myeloperoxidase, and nitric oxide synthases (NOS) [7–10]. Among these, NOX and NOS are associated with age-related diseases, DNA damage, and mitochondrion dysfunction, therefore influencing epigenetic change.

Genetic inheritance plays an important role in longevity and in age-related diseases [1]. Oxidation or histone acetylation results in altered protein homeostasis, DNA damage, and epigenetic changes, occurring in aged tissues [11]. Histone acetyltransferases (HATs) and histone deacetylases (HDACs) are two classes of enzymes regulating histone acetylation and deacetylation. Deacetylation of HDACs results in positive charges in the condensation of chromatin and thereby turns off gene transcription [12]. Among the HDAC superfamilies, HDAC4 is of interest since this enzyme is located both in the nucleus and cytoplasm and may act on more than simply cellular histones. This factor alone suggests that HDAC4 could have the potential in the treatment of neurodegeneration or CVDs.

1.1. The Subcellular Location and Substrates of HDAC4. In mammals, there are 18 types of HDACs recognized, and these are divided into classes I, II, III, and IV based on structure and homology with yeast HDACs. Class I types consist of HDACs 1, 2, 3, and 8, which are expressed and located in

the nucleus [13]. Class III is composed of a family of sirtuins, and their activation is dependent on NAD^+. HDAC11 is the only member of class IV and having structural similarities to class I HDACs. Class II proteins can be further divided into two subgroups: class IIa (HDACs 4, 5, 7, and 9) and class IIb consisting of HDACs 6 and 10. Interestingly, only class II HDACs exhibit tissue-specific patterns of expression. For example, HDAC4, which will be mainly discussed in this paper, is highly expressed in the brain, heart, and skeletal muscle [14].

In contrast to class I HDACs, HDAC4 shuttles between the nucleus and cytoplasm. The location of HDAC4 plays an important function in dictating the physiology and pathological role of this protein within cells and tissues. HDAC4 has the tendency to be maintained in the cytoplasm in neurons and in the nucleus of myoblasts. The key to the subcellular location of HDAC4 is its phosphorylation status. Phosphorylated HDAC4 binds to the chaperone protein 14-3-3, inducing nuclear export [15]. Phosphorylation of HDAC4 can be mediated by a diverse array of kinases, namely, calcium/calmodulin-dependent protein kinase (CaMK) [16], extracellular signal-regulated kinases 1 and 2 (ERK1/2) [16], protein kinase A (PKA), and glycogen synthase kinase 3 (GSK3) [17]. CaMK play a significant role in the maintenance of neurons and in the export of HDAC4 driven by calcium influx induced by synaptic activity in neurons [18]. Serine residues at positions 210, 246, 350, 467, and 632 are key phosphorylation sites in this protein [16, 19]. In addition, ROS can also induce nuclear export. In this instance, NOX4 produces H_2O_2 which directly oxidizes cysteine residues 274/276 in DnaJb5 and cysteine-667/669 in HDAC4, to promote nuclear targeting of HDAC4 export [20, 21]. Interestingly, proteolytic cleavage can also influence the location of HDAC4 in cells. Following cleavage by caspases, HDAC4 leaves the nuclear localization signal containing fragments accumulated in the nucleus [22, 23]. The fragments lose the C-terminal catalytic domain but retain the combination with MEF2C. Moreover, the fragments show an increased repressive effect on Runx2- and SRF-dependent transcription (Figure 1) [24].

Consistent with its cellular location, HDAC4 is involved in removing acetyl groups from both histones and nonhistone proteins with a zinc-containing catalytic domain. Unlike class I HDACs, HDAC4 only gains deacetylase activity only when interacting with HDAC3 and RbAp48 [15]. The catalytic domain tends to form a multiprotein functional complex. Deacetylation of histone H3 and histone H4 suppresses gene expression. In addition, heat shock protein 70 (Hsp70) can be acetylated at lysine 77. Hsp70 is acetylated by ARD1 in the early cellular stress response and deacetylated by HDAC4 in the late. Deacetylated Hsp70 contributes to protein degradation [25]. Transcription factors are another kind of substrates deacetylated by HDAC4. Runx-2 and HIF-1α are known transcription factors being deacetylated by HDAC4. Acetylated Runx-2 inhibits Smurf1-mediated degradation, but deacetylated HIF-1α shows increased stability (Figure 2) [26–29].

In addition to its catalytic function, HDAC4 can directly interact with other cellular proteins. For example, HDAC4 directly binds to and represses MEF2-mediated expression of GATA4 and Nkx2-5. As a result, HDAC4 prevents myogenesis. The repression of gene transcription by the MEF-2/HDAC complexes is suppressed due to CaMK-induced translocation of HDAC4 and HDAC5 to the cytoplasm.

2. HDAC4 Promotes Age-Related Diseases

Numerous studies show that HDAC4 has a broad interaction with different kinds of proteins and is involved in several physiological pathways such as myogenesis and oxidative stress. This sensitive balance means that HDAC4 plays important roles in growth and development. However, dysfunction of HDAC4, which often occurs during aging, may precipitate conditions like hypertension, cardiovascular diseases (CVDs), and neurodegeneration.

Vascular calcification is the pathological accumulation of calcium phosphate crystals in the medial and intimal layers of vascular walls and is tightly linked with metabolic diseases such as chronic kidney disease, diabetes, and vascular diseases viz. atherosclerosis [30]. Pathologically, there are two major forms of vascular calcification with both existing in the same clinical condition. The first type is intimal calcification associated with atherosclerosis-linked lipid and cholesterol accumulation under the injured endothelium. The second type is medial calcification, also known as Mönckeberg's sclerosis, which involves the deposition of minerals within the vascular smooth muscle layers [31]. Ting and colleagues revealed novel findings on the involvement of HDACs and their modifiers in the development of vascular calcification. In human aortic smooth muscle cells, inhibition of HDAC mitigates the effect of Notch protein to increase smooth muscle α-actin levels, indicating that HDAC activity is required for Notch signaling during differentiation [32]. HDAC4 and HDAC5 are regulated in a CaMKII-dependent manner in vascular smooth muscle cells [33, 34]. Inhibition of HDAC using butyrate abrogates the activation of Akt. This results in differential effects on the downstream targets of Akt, promoting signaling cross-talk and resulting in vascular smooth muscle growth through proliferation arrest [35]. RUNX2 is one of the downstream targets of Akt signaling via hydrogen peroxide activation and has an increased expression level in vascular calcification [36]. HIF-1α promotes the calcification and osteogenesis of vascular smooth muscle cells to build extracellular matrix calcification. HIF-1α is downregulated by ROS scavengers and HDAC4 inhibitors [27, 37, 38]. Also, HIF-1α is reported to be a key transcription factor in mitochondrial dysfunction in hypoxia response [39]. These results show that ROS and HDAC4 have a synergistic effect on vascular aging and calcification. Researchers at Yale University have shown that HDAC activity is associated with hypertension by increasing MEF2 activity in endothelial cells following treatment with a class IIa histone deacetylase inhibitor [34]. This innovation may be valuable as a treatment solution for pulmonary hypertension, by offering a means of restoring MEF2 activity using class IIa histone deacetylase inhibitors. Therefore, the critical function of HDACs in vascular biology could be exploited to employ HDACs as a molecular target for treating hypertension [40].

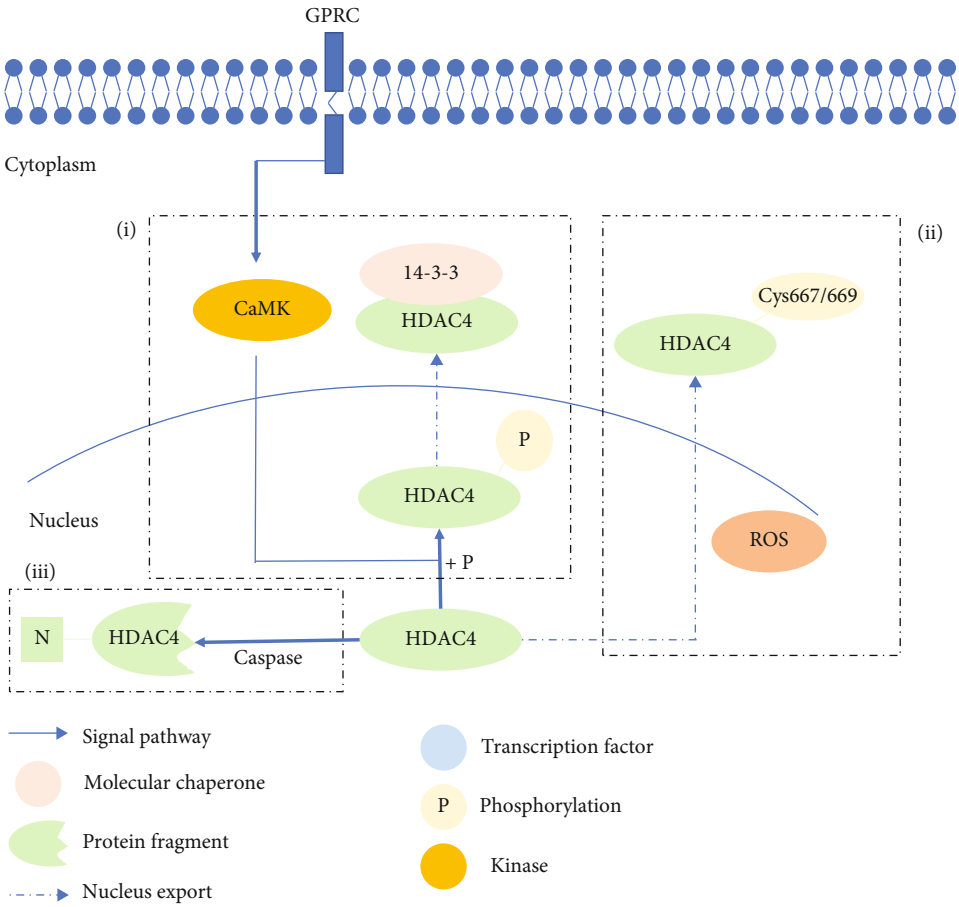

Figure 1: The scheme of HDAC4 partitioning between the nucleus and cytoplasm. (a) HDAC4 is phosphorylated by a kinase like CaMK and then combines 14-3-3, inducing nucleus export. (b) Oxidation of Cys667/669 of HDAC4 also promotes nuclear export. (c) The cleavage of HDAC4 causes N-term retention in the nucleus, and the N-terminal sequence has functional activity.

CVD is highly prevalent and is the leading cause of mortality and morbidity in developed countries. CVD refers to a broad spectrum of diseases affecting the cardiovascular system and includes the heart and blood vessels. One common condition is atherosclerosis, a progressive disease in which the inner layers of the artery walls become thick and irregular because of the deposition of fat, cholesterol, and other substances. Interestingly, HDAC4 plays a vital role in mediating cardiovascular diseases since (1) Ca^{2+}/calmodulin-dependent protein kinase- (CaMK-) II promotes hypertrophic growth via phosphorylation of HDAC4 in cultured cardiomyocytes, (2) activation of HDAC4 promotes angiotensin II-induced vascular smooth muscle hypertrophy, and (3) CaMKII-mediated cardiac hypertrophy can be altered by interfering with the HDAC4-MEF-2 signaling pathway [41]. This link is likely due to HDAC4's ability to promote reactive oxygen species- (ROS-) dependent vascular inflammation and the development of hypertension in spontaneously hypertensive rats [33]. Similarly, in a mouse model of vascular inflammation, Ang II-induced production of proinflammatory mediators, such as IL-6, VCAM-1, COX2, and iNOS, is attenuated by knockdown of HDAC4. HDAC4 is activated by Ang II and deacetylates transcription factor FoxO3a, inducing upregulation of LC3-II, Beclin 1, and Atg5. In addition, to determine whether HDAC4 mediates the inflammatory response, Tasquinimod (Taq), an inhibitor of HDAC4, was tested [42]. The levels of proinflammatory mediators decrease significantly in rat primary endothelial cells cotreated with Ang II/Taq but increase in Ang II-treated cells. Immunofluorescence further confirmed that treatment with siRNA HDAC4 or Taq decreases the expression of HDAC4 and VCAM-1 proteins. The Ang II-induced inflammatory response is alleviated by the inhibition of HDAC4 (see Figure 3). In addition, ROS are critical components of Ang II function [43]. Among the various forms of ROS, superoxide anion ($^{\cdot}O2^{-}$), hydrogen peroxide (H_2O_2), nitric oxide (NO), and peroxynitrite ($ONOO^{-}$) are particularly important in the cardiovascular system [44]. In the cardiovascular system, NOX is the main producer of vascular ROS, and NOX4 is induced by Ang II [45]. Interestingly, NOX4-produced H_2O_2 also influences the location of HDAC4.

Vascular inflammation is significantly correlated with hypertension and CVD. Vascular injury or damage accumulated in vascular senescence also results in vascular endothelial cell proliferation and migration, causing hypertrophic growth [46]. Vascular inflammation is observed in the two situations [47]. In the first, Smyd3 (SET and MYND domain-containing protein 3), a methyltransferase inducing trimethylation of lysine 4 on histone 3 (H3K4me3),

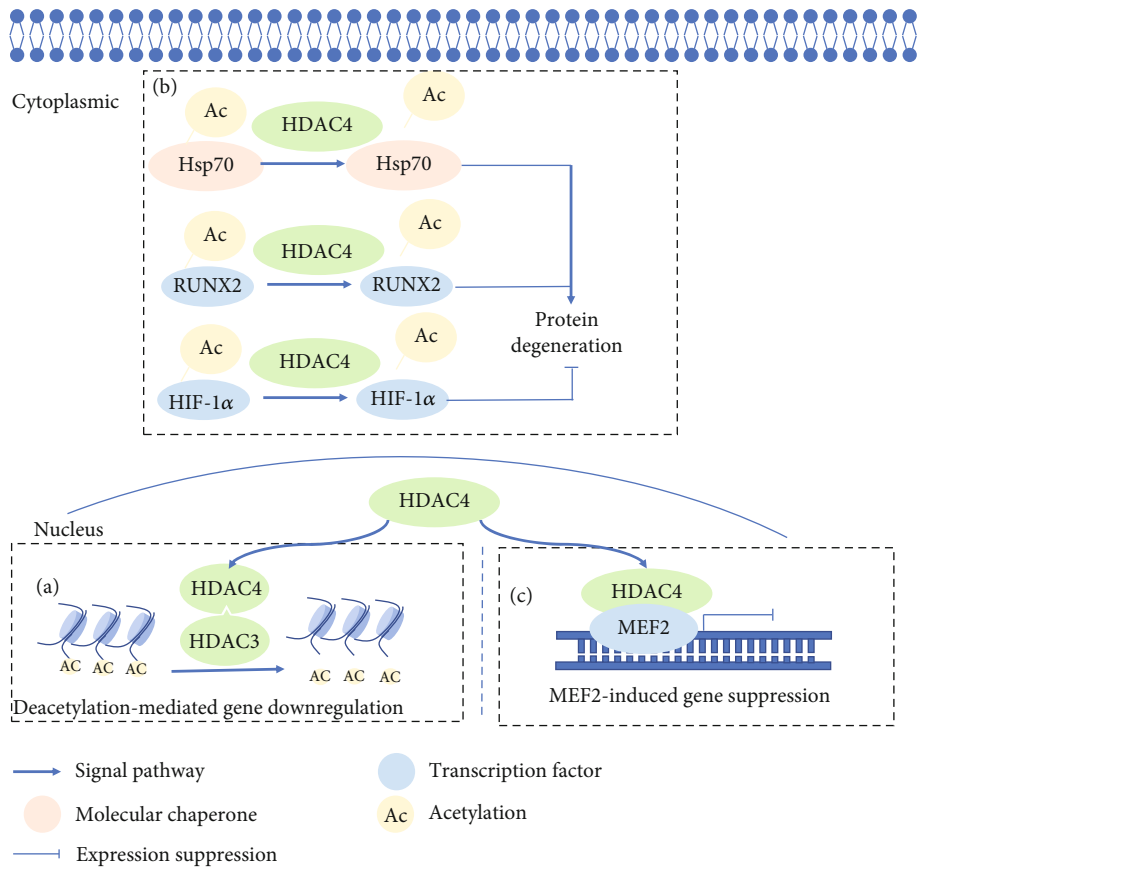

Figure 2: A schematic of HDAC4 function and interaction with cellular substrates. (a) HDAC4 deacetylates histones H3 and H4, tightening the linkage between DNA and nucleosomes and turning off gene transcription; (b) HDAC4 deacetylates nonhistone proteins like Hsp70 and transcription factors therefore altering protein degeneration; (c) HDAC4 binds to MEF2 and then suppresses gene transcription, playing a vital role in muscle-related development and diseases.

participates in Ang II-induced vascular senescence. Knockout of Smyd3 in mice can significantly alleviate Ang II-induced vascular senescence. Proinflammatory mediators such as VCAM-1 and iNOS are upregulated in Ang II-induced WT mice but blocked in Smyd3$^{-/-}$ mice [48, 49]. In a vascular injury model, JMJD3 (Jumonji domain-containing protein 3), a histone demethylase inducing demethylation of lysine 27 on histone 3 (H3K27), induces increased expression of NOX4, Atg5, Beclin 1, and iNOS, respectively. Changes in protein expression levels indicate oxidative stress and vascular inflammation (Figure 3) [50, 51].

Ang II-induced vascular injury indicates a crucial role of immune cells in disease progression. The activated macrophages and T cells regulate vascular inflammation driving vascular injury. Macrophage colony-stimulating factor (m-CSF) deficiency reduces the number of vascular macrophages in Ang II-induced endothelial dysfunction, vascular inflammation, and hypertension [52]. The evaluated expression of SMYD3 promotes the activation of ALOX-15, which acts as a marker of anti-inflammatory macrophages [53]. Meanwhile, JMJD3 is also involved in the profibrotic signature of macrophage-derived foam cells via RNA sequencing [54]. In addition, $\gamma\delta$ T cells mediate Ang II–induced vascular injury. Comparison of TCR$\delta^{-/-}$ between WT mice showed the CD4$^+$ CD69$^+$ and CD4$^+$ CD69$^+$ T cells activated in WT mice and blunting in TCR$\delta^{-/-}$ mice [55]. Vascular inflammation is also associated with many forms of neurodegenerations, including Alzheimer's disease, Parkinson's disease, and amyotrophic lateral sclerosis [56]. Alzheimer's disease (AD) is the most common form of dementia, a brain degenerative disease affecting nearly 10% of the population over 65 years of age [57, 58]. Amyloid-β (Aβ) is widely considered a key contributor to the pathophysiology of AD and induces brain inflammation. Inflammation in endothelial cells is characterized by the expression of VCAM-1 and ICAM-1. The elevated expression level of NLRP3 has been observed in human brain and model mice, activating the production of proinflammatory cytokines like IL-1β, IL-18, and gasdermin D [59, 60]. In addition, the elevated expression level of HDAC4 was confirmed in the brain of AD patients and in mouse models. Indeed, the oral administration of Taq increases the levels of Syn2 and Homer1, which are upregulated in wide mice compared to 3xTg-AD mice [61–64] (Figure 4).

In other neurodegenerative conditions like Parkinson's disease (PD), HDAC4 may also be important. PD is the second most common neurodegenerative disorder affecting approximately 0.2% of the global population and 1% of people aged over 60 [65]. In a recent case-control study involving 33 patients and 27 healthy subjects, it was shown that high expression levels of VCAM-1 and angiogenic

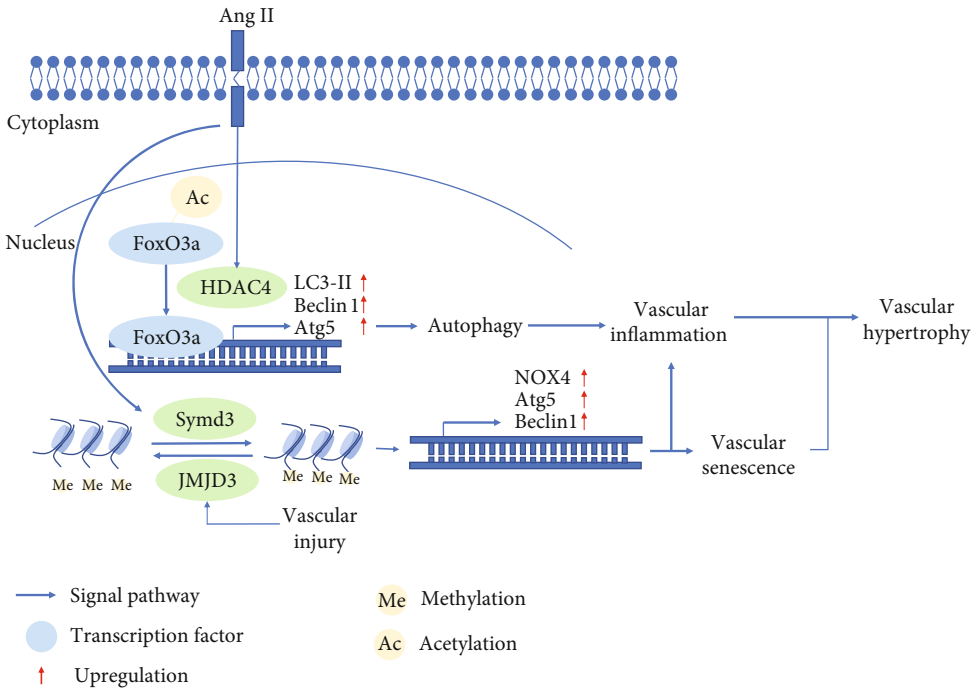

Figure 3: Epigenetic modification in vascular diseases. Ang II induces the expression of HDAC4 and Symd3. The former deacetylates FoxO3a, upregulating the levels of LC3 II, Atg5, and Beclin 1. The latter methylates H3K4 inducing NOX4, Atg5, and Beclin 1 expression. HDAC4 and Symd3 both mediate vascular inflammation and senescence. JMJD3 demethylates H3K27 and induces NOX4, Atg5, and Beclin 1 expression, resulting in the pathological features of vascular senescence and inflammation. All of these may lead to vascular hypertrophy.

microRNAs were linked to vascular inflammation [66]. The A53T mutant α-synuclein induces nuclear accumulation of HDAC4, promoting neuronal apoptosis through suppressing the activity of MEF2 [67] (Figure 4). Though there is no HDAC4 inhibitor for therapeutic purposes, the nuclear accumulation of HDAC4 discloses avenues for possible intervention using therapeutics.

In addition, other conditions like Friedreich's ataxia (FRDA), spinal muscular atrophy (SMA), and amyotrophic lateral sclerosis (ALS) are also vascular inflammation-associated neurodegenerations [68, 69]. HDAC inhibitors increase FXN expression by ~15% in FRDA and ameliorate the disease phenotype in animal models [70–73]. The severity of SMA is inversely correlated with the relative amount of SMN protein. Several inhibitors including butyrate, valproate, phenyl-butyrate, and vorinostat, class I and II HDAC inhibitors, are effective in upregulating the expression of SMN2 in fibroblasts obtained from patients suffering from SMA, which is associated with improved survival, weight loss, and motor behavior [74–78]. In ALS research, two studies revealed that the pan-HDAC inhibitor TSA or sodium phenylbutyrate ameliorates axonal degeneration leading to motoneuron-related death and enhancing the motor functions in the $SOD1^{G93A}$ mouse model [79, 80] (Figure 4).

3. The Research and Development of HDAC4 Inhibitors

HDAC4 inhibitors have been proved effective for cancer, CVDs, and neurodegeneration. The synthesis of HDAC4 inhibitors has been a subject of clinical research for several decades. The specificity of inhibitors has also developed over time from generic pan-HDAC inhibitors to the more refined class-specific inhibitors.

Trichostatin A (TSA) is an archetypal classical HDAC inhibitor, which has been used widely by researchers. TSA is a pan-HDAC inhibitor, which inhibits both class I and class II HDACs. TSA was originally reported as a fungistatic antibiotic obtained from culture broths of *Streptomyces platensis*. Other inhibitors have also been reported and include vorinostat. This compound is also known as suberoylanilide hydroxamic acid (SAHA) and was designed and optimized based on similarity to the structure of TSA. Vorinostat has been widely used to treat cutaneous T cell lymphoma. As summarized, the synthesis of SAHA indicates that natural products could be a possible source for the identification and development of highly selective HDAC4 inhibitors.

Other compounds of interest include LMK235 (N-((6-(hydroxyamino)-6-oxohexyl)oxy)-3,5-dimethylbenzamide), a potent hydroxamate-based HDAC inhibitor. LMK235 specifically inhibits HDAC4 and shows equipotent efficacy to HDAC4 as pan-HDAC inhibitors like SAHA [81]. Moreover, two class IIa HDAC inhibitors, TMP195 and TMP269, which both contain a common metal-binding group, have increased specificity [82].

Looking to the future, multifold HDAC4 inhibitors are currently in various development (R&D) pipelines. Of the available research, these molecules are showing promise in the treatment of different types of cancer, autoimmune diseases, peripheral pain, psychiatric disorders, and inflammation.

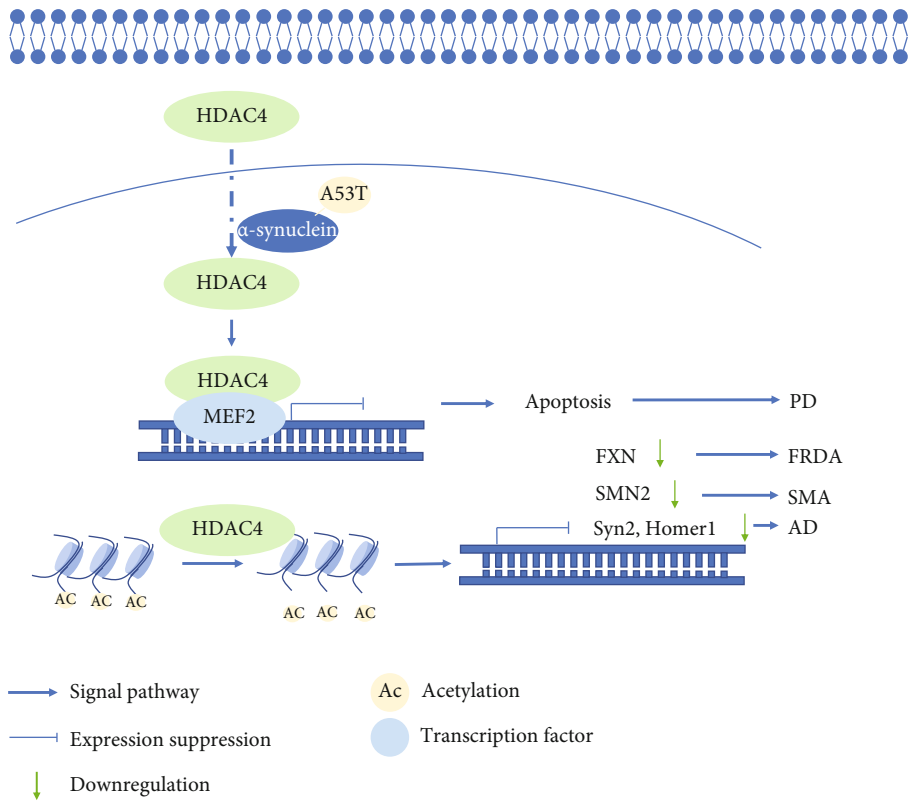

Figure 4: HDAC4 mediated neurodegeneration. HDAC4 deacetylates histones, subsequently tightens the linkage between nucleosomes and DNA, and represses the levels of FXN, SMN2, Syn2, and Homer1. These gene expression changes mediate FRDA, SMA, and AD. A53T mutant α-synuclein accumulates HDAC4 transport into the nucleus, which binds to MEF2 mediating neuron apoptosis and leading to PD.

BMN-290, an HDAC4i inhibitor developed by Scripps Research Institute and BioMarin Pharmaceutical Inc., has been assessed for the treatment of neurodegenerative diseases The compound reverses FXN silencing and is in the preclinical stage. Two other HDAC4 inhibitors, mocetinostat dihydrobromide and a class IIa HDAC inhibitor, both developed by MethylGene Inc., are undergoing extensive clinical trials for the treatment of multiple cancers including advanced solid tumor and metastatic non-small-cell lung cancer. The former compound was designed to target HDACs 4, 5, and 7, while the latter was designed as HDAC 1, 2, 3, 4, 7, and 11 inhibitors. In addition, the novel HDAC4 selective inhibitor, CHDI-00381817, is being investigated by the Cure Huntington's Disease Initiative (CHDI) foundation for its potential use in treating Huntington's disease (HD) (Table 1). These four HDAC4 inhibitors are more selective than TSA and SAHA, but some of these drugs could be further developed to enhance selectivity.

Another four HDAC4 inhibitors are under preclinical stage evaluation. SIK3 is a checkpoint inhibitor, is developed by iOmx Therapeutics AG, and is designed as a HDAC4 inhibitor. Similarly, KYAN-001, developed by Georgetown University and Kyan Therapeutics Inc., is designed as a HDAC4- and HDAC6-specific inhibitor. These two molecules are both aimed at cancer therapy. KRA-1641 is developed by Karus Therapeutics Ltd., and a histone deacetylase-4 inhibitor (oral, neurodegenerative diseases/amyotrophic lateral sclerosis) is developed by Acetylon Pharmaceuticals Inc. The two are HDAC4-specific inhibitors.

3.1. Our Work and Hypothesis. In a recent study, we collected the chemical structures of several HDAC4 inhibitors from patent documents and tried to evaluate their characteristics related to clinical use. Based on the information, we attempted to design several novel selective HDAC4 inhibitors. The structures of these HDAC4 inhibitors can be divided into four groups: A, B, C, and D, as shown in Figure 5 [79, 83]. Small molecules with structures similar to HDAC4 were considered possible HDAC4 inhibitors. Different functional groups including OCH_3, OH, $N(CH_3)_2$, NO_2, and small alkyl chains were added to the compounds to increase their affinity for HDAC4. Initially, these molecules were screened using the molecular operating environment software. The docking results obtained from the software predicted that these small molecules would inhibit HDAC4, which remains to be further confirmed by *in vitro* and *in vivo* studies.

4. Discussion

Here, we report on the role of HDAC4 and its utility as a potential therapeutic target in the treatment of age-related diseases. Histone deacetylation, nonhistone deacetylation, and protein complexes are induced by HDAC4 and

Table 1: HDAC4 inhibitors in the research and development pipelines.

Drug ID	Representative structure(s)	IC50
LMK-235	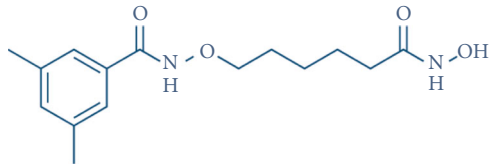	11.9 and 4.2 nM against HDAC4 and HDAC5
TMP-195	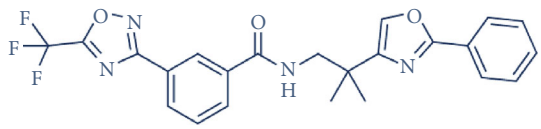	59, 60, 26, and 15 nM against HDACs 4, 5, 7, and 9
TMP-269	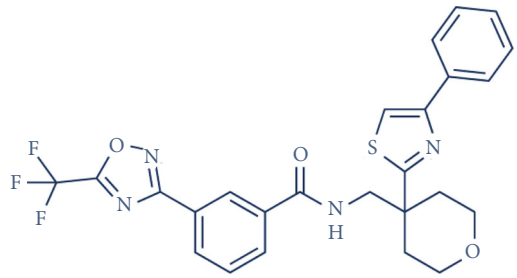	157, 97, 43, and 23 nM against HDACs 4, 5, 7, and 9
BMN-290	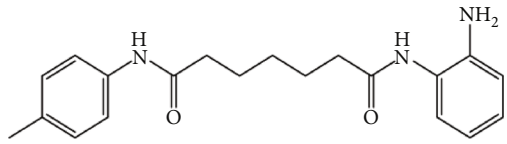	NA
Mocetinostat dihydrobromide (MG-0103)	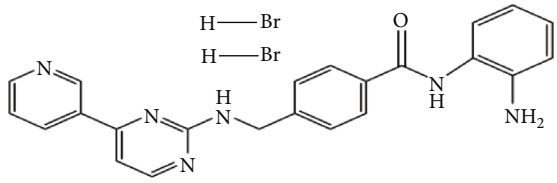	0.05, 0.2, 1, and 20 μM against HDACs 1, 2, 4, 6, and 8, respectively
Class IIa HDAC inhibitors, MethylGene	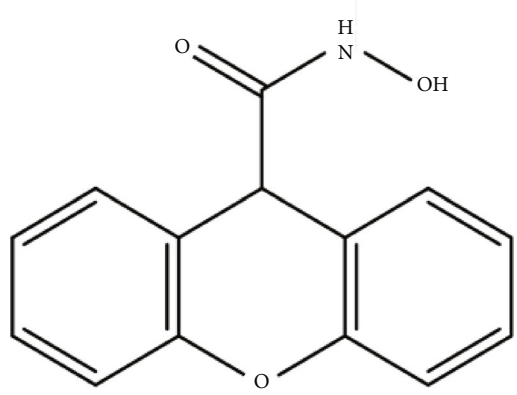	0.25, 0.11, and 0.05 μM against HDACs 4, 5, and 7, respectively

Table 1: Continued.

Drug ID	Representative structure(s)	IC50
CHDI-00381817	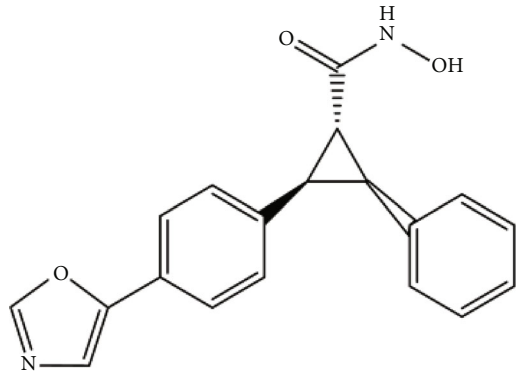	0.02 μM against HDAC4

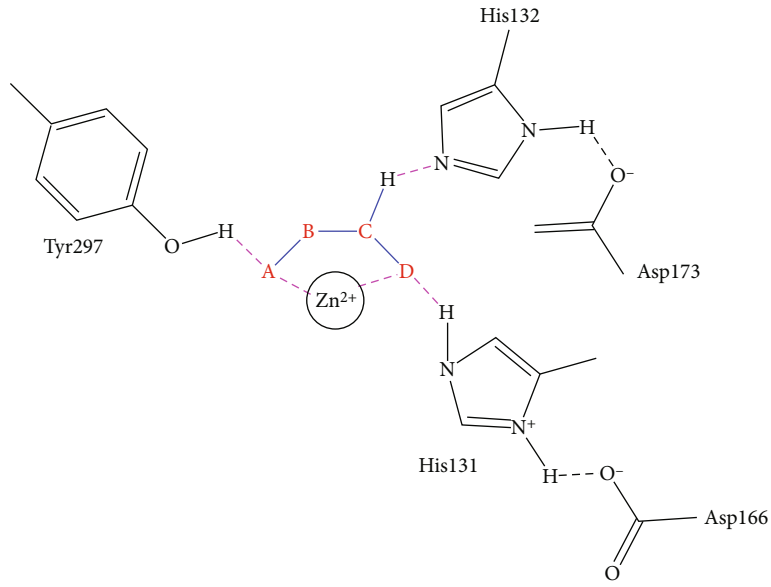

Figure 5: The structures of HDAC are divided into groups A, B, C, and D for the attachment or binding of histone deacetylases (HDACs). Group A inhibitors are soft, with nonbonding electron-pair donors that coordinate the zinc ion and H-bond acceptor to accept a hydrogen bond from tyrosine –OH. An H-bond could be donated to the phenol oxygen atom of Tyr297. Group B links the zinc-chelating moiety to the spacer and hence is at least trivalent. Group C includes H-bond donors to residue His132; consequently, they are trivalent or of higher valency. Group D includes proton donors that protonate His131, subsequently accepting an ionic H-bond from it and forming a strong interaction with the zinc ion.

participate in aging and neurodegeneration. HDAC4 is regulated by variable intercellular features including abundance, posttranscriptional regulation, and location. ROS determines HDAC4 location and accumulates in the nucleus/cytoplasm in aging and neurodegeneration. ROS induces DNA damage, apoptosis, and protein degradation, all of which cause DNA structural variation. In addition, the level of ROS is influenced by HDAC inhibitors. These mechanisms indicate associations between ROS and HDAC4.

Hypertension, CVD, and neurodegenerations are reported to be related to inflammation. Indeed, vascular inflammation is largely driven via injury and aging processes. Vascular injury induced by stroke is linked to vascular inflammation and induced PD. However, the linkage between damage accumulation along with aging and disease has not been fully explored. What is known is that the epigenetic landscape and oxidative stress are intimately linked and likely play a role in age-related diseases. It is likely that HDAC4 is important in these processes. Indeed, the activity and location of HDAC4 both act on age-related diseases. The activity of HDAC4 relates to muscle disease, and the location preferably relates to neurodegeneration. Hence, HDAC4 inhibitors may show promise as potential therapeutics.

HDAC4 inhibitors have been recognized as a potential therapeutic approach for several diseases. Small molecules with similar structures to existing HDAC4 inhibitors could

be considered possible new HDAC4 inhibitors. For example, SAHA has a similar structure to TSA. Derivatives of hydroxamate and trifluoromethyl oxadiazole should also be considered potential inhibitors. However, most HDAC4 inhibitor research and associated clinical trials largely focus on cancer treatment. Therefore, in the future, it may be timely to assess HDAC4 inhibitors in neurodegenerative conditions. Since the therapeutic drug has already been developed, potential use in neurodegenerations could be evaluated [84]. Our group also designed and synthesized novel HDAC4 inhibitors from natural products, and the work will be published soon.

The dysfunction of HDAC4 causes diseases, but normal HDAC4 plays a critical role in differentiation and development. HDAC4 is required for learning, memory, and synaptic plasticity [85]. Although the research for HDAC4 has proceeded for over 20 years, there are still lots of research gaps remaining. The lack of HDAC4-specific inhibitors and the abundant posttranscriptional regulation make the verification a complicated work. Further studies will elucidate the mechanisms of HDAC4 and provide more feasible drug design groups.

Conflicts of Interest

The authors declared that there is no conflict of interest regarding the publication of this paper.

Authors' Contributions

All authors contributed to the article and approved the submitted version.

Acknowledgments

This work was supported by the Macau Science and Technology Development Fund (FDCT (0007/2019/AKP, 0021/2020/AGJ, and 0011/2020/A1)), the funding of Innovative research team of high-level local universities in Shanghai and a key laboratory program of the Education Commission of Shanghai Municipality (ZDSYS14005) and the National Natural Science Foundation of China (No. 81973320).

References

[1] T. Wyss-Coray, "Ageing, neurodegeneration and brain rejuvenation," *Nature*, vol. 539, pp. 180–186, 2016.

[2] A. Elobeid, S. Libard, M. Leino, S. N. Popova, and I. Alafuzoff, "Altered proteins in the aging brain," *Journal of Neuropathology and Experimental Neurology*, vol. 75, no. 4, pp. 316–325, 2016.

[3] X. Li, C. Wu, J. Lu et al., "Cardiovascular risk factors in China: a nationwide population-based cohort study," *The Lancet Public Health*, vol. 5, no. 12, pp. e672–e681, 2020.

[4] B. J. North and D. A. Sinclair, "The intersection between aging and cardiovascular disease," *Circulation Research*, vol. 110, no. 8, pp. 1097–1108, 2012.

[5] W. Zhang, M. Song, J. Qu, and G. H. Liu, "Epigenetic modifications in cardiovascular aging and diseases," *Circulation Research*, vol. 123, no. 7, pp. 773–786, 2018.

[6] M. A. Evans, S. Sano, and K. Walsh, "Cardiovascular disease, aging, and clonal hematopoiesis," *Annual Review of Pathology*, vol. 15, pp. 419–438, 2020.

[7] K. Bedard and K.-H. Krause, "The NOX family of ROS-generating NADPH oxidases: physiology and pathophysiology," *Physiological Reviews*, vol. 87, no. 1, pp. 245–313, 2007.

[8] R. Radi, H. Rubbo, K. Bush, and B. A. Freeman, "Xanthine oxidase binding to glycosaminoglycans: kinetics and superoxide dismutase interactions of immobilized xanthine oxidase-heparin complexes," *Archives of Biochemistry and Biophysics*, vol. 339, no. 1, pp. 125–135, 1997.

[9] S. J. Klebanoff, "Myeloperoxidase: friend and foe," *Journal of Leukocyte Biology*, vol. 77, no. 5, pp. 598–625, 2005.

[10] C. Nathan, Q. Xie Beatrice, and S. Seaver, "Nitric oxide synthases: roles, tolls, and controls," *Cell*, vol. 78, no. 6, pp. 915–918, 1994.

[11] R. Di Micco, V. Krizhanovsky, D. Baker, and F. d'Adda di Fagagna, "Cellular senescence in ageing: from mechanisms to therapeutic opportunities," *Nature Reviews Molecular Cell Biology*, vol. 22, no. 2, pp. 75–95, 2021.

[12] S. Parbin, S. Kar, A. Shilpi et al., "Histone deacetylases," *Journal of Histochemistry and Cytochemistry*, vol. 62, no. 1, pp. 11–33, 2014.

[13] S. A. M. Thiagalingam, K. H. Cheng, H. J. Lee, N. Mineva, A. Thiagalingam, and J. F. Ponte, "Histone deacetylases: unique players in shaping the epigenetic histone code," *Annals of the New York Academy of Sciences*, vol. 983, no. 1, pp. 84–100, 2003.

[14] A. H. Wang, N. R. Bertos, M. Vezmar et al., "HDAC4, a human histone deacetylase related to yeast HDA1, is a transcriptional corepressor," *Molecular and Cellular Biology*, vol. 19, no. 11, pp. 7816–7827, 1999.

[15] A. H. Wang, M. J. Kruhlak, J. Wu et al., "Regulation of histone deacetylase 4 by binding of 14-3-3 proteins," *Molecular and Cellular Biology*, vol. 20, no. 18, pp. 6904–6912, 2000.

[16] X. Zhao, A. Ito, C. D. Kane et al., "The modular nature of histone deacetylase HDAC4 confers phosphorylation- dependent intracellular trafficking," *Journal of Biological Chemistry*, vol. 276, no. 37, pp. 35042–35048, 2001.

[17] N. Cernotta, A. Clocchiatti, C. Florean, and C. Brancolini, "Ubiquitin-dependent degradation of HDAC4, a new regulator of random cell motility," *Molecular Biology of the Cell*, vol. 22, no. 2, pp. 278–289, 2011.

[18] S. Chawla, P. Vanhoutte, F. J. L. Arnold, C. L. H. Huang, and H. Bading, "Neuronal activity-dependent nucleocytoplasmic shuttling of HDAC4 and HDAC5," *Journal of Neurochemistry*, vol. 85, no. 1, pp. 151–159, 2003.

[19] C. Xu, J. Jin, C. Bian et al., "Sequence-specific recognition of a PxLPxI/L motif by an ankyrin repeat tumbler lock," *Science Signaling*, vol. 5, no. 226, p. ra39, 2012.

[20] T. Ago, T. Liu, P. Zhai et al., "A redox-dependent pathway for regulating class II HDACs and cardiac hypertrophy," *Cell*, vol. 133, no. 6, pp. 978–993, 2008.

[21] S. Matsushima, J. Kuroda, T. Ago et al., "Increased oxidative stress in the nucleus caused by Nox4 mediates oxidation of HDAC4 and cardiac hypertrophy," *Circulation Research*, vol. 112, no. 4, pp. 651–663, 2013.

[22] F. Liu, M. Dowling, X. J. Yang, and G. D. Kao, "Caspase-mediated specific cleavage of human histone deacetylase 4," *Journal of Biological Chemistry*, vol. 279, no. 33, pp. 34530–34546, 2004.

[23] G. Paroni, A. Fontanini, N. Cernotta et al., "Dephosphorylation and caspase processing generate distinct nuclear pools of histone deacetylase 4," *Molecular and Cellular Biology*, vol. 27, no. 19, pp. 6718–6732, 2007.

[24] E. Kozhemyakina, T. Cohen, T.-P. Yao, and A. B. Lassar, "Parathyroid hormone-related peptide represses chondrocyte hypertrophy through a protein phosphatase 2A/histone deacetylase 4/MEF2 pathway," *Molecular and Cellular Biology*, vol. 29, no. 21, pp. 5751–5762, 2009.

[25] J. H. Seo, J. H. Park, E. J. Lee et al., "ARD1-mediated Hsp70 acetylation balances stress-induced protein refolding and degradation," *Nature Communications*, vol. 7, no. 1, 2016.

[26] E. J. Jeon, K. Y. Lee, N. S. Choi et al., "Bone morphogenetic protein-2 stimulates Runx2 acetylation," *Journal of Biological Chemistry*, vol. 281, no. 24, pp. 16502–16511, 2006.

[27] H. Geng, C. T. Harvey, J. Pittsenbarger et al., "HDAC4 protein regulates HIF1α protein lysine acetylation and cancer cell response to hypoxia," *Journal of Biological Chemistry*, vol. 286, no. 44, pp. 38095–38102, 2011.

[28] D. Z. Qian, S. K. Kachhap, S. J. Collis et al., "Class II histone deacetylases are associated with VHL-independent regulation of hypoxia-inducible factor 1α," *Cancer Research*, vol. 66, no. 17, pp. 8814–8821, 2006.

[29] H. W. Seo, E. J. Kim, H. Na, and M. O. Lee, "Transcriptional activation of hypoxia-inducible factor-1α by HDAC4 and HDAC5 involves differential recruitment of p300 and FIH-1," *FEBS Letters*, vol. 583, no. 1, pp. 55–60, 2009.

[30] A. S. A. Bardeesi, J. Gao, K. Zhang et al., "A novel role of cellular interactions in vascular calcification," *Journal of Translational Medicine*, vol. 15, no. 1, pp. 1–8, 2017.

[31] D. Proudfoot and C. M. Shanahan, "Biology of calcification in vascular cells: intima versus media," *Herz*, vol. 26, no. 4, pp. 245–251, 2021.

[32] D. J. Farrar, M. G. Bond, W. A. Riley, and J. K. Sawyer, "Anatomic correlates of aortic pulse wave velocity and carotid artery elasticity during atherosclerosis progression and regression in monkeys," *Circulation*, vol. 83, no. 5, pp. 1754–1763, 1991.

[33] Y. Tang, J. M. Boucher, and L. Liaw, "Histone deacetylase activity selectively regulates notch-mediated smooth muscle differentiation in human vascular cells," *Journal of the American Heart Association*, vol. 1, no. 3, 2012.

[34] R. Ginnan, L. Y. Sun, J. J. Schwarz, and H. A. Singer, "MEF2 is regulated by CaMKIIδ2 and a HDAC4-HDAC5 heterodimer in vascular smooth muscle cells," *Biochemical Journal*, vol. 444, no. 1, pp. 105–114, 2012.

[35] O. P. Mathew, K. Ranganna, J. Mathew et al., "Cellular effects of butyrate on vascular smooth muscle cells are mediated through disparate actions on dual targets, histone deacetylase (HDAC) activity and Pi3k/Akt signaling network," *International Journal of Molecular Sciences*, vol. 20, no. 12, p. 2902, 2019.

[36] C. H. Byon, A. Javed, Q. Dai et al., "Oxidative stress induces vascular calcification through modulation of the osteogenic transcription factor Runx2 by AKT signaling," *Journal of Biological Chemistry*, vol. 283, no. 22, pp. 15319–15327, 2008.

[37] Y. Zhu, W. Q. Ma, X. Q. Han, Y. Wang, X. Wang, and N. F. Liu, "Advanced glycation end products accelerate calcification in VSMCs through HIF-1α/PDK4 activation and suppress glucose metabolism," *Scientific Reports*, vol. 8, no. 1, pp. 1–12, 2018.

[38] N. Escobales, R. E. Nuñez, S. Jang et al., "Mitochondria-targeted ROS scavenger improves post-ischemic recovery of cardiac function and attenuates mitochondrial abnormalities in aged rats," *Journal of Molecular and Cellular Cardiology*, vol. 77, pp. 136–146, 2014.

[39] H. Zhang, M. Bosch-Marce, L. A. Shimoda et al., "Mitochondrial autophagy is an HIF-1-dependent adaptive metabolic response to hypoxia," *Journal of Biological Chemistry*, vol. 283, no. 16, pp. 10892–10903, 2008.

[40] M. Haberland, R. L. Montgomery, and E. N. Olson, "The many roles of histone deacetylases in development and physiology: implications for disease and therapy," *Nature Reviews Genetics*, vol. 10, no. 1, pp. 32–42, 2009.

[41] H. Li, W. Li, A. K. Gupta, P. J. Mohler, M. E. Anderson, and I. M. Grumbach, "Calmodulin kinase II is required for angiotensin II-mediated vascular smooth muscle hypertrophy," *American Journal of Physiology. Heart and Circulatory Physiology*, vol. 298, pp. 688–698, 2010.

[42] D. Yang, C. Xiao, F. Long et al., "HDAC4 regulates vascular inflammation via activation of autophagy," *Cardiovascular Research*, vol. 114, pp. 1016–1028, 2018.

[43] R. M. Touyz, "Reactive oxygen species and angiotensin II signaling in vascular cells: implications in cardiovascular disease," vol. 37, no. 8, pp. 1263–1273, 2004.

[44] Y. Taniyama and K. K. Griendling, "Reactive oxygen species in the vasculature," *Hypertension*, vol. 42, no. 6, pp. 1075–1081, 2003.

[45] R. M. Touyz, X. Chen, F. Tabet et al., "Expression of a functionally active gp91phox-containing neutrophil-type NAD(P)H oxidase in smooth muscle cells from human resistance arteries," *Circulation Research*, vol. 90, no. 11, pp. 1205–1213, 2002.

[46] M. Zhu, Q. Ding, Z. Lin, X. Chen, S. Chen, and Y. Zhu, "New insights of epigenetics in vascular and cellular senescence," *Journal of Translational Internal Medicine*, vol. 9, no. 4, pp. 239–248, 2021.

[47] Z. Lin, Q. Ding, X. Li et al., "Targeting epigenetic mechanisms in vascular aging," *Frontiers in Cardiovascular Medicine*, vol. 8, 2022.

[48] X. L. Luo, D. Yang, W. J. Wu et al., "Critical role of histone demethylase Jumonji domain-containing protein 3 in the regulation of neointima formation following vascular injury," *Cardiovascular Research*, vol. 114, no. 14, pp. 1894–1906, 2018.

[49] A. Mongelli and C. Gaetano, "JMJD3 and vascular injury: the emperor's new clothes," *Cardiovascular Research*, vol. 114, pp. 1825–1827, 2018.

[50] D. Yang, G. Wei, F. Long et al., "Histone methyltransferase Smyd 3 is a new regulator for vascular senescence," *Aging Cell*, vol. 19, no. 9, 2020.

[51] D. Yang, Z. Su, G. Wei et al., "H3K4 methyltransferase Smyd3 mediates vascular smooth muscle cell proliferation, migration, and neointima formation," *Arteriosclerosis, Thrombosis, and Vascular Biology*, vol. 41, no. 6, pp. 1901–1914, 2021.

[52] C. de Ciuceis, F. Amiri, P. Brassard, D. H. Endemann, R. M. Touyz, and E. L. Schiffrin, "Reduced vascular remodeling, endothelial dysfunction, and oxidative stress in resistance arteries of angiotensin II-infused macrophage colony-stimulating factor-deficient mice," *Arteriosclerosis, Thrombosis, and Vascular Biology*, vol. 25, no. 10, pp. 2106–2113, 2005.

[53] N. A. Kittan, R. M. Allen, A. Dhaliwal et al., "Cytokine induced phenotypic and epigenetic signatures are key to establishing

specific macrophage phenotypes," *PLoS One*, vol. 8, no. 10, p. e78045, 2013.

[54] A. E. Neele, K. H. M. Prange, M. A. Hoeksema et al., "Macrophage Kdm6b controls the pro-fibrotic transcriptome signature of foam cells," *Epigenomics*, vol. 9, no. 4, pp. 383–391, 2017.

[55] A. Caillon, M. O. R. Mian, J. C. Fraulob-Aquino et al., "$\Gamma\gamma\delta$ T cells mediate angiotensin II-induced hypertension and vascular injury," *Circulation*, vol. 135, no. 22, pp. 2155–2162, 2017.

[56] C. K. Glass, K. Saijo, B. Winner, M. C. Marchetto, and F. H. Gage, "Mechanisms underlying inflammation in neurodegeneration," *Cell*, vol. 140, no. 6, pp. 918–934, 2010.

[57] H. C. Hendrie, "Epidemiology of dementia and Alzheimer's disease," *American Journal of Geriatric Psychiatry*, vol. 6, no. 2, 1998.

[58] A. D. Korczyn, "The amyloid cascade hypothesis," *Alzheimer's and Dementia*, vol. 4, no. 3, pp. 176–178, 2008.

[59] M. T. Heneka, M. P. Kummer, A. Stutz et al., "NLRP3 is activated in Alzheimer's disease and contributes to pathology in APP/PS1 mice," *Nature*, vol. 493, no. 7434, pp. 674–678, 2013.

[60] E. F. Fang, Y. Hou, K. Palikaras et al., "Mitophagy inhibits amyloid-β and tau pathology and reverses cognitive deficits in models of Alzheimer's disease," *Nature Neuroscience*, vol. 22, no. 3, pp. 401–412, 2019.

[61] F. J. Jahed, R. Rahbarghazi, H. Shafaei, A. Rezabakhsh, and M. Karimipour, "Application of neurotrophic factor-secreting cells (astrocyte - like cells) in the in-vitro Alzheimer 's disease-like pathology on the human neuroblastoma cells," *Brain Research Bulletin*, vol. 172, pp. 180–189, 2021.

[62] L. Nie, J. Xia, H. Li et al., "Ginsenoside Rg1 ameliorates behavioral abnormalities and modulates the hippocampal proteomic change in triple transgenic mice of Alzheimer's disease," *Oxidative Medicine and Cellular Longevity*, vol. 2017, 17 pages, 2017.

[63] C. Chen, P. Liu, J. Wang et al., "Dauricine attenuates spatial memory impairment and Alzheimer-like pathologies by enhancing mitochondrial function in a mouse model of Alzheimer's disease," *Frontiers in Cell and Developmental Biology*, vol. 8, 2021.

[64] K.-P. Lin, R.-S. Liu, and B.-H. Yang, "Springer Proceedings in Physics 272 Future Trends and Challenges of Molecular Imaging and AI Innovation Proceedings of FASMI 2020," https://linkspringer.com/bookseries/361.

[65] O. B. Tysnes and A. Storstein, "Epidemiology of Parkinson's disease," *Journal of Neural Transmission*, vol. 124, no. 8, pp. 901–905, 2017.

[66] C. C. Yu, H. L. Chen, M. H. Chen et al., "Vascular inflammation is a risk factor associated with brain atrophy and disease severity in Parkinson's disease: a case-control study," *Oxidative Medicine and Cellular Longevity*, vol. 2020, 12 pages, 2020.

[67] Q. Wu, X. Yang, L. Zhang, Y. Zhang, and L. Feng, "Nuclear accumulation of histone deacetylase 4 (HDAC4) exerts neurotoxicity in models of Parkinson's disease," *Molecular Neurobiology*, vol. 54, no. 9, pp. 6970–6983, 2017.

[68] J. G. Lees, M. Napierala, A. Pébay, M. Dottori, and S. Y. Lim, "Cellular pathophysiology of Friedreich's ataxia cardiomyopathy," *International Journal of Cardiology*, vol. 346, pp. 71–78, 2022.

[69] A. K. Shetty, R. Upadhya, L. N. Madhu, and M. Kodali, "Novel insights on systemic and brain aging, stroke, amyotrophic lateral sclerosis, and Alzheimer's disease," *Aging and Disease*, vol. 10, no. 2, pp. 470–482, 2019.

[70] E. Soragni, C. Xu, H. L. Plasterer, V. Jacques, J. R. Rusche, and J. M. Gottesfeld, "Rationale for the development of 2-aminobenzamide histone deacetylase inhibitors as therapeutics for Friedreich ataxia," *Journal of Child Neurology*, vol. 27, no. 9, pp. 1164–1173, 2012.

[71] M. Rai, E. Soragni, K. Jenssen et al., "HDAC inihibitors correct frataxin deficiency in a Friedreich ataxia mouse model," *PLoS One*, vol. 3, no. 4, 2008.

[72] C. Sandi, R. M. Pinto, S. al-Mahdawi et al., "Prolonged treatment with pimelic o -aminobenzamide HDAC inhibitors ameliorates the disease phenotype of a Friedreich ataxia mouse model," *Neurobiology of Disease*, vol. 42, no. 3, pp. 496–505, 2011.

[73] J. P. Sarsero, L. Li, H. Wardan, K. Sitte, R. Williamson, and P. A. Ioannou, "Upregulation of expression from the FRDA genomic locus for the therapy of Friedreich ataxia," *Journal of Gene Medicine*, vol. 5, no. 1, pp. 72–81, 2003.

[74] L. Brichta, Y. Hofmann, E. Hahnen et al., "Valproic acid increases the SMN2 protein level: a well-known drug as a potential therapy for spinal muscular atrophy," *Human Molecular Genetics*, vol. 12, no. 19, pp. 2481–2489, 2003.

[75] C. Andreassi, C. Angelozzi, F. D. Tiziano et al., "Phenylbutyrate increases SMN expression _in vitro_ : relevance for treatment of spinal muscular atrophy," *European Journal of Human Genetics*, vol. 12, no. 1, pp. 59–65, 2004.

[76] J.-G. Chang, H.-M. Hsieh-Li, Y.-J. Jong, N. M. Wang, C.-H. Tsai, and H. Li, "Treatment of spinal muscular atrophy by sodium butyrate," *Proceedings of the National Academy of Sciences*, vol. 98, no. 17, pp. 9808–9813, 2001.

[77] A. M. Avila, B. G. Burnett, A. A. Taye et al., "Trichostatin A increases SMN expression and survival in a mouse model of spinal muscular atrophy," *Journal of Clinical Investigation*, vol. 117, no. 3, pp. 659–671, 2007.

[78] M. Riessland, B. Ackermann, A. Förster et al., "SAHA ameliorates the SMA phenotype in two mouse models for spinal muscular atrophy," *Human Molecular Genetics*, vol. 19, no. 8, pp. 1492–1506, 2010.

[79] Y. E. Yoo and C. P. Ko, "Treatment with trichostatin A initiated after disease onset delays disease progression and increases survival in a mouse model of amyotrophic lateral sclerosis," *Experimental Neurology*, vol. 231, no. 1, pp. 147–159, 2011.

[80] L. G. Bilsland, E. Sahai, G. Kelly, M. Golding, L. Greensmith, and G. Schiavo, "Deficits in axonal transport precede ALS symptoms in vivo," *Proceedings of the National Academy of Sciences of the United States of America*, vol. 107, no. 47, pp. 20523–20528, 2010.

[81] L. Marek, A. Hamacher, F. K. Hansen et al., "Histone deacetylase (HDAC) inhibitors with a novel connecting unit linker region reveal a selectivity profile for HDAC4 and HDAC5 with improved activity against chemoresistant cancer cells," *Journal of Medicinal Chemistry*, vol. 56, no. 2, pp. 427–436, 2013.

[82] M. Lobera, K. P. Madauss, D. T. Pohlhaus et al., "Selective class IIa histone deacetylase inhibition via a nonchelating zinc-binding group," *Nature Chemical Biology*, vol. 9, no. 5, pp. 319–325, 2013.

[83] H. Ryu, K. Smith, S. I. Camelo et al., "Sodium phenylbutyrate prolongs survival and regulates expression of anti- apoptotic genes in transgenic amyotrophic lateral sclerosis mice," *Journal of Neurochemistry*, vol. 93, no. 5, pp. 1087–1098, 2005.

[84] A. S. Dickey, D. N. Sanchez, M. Arreola et al., "PPARδ activation by bexarotene promotes neuroprotection by restoring bioenergetic and quality control homeostasis," *Science Translational Medicine*, vol. 9, no. 419, p. eaal2332, 2017.

[85] Y. Zhu, M. Huang, E. Bushong et al., "Class IIa HDACs regulate learning and memory through dynamic experience-dependent repression of transcription," *Nature Communications*, vol. 10, no. 1, pp. 1–14, 2019.

Hindawi
Oxidative Medicine and Cellular Longevity
Volume 2022, Article ID 6849304, 35 pages
https://doi.org/10.1155/2022/6849304

Research Article

Identification of Prognostic and Tumor Microenvironment by Shelterin Complex-Related Signatures in Oral Squamous Cell Carcinoma

Suwei Zhang,[1] **Hanhui Yu**,[2] **Jiazhen Li**,[1] **Liang Zhao**,[3] **Lei Tan**,[3] **Qiang Song**,[4] **and Cong Sun**[3]

[1]*Department of Clinical Laboratory, Shantou Central Hospital, Shantou, Guangdong Province 515041, China*
[2]*Department of Neurosurgery, Shantou Central Hospital, Shantou, Guangdong Province 515041, China*
[3]*Department of Stomatology, The First Affiliated Hospital of Xi'an Jiaotong, Xi'an, Shanxi Province 710061, China*
[4]*Department of Structural Heart Disease, The First Affiliated Hospital of Xi'an Jiaotong University, Xi'an, Shanxi Province 710061, China*

Correspondence should be addressed to Cong Sun; suncong@m.poe.edu.pl

Received 19 January 2022; Accepted 24 May 2022; Published 15 June 2022

Academic Editor: Natalia Krasteva

Oral squamous cell carcinoma (OSCC) is a common malignant tumor of the oral cavity. Shelterin complex gene (SG) has an important role in regulating telomere structure and length. SG is considered promising as a novel prognostic marker for cancer and a potential target for tumor therapy. However, SGs have not been systematically studied in OSCC. We analyzed SGs based on public data from OSCC patients and showed that SGs are closely associated with the prognosis of OSCC patients. Two different subtypes of SGs were identified in the TCGA and GEO cohorts, and LASSO regression analysis was used to further construct an SGs-related prognostic model. Randomized cohorts and different clinical subgroups validated the model's accuracy. The assessment of clinical characteristics, tumor mutational burden (TMB), and tumor microenvironment (TME) between high- and low-risk scores groups showed lower TMB, more abundant immune cell infiltration, and better prognosis in the low-risk group. According to the IPS analysis, patients in the low-risk group were more responsive to immunotherapy. This study establishes a foundation for research on SG and confirms that risk scores can predict prognosis and guide clinical treatment in OSCC patients.

1. Introduction

Telomeres are specialized nucleotide arrays located at the ends of linear chromosomes. As a result of shelterin being able to lengthen telomeres and protect the ends, malignant cells have bypassed senescence, which results in genomic instability [1–3]. The DNA damage signaling pathways inhibited by shelterin include classical NHEJ, ATM and ATR signaling, alternate NHEJ, resection, and homologous recombination. There are six proteins in the shelterin complex, including TERF2-interacting protein 1 (TERF2IP), TERF1 and TERF2 (telomeric repeat-binding proteins), adrenocortical dysplasia protein homolog (ACD), POT1 (patent for telomere protection), and TIF2 (TERF1-interacting protein 2) [4–6].

One of the most common oral cancers is OSCC (oral squamous cell carcinoma), with more than 350,000 diagnoses each year, corresponding to roughly 2% of all tumor diagnoses [7, 8]. OSCC patients have a low 5-year survival rate (less than 60%), and there are no optimal clinical treatment options [9, 10]. Therefore, novel treatment targets are urgently needed to improve. A more reliable prognostic model is also needed to make treatment more feasible.

Shelterin complex genes (SGs) have been implicated in cancer development in previous studies [11, 12]. Li et al. found that telomere dysfunction and cellular senescence could be

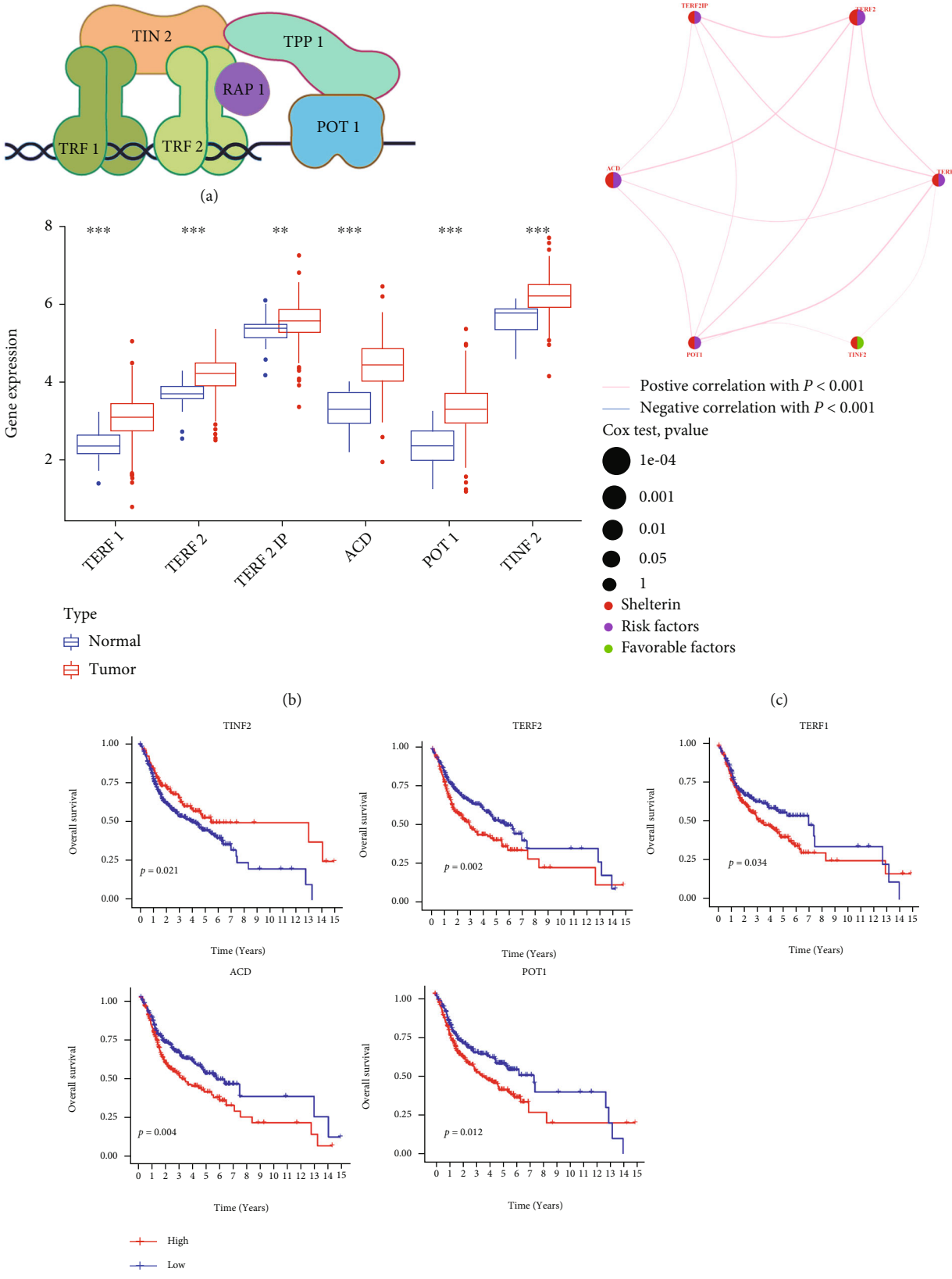

Figure 1: Continued.

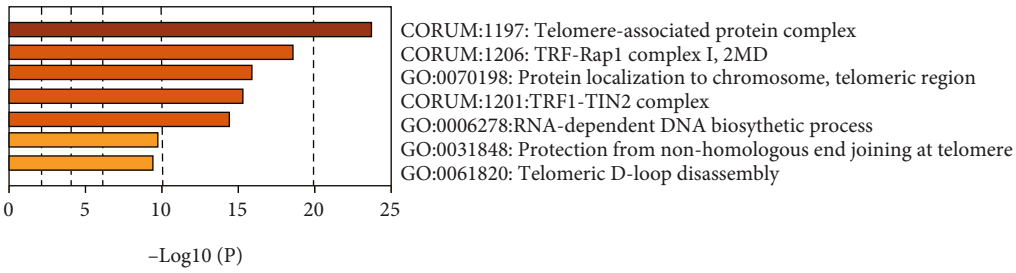

(e)

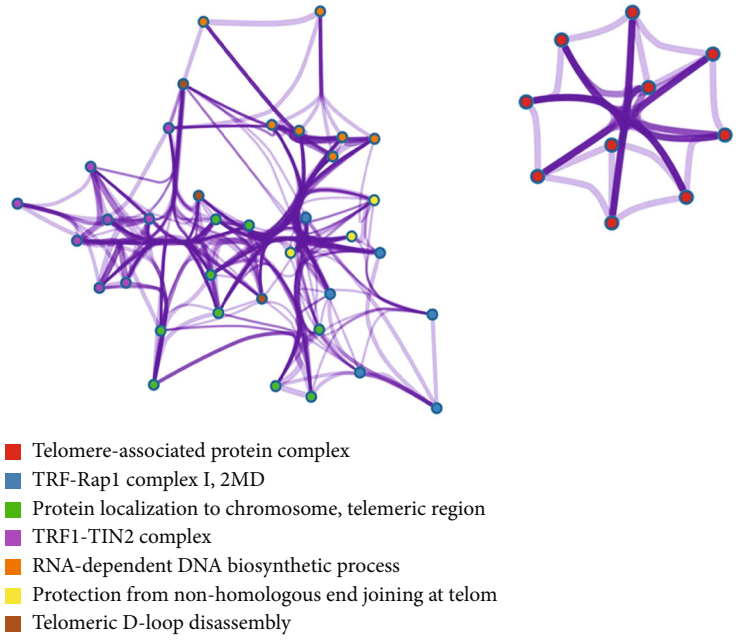

(f)

Figure 1: SGs in OSCC have distinct characteristics and differences. (a) Schematic illustration of shelterin complex. The shelterin complex is composed of six core proteins, including TERF2-interacting protein 1 (TERF2IP), telomeric repeat-binding factors 1 and 2 (TERF1 and TERF2), adrenocortical dysplasia protein homolog (ACD), protection of telomeres 1 (POT1), and TERF1-interacting protein 2 (TINF2). (b) The mRNA expression levels of SGs were compared between normal and tumor samples. $*P < 0.05$, $**P < 0.01$, and $*** P < 0.001$. (c) A network of correlations including SGs. The lines connecting SGs represented their interaction with each other. The size of each circle represented the prognosis effect of each regulator and scaled by P value. Favorable factors for patients' survival were indicated by a green dot in the right half of the circle and risk factors indicated by the purple dot in the right half of the circle. (d) The results of survival analysis showed the relationship between the expression level of SGs and the prognosis of OSCC patients. (e) The image showed the histogram of the enriched pathways associated with the SGs. The abscissa was the value of -Log10P and longitudinal which were different enrichment pathways, sorted by the value of -Log10P. (f) The image showed the network of enriched terms. Each node represented an enriched term and was colored by its cluster ID.

Table 1: The functional enrichment analysis of SGs.

GO	Description	Count	Log10(P)	Log10(q)
CORUM:1197	Telomere-associated protein complex	6	-24.02	-19.99
CORUM:1206	TRF-Rap1 complex I, 2MD	5	-18.77	-15.38
GO:0070198	Protein localization to chromosome, telomeric region	5	-15.90	-12.94
CORUM:1201	TRF1-TIN2 complex	4	-15.36	-12.53
GO:0006278	RNA-dependent DNA biosynthetic process	5	-14.47	-11.72
GO:0031848	Protection from non-homologous end joining at telomere	3	-9.82	-7.26
GO:0061820	Telomeric D-loop disassembly	3	-9.44	-6.90

"Count" is the number of genes in the given ontology term. "Log10(P)" is the P value in log base 10. "Log10(q)" is the multitest adjusted P value in log base 10.

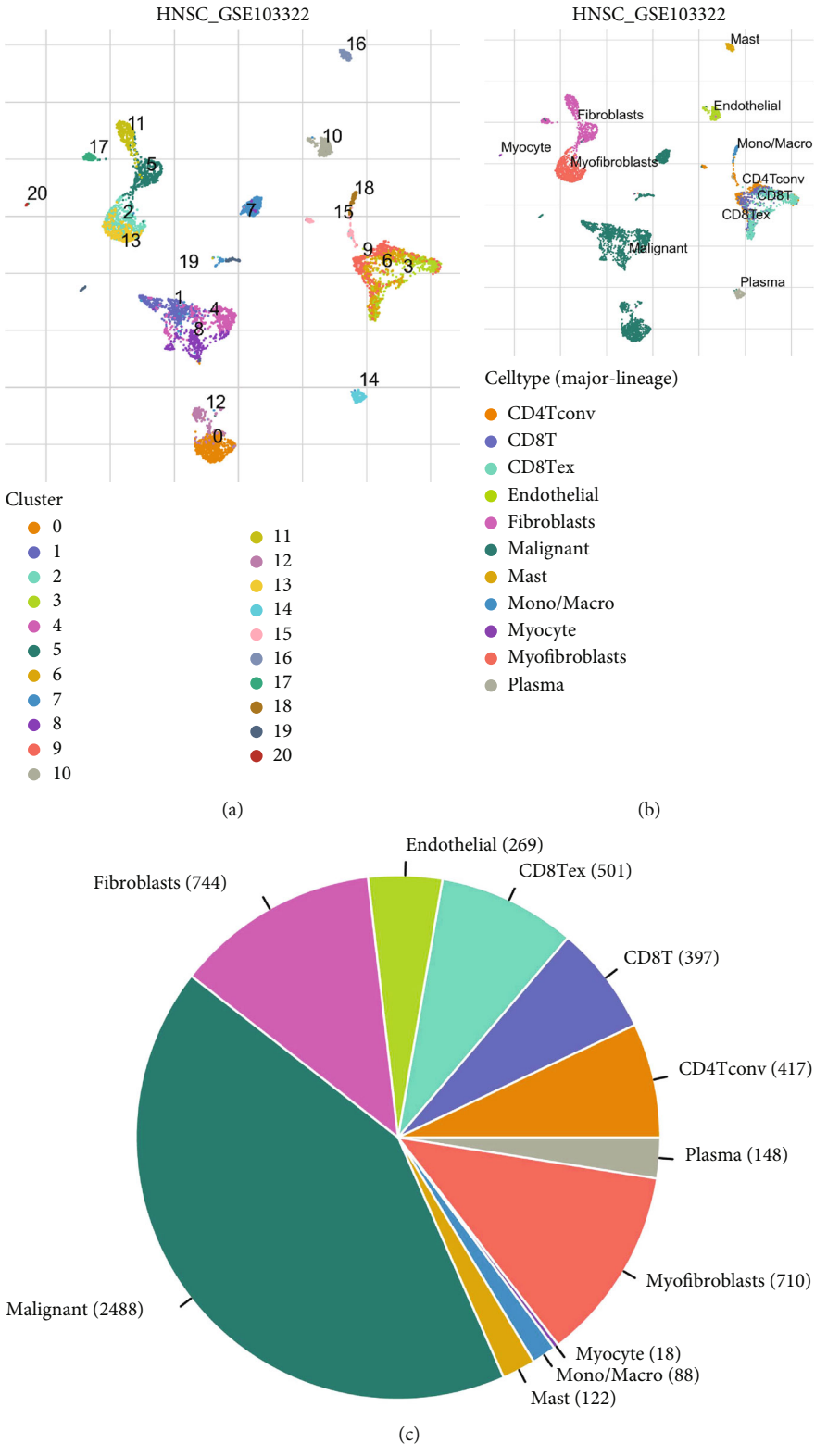

Figure 2: Continued.

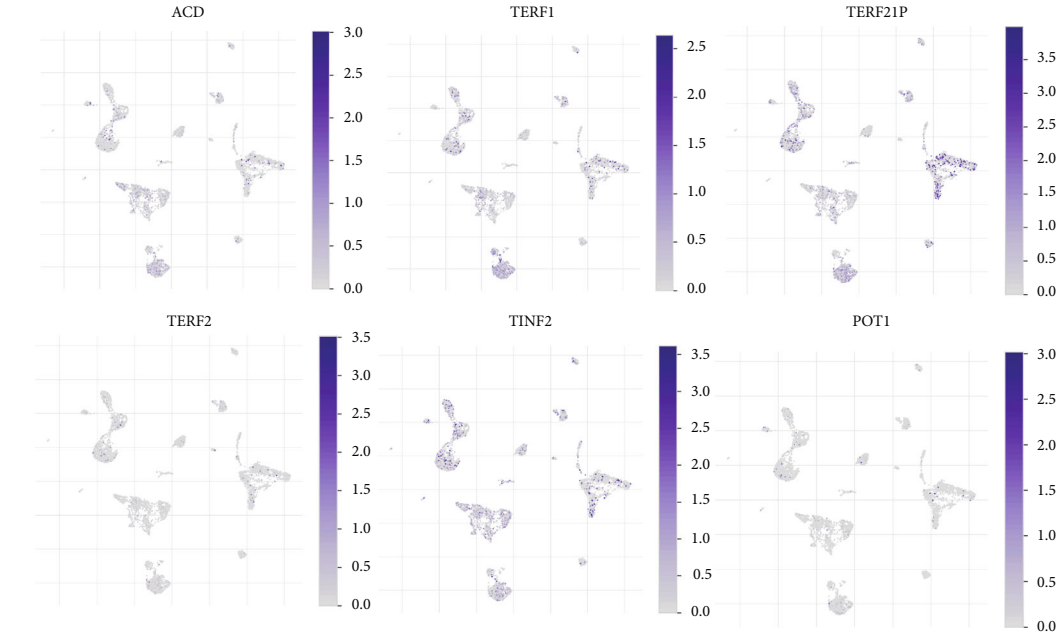

(d)

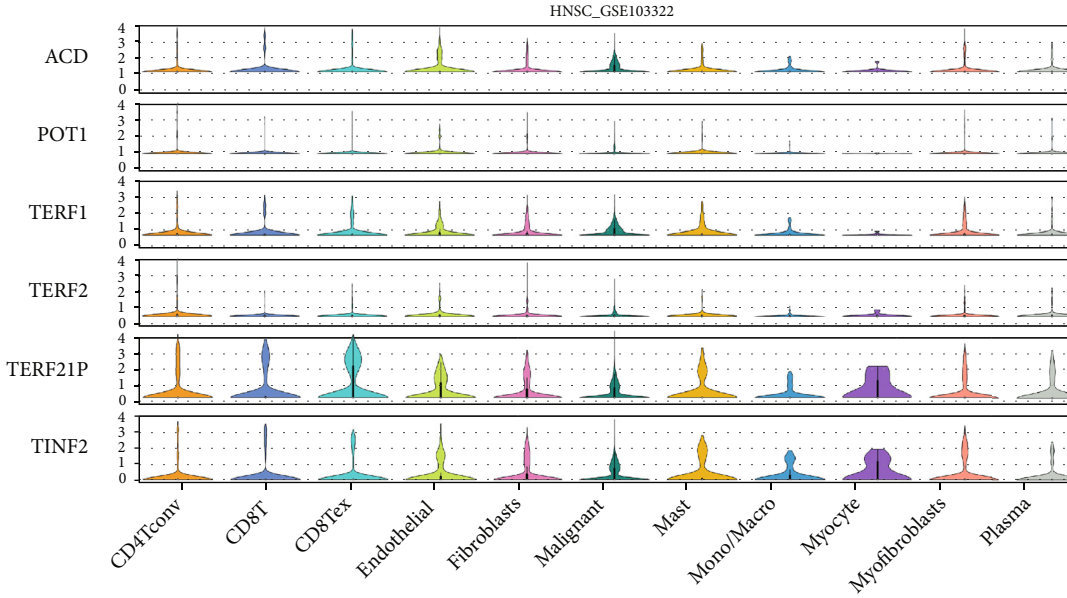

(e)

Figure 2: Analysis of the expression distribution of SGs based on single-cell data. The overview tab of the GSE103322 dataset. Two UMAP plots with cells colored by cluster ID (a) and cell type (b) are displayed. (c) The pie plot shows the cell number distribution of each cell type. (d) The expression of SGs is visualized at single-cell and cell-type resolution. (e) Violin plots visualize the distribution of SGs across different cell types.

induced by targeting POT1 with MiR-185 [13]. During gallbladder cancer development, the telomere length of the SG is also significantly altered [14]. SG is considered promising as a novel prognostic marker for cancer and a potential target for tumor therapy. In OSCC, its role is not yet fully understood. We must comprehensively evaluate immunocellular infiltration characteristics in the SG-regulated tumor microenvironment (TME) in order to better understand the microenvironment of OSCC and to develop personalized treatments.

In order to predict prognosis and guide treatment, it was of primary importance to comprehensively evaluate the expression patterns of SGs in OSCC and develop a prognostic risk scoring model for SGs. Risk scores were used to assess tumor mutational burden, tumor microenvironment, immunotherapy response, drug sensitivity, and clinical prognosis in OSCC patients. Findings from these studies may provide new perspectives on how to better understand and treat SGs in OSCC.

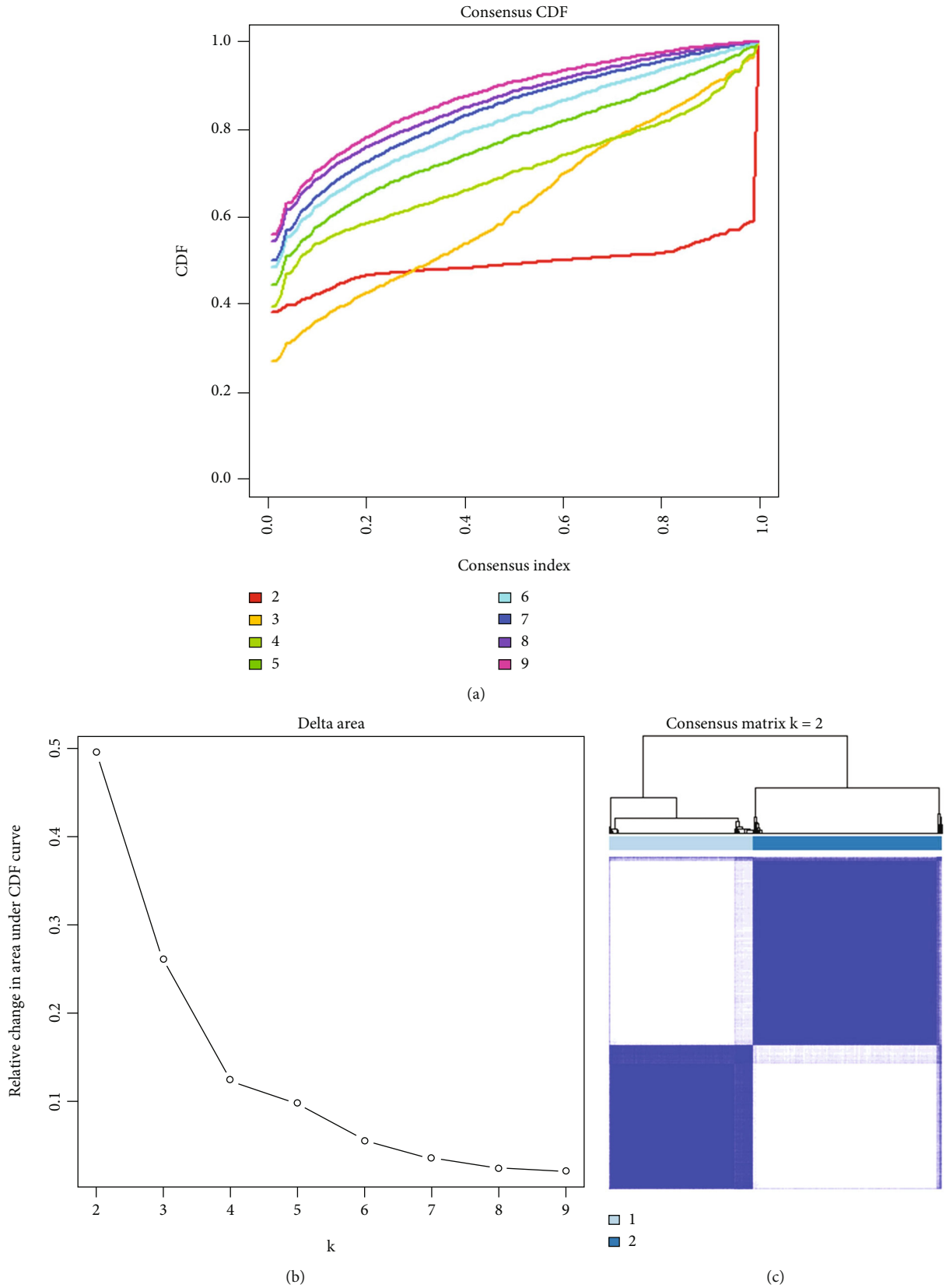

Figure 3: Continued.

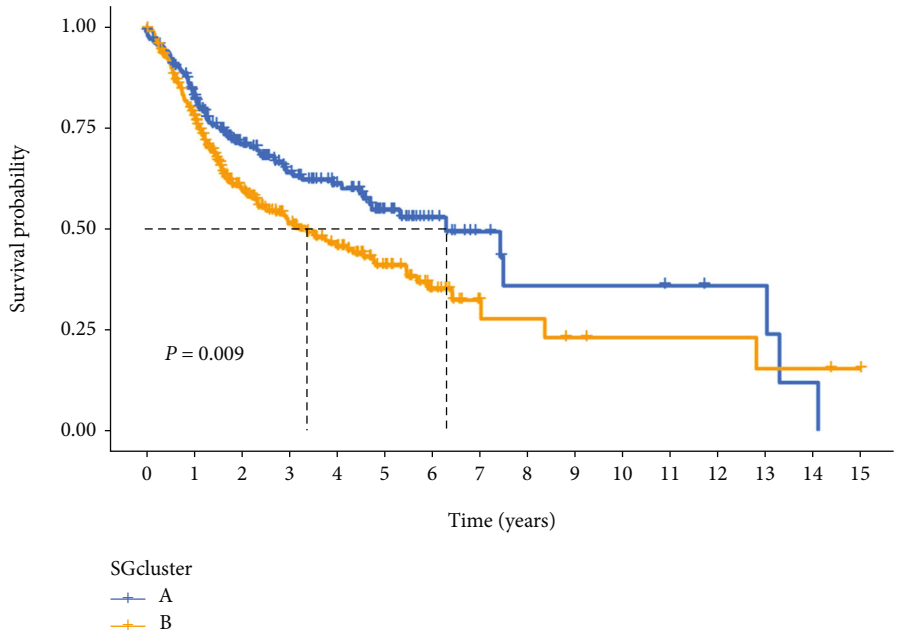

(d)

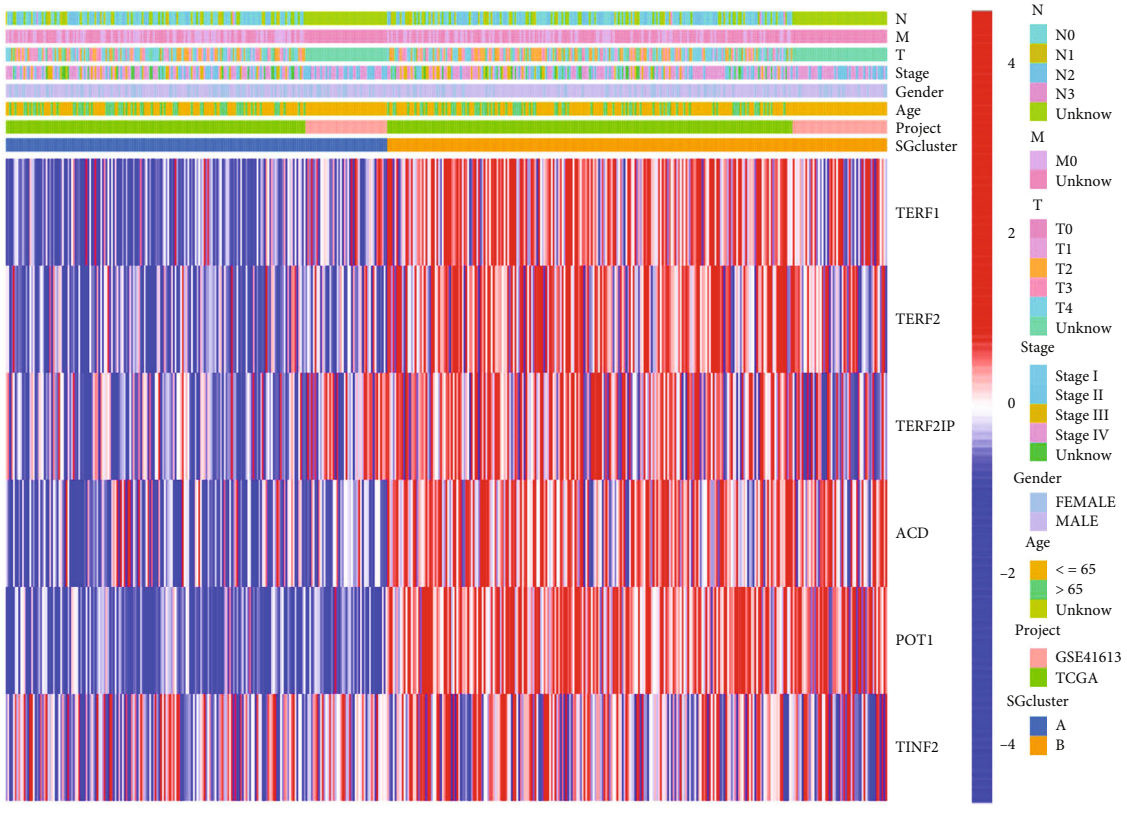

(e)

Figure 3: Continued.

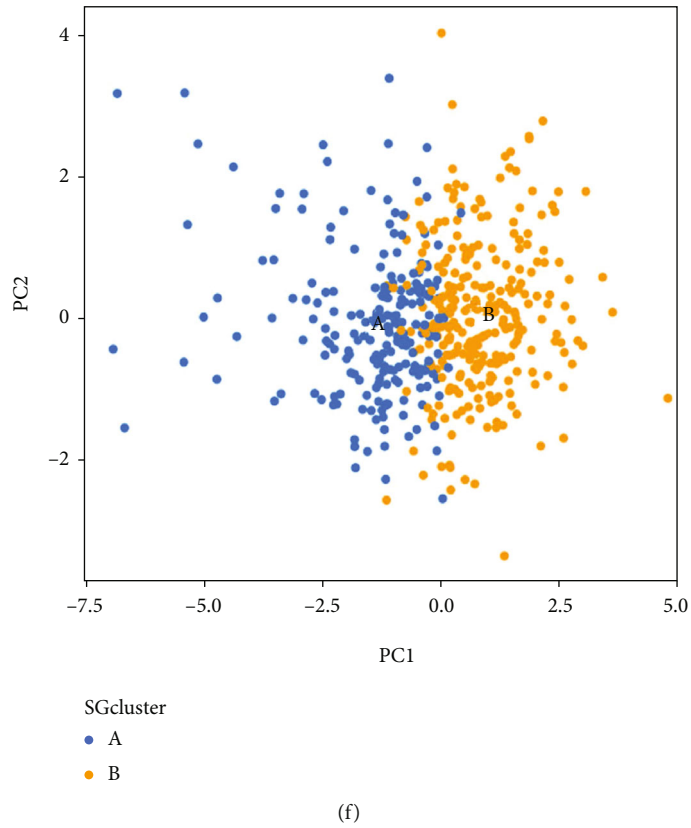

(f)

Figure 3: Subgroups of OSCC defined by genes involved in pyroptosis. (a) CDF curves of the consensus score ($k = 2 – 9$) in the two cohorts. (b) Relative change in the area under the CDF curve ($k = 2 – 9$) in the two cohorts. (c) Patients in two cohorts were grouped into two clusters according to the consensus clustering matrix ($k = 2$). (d) Kaplan–Meier survival analyses of the patients with SGCluster A and SGCluster B. (e) The two cluster heat maps based on SGs with clinical characteristics. Unknown: data not available. (f) PCA plot for OSCC patients based on the SGCluster.

2. Methods

2.1. OSCC Data Preparation. OSCC patient-related data were retrieved from TCGA (https://portal.gdc.cancer.gov/) and GEO databases (https://www.ncbi.nlm.nih.gov/geo/). TCGA-OSCC data (workflow type, HTSeq-FPKM) were obtained from the TCGA-HNSCC project. In the subsequent analysis, FPKM values were transformed using log2 (FPKM +1) [15, 16]. Gene Expression Omnibus data for GSE41613 was obtained from (GEO, https://www.ncbi.nlm.nih.gov/geo/query/acc.cgi?acc=GSE41613) database, Platform: GPL570. An RMA normalization was carried out on the GSE41613 datasets. From GSE103322, we derived the data on single cells RNA-seq from oral cancer (http://www.ncbi.nlm.nih.gov/geo/query/acc.cgi?acc=GSE103322). Cells from 18 patients with oral tumors made up 5902 single cells [17]. Public databases listed above are freely accessible, and the study followed their publication guidelines and data access policies.

2.2. Identification of Differentially Expressed SGs. By analyzing TCGA-OSCC and GSE41613 samples, we aimed to determine which SGs differed in expression between normal and tumor tissues. The SVA package was used to normalize RNA expression profiles and eliminate batch effects on TCGA and GEO data [18]. Researchers have used the R package "limma" to identify SGs that show a significant difference ($P > 0.05$) between normal tissue and tumor tissue [19]. The Metascape database (https://metascape.org/gp/index.html#/main/step1) contains gene annotations and analyses [20]; this study used Metascape to perform enrichment analyses on SGs.

2.3. SGs-Based Classifications of OSCC Patients in the TCGA-OSCC and GSE41613 Cohorts. We identified the distinct patterns of SG expression in OSCC patients by using consensus clustering based on their expression levels to classify them further. The above steps were performed through the R package "ConsensusClusterPlus" and repeated 1000 times to ensure clustering stability [21, 22]. The CDF curve for the consensus heat map is determined by the area's relative change and the consensus heat map's consensus score. To determine the prognosis of patients with different OSCC, a Kaplan-Meier survival analysis was performed.

2.4. Gene Set Variation Analysis (GSVA). Functional enrichment analysis of SGs clusters was conducted using the "GSVA" R package [23]. ClusterProfiler was used for functional annotation, and the MSigDB gene set file obtained from the GSEA-MSigDB database (https://www.gsea-

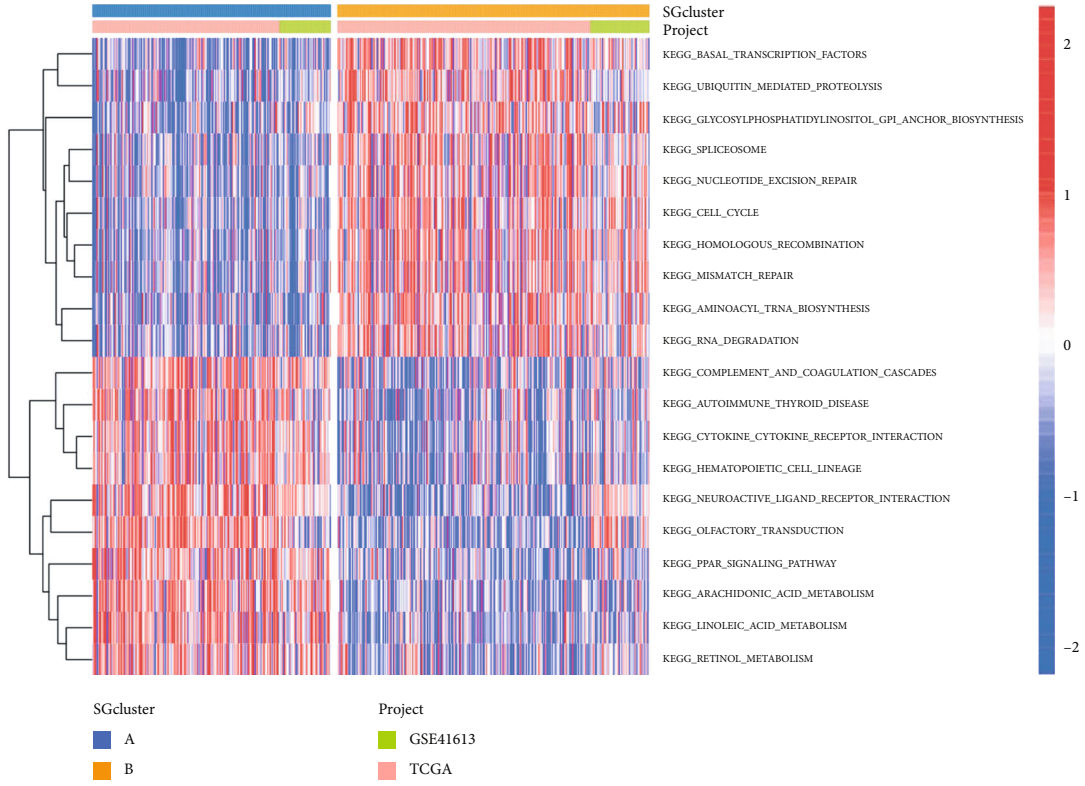

(a)

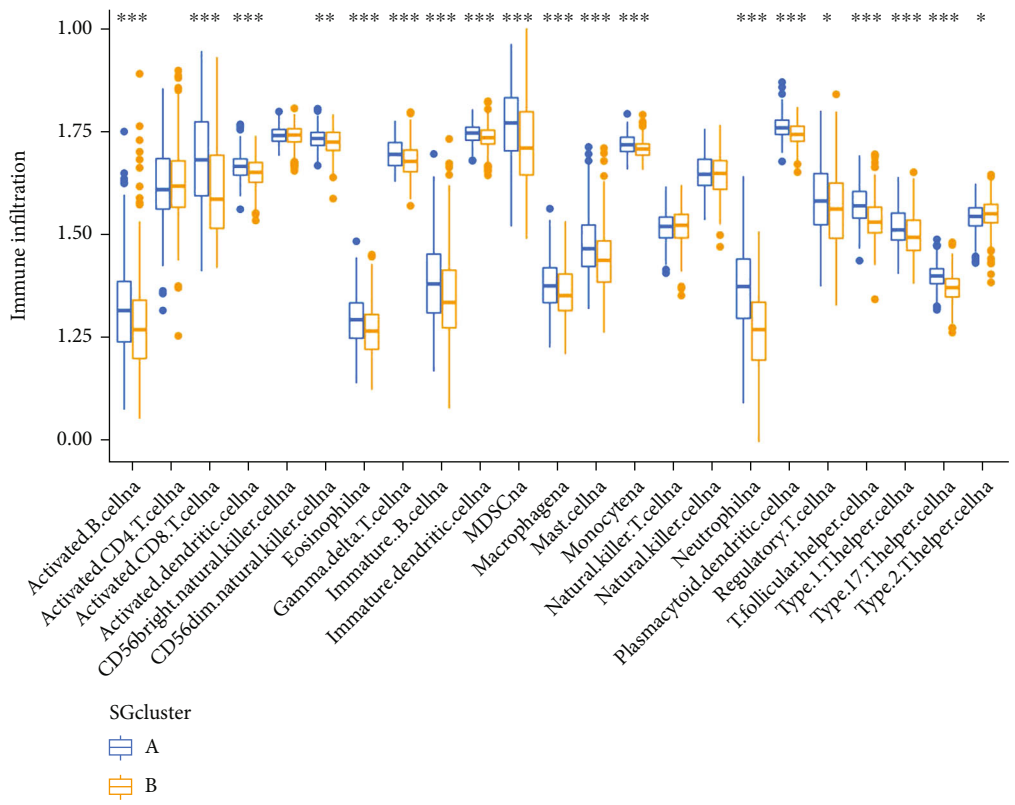

(b)

Figure 4: Continued.

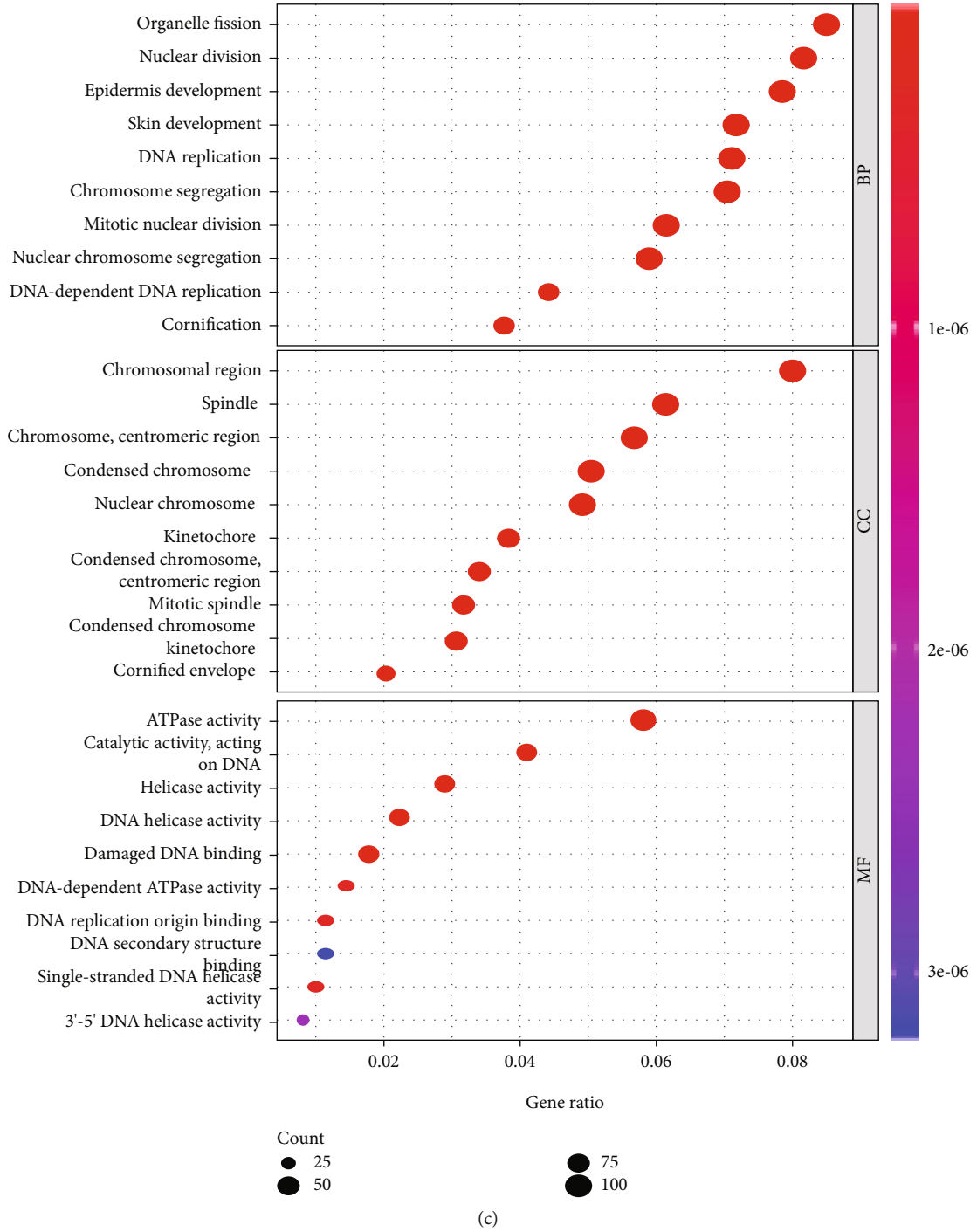

(c)

Figure 4: Continued.

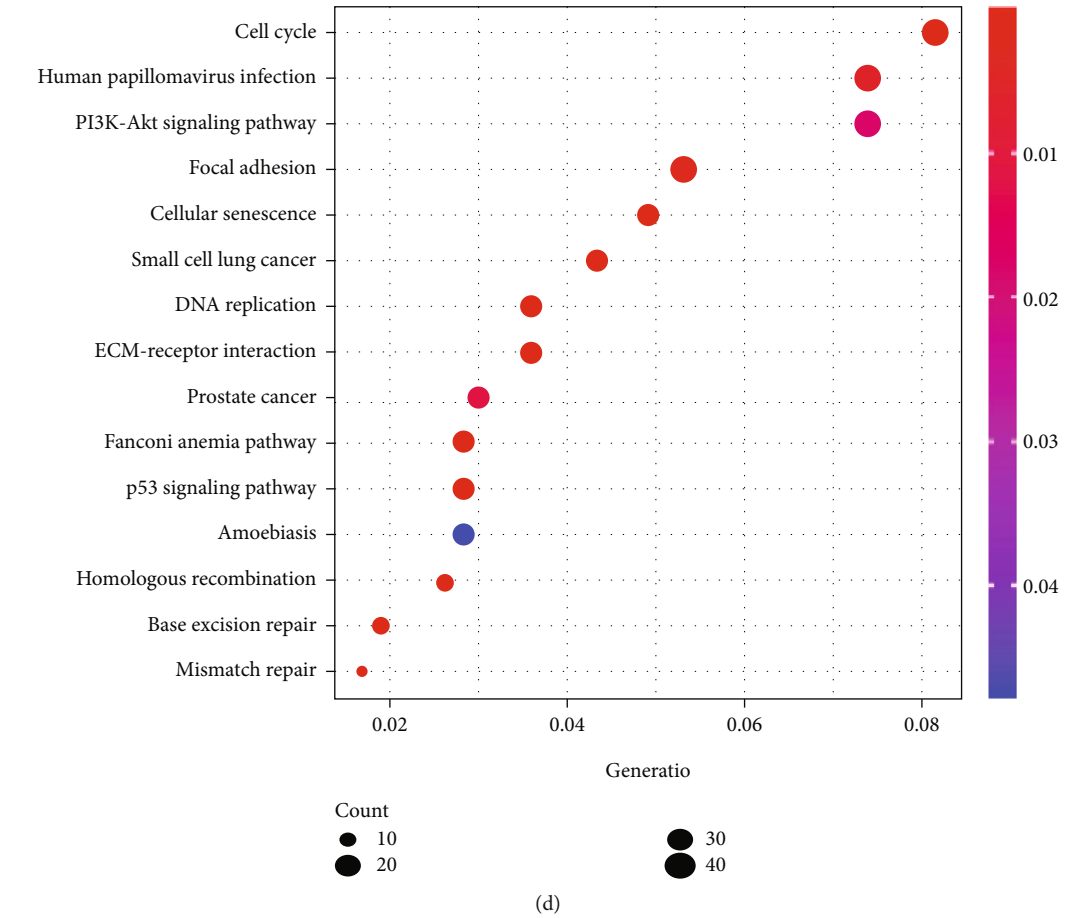

(d)

Figure 4: Different analyses between SGCluster A and SGCluster B. (a) Heat mapping was used to visualize the biological process by GSVA analysis in the 2 clusters. (b) Analysis of immune infiltrating cells between SGCluster A and SGCluster B. $*P < 0.05$, $**P < 0.01$, and $***P < 0.001$. GO (c) and KEGG (d) enrichment analysis of DEGs between SGCluster A and SGCluster B.

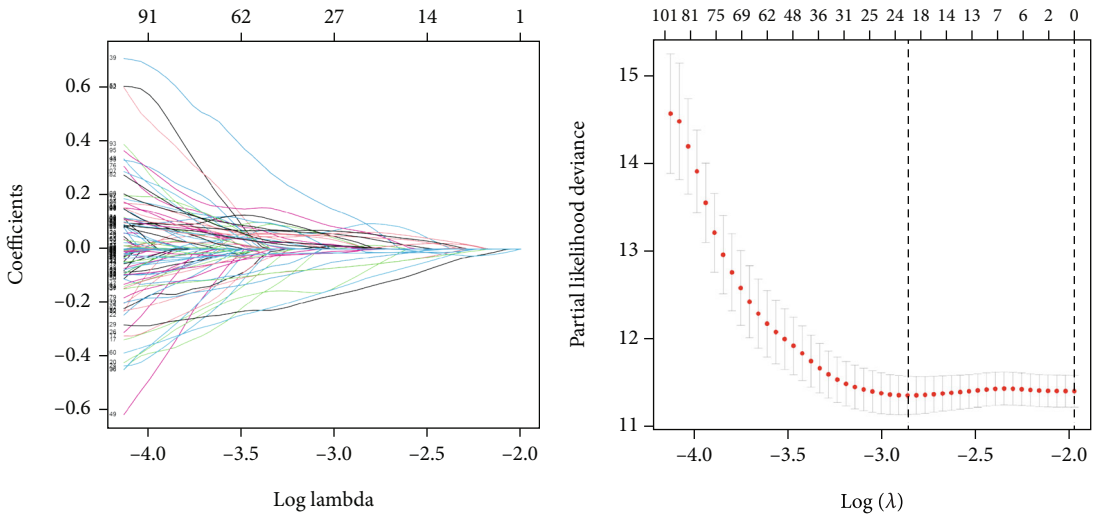

(a) (b)

Figure 5: Continued.

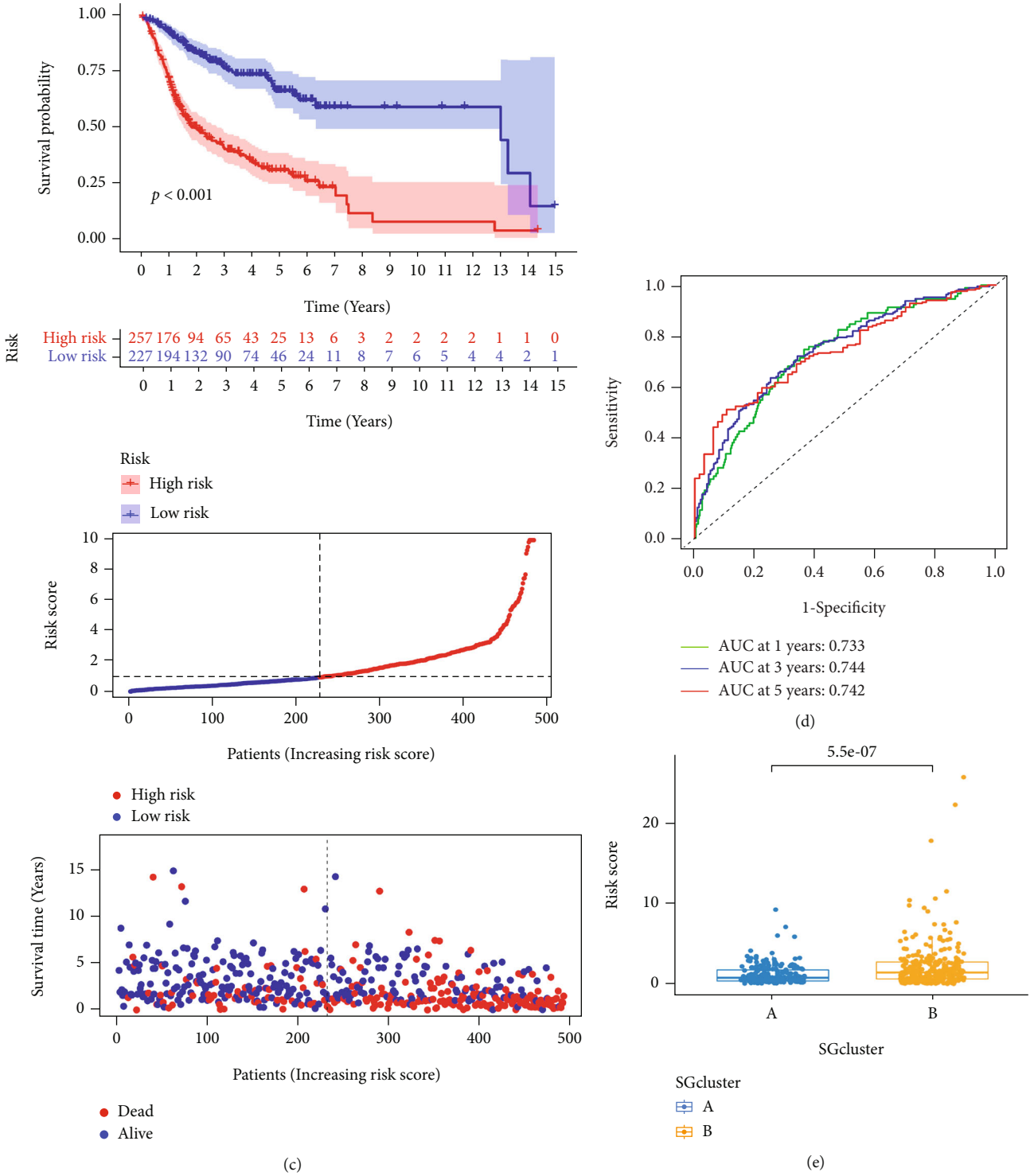

Figure 5: Continued.

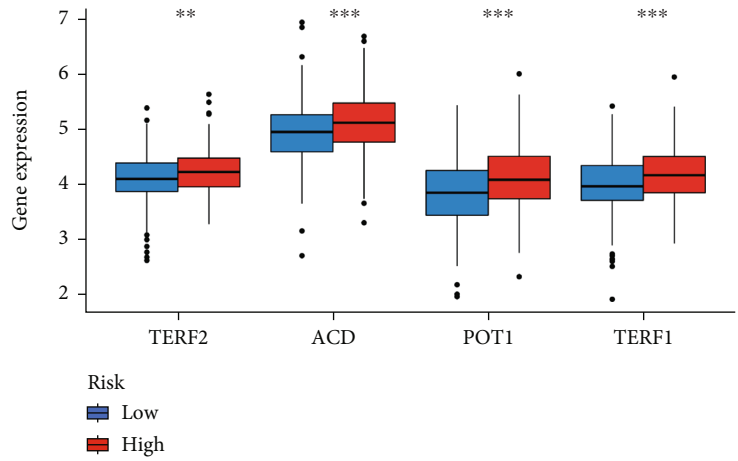

(f)

Figure 5: Construction of SGs-related risk signature. (a) Validation was performed for tuning parameter selection through the least absolute shrinkage and selection operator (LASSO) regression model for overall survival (OS). (b) Cross-validation for tuning parameter selection in the lasso regression. (c) SGs-related prognostic model constructed in total OSCC patients. (d) Plots of the AUC for time-dependent ROC performance. (e) SGCluster B has a higher risk score. (f) Expression levels of SGs genes in high- and low-risk groups.

msigdb.org/) was used to obtain the gene set (c2.cp.kegg.v7.2.symbols.gmt).

2.5. Construction of an SG-Related Risk Scores Model. SG-related patterns are differentiated by differently expressed genes (DEGs). Subsequently, DEGs with $P < 0.05$ were also included in the univariate Cox regression test utilizing the selection operator (LASSO) algorithm for dimensionality reduction and least absolute shrinkage [24–26]. Based on standardized expression levels and coefficients, each patient was assigned a risk score (RS). A median risk score was used to group patients into high- and low-risk groups. Using the R package "survminer," survival analysis was conducted between groups of high- and low-risk individuals. Analyses of multivariate and univariate Cox regression were also performed to determine the prognostic value of risk scores.

2.6. Tumor Mutation Burdens (TMB). In order to summarize OSCC patients' mutations, we used the COSMIC (Catalogue of Somatic Mutations in Cancer, https://cancer.sanger.ac.uk/cosmic) and then gathered genomic mutation data of TCGA-OSCC for further analysis [27, 28].

2.7. Evaluation of the Chemotherapy and Immunotherapy Response Based on RS. For predicting the IC50 of chemotherapy drugs for OSCC patients from TCGA, the "pRRophetic" package was used to explore their sensitivity to different treatments. We compared the high-risk and low-risk groups. The "ESTIMATE" package was used to calculate the stromal scores, ESTIMATE scores, immune scores, and tumor purity. Additionally, we assessed immune cell infiltration levels in the TME by using the ssGSEA algorithm in the R "GSVA" package. From The Cancer Immunome Atlas (TCIA), we downloaded immunophenotype scores (IPS) from the TCGA-OSCC project. The higher the IPS, the better the accuracy of the more accurate result [29, 30].

2.8. Statistical Analysis. Statistical analyses were carried out using R version 4.1.0, GraphPad Prism 8, and SPSS 23.0. We used the cluster profile package to examine GO, KEGG, and functional annotation enrichment. The ROC curve analysis was conducted using the "timeROC," "survminer," and "survival" R packages. The volcano and heat map were developed by R software's "ggplots" package. *P* values for all statistical analyses were two-sided, and a significance level of $P < 0.05$ was considered.

3. Results

3.1. Identification of SGs between Normal and Tumor Tissues in OSCC. The shelterin complex consists of six proteins (Figure 1(a)), termed TRF1, TRF2, RAP1, TPP1, POT1, and TIN2, and abnormal expression of shelterin has been observed in various types of cancers. However, the study of shelterin genes in OSCC is unclear. Compared with normal tissues, we found that all 6 SGs were significantly highly expressed in the tumor group (Figure 1(b)). The comprehensive landscape of the interactions between 6 SGs in OSCC patients is illustrated in the network. A positive correlation was found between the 6 SGs, many of which were risk factors for OSCC (Figure 1(c)). The occurrence and development of OSCC may be influenced by crosstalk. According to the survival analysis, high expression levels of TERF1, TERF2, ACD, and POT1 contributed to poor prognosis, while high expression level of TINF2 had a better survival advantage (Figure 1(d)). The functional enrichment analysis of SGs was performed through the Metascape website, and the results showed that SGs were mainly enriched in telomere-related pathways, such as telomere-associated protein complex, protection from nonhomologous end joining at telomere, RNA-dependent DNA biosynthetic process, and telomeric D-loop disassembly (Figure 1(e); Table 1). Enriched terms were selected and rendered as a network plot (Figure 1(f)).

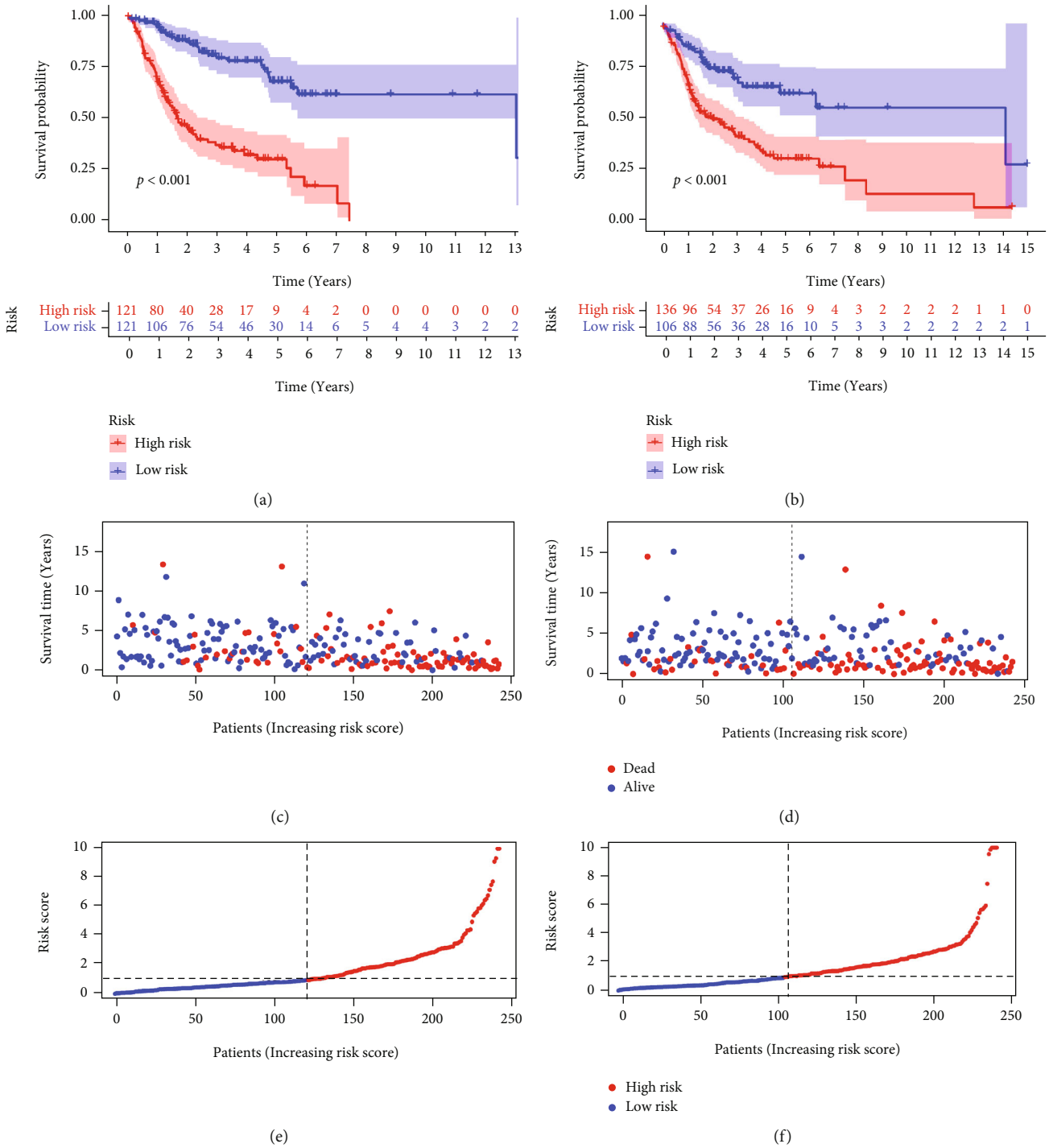

Figure 6: Continued.

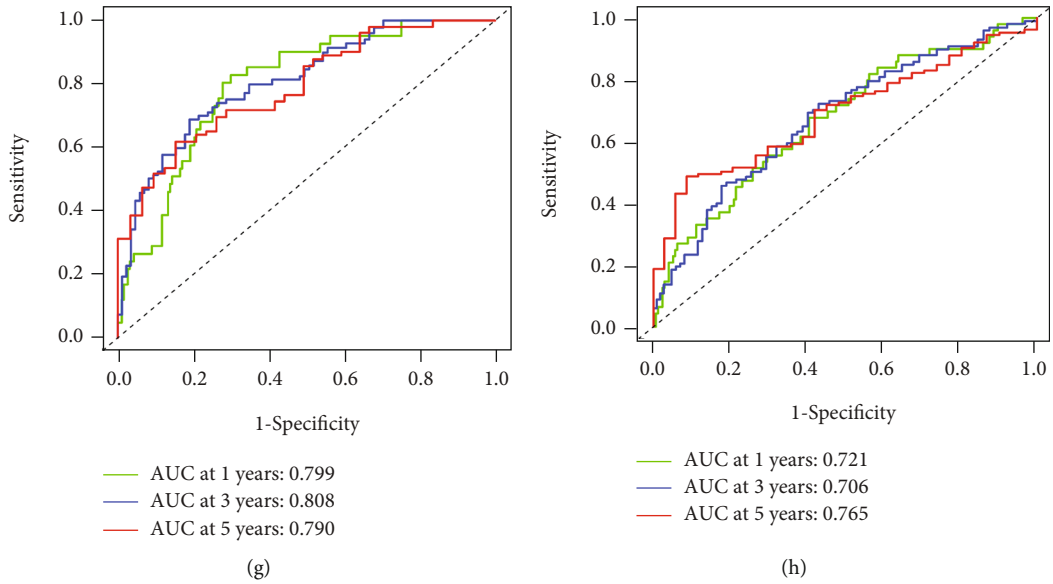

Figure 6: Verification of SGs-related risk signatures. Validation cohort 1 (a, c, e, and g), and the validation cohort 2 (b, d, f, and h). (a, b) Kaplan–Meier survival curve. (c, d) Survival statuses of high-risk and low-risk patients. (e, f) The distribution of the risk scores. (g, h) Plots of the AUC for time-dependent ROC performance.

3.2. Analysis of the Expression Distribution of SGs Based on Single-Cell Data. We obtained 5902 single-cell data from 18 oral tumor patients from GSE103322 to determine the expression distribution of SGs in different cell types. Using TISCH (Tumor Immune Single-cell Hub) database, we visualized them. Findings revealed that these cells were divided into 20 clusters (Figure 2(a)). Primary cell types include CD4Tconv, CD8T, CD8Tex, endothelial, fibroblasts, malignant, Mast, mono/macro, myocyte, myofibroblasts, and plasma (Figure 2(b)). Among them, malignant enrichment was the most, and fibroblasts in the second (Figure 2(c)). Then we further visualized the expression levels of SGs at single-cell resolution (Figure 2(d)), and we found that TERF2I1 and TINF2 gene expression distribution were the most enriched, mainly distributed on CD8Tex, endothelial, fibroblasts, Mast, mono/macro, and myocyte (Figure 2(e)).

3.3. Classification of Tumors Based on SGs. Based on the expression levels of SGs, we conducted a consensus clustering analysis on OSCC patients to better understand the role of SGs in OSCC. When we increased the clustering variable (k) from 2 to 9, we found the highest correlation between OSCC patients and other groups when $k = 2$ (Figures 3(a)–3(c)). Kaplan-Meier analysis revealed that SGCluster A had a significantly greater overall survival time (OS) than SGCluster B ($P = 0.009$, Figure 3(d)). Our heat map compares the SGs expression and clinical characteristics between the two clusters. Based on the heat map, we found that except for TINF2, the rest of the SGs were significantly enriched in SGCluster B (Figure 3(e)). The PCA analysis demonstrated that the SGs-based classification pattern could classify OSCC patients into two distinct subgroups (Figure 3(f)). The GSVA enrichment analysis explored the biological differences between these two clusters (Figure 4(a)). SGCluster A is significantly enriched for cancer and immune-related pathways, such as complement and coagulation cascades, autoimmune thyroid disease, ppar signaling pathway, olfactory transduction, cytokine receptor interaction, hematopoietic cell lineage, neuroactive ligand-receptor interaction, arachidonic acid metabolism, linoleic acid metabolism, and retinol metabolism. SGCluster B is enriched in nucleotide excision repair, cell cycle, glycosylphosphatidylinositol GPI anchor biosynthesis spliceosome, basal transcription factors, mismatch repair, aminoacyl-tRNA biosynthesis, homologous recombination, ubiquitin-mediated proteolysis, and RNA degradation. We also analyzed the level of immune infiltrating cells between the two subgroups (Figure 4(b)). We found that SGCluster A exhibited a greater enrichment of immune cells, such as activated B cells, CD8 T cells, eosinophilia, macrophage, Mast cell, and neutrophil, which may also be the one reason why SGCluster A has a better prognosis.

In addition, we identified 1329 DEGs between SGCluster A and SGCluster B (Supplementary file 1) and performed functional enrichment analysis on them. The DEGs enriched in GO pathways were mainly involved in DNA replication, DNA helicase activity, condensed chromosome, nuclear chromosome, kinetochore, and DNA replication (Figure 4(c)). In the KEGG enrichment analysis, DEGs were mostly enriched in pathways related to cell cycle, DNA replication, and cellular senescence, such as cell cycle, cellular senescence, ECM-receptor interaction, base excision repair, p53 signaling pathway, and PI3K-Akt signaling pathway (Figure 4(d)).

3.4. Development and Validation of an SGs-Related Risk Signature. Based on DEGs between SGCluster A and SGCluster B, we developed a prognostic model to explore further the application of SGs in OSCC patients' prognosis and treatment. To screen DEGs for genes associated with

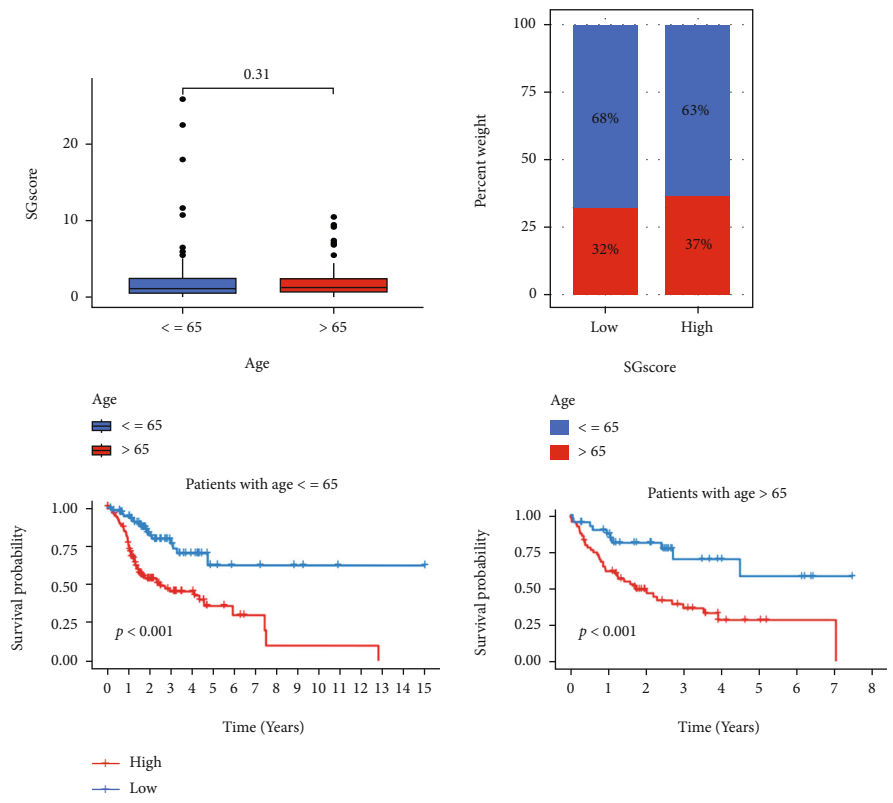

(a)

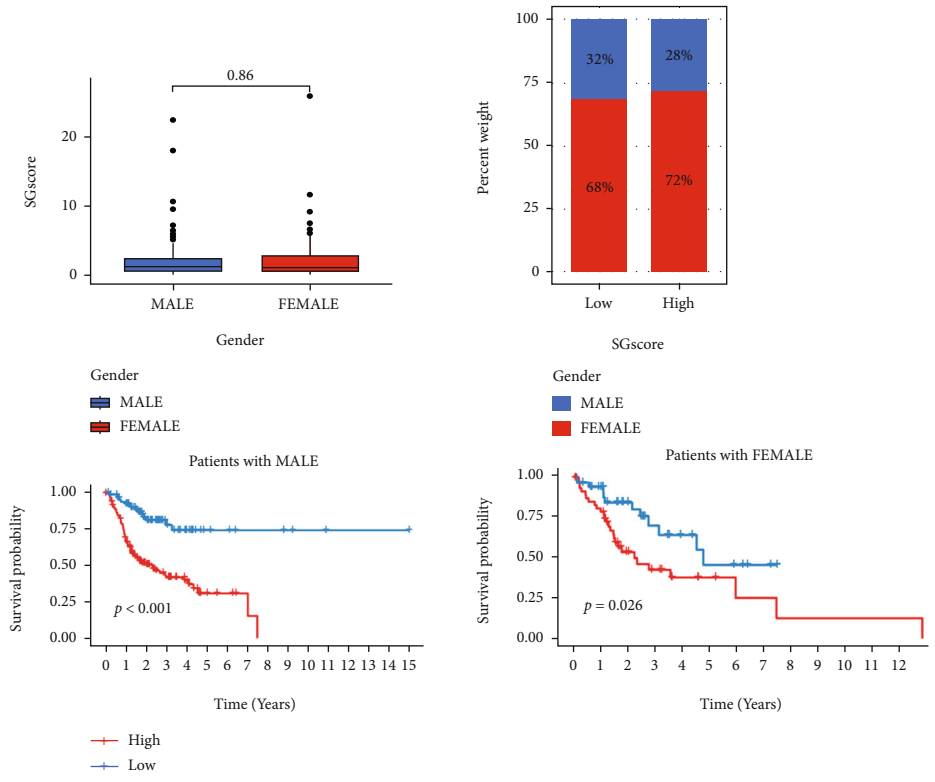

(b)

Figure 7: Continued.

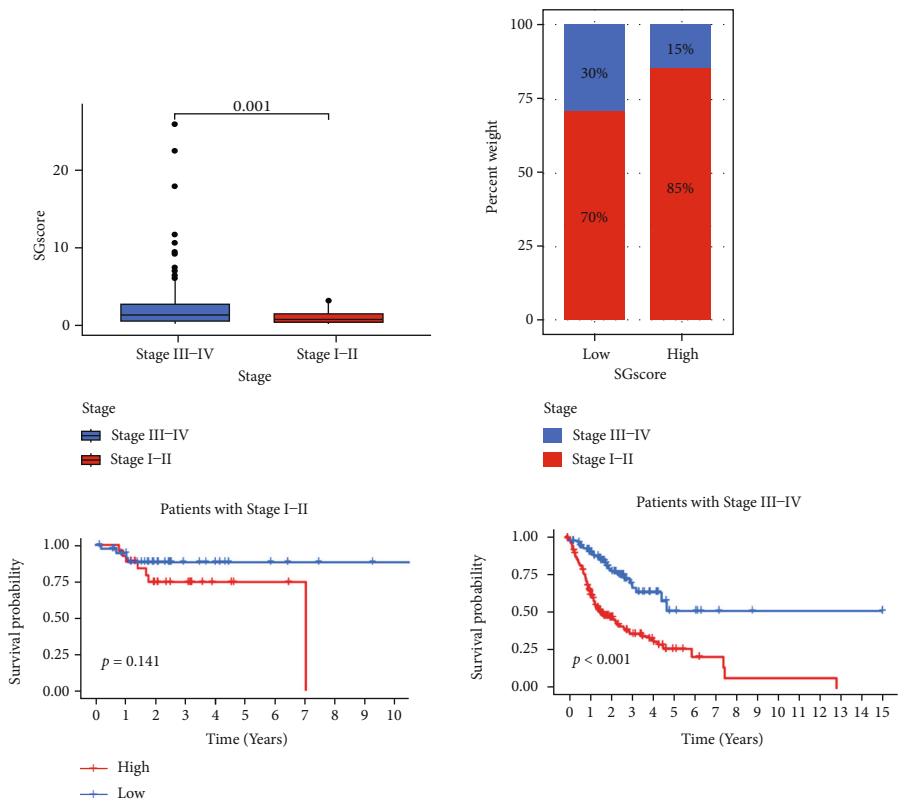

(c)

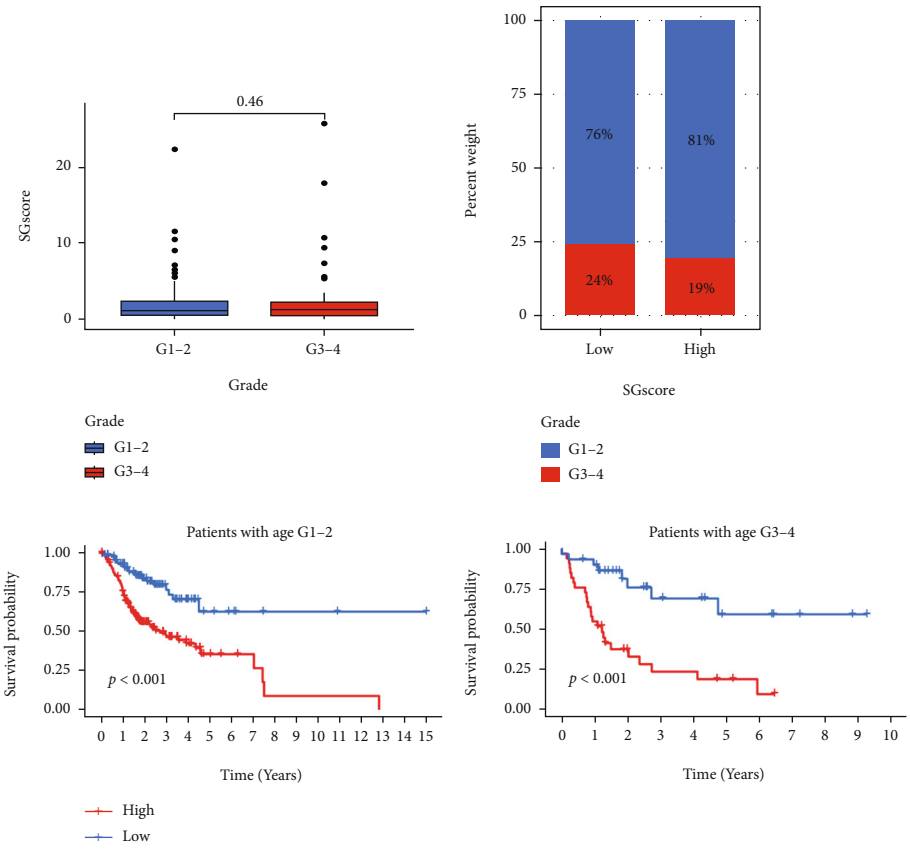

(d)

Figure 7: Continued.

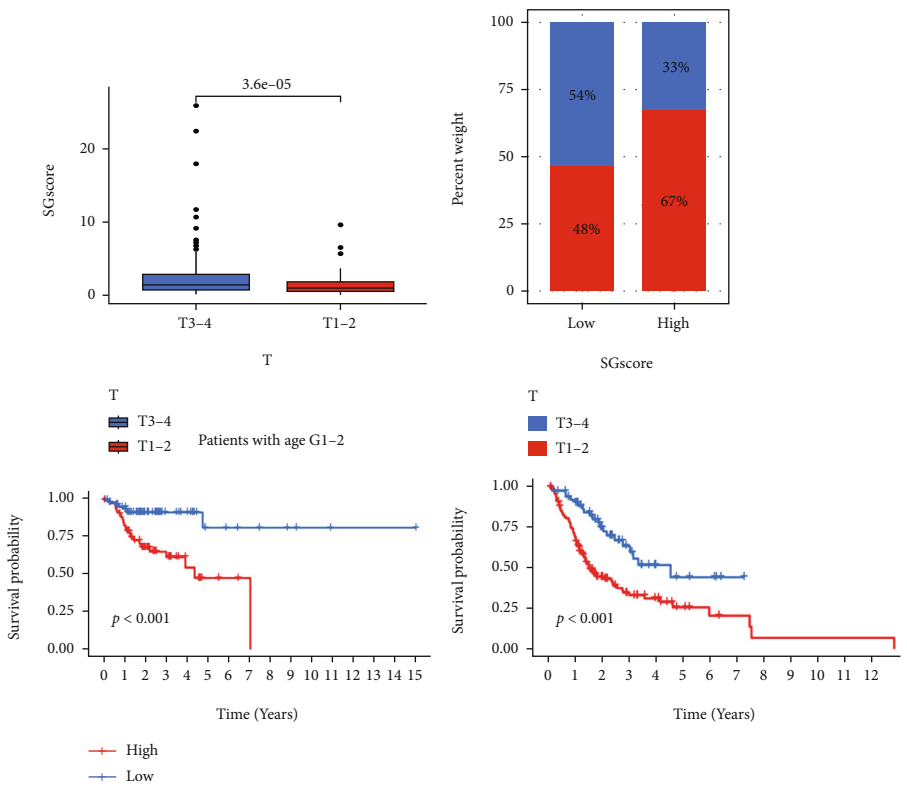

(e)

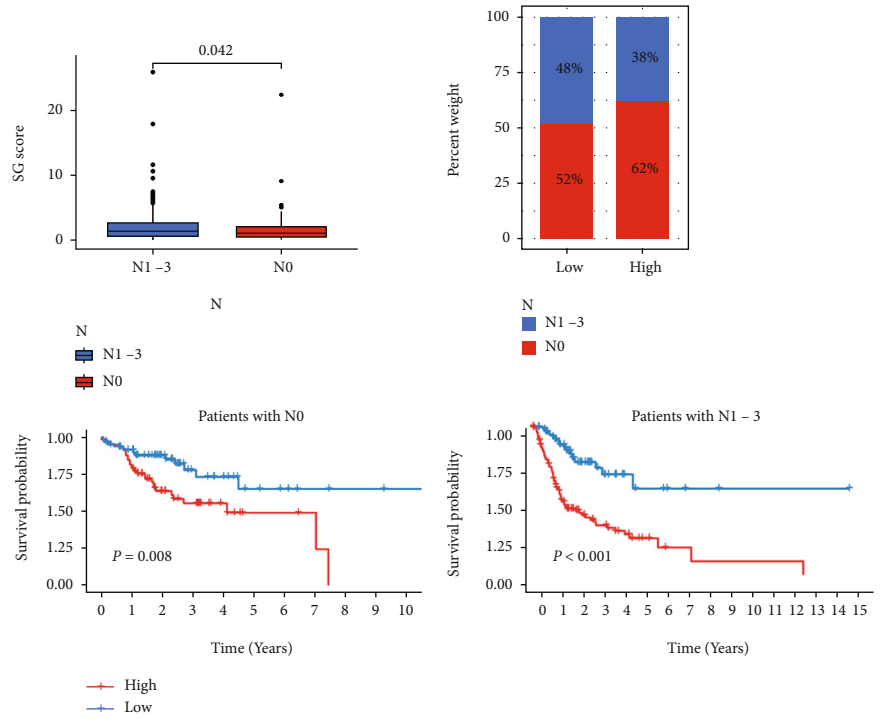

(f)

Figure 7: Relationship between risk scores and clinical characteristics. Relationship between risk score and age (a), gender (b), stage (c), grade (d), T (e), and N (f).

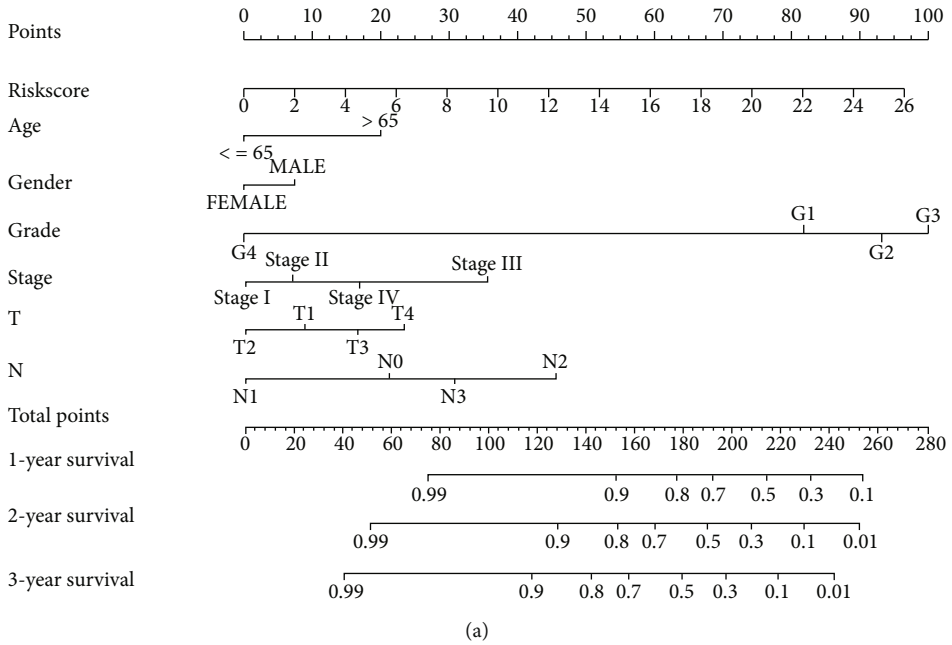

(a)

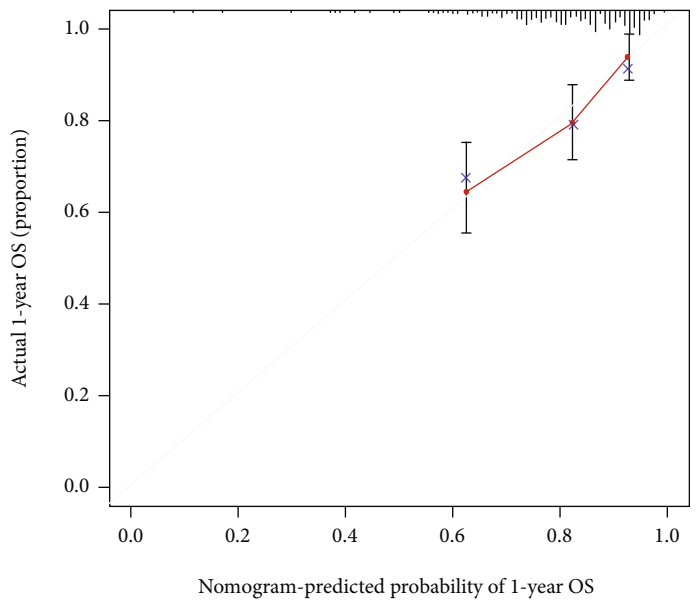

(b)

Figure 8: Continued.

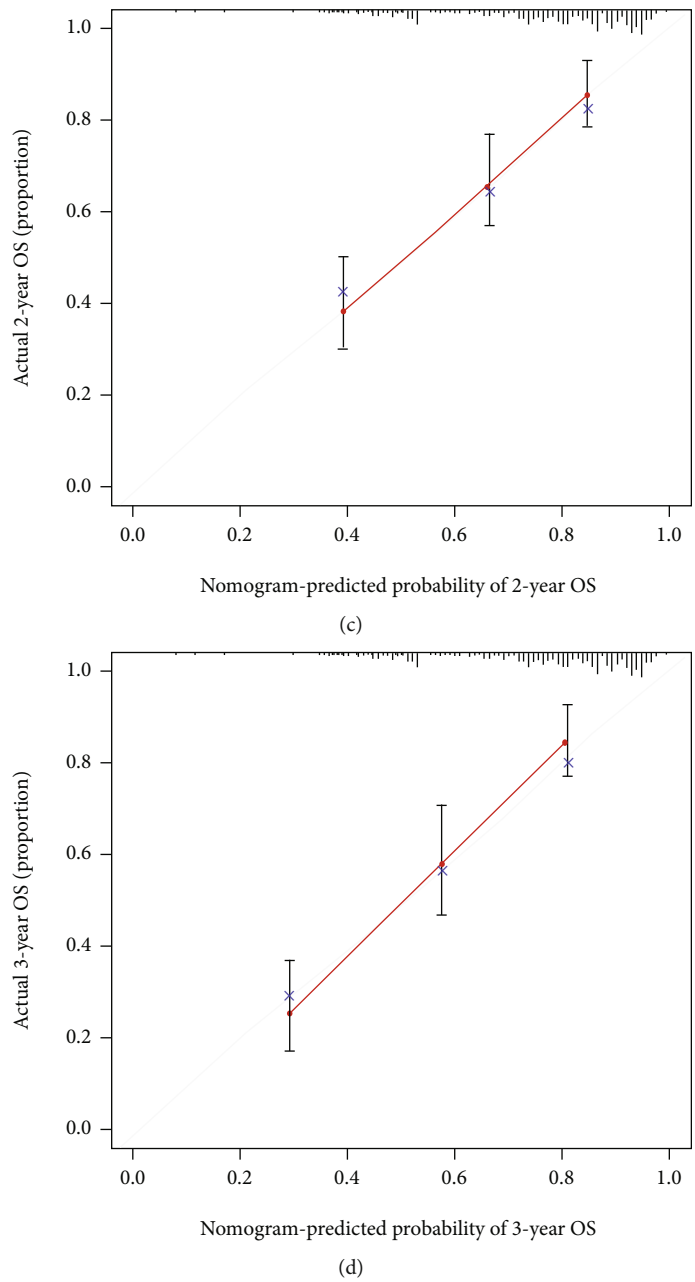

Figure 8: Nomogram to predict the 1-year, 2-year, and 3-year overall survival rates of OSCC patients. (a) A nomogram for predicting survival. Nomogram calibration plots for predicting OS at 1 (b), 2 (c), and 3 (d) years.

prognosis, we performed a univariate Cox analysis (Supplementary file 2). Based on the results of the LASSO algorithm, the best prognostic genes were identified in OSCC patients (Figures 5(a) and 5(b)). We constructed multivariate Cox prediction signatures based on the prognostic genes identified with LASSO. The final analysis identified 14 genes associated with risk. Patients with OSCC were classified into low- and high-risk categories based on their median risk score. According to Kaplan-Meier plots, low-risk patients tend to have a better prognosis (Figure 5(c)). We constructed time-dependent ROC curves to evaluate the model's predictive ability, with AUCs reaching 0.733 after 1 year, 0.744 after 2 years, and 0.742 after 5 years (Figure 5(d)). The results indicate that the model is a good predictor. In addition, we evaluated the risk scores of SGCluster A and SGCluster B. We found that SGCluster A has a lower risk score (Figure 5(e)), supporting our previous findings that SGCluster A has a better outcome (Figure 3(d)). Figure 5(f) shows the expression levels of specific SGs in high-risk and low-risk groups, in which TERF1, TERF2, ACD, and POT1 are all significantly highly expressed in the high-risk population (Figure 5(f)).

To further test the model's robustness, OSCC patients were randomly assigned to validation cohort 1 (Figures 6(a)–6(c), and 6(e)) and validation cohort 2 (Figures 6(b)–6(d), and 6(f)). We calculated the risk score

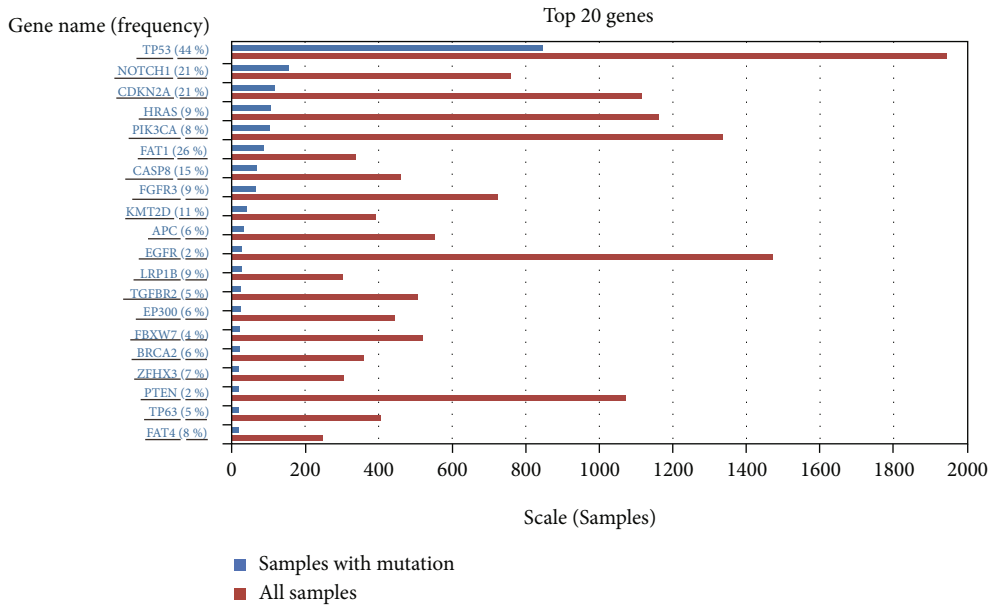

(a)

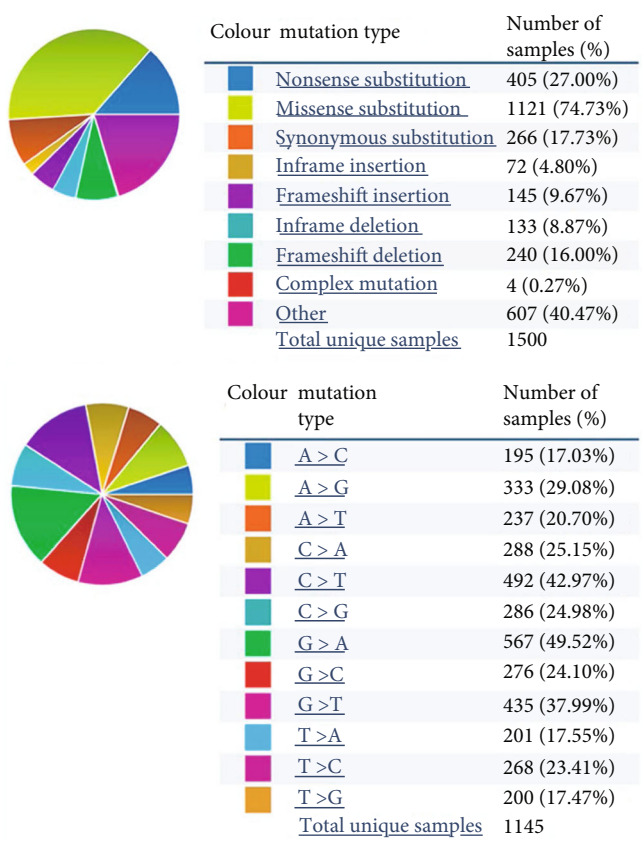

Colour	mutation type	Number of samples (%)
	Nonsense substitution	405 (27.00%)
	Missense substitution	1121 (74.73%)
	Synonymous substitution	266 (17.73%)
	Inframe insertion	72 (4.80%)
	Frameshift insertion	145 (9.67%)
	Inframe deletion	133 (8.87%)
	Frameshift deletion	240 (16.00%)
	Complex mutation	4 (0.27%)
	Other	607 (40.47%)
	Total unique samples	1500

Colour	mutation type	Number of samples (%)
	A > C	195 (17.03%)
	A > G	333 (29.08%)
	A > T	237 (20.70%)
	C > A	288 (25.15%)
	C > T	492 (42.97%)
	C > G	286 (24.98%)
	G > A	567 (49.52%)
	G >C	276 (24.10%)
	G >T	435 (37.99%)
	T >A	201 (17.55%)
	T >C	268 (23.41%)
	T >G	200 (17.47%)
	Total unique samples	1145

(b)

Figure 9: Continued.

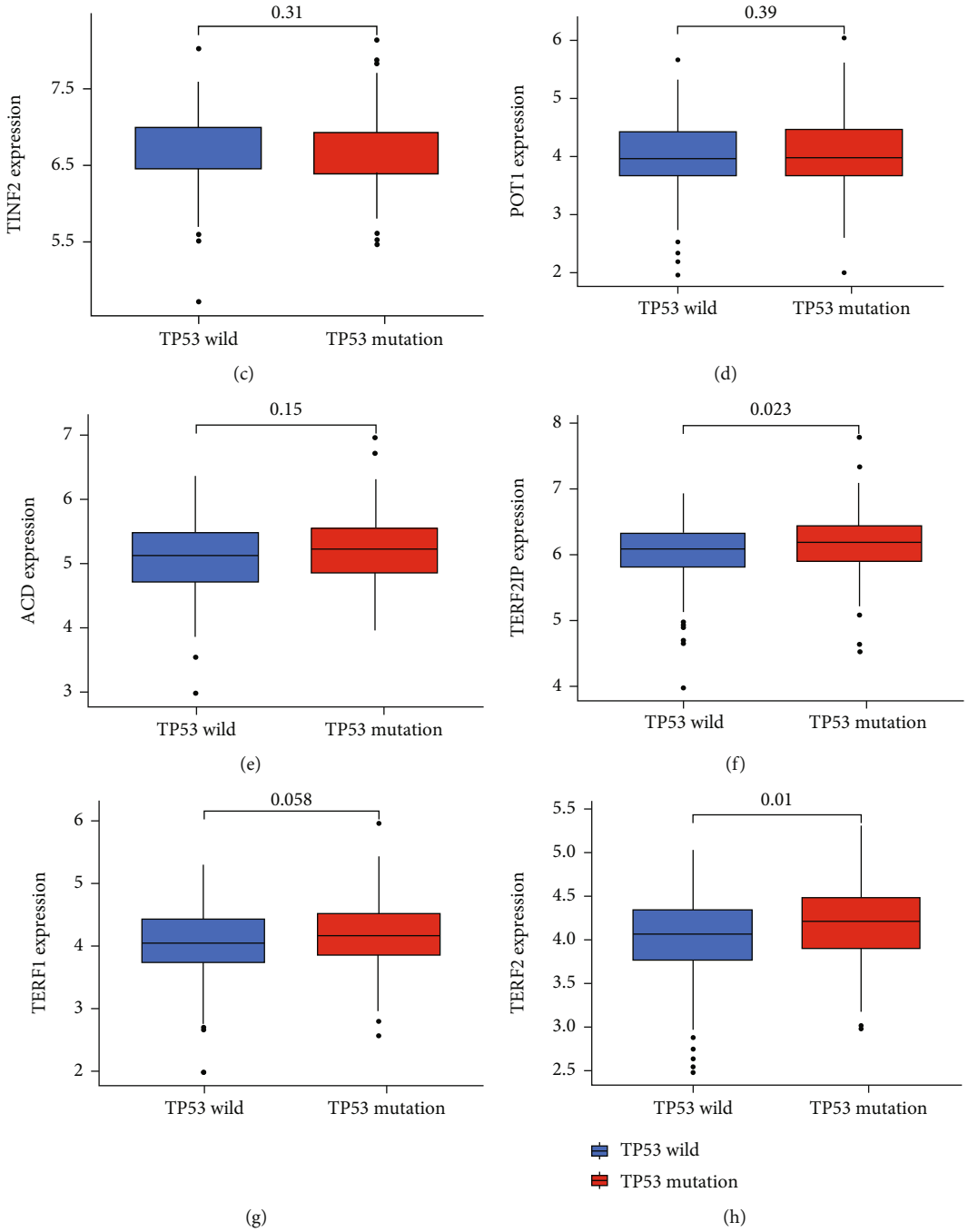

Figure 9: Continued.

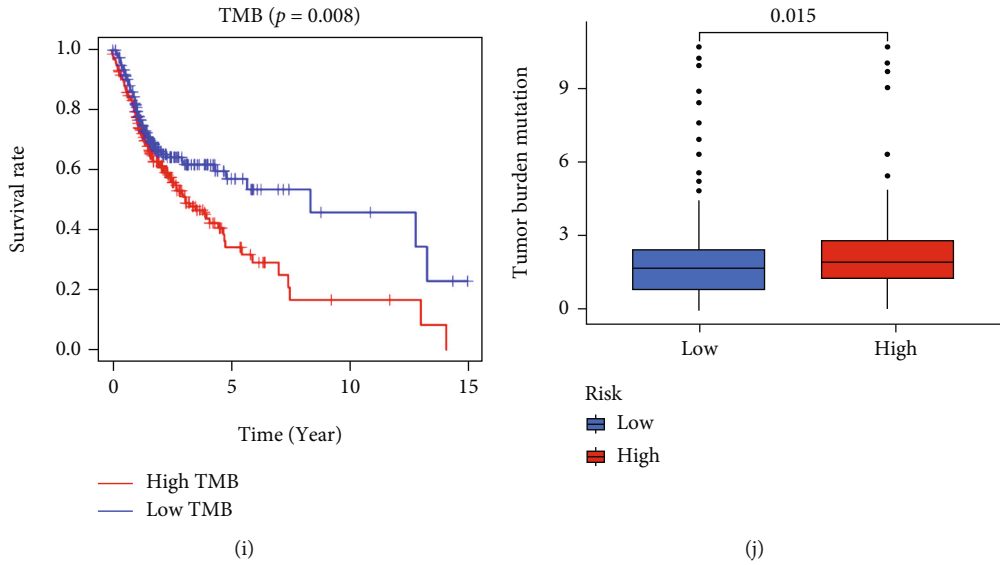

Figure 9: Relationship between risk score and TMB. COSMIC database analysis of OSCC mutation distributions (a) and its types (b). (c–h) Correlation analysis of TP53 mutation and gene expression level of SGs. (i) High TMB scores are associated with poorer outcomes. (j) Distribution of TMB in high- and low-risk score groups.

using the same algorithm, and we found that greater risk was associated with a worse outcome (Figures 6(a) and 6(b)). The AUC confirmed the reliability of the model results for both the validation cohort 1 (Figure 6(g); AUC at one, three, and five years were 0.799, 0.808, and 0.790, respectively) and the validation cohort 2 (Figure 6(h); AUC at 1, 3, and 5 years were 0.721, 0.706, and 0.765, respectively).

3.5. Relationship between Risk Scores and Clinical Characteristics. We analyzed the relationship between clinical characteristics (age, gender, stage, grade, T, and N) and risk scores to validate the accuracy of risk scores further and identify their role (Figures 7(a)–7(f)). A significant association was found between risk scores and stage (Figure 7(c)), T stage (Figure 7(e)), and N stage (Figure 7(f)), and patients with poorer clinical characteristics (stages III-IV, N1-3) tended to have higher risk scores. In addition, we found that risk score remained an excellent predictor (patients with age ≤65, age >65, MALE, FEMALE, stages III-IV, G1-2, G3-4, T1-2, T3-4, N0, and N1-3). We created risk scores as well as nomograms to extend their clinical application. Each patient was assigned a total score based on the scores of the item indicators, and patients with higher total scores had poorer clinical outcomes (Figure 8(a)). Calibrating the nomogram was good predictive power (Figures 8(b)–8(d)).

3.6. SGs-Related Risk Scores Could Predict and Represent Tumor Mutational Burden (TMB). According to an increasing amount of evidence, TMB may be a catalyst for tumor progression. Using the COSMIC database, we analyzed the mutation status of OSCC. The most common mutation types in OSCC were missense, G > A, and C > T mutations (Figures 9(a) and 9(b)). According to the TCGA data, TP53 is the gene with the highest mutation rate in OSCC, so we looked into the relationship between TP53 mutations and gene expression levels in this tumor (Figures 9(c)–9(h)), determining that the TP53 mutation group has a higher level of TERF2IP (Figure 9(f)) and TERF2 (Figure 9(h)) expression. In addition, high TMB scores are associated with a worse prognosis (Figure 9(i)). This resulted in a higher TMB score in the high-risk group (Figure 9(j)), indicating the importance of the risk score in TMB.

3.7. The Role of Risk Scores in the Tumor Microenvironment (TME). The application of the ssGSEA algorithm allowed us to estimate immune cell infiltration in the high-risk and low-risk groups. Results revealed that the low-risk group had more immune cells present (Supplementary Figure 1); the resting Mast cells, CD4 memory activated T cells, CD8 naive B cells, T cell regulatory (Tregs) cells, plasma cells, and T cell CD8 were all negatively correlated with risk. The risk scores were positively correlated with macrophages M0, CD4 memory resting T cells, NK cells resting, and Mast cells activated (Figure 10(a)). Furthermore, we used ESTIMATE (Figures 10(d)–10(g)). ssGSEA algorithms (Figure 10(c)) were used to analyze the TME of OSCC. The low-risk group had a higher immune score, immune-infiltrating cells, and immune pathways (Figure 10(d)).

3.8. Exploring the Application Value of Risk Score in Clinical Treatment. Risk scores related to SGs have been found to play an important role in TMB and TME. In order to further explore the clinical utility of risk scores, we performed univariate and multivariate Cox analyses to identify their prognostic value. Based on the findings, OSCC patients' risk score was an independent prognostic factor (Figure 11(a)). A wide variety of tumors have been treated with immunotherapy. Through the TCIA database, OSCC patients' IPS data were examined to determine the risk score's role in immunotherapy (Figures 11(b)–11(g)). In low-risk patients, CTLA4 expression was significantly high (Figure 11(c)).

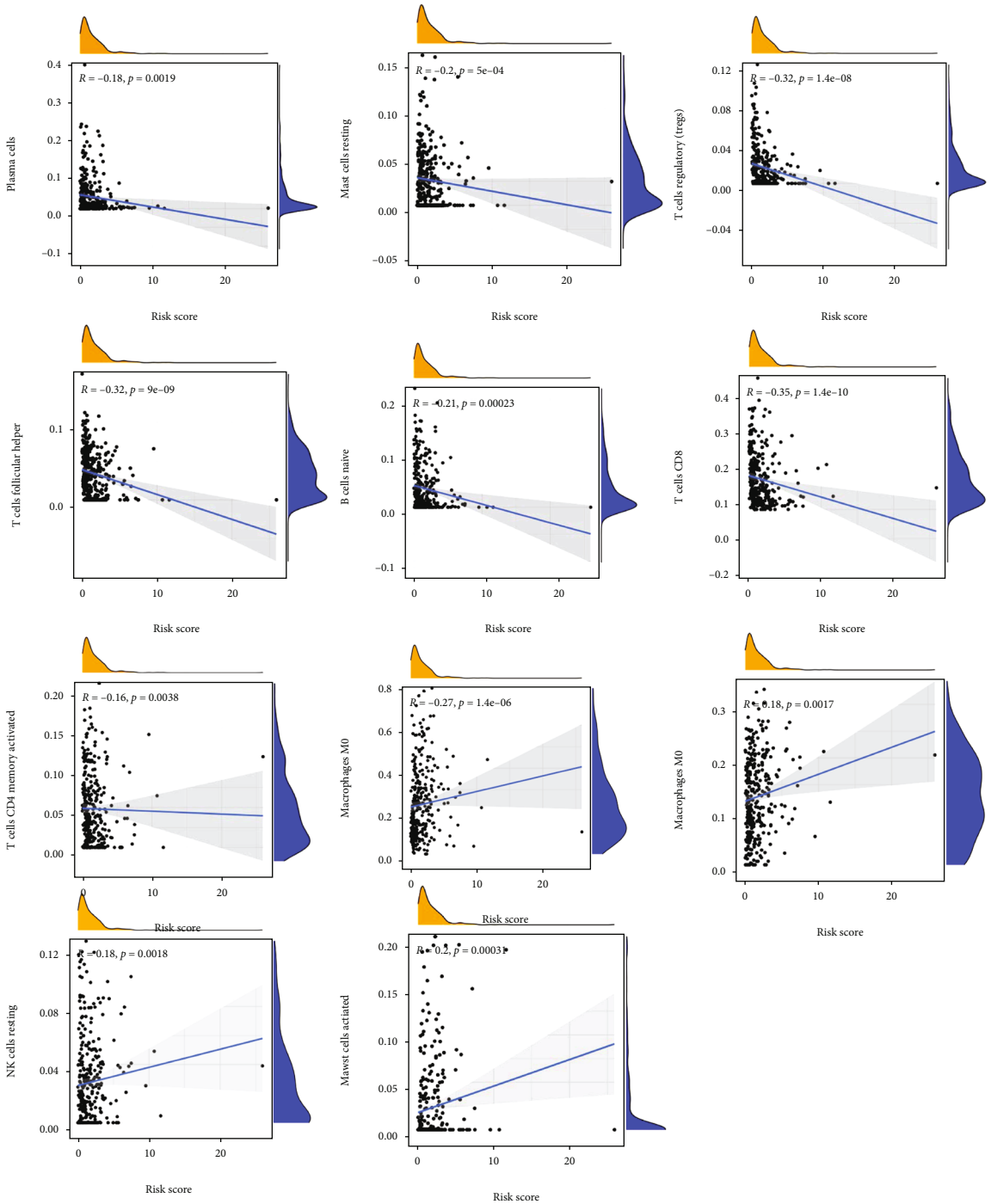

(a)

Figure 10: Continued.

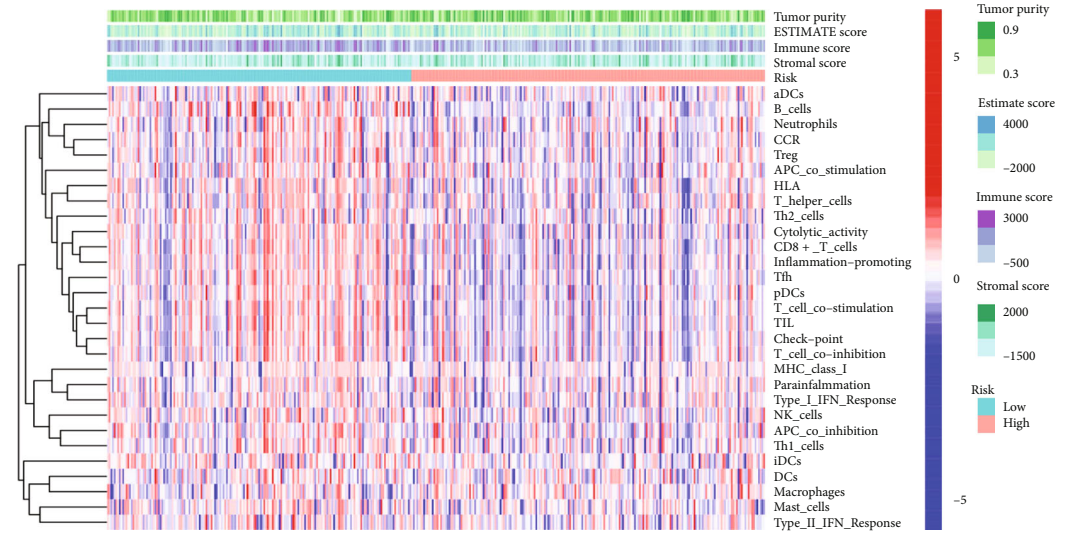

(b)

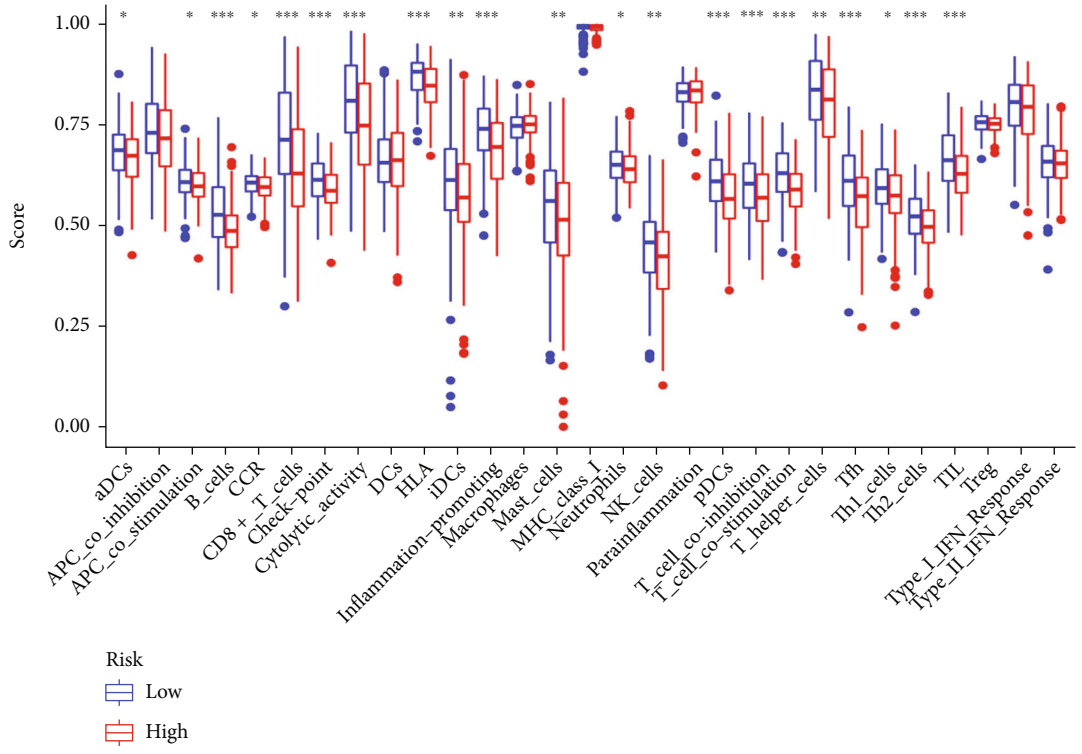

(c)

Figure 10: Continued.

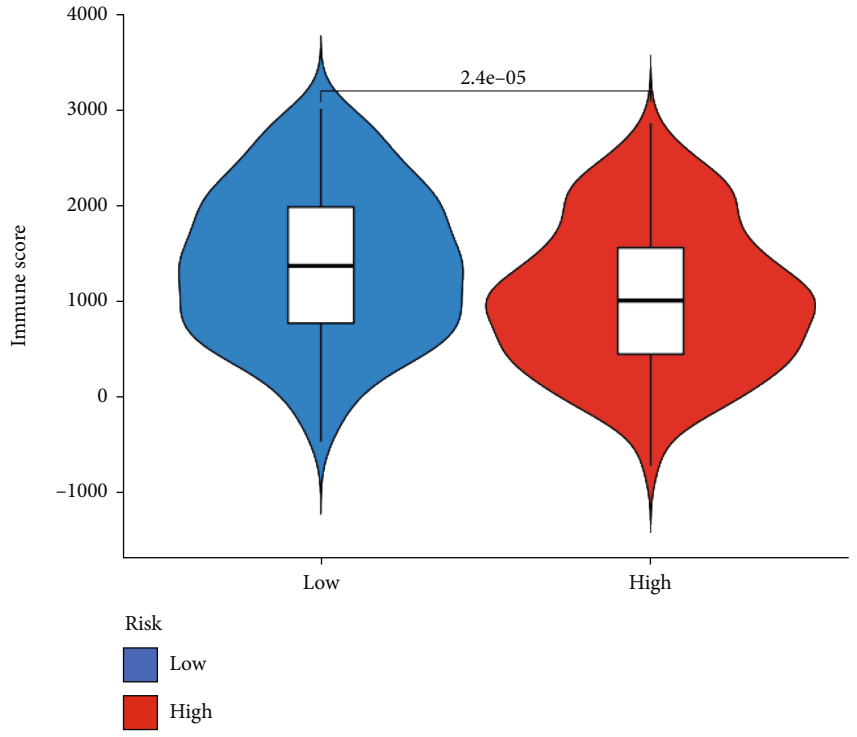

(d)

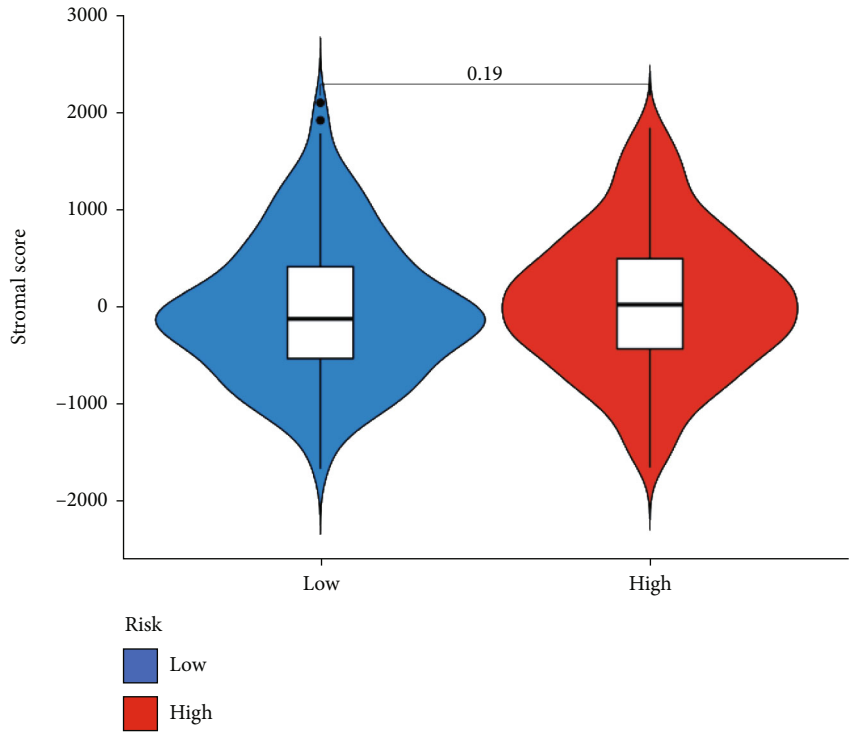

(e)

Figure 10: Continued.

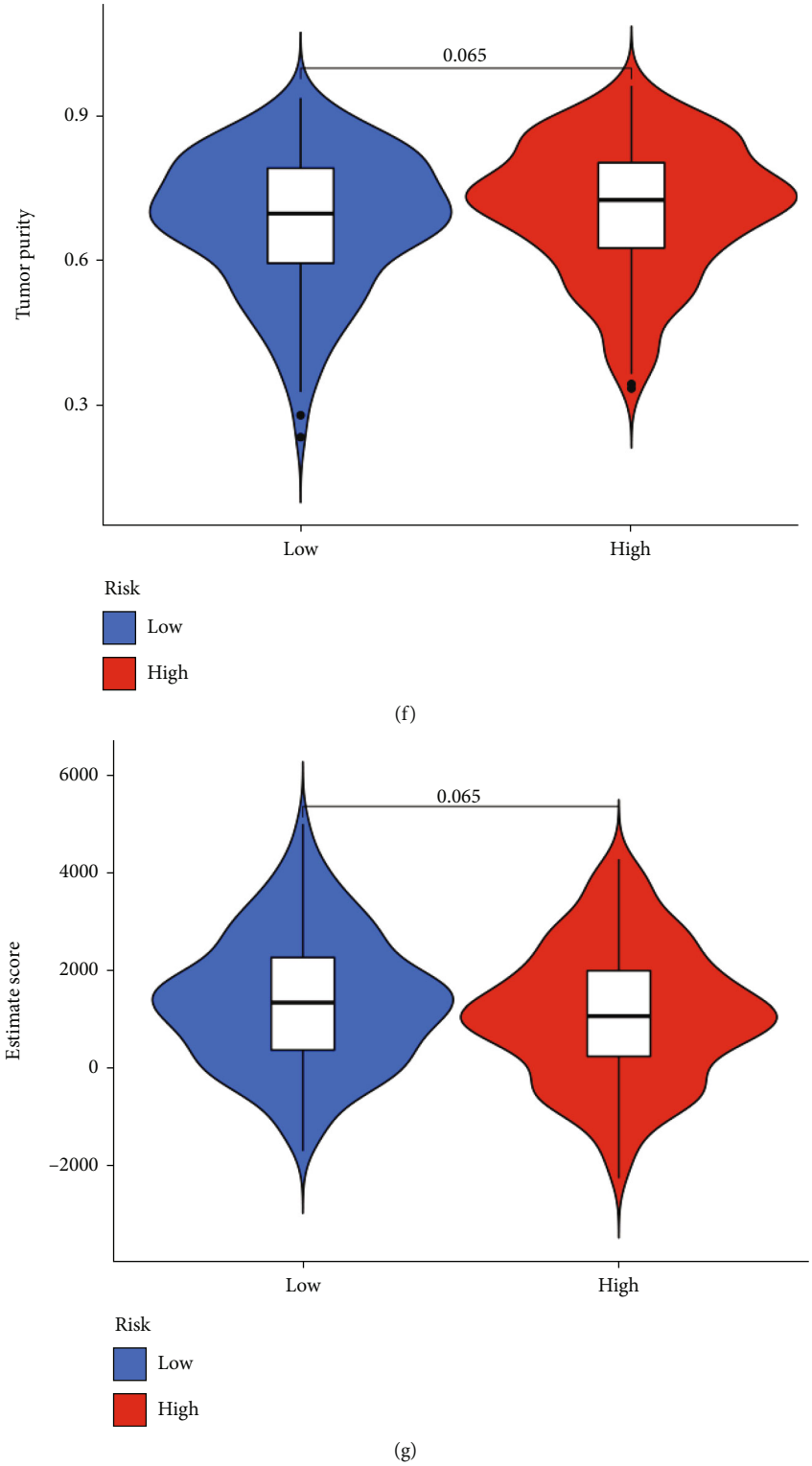

Figure 10: The relationship between risk score and TME. (a) Correlation analysis of immune infiltrating cells and risk score. (b) Heat map of the relationship between microenvironment and risk score. (c) Enrichment analysis of immune cells and immune-related pathways in high- and low-risk groups. $*P < 0.05$, $**P < 0.01$, and $*** P < 0.001$. Comparison of immune score (d), stromal score (e), tumor purity (f), and ESTIMATE score (g) in high- and low-risk groups.

Accordingly, the IPS score showed that low-risk patients received immunotherapy more readily than high-risk patients (Figures 11(d)–11(g)), which could help our clinical treatment. GSEA enrichment analysis revealed the high-risk groups tended to be enriched for the following: dilated cardiomyopathy, ECM receptor interaction, metabolism of

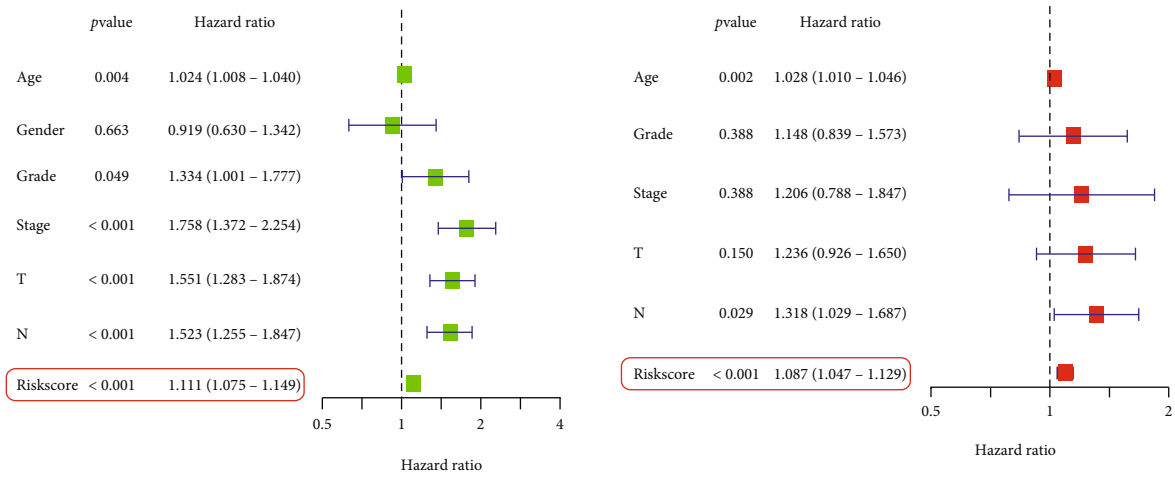

(a)

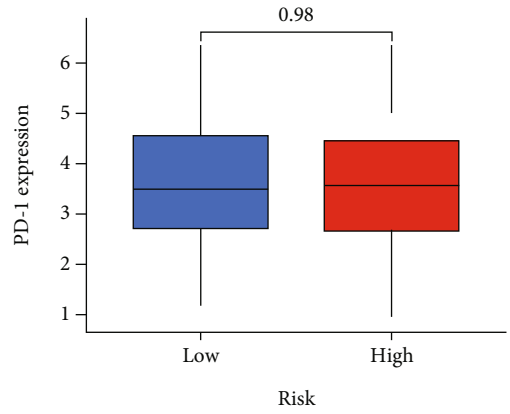

(b)

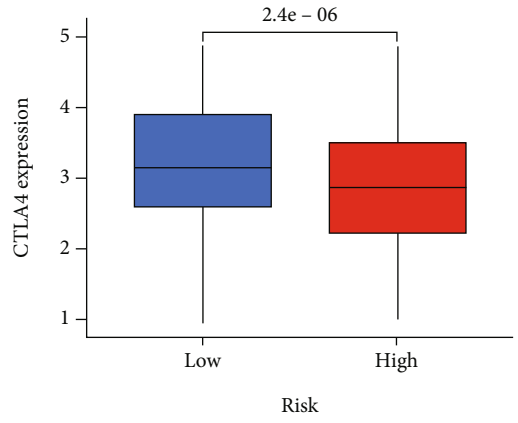

(c)

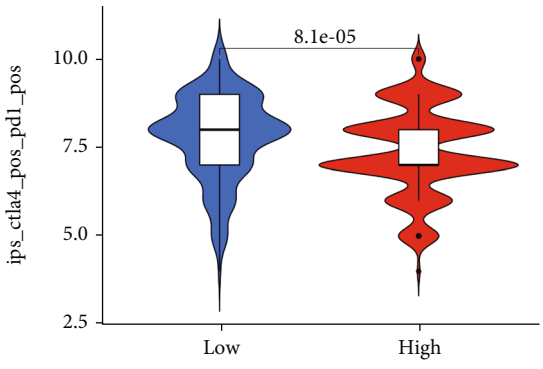

(d)

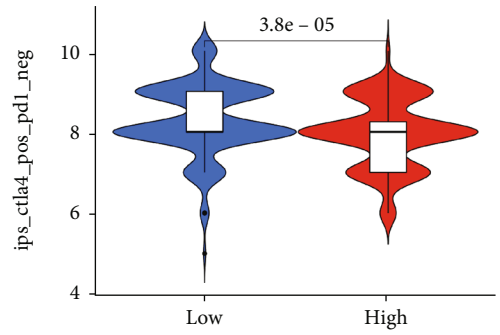

(e)

Figure 11: Continued.

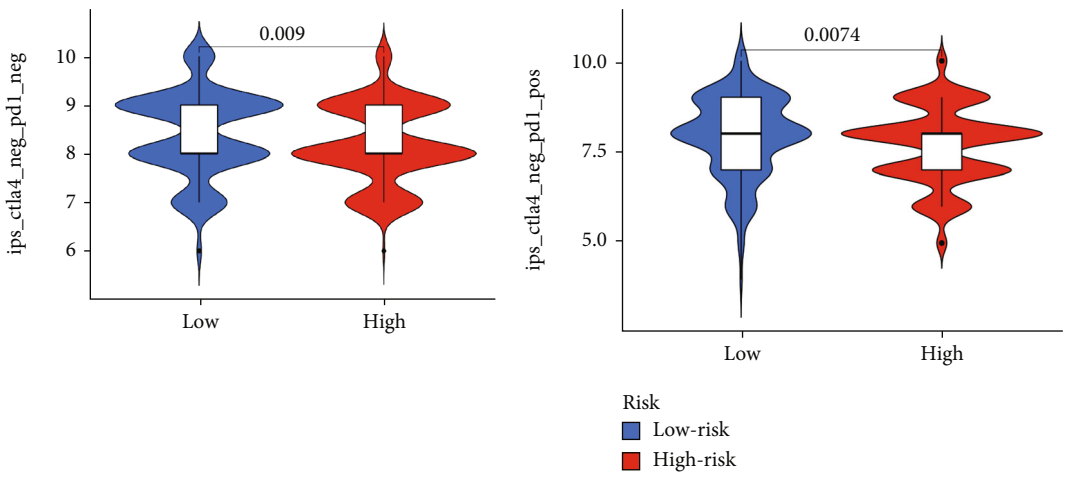

(f) (g)

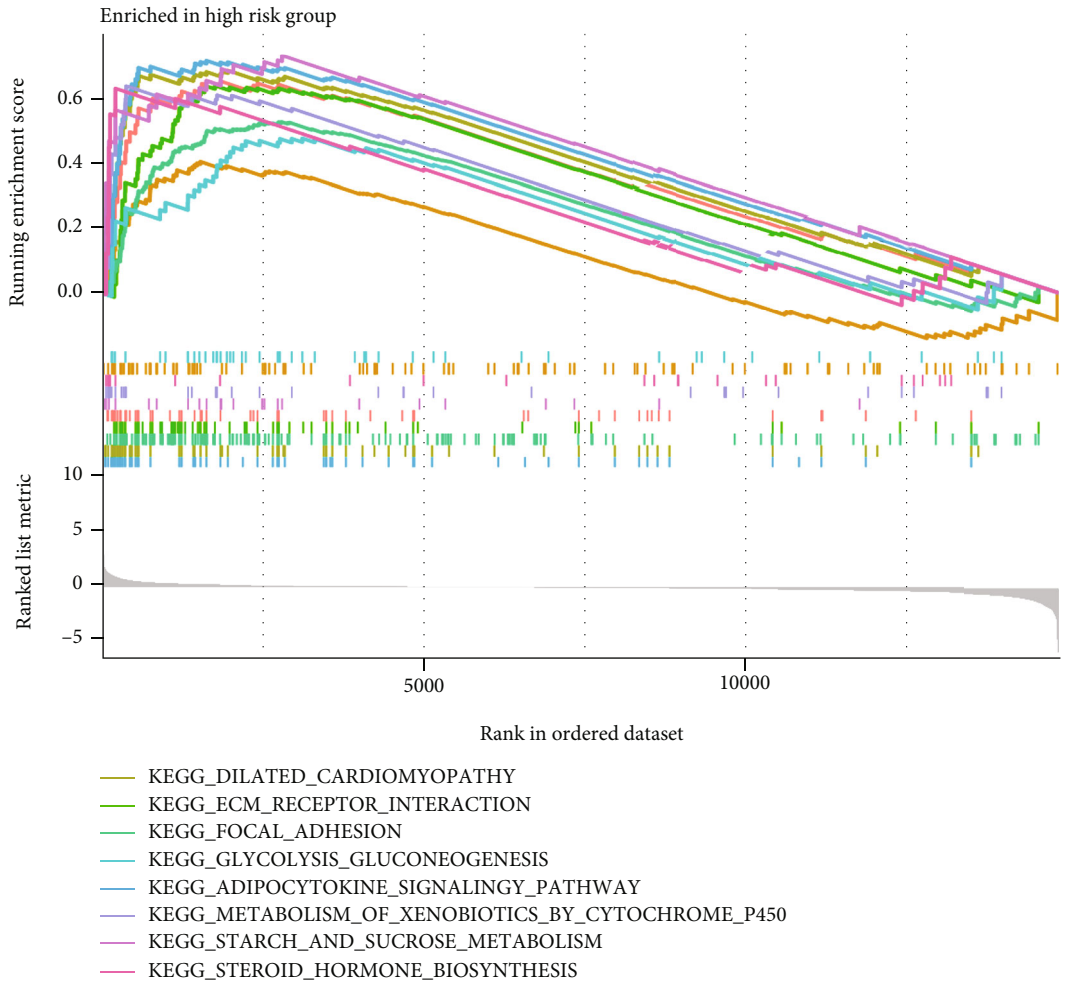

(h)

Figure 11: Continued.

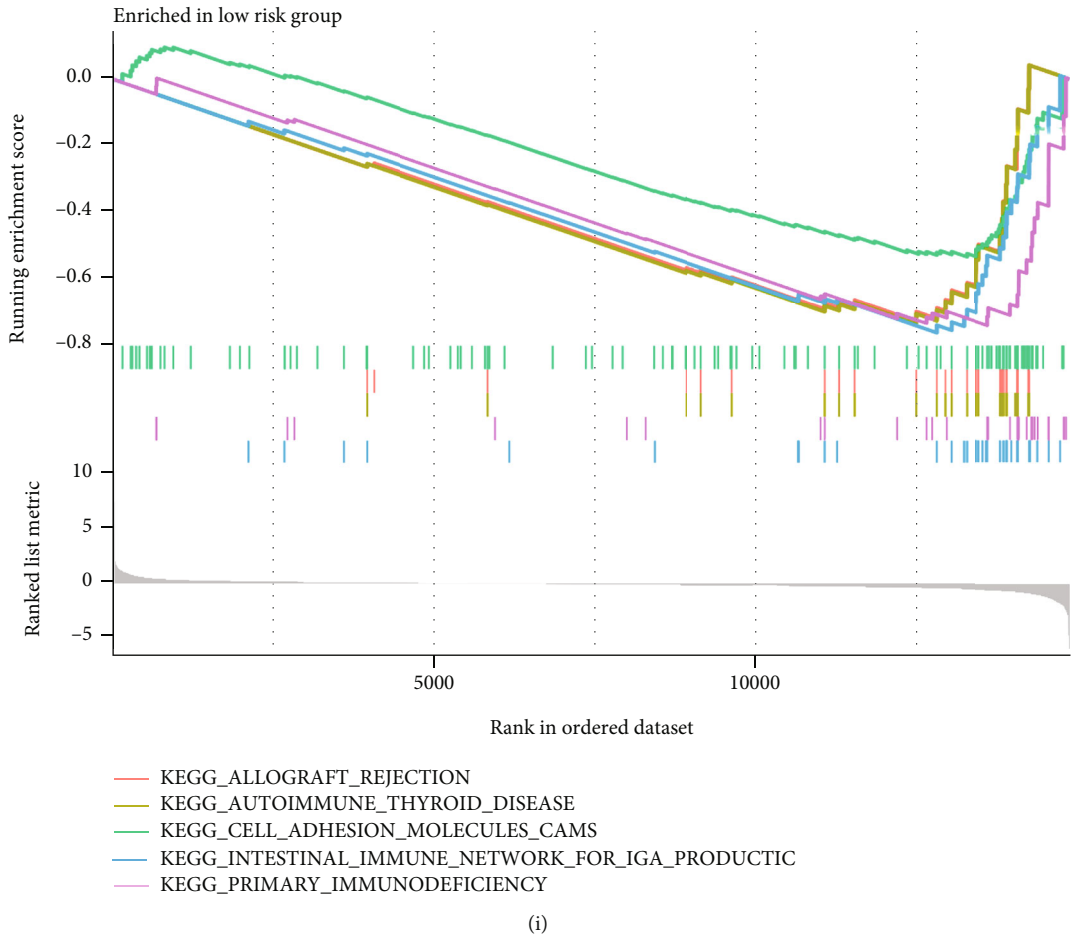

(i)

Figure 11: Application of risk score in clinical treatment. (a) The risk score is an independent prognostic indicator in OSCC patients. (b) Expression levels of PD1 in high- and low-risk groups. (c) Expression levels of CTLA4 in high- and low-risk groups. (d) CTLA4+PD1+. (e) CTLA4+ PD1−. (f) CTLA4− PD1−. (g) CTLA4− PD1+. (h) GSEA enrichment results for the high-risk group. (i) GSEA enrichment results for the high-risk group.

xenobiotics by cytochrome p450, focal adhesion, adipocytokine signaling pathway, starch, sucrose metabolism, and steroid hormone biosynthesis (Figure 11(h)). Low-risk group members were primarily enriched for allograft rejection, an intestinal immune network for igan production, cell adhesion molecules, primary immunodeficiency, and autoimmune thyroid disease (Figure 11(i)). Based on the GDSC database, we also evaluated the response of chemotherapeutic agents in high and low patients (Genomics of Drug Sensitivity in Cancer, https://www.cancerrxgene.org/). Using ridge regression, we estimated the half-maximal inhibitory concentration (IC50) of samples. We calculated the prediction accuracy using the R package "pRRophetic" (Figures 12(a)–12(p)). In light of the above results, we believe that risk scores based on SGs may be useful for guiding clinical treatment.

4. Discussion

Tumor growth and metastasis are influenced by SGs that regulate viability, apoptosis, proliferation, adhesion, migration, and metastasis [31–33]. It has also been proposed that mutations in SGs may also be associated with the acquisition of somatic aberrations that accelerate cancer development [34–36]. More importantly, SGs promote or inhibit the growth of tumors by influencing the tumor compartment and its microenvironment. SGs have been extensively studied as therapeutic targets for cancer.

We examined the expression of SGs and their prognostic characteristics in OSCC patients, concluding that three of the six SGs were significantly elevated. Additionally, 4 were identified as OSCC risk factors (TERF1, TERF2, ACD, and POT1). As a result of the functional enrichment analysis, they were largely enriched in pathways related to telomeres (such as telomere-associated protein complex, protection from nonhomologous end joining at telomere, RNA-dependent DNA biosynthetic process, and telomeric D-loop disassembly). Several cancer types require telomere-associated proteins to maintain normal telomere function [33, 37, 38]. To further explore the role of SGs in OSCC, a consensus clustering analysis was conducted on OSCC patients based on their SG expression levels. We found that OSCC patients could be divided into two subgroups (SGCluster A and SGCluster B). Furthermore, SGCluster A has a higher enrichment of immune infiltrating cells, which

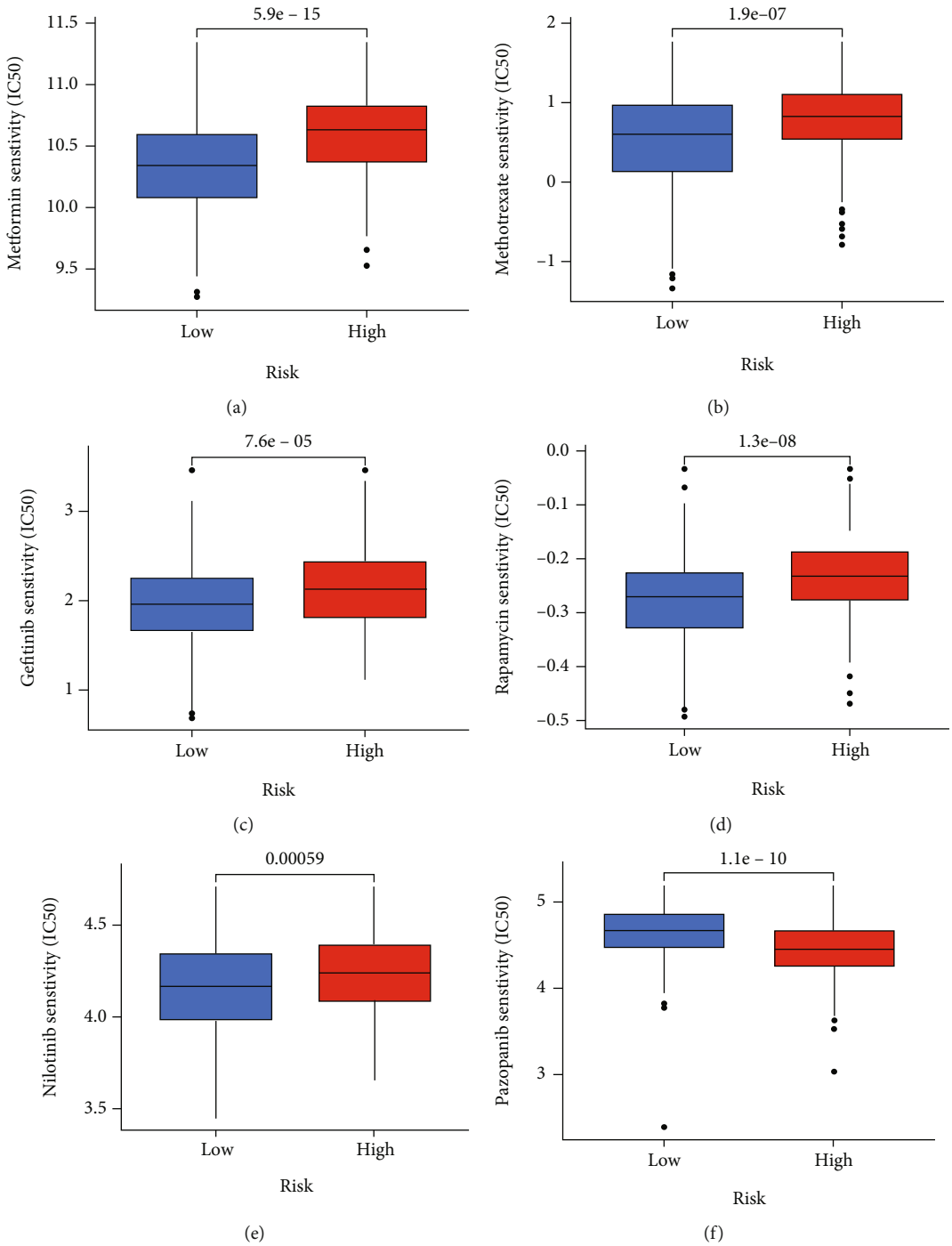

Figure 12: Continued.

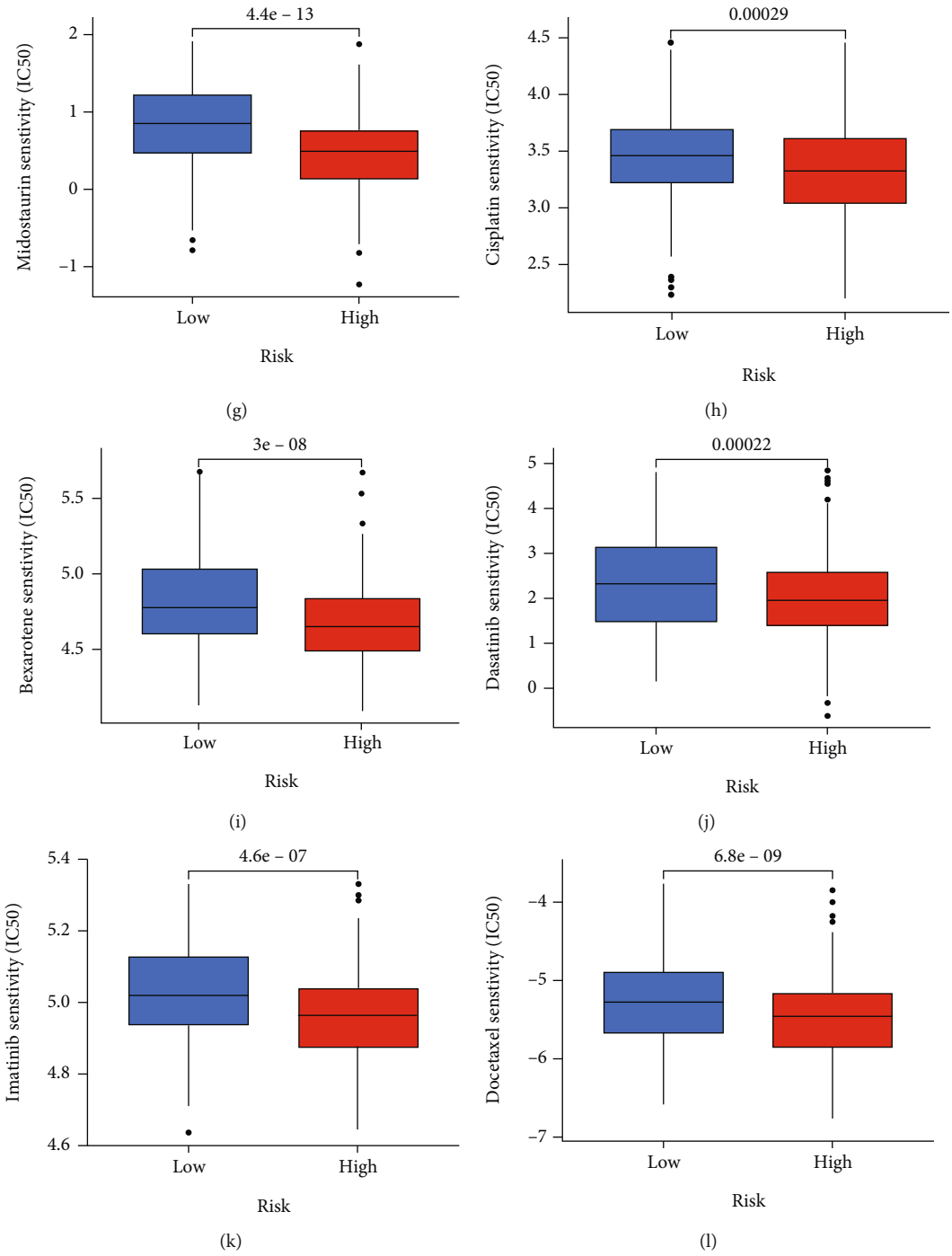

Figure 12: Continued.

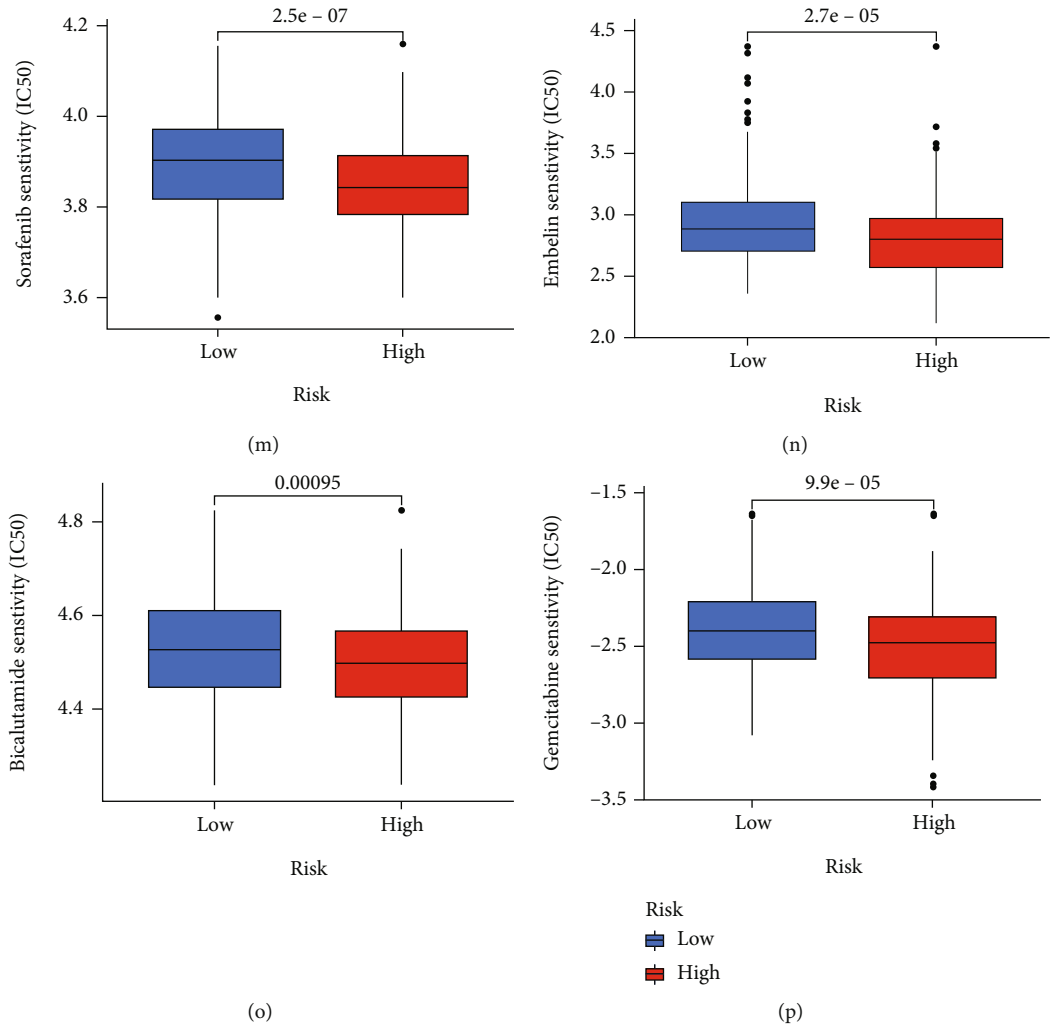

Figure 12: (a–p) Analysis of drug sensitivity in high and low risk groups.

may be one of the reasons for its better prognosis. Furthermore, we explored the differences between the two subgroups and identified 1329 DEGs. We identified DEGs based on GO and KEGG enrichment analysis, which, as expected, significantly correlated with pathways relating to cell cycle, senescence, apoptosis, chromosomes, and tumorigenesis development.

We developed prognostic models based on these DEGs. In order to expand the use of SGs in prognosis and clinical treatment for OSCC patients, we tested their stability and accuracy among randomized cohorts and different clinical subgroups. As a result, the model accurately predicted patients' prognoses. Notably, patients in the low-risk group tended to have lower TMB and more abundant immune-infiltrating cells, including Mast cells resting, T cells CD4 memory activated, T cells follicular helper, T cells regulatory (Tregs), plasma cells, T cells CD8, and B cells naive. Previous studies have suggested that highly abundant TME may be more sensitive to immunotherapy. In order to identify high- and low-risk immunotherapy groups, we calculated IPS scores. We found that low-risk groups tended to have higher IPS scores, representing the low-risk groups more sensitive to immunotherapy. The drug sensitivity analysis revealed that various chemotherapeutic drugs are more or less sensitive to high- and low-risk groups of patients. The findings of our study can help treat the OSCC patients and update the study of SGs. We believe that the risk scores can be used to predict OSCC prognosis and help predict patients' clinical response to immunotherapy.

However, there are several limitations to this study. The majority of the data we used came from public databases, so more experiments are required to verify the findings. In addition, studies reporting on SGs' role in OSCC are few, and our study only provides theoretical foundations for future experimental testing.

5. Conclusion

In summary, we systematically examined the expression levels and prognostic relevance of SGs in OSCC. In addition, a risk score model for SGs was constructed to evaluate the prognosis and TME of OSCC. Using risk scores, it is possible to predict OSCC prognosis and assess TME and

immunotherapy responses. Risk scores allow for more individualized clinical treatment and will assist in guiding medical practice.

Abbreviations

OSCC: Oral squamous cell carcinoma
GEO: Gene Expression Omnibus
TCGA: The Cancer Genome Atlas
OS: Overall survival
ROC: Receiver operating characteristic
TMB: Tumor mutational burden
TME: Tumor microenvironment
GO: Gene ontology
KEGG: Kyoto Encyclopedia of Genes and Genomes
DEGs: Differentially expressed genes
SGs: Shelterin complex genes.

Data Availability

The data sets analyzed during the current study are available in the TCGA (https://portal.gdc.cancer.gov/) and GEO repository (https://www.ncbi.nlm.nih.gov/geo/).

Conflicts of Interest

The authors declare that there are no competing interests associated with the manuscript.

Authors' Contributions

SZ and CS designed the study and wrote the manuscript. HY, JL, LZ, LT, and QS analyzed data and contributed to writing the manuscript. All the authors have approved the manuscript.

Supplementary Materials

Supplementary Figure 1: immune infiltrating cells in high and low risk groups. $*P < 0.05$, $**P < 0.01$, and $***P < 0.001$. Supplementary file 1: 1329 DEGs between SGCluster A and SGCluster B. Supplementary file 2: result of univariate Cox analysis. *(Supplementary Materials)*

References

[1] J. W. Shay, "Telomeres and aging," *Current Opinion in Cell Biology*, vol. 52, pp. 1–7, 2018.

[2] E. M. Smith, D. F. Pendlebury, and J. Nandakumar, "Structural biology of telomeres and telomerase," *Cellular and Molecular Life Sciences*, vol. 77, no. 1, pp. 61–79, 2020.

[3] S. M. Mir, S. Samavarchi Tehrani, G. Goodarzi et al., "Shelterin complex at telomeres: implications in ageing," *Clinical Interventions in Aging*, vol. 15, no. 15, pp. 827–839, 2020.

[4] C. B. Storti, R. A. de Oliveira, M. de Carvalho et al., "Telomere-associated genes and telomeric lncRNAs are biomarker candidates in lung squamous cell carcinoma (LUSC)," *Experimental and Molecular Pathology*, vol. 112, article 104354, 2020.

[5] S. Kabir, D. Hockemeyer, and T. de Lange, "TALEN gene knockouts reveal no requirement for the conserved human shelterin protein Rap1 in telomere protection and length regulation," *Cell Reports*, vol. 9, no. 4, pp. 1273–1280, 2014.

[6] J. K. Alder, C. E. Barkauskas, N. Limjunyawong et al., "Telomere dysfunction causes alveolar stem cell failure," *Proceedings of the National Academy of Sciences*, vol. 112, no. 16, pp. 5099–5104, 2015.

[7] A. W. Y. Chai, K. P. Lim, and S. C. Cheong, "Translational genomics and recent advances in oral squamous cell carcinoma," *Seminars in Cancer Biology*, vol. 61, pp. 71–83, 2020.

[8] J. Wang, Y. Wang, F. Kong et al., "Identification of a six-gene prognostic signature for oral squamous cell carcinoma," *Journal of Cellular Physiology*, vol. 235, no. 3, pp. 3056–3068, 2020.

[9] G. Z. Huang, Q. Q. Wu, Z. N. Zheng, T. R. Shao, and X. Z. Lv, "Identification of candidate biomarkers and analysis of prognostic values in oral squamous cell carcinoma," *Frontiers in Oncology*, vol. 9, no. 9, article 1054, 2019.

[10] Z. Ling, B. Cheng, and X. Tao, "Epithelial-to-mesenchymal transition in oral squamous cell carcinoma: challenges and opportunities," *International Journal of Cancer*, vol. 148, no. 7, pp. 1548–1561, 2021.

[11] Z. Luo, W. Liu, P. Sun, F. Wang, and X. Feng, "Pan-cancer analyses reveal regulation and clinical outcome association of the shelterin complex in cancer," *Briefings in Bioinformatics*, vol. 22, no. 5, article bbaa441, 2021.

[12] S. G. Fernandes, R. Dsouza, G. Pandya et al., "Role of telomeres and telomeric proteins in human malignancies and their therapeutic potential," *Cancers*, vol. 12, no. 7, article 1901, 2020.

[13] T. Li, Z. Luo, S. Lin et al., "MiR-185 targets POT1 to induce telomere dysfunction and cellular senescence," *Aging (Albany NY)*, vol. 12, no. 14, pp. 14791–14807, 2020.

[14] S. S. Poojary, G. Mishra, T. D. Singh, S. Gupta, B. R. Shrivastav, and P. K. Tiwari, "Telomere length variation and expression analysis of shelterin complex genes during gallbladder carcinogenesis," *Journal of Cancer Research and Therapeutics*, vol. 13, no. 2, pp. 235–239, 2017.

[15] X. T. Zhao, Y. Zhu, J. F. Zhou, Y. J. Gao, and F. Z. Liu, "Development of a novel 7 immune-related genes prognostic model for oral cancer: a study based on TCGA database," *Oral Oncology*, vol. 112, article 105088, 2021.

[16] J. Wu, Y. Zhu, M. Luo, and L. Li, "Comprehensive analysis of pyroptosis-related genes and tumor microenvironment infiltration characterization in breast cancer," *Frontiers in Immunology*, vol. 12, no. 12, article 748221, 2021.

[17] S. V. Puram, I. Tirosh, A. S. Parikh et al., "Single-cell transcriptomic analysis of primary and metastatic tumor ecosystems in head and neck cancer," *Cell*, vol. 171, no. 7, pp. 1611–1624, 2017.

[18] J. T. Leek, W. E. Johnson, H. S. Parker, A. E. Jaffe, and J. D. Storey, "The sva package for removing batch effects and other unwanted variation in high-throughput experiments," *Bioinformatics*, vol. 28, no. 6, pp. 882-883, 2012.

[19] M. E. Ritchie, B. Phipson, D. Wu et al., "limma powers differential expression analyses for RNA-sequencing and microarray studies," *Nucleic Acids Research*, vol. 43, no. 7, pp. e47–e47, 2015.

[20] Y. Zhou, B. Zhou, L. Pache et al., "Metascape provides a biologist-oriented resource for the analysis of systems-level datasets," *Nature Communications*, vol. 10, no. 1, pp. 1–10, 2019.

[21] C. Tao, K. Huang, J. Shi, Q. Hu, K. Li, and X. Zhu, "Genomics and prognosis analysis of epithelial-mesenchymal transition in glioma," *Frontiers in Oncology*, vol. 10, no. 10, article 183, 2020.

[22] J. Zheng, T. Zhang, W. Guo et al., "Integrative analysis of multi-omics identified the prognostic biomarkers in acute myelogenous leukemia," *Frontiers in Oncology*, vol. 10, no. 10, article 591937, 2020.

[23] S. Hänzelmann, R. Castelo, and J. Guinney, "GSVA: gene set variation analysis for microarray and RNA-seq data," *BMC Bioinformatics*, vol. 14, no. 1, pp. 1–15, 2013.

[24] M. Zhang, K. Zhu, H. Pu et al., "An immune-related signature predicts survival in patients with lung adenocarcinoma," *Frontiers in Oncology*, vol. 9, no. 9, article 1314, 2019.

[25] Z. Ye, M. Zheng, Y. Zeng et al., "Bioinformatics analysis reveals an association between cancer cell stemness, gene mutations, and the immune microenvironment in stomach adenocarcinoma," *Frontiers in Genetics*, vol. 11, no. 11, article 595477, 2020.

[26] Q. Wan, C. Liu, C. Liu, W. Liu, X. Wang, and Z. Wang, "Discovery and validation of a metastasis-related prognostic and diagnostic biomarker for melanoma based on single cell and gene expression datasets," *Frontiers in Oncology*, vol. 10, no. 10, article 585980, 2020.

[27] J. G. Tate, S. Bamford, H. C. Jubb et al., "COSMIC: the catalogue of somatic mutations in cancer," *Nucleic Acids Research*, vol. 47, no. D1, pp. D941–D947, 2019.

[28] L. B. Alexandrov, J. Kim, N. J. Haradhvala et al., "The repertoire of mutational signatures in human cancer," *Nature*, vol. 578, no. 7793, pp. 94–101, 2020.

[29] P. Charoentong, F. Finotello, M. Angelova et al., "Pan-cancer immunogenomic analyses reveal genotype-immunophenotype relationships and predictors of response to checkpoint blockade," *Cell Reports*, vol. 18, no. 1, pp. 248–262, 2017.

[30] P. Wu, W. Sun, and H. Zhang, "An immune-related prognostic signature for thyroid carcinoma to predict survival and response to immune checkpoint inhibitors," *Cancer Immunology, Immunotherapy*, vol. 71, no. 3, pp. 747–759, 2022.

[31] ICGC/TCGA, "Pan-cancer analysis of whole genomes," *Nature*, vol. 578, no. 7793, pp. 82–93, 2020.

[32] A. E. Bilsland, C. J. Cairney, and W. N. Keith, "Targeting the telomere and shelterin complex for cancer therapy: current views and future perspectives," *Journal of Cellular and Molecular Medicine*, vol. 15, no. 2, pp. 179–186, 2011.

[33] L. Bejarano, G. Bosso, J. Louzame et al., "Multiple cancer pathways regulate telomere protection," *EMBO Molecular Medicine*, vol. 11, no. 7, article e10292, 2019.

[34] M. Qian, S. Wang, X. Guo et al., "Hypoxic glioma-derived exosomes deliver microRNA-1246 to induce M2 macrophage polarization by targeting TERF2IP via the STAT3 and NF-κB pathways," *Oncogene*, vol. 39, no. 2, pp. 428–442, 2020.

[35] A. Cicconi and S. Chang, "Shelterin and the replisome: at the intersection of telomere repair and replication," *Current Opinion in Genetics & Development*, vol. 60, pp. 77–84, 2020.

[36] L. G. Aoude, A. L. Pritchard, C. D. Robles-Espinoza et al., "Nonsense mutations in the shelterin complex genes ACD and TERF2IP in familial melanoma," *Journal of the National Cancer Institute*, vol. 107, no. 2, article dju408, 2015.

[37] M. K. Graham and A. Meeker, "Telomeres and telomerase in prostate cancer development and therapy," *Nature Reviews Urology*, vol. 14, no. 10, pp. 607–619, 2017.

[38] H. Samavat, X. Xun, A. Jin, R. Wang, W. P. Koh, and J. M. Yuan, "Association between prediagnostic leukocyte telomere length and breast cancer risk: the Singapore Chinese Health Study," *Breast Cancer Research*, vol. 21, no. 1, pp. 1–10, 2019.

Hindawi
Oxidative Medicine and Cellular Longevity
Volume 2022, Article ID 2905663, 11 pages
https://doi.org/10.1155/2022/2905663

Review Article

Research Progress on G-Quadruplexes in Human Telomeres and Human Telomerase Reverse Transcriptase (hTERT) Promoter

Wei Gu,[1] Zihan Lin,[1] Shengchao Zhao,[1,2] Guanzhen Wang,[1,2] Ziyi Shen,[1] Wei Liu,[2] Yi Cai,[3] Kaibo Wang,[4] Chunpeng Craig Wan,[5] and Tingdong Yan[1]

[1]*School of Life Sciences, Shanghai University, Shanghai 200444, China*
[2]*University and College Key Lab of Natural Product Chemistry and Application in Xinjiang, School of Chemistry and Environmental Science, Yili Normal University, Yining 835000, China*
[3]*Guangzhou Municipal and Guangdong Provincial Key Laboratory of Molecular Target & Clinical Pharmacology, The NMPA and State Key Laboratory of Respiratory Disease, School of Pharmaceutical Sciences and the Fifth Affiliated Hospital, Guangzhou Medical University, Guangzhou 511436, China*
[4]*Jiangsu Key Laboratory of Bioactive Natural Product Research and State Key Laboratory of Natural Medicines, China Pharmaceutical University, Nanjing 210009, China*
[5]*Jiangxi Key Laboratory for Postharvest Technology and Nondestructive Testing of Fruits & Vegetables, College of Agronomy, Jiangxi Agricultural University, Nanchang 330045, China*

Correspondence should be addressed to Yi Cai; yicaisysu@163.com, Chunpeng Craig Wan; chunpengwan@jxau.edu.cn, and Tingdong Yan; yantdntu2018@163.com

Received 1 March 2022; Accepted 19 May 2022; Published 6 June 2022

Academic Editor: Milena Georgieva

The upregulation telomerase activity is observed in over 85-90% of human cancers and provides an attractive target for cancer therapies. The high guanine content in the telomere DNA sequences and the hTERT promoter can form G-quadruplexes (G4s). Small molecules targeting G4s in telomeres and hTERT promoter could stabilize the G4s and inhibit hTERT expression and telomere extension. Several G4 ligands have shown inhibitory effects in cancer cells and xenograft mouse models, indicating these ligands have a potential for cancer therapies. The current review article describes the concept of the telomere, telomerase, and G4s. Moreover, the regulation of telomerase and G4s in telomeres and hTERT promoter is discussed as well. The summary of the small molecules targeting G4s in telomeric DNA sequences and the hTERT promoter will also be shown.

1. Telomeres and Telomerase

Telomeres are dynamic nucleoprotein structures situated at the terminus of linear chromosomes and are the critical parts of chromosome structures in eukaryotic cells. Telomeres consist of highly conserved tandem DNA repeats which are linked with certain telomeric proteins. The repetitive sequences are conserved in over 90 eukaryotes, including mammals [1]. Binding of telomeric sequence-specific binding protein and their associated factors form a cap at the end of the linear chromosome. TRF1, TRF2, RAP1, TIN2, TPP1, and POT1 bind with telomeres, which form shelterin complex to prevent telomeres from end-end fusion, degradation, and recombination. TRF1 and TRF2 directly interact with double-stranded TTAGGG repeats, while POT1 interacts with 3′ single-stranded overhangs [2, 3]. The telomeric 3′ single-stranded overhangs form t-loop regulated by CDK phosphorylation of TRF2 during the cell cycle [4]. DNA replication follows two processes which are semiconservative replication and semidiscontinuous replication. In this procedure, DNA polymerase synthesizes a new DNA chain in the 5′ to 3′ direction with the help of tRNA primers. After the removal of tRNA primers, about 50-200 bp of telomeres DNA sequence will be lost at the 5′ end of the newly synthesized DNA strand [3, 5]. In stem cells and germ cells, the length of telomeres is often longer

than that of somatic cells, which is because these cells have high telomerase activity and the telomerase is naturally silenced in the majority of somatic cells [6]. The literature indicates that telomerase is transiently expressed in the S phase during the normal cell division cycle to maintain the $3'$ overhang of telomeres. When the $3'$ overhang is destroyed or shortens to a critical limit, the telomere-binding proteins fail to protect the chromosomal ends, and this will lead to the uncapping of telomere and induction of DNA damage responses [6]. Furthermore, this will lead to cell cycle arrest and induction of cellular senescence and apoptosis through p53 and other signaling pathways [7–11].

Telomerase is a ribonucleoprotein complex with reverse transcriptase activity, and its function is to extend the length of the telomere. Telomerase activity can be detected in tissues from the fetal to the newborn. But after birth, the telomerase activity in somatic cells is lost. Telomerase is expressed in the ovary and testis in the reproductive system, but not in mature sperm and ovum [12]. Telomerase contains two essential subunits, the protein subunit human telomerase reverse transcriptase (hTERT) and the RNA subunit which is human telomerase RNA (hTERC or hTER). hTER contains a templating region ($5'$-CUAACCCUAAC-$3'$) that is necessary for the hTERT to copy the newly synthesized telomere sequence at the terminus of the chromosome [13] (Figure 1). The activity of telomerase is strictly regulated, which affects the cell fate by maintaining the stability of the telomere structure. If the activity of telomerase is only half of the normal level, it will lead to the shortening of telomeres [14]. The upregulation of telomerase activity in cancer cells is necessary for the telomere maintenance in tumor cells and underlies the ability of cancer cells to divide continuously. Interestingly, the telomere length of cancer cells is often shorter than normal cells, perhaps because the cells divide rapidly at an early stage of tumor development that exceeds the ability of telomerase synthesis [14]. About 85-90% of cancer cells obtained the ability of self-renewal and proliferation through activation of telomerase. Besides, there are about 5-10% of cancer cells use alternative lengthening of telomeres (ALT) to maintain telomeres [15]. Bodnar et al. reported that transferring of exogenous hTERT can exceed their normal lifespan and maintain normal human cells in a phenotypically youthful state, which could have important applications in telomere-related diseases and antiaging research [16]. Telomerase, as the key molecule to maintain telomeres, is of great significance for the regulation of cell senescence and cell division. A large number of studies have focused on the regulation of telomerase activity, hoping to develop new strategies to achieve targeted telomerase inhibition for cancer therapy and telomerase activation for the intervention in human aging.

2. Regulation of Human Telomerase

hTERT and hTER are two main targets for telomerase regulation. hTERT synthesizes the telomere DNA sequence using the hTER RNA motif as a template. For the RNA template sequence in hTER, the corresponding antisense oligonucleotide can be combined with it to inhibit the activity of telomerase. In somatic cells, telomerase lost function because of hTERT gene silencing, not hTER. hTER is universally expressed in all tissues and not a limiting factor for telomerase activity. It is noteworthy that hTER is highly expressed in cancer cells and germ cells to maintain the high telomerase [13]. Because telomerase is so important in human cancer and aging, numerous studies focus on the regulation of telomerase. The regulation of telomerase is a complex biological process and involves regulation of hTERT expression, regulation of hTERT translation, regulation of hTERT by epigenetic means, chromosome rearrangement, and miRNAs [17–19]. hTERT promoter covers about 3.5 kb upstream of the transcription start site, and there are multiple transcription factor binding sites such as SP1 and c-MYC that have been identified by methods such as reporter assay, ChIP, and EMSA. Enhancers located in the -20 kb upstream of the transcription start site (TSS) region also play important role in the regulation of hTERT [17–19]. Recently, studies reported that there are two gain-of-function mutations (C228T and C250T) in the hTERT promoter region, which cause telomerase activation and drive tumorigenesis in human cancer such as melanoma, glioma, liver cancer, and urothelial cancer [20–23], which provided an attractive target for cancer therapy. It has been proved that there are 12 consecutive G-tracts in the promoter sequence from -100 to -168 form special G4 structures, which inhibit the expression of hTERT. Small molecules binding to G4 structure could decrease the expression of hTERT and inhibit cancer cell proliferation.

3. G-Quadruplex Structure and Its Regulation

G-quartet is a very stable planar structure that consists of four guanines by Hoogsteen bond to form hydrogen bonds and metal ions like K^+ (Figures 2(a) and 2(b)). Following the literature, it is evident that $K^+ > Na^+ > Li^+$ plays an important role in the maintenance of the G-quartet structure. Two or more π–π stacked G-quartets form G4 structure [24–26]. G4 is found in DNA and RNA sequences which are rich in GC bases. G4 is an atypical secondary structure of DNA, continuous G-rich DNA sequences containing multiple G-tracts are folded to form intramolecular G4 in single DNA, and double-stranded DNA can form interstrand G4 [26] (Figure 2(c)–2(e)). There is another atypical nucleic acid secondary structure named i-motif, formed by four cytosines that has been proved to exist in the double-stranded DNA sequence with GC bases rich. Further studies showed that the formation of i-motif and G4 is interdependent in human cells [27, 28]. There are many proposed methods for G4 research: the possibility of G4 formation is predicted and analyzed based on the base sequence of the target DNA fragment; the nucleic acid sequence designed and synthesized in vitro can be determined to form the G4 structure through physical and chemical methods such as circular dichroism, X-ray, nuclear magnetic resonance, and gel migration analysis; Thioflavin T can bind specifically to G4 and enhance Thioflavin T fluorescence; G4 dimer can enhance the fluorescence intensity of Thioflavin

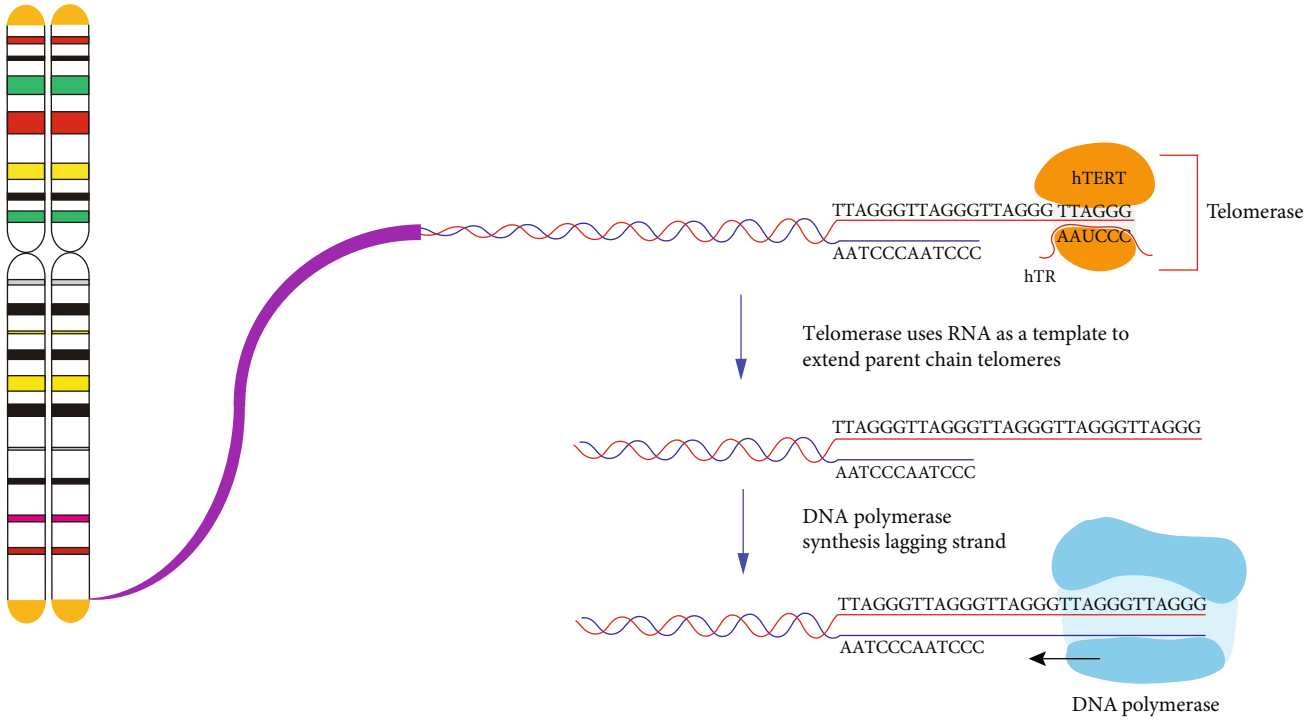

Figure 1: Telomere elongation by telomerase. Telomerase reverse transcriptase synthesizes telomeres DNA sequence which requires hTER as an RNA template and DNA polymerase to complete telomere elongation [1, 13].

T dramatically as compared to monomeric G4 [29, 30]; it is a mature and common method to study the biological function of G4 through molecular cloning and luciferase reporter assay [31, 32]. G4s are not randomly distributed on the DNA sequence; it is found that G4s mainly exist in the promoter of the genes and the chromatin terminal telomere DNA by G4-specific antibodies and genome sequencing. Generally, the DNA sequence that forms the G-4 has a similar base arrangement. $G_{3\text{-}5}N_{1\text{-}7}G_{3\text{-}5}N_{1\text{-}7}G_{3\text{-}5}N_{1\text{-}7}G_{3\text{-}5}$ is the general motif of the G4 structure, which can help us to predict and analyze the possible sequence of G4. Previously, a relatively simple algorithm was used to search for this consensus sequence in the genome sequence, and more than 300,000 possible DNA G4 sites were identified from the human genome. Recently, more than 700,000 potential G4 sites were identified in the human genome by G4 ChIP-seq. Interestingly, more than 40% of human gene promoter regions contain at least one G4 motif [33–35], suggesting the important function of G4 in the regulation of gene expression. Cancer is one of the most threatening diseases to human health, and its pathogenic mechanism is very complicated. Studies have found that many proteins with important functions are involved in tumorigenesis. If G4s are involved in the gene expression, studying the relationship between G4 and oncogene expression can help us to understand the mechanism of tumorigenesis and provide targets for cancer therapy. Myc is a proto-oncogene, as a transcription factor that participates in the regulation of cell proliferation, metabolism, apoptosis, and other important processes. Upexpression of Myc has been observed in up to 80% of solid tumors, such as gastric cancer, ovarian cancer, and breast cancer [36, 37]. In vivo, there is a sequence containing six G-tracts with different numbers of G formed G4 structure in the promoter of Myc, which could inhibit the expression of Myc. After treatment with G4 stabilizers such as TMPyP4, the expression of MYC was significantly reduced [38]. Not only in the proto-oncogene but also the promoter of some tumor suppressor genes may also form G4. In most cases, G4 downregulates gene expression by preventing transcription factors from binding to gene promoters or hindering the sliding of RNA polymerase along with DNA. However, G4 structure can not only inhibit gene expression but G4 formed in the promoter may promote gene expression. As a deubiquitinating enzyme, BAP1 is also considered an antioncogene. There is a G4 structure in the promoter of BAP1, and it upregulates the expression of BAP1, which in turn achieves the antitumor effect. In addition, in the promoter of relaxin and OCT, the G4 structure also promotes gene expression [39–41].

After G4 is formed in the DNA sequence, it does not become a stable structure on the genome. There are more than 20 helicases such as FANCJ and Pif1 that can bind and untie G4s in the cells. Pif1 can untie G4s after the small-molecule G4 ligands bind to G4s [42]. This suggests that small-molecule ligands targeting G4s in the promoter of genes may not achieve the expected effect of gene regulation under the action of helicases. In addition to the gene promoters, another important region where G4s exist is the chromatin terminal telomeres DNA. The G4s were first discovered in the G-rich single-stranded G-tail structure in the $3'$ end of the telomere DNA. Telomeres play an essential role in tumor proliferation, so numerous studies have linked

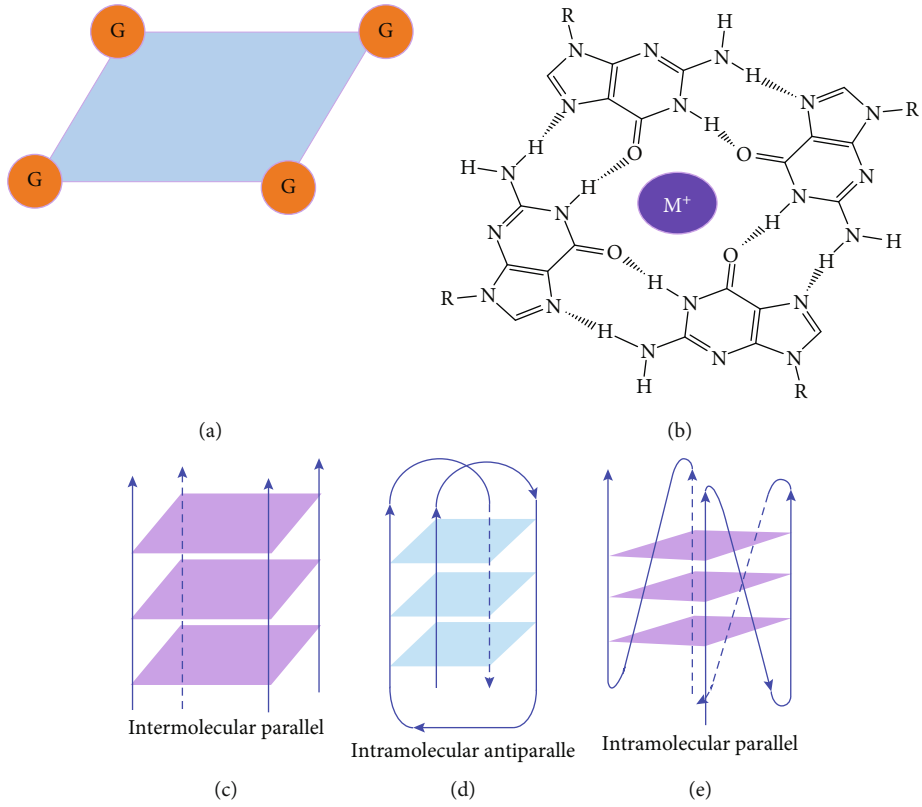

FIGURE 2: The structure of G-quartet and common G4 types. (a) Guanines form the planar structure of G-quartet. (b) G-quartet stabilized by hydrogen and cation like K^+ and Na^+. (c–e) Illustration of common G4 types [34].

G4s to the inhibition of telomere elongation, through G4 ligands to stabilize the structure of telomere terminal G4 and inhibit the proliferation of cancer cells [43–45].

4. G-Quadruplex Structures in Telomeres and hTERT Promoter

G4 structures can be formed in telomere DNA sequence and hTERT promoter, which suggests G4 is a potential target to inhibit telomere elongation and telomerase activity. The telomere terminal repeat sequence TTAGGG is highly rich in guanine, and there are often G4s at the telomere, especially in $3'$ overhang. Generally, telomerase needs helicase to untie the G4 structure before the elongation of the telomere. If some G4 ligands bind and stabilize the G4s at the end of telomeres, the helicase cannot perform its function, and the G4s blocking the telomerase bind with telomere. In the subsequent cell division, the telomere length will gradually shorten and eventually trigger replication senescence [11, 46] (Figure 3). Such drugs can also cause the depolymerization of the telomere terminal protein complex. When telomere is destroyed, the telomere-binding proteins can no longer protect the chromosome end, and this will induce DNA damage response and lead to cellular senescence and apoptosis [47]. This method has attracted a lot of attention and maybe a promising treatment for targeting telomeres because this kind of drug can directly affect telomeres, and they have a faster effect which acts as a revival of telomerase activity.

Another method is to stabilize the G4 structure in the hTERT promoter and reduce the expression of hTERT, thereby reducing the telomerase activity and preventing cells from synthesizing telomere end repeat sequences and leading to aging and apoptosis (Figure 3). The hTERT promoter G4 is a potential drug target, and further studying its structure will be helpful for drug development. Currently, there are two widely accepted models for hTERT promoter G4s. In the first model, Monsen et al. and Chaires et al. provided that there is a three-parallel G4 conformation in the wild-type hTERT promoter. The triple parallel quadruple structure consists of 1-4 G-tracts, 5-8 G-tracts, and 9-12 G-tracts, folding into a compact stacked three-G-4 conformation [48, 49]. The second model suggested that the 5-8 G-tracts alone may not easily form G4, but the 5-8 G-tracts and the 9-12 G-tracts form G4 and connected the 1-4 G beam by the 26 bp length hairpin structure. In the other words, the numbers 1-4 and 5, 6, 11, and 12 G-tracts formed two typical stable parallel G4 structures called G4 dimer in the hTERT promoter [50–52] (Figure 4). Both models believed that the 1-4 G-tracts alone forms a G4, which is a hybrid structure of parallel and antiparallel (3 + 1) [50]. The first model has been verified in various physical and chemical methods in vitro, and the second model has more support from drug experiments. Considering the complexity of the *in vivo* environment, the existing model of the G4s in the hTERT

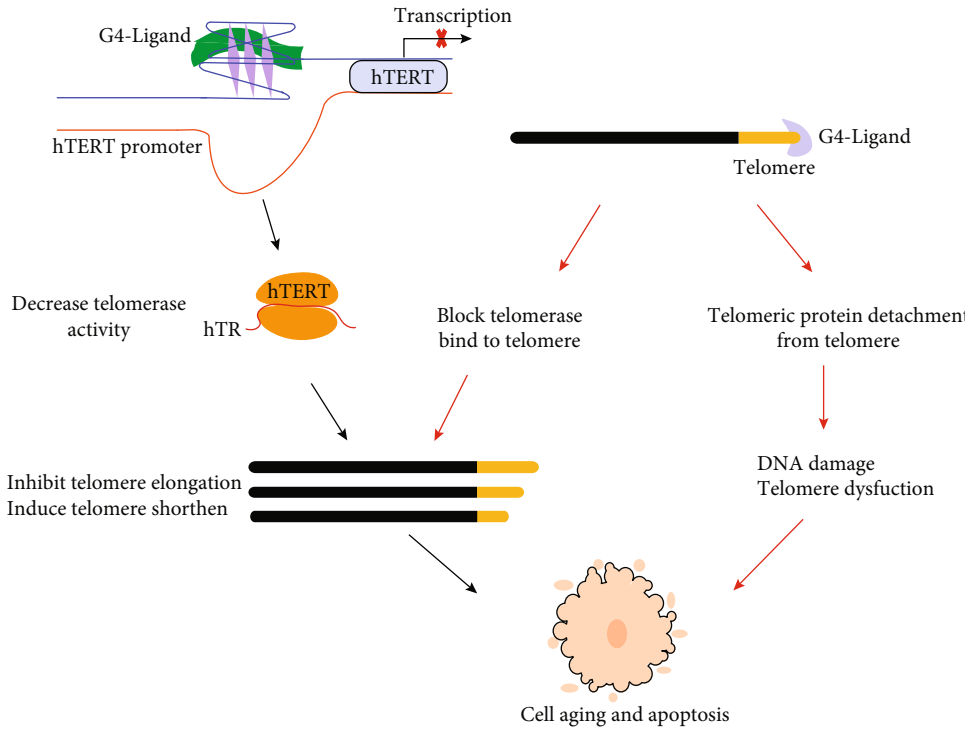

Figure 3: The mechanism of telomere and telomerase promoter G4 ligands inhibit cancer cells growth. The black arrows indicate that G4 ligands targeting hTERT promotor G4 shorten telomere, and this is a slow effect that induces cell death. The telomeric G4 ligand bind telomere could quickly inhibit the growth of cancer cells which is indicated by red arrows [11, 26].

promoter may require more study to verify. The drugs targeting hTERT promoter G4 need to regulate gene expression to shorten the effect of telomeres and inhibit proliferation; it will take a long term to see the effects [53]. Although G4 ligand drugs have shown attractive prospects, both the telomere structure and the complexity of G4 require further study. Some small molecular G4 ligands have good antitumor effects in vitro and animal models, but the mechanism needs further study. Because of the lack of clinical research data to support, G4 ligands still have a long way to be used as a clinical drug.

5. Small Molecules Targeting G4s in Telomeres and hTERT Promoter

The cationic porphyrin TMPyP4 can bind and stabilize the G4s in the human telomere sequence, thereby hindering the binding of telomerase to the telomere. TMPyP4 shows the inhibitory effect on breast cancer and prostate cancer as well as decreases telomerase activity at the cellular and animal levels. However, TMPyP4 can also bind G4 in the promoter of c-Myc and inhibit the expression of c-Myc. c-Myc is a transcription factor of hTERT, so TMPyP4 can indirectly decrease the expression of hTERT by downregulation of c-Myc [54]. TMPyP4 leads to telomere DNA damage response and activates cellular senescence and apoptosis [55, 56]. Telomestatin can bind to telomere G4, showing both high quadruplex affinity and telomerase inhibitory potency. Telomestatin inhibits telomerase activity and tumor growth in a leukemia xenograft mouse model [57, 58]. BRACO19 is one of the most potent inhibitors of telomerase, with high specificity for telomeres G4 and induce telomere DNA damage and cellular senescence by inducing stable telomere G4, hindering terminal protein complex to detach. BRACO19 showed a strong inhibitory effect and short treatment time; it can have about 90% inhibitory effect in the uterine tumor xenograft mouse model [54, 59]. BRACO-19 suppresses proliferation and reduces telomerase activity on glioma cells and has no effect on normal human astrocytes, showing good selectivity for tumor cells. The excellent performance also makes BRACO19 one of the most promising drugs for clinical application [60]. Pyridostatin can stabilize telomere G4 and compete with POT1 for telomere binding. After POT1 dissociates from telomeres, it induces a DNA damage response, leading to the death of cancer cells [61]. RHPS4 is an acridine derivative, and it induces a strong telomere damage response and cell apoptosis by binding to telomere G4 to cause the dissociation of POT1 from the telomere. It can also reduce hTERT expression and inhibit telomerase activity, causing telomere length shortening. RHPS4 had a good inhibitory effect on tumor cell lines and xenograft mouse models and has almost nonspecific damage to nontumor tissues. In further drug combination studies, it was found that the combination of RHPS4 with paclitaxel showed a synergistic effect on uterine tumors [53, 62]. Although most cancers have acquired the ability to immortalize through the reexpression of telomerase, about 20% of tumor cells can be detected mutations in the hTERT promoter, and these mutations cause the upregulation of hTERT expression and telomerase activity [63]. Two highly

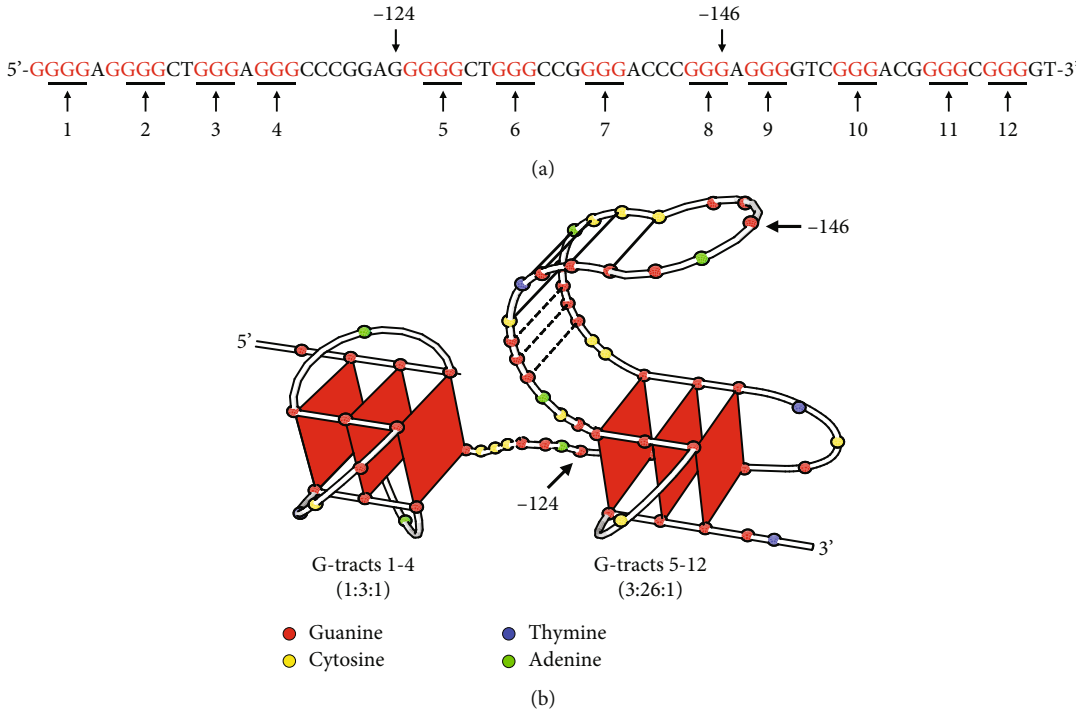

Figure 4: The G4s in hTERT core promotor. (a) The 12 consecutive G-tracts in the hTERT promoter can form G4s. (b) The hairpin structure model of G4s in hTERT core promoter [52].

abundant hotspot mutations, G>A mutations at 124 and 146 sites, were found in the gene-sequencing analysis in various tumor cells. Further studies confirmed that these two mutations inhibited the formation and stabilization of G4 which is formed by the numbers 5, 6, 11, and 12 G-tracts in the hTERT promoter, thereby upregulating hTERT expressed in tumor cells. The propylguanidino-acridine derivative GTC365 directly binds the G4 formed by the 5th, 6th, 11th, and 12th G tetrad fold in the hTERT promoter and reduces the expression of hTERT. GTC365 can also strengthen the stability of G4 and help G4 to inhibit hTERT expression, reducing telomere length and promoting cancer cellular senescence and apoptosis. In melanoma cells, the GTC365 shows the therapeutic potential of decreasing the hTERT expression. GTC365 inhibits tumor growth which is significantly better than BRACO19, especially when cancer cells are treated with low concentration [52]. RG260 contains benzoylphenylurea (BPU) which can bind to hairpin structure between quadruplets of promoter but lacks the acridine moiety of GTC365 that binds to the quadruples. RG260 targets the hairpin structure in the hTERT G4s, induces 9-12 G bundles to form a G4, and reduces hTERT expression. In prostate cancer, RG260 and its derivatives may induce oxidative stress and human prostate tumor cell apoptosis through mitochondrial damage, without harming normal human prostate epithelial cells. In subsequent *in vivo* xenografts, RG260 derivatives caused significant growth inhibition of prostate cancer [64]. Triazinel 12459 shows good therapeutic potential in lymphoma. On the one hand, inducing the formation of telomere G4 will cause the dysfunction of telomerase and further lead to telomere shortening and apoptosis. On the other hand, it can affect the splicing of hTERT mRNA and affect the telomerase activity by downregulating the hTERT mRNA expression [65, 66]. Thiazole orange is a G4 ligand. By modifying its side chain with different amino acids, it was found that various derivatives have strong inhibitory effects on telomerase activity in vitro. Among them, thiazole orange-spermine conjugate has a similar effect to BRACO19. But the role of these derivatives in cancer cells and mouse models needs further study [67]. BMPQ-1 with the 5H-pyrazolo [4,3-c] quinoline core has strong selectivity for the G4 at the end of the telomere and can stabilize G4 at the $3'$ overhang of the telomere. BMPQ-1 can induce the formation of telomere G4, causing telomere dysfunction and DNA damage response, followed by cell senescence and apoptosis. The BMPQ-1 also showed good tumor-suppressing effects in lung, liver, and gastric cancer cells and human colon adenocarcinoma xenograft mouse models, even better than of the classical G4 ligand BRACO19 [68]. In traditional Chinese medicine, many natural compounds have been found to have the ability to stabilize G4 in telomeres and hTERT promoter, and the modified derivatives of these natural products have stronger effects. Natural compounds have the advantages of being extensive, easy to extract, and lower toxicity, so more effective G4 ligands can be found from there. Alkaloids, as a natural medicine research focus, are expected to provide stable G4 drug molecules. Berberine is isolated from the Chinese herbal medicine *Rhizoma Coptidis*, a natural isoquinoline alkaloid, which has anti-inflammatory, antibacterial, and anticancer effects. Berberine is also used in chronic diseases, protects cardiovascular issues, and

Table 1: Small molecules targeting G4s in telomeres and hTERT promoter.

Compound	Chemical structure	Main tumor cell type
GTC365	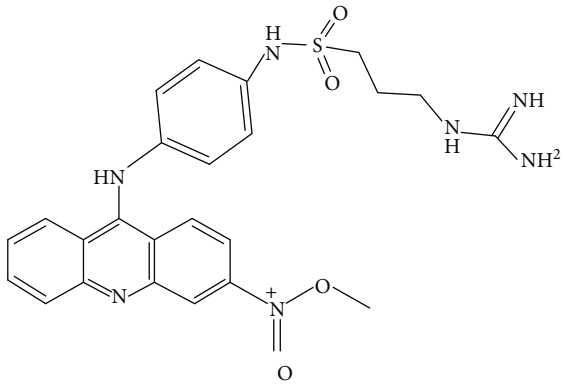	Melanoma [52]
TMPyP4	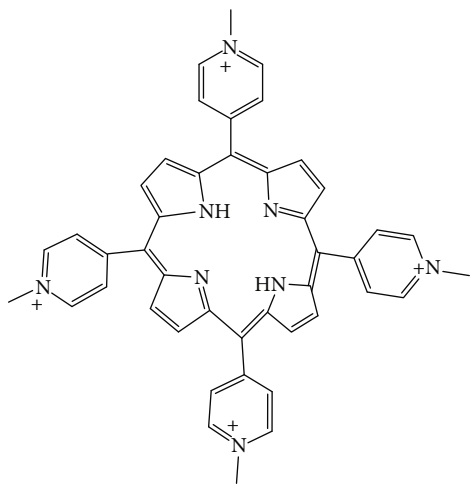	Mammary cancer, prostatic cancer [55]
Telomestatin	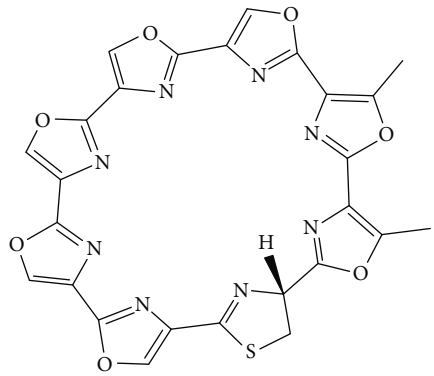	Lymphoma [59]
BRACO19	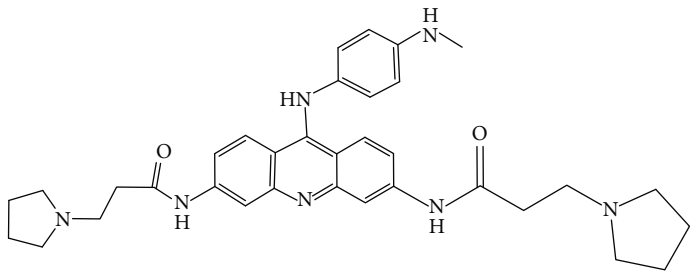	Uterine carcinoma [60], Glioma [61]

Table 1: Continued.

Compound	Chemical structure	Main tumor cell type
RHPS4	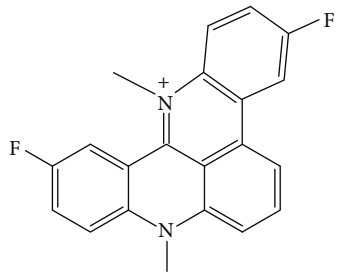	Breast carcinoma [63]
BMPQ-1	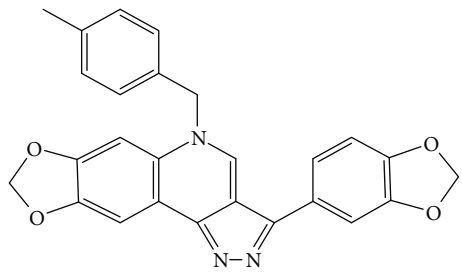	Lung cancer, liver cancer, and colon adenocarcinoma [69]
Berberine	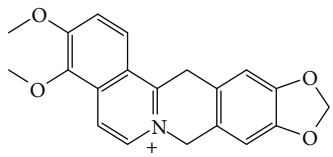	Cervical cancer, colorectal cancer [71, 72]

lowers blood lipids and blood sugar levels [69]. Researchers found that berberine can inhibit the proliferation of several cancer cells such as cervical cancer and has little or no toxicity in normal cells. Berberine inhibits tumor growth by inducing and increasing G4 stability and decreasing telomerase activity. The berberine derivatives which are alkyl-substituted at positions C-9 and C-13 have strong specificity for telomere G4 [70–72]. In vitro physicochemical properties, studies on the ability of other natural alkaloids to induce and stabilize G4 have shown that the interaction between benzophenanthridine alkaloids and telomere G4s is stronger than isoquinoline alkaloids. However, there is a lack of research at the cell and animal levels. Further study needs to be done to find more effective pharmaceutical ingredients to stabilize G4 in telomeres and hTERT promoter from natural products [73, 74] (Table 1).

6. Conclusion and Perspectives

Numerous studies have confirmed that telomere and telomerase are associated with cancer, neurological diseases, aging, and other diseases. The upregulation of telomerase activity in cancer cells is necessary for the telomere maintenance in cancer cells and underlies the ability of cancer cells to divide continuously. Therefore, telomerase has become a potential target for cancer therapy. However, telomerase inhibition may also cause undesirable effects on stem cells and progenitor cells. Recent studies showed that two mutations in the hTERT promoter can upregulate hTERT expression in glioblastoma, melanoma, and liver cancer. These mutations abrogate the G4-folding process and result in activation of hTERT, suggesting a potential specific target for cancer therapy. G4 has been confirmed to exist in the hTERT promoter, so it is possible to target hTERT promoter G4 for therapy. Although several drugs targeting the G4 have achieved good results in vitro and mouse models, G4 ligand drugs are still a long way away from clinical application. The first problem that needs to be resolved is the specificity of the G4 ligand drugs. Some drugs targeting G4 in the promoter may bring us other side effects while suppressing tumors. The development of G4 drugs targeting telomeres and hTERT promoter with clinical application prospects not only has a strong effect on tumor cells but also has a specific binding target to avoid any unnecessary binding to other molecules for modulation of certain gene expressions. Resistance is an important factor limiting the use of most anticancer drugs. After treatment with G4 ligands, some cancer cells develop resistance and even increase the expression of telomerase [65]. The ligand targeting G4 in the hTERT promoter takes time to show the inhibition effect. Although it hinders the function of telomerase to lengthen telomeres, cancer cells continue to proliferate until the length of telomeres is shortened to the critical limit. Considering the different stages of the tumor, only the use of G4 ligand drugs may not be able to achieve the optimal antitumor effect. The combination of G4 ligand drugs with other clinical used drugs may achieve better therapeutic effects. With the improvement of drug design and the further study of the mechanism of G4s, new G4 ligand drugs that target telomeres and hTERT promoter will make progress in

solving specificity, safety, and drug resistance, and breakthroughs will be made in clinical experiments soon.

Data Availability

The data used to support the findings of this study are available from the corresponding author upon request.

Consent

Written informed consent was obtained from the study participants.

Conflicts of Interest

The authors declare that they have no conflicts of interest.

Acknowledgments

This work was supported by grants from the National Natural Science Foundation of China (No. 31972899), by the Program for Professor of Special Appointment (Eastern Scholar) at Shanghai Institutions of Higher Learning, and by the Shanghai Overseas Talents Introduction Program.

References

[1] J. W. Shay and W. E. Wright, "Telomeres and telomerase: three decades of progress," *Nature Reviews. Genetics*, vol. 20, no. 5, pp. 299–309, 2019.

[2] H. Xin, D. Liu, and Z. Songyang, "The telosome/shelterin complex and its functions," *Genome Biology*, vol. 9, no. 9, p. 232, 2008.

[3] K. J. Turner, V. Vasu, and D. K. Griffin, "Telomere biology and human phenotype," *Cell*, vol. 8, no. 1, p. 73, 2019.

[4] G. Sarek, P. Kotsantis, P. Ruis et al., "CDK phosphorylation of TRF2 controls t-loop dynamics during the cell cycle," *Nature*, vol. 575, no. 7783, pp. 523–527, 2019.

[5] C. J. Webb, Y. Wu, and V. A. Zakian, "DNA repair at telomeres: keeping the ends intact," *Cold Spring Harbor Perspectives in Biology*, vol. 5, no. 6, p. 5, 2013.

[6] K. Masutomi, E. Y. Yu, S. Khurts et al., "Telomerase maintains telomere structure in normal human cells," *Cell*, vol. 114, no. 2, pp. 241–253, 2003.

[7] P. Martinez and M. A. Blasco, "Telomere-driven diseases and telomere-targeting therapies," *The Journal of Cell Biology*, vol. 216, no. 4, pp. 875–887, 2017.

[8] W. E. Wright, V. M. Tesmer, K. E. Huffman, S. D. Levene, and J. W. Shay, "Normal human chromosomes have long G-rich telomeric overhangs at one end," *Genes & Development*, vol. 11, no. 21, pp. 2801–2809, 1997.

[9] M. Z. Levy, R. C. Allsopp, A. B. Futcher, C. W. Greider, and C. B. Harley, "Telomere end-replication problem and cell aging," *Journal of Molecular Biology*, vol. 225, no. 4, pp. 951–960, 1992.

[10] J. J. Jacobs and T. de Lange, "Significant role for $p16^{INK4a}$ in p53-independent telomere-directed senescence," *Current Biology*, vol. 14, no. 24, pp. 2302–2308, 2004.

[11] A. N. Guterres and J. Villanueva, "Targeting telomerase for cancer therapy," *Oncogene*, vol. 39, no. 36, pp. 5811–5824, 2020.

[12] W. E. Wright, M. A. Piatyszek, W. E. Rainey, W. Byrd, and J. W. Shay, "Telomerase activity in human germline and embryonic tissues and cells," *Developmental Genetics*, vol. 18, no. 2, pp. 173–179, 1996.

[13] J. Feng, W. D. Funk, S. S. Wang et al., "The RNA component of human telomerase," *Science*, vol. 269, no. 5228, pp. 1236–1241, 1995.

[14] E. H. Blackburn, C. W. Greider, and J. W. Szostak, "Telomeres and telomerase: the path from maize, Tetrahymena and yeast to human cancer and aging," *Nature Medicine*, vol. 12, no. 10, pp. 1133–1138, 2006.

[15] T. M. Bryan, A. Englezou, L. Dalla-Pozza, M. A. Dunham, and R. R. Reddel, "Evidence for an alternative mechanism for maintaining telomere length in human tumors and tumor-derived cell lines," *Nature Medicine*, vol. 3, no. 11, pp. 1271–1274, 1997.

[16] A. G. Bodnar, M. Ouellette, M. Frolkis et al., "Extension of lifespan by introduction of telomerase into normal human cells," *Science*, vol. 279, no. 5349, pp. 349–352, 1998.

[17] S. C. Akincilar, B. Unal, and V. Tergaonkar, "Reactivation of telomerase in cancer," *Cellular and Molecular Life Sciences*, vol. 73, no. 8, pp. 1659–1670, 2016.

[18] Y. S. Cong, W. E. Wright, and J. W. Shay, "Human telomerase and its regulation," *Microbiology and Molecular Biology Reviews*, vol. 66, no. 3, pp. 407–425, 2002.

[19] T. Yan, W. F. Ooi, A. Qamra et al., "HoxC5 and miR-615-3p target newly evolved genomic regions to repress hTERT and inhibit tumorigenesis," *Nature Communications*, vol. 9, no. 1, p. 100, 2018.

[20] F. W. Huang, E. Hodis, M. J. Xu, G. V. Kryukov, L. Chin, and L. A. Garraway, "Highly recurrent TERT promoter mutations in human melanoma," *Science*, vol. 339, no. 6122, pp. 957–959, 2013.

[21] S. Horn, A. Figl, P. S. Rachakonda et al., "TERT promoter mutations in familial and sporadic melanoma," *Science*, vol. 339, no. 6122, pp. 959–961, 2013.

[22] P. J. Killela, Z. J. Reitman, Y. Jiao et al., "TERT promoter mutations occur frequently in gliomas and a subset of tumors derived from cells with low rates of self-renewal," *Proceedings of the National Academy of Sciences of the United States of America*, vol. 110, no. 15, pp. 6021–6026, 2013.

[23] J. C. Nault, M. Mallet, C. Pilati et al., "High frequency of telomerase reverse-transcriptase promoter somatic mutations in hepatocellular carcinoma and preneoplastic lesions," *Nature Communications*, vol. 4, no. 1, p. 2218, 2013.

[24] S. Burge, G. N. Parkinson, P. Hazel, A. K. Todd, and S. Neidle, "Quadruplex DNA: sequence, topology and structure," *Nucleic Acids Research*, vol. 34, no. 19, pp. 5402–5415, 2006.

[25] J. T. Davis, "G-quartets 40 years later: from 5'-GMP to molecular biology and supramolecular chemistry," *Angewandte Chemie (International Ed. in English)*, vol. 43, no. 6, pp. 668–698, 2004.

[26] S. Balasubramanian, L. H. Hurley, and S. Neidle, "Targeting G-quadruplexes in gene promoters: a novel anticancer strategy?," *Nature Reviews. Drug Discovery*, vol. 10, no. 4, pp. 261–275, 2011.

[27] M. Zeraati, D. B. Langley, P. Schofield et al., "I-motif DNA structures are formed in the nuclei of human cells," *Nature Chemistry*, vol. 10, no. 6, pp. 631–637, 2018.

[28] J. J. King, K. L. Irving, C. W. Evans et al., "DNA G-quadruplex and i-motif structure formation is interdependent in human

cells," *Journal of the American Chemical Society*, vol. 142, no. 49, pp. 20600–20604, 2020.

[29] R. A. de la Faverie, A. Guedin, A. Bedrat, L. A. Yatsunyk, and J. L. Mergny, "Thioflavin T as a fluorescence light-up probe for G4 formation," *Nucleic Acids Research*, vol. 42, no. 8, p. e65, 2014.

[30] S. Jing, Q. Liu, Y. Jin, and B. Li, "Dimeric G-quadruplex: an effective nucleic acid scaffold for lighting up Thioflavin T," *Analytical Chemistry*, vol. 93, no. 3, pp. 1333–1341, 2021.

[31] M. Adrian, B. Heddi, and A. T. Phan, "NMR spectroscopy of G-quadruplexes," *Methods*, vol. 57, no. 1, pp. 11–24, 2012.

[32] R. Hansel-Hertsch, J. Spiegel, G. Marsico, D. Tannahill, and S. Balasubramanian, "Genome-wide mapping of endogenous G-quadruplex DNA structures by chromatin immunoprecipitation and high-throughput sequencing," *Nature Protocols*, vol. 13, no. 3, pp. 551–564, 2018.

[33] J. L. Huppert and S. Balasubramanian, "G-quadruplexes in promoters throughout the human genome," *Nucleic Acids Research*, vol. 35, no. 2, pp. 406–413, 2007.

[34] D. Varshney, J. Spiegel, K. Zyner, D. Tannahill, and S. Balasubramanian, "The regulation and functions of DNA and RNA G-quadruplexes," *Nature Reviews. Molecular Cell Biology*, vol. 21, no. 8, pp. 459–474, 2020.

[35] J. L. Huppert and S. Balasubramanian, "Prevalence of quadruplexes in the human genome," *Nucleic Acids Research*, vol. 33, no. 9, pp. 2908–2916, 2005.

[36] M. Liu, B. Yao, T. Gui et al., "PRMT5-dependent transcriptional repression of c-Myc target genes promotes gastric cancer progression," *Theranostics*, vol. 10, no. 10, pp. 4437–4452, 2020.

[37] Y. Fallah, J. Brundage, P. Allegakoen, and A. N. Shajahan-Haq, "MYC-driven pathways in breast cancer subtypes," *Biomolecules*, vol. 7, no. 4, p. 53, 2017.

[38] A. Siddiqui-Jain, C. L. Grand, D. J. Bearss, and L. H. Hurley, "Direct evidence for a G-quadruplex in a promoter region and its targeting with a small molecule to repress c-MYC transcription," *Proceedings of the National Academy of Sciences of the United States of America*, vol. 99, no. 18, pp. 11593–11598, 2002.

[39] D. Renciuk, J. Ryneš, I. Kejnovská et al., "G-quadruplex formation in the Oct4 promoter positively regulates Oct4 expression," *Biochim Biophys Acta Gene Regul Mech*, vol. 1860, no. 2, pp. 175–183, 2017.

[40] H. P. Gu, S. Lin, M. Xu et al., "Up-regulating relaxin expression by G-quadruplex interactive ligand to achieve antifibrotic action," *Endocrinology*, vol. 153, no. 8, pp. 3692–3700, 2012.

[41] Y. Li, X. Zhang, Y. Gao, J. Shi, L. Tang, and G. Sui, "G-quadruplexes in the BAP1 promoter positively regulate its expression," *Experimental Cell Research*, vol. 369, no. 1, pp. 147–157, 2018.

[42] R. Zhou, J. Zhang, M. L. Bochman, V. A. Zakian, and T. Ha, "Periodic DNA patrolling underlies diverse functions of Pif1 on R-loops and G-rich DNA," *eLife*, vol. 3, article e02190, 2014.

[43] H. J. Lipps and D. Rhodes, "G-quadruplex structures: in vivo evidence and function," *Trends in Cell Biology*, vol. 19, no. 8, pp. 414–422, 2009.

[44] N. Lipinska, A. Romaniuk, A. Paszel-Jaworska, E. Toton, P. Kopczynski, and B. Rubis, "Telomerase and drug resistance in cancer," *Cellular and Molecular Life Sciences*, vol. 74, no. 22, pp. 4121–4132, 2017.

[45] A. Zhao, S. E. Howson, C. Zhao et al., "Chiral metallohelices enantioselectively target hybrid human telomeric G-quadruplex DNA," *Nucleic Acids Research*, vol. 45, no. 9, pp. 5026–5035, 2017.

[46] W. C. Drosopoulos, S. T. Kosiyatrakul, and C. L. Schildkraut, "BLM helicase facilitates telomere replication during leading strand synthesis of telomeres," *The Journal of Cell Biology*, vol. 210, no. 2, pp. 191–208, 2015.

[47] R. Sanchez-Vazquez, P. Martinez, and M. A. Blasco, "AKT-dependent signaling of extracellular cues through telomeres impact on tumorigenesis," *PLoS Genetics*, vol. 17, no. 3, article e1009410, 2021.

[48] R. C. Monsen, L. DeLeeuw, W. L. Dean et al., "The hTERT core promoter forms three parallel G-quadruplexes," *Nucleic Acids Research*, vol. 48, no. 10, pp. 5720–5734, 2020.

[49] J. B. Chaires, J. O. Trent, R. D. Gray et al., "An improved model for the hTERT promoter quadruplex," *PLoS One*, vol. 9, no. 12, article e115580, 2014.

[50] R. Leão, J. D. Apolónio, D. Lee, A. Figueiredo, U. Tabori, and P. Castelo-Branco, "Mechanisms of human telomerase reverse transcriptase (hTERT) regulation: clinical impacts in cancer," *Journal of Biomedical Science*, vol. 25, no. 1, p. 22, 2018.

[51] S. L. Palumbo, S. W. Ebbinghaus, and L. H. Hurley, "Formation of a unique end-to-end stacked pair of G-quadruplexes in the hTERT core promoter with implications for inhibition of telomerase by G-quadruplex-interactive ligands," *Journal of the American Chemical Society*, vol. 131, no. 31, pp. 10878–10891, 2009.

[52] H. J. Kang, Y. Cui, H. Yin et al., "A pharmacological chaperone molecule induces cancer cell death by restoring tertiary DNA structures in mutant hTERT promoters," *Journal of the American Chemical Society*, vol. 138, no. 41, pp. 13673–13692, 2016.

[53] P. Phatak, J. C. Cookson, F. Dai et al., "Telomere uncapping by the G-quadruplex ligand RHPS4 inhibits clonogenic tumour cell growth in vitro and in vivo consistent with a cancer stem cell targeting mechanism," *British Journal of Cancer*, vol. 96, no. 8, pp. 1223–1233, 2007.

[54] S. Neidle, "Human telomeric G-quadruplex: the current status of telomeric G-quadruplexes as therapeutic targets in human cancer," *The FEBS Journal*, vol. 277, no. 5, pp. 1118–1125, 2010.

[55] J. F. Riou, L. Guittat, P. Mailliet et al., "Cell senescence and telomere shortening induced by a new series of specific G-quadruplex DNA ligands," *Proceedings of the National Academy of Sciences of the United States of America*, vol. 99, no. 5, pp. 2672–2677, 2002.

[56] S. Neidle, "Quadruplex nucleic acids as novel therapeutic targets," *Journal of Medicinal Chemistry*, vol. 59, no. 13, pp. 5987–6011, 2016.

[57] N. Temime-Smaali, L. Guittat, A. Sidibe, K. Shin-ya, C. Trentesaux, and J. F. Riou, "The G-quadruplex ligand telomestatin impairs binding of topoisomerase IIIalpha to G-quadruplex-forming oligonucleotides and uncaps telomeres in ALT cells," *PLoS One*, vol. 4, no. 9, article e6919, 2009.

[58] T. Tauchi, K. Shin-ya, G. Sashida et al., "Telomerase inhibition with a novel G-quadruplex-interactive agent, telomestatin: in vitro and in vivo studies in acute leukemia," *Oncogene*, vol. 25, no. 42, pp. 5719–5725, 2006.

[59] A. M. Burger, F. Dai, C. M. Schultes et al., "The G-quadruplex-interactive molecule BRACO-19 inhibits tumor growth, consistent with telomere targeting and interference with

telomerase function," *Cancer Research*, vol. 65, no. 4, pp. 1489–1496, 2005.

[60] G. Zhou, X. Liu, Y. Li et al., "Telomere targeting with a novel G-quadruplex-interactive ligand BRACO-19 induces T-loop disassembly and telomerase displacement in human glioblastoma cells," *Oncotarget*, vol. 7, no. 12, pp. 14925–14939, 2016.

[61] R. Rodriguez, S. Müller, J. A. Yeoman, C. Trentesaux, J. F. Riou, and S. Balasubramanian, "A novel small molecule that alters shelterin integrity and triggers a DNA-damage response at telomeres," *Journal of the American Chemical Society*, vol. 130, no. 47, pp. 15758-15759, 2008.

[62] E. Salvati, C. Leonetti, A. Rizzo et al., "Telomere damage induced by the G-quadruplex ligand RHPS4 has an antitumor effect," *The Journal of Clinical Investigation*, vol. 117, no. 11, pp. 3236–3247, 2007.

[63] K. Chiba, J. Z. Johnson, J. M. Vogan, T. Wagner, J. M. Boyle, and D. Hockemeyer, "Cancer-associated TERT promoter mutations abrogate telomerase silencing," *eLife*, vol. 4, 2015.

[64] J. H. Song, H. J. Kang, L. A. Luevano et al., "Small-molecule-targeting hairpin loop of hTERT promoter G-quadruplex induces cancer cell death," *Cell Chemical Biology*, vol. 26, no. 8, pp. 1110–1121.e4, 2019, e4.

[65] D. Gomez, N. Aouali, A. Londoño-Vallejo et al., "Resistance to the short term antiproliferative activity of the G-quadruplex ligand 12459 is associated with telomerase overexpression and telomere capping alteration," *The Journal of Biological Chemistry*, vol. 278, no. 50, pp. 50554–50562, 2003.

[66] D. Gomez, T. Lemarteleur, L. Lacroix, P. Mailliet, J. L. Mergny, and J. F. Riou, "Telomerase downregulation induced by the G-quadruplex ligand 12459 in A549 cells is mediated by hTERT RNA alternative splicing," *Nucleic Acids Research*, vol. 32, no. 1, pp. 371–379, 2004.

[67] S. Wang, D. Yang, M. Singh et al., "Thiazole orange - spermine conjugate: a potent human telomerase inhibitor comparable to BRACO-19," *European Journal of Medicinal Chemistry*, vol. 175, pp. 20–33, 2019.

[68] C. Gao, Z. Liu, H. Hou et al., "BMPQ-1 binds selectively to (3+1) hybrid topologies in human telomeric G-quadruplex multimers," *Nucleic Acids Research*, vol. 48, no. 20, pp. 11259–11269, 2020.

[69] A. F. Cicero and A. Baggioni, "Berberine and its role in chronic disease," *Advances in Experimental Medicine and Biology*, vol. 928, pp. 27–45, 2016.

[70] L. Fu, W. Chen, W. Guo et al., "Berberine targets AP-2/hTERT, NF-kappaB/COX-2, HIF-1alpha/VEGF and cytochrome-c/caspase signaling to suppress human cancer cell growth," *PLoS One*, vol. 8, no. 7, article e69240, 2013.

[71] J. Becher, D. V. Berdnikova, H. Ihmels, and C. Stremmel, "Synthesis and investigation of quadruplex-DNA-binding, 9-O-substituted berberine derivatives," *Beilstein Journal of Organic Chemistry*, vol. 16, pp. 2795–2806, 2020.

[72] F. Papi, C. Bazzicalupi, M. Ferraroni et al., "Pyridine derivative of the natural alkaloid berberine as human telomeric G4-DNA binder: a solution and solid-state study," *ACS Medicinal Chemistry Letters*, vol. 11, no. 5, pp. 645–650, 2020.

[73] X. Ji, H. Sun, H. Zhou, J. Xiang, Y. Tang, and C. Zhao, "The interaction of telomeric DNA and C-myc22 G-quadruplex with 11 natural alkaloids," *Nucleic Acid Therapeutics*, vol. 22, no. 2, pp. 127–136, 2012.

[74] F. Papi, M. Ferraroni, R. Rigo et al., "Role of the benzodioxole group in the interactions between the natural alkaloids chelerythrine and coptisine and the human telomeric G-quadruplex DNA. A multiapproach investigation," *Journal of Natural Products*, vol. 80, no. 12, pp. 3128–3135, 2017.

Hindawi
Oxidative Medicine and Cellular Longevity
Volume 2022, Article ID 9144644, 18 pages
https://doi.org/10.1155/2022/9144644

Research Article

Senotherapy Protects against Cisplatin-Induced Ovarian Injury by Removing Senescent Cells and Alleviating DNA Damage

Dingfu Du,[1,2,3,4,5] Xianan Tang,[1,3,4] Yufeng Li,[1,6] Yueyue Gao,[1,3,4] Runhua Chen,[1,3,4] Qian Chen,[1,3,4] Jingyi Wen,[1,3,4] Tong Wu,[1,3,4] Yan Zhang,[1,3,4] Huan Lu,[1,3,4] Jinjin Zhang,[1,3,4] and Shixuan Wang[1,3,4]

[1]*Department of Obstetrics and Gynecology, Tongji Hospital, Tongji Medical College, Huazhong University of Science and Technology, Wuhan, Hubei 430030, China*
[2]*Sun Yat-sen University Cancer Center, State Key Laboratory of Oncology in South China, Collaborative Innovation Center of Cancer Medicine, Guangzhou, Guangdong 510000, China*
[3]*National Clinical Research Center for Obstetrical and Gynecological Diseases, Wuhan, Hubei 430030, China*
[4]*Key Laboratory of Cancer Invasion and Metastasis, Ministry of Education, Wuhan, Hubei 430030, China*
[5]*Department of Head and Neck Surgery, Sun Yat-sen University Cancer Center, Guangzhou, Guangdong 510000, China*
[6]*Reproductive Medicine Center, Tongji Hospital, Tongji Medical College, Huazhong University of Science and Technology, Wuhan, Hubei 430030, China*

Correspondence should be addressed to Jinjin Zhang; jinjinzhang@tjh.tjmu.edu.cn and Shixuan Wang; shixuanwang@tjh.tjmu.edu.cn

Dingfu Du and Xianan Tang contributed equally to this work.

Received 2 March 2022; Accepted 2 May 2022; Published 3 June 2022

Academic Editor: Milena Georgieva

Ovarian damage induced by platinum-based chemotherapy seriously affects young women with cancer, manifesting as infertility, early menopause, and premature ovarian insufficiency. However, effective prevention strategies for such damage are lacking. Senescent cells may be induced by chemotherapeutic agents. We hypothesized that cisplatin can lead to senescence in ovarian cells during the therapeutic process, and senolytic drugs can protect animals against cisplatin-induced ovarian injury. Here, we demonstrated the existence of senescent cells in cisplatin-treated ovaries, identified the senescence-associated secretory phenotype, and observed significant improvement of ovarian function by treatment with metformin or dasatinib and quercetin (DQ) independently or in combination. These senotherapies improved both oocyte quality and fertility, increased the ovarian reserve, and enhanced hormone secretion in cisplatin-exposed mice. Additionally, attenuated fibrosis, reorganized subcellular structure, and mitigated DNA damage were observed in the ovaries of senotherapeutic mice. Moreover, RNA sequencing analysis revealed upregulation of the proliferation-related genes *Ki*, *Prrx2*, *Sfrp4*, and *Megfl0*; and the antioxidative gene *H2-Q10* after metformin plus DQ treatment. Gene ontology analysis further revealed that combining senotherapies enhanced ovarian cell differentiation, development, and communication. In this study, we demonstrated that metformin plus DQ recovered ovarian function to a greater extent compared to metformin or DQ independently, with more follicular reserve, increased pups per litter, and reduced DNA damage. Collectively, our work indicates that senotherapies might prevent cisplatin-induced ovarian injury by removing senescent cells and reducing DNA damage, which represent a promising therapeutic avenue to prevent chemotherapy-induced ovarian damage.

1. Introduction

With the rapid development of modern medicine, multiple cancers have been rapidly, accurately diagnosed and treated in the early stage. Thus, the survival time of cancer patients has been significantly prolonged [1]. Acute lymphoblastic leukemia and breast cancer are the most common malignancies among female populations of adolescent and reproductive ages, respectively. The 10-year survival rate of the former exceeds 80%, and the five-year survival rate of the latter has reached 70% [2, 3]. Since a variety of tumor incidences gradually approach the young population, the quality of life of cancer survivors has become a growing problem needing urgently to be solved.

At present, chemotherapy remains the most prevalent treatment for cancer. Cisplatin is a first-line drug extensively used for various solid tumors, such as acute lymphoblastic leukemia, breast cancer, and cervical cancer, and it has been widely studied for its multisystem side effects [4]. Female gonads are particularly sensitive to cisplatin. Evidence suggests that the principal manifestation of cisplatin-induced ovarian damage is a loss of the healthy ovarian reserve and female fertility, frequently accompanied by increased atretic follicles [5]. The precise mechanisms underlying this drug's ovarian toxicity involve irreversible DNA damage, overloaded oxidative stress, and uncontrolled apoptosis activation [5–7]. Fertility-preservation strategies, such as ovarian tissue cryopreservation, embryo cryopreservation, stem cell transplantation, and oocyte donation, might benefit a proportion of tumor survivors. However, practical problems, such as safety and ethical issues, have restricted their wide use [8, 9]. Currently, no better method exists for recovering cisplatin-induced ovarian damage, and effective interventions can only be carried out if the involved mechanisms are uncovered.

Cellular senescence can be triggered by various stress stimuli and is characterized by permanent cell cycle arrest, macromolecular damage, deregulated cell metabolism, and a particular senescence-associated secretory phenotype (SASP), which can be detected by short, dysfunctional telomeres, persistent DNA damage response (DDR), $P16^{link4a}$ expression, β-galactoside (β-gal) staining, and SASP [10, 11]. Cellular senescence inevitably occurs in normal aging tissues, and lingering senescent cells impair tissue homeostasis, further rendering aged tissues dysfunctional and vulnerable to stress [12]. Based on this theory, animal studies are in progress to evaluate the benefits of senotherapies in age-associated disorder prevention and healthy lifespan extension, and several approaches have been offered either involving the removal of senescent cells (such as dasatinib plus quercetin [DQ]) or the inhibition of SASP (such as metformin) secretions [13]. Recent evidence has reported that DQ induces selective apoptosis of senescent cells (SNCs), preserves organ function, prevents age-related pathologies, and increases lifespan [14–16]. Metformin, a traditional anti-hyperglycemic agent, was recently identified to possess a senomorphic effect and the potential to fight against age-related diseases [17–19]. In addition to natural aging, studies into genotoxic agents, such as cisplatin, cyclophosphamide, and doxorubicin, have acknowledged their senescence-promoting effects [10, 20–22]. Surveys of cisplatin have shown that this chemotherapy could induce SNCs in normal tissues such as the kidneys and neurons, which are involved in the pathogenesis of acute kidney injury and peripheral neuropathy [23, 24]. To date, few attempts have been made to identify whether SNCs exist in cisplatin-exposed ovaries and whether senotherapies could protect against cisplatin-induced ovarian damage.

In our present research, we hypothesized that cisplatin might induce ovarian cell senescence and senotherapies may effectively restore ovarian reserve and function. Our study confirmed that DNA damage and SNCs were involved in the ovarian damage induced by cisplatin. Treatment with metformin or DQ alone or both in combination alleviated cisplatin-induced ovarian dysfunction by removing SNCs, inhibiting SASP secretion and blocking apoptosis. Our work uncovers a novel mechanism for cisplatin-induced ovarian damage and reveals that senotherapies targeting senescent cells may be a potential fertility-preservation avenue for female cancer patients.

2. Methods and Materials

2.1. In Vitro Primary Granulosa Cells (GCs) Culture and Drug Administration. Ovaries were isolated from euthanized 3-week-old female C57BL/6 mice and punctured thoroughly to release GCs. The harvested GCs were centrifuged at 800 revolutions per minute (rpm) for 5.5 minutes, incubated in DMEM/F12 (12400-024; Gibco Laboratories, Gaithersburg, MD, USA) culture medium, and then divided into 4 groups. The GCs of the blank control group (NC group) were treated with DMEM/F12 growth medium without any other treatment. For the cisplatin group (Cis group), cisplatin plus metformin group (Cis+M group), and cisplatin plus DQ group (Cis+DQ group), cisplatin (30 μmol/L) was added to the medium after GC attachment. Following 24 hours, the whole medium of each group was replaced. GCs in the NC group and Cis group were cultured in DMEM/F12 growth medium for another 24 hours, and the other two groups were treated with metformin (5 mmol/L) or D+Q (D: 1 nmol/L; Q: 20 μmol/L) for another 24 hours.

2.2. Cell Culture Medium Cytokine Detection. After drug administration, the cell culture medium of the NC group and Cis group was collected. The cytokines accumulated in culture medium after different medications were determined using a Luminex mouse 23 cytokine array (Wayen Biotechnologies, Shanghai, China).

2.3. Animal Care and Drug Administration. One hundred sex-mature 6-week-old C57BL/6 female mice were provided by the Tongji Hospital Experimental Animal Center, which is affiliated with the Tongji Medical College of Huazhong University. Animals were acclimated to the environment for one week before drug administration on an alternating 12-hour light/dark cycle with free access to food and water. Then, 20 mice were administered dasatinib (5 mg/kg) and

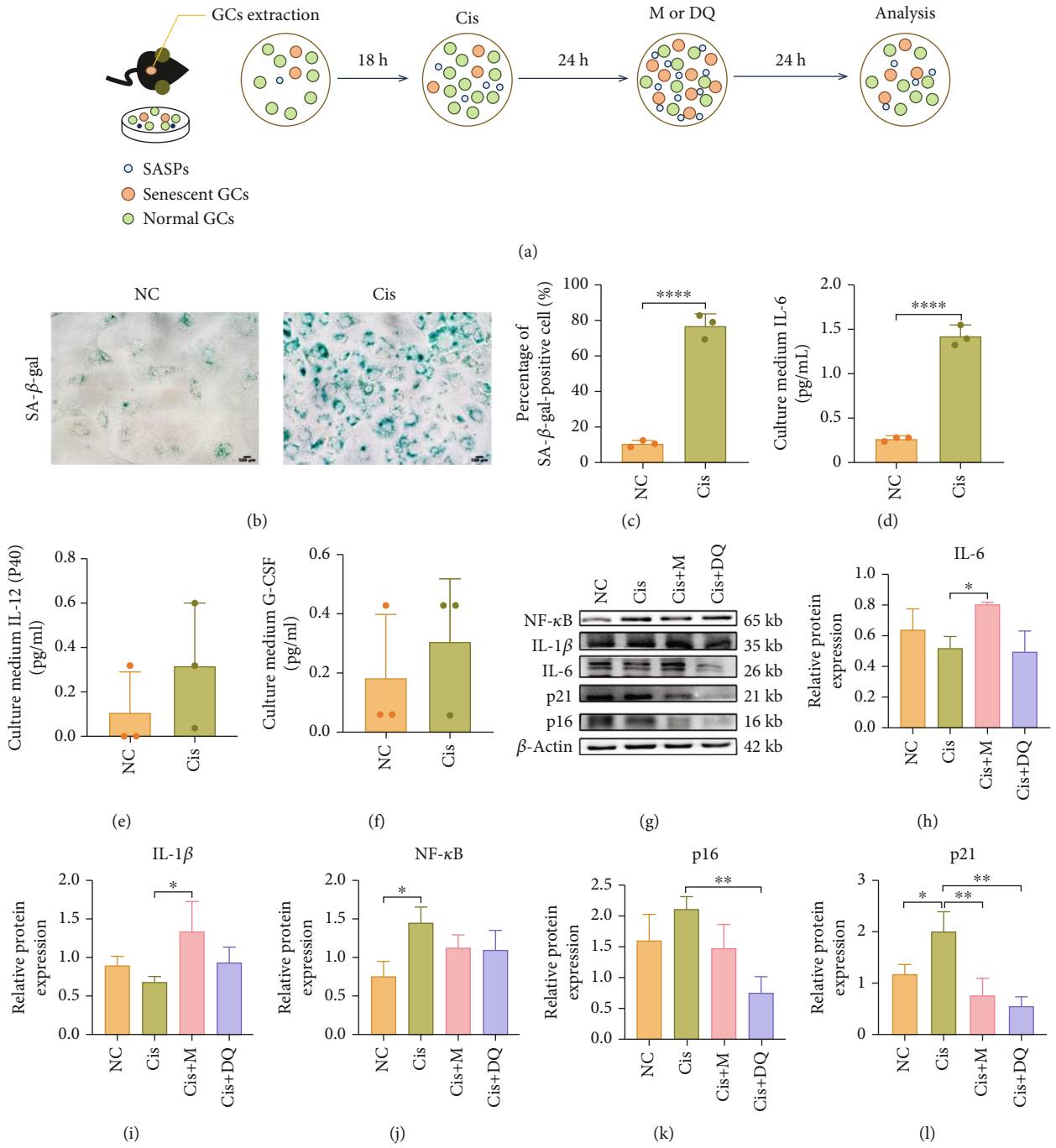

Figure 1: Metformin and DQ independently reduced senescent granulosa cells and SASP caused by cisplatin in vitro. (a) Flowchart of primary GCs in vitro experiment. (b, c) Light microscopic images of SA-β-gal-stained GCs after cisplatin administration and quantitative analysis of SA-β-gal–positive GCs ($n=3$). Scar bars are marked on respective images. (d–f) Cytokines accumulated in cell culture medium of the NC and Cis groups. (g–l) The protein levels of senescence-associated markers and SASP were analyzed by western blotting ($n=3$). Results are presented using mean ± standard deviation values. $*p<0.05$, $**p<0.01$, $****p<0.0001$.

quercetin (50 mg/kg) intragastrically 2 times weekly for 4 weeks and/or received metformin-containing water (2 mg/mL) or pure water over a period of 4 weeks (Cis+DQ, Cis+M, cisplatin plus metformin, and DQ [Cis+M+DQ] groups, 20 mice per group, 60 mice in total). One week after senotherapy administration, the aforementioned 60 mice were simultaneously subjected to intraperitoneal injection with 2.5 mg/kg of cisplatin 3 times weekly for the next 3 weeks. Another 20 mice received saline or cisplatin injection only at 7 weeks of age (NC and Cis groups, 20 mice per group, 40 mice in total). All animal operations were performed in compliance with the guide approved by the ethics

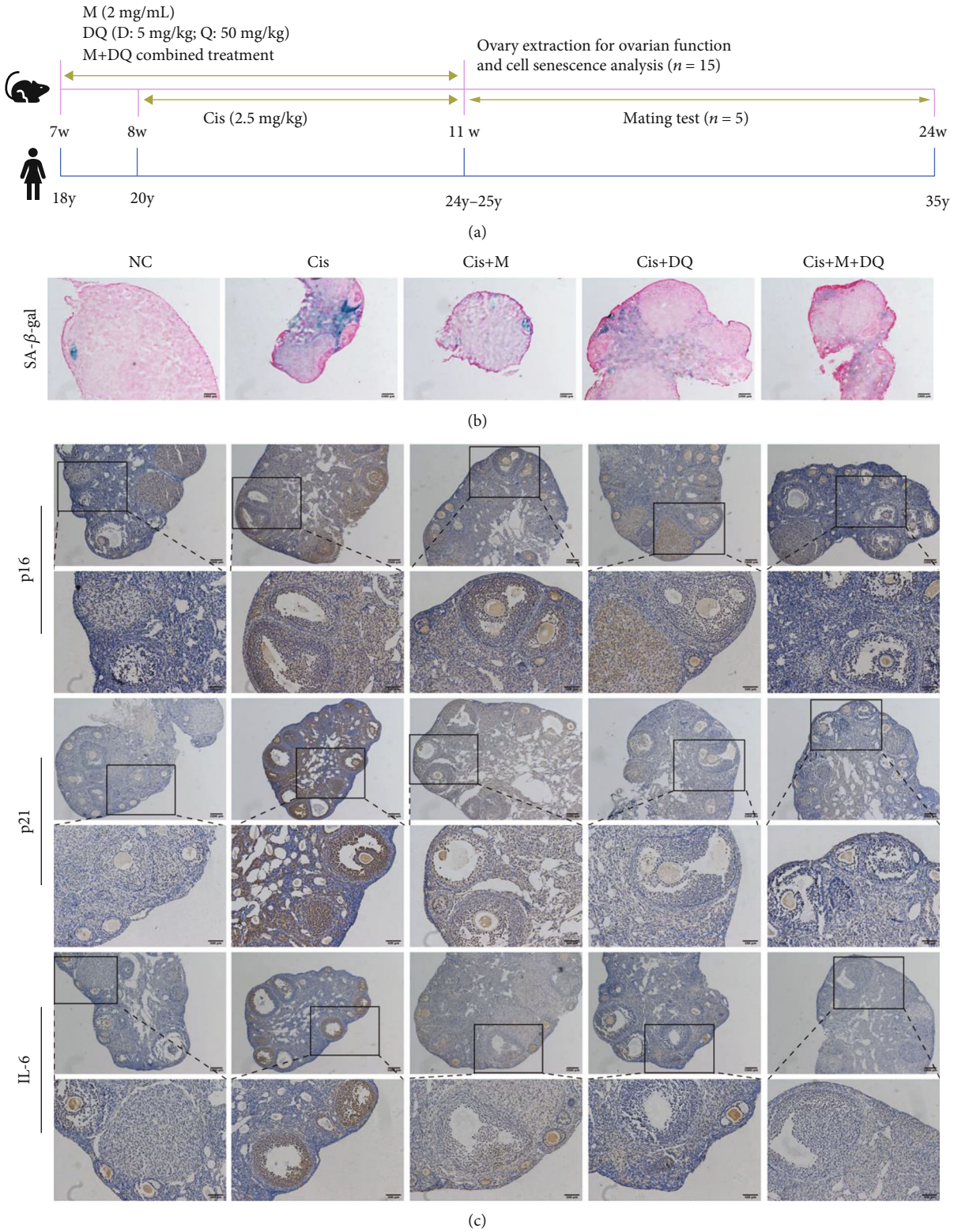

Figure 2: Continued.

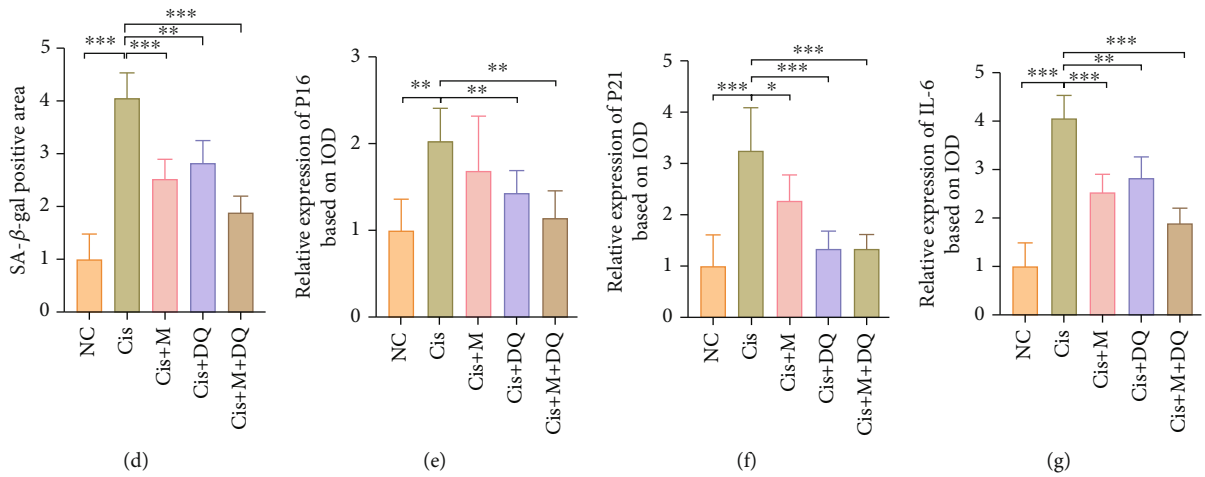

FIGURE 2: Metformin or DQ alone or in combination with each other alleviated the senescent stress induced by cisplatin in vivo. (a) Flowchart of drug administration animal experiment. (b, c) Light microscopic images of SA-β-gal staining and $P16^{link4a}$, $P21^{WAF1/Cip1}$, and IL-6 IHC staining after different medications. Scar bars are marked on respective images ($n=3$). (d–g) Quantitative analysis of SA-β-gal–positive area and $P16^{link4a}$-, $P21^{WAF1/Cip1}$-, and IL-6-postive IOD ($n=3$). Results are presented using mean ± standard deviation values. $*p < 0.05$, $**p < 0.01$, $***p < 0.001$.

committee of Tongji Hospital, Tongji Medical College, Huazhong University of Science and Technology, in the People's Republic of China.

2.4. Senescence-Associated- (SA-) β-Gal Staining. SA-β-gal staining of GCs or frozen ovarian slices was conducted according to the product manual. In brief, for GCs, samples were prewashed with phosphate-buffered saline and then fixed with the fixative solution provided in the Senescence β-Galactosidase Staining Kit (C0602; Beyotime Biotechnology, Haimen, China). For frozen ovarian sections, ovarian slices were rewarmed first and then processed for the staining step.

2.5. Sirius red Staining. A series of representative ovarian sections in different medication groups were chosen to identify the fibrosis level using Sirius red staining. Initially, we dewaxed and hydrated the ovarian slices and processed them with 10-minute celestine blue staining. After 3 washes with ddH_2O, the ovarian sections were subjected to Sirius red solution for 30 minutes. Following another round of dehydration, we mounted ovarian slices with neutral resins for subsequent imaging and quantitative analysis.

2.6. Immunoblot and Quantitative Analyses. In brief, total ovarian proteins or proteins from cell lysates were extracted and separated by 10% sodium dodecyl sulphate–polyacrylamide gel electrophoresis (SDS-PAGE) gel or 12% SDS–PAGE gel according to the molecular weight of the proteins to be measured. Targeted proteins were subsequently transferred to polyvinylidene fluoride membranes and blocked with rapid blocking buffer for 30 minutes. After 3 washes with Tris-Buffered Saline and Tween 20 (TBST), targeted proteins were incubated with specific primary antibodies against nuclear factor kappa-light-chain-enhancer of activated B-cells (NF-κB) (Cat# 10745-1-AP, 1 : 1000; Proteintech, Rosemont, IL, USA), $P16^{link4a}$ (Cat# 10883-1-AP, 1 : 500; Proteintech, Rosemont, IL, USA), $P21^{WAF1/Cip1}$ (Cat# A1438, 1 : 1000; ABclonal Technology, Woburn, MA, USA), interleukin (IL)-6 (Cat# A0286, 1 : 1000; ABclonal Technology, Woburn, MA, USA), IL-1β (Cat# A19635, 1 : 500; ABclonal Technology, Woburn, MA, USA), proliferating cell nuclear antigen (PCNA) (Cat# sc-56, 1 : 1000; Santa Cruz Biotechnology, Dallas, TX, USA), heme oxygenase (HO)-1 (Cat# 10701-1-AP, 1 : 1000; ABclonal Technology, Woburn, MA, USA), and superoxide dismutase (SOD) 2 (Cat# Ag21388; ABclonal Technology, Woburn, MA, USA) diluted in TBST overnight in a 4°C refrigerator. After 30 minutes of rewarming, target blots were washed with TBST 3 times and incubated with appropriate secondary antibodies for 1 hour the next day. Ultimately, blots were imaged using the chemiluminescence method after 3 washes.

2.7. Immunohistochemistry (IHC) and Immunofluorescence (IF) Staining. Three representative sections of ovaries in distinct groups were selected for IHC and IF analyses. The former was used to detect the localization and quantitative expressions of ovarian $P16^{link4a}$, $P21^{WAF1/Cip1}$, IL-6, and 8-hydroxy-2 deoxyguanosine (8-OHdG) (Cat# sc-393871, 1 : 100; Santa Cruz Biotechnology, Dallas, TX, USA), and the latter was applied to identify zona pellucida protein 3 (ZP3) protein expression (ab70384, 1 : 100; Abcam, Cambridge, UK). IHC and IF were performed using routine protocols as previously described [25].

2.8. Terminal Deoxynucleotidyl Transferase dUTP Nick End Labeling (TUNEL) Cell Apoptosis Analysis and 5-Ethynyl-2′-Deoxyuridine (EdU) Cell Proliferation Analysis. Ovarian sections were first dewaxed and hydrated, and then we performed staining steps according to the manuals of the Colorimetric TUNEL Apoptosis Assay Kit (C1098; Beyotime Biotechnology, Haimen, China) and BeyoClick™ EdU Cell Proliferation Kit with Alexa Fluor 488 (C0071S; Beyotime Biotechnology, Haimen, China).

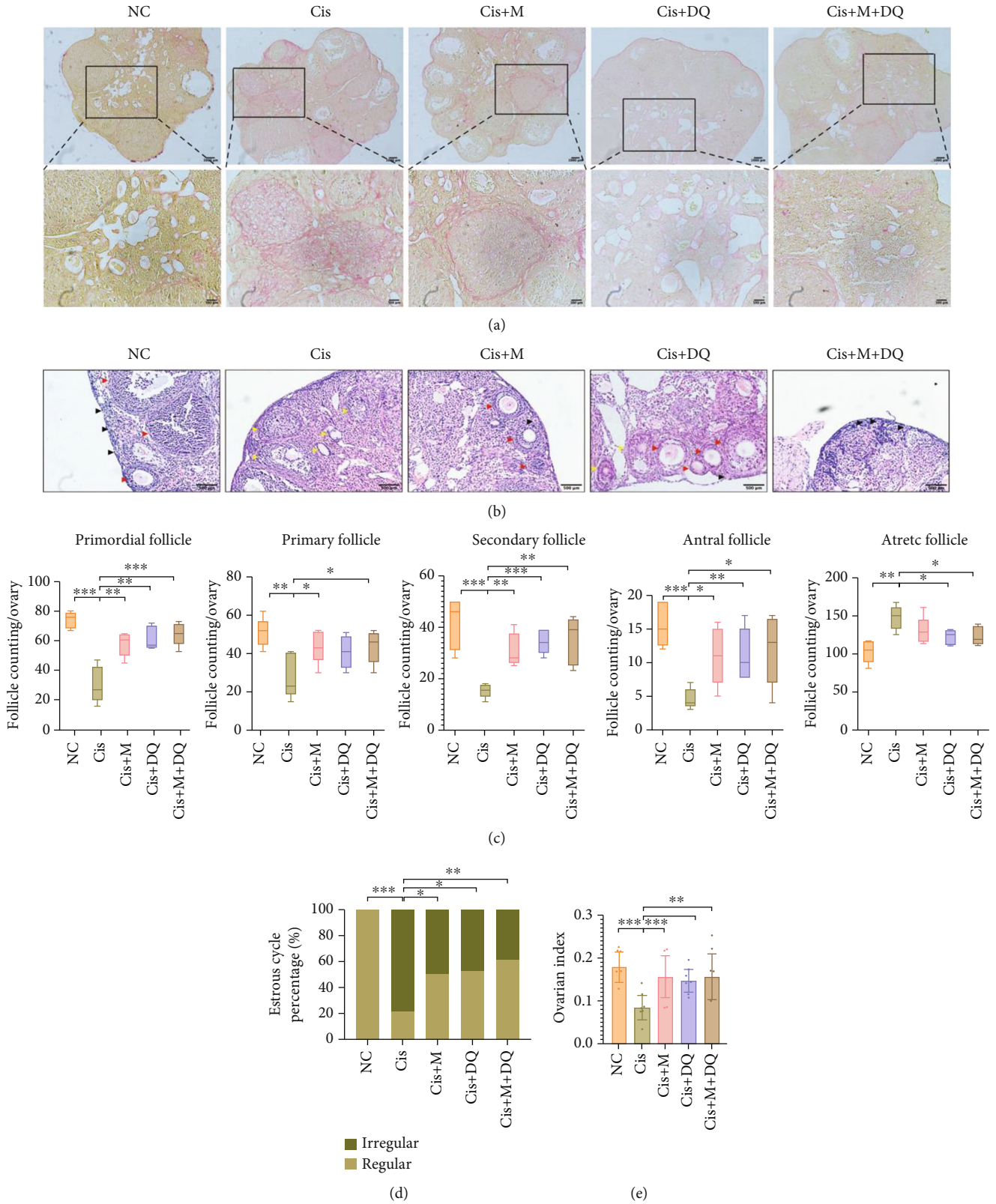

Figure 3: Continued.

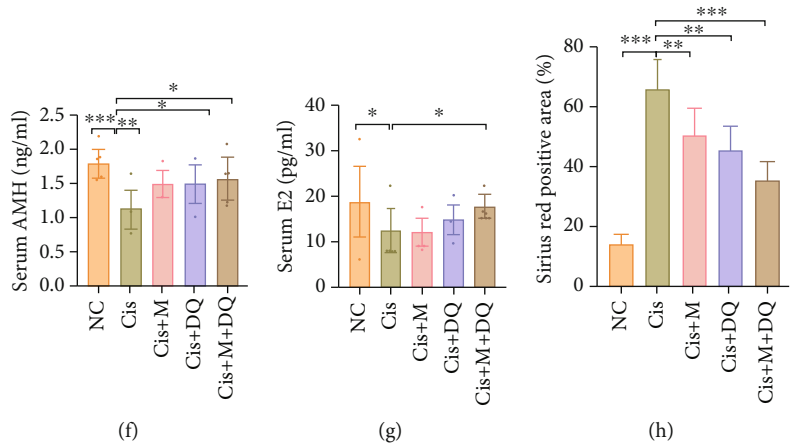

Figure 3: Metformin and DQ alone or with each other improved healthy ovarian reserve and function in cisplatin-treated mice. (a, h) Representative images of Sirius red stained ovaries and quantitative analysis of Sirius red positive area. Scar bars were marked on respective images ($n=3$). (b, c) HE staining of ovarian sections and quantitative counting of follicles at different levels ($n=5$). *Black arrow*: primordial follicle; *red arrow*: primary follicle, secondary follicle and antral follicle; *yellow arrow*: atretic follicle. (d) Regular and irregular estrous cycle percentage of different medication groups ($n=6$). (e) Mice ovarian index in different medication groups ($n=10$). (f, g) Serum AMH ($n=8$) and E_2 ($n=7$) of following the administration of different drugs. Results are presented using mean ± standard deviation values. $*p<0.05$, $**p<0.01$, $***p<0.001$.

2.9. Transmission Electron Microscope. Three ovaries per group were preserved in electron microscope preservation solution (G1102; Servicebio, Wuhan, China). Transmission electron microscopy images of each ovary sample were taken by ServiceBio (Wuhan, China).

2.10. Estrous Cycle Analysis. Vaginal smears of all animals were sampled at 9:00 a.m. for 15 consecutive days from the day drug administration was finished. Vaginal secretions were collected with saline and then spread on slides, followed by hematoxylin and eosin (HE) staining after air drying. Then, the stage of the estrous cycle was determined by cytology by 2 people separately under a microscope.

2.11. Follicle Counting. Five ovaries from distinct individuals in each group were obtained for follicle counting. Dissected ovaries were preserved in 4% paraformaldehyde and then cut into 5 μm pieces. Follicles at different levels were counted by 2 people separately. The detailed procedures were performed as previously described [26].

2.12. Serum Anti-Müllerian Hormone (AMH) and Estradiol (E_2) Determination. Nonhemolytic blood samples of female mice were collected before sacrifice. Levels of serum AMH and E_2 were determined using the Mouse AMH ELISA Kit and Mouse E_2 ELISA Kit according to the manufacturer's instructions (CSB-E13156 m and CSB-E05109 m; Cusabio Technology LLC, Houston, TX, USA).

2.13. Mating Test. Five female mice in each group were randomly selected for the mating test. The mating test began once the drug administration ended. In brief, 10 days were designated as a mating cycle, and 2 female mice with 1 male mouse were arranged in one cage for mating. We tested the vaginal plugs every morning at 9:00 a.m. to evaluate for a pregnant outcome. The pregnant mice were then allocated to an independent cage, and their pup conditions were recorded. Ten days later, nonpregnant mice were marked and separated from male mice. After the first round parturition ended, another mating cycle was repeated. The duration of the mating test was 6 months in total.

2.14. Statistical Analysis. Statistical analyses were conducted using the SPSS 26.0 software (IBM Corporation, Armonk, NY, USA). Group differences of continuous variables were calculated using one-way analysis of variance (nonparametric tests). Group differences in regular cycle numbers were analyzed using chi-squared analysis. $p<0.05$ was considered statistically significant.

3. Results

3.1. Confirmation of Senescent Ovarian Cells Induced by Cisplatin and Alleviated by Senotherapies. To determine whether cisplatin could induce ovarian cell senescence, we exposed ovarian GCs of female mice to cisplatin in vitro. The flowchart of in vitro experiment is shown in Figure 1 (a). We first screened senescent stress via SA-β-gal staining. As shown in Figures 1(b) and 1(c), SA-β-gal–positive staining was remarkably increased in cisplatin-treated GCs relative to the control group ($p<0.05$). To better investigate the secretory phenotype, cell culture medium following cisplatin administration was collected and determined using a Luminex mouse 23 cytokine array (Wayen Biotechnologies, Shanghai, China). Compared to the control, IL-6 obviously accumulated in the Cis group culture medium ($p<0.05$, Figure 1(d)). Other inflammatory cytokines, such as granulocyte colony-stimulating factor (G-CSF) and IL-12 (P40), showed an upward trend following cisplatin administration without statistical significance (Figures 1(e) and 1(f)). The above results indicated that cisplatin might induce granular cell senescence.

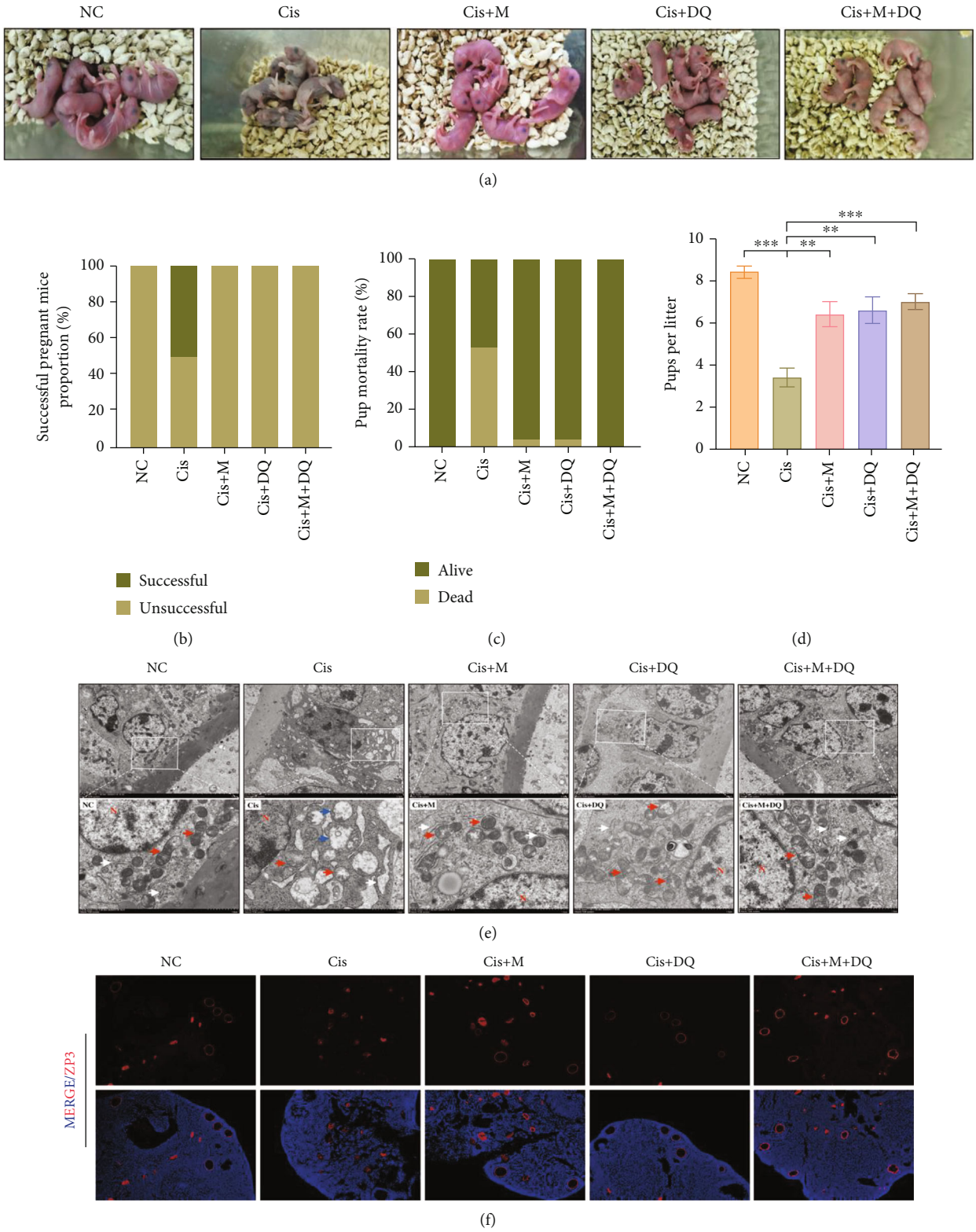

Figure 4: Metformin or DQ alone or in combination with each other pretreatment reorganized the ovarian subcellular structure and preserved mice fertility. (a) General state of pups in different groups. (b–d) Successful pregnant rate, pup mortality rate, and pups per litter of the different drug-administration groups ($n=5$). (e) Transmission electron microscopy images revealed subcellular morphologies of different medication-treated ovaries ($n=3$). Red arrow: mitochondria; white arrow: endoplasmic reticulum (ER); blue arrow: vacuolated cytoplasm; N: nucleus of the GC. The low magnification was 3,000x and the high magnification (insets) was 10,000x. (f) Immunofluorescence of ZP3 in ovaries treated with different medication regimens ($n=3$). Results are presented using mean ± standard deviation values. $**p < 0.01$, $***p < 0.001$.

To further explore whether senotherapies metformin and/or DQ may alleviate the senescence stress caused by cisplatin in vitro, we undertook western blot analysis of senescence-related markers. Quantitative analysis of senescence-related proteins in each group revealed significant upregulation of the senescence marker $P21^{WAF1/Cip1}$ and activation of NF-κB in cisplatin-exposed GCs lysates ($p < 0.05$, Figures 1(g)–1(l)); however, another senescence effector, $P16^{link4a}$, only shows an increased tendency (Figure 1(k)). Conversely, DQ administration led to an obvious downregulation of the senescence markers $P21^{WAF1/Cip1}$ and $P16^{link4a}$ ($p < 0.05$) (Figures 1(k) and 1(l)), and metformin treatment only reduced $P21^{WAF1/Cip1}$ expression ($p < 0.05$, Figure 1(l)), suggesting metformin had a less profound senolytic effect than DQ. Western blot analysis of the SASP markers indicated that metformin excessively prohibited inflammatory cytokine secretion, and IL-6 and IL-1β in cell lysates were highly enriched after metformin treatment ($p < 0.05$, Figures 1(h) and 1(i)). Collectively, these results indicated that metformin and DQ variously attenuated the cisplatin-induced ovarian cell senescence burden in vitro. Of note, DQ exhibited a prominent senescent GC elimination capacity, and metformin probably acted via effective blockage of SASP secretion.

3.2. Removal of Senescent Cells by Metformin or DQ Alone or Both in Combination following Cisplatin Chemotherapy. To further reveal whether metformin and/or DQ intervention could mitigate senescent stress in vivo, we established a cisplatin-induced ovarian damage animal model to assess SNCs after the aforementioned medication. The flowchart of the animal experiment is shown in Figure 2(a). SA-β-gal staining of ovarian sections showed a trend consistent with that of the in vitro experiments. In particular, enlarged SA-β-gal–positive staining of mouse ovaries was recorded after cisplatin administration, and metformin and/or DQ invention resulted in various shrinkages of the SA-β-gal–positive staining area in the ovaries ($p < 0.05$, Figures 2(b) and 2(d)). Likewise, we determined senescence-associated markers in ovaries post cisplatin exposure. IHC results revealed remarkably increased positive expressions of $P16^{link4a}$, $P21^{WAF1/Cip1}$, and IL-6 in cisplatin-treated ovaries, suggesting that senescence stress was also induced by cisplatin in vivo (Figure 2(c)). Alone or combined treatment with metformin and DQ significantly inhibited the expression of $P16^{link4a}$, $P21^{WAF1/Cip1}$, and IL-6 (Figure 2(c)). Quantitative analysis of integral optical density (IOD) indicated that metformin plus DQ treatment removed the maximum senescence signal ($p < 0.05$, Figures 2(e)–2(g)). In summary, these data validated that senescent cells do exist in cisplatin-treated mouse ovaries, and ovarian senescent stress induced by cisplatin can be effectively removed by metformin and/or DQ treatment in vivo. In particular, metformin plus DQ treatment maximally eliminated the senescent burden in the cisplatin-exposed ovarian setting.

3.3. Reversal of Ovarian Function by Metformin or DQ Alone or Both in Combination against Cisplatin-Induced Damage. To further uncover whether metformin and/or DQ senotherapies protect ovaries from cisplatin-induced ovarian dysfunction, we undertook ovarian fibrosis evaluation, ovarian follicle counting, and estrous cycle and serum hormone determination in each group. Series of ovarian Sirius red staining indicated obvious fibrosis in cisplatin-treated ovaries, which was significantly alleviated following metformin and/or DQ administration ($p < 0.05$, Figures 3(a) and 3(h)). Ovarian follicle counting directly reflected the ovarian reserve. In this study, primordial follicles and growing follicles were largely reduced in cisplatin-treated ovaries, and atretic follicles were significantly elevated ($p < 0.05$, Figure 3(c)). However, metformin and/or DQ treatment restored the growth and development of ovarian follicles (Figure 3(c)). Notably, combination administration of both maximally preserved ovarian reserve and prohibited follicle atresia caused by cisplatin ($p < 0.05$, Figure 3(c)).

The estrous cycle is thought to be a reflection of ovarian endocrine function. We next assessed irregular estrous cycle frequencies in each group. Remarkably, cisplatin treatment disturbed estrous cycles in mice, as the percentage of irregular estrous cycles was up to 78.9% ($p < 0.05$, Figure 3(d)), with irregular estrous cycle rates of 50%, 47.4%, and 38.9% in the Cis+M group, Cis+DQ group, and Cis+M+DQ group, respectively ($p < 0.05$, Figure 3(d)). Moreover, the ovarian index was obviously reduced in cisplatin-treated mice, whereas senotherapies (Cis+M, Cis+DQ, and Cis+M+DQ) led to a significant recovery ($p < 0.05$, Figure 3(e)). To evaluate murine ovarian endocrine function post medication accurately, we measured the serum concentrations of E_2 and AMH. Consistent with previous reports, serum E_2 levels dramatically decreased after cisplatin exposure ($p < 0.05$, Figure 3(g)). Combination treatment with metformin and DQ reversed the decline in serum E_2 levels in mice; however, no significant improvement in serum E_2 levels was observed in the Cis+M and Cis+DQ groups (Figure 3(g)). Markedly decreased serum AMH (a predictive biological marker of ovarian reserve) in cisplatin-treated mice was also observed, while elevated serum AMH was recognized in the Cis+M, Cis+DQ, and Cis+M+DQ groups compared with cisplatin-exposed mice ($p < 0.05$, Figure 3(f)). Similarly, serum AMH was significantly improved in the Cis+M+DQ group, albeit remaining barely different from the NC group mice (Figure 3(f)). Taken together, cisplatin severely impaired mouse ovarian health reserve and function, and senotherapies metformin and/or DQ effectively reversed the injury.

3.4. Preservation of Fertility and Reshaping of Ovarian Subcellular Structure by Metformin or DQ Pretreatment. To identify whether metformin and/or DQ mitigates cisplatin-induced reproductive dysfunction and oocyte impairment, we performed a mating test. The general status of pups in each medication group is shown in Figure 4(a). The successful pregnancy rate in cisplatin-treated mice was significantly lower than that in the NC group, which was recovered in the Cis+M, Cis+DQ, and Cis+M+DQ groups (Figure 4(b)). Meanwhile, the pup mortality rate of cisplatin-treated mice increased compared to that of NC mice, and administration of metformin or DQ alone or both in combination seemed to decrease pup mortality (Figure 4(c)). Additionally, the

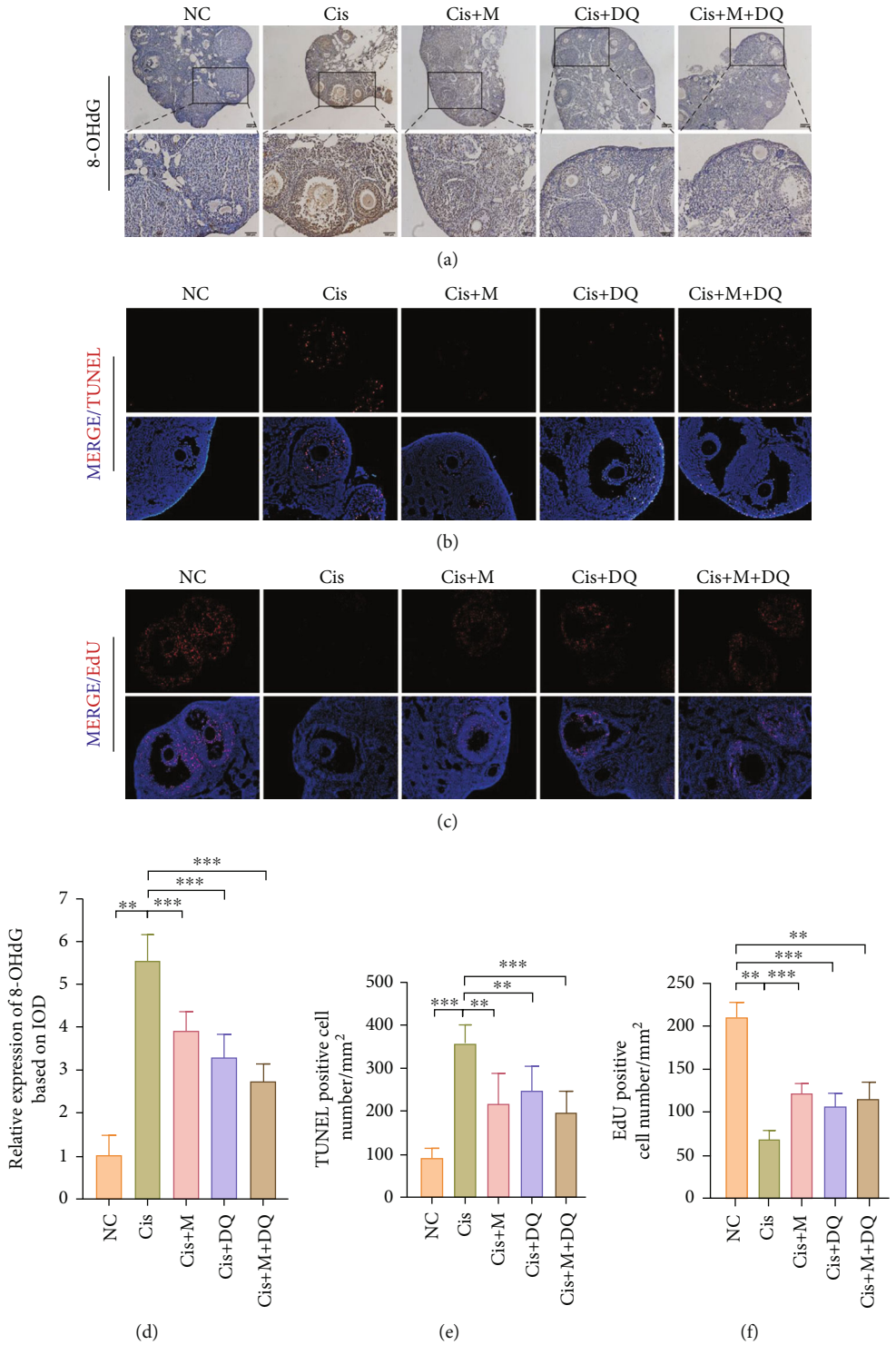

Figure 5: Continued.

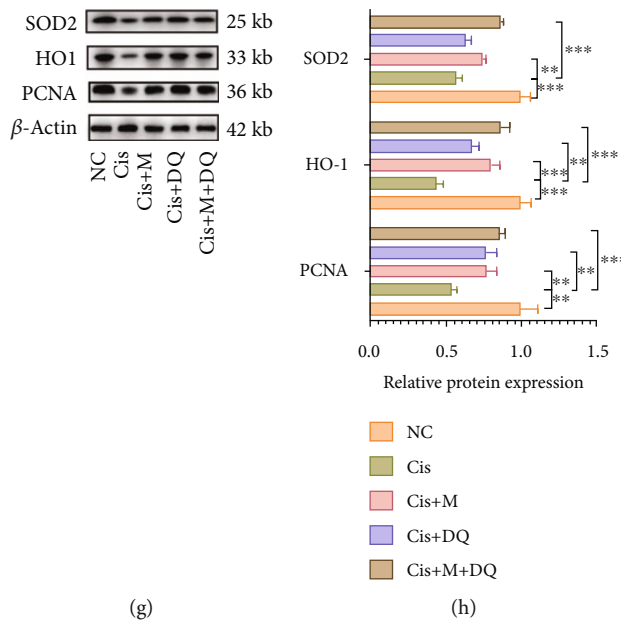

Figure 5: Metformin and DQ alleviate cisplatin-induced ovarian DNA damage. (a, d) Representative images of 8-OHdG immunohistochemical staining after different medications and quantitative analysis of 8-OHdG–positive expression based on IOD (n =3). (b, c, e, f) TUNEL and EdU fluorescence of ovarian sections after different medications and determination of TUNEL- and EdU-positive cell numbers (n =3). (g, h) Western blot analysis of SOD2, HO1, and PCNA protein expressions in ovaries treated with different medication regimens (n =3). Results are presented using mean ± standard deviation values. $**p < 0.01$, $***p < 0.001$.

average pup number per litter in the Cis+M, Cis+DQ, and Cis+M+DQ groups mice was significantly greater than that in cisplatin-treated mice ($p < 0.05$, Figure 4(d)). Notably, the number of pups per litter was indistinguishable between the combo medication group and the NC group (Figure 4(d)).

Healthy follicles constitute the elementary units of female ovaries. GCs serve as vital compartments of the follicle unit, suffering severe damage during cisplatin exposure. To disclose the influence of SNCs on granular subcellular structure, transmission electron microscopy was conducted to record subcellular morphologic alternations of GCs in distinct groups (Figure 4(e)). The majority of GCs were well aligned with integrated nuclear membranes, visible nucleoli, and evenly distributed chromatin in the NC group. Abundant good shapes of the subcellular organelles were captured by cameras, including oval and complete mitochondria with clear cristae and plentiful and enlarged reticulum with ribosome attachments, suggestive of functional protein synthesis. Conversely, the GCs in the Cis group showed a morphology of severely damaged subcellular ultrastructure, characterized by expansive perinuclear space, inhomogeneous distributed chromatin, increased heterochromatin, and even emergence of plasmarrhexis. The functional organelles also suffered from cisplatin exposure. We noticed that mitochondria were dissolved into vacuoles accompanied by discrete cristae, and the endoplasmic reticulum was swollen and even ruptured in cisplatin-exposed GCs. However, metformin, DQ, and metformin plus DQ combined treatment attenuated the subcellular deterioration caused by cisplatin. Compared to cisplatin-treated GCs, the distribution of chromatin was relatively uniform, along with rare heterochromatin, clear nuclear membrane, and limited perinuclear space after senotherapies. The subcellular organelles of the senotherapeutic groups appeared to have a good outline under transmission electron microscopy. The above results illustrated that cisplatin exerted a robust toxic effect on granular subcellular structure, and metformin, DQ, and metformin plus DQ in combination may counteract the subcellular toxic effect caused by cisplatin.

Essentially, oocyte quality is the primary determinant of female fertility and reproductive health. Previous literature has reported the direct impairment of oocytes caused by cisplatin [27]. Ovarian section ZP3 IF was further applied to assess oocyte quality via evaluation of zona pellucida conditions. Remarkably reduced healthy follicles but increased shrinking atretic follicles in cisplatin-treated ovaries were recorded via ZP3 staining. The administration of metformin and/or DQ was associated with an upregulation of normal ZP3 staining, indicating a restoration of oocyte quality following senotherapies (Figure 4(f)). These above results indicated that metformin and/or DQ administration reorganized the granular subcellular structure, preserved female mice fertility, and prohibited oocyte deterioration after cisplatin treatment.

3.5. Alleviation of Cisplatin-Induced Ovarian DNA Damage by Metformin or DQ Alone or Both in Combination. As reported, DDR is an important inducer of cellular senescence [28]. Previous studies have acknowledged DNA damage in other tissues caused by cisplatin and the emerging therapeutic effects of senolytics and senomorphics on organ dysfunction [13, 29]. Thus, we measured DNA damage levels via 8-OHdG IHC staining to identify the possible ovarian genotoxicity caused by cisplatin and the protective

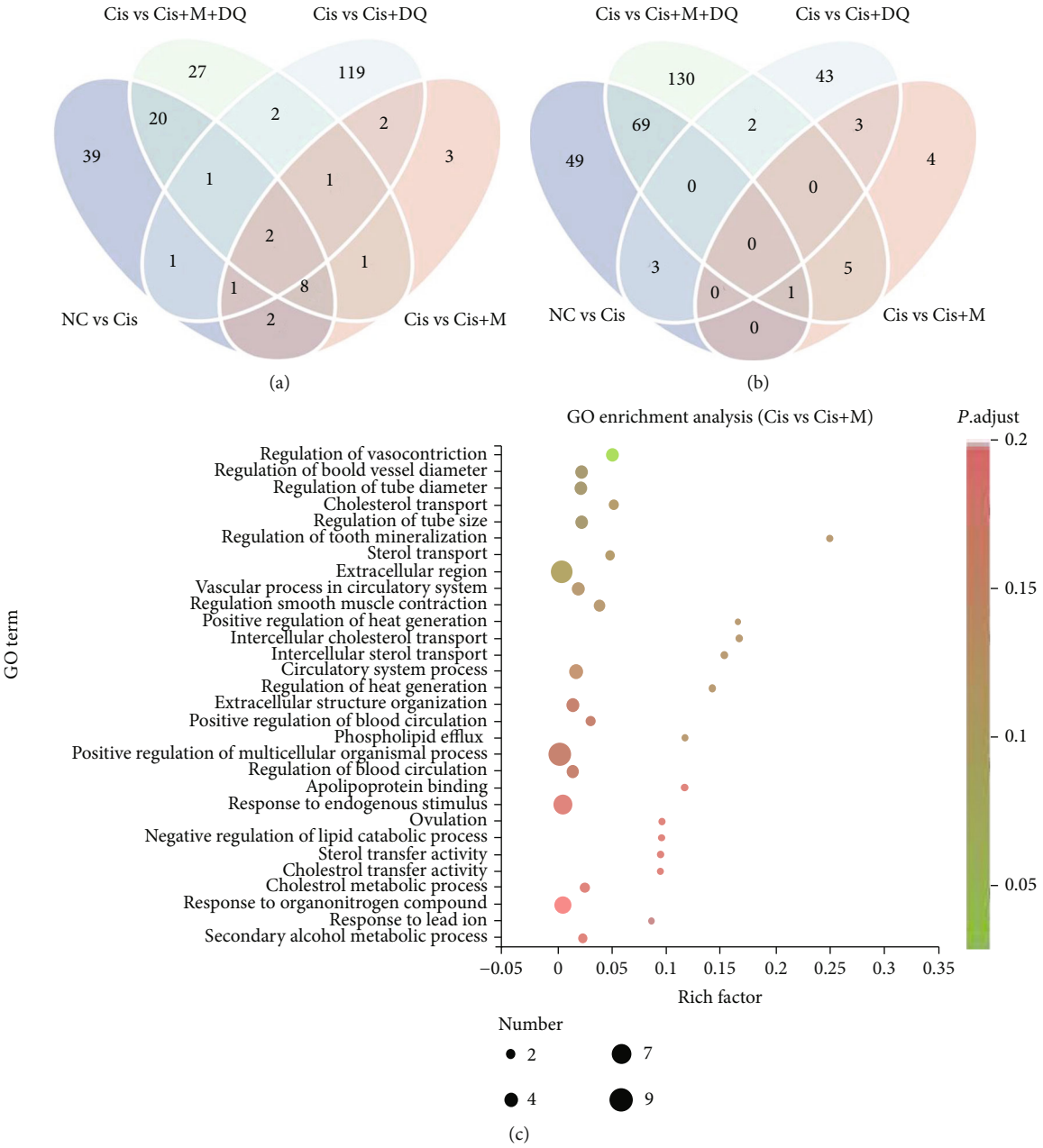

Figure 6: Continued.

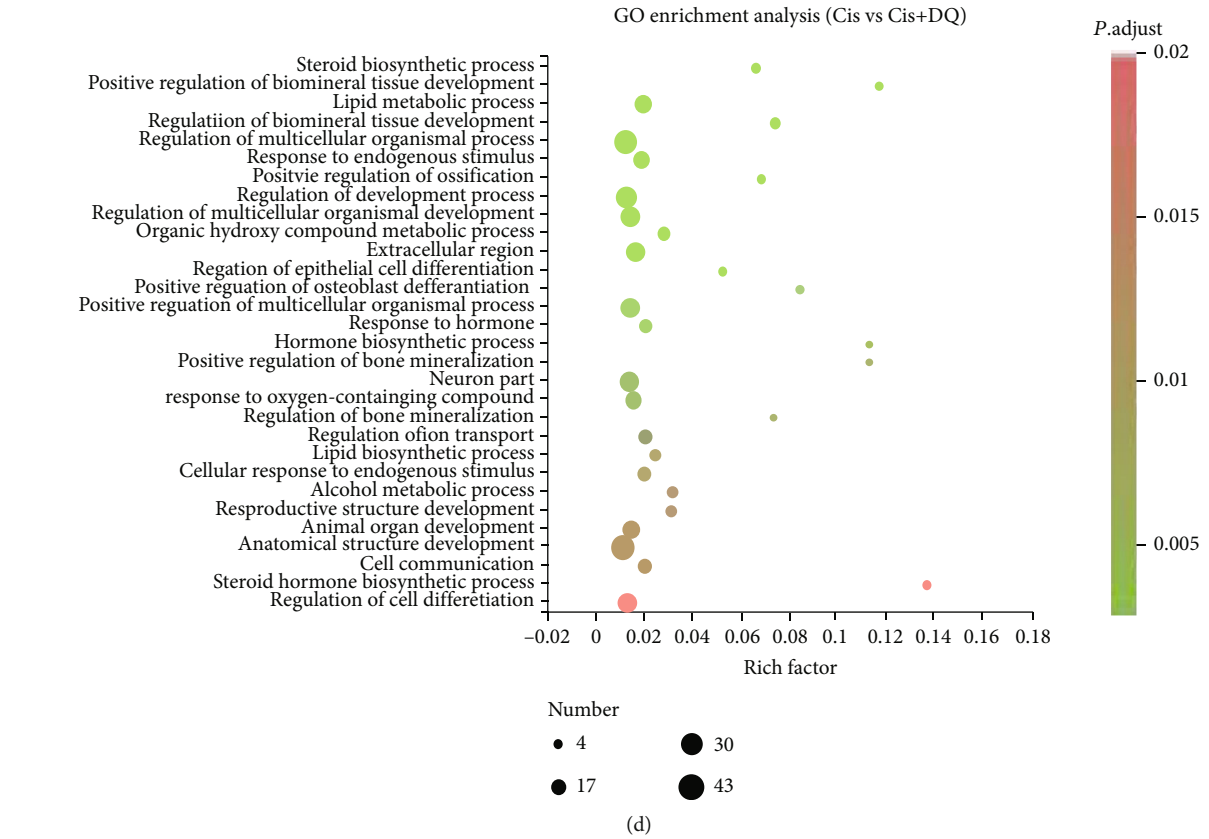

(d)

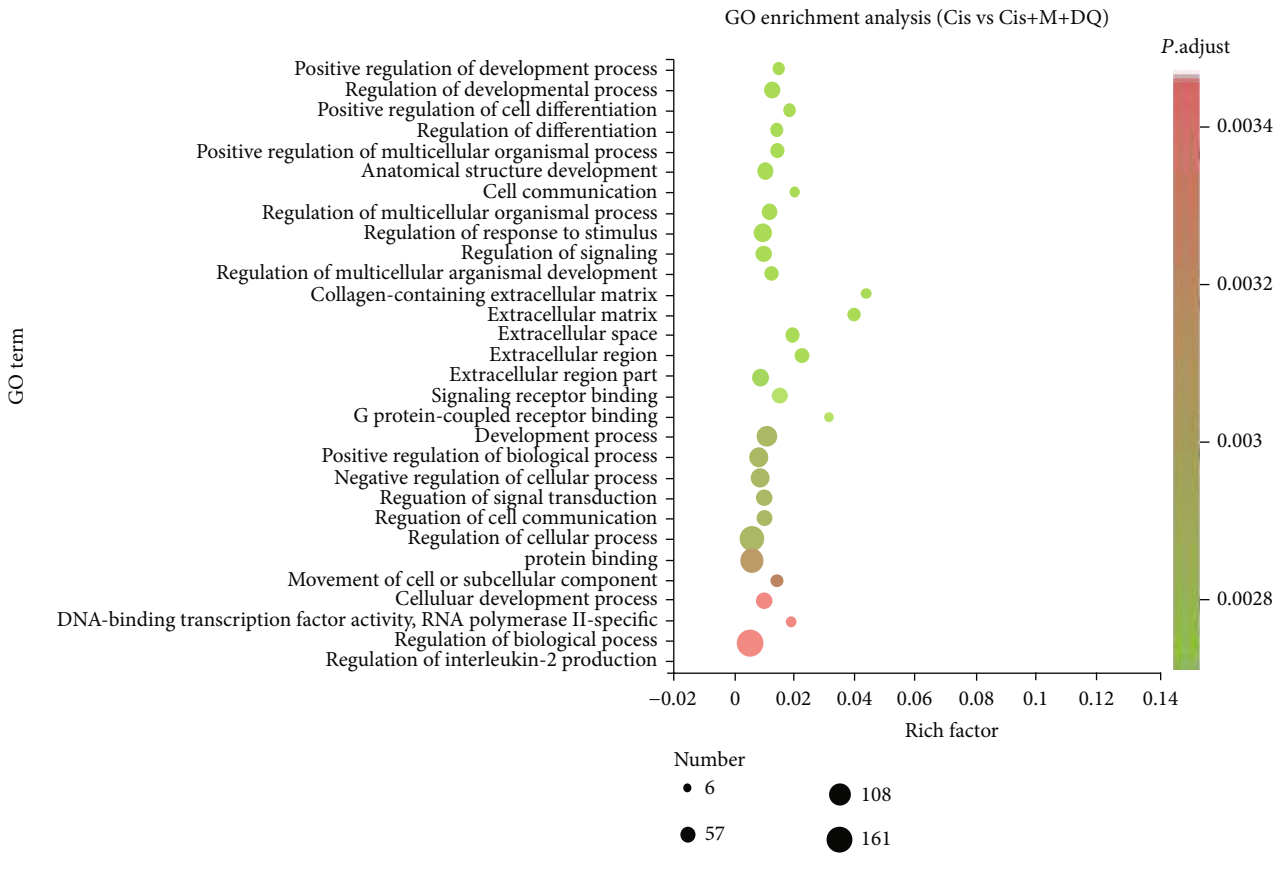

(e)

Figure 6: Continued.

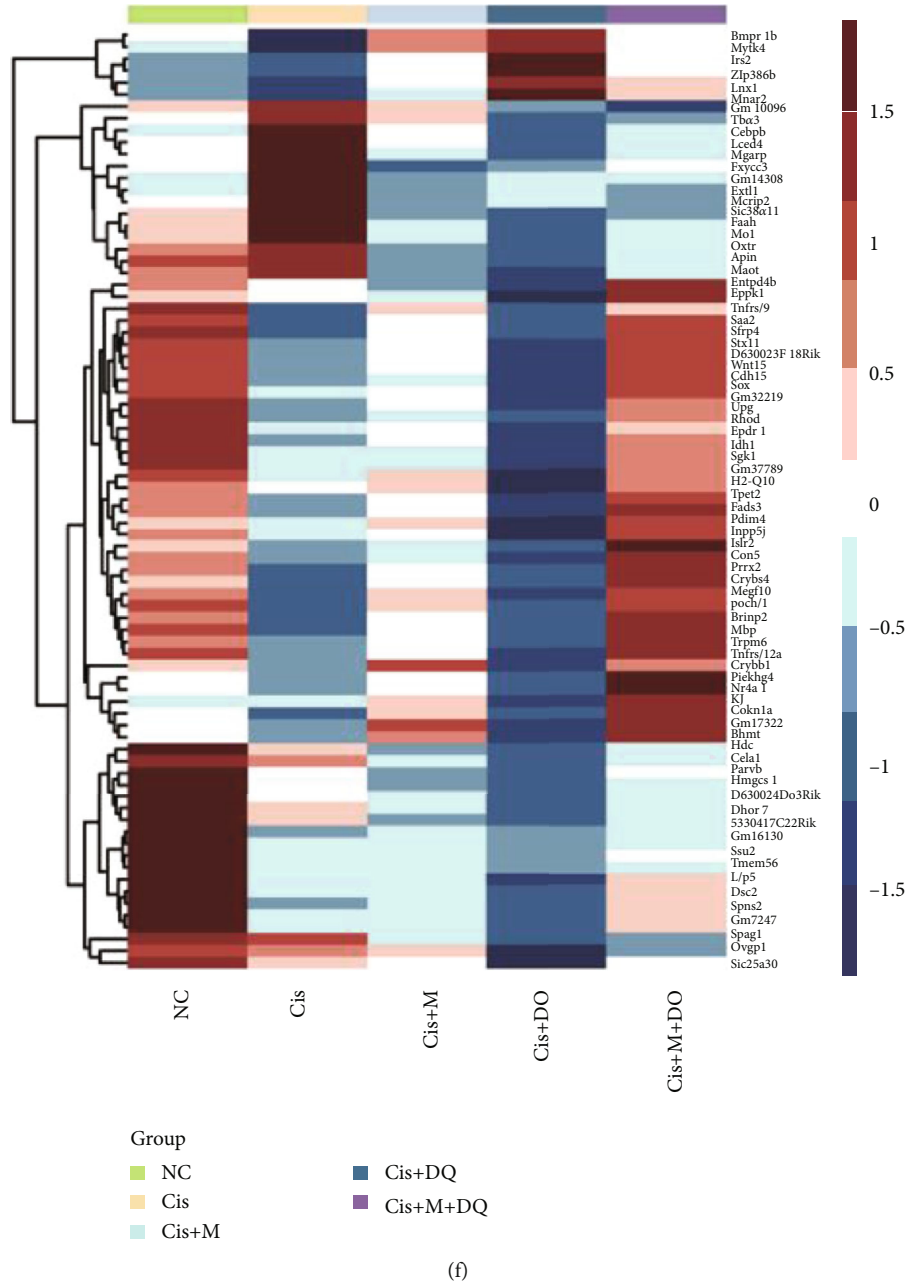

(f)

Figure 6: Senotherapeutic treatment positively regulates cell development. (a, b) Venn diagrams of rescued DEGs. (a) The number of cisplatin enhanced genes downregulated by senotherapies. (b) The number of cisplatin downregulated genes recovered by senotherapies. (c–e) GO terms enriched based on DEGs between the Cis group and different senotherapeutic groups. (f) Heat map of DEGs ovaries treated with different medication regimens (n =3).

effects of senotherapeutic agents. Increased positive staining of 8-OHdG was observed in the Cis group, and western blot analysis revealed a significant decline in the antioxidative markers HO-1 and SOD2 in ovaries following cisplatin chemotherapy, indicating dramatic DNA oxidative injury and unmatched antioxidative capacity in cisplatin-treated ovaries ($p < 0.05$, Figures 5(a), 5(d), 5(g), and 5(h)). The above indexes were variously restored in ovaries treated by Cis +M, Cis+DQ, and Cis+M+DQ; among these, the combination treatment (Cis+M+DQ) ensured the largest elimination of ovarian DNA oxidative damage.

Additionally, the senolytics are suggested to take effect via the modulation of cell apoptosis [30]. To determine whether cisplatin-induced cell senescence affected ovarian cell viability, we performed TUNEL- and EdU-specific staining of ovarian sections to assess the status of cell apoptosis and proliferation in ovaries subjected to distinct treatments. Cisplatin chemotherapy resulted in severe apoptosis of ovarian cells (primarily GCs, small fraction of interstitial cells), while metformin, DQ, and metformin plus DQ co-administration treatment decreased the TUNEL staining ($p < 0.05$, Figures 5(b) and 5 (e)). Positive EdU staining was almost invisible in cisplatin-

treated ovaries; however, metformin, DQ, metformin+DQ combined treatment led to a notable recovery, as shown in Figures 5(c)–5(f). Statistical counting of the number of EdU–positive cells per square millimeter and quantitative analysis of PCNA proteins revealed cisplatin excessively activated the ovarian cell apoptosis, whereas metformin, DQ, and metformin plus DQ treatment reversed this process and restored ovarian cells proliferation to various degrees ($p < 0.05$, Figure 5(f)–5(h)). Notably, metformin plus DQ treatment exhibited the best cell protective capacity. In summary, metformin and/or DQ effectively protected ovaries from cisplatin-induced DNA damage.

3.6. Positive Regulation of Cell Development in Cisplatin-Induced Ovaries by Senotherapeutic Treatment. To explore the molecular events induced by senotherapies in cisplatin-treated ovaries, we employed transcriptome sequencing of ovaries in the different drug-administration groups. Venn diagrams show the number of differentially expressed genes (DEGs) between NC and Cis ovaries along with the rescued genes in different senotherapeutic groups (Figures 6(a) and 6(b)). Specifically, cisplatin exposure resulted in the downregulation of 73 genes in the ovaries, among which metformin, senolytic DQ, and metformin and DQ together rescued 1, 3, and 70 of them, respectively (Figure 6(b)). Thirty-five cisplatin-upregulated genes were modulated following senotherapies—in particular, metformin, senolytic DQ, and metformin and DQ together reset 13, 5, and 31 of them (Figure 6(a)). A heat map unveils the specific DEGs involved. In comparison to Cis-treated ovaries, cell proliferation-related DEGs, including *Ki*, *Prrx2*, *Sfrp4*, and *Megfl0*, and the antioxidative gene *H2-Q10*, were significantly upregulated in ovaries of the Cis+M+DQ group (Figure 6(f)). *Tnfrsf9* and another proliferation activator of endothelial cells, *Tnfrsf12a*, were modulated upwards following single metformin treatment (Figure 6(f)). Strikingly, senolytic DQ treatment downregulated the inflammatory-related gene *Cebpb* and the fibrosis-related gene *Loxl4* (Figure 6(f)). Moreover, DEGs between Cis-treated ovaries and different senotherapeutic groups were enriched in a series of gene ontology (GO) terms related to multiple cellular processes (Figures 6(c)–6(e)). Compared to the Cis group, senolytic DQ co-administration led to a significant enhancement of steroid hormone and lipid biosynthesis, and the genes associated with the cell-development process were also enriched after DQ treatment (Figure 6(d)). In addition, combination senotherapies (Cis+M+DQ group) facilitated cell differentiation, cell development, and cell signal communication (Figure 6(e)). The above comparative analysis of cisplatin and senotherapeutic DEGs in the ovaries supports the promotion effects of senotherapies on steroid hormone, cell proliferation, differentiation, and cell communication pathways, all of which are pathways that may contribute to fertility preservation in female cancer survivors.

4. Discussion

To date, chemotherapy is still the prevalent treatment for tumors and, among the available drugs, cisplatin is widely used in clinical practice. Cisplatin-induced ovarian damage primarily manifests as a loss of the healthy ovarian reserve and increased atretic follicles [5]. Currently, no effective medications are available to prevent such ovarian damage.

The underlying mechanisms of cisplatin-induced ovarian dysfunction involve irreversible DNA damage, overloaded oxidative stress, and uncontrolled apoptosis activation [5–7]. Recent evidence suggests that cisplatin not only leads to senescence of tumor cells but also affects peripheral nontumor renal and neuronal tissues [23, 24]. However, it remains unclear whether SNCs exist in cisplatin-exposed normal ovarian tissues. In our present study, we confirmed that cisplatin administration could induce ovarian cell senescence both in vitro and in vivo, and we further discovered that metformin and DQ treatment may improve cisplatin-injured ovarian function by removing senescent ovarian cells and reducing DNA damage.

DQ, a well-known senolytic, has shown a broad-spectrum senescent cell-killing effect. Emerging evidence suggests that senolytics targeting cell senescence may blaze a new trail for age-related diseases [13]. The cocktail of DQ has been reported to improve murine cardiac function and exercise capacity, thus delaying murine aging [30]. Metformin has been a widely used oral hypoglycemic medication for type 2 diabetes mellitus for five decades, and its nonglycemic benefits, including a prominent SASP elimination efficiency, have been consecutively identified in various in vitro and in vivo models [18, 19, 31]. In our present study, we confirmed the distinct senescence-removal effect and ovarian-preservation efficiency of metformin and/or DQ. Consistent with previous studies, metformin displayed a better SASP-inhibition ability, since western blot analysis showed a remarkable accumulation of SASP in cell lysates following metformin treatment. Importantly, dramatic downregulation of the senescent marker $P21^{WAF1/Cip1}$ was observed in Cis+DQ and Cis+M GCs, indicating a considerable senolytic capacity of DQ and metformin in the ovarian setting. Notably, in addition to SASP prohibition, metformin benefits ovaries by promoting *Sirt1* expression, preventing ovarian oxidative damage, reducing degenerating follicles and interstitial cells, and improving ovarian angiogenesis [32, 33]. Understandably, metformin plus DQ combination treatment produced a synergistic effect in cisplatin-exposed ovarian protection considering the complementary anti-aging targets of these 3 drugs. These data also supported the notion that the cell senescence burden is negatively correlated with ovarian health reserve and may probably work as a useful marker to predict female fecundity after cisplatin chemotherapy.

A hallmark of senescent cells is the secretion of SASPs or the senescence messaging secretome [10]. SASPs serve as mediators and spread senescence or senescence phenotypes in autocrine and paracrine fashions, thus interfere with cell viability and induce apoptosis [34]. We first set out to determine the SASPs secreted by senescent GCs following cisplatin exposure in vitro. A mouse cytokine array indicated significant elevation of inflammatory cytokine secretion in the cisplatin-exposed group; in particular, representative

SASP IL-6 tripled over that in the NC group after cisplatin administration. The senomorphic agent metformin prominently alleviated SASP secretion after cisplatin exposure, since IL-6 and IL-1β were remarkably accumulated in cell lysates of Cis+M GCs compared to Cis-treated GCs. DQ showed a less profound influence on senescent granular SASP secretion, and IL-1β quantitative analysis showed an upwards tendency in cell lysates but reached no statistical significance compared to the Cis group. In addition, an in vivo animal experiment further demonstrated that cisplatin-induced ovarian cell senescence was not confined to GCs, since SA-β-gal staining and $P16^{link4a}$- and $P21^{WAF1/Cip1}$-positive staining were also present in ovarian theca-interstitial cells. However, to determine whether theca-interstitial cell senescence is attributed to direct cisplatin damage or influenced by the SASP paracrine activity of GCs, further investigation is required.

In addition to the senescence removal of metformin and DQ discovered in our study, we surprisingly uncovered a metformin and/or DQ anti-DNA damage capacity in cisplatin-damaged ovaries. The antioxidative proteins SOD2 and HO-1 were significantly upregulated in the ovaries of the senotherapeutic groups, while subtle TUNEL staining and obvious EdU IF were noted in Cis+M, Cis +DQ, and Cis+M+DQ follicle units. Quantitative analysis of PCNA protein expression also revealed marked elevation after single or combined application of senotherapeutics. Transcriptome sequencing analysis further proved that the proportions of cisplatin-modulated genes could be rescued with single or combined senotherapies; of note, combination treatment rescued the largest proportion of genes. As expected, the heat map showed that cell proliferation-associated genes, such as *Ki*, *Prrx2*, *Sfrp4*, and *Megfl0*; and the antioxidative gene *H2-Q10* were remarkably enhanced in Cis+M+DQ ovaries. Except for senolytic efficiency, DQ probably exerted anti-inflammatory and antifibrosis effects since related genes were upregulated following DQ co-administration. GO enrichment analysis revealed that the biological processes enhanced after combination treatment were positive regulation of cell development, cell differentiation, and cell communication. Taken together, these data verified that senotherapies not only fight against cell senescence but also participate in multiple cellular processes and promote ovarian cell survival after chemotherapy in multiple ways.

Several limitations of our study should be declared here. First, we did not comprehensively detect all senescence-related markers in mouse ovarian tissue and GCs. Future studies are required to cover more SASPs and senescence markers. Second, we did not confirm our discovery in clinical samples, and associated experiments will be undertaken in the near future.

In summary, our present study demonstrated that cellular senescence is involved in cisplatin-induced ovarian dysfunction and clearance of senescent cells by independent or combined administration of metformin and/or DQ ameliorated cisplatin-induced ovarian dysfunction in mice. Metformin plus DQ therapy further attenuated cisplatin-induced DNA damage. Transcriptomic sequencing revealed that the proportions of cisplatin-altered genes were rescued and biological processes, such as cell differentiation, cell development, and cell signal communication, were significantly upregulated after combination treatment. Additionally, we discovered synergistic effects of metformin and DQ in cisplatin-induced ovarian failure. Our work provides a previously unreported mechanism for cisplatin-induced ovarian damage and reveals that senotherapies targeting senescent cells could partially reverse this damage and may represent a promising therapeutic avenue to prevent chemotherapy-induced fertility loss.

5. Conclusion

In conclusion, our work demonstrates that senotherapies might prevent cisplatin-induced ovarian injury by removing senescent cells and reducing DNA damage, which may serve as a promising therapeutic avenue to prevent chemotherapy-induced ovarian damage.

Abbreviations

DQ: Dasatinib and quercetin
SASP: Senescence-associated secretory phenotype
DDR: DNA damage response
β-gal: β-Galactoside
SNCs: Senescent cells
GCs: Granulosa cells
rpm: Revolutions per minute
SDS-PAGE: Sodium dodecyl sulphate–polyacrylamide gel electrophoresis
TBST: Tris-Buffered Saline and Tween 20
NF-κB: Nuclear factor kappa-light-chain-enhancer of activated B-cells
IL: Interleukin
PCNA: Proliferating cell nuclear antigen
HO: Heme oxygenase
SOD: Superoxide dismutase
IHC: Immunohistochemistry
IF: Immunofluorescence
8-OHdG: 8-hydroxy-2 deoxyguanosine
ZP3: Zona pellucida protein 3
TUNEL: Terminal deoxynucleotidyl transferase dUTP nick end labeling
EdU: 5-Ethynyl-2′-deoxyuridine
HE: Hematoxylin and eosin
AMH: Anti-Müllerian hormone
E_2: Estradiol
G-CSF: Granulocyte colony-stimulating factor
IOD: Integral optical density
DEG: Differentially expressed genes
GO: Gene ontology.

Data Availability

The data that support the findings of this study are available from the corresponding author upon reasonable request.

Disclosure

The funders had no role in the study design, data collection, analysis, and interpretation of the data or in writing the manuscript.

Conflicts of Interest

The authors declare that they have no conflicts of interest.

Authors' Contributions

Dingfu Du, Jinjin Zhang, and Shixuan Wang designed the experiments. Dingfu Du and Xianan Tang accomplished the molecular-biological experiments in vitro and in vivo. Yueyue Gao, Runhua Chen, and Huan Lu took the responsibility of animal drug administration and data analysis. Qian Chen, Jingyi Wen, Tong Wu, and Yan Zhang revised the manuscript. Dingfu Du and Xianan Tang contributed equally to this work.

Acknowledgments

This work was supported by grants from the National Natural Science Foundation of China (NO. 82001498, NO. 81873824, and NO. 82002768) and the Natural Science Foundation of Hubei Province (NO. 2020CFB544).

References

[1] H. Sung, J. Ferlay, R. L. Siegel et al., "Global cancer statistics 2020: GLOBOCAN estimates of incidence and mortality worldwide for 36 cancers in 185 countries," *CA: a Cancer Journal for Clinicians*, vol. 71, no. 3, pp. 209–249, 2021.

[2] E. Taylan and K. H. Oktay, "Current state and controversies in fertility preservation in women with breast cancer," *World J Clin Oncol.*, vol. 8, no. 3, pp. 241–248, 2017.

[3] N. Bhakta, Q. Liu, K. K. Ness et al., "The cumulative burden of surviving childhood cancer: an initial report from the St Jude Lifetime Cohort Study (SJLIFE)," *Lancet*, vol. 390, no. 10112, pp. 2569–2582, 2017.

[4] L. Qi, Q. Luo, Y. Zhang, F. Jia, Y. Zhao, and F. Wang, "Advances in toxicological research of the anticancer drug cisplatin," *Chemical Research in Toxicology*, vol. 32, no. 8, pp. 1469–1486, 2019.

[5] N. Spears, F. Lopes, A. Stefansdottir et al., "Ovarian damage from chemotherapy and current approaches to its protection," *Human Reproduction Update*, vol. 25, no. 6, pp. 673–693, 2019.

[6] Q. N. Nguyen, N. Zerafa, S. H. Liew et al., "Loss of PUMA protects the ovarian reserve during DNA-damaging chemotherapy and preserves fertility," *Cell death & disease*, vol. 9, no. 6, p. 9, 2018.

[7] L. S. Ayres, M. Berger, I. C. L. de Oliveira Durli et al., "Kallikrein-kinin system and oxidative stress in cisplatin-induced ovarian toxicity," *Reproductive Toxicology*, vol. 93, pp. 1–9, 2020.

[8] M. M. Dolmans and D. D. Manavella, "Recent advances in fertility preservation," *The Journal of Obstetrics and Gynaecology Research*, vol. 45, no. 2, pp. 266–279, 2019.

[9] M. Harada and Y. Osuga, "Fertility preservation for female cancer patients," *Fertility and sterility*, vol. 94, no. 1, pp. 28–33, 2019.

[10] V. Gorgoulis, P. D. Adams, A. Alimonti et al., "Cellular senescence: defining a path forward," *Cell*, vol. 179, no. 4, pp. 813–827, 2019.

[11] S. He and N. E. Sharpless, "Senescence in health and disease," *Cell*, vol. 169, no. 6, 2017.

[12] B. G. Childs, M. Durik, D. J. Baker, and J. M. Van Deursen, "Cellular senescence in aging and age-related disease: from mechanisms to therapy," *Nature Medicine*, vol. 21, no. 12, pp. 1424–1435, 2015.

[13] J. Martel, D. M. Ojcius, C. Y. Wu et al., "Emerging use of senolytics and senomorphics against aging and chronic diseases," *Medicinal Research Reviews*, vol. 40, no. 6, pp. 2114–2131, 2020.

[14] M. Ogrodnik, S. Miwa, T. Tchkonia et al., "Cellular senescence drives age-dependent hepatic steatosis," *Nature Communications*, vol. 8, no. 1, 2017.

[15] J. Iske, M. Seyda, T. Heinbokel et al., "Senolytics prevent mt-DNA-induced inflammation and promote the survival of aged organs following transplantation," *Nature communications*, vol. 11, no. 1, pp. 1–13, 2020.

[16] M. Xu, T. Pirtskhalava, J. N. Farr et al., "Senolytics improve physical function and increase lifespan in old age," *Nature medicine*, vol. 24, no. 8, pp. 1246–1256, 2018.

[17] D. Chen, D. Xia, Z. Pan et al., "Metformin protects against apoptosis and senescence in nucleus pulposus cells and ameliorates disc degeneration in vivo," *Cell death & disease*, vol. 7, 2016.

[18] C. Hansel, S. Barr, A. V. Schemann et al., "Metformin protects against radiation-induced acute effects by limiting senescence of bronchial-epithelial cells," *International Journal of Molecular Sciences*, vol. 22, no. 13, p. 7064, 2021.

[19] Q. Hu, J. Peng, L. Jiang et al., "Metformin as a senostatic drug enhances the anticancer efficacy of CDK4/6 inhibitor in head and neck squamous cell carcinoma," *Cell death & disease*, vol. 11, no. 10, p. 11, 2020.

[20] A. Palaniyappan, "Cyclophosphamide induces premature senescence in normal human fibroblasts by activating MAP kinases," *Biogerontology*, vol. 10, no. 6, pp. 677–682, 2009.

[21] A. M. Meredith and C. R. Dass, "Increasing role of the cancer chemotherapeutic doxorubicin in cellular metabolism," *The Journal of Pharmacy and Pharmacology*, vol. 68, no. 6, pp. 729–741, 2016.

[22] T. Nacarelli, T. Fukumoto, J. A. Zundell et al., "NAMPT inhibition suppresses cancer stem-like cells associated with therapy-induced senescence in ovarian cancer," *Cancer Research*, vol. 80, no. 4, pp. 890–900, 2020.

[23] A. Calls, A. Torres-Espin, X. Navarro, V. J. Yuste, E. Udina, and J. Bruna, "Cisplatin-induced peripheral neuropathy is associated with neuronal senescence-like response," *Neuro-Oncology*, vol. 23, no. 1, pp. 88–99, 2021.

[24] C. Li, N. Xie, Y. Li, C. Liu, F. F. Hou, and J. Wang, "N-acetylcysteine ameliorates cisplatin-induced renal senescence and renal interstitial fibrosis through sirtuin1 activation and p53 deacetylation," *Free Radical Biology and Medicine*, vol. 130, pp. 512–527, 2019.

[25] Y. Ma, M. Qi, Y. An et al., "Autophagy controls mesenchymal stem cell properties and senescence during bone aging," *Aging Cell*, vol. 17, no. 1, pp. 1–12, 2018.

[26] X.-m. Zhang, L. Li, J.-j. Xu et al., "Rapamycin preserves the follicle pool reserve and prolongs the ovarian lifespan of female rats via modulating mTOR activation and sirtuin expression," *Gene*, vol. 523, no. 1, pp. 82–87, 2013.

[27] Q. N. Nguyen, N. Zerafa, S. H. Liew, J. K. Findlay, M. Hickey, and K. J. Hutt, "Cisplatin- and cyclophosphamide-induced primordial follicle depletion is caused by direct damage to oocytes," *Molecular Human Reproduction*, vol. 25, no. 8, pp. 433–444, 2019.

[28] J. M. Van Deursen, "The role of senescent cells in ageing," *Nature Publishing Group*, vol. 509, no. 7501, pp. 439–446, 2014, Available from:.

[29] W. J. Wang, X. M. Chen, and G. Y. Cai, "Cellular senescence and the senescence-associated secretory phenotype: potential therapeutic targets for renal fibrosis," *Experimental Gerontology*, vol. 151, p. 111403, 2021.

[30] Y. Zhu, T. Tchkonia, T. Pirtskhalava et al., "The achilles' heel of senescent cells: from transcriptome to senolytic drugs," *Aging Cell*, vol. 14, no. 4, pp. 644–658, 2015.

[31] N. Noren Hooten, A. Martin-Montalvo, D. F. Dluzen et al., "Metformin-mediated increase in DICER1 regulates microRNA expression and cellular senescence," *Aging Cell*, vol. 15, no. 3, pp. 572–581, 2016.

[32] X. Qin, D. Du, Q. Chen et al., "Metformin prevents murine ovarian aging," *Aging (Albany NY)*, vol. 11, no. 11, pp. 3785–3794, 2019.

[33] R. R. Mahamed, C. C. Maganhin, G. R. S. Sasso, M. de Jesus Simões, M. C. P. Baracat, and E. C. Baracat, "Metformin improves ovarian follicle dynamics by reducing theca cell proliferation and CYP-17 expression in an androgenized rat model," *J Ovarian Res. Journal of Ovarian Research*, vol. 11, pp. 1–10, 2018.

[34] J. C. Acosta, A. Banito, T. Wuestefeld et al., "A complex secretory program orchestrated by the inflammasome controls paracrine senescence," *Nature Publishing Group*, vol. 15, no. 8, pp. 978–990, 2013, Available from:.

Hindawi
Oxidative Medicine and Cellular Longevity
Volume 2022, Article ID 2713483, 13 pages
https://doi.org/10.1155/2022/2713483

Review Article

Cellular and Molecular Mechanisms Involved in Hematopoietic Stem Cell Aging as a Clinical Prospect

Soheila Montazersaheb,[1] **Ali Ehsani**,[2] **Ezzatollah Fathi**,[3] **and Raheleh Farahzadi**[4]

[1]*Molecular Medicine Research Center, Tabriz University of Medical Sciences, Tabriz, Iran*
[2]*Student Research Committee, Tabriz University of Medical Sciences, Tabriz, Iran*
[3]*Department of Clinical Sciences, Faculty of Veterinary Medicine, University of Tabriz, Tabriz, Iran*
[4]*Hematology and Oncology Research Center, Tabriz University of Medical Sciences, Tabriz, Iran*

Correspondence should be addressed to Ezzatollah Fathi; ez.fathi@tabrizu.ac.ir and Raheleh Farahzadi; farahzadir@tbzmed.ac.ir

Received 1 January 2022; Revised 28 February 2022; Accepted 22 March 2022; Published 1 April 2022

Academic Editor: Natalia Krasteva

There is a hot topic in stem cell research to investigate the process of hematopoietic stem cell (HSC) aging characterized by decreased self-renewal ability, myeloid-biased differentiation, impaired homing, and other abnormalities related to hematopoietic repair function. It is of crucial importance that HSCs preserve self-renewal and differentiation ability to maintain hematopoiesis under homeostatic states over time. Although HSC numbers increase with age in both mice and humans, this cannot compensate for functional defects of aged HSCs. The underlying mechanisms regarding HSC aging have been studied from various perspectives, but the exact molecular events remain unclear. Several cell-intrinsic and cell-extrinsic factors contribute to HSC aging including DNA damage responses, reactive oxygen species (ROS), altered epigenetic profiling, polarity, metabolic alterations, impaired autophagy, Janus kinase/signal transducer and activator of transcription (JAK/STAT) pathway, nuclear factor- (NF-) κB pathway, mTOR pathway, transforming growth factor-beta (TGF-β) pathway, and wingless-related integration site (Wnt) pathway. To determine how deficient HSCs develop during aging, we provide an overview of different hallmarks, age-related signaling pathways, and epigenetic modifications in young and aged HSCs. Knowing how such changes occur and progress will help researchers to develop medications and promote the quality of life for the elderly and possibly alleviate age-associated hematopoietic disorders. The present review is aimed at discussing the latest advancements of HSC aging and the role of HSC-intrinsic factors and related events of a bone marrow niche during HSC aging.

1. Introduction

Hematopoiesis is defined as a continuous process by which hematopoietic stem cells (HSCs) replenish diverse types of blood cells such as erythrocytes, B and T lymphocytes, myeloid cells, natural killer (NK) cells, dendritic cells (DCs), mast cells, and platelets during the lifespan of an organism [1, 2] (Figure 1). HSCs are the first isolated and identified stem cells and, more importantly, are still the most studied stem cells. Based on repopulation capacity, HSC pool is divided into three distinct types, including long-term repopulating HSCs (LT-HSCs), short-term repopulating HSCs (ST-HSCs), and multipotent progenitors (MPPs). These progenitors are identified based on cell surface markers and fluorescence-activated cell sorting (FACS) analysis. All murine HSCs are characterized by the lack of lineage-specific surface markers (Lin^-), overexpression of stem cell antigen-1 $(Sca\text{-}1)^+$, and $c\text{-}Kit^+$ (LSKs), referring to $Lin^- Sca1^{++} Kit^+$ or LSK. In addition, it was found that murine HSCs have some primitive markers, including CD48 (Slamf2), CD150 (Slamf1), Flt3, and CD34 [3].

HSCs have the capacity to self-renew and differentiate into diverse types of immune cells, but, similar to adult stem cells, they are susceptible to aging-related stresses. Despite the increasing numbers of human HSCs during aging, a decrease in the self-renewal ability and reconstitution

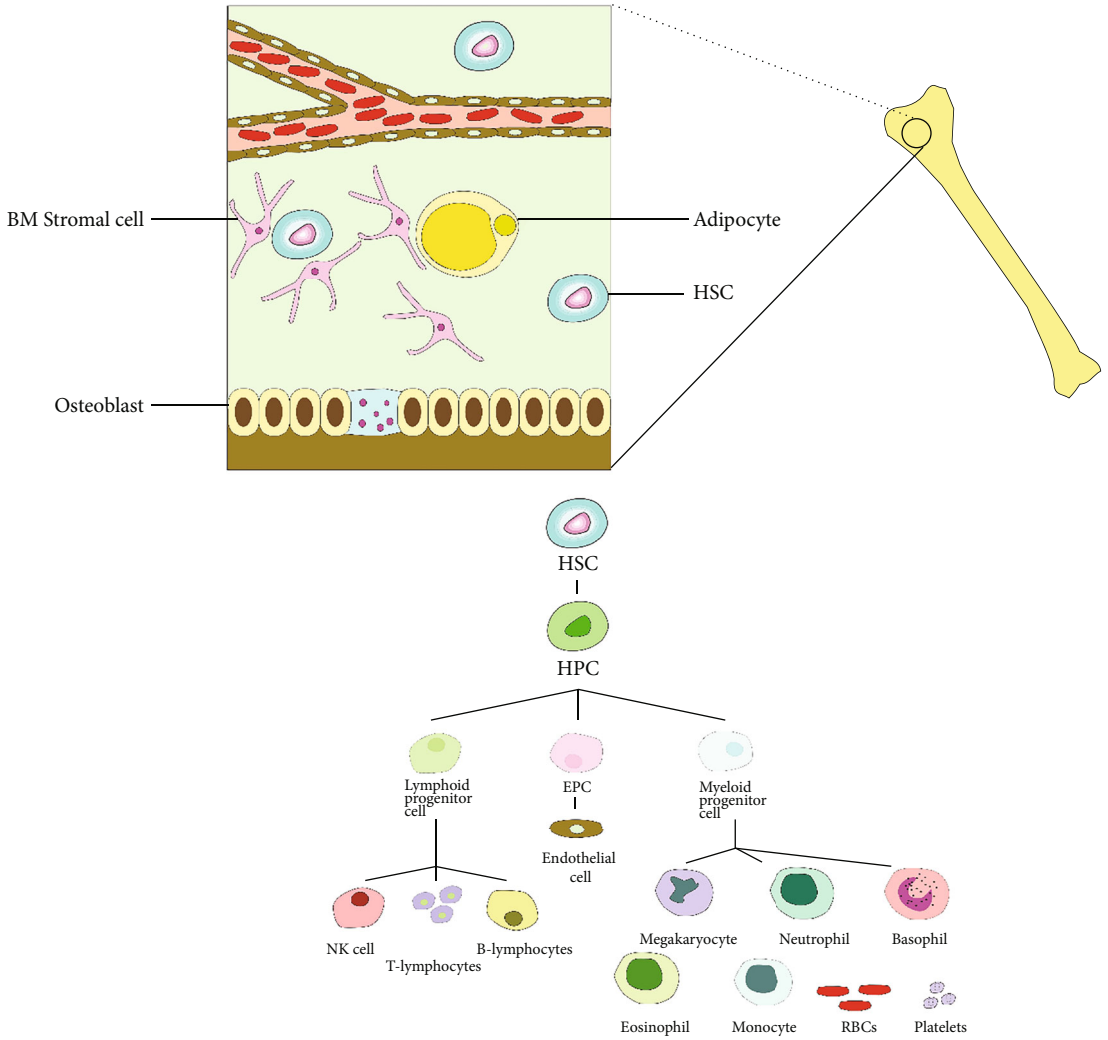

Figure 1: The BM niches. The BM hosts two kinds of adult stem cells, including MSCs and HSCs. The HSCs can give rise to the HPCs which in turn give rise to the lymphoid progenitor cells and the myeloid progenitor cells.

potential of HSCs was observed after transplantation [4]. Upon aging, this gradual loss of the self-renewal and reconstitution potential makes HSCs distinct from pluripotent embryonic stem cells (ESCs) and induced pluripotent stem cells (iPSCs) [5]. Besides, aged human HSCs displayed profound epigenetic reprogramming by targeting cancer pathways, predisposing them to leukemia [6].

Several cell-intrinsic and cell-extrinsic factors contribute to HSC aging. The functional alterations of HSCs with aging are regulated mainly by various cell-intrinsic signals such as DNA damage, reactive oxygen species (ROS), epigenetic changes, and changes in polarity. Furthermore, hematopoietic niche-derived cell-extrinsic factors have a substantial role in the function and maintenance of HSCs [7, 8]. A better understanding of the molecular mechanisms responsible for HSC aging will enable the scientific community to enhance the regenerative capacity and function of healthy HSCs and delay the aging process of the hematopoietic system in the elderly [9].

Given that HSC aging is accompanied by its dysfunction, several studies have investigated the mechanisms behind this. HSC aging is associated with altered expression of some genes and mutations of specific genes [5, 10]. Furthermore, inhibition of specific pathways, such as the mammalian target of rapamycin (mTOR) and p38 mitogen-activated protein kinase (P38 MAPK) signaling pathways, is involved in the aging of HSCs [11]. Additionally, disturbances in epigenetic profiles contribute to the functional decline of HSCs during aging [12]. Various factors within the HSC niche play a crucial role during aging, for instance, cytokines and enzymes [13]. This review compares the distinct biological hallmarks, signaling pathways, and epigenetic profiles of young and aged HSCs. Due to the strong association between hematological malignancies and aging, this review also highlights the relationship between molecular mechanisms and functional alteration and finally may offer important clinical insights.

2. Hallmarks of HSC Aging

2.1. Repopulation Capacity Defects. It is known that the number of HSCs in bone marrow (BM) is increased by 2

to 10 times as mice and humans age. Nevertheless, the reasons that underlie this aging-associated increase in the HSC number are still vague. This can be due to a possible compensatory mechanism of HSCs to deal with the functional loss [14]. Even though both young and aged HSCs have a similar cell division frequency, an increase in the frequency of symmetric cell divisions may also contribute to an increased number and functional defects in aged HSCs. Besides, several studies indicated that aged HSCs exhibit less quiescence and undergo more cell division [4]; thus, they accumulate more oxidative DNA damage than young HSCs [15]. These factors limit the self-renewal and reconstitution ability of aged human HSCs in the hematopoietic system.

A growing body of evidence showed myeloid-biased differentiation in aged human HSCs [3]. Adelman et al. found that transplantation of young HSCs into aged niches led to homing deficit and reduced differentiation with a bias toward the myeloid lineage [6]. In contrast, there was a limited and incomplete rejuvenation of aged HSCs in the young BM niche [7, 8].

To verify the functional difference between aged HSCs and young, the long-term self-renewal and multilineage capacity of HSCs were determined by a competitive transplantation analysis as a gold standard. In this method, HSCs with BM cells were mixed in order to restore immunity of postirradiation recipient animals [14]. As reported by several investigations, aged HSCs had a diminished repopulation capacity [4]. This evidence implies that the increased number of aged HSCs cannot compensate for immune cells' impaired function and immune homeostasis in aged populations.

2.2. Aged HSC Rejuvenation Strategies. HSCs' function declines during aging, but whether this dysfunctionality can be reversible remains vague. Villeda et al. found that exposing old animals with young blood improved the age-related phenotype and reversed preexisting effects of brain aging [16]. This part summarizes some rejuvenation approaches to restore at least the partial function of aged HSC (Table 1). HSC aging is linked with alterations in various gene expressions. The special AT-rich sequence binding protein 1 (Satb1) is an oncogenic driver with potential therapeutic targeting. The reduced level of Satb1 was observed in aged HSCs, and thereby, forced Satb1 overexpression could partially restore the function [17]. In addition, it was found that sirtuins 3 [18] and 7 [19] were suppressed with age. Therefore, upregulation of these regulators might improve the HSC regenerative capacity.

Another approach for rejuvenating aged HSCs relies on the inhibition of the mTOR pathway [20]. mTOR is a crucial regulator of cellular metabolism that acts as a nutrient-sensing and links to cell growth, proliferation, and survival. Nutrient-sensing pathways are a significant determinant of longevity [21]. As mentioned earlier, stem cells are maintained in a quiescent state before activation; thereby, they reduce transcriptional, translational, and metabolic activity by suppressing mTOR activity [22]. Considering the central role of mTOR in age-related disease, inhibition of mTOR by rapamycin or other gene modulatory agents can ameliorate age-related pathologies [23]. It is well known that fasting and refeeding regimens have rejuvenating effects on the hematopoietic system. Cheng et al. reported that extended fasting could regenerate HSCs by reducing protein kinase A (PKA) activity and circulating IGF-1 levels [24]. Moreover, the rejuvenation of aged HSCs can also be affected by diverse pharmacological agents as well as changes in the BM niche, as shown in Table 1.

2.3. Homing Defect and Increased Mobilization. Throughout adulthood, HSCs are located in the marrow cavity of all long bones and coexist with other cells in a well-organized structure called niche. It has been revealed that engraftment of HSC into nonmyeloablative recipients led to a spatially localized niche of stem cells. In contrast, other transplanted BM cells became flattened on the bone lining in the periosteum of the bone. Nilsson et al. showed that whole BM transplant containing cells of the bone lineage could engraft and turn into the competent osteoblasts producing the bone matrix [34]. Several lines of evidence demonstrated that osteoblastic cells have a regulatory role in the niche and function of HSCs via the Notch activation pathway [35].

Live imaging-based techniques revealed distinct populations of hematopoietic cells in different regions, depending on their differentiation stage [36]. It is worth noting that transplanted HSCs were more prone to settle in the endosteum of irradiated recipients, while nonirradiated mice had random distributions [37]. Successful treatment of a broad spectrum of blood disorders and malignant diseases such as leukemia, lymphoma, and myeloma relies on the homing and trafficking ability of donor HSCs into the BM of the host [38]. Liang et al. reported harmful effects of aging on homing ability and engraftment of HSCs. According to their findings, aged mouse HSCs had a threefold lower homing efficiency than young HSCs [39].

Another similar report displayed the decreased homing potential of aged HSCs in BM compared to the young counterparts [40]. Systemically administered cytokines or cytotoxic agents could induce mobilization of HSCs from the BM into the peripheral blood (PB), which subsequently could be collected for HSC transplantation and treatment of immune deficiencies and malignancies [41]. A body of growing evidence has revealed the crucial role of Granulocyte Colony-Stimulating Factor (G-CSF) in mobilizing hematopoietic cells from the BM into the PB. It was reported that mice treated with G-CSF exhibited a higher level of all lineage progenitors in the spleen [42, 43]. In other words, hematopoietic progenitor cell (HPC) mobilization was noticeably impaired in mice deficient with the G-CSF receptor (G-CSFR). Given the expression of G-CSFR on mature hematopoietic cells, it can be assumed that G-CSFR signals have a fundamental role in HPC mobilization [42]. However, Liu et al. reported that G-CSFR expression on HPCs was not necessary for their mobilization, indicating the indirect effect of G-CSF on hematopoietic cells for HSC mobilization [44].

Xing et al. reported that upon stimulation with G-CSF, mobilization of hematopoietic stem and progenitor cells (HSPCs) from BM into the PB was strongly dependent on deadhesion of HSPCs from the niche. They showed that

Table 1: Rejuvenation approaches in aged HSCs.

Rejuvenation approach	Mechanism of action	Outcomes	Ref
Satb1 upregulation	Genetic modulation	Promote reconstituting and lymphopoietic potential of aged HSCs	[17]
Sirtuin 3 upregulation	Genetic modulation	Enhancement of the regenerative potential of aged HSCs	[18]
Sirtuin 7 upregulation	Genetic modulation	Restoring mitochondrial dysregulation Reduce myeloid bias	[19]
Curcumin	Pharmacological modalities	Boost the regenerative potential of aged HSCs Restore the engraftment ability	[25]
Microvesicles from young MSC	Pharmacological modalities	Rejuvenate the aged HSCs Restore function via transferring microvesicles containing autophagy-related mRNAs	[26]
Extended fasting	Pharmacological modalities	Decreasing circulating IGF-1 levels and PKA activity	[24]
cdc42 inhibitor (CASIN)	Pharmacological modalities	Promote rejuvenation capacity of the HSC Reverting a normal phenotype Restore the cellular function of aged HSCs	[27]
p38/MAPK inhibitor (TN13)	Pharmacological modalities	Rejuvenating aged HSCs through reducing ROS	[28]
p38/MAPK inhibitor (SB203580)	Pharmacological modalities	Restore the repopulating potential Maintenance of HSC quiescence	[29]
BCL-2and BCL-xL inhibitor (ABT263)	Pharmacological modalities	Depletion of senescent HSCs Improve reconstitution potential	[30]
mTOR inhibitor (rapamycin)	Pharmacological modalities	Increasing regenerative capacity of HSCs Extending the life span	[31]
RANTES/CCL5 knockout	Targeting the BM niche	Decrease myeloid bias Improve the engraftment potential after transplantation	[32]
Bone marrow transplant	Changing the BM niche	Restoring the normal phenotype	[33]

Special AT-rich sequence binding protein 1: Satb1; cell division control protein 42 homolog: Cdc42; mammalian target of rapamycin: mTOR.

aged mice exhibited a 5-fold increase in HSC mobilization in a mouse model of G-CSF-induced mobilization [45].

2.4. Skewing in Lineage Distribution. Under the normal physiologic conditions, HSCs differentiate into myeloid and lymphoid lineages, maintaining a balanced pattern and controlled production. On the other hand, a higher prevalence of anemia and compromised adaptive immunity occur in older adults. The reasons behind this are related to the impaired function of T and B lymphocytes due to the involution of the thymus and a low number of aged lymphoid progenitors [46]. Indeed, aging can drive HSC differentiation toward myeloid lineage with high myeloid cells in PB. There is a severe upregulation in the age-associated genes in myeloid malignancies [47]. During aging, myeloid cells are preserved, while B lymphoid cells are decreased, resulting in a skew in the myeloid to lymphoid ratio (myeloid/lymphoid) [48]. This skewing may explain a higher incidence of myeloid versus lymphoid malignancies in aged subjects [49].

In this context, Sudo et al. reported that despite less differentiation in aged HSCs, they still exhibited self-renewal potential to regenerate blood cells. According to their study, HSC levels gradually increased with age due to the constant self-renewal of HSCs [50]. As evidenced by aged mice, myeloid progenitor numbers showed relative expansion compared to the young mice, a characteristic of aged HSCs known to be cell autonomous [51]. Collectively, the expression of myeloid-specific genes is upregulated during HSC aging, whereas lymphoid-specific genes are downregulated [52].

2.5. The Cell-Intrinsic Mechanisms of HSC Aging. As discussed earlier, the decline of HSC functioning with age is thought to be driven by a variety of molecular and cell-intrinsic mechanisms [14]. Although mechanistically, it is possible to separately discuss these multiple aging pathways, they are highly interconnected and interdependent (Figure 2).

2.6. DNA Damage Responses and Genetic Mutations in HSC Aging. Unlike proliferating progenitors, which rely on reliable homologous recombination (HR) pathways to repair DNA damage, quiescent HSCs use the error-prone nonhomologous end joining (NHEJ) repair pathway, making them prone to DNA damage [53]. Several studies have demonstrated an increase of 2-3-fold in accumulated DNA damage in aged HSCs, as identified by staining of H2A histone family member X (H2AX) foci, DNA mutation frequency, the alkaline comet assay, and the LOH assay [54–56]. Relying on these findings, it can be explained that the elderly are more likely to acquire mutations, age-related clonal hematopoiesis, and a higher risk of myeloid malignancies [57, 58]. It was identified that DNA damage has a crucial

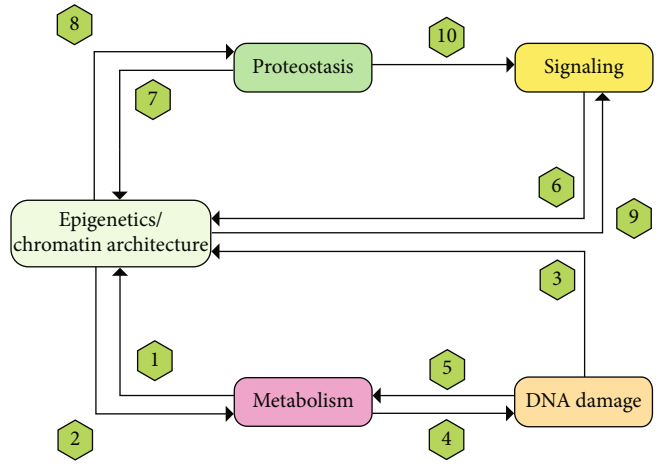

Figure 2: Interconnections between different biological processes involved in intrinsic HSC aging.

role in driving HSC aging. It was evidenced by the premature aging phenotype of HSCs isolated from mice lacking the DNA repair components [59, 60].

DNA damage in HSCs may result from errors during DNA synthesis or/and by endogenous factors, such as elevated ROS levels or environmental stressors [61]. Indeed, DNA damage impairs HSC function by inducing DNA damage repair and activating cell cycle checkpoints such as CD53-p21-mediated cell cycle arrest [62]. Besides, overexpression of senescence-associated of p16Ink protein [15] and proapoptotic proteins such as PUMA (as an essential factor for p53-dependent apoptosis) [53] can impair HSC function. Beerman and his colleagues showed that HSCs isolated from old mice had consistent evidence of DNA strand breaks, demonstrating that HSCs are not uniquely genoprotected with age [56]. According to a recent report, aged HSCs also displayed more replication errors [63].

2.7. Reactive Oxygen Species. In the BM, HSCs are located within hypoxic niches which may protect them against oxidative stress and promote self-renewal potential [64]. Since HSCs are quiescent and maintain low metabolic requirements, they produce low levels of ROS. However, it has been shown that ROS levels increase as HSCs age, resulting in oxidative stress in HSCs [65, 66]. In addition to ROS levels increasing during aging, it also contributes to increased proliferation rate, senescence, and apoptosis. The self-renewal potential of HSCs exposed to low ROS levels was higher, as evidenced by serial transplantations. By contrast, exposing HSCs to a higher level of ROS results in self-renewal failure, accompanied by upregulation of mTOR and p38 mitogen-activated protein kinase activity [67].

According to a study in the three mouse models (young, middle, and aged), mitochondria and NADPH oxidase were the main ROS-generating sources in the three groups, while cytochrome P450 contributed to the aged and middle groups and xanthine oxidase only to the aged one. Besides, DNA damage and apoptosis were detected in the middle and aged mice. Also, old mice exhibited shorter telomere length. As evidenced, telomere shortening occurs with age, playing an essential role in myeloid skewing [68]. With these backgrounds, oxidative stress might contribute to HSC dysfunction during the aging process [69, 70].

Previous publications have reported that ROS plays a significant role in regulating HSC aging. It has been found that transcription factors of forkhead box O (FOXO) family such Foxo1, Foxo3a, and Foxo4 have an essential role in regulating HSC pools, progenitors, and ROS-mediated activity in HSCs [71].

Several lines of evidence revealed overexpression of hypoxia-inducible factor-1α (HIF-1α) in HSCs. Interestingly, HIF-1α could switch HSC cellular metabolism from mitochondrial respiration into glycolysis, ultimately reducing ROS production. Indeed, HIF-1α deletion in HSCs could induce ROS generation and negatively impact long-term repopulation ability [72].

2.8. Altered Epigenetic Profiling. The term epigenetics refers to changes in gene expression without affecting the DNA sequence. In other words, it is a change in phenotype without changing the genotype. Epigenetic regulation is a key mechanism that maintains the multipotency and self-renewal of HSCs. This process is mediated by DNA methylation or histone modification (methylation/acetylation) to preserve self-renewal gene expression and suppress involved genes in differentiation and lineage fate [73, 74]. It is well documented that DNA methyltransferase 1 (Dnmt1) is a crucial regulator of HSCs and exerts its effect by reestablishing existing DNA methylation profiles during the cell replication. This is possibly mediated by recognizing hemimethylated DNA and maintaining preexisting DNA methylation patterns of the parent strand on the daughter strand [75]. Dnmt3a/3b is involved in de novo DNA methyltransferase and establishes new DNA methylation during the development and differentiation of stem cells [76, 77].

Compelling evidence indicates that Dnmt1-deficient mice had a reduction in HSC number and function [78]. However, in Dnmt3a-knockout mice, HSCs could grow and self-renew more efficiently and are surprisingly enhanced in mice with Dnmt3a/3b double-knockout [76, 79]. A growing body of study suggests that altered epigenetic profiles are strongly associated with HSC aging. The global

DNA methylation of old HSCs is generally stable or slightly higher than that of young HSCs. These epigenetic alterations could affect not only self-renewal genes but also contribute to age-dependent functional decline and myeloid-biased differentiation. This is possibly due to the regulation of gene expression levels in differentiated progeny [6, 80]. In addition, age-related epigenetic alterations of HSCs are strongly linked with a proliferation history, indicating that epigenetic memory loss is driven by proliferation [12]. A proliferation-driven HSC aging occurs by switching HSCs from a dormant state and multipotency to activation and lineage priming. This process is mediated by a series of factors through inducing the epigenetic switch such as Ezh1-to-Ezh2 PRC2 [80], decreasing the level of Dnmt1, Dnmt3b, and all three Tet enzymes, as well as the involvement of critical modulators of chromatin states such as Bmi, Eed, Suz12, Jarid1b, Kat6b, Sirt1, and Suv39H1 [80, 81].

As discussed earlier, aged human HSCs have a profound epigenetic reprogramming by targeting cancer-related pathways, predisposing to leukemia [6]. In this context, it was reported that redistribution of DNA methylation and decrease in H3K27ac, H3K4me1, and H3K4me3 levels predisposed cells to age-related acute myeloid leukemia (AML) as compared to the young HSCs [82].

2.9. Polarity. Asymmetric distribution of specific proteins known as "increased polarity" has been recognized as a prominent characteristic of aged HSCs, while this feature is less obvious in young HSCs [83]. The cell division control protein 42 homolog (Cdc42) is believed to be responsible for the unequal distribution of these proteins. Cell Cdc42 switches an inactive GDP-bound state to an active GTP-bound state in response to different signals. Besides, this molecule can regulate actin polymerization and organization of tubulin, affecting cell-cell and cell-extracellular matrix adhesion and the polarity in various cell types [27, 83]. With this notion, the application of Cdc42 inhibitors can restore the polarity in aged HSCs and improve their function after transplantation [84]. According to Florian et al., the elevated activity of Cdc42 is linked to the aging of HSCs and the loss of polarity of aged HSCs [85]. In aged HSCs, constitutive activation of Cdc42 induced premature aging of HSCs by depolarizing Cdc42 and tubulin. Pharmacological inhibition of Cdc42 activity could restore the cellular function of aged HSCs [86], although it is not clear whether the acute reversal of asymmetry in protein distribution has long-term effects on the function of HSC.

2.10. Metabolic Alterations and Impaired Autophagy. As described above, HSCs maintain a low metabolic rate and glycolytic activity. A young HSC undergoes an oxidative metabolic change following activation, which can be reversed by returning to the quiescent state. In contrast, the basal metabolism of aged HSC shifts towards oxidative metabolism [87], which leads to an increase in ROS levels and a decrease in regenerative capacity [88]. As a response to metabolic stress, cells engage autophagy, a "housekeeping" mechanism for the self-degradation of cellular components [89]. In this process, organelles or portions of the cytosol are enclosed within double-membrane vesicles, which are subsequently fused with the lysosome where degradation occurs [90]. It has been well documented that the deregulation of autophagy is associated with aging and various age-related diseases such as cancer [91] (Figure 3).

3. Alterations in the Intrinsic Signaling Pathways Present in HSC Aging

Several studies have found that age-related decline in the functional capacity of HSCs is associated with multiple signaling pathways. Signaling pathways that contribute to HSC aging include Janus kinase/signal transducer and activator of transcription (JAK/STAT) pathway, nuclear factor-(NF-) κB, mTOR, transforming growth factor-beta (TGF-β), and wingless-related integration site (Wnt) (Figure 4) [92].

3.1. The Signaling Pathways of JAK/STAT, NF-κB, and mTOR involved in HSC Aging. JAK/STAT signaling cascade is a highly conserved event that regulates biological processes such as immune responses, regeneration, and homeostasis [93]. Besides, this pathway controls stem cell dynamics and senescence. Using a single-cell transcriptome, a previous study by Kirschner et al. found that the JAK/STAT signaling pathway had a crucial role in stem cell exhaustion during aging. They detected a divergent subpopulation of old HSCs with a p53 signature. p53 has a substantial role in hematopoietic aging. Increasing p53 activity decreases the function and proliferation of HSCs, while decreasing p53 levels has the opposite effect. The relationship between p53 signaling and JAK/STAT was investigated through constitutive activation of JAK2 (V617F) and p53-positive expansion in aged mice. JAK2- (V617F-) mediated proliferative activity showed a critical role in the p53-induced functional decline in aged HSCs [94]. Additionally, it is well established that NF-κB-mediated activity has a substantial regulatory role in HSC aging [95]. In a study carried out by Stein et al., they identified the role of the NF-κB subunit RelA/p65 in HSC regulation in mice lacking RelA/p65. p65 is the main regulator of hematopoietic development [96]. Loss of p65 led to a severe functional defect in HSCs. Besides, there was an increase in HSPC cycling, differentiation deficits, and extramedullary hematopoiesis [97]. Chen and Kerr reported that aged HSPCs exhibited elevated activity of NF-κB that resulted in increased differentiation and loss of self-renewal [74]. Rad21/cohesin is a critical mediator of NF-κB signaling and is necessary for normal differentiation; however, it can limit HSCs' self-renewal during the aging process in an NF-κB-dependent manner. In this context, old HSCs displayed failure in downregulating Rad21/cohesin and differentiation signals. Collectively, these findings indicate that aged HSCs have increased NF-κB activity [98].

As discussed in the previous part, the mTOR pathway is a robust regulator of cellular function that integrates a wide variety of signals received from mitogens, nutrients, and energy levels [99]. It is well accepted that mTOR inhibition enhances lifespan, but the mechanism of action by which this occurs is still vague. Growing evidence has shown that hyperactivity of mTOR is strongly linked with age-

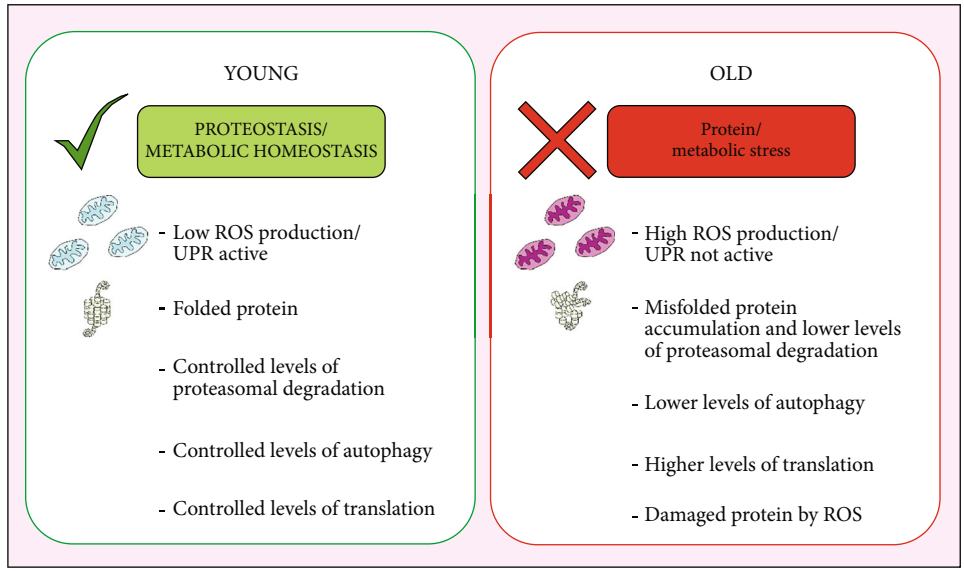

Figure 3: Metabolic homeostasis and proteostasis during aging in HSC.

associated disorders [20]. Furthermore, several studies have demonstrated that mTOR inhibition with rapamycin attenuated the pathological processes [100]. Bitto et al. reported that three months of rapamycin therapy could inhibit the mTOR pathway and extend the lifespan up to 60% in middle-aged mice [101]. Chen et al. found that HSCs from aged mice had higher phosphorylated (p-)mTOR and mTOR activity than those HSCs from young mice. According to their results, intraperitoneal injection of rapamycin at a dose of 4 mg/kg every other day for six weeks in aged mice extended the life span. These data implicated the efficacy of rapamycin in restoring HSC functions in the old mice [102].

3.2. The Role of the TGF-β Signaling Pathway in HSC Aging. The transforming growth factor-β (TGF-β) pathway is fundamental for many cellular functions. This pathway also regulates HSC features such as self-renewal, differentiation, and quiescence [103]. Given the regulatory role of TGF-β potential in differentiation among HSC subtypes, Challen and colleagues reported that TGF-β1 could stimulate the proliferation of myeloid-biased HSCs in young mice and prevented the turnover of lymphoid-biased HSCs [104].

On the contrary, it was demonstrated that old mice treated with TGF-β1 produced fewer myeloid cells. Indeed, aged HSCs exhibited more responsiveness to TGF-β1 than young HSCs [105]. Genome-wide transcriptome analysis during HSC aging demonstrated the downregulation of regulatory genes involved in the TGF-β pathway (Smad4, Nr4a1, Endoglin, Cepba, Jun, Spectrin b2, and Junb), indicating a decline of TGF-β signaling with aging [106].

3.3. The Wnt Pathway. As described earlier, polarity is linked with specific functions of HSC, including migration and division. However, polarity loss is associated with an impairment of self-renewal capacity, accompanied by alteration in HSC differentiation [92]. In addition, there is an elevated level of Cdc42 in aged HSCs, which is associated with loss of polarity [86]. According to further research on the Cdc42 polarity pathway, HSC aging is caused by changes in Wnt signaling, from canonical to noncanonical [107]. It has been identified that treatment with Wnt5a led to a series of events including activation of Cdc42, induction of aging-associated polarity, a decline in regenerative potential, and modification of myeloid-lymphoid differentiation in young HSCs [107].

3.4. Other Pathways. G-CSF transiently upregulates stromal cell-derived factor-1 (SDF-1) and activates CXC chemokine receptor-4 (CXCR4) signaling that results in hepatocyte growth factor (HGF) production. HGF can bind to c-Met and activate c-Met signaling, regulating the mTOR-FOXO3a signaling pathway [108]. Furthermore, G-CSF signaling can facilitate ROS production and HSC egress from BM [109].

4. HSC Aging Occurs through Changes in the Extrinsic Factors

In addition to intrinsic mechanisms, some studies have found that extrinsic factors also contributed to HSC aging [110]. HSC function is strongly affected by the BM microenvironment. Megakaryocytes promote HSC quiescence within this niche [111]. Li et al. provided insights regarding the mechanism of homing HSPC. They reported that the vascular cell adhesion molecule-1^+ (VCAM-1) macrophage with patrolling properties interacted with and homed HSPCs into a vascular niche [112]. In another study by Chow et al., $CD169^+$ macrophages in the BM enhanced the retention of HSPCs [113]. Furthermore, Winkler et al. demonstrated that phagocytic macrophages with the unusual $F4/80^+Ly^-6G^+CD11b^+$ phenotype could maintain HSC niches, and more importantly, the loss of these macrophages could mobilize HSCs [114]. A previous study found that regulatory T cells that highly expressed CD150 could maintain a quiescent state, HSC numbers, and immune privilege by the adenosine pathway [115]. Along with the hematopoietic cells mentioned

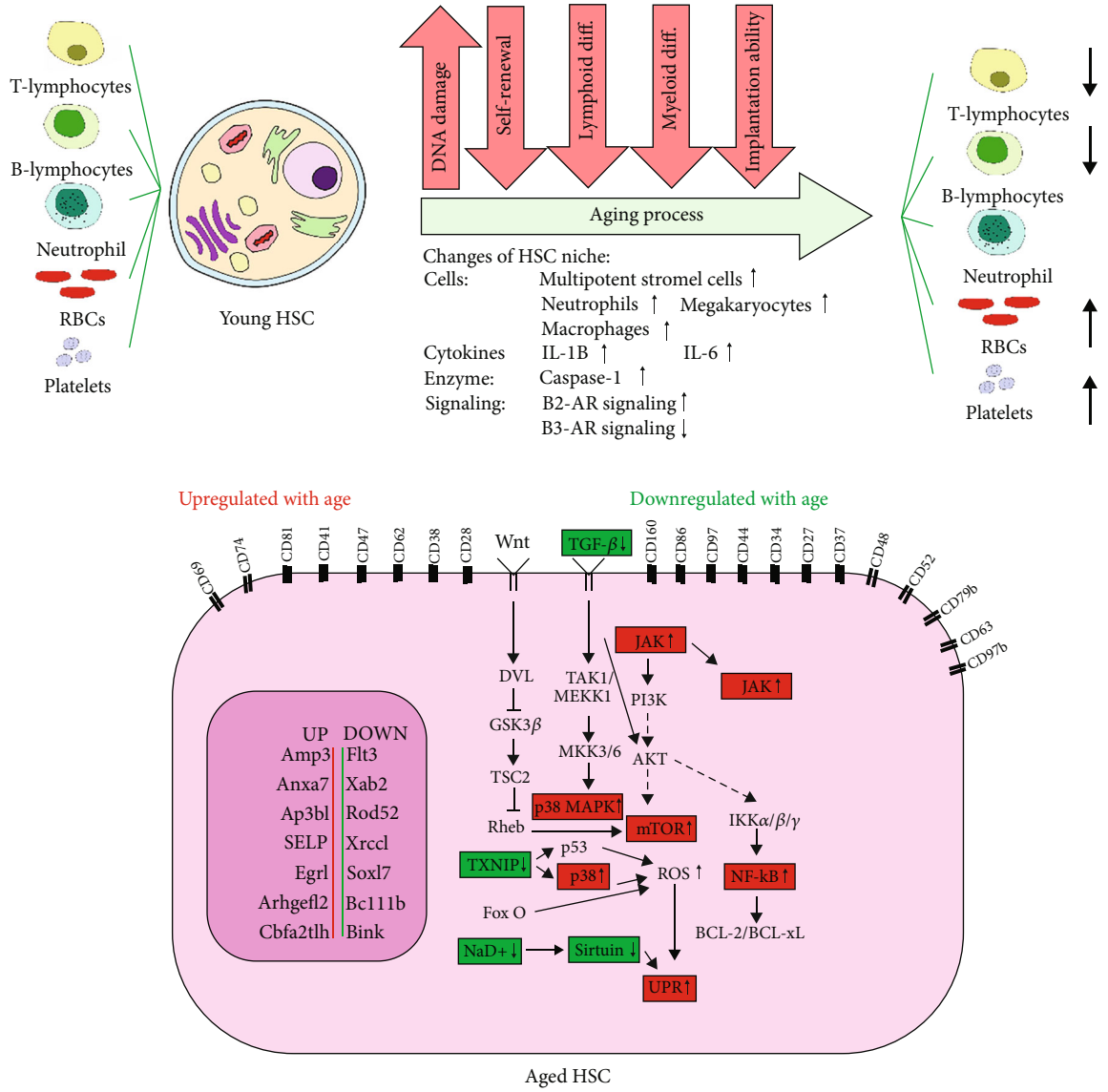

Figure 4: Functional alterations and HSC aging mechanisms. Aging affects HSC functions, including decreasing self-renewal ability and myeloid/platelet-biased differentiation and impairing implantation ability. The intrinsic mechanisms are illustrated at the gene level, signaling pathway level, and epigenetic level.

above, several nonhematopoietic cells such as mesenchymal stromal cells (MSCs), perivascular cells, and arterial and sinusoidal endothelial cells have a pivotal role in the HSC niche [116, 117].

The sympathetic nervous system (SNS) regulates HSC trafficking and orchestrates adrenergic neurotransmission into the microenvironment on circadian rhythms [118]. Here, we summarize how HSC environment, the SNS, and other related factors affect HSC aging.

The research of Maryanovich et al. in 2018 proved that HSC aging significantly relied on the innervation of the BM by SNS, since the loss of SNS nerves or adrenoreceptor $\beta 3$ signaling (ADR$\beta 3$) resulted in premature HSC aging. Remarkably, in an in vivo setting, supplementation of a sympathomimetic with selective effect on ADR$\beta 3$ significantly rejuvenated the function of aged HSCs. These findings suggested that maintenance of SNS innervation of BM may offer new strategies for HSC rejuvenation [119].

Megakaryocytes also exhibit the potential of inhibiting HSC proliferation. As mentioned above, both HSCs and megakaryocytes increase during aging. HSCs are located further from megakaryocytes; thereby, it seems that decreased interactions between HSCs and megakaryocytes may be involved in premature hematopoietic aging. In other words, the distance between HSCs and megakaryocytes could regulate HSC proliferation and enhance ADR$\beta 3$ during physiological aging. In this regard, Ho et al. identified that β-adrenergic signals promoted megakaryopoiesis during aging. They showed that HSC-supporting niches declined near the bone during natural aging; however, they expanded away from it. Increasing noradrenergic innervation of the BM raises interleukin-6-dependent megakaryopoiesis through

the β2-adrenergic receptors (ARs). Besides, reduction of β3-AR-Nos1 activity is associated with niche alterations in aging, leading to myeloid expansion and impaired lymphoid differentiation [120]. Frisch et al. also found that the dysfunction of aged macrophages was associated with HSC platelet bias and an increase in senescent neutrophils in aged mice compared to younger counterparts. Aged macrophages from the marrow of old mice and humans displayed an activated phenotype and overexpression of inflammatory markers such as IL-1β. Altogether, it can be assumed that overexpression of IL-1β and caspase-1 in the aged mouse BM niche has a contributory role in age-related lineage skewness of HSCs [13].

5. Conclusion

This paper summarizes the hallmarks of HSC aging pertaining to repopulating capacity, homing ability, mobilization, and lineage skewing. Multiple cell-intrinsic factors contribute to HSC aging, such as genetic mutations and DNA damage, ROS production, epigenetic alterations, polarity, clonality, metabolic changes, and impaired autophagic activity. Numerous studies using knockout and transgenic animal models have demonstrated that epigenetic factors are crucial for maintaining proper HSC function. In general, several cell-extrinsic factors, such as HSC-surrounding niches such as megakaryocytes, MSCs, macrophages, and neutrophils, impact HSC aging. β-Adrenergic nerve signals, cytokines such as IL-6 and IL-1β, and enzymes like caspase-1 also influence HSC aging. Furthermore, inhibition of specific pathways, such as the mTOR and P38 MAPK signaling pathways, is involved in the aging of HSCs.

The interconnections between these processes will be crucial in deciphering how aging affects stem cells. Most of the aging mechanisms reviewed in this paper have been investigated in mouse or nonhuman systems. However, we would like to highlight the progress that has been made to date and the importance of pursuing an integrated approach to connect all underlying factors that affect HSC upon aging. Accordingly, a more comprehensive perspective regarding this process might be the key to bridging the gap between translation and the human system. Therefore, future work should emphasize the mechanisms of the HSC niche during aging. Moreover, expanding long-term HSCs *in vitro* is still a challenge, and the findings of HSC aging could be applied to this challenge.

Conflicts of Interest

The authors declare that there is no conflict of interest regarding the publication of this paper.

Authors' Contributions

Ezzatollah Fathi and Raheleh Farahzadi contributed equally to this work.

References

[1] S. Akunuru and H. Geiger, "Aging, clonality, and rejuvenation of hematopoietic stem cells," *Trends in Molecular Medicine*, vol. 22, no. 8, pp. 701–712, 2016.

[2] B. M. Moehrle and H. Geiger, "Aging of hematopoietic stem cells: DNA damage and mutations?," *Experimental Hematology*, vol. 44, no. 10, pp. 895–901, 2016.

[3] J. Lee, S. Yoon, I. Choi, and H. Jung, "Causes and mechanisms of hematopoietic stem cell aging," *International Journal of Molecular Sciences*, vol. 20, no. 6, p. 1272, 2019.

[4] W. W. Pang, S. L. Schrier, and I. L. Weissman, "Age-associated changes in human hematopoietic stem cells," in *Seminars in Hematology*, Elsevier, 2017.

[5] G. de Haan and S. S. Lazare, "Aging of hematopoietic stem cells," *Blood, The Journal of the American Society of Hematology*, vol. 131, no. 5, pp. 479–487, 2018.

[6] E. R. Adelman, H. T. Huang, A. Roisman et al., "Aging human hematopoietic stem cells manifest profound epigenetic reprogramming of enhancers that may predispose to leukemia," *Cancer Discovery*, vol. 9, no. 8, pp. 1080–1101, 2019.

[7] S. J. Morrison and D. T. Scadden, "The bone marrow niche for haematopoietic stem cells," *Nature*, vol. 505, no. 7483, pp. 327–334, 2014.

[8] S. E. Latchney and L. M. Calvi, "The aging hematopoietic stem cell niche: phenotypic and functional changes and mechanisms that contribute to hematopoietic aging," in *Seminars in Hematology*, Elsevier, 2017.

[9] E. Mejia-Ramirez and M. C. Florian, "Understanding intrinsic hematopoietic stem cell aging," *Haematologica*, vol. 105, no. 1, pp. 22–37, 2020.

[10] M. Wahlestedt, C. J. Pronk, and D. Bryder, "Concise review: hematopoietic stem cell aging and the prospects for rejuvenation," *Stem Cells Translational Medicine*, vol. 4, no. 2, pp. 186–194, 2015.

[11] B. Chatterjee and S. S. Thakur, "Aging of hematopoietic stem cells: insight into mechanisms and consequences," in *Stem Cells and Aging*, pp. 103–111, Elsevier, 2021.

[12] I. Beerman, C. Bock, B. S. Garrison et al., "Proliferation-dependent alterations of the DNA methylation landscape underlie hematopoietic stem cell aging," *Cell Stem Cell*, vol. 12, no. 4, pp. 413–425, 2013.

[13] B. J. Frisch, C. M. Hoffman, S. E. Latchney et al., "Aged marrow macrophages expand platelet-biased hematopoietic stem cells via interleukin-1B," *JCI insight*, vol. 4, no. 10, 2019.

[14] H. Geiger, G. De Haan, and M. C. Florian, "The ageing haematopoietic stem cell compartment," *Nature Reviews Immunology*, vol. 13, no. 5, pp. 376–389, 2013.

[15] T. Yahata, T. Takanashi, Y. Muguruma et al., "Accumulation of oxidative DNA damage restricts the self-renewal capacity of human hematopoietic stem cells," *Blood, The Journal of the American Society of Hematology*, vol. 118, no. 11, pp. 2941–2950, 2011.

[16] S. A. Villeda, K. E. Plambeck, J. Middeldorp et al., "Young blood reverses age-related impairments in cognitive function and synaptic plasticity in mice," *Nature medicine*, vol. 20, no. 6, pp. 659–663, 2014.

[17] Y. Doi, T. Yokota, Y. Satoh et al., "Variable SATB1 levels regulate hematopoietic stem cell heterogeneity with distinct lineage fate," *Cell reports*, vol. 23, no. 11, pp. 3223–3235, 2018.

[18] K. Brown, S. Xie, X. Qiu et al., "SIRT3 reverses aging-associated degeneration," *Cell reports*, vol. 3, no. 2, pp. 319–327, 2013.

[19] A. Wronska, A. Lawniczak, P. M. Wierzbicki, and Z. Kmiec, "Age-related changes in sirtuin 7 expression in calorie-restricted and refed rats," *Gerontology*, vol. 62, no. 3, pp. 304–310, 2016.

[20] H. Fernandes, J. Moura, and E. Carvalho, "mTOR signaling as a regulator of hematopoietic stem cell fate," *Stem Cell Reviews and Reports*, vol. 17, no. 4, pp. 1312–1322, 2021.

[21] D. Papadopoli, K. Boulay, L. Kazak et al., "mTOR as a central regulator of lifespan and aging," *F1000Research*, vol. 8, p. 998, 2019.

[22] M. Ermolaeva, F. Neri, A. Ori, and K. L. Rudolph, "Cellular and epigenetic drivers of stem cell ageing," *Nature Reviews Molecular Cell Biology*, vol. 19, no. 9, pp. 594–610, 2018.

[23] Y. Zhang, J. Zhang, and S. Wang, "The role of rapamycin in healthspan extension via the delay of organ aging," *Ageing Research Reviews*, vol. 70, article 101376, 2021.

[24] C.-W. Cheng, G. B. Adams, L. Perin et al., "Prolonged fasting reduces IGF-1/PKA to promote hematopoietic-stem-cell-based regeneration and reverse immunosuppression," *Cell stem cell*, vol. 14, no. 6, pp. 810–823, 2014.

[25] P. Shinde, R. Kuhikar, R. Kulkarni, N. Khan, L. Limaye, and V. Kale, "Curcumin restores the engraftment capacity of aged hematopoietic stem cells and also reduces PD-1 expression on cytotoxic T cells," *Journal of tissue engineering and regenerative medicine*, vol. 15, no. 4, pp. 388–400, 2021.

[26] R. Kulkarni, M. Bajaj, S. Ghode, S. Jalnapurkar, L. Limaye, and V. P. Kale, "Intercellular transfer of microvesicles from young mesenchymal stromal cells rejuvenates aged murine hematopoietic stem cells," *Stem Cells*, vol. 36, no. 3, pp. 420–433, 2018.

[27] A. Amoah, A. Keller, R. Emini et al., "Aging of human hematopoietic stem cells is linked to changes in Cdc 42 activity," *Haematologica*, vol. 107, no. 2, pp. 393–402, 2022.

[28] H. Jung, D. O. Kim, J. E. Byun et al., "Thioredoxin-interacting protein regulates haematopoietic stem cell ageing and rejuvenation by inhibiting p 38 kinase activity," *Nature Communications*, vol. 7, no. 1, pp. 1–12, 2016.

[29] L. Lu, Y. Y. Wang, J. L. Zhang, D. G. Li, and A. M. Meng, "p 38 MAPK inhibitor insufficiently attenuates HSC senescence administered long-term after 6 Gy total body irradiation in mice," *International Journal of Molecular Sciences*, vol. 17, no. 6, p. 905, 2016.

[30] J. Chang, Y. Wang, L. Shao et al., "Clearance of senescent cells by ABT263 rejuvenates aged hematopoietic stem cells in mice," *Nature medicine*, vol. 22, no. 1, pp. 78–83, 2016.

[31] K. Saraswat, R. Kumar, and S. I. Rizvi, "Inhibition of mTOR signalling: a potential anti-aging drug strategy," in *Molecular Basis and Emerging Strategies for Anti-Aging Interventions*, pp. 151–160, Springer, 2018.

[32] A. V. Ergen, N. C. Boles, and M. A. J. B. Goodell, "The Journal of the American Society of HematologyRantes/Ccl 5 influences hematopoietic stem cell subtypes and causes myeloid skewing," vol. 119, no. 11, pp. 2500–2509, 2012.

[33] W. Kuribayashi, A. Iwama, and M. Oshima, "Incomplete rejuvenation of aged HSCs in young bone marrow niche," *Experimental Hematology*, vol. 76, p. S72, 2019.

[34] S. K. Nilsson, M. S. Dooner, H. U. Weier et al., "Cells capable of bone production engraft from whole bone marrow transplants in nonablated mice," *The Journal of experimental medicine*, vol. 189, no. 4, pp. 729–734, 1999.

[35] J. Zhang, C. Niu, L. Ye et al., "Identification of the haematopoietic stem cell niche and control of the niche size," *Nature*, vol. 425, no. 6960, pp. 836–841, 2003.

[36] C. Lo Celso, H. E. Fleming, J. W. Wu et al., "Live-animal tracking of individual haematopoietic stem/progenitor cells in their niche," *Nature*, vol. 457, no. 7225, pp. 92–96, 2009.

[37] Y. Xie, T. Yin, W. Wiegraebe et al., "Detection of functional haematopoietic stem cell niche using real-time imaging," *Nature*, vol. 457, no. 7225, pp. 97–101, 2009.

[38] M. J. Domingues, S. K. Nilsson, and B. Cao, "New agents in HSC mobilization," *International journal of hematology*, vol. 105, no. 2, pp. 141–152, 2017.

[39] Y. Liang, G. Van Zant, and S. J. Szilvassy, "Effects of aging on the homing and engraftment of murine hematopoietic stem and progenitor cells," *Blood*, vol. 106, no. 4, pp. 1479–1487, 2005.

[40] H. E. Broxmeyer, Y. Liu, R. Kapur et al., "Fate of hematopoiesis during aging. What do we really know, and what are its implications?," *Stem cell reviews and reports*, vol. 16, pp. 1020–1048, 2020.

[41] J. Tay, J.-P. Levesque, and I. G. Winkler, "Cellular players of hematopoietic stem cell mobilization in the bone marrow niche," *International journal of hematology*, vol. 105, no. 2, pp. 129–140, 2017.

[42] L. J. Bendall and K. F. Bradstock, "G-CSF: From granulopoietic stimulant to bone marrow stem cell mobilizing agent," *Cytokine & growth factor reviews*, vol. 25, no. 4, pp. 355–367, 2014.

[43] J. M. Bernitz, M. G. Daniel, Y. S. Fstkchyan, and K. Moore, "Granulocyte colony-stimulating factor mobilizes dormant hematopoietic stem cells without proliferation in mice," *The Journal of the American Society of Hematology*, vol. 129, no. 14, pp. 1901–1912, 2017.

[44] F. Liu, J. Poursine-Laurent, and D. C. J. B. Link, "Expression of the G-CSF receptor on hematopoietic progenitor cells is not required for their mobilization by G-CSF," *The Journal of the American Society of Hematology*, vol. 95, no. 10, pp. 3025–3031, 2000.

[45] Z. Xing, M. A. Ryan, D. Daria et al., "Increased hematopoietic stem cell mobilization in aged mice," *Blood*, vol. 108, no. 7, pp. 2190–2197, 2006.

[46] H. Geiger and K. L. Rudolph, "Aging in the lympho-hematopoietic stem cell compartment," *Trends in immunology*, vol. 30, no. 7, pp. 360–365, 2009.

[47] E. M. Groarke and N. S. Young, "Aging and hematopoiesis," *Clinics in geriatric medicine*, vol. 35, no. 3, pp. 285–293, 2019.

[48] W. W. Pang, E. A. Price, D. Sahoo et al., "Human bone marrow hematopoietic stem cells are increased in frequency and myeloid-biased with age," *Proceedings of the National Academy of Sciences*, vol. 108, no. 50, pp. 20012–20017, 2011.

[49] R. A. Signer, E. Montecino-Rodriguez, O. N. Witte, J. McLaughlin, and K. Dorshkind, "Age-related defects in B lymphopoiesis underlie the myeloid dominance of adult leukemia," *Blood, The Journal of the American Society of Hematology*, vol. 110, no. 6, pp. 1831–1839, 2007.

[50] K. Sudo, H. Ema, Y. Morita, and H. Nakauchi, "Age-associated characteristics of murine hematopoietic stem cells," *The Journal of experimental medicine*, vol. 192, no. 9, pp. 1273–1280, 2000.

[51] I. Beerman, D. Bhattacharya, S. Zandi et al., "Functionally distinct hematopoietic stem cells modulate hematopoietic lineage potential during aging by a mechanism of clonal expansion," *Proceedings of the National Academy of Sciences*, vol. 107, no. 12, pp. 5465–5470, 2010.

[52] A. Rundberg Nilsson, S. Soneji, S. Adolfsson, D. Bryder, and C. J. Pronk, "Human and murine hematopoietic stem cell aging is associated with functional impairments and intrinsic megakaryocytic/erythroid bias," *PloS one*, vol. 11, no. 7, article e0158369, 2016.

[53] M. Mohrin, E. Bourke, D. Alexander et al., "Hematopoietic stem cell quiescence promotes error-prone DNA repair and mutagenesis," *Cell Stem Cell*, vol. 7, no. 2, pp. 174–185, 2010.

[54] J. Flach, S. T. Bakker, M. Mohrin et al., "Replication stress is a potent driver of functional decline in ageing haematopoietic stem cells," *Nature*, vol. 512, no. 7513, pp. 198–202, 2014.

[55] C. E. Rübe, A. Fricke, T. A. Widmann et al., "Accumulation of DNA damage in hematopoietic stem and progenitor cells during human aging," *PloS one*, vol. 6, no. 3, article e17487, 2011.

[56] I. Beerman, J. Seita, M. A. Inlay, I. L. Weissman, and D. J. Rossi, "Quiescent hematopoietic stem cells accumulate DNA damage during aging that is repaired upon entry into cell cycle," *Cell Stem Cell*, vol. 15, no. 1, pp. 37–50, 2014.

[57] G. Genovese, A. K. Kähler, R. E. Handsaker et al., "Clonal hematopoiesis and blood-cancer risk inferred from blood DNA sequence," *New England Journal of Medicine*, vol. 371, no. 26, pp. 2477–2487, 2014.

[58] K. Bolton, "Update on clonal hematopoiesis," *Clinical Lymphoma Myeloma and Leukemia*, vol. 21, pp. S32–S33, 2021.

[59] B. Schumacher, J. Pothof, J. Vijg, and J. H. J. Hoeijmakers, "The central role of DNA damage in the ageing process," *Nature*, vol. 592, no. 7856, pp. 695–703, 2021.

[60] D. Delia and S. Mizutani, "The DNA damage response pathway in normal hematopoiesis and malignancies," *International Journal of Hematology*, vol. 106, no. 3, pp. 328–334, 2017.

[61] D. Walter, A. Lier, A. Geiselhart et al., "Exit from dormancy provokes DNA-damage-induced attrition in haematopoietic stem cells," *Nature*, vol. 520, no. 7548, pp. 549–552, 2015.

[62] B. Kolaczkowski and J. W. Thornton, "Performance of maximum parsimony and likelihood phylogenetics when evolution is heterogeneous," *Nature*, vol. 431, no. 7011, pp. 980–984, 2004.

[63] T. McNeely, M. Leone, H. Yanai, and I. Beerman, "DNA damage in aging, the stem cell perspective," *Human Genetics*, vol. 139, no. 3, pp. 309–331, 2020.

[64] B. Wielockx, T. Grinenko, P. Mirtschink, and T. Chavakis, "Hypoxia pathway proteins in normal and malignant hematopoiesis," *Cell*, vol. 8, no. 2, p. 155, 2019.

[65] F. Chen, Y. Liu, N. K. Wong, J. Xiao, and K. F. So, "Oxidative stress in stem cell aging," *Cell Transplantation*, vol. 26, no. 9, pp. 1483–1495, 2017.

[66] T. Simsek, F. Kocabas, J. Zheng et al., "The distinct metabolic profile of hematopoietic stem cells reflects their location in a hypoxic niche," *Cell Stem Cell*, vol. 7, no. 3, pp. 380–390, 2010.

[67] A. Ludin, S. Gur-Cohen, K. Golan et al., "Reactive oxygen species regulate hematopoietic stem cell self-renewal, migration and development, as well as their bone marrow microenvironment," *Antioxidants & Redox Signaling*, vol. 21, no. 11, pp. 1605–1619, 2014.

[68] M. L. Porto, B. P. Rodrigues, T. N. Menezes et al., "Reactive oxygen species contribute to dysfunction of bone marrow hematopoietic stem cells in aged C57BL/6 J mice," *Journal of Biomedical Science*, vol. 22, no. 1, pp. 1–13, 2015.

[69] K. L. Rudolph, S. Chang, H. W. Lee et al., "Longevity, stress response, and cancer in aging telomerase-deficient mice," *Cell*, vol. 96, no. 5, pp. 701–712, 1999.

[70] A. Samimi, H. Kalantari, M. Z. Lorestani, R. Shirzad, and N. Saki, "Oxidative stress in normal hematopoietic stem cells and leukemia," *APMIS*, vol. 126, no. 4, pp. 284–294, 2018.

[71] V. Menon and S. Ghaffari, "Transcription factors FOXO in the regulation of homeostatic hematopoiesis," *Current Opinion in Hematology*, vol. 25, no. 4, pp. 290–298, 2018.

[72] W. W. Wheaton and N. S. Chandel, "Hypoxia. 2. Hypoxia regulates cellular metabolism," *American Journal of Physiology-Cell Physiology*, vol. 300, no. 3, pp. C385–C393, 2011.

[73] H. Kunimoto and H. Nakajima, "Epigenetic dysregulation of hematopoietic stem cells and preleukemic state," *International Journal of Hematology*, vol. 106, no. 1, pp. 34–44, 2017.

[74] D. Chen and C. Kerr, "The epigenetics of stem cell aging comes of age," *Trends in Cell Biology*, vol. 29, no. 7, pp. 563–568, 2019.

[75] X. Li, D. Liu, L. Zhang et al., "The comprehensive DNA methylation landscape of hematopoietic stem cell development," *Cell discovery*, vol. 7, no. 1, pp. 1–4, 2021.

[76] J. J. Trowbridge and S. H. Orkin, "Dnmt 3a silences hematopoietic stem cell self-renewal," *Nature Genetics*, vol. 44, no. 1, pp. 13-14, 2012.

[77] R. Ramabadran, J. Wang, A. Guzman et al., "Loss of de novo DNA methyltransferase DNMT3A impacts alternative splicing in hematopoietic stem cells," *Blood*, vol. 130, 2017.

[78] G. L. Sen, J. A. Reuter, D. E. Webster, L. Zhu, and P. A. Khavari, "DNMT1 maintains progenitor function in self-renewing somatic tissue," *Nature*, vol. 463, no. 7280, pp. 563–567, 2010.

[79] J. J. Lugus, C. Park, Y. D. Ma, and K. Choi, "Both primitive and definitive blood cells are derived from Flk-1+ mesoderm," *Blood, The Journal of the American Society of Hematology*, vol. 113, no. 3, pp. 563–566, 2009.

[80] J. M. Bernitz, K. Rapp, M. G. Daniel et al., "Memory of divisional history directs the continuous process of primitive hematopoietic lineage commitment," *Stem Cell Reports*, vol. 14, no. 4, pp. 561–574, 2020.

[81] B. Carter and K. Zhao, "The epigenetic basis of cellular heterogeneity," *Nature Reviews Genetics*, vol. 22, no. 4, pp. 235–250, 2021.

[82] E. Mejia-Ramirez, H. Geiger, and M. C. Florian, "Loss of epigenetic polarity is a hallmark of hematopoietic stem cell aging," *Human Molecular Genetics*, vol. 29, no. R2, pp. R248–R254, 2020.

[83] M. C. Florian, M. Klose, M. Sacma et al., "Aging alters the epigenetic asymmetry of HSC division," *PLoS biology*, vol. 16, no. 9, article e2003389, 2018.

[84] H. Geiger and H. Zheng, "Cdc42 and aging of hematopoietic stem cells," *Current opinion in hematology*, vol. 20, no. 4, p. 295, 2013.

[85] R. Kandi, K. Senger, A. Grigoryan et al., "Cdc42-Borg4-Septin7 axis regulates HSC polarity and function," *EMBO Reports*, vol. 22, no. 12, article e52931, 2021.

[86] M. C. Florian, K. Dörr, A. Niebel et al., "Cdc42 activity regulates hematopoietic stem cell aging and rejuvenation," *Cell stem cell*, vol. 10, no. 5, pp. 520–530, 2012.

[87] E. V. Verovskaya, P. V. Dellorusso, and E. Passegué, "Losing sense of self and surroundings: hematopoietic stem cell aging and leukemic transformation," *Trends in molecular medicine*, vol. 25, no. 6, pp. 494–515, 2019.

[88] N. S. Chandel, H. Jasper, T. T. Ho, and E. Passegue, "Metabolic regulation of stem cell function in tissue homeostasis and organismal ageing," *Nature cell biology*, vol. 18, no. 8, pp. 823–832, 2016.

[89] L. You, S. Jin, L. Zhu, and W. Qian, "Autophagy, autophagy-associated adaptive immune responses and its role in hematologic malignancies," *Oncotarget*, vol. 8, no. 7, p. 12374, 2017.

[90] T. T. Ho, M. R. Warr, E. R. Adelman et al., "Autophagy maintains the metabolism and function of young and old stem cells," *Nature*, vol. 543, no. 7644, pp. 205–210, 2017.

[91] S. Talukdar, S. K. Das, L. Emdad, and P. B. Fisher, "Autophagy and senescence: insights from normal and cancer stem cells," *Advances in Cancer Research*, vol. 150, pp. 147–208, 2021.

[92] A. K. Singh, M. J. Althoff, and J. A. Cancelas, "Signaling pathways regulating hematopoietic stem cell and progenitor aging," *Current stem cell reports*, vol. 4, no. 2, pp. 166–181, 2018.

[93] C. Schubert, M. Allhoff, S. Tillmann et al., "Differential roles of STAT1 and STAT2 in the sensitivity of JAK2V617F-vs. BCR-ABL-positive cells to interferon alpha," *Journal of hematology & oncology*, vol. 12, no. 1, pp. 1–16, 2019.

[94] K. Kirschner, T. Chandra, V. Kiselev et al., "Proliferation drives aging-related functional decline in a subpopulation of the hematopoietic stem cell compartment," *Cell reports*, vol. 19, no. 8, pp. 1503–1511, 2017.

[95] V. A. García-García, J. P. Alameda, A. Page, and M. L. Casanova, "Role of NF-κB in ageing and age-related diseases: lessons from genetically modified mouse models," *Cells*, vol. 10, no. 8, p. 1906, 2021.

[96] M. M. Nakagawa, H. Chen, and C. V. Rathinam, "Constitutive activation of NF-κB pathway in hematopoietic stem cells causes loss of quiescence and deregulated transcription factor networks," *Frontiers in Cell and Developmental Biology*, vol. 6, no. 143, pp. 1–14, 2018.

[97] S. J. Stein and A. S. Baldwin, "Deletion of the NF-κB subunit p 65/Rel A in the hematopoietic compartment leads to defects in hematopoietic stem cell function," *The Journal of the American Society of Hematology*, vol. 121, no. 25, pp. 5015–5024, 2013.

[98] Z. Chen, E. M. Amro, F. Becker et al., "Cohesin-mediated NF-κB signaling limits hematopoietic stem cell self-renewal in aging and inflammation," *Journal of Experimental Medicine*, vol. 216, no. 1, pp. 152–175, 2019.

[99] F. Boutouja, C. M. Stiehm, and H. W. Platta, "mTOR: a cellular regulator interface in health and disease," *Cells*, vol. 8, no. 1, p. 18, 2019.

[100] Z. Chrienova, E. Nepovimova, and K. Kuca, "The role of mTOR in age-related diseases," *Journal of Enzyme Inhibition and Medicinal Chemistry*, vol. 36, no. 1, pp. 1679–1693, 2021.

[101] A. Bitto, T. K. Ito, V. V. Pineda et al., "Transient rapamycin treatment can increase lifespan and healthspan in middle-aged mice," *elife*, vol. 5, article e16351, 2016.

[102] C. Chen, Y. Liu, Y. Liu, and P. Zheng, "mTOR regulation and therapeutic rejuvenation of aging hematopoietic stem cells," *Science signaling*, vol. 2, no. 98, p. ra75, 2009.

[103] U. Blank and S. J. B. Karlsson, "TGF-β signaling in the control of hematopoietic stem cells," *The Journal of the American Society of Hematology*, vol. 125, no. 23, pp. 3542–3550, 2015.

[104] G. A. Challen, N. C. Boles, S. M. Chambers, and M. A. Goodell, "Distinct hematopoietic stem cell subtypes are differentially regulated by TGF-β1," *Cell stem cell*, vol. 6, no. 3, pp. 265–278, 2010.

[105] R. Quéré, L. Saint-Paul, V. Carmignac et al., "Tif1γ regulates the TGF-β1 receptor and promotes physiological aging of hematopoietic stem cells," *Proceedings of the National Academy of Sciences*, vol. 111, no. 29, pp. 10592–10597, 2014.

[106] D. Sun, M. Luo, M. Jeong et al., "Epigenomic profiling of young and aged HSCs reveals concerted changes during aging that reinforce self-renewal," *Cell stem cell*, vol. 14, no. 5, pp. 673–688, 2014.

[107] M. C. Florian, K. J. Nattamai, K. Dörr et al., "A canonical to non-canonical Wnt signalling switch in haematopoietic stem-cell ageing," *Nature*, vol. 503, no. 7476, pp. 392–396, 2013.

[108] M. Tesio, K. Golan, S. Corso et al., "Enhanced c-Met activity promotes G-CSF–induced mobilization of hematopoietic progenitor cells via ROS signaling," *Blood, The Journal of the American Society of Hematology*, vol. 117, no. 2, pp. 419–428, 2011.

[109] J. Lee, Y. S. Cho, H. Jung, and I. Choi, "Pharmacological regulation of oxidative stress in stem cells," *Oxidative Medicine and Cellular Longevity*, vol. 2018, 13 pages, 2018.

[110] T. Y. Wong, M. A. Solis, Y. H. Chen, and L. L. Huang, "Molecular mechanism of extrinsic factors affecting anti-aging of stem cells," *World journal of stem cells*, vol. 7, no. 2, pp. 512–520, 2015.

[111] I. Bruns, D. Lucas, S. Pinho et al., "Megakaryocytes regulate hematopoietic stem cell quiescence through CXCL4 secretion," *Nature medicine*, vol. 20, no. 11, pp. 1315–1320, 2014.

[112] D. Li, W. Xue, M. Li et al., "VCAM-1+ macrophages guide the homing of HSPCs to a vascular niche," *Nature*, vol. 564, no. 7734, pp. 119–124, 2018.

[113] A. Chow, D. Lucas, A. Hidalgo et al., "Bone marrow CD169+ macrophages promote the retention of hematopoietic stem and progenitor cells in the mesenchymal stem cell niche," vol. 208, no. 2, pp. 261–271, 2011.

[114] I. G. Winkler, N. A. Sims, A. R. Pettit et al., "Bone marrow macrophages maintain hematopoietic stem cell (HSC) niches and their depletion mobilizes HSCs," *Blood, The Journal of the American Society of Hematology*, vol. 116, no. 23, pp. 4815–4828, 2010.

[115] Y. Hirata, K. Furuhashi, H. Ishii et al., "CD150high bone marrow Tregs maintain hematopoietic stem cell quiescence and immune privilege via adenosine," *Cell stem cell*, vol. 22, no. 3, pp. 445–453.e5, 2018.

[116] A. P. Kusumbe, S. K. Ramasamy, T. Itkin et al., "Age-dependent modulation of vascular niches for haematopoietic stem cells," *Nature*, vol. 532, no. 7599, pp. 380–384, 2016.

[117] M. Acar, K. S. Kocherlakota, M. M. Murphy et al., "Deep imaging of bone marrow shows non-dividing stem cells are mainly perisinusoidal," *Nature*, vol. 526, no. 7571, pp. 126–130, 2015.

[118] C. Fielding and S. Méndez-Ferrer, "Neuronal regulation of bone marrow stem cell niches," *F1000Research*, vol. 9, p. 614, 2020.

[119] M. Maryanovich, A. H. Zahalka, H. Pierce et al., "Adrenergic nerve degeneration in bone marrow drives aging of the hematopoietic stem cell niche," *Nature Medicine*, vol. 24, no. 6, pp. 782–791, 2018.

[120] Y.-H. Ho, R. del Toro, J. Rivera-Torres et al., "Remodeling of bone marrow hematopoietic stem cell niches promotes myeloid cell expansion during premature or physiological aging," *Cell Stem Cell*, vol. 25, no. 3, pp. 407–418.e6, 2019.

Hindawi
Oxidative Medicine and Cellular Longevity
Volume 2022, Article ID 5910575, 35 pages
https://doi.org/10.1155/2022/5910575

Research Article

CCNA2 as an Immunological Biomarker Encompassing Tumor Microenvironment and Therapeutic Response in Multiple Cancer Types

Aimin Jiang,[1] **Ye Zhou**,[1] **Wenliang Gong**,[1] **Xin Pan**,[2] **Xinxin Gan**,[1] **Zhenjie Wu**,[1] **Bing Liu**,[3] **Le Qu**,[2] **and Linhui Wang**[1]

[1]*Department of Urology, Changhai Hospital, Naval Medical University (Second Military Medical University), Shanghai, China*
[2]*Department of Urology, Affiliated Jinling Hospital, Medical School of Nanjing University, Nanjing, Jiangsu Province, China*
[3]*Department of Urology, The Third Affiliated Hospital of Second Military Medical University, Shanghai, China*

Correspondence should be addressed to Bing Liu; 13501616398@163.com, Le Qu; septsoul@smmu.edu.cn, and Linhui Wang; wanglinhuicz@163.com

Received 24 January 2022; Accepted 9 March 2022; Published 31 March 2022

Academic Editor: Milena Georgieva

Background. Cancer is a major threat to human health worldwide. Although recent innovations and advances in early detection and effective therapies such as targeted drugs and immune checkpoint inhibitors have saved more lives of cancer patients and improved their quality of life, our knowledge about cancer remains largely unknown. CCNA2 belongs to the cell cyclin family and has been demonstrated to be a tumorigenic gene in multiple solid tumor types. The aim of the present study was to make a comprehensive analysis on the role of CCNA2 at a pancancer level. *Methods*. Multidatabases were collected to evaluate the different expression, prognostic value, DNA methylation, tumor mutation burden, microsatellite instability, mismatch repair, tumor immune microenvironment, and drug sensitivity of CCNA2 across pancancer. IHC was utilized to validate the expression and prognostic value of CCNA2 in ccRCC patients from SMMU cohort. *Results*. CCNA2 was differentially expressed in most cancer types vs. normal tissues. CCNA2 may significantly influence the prognosis of multiple cancer types, especially clear cell renal cell carcinoma (ccRCC). CCNA2 was also frequently mutated in most cancer types. Notably, CCNA2 was significantly correlated with immune cell infiltration and immune checkpoint inhibitory genes. In addition, CCNA2 was also strongly related to drug resistance. *Conclusion*. CCNA2 may prove to be a new biomarker for prognostic prediction, tumor immunity assessment, and drug susceptibility evaluation in pancancer level, especially in ccRCC.

1. Introduction

Cancer is one of the major diseases threatening human health [1]. With the continuous development of medical technology, the screening and treatment of cancer have improved constantly and remarkably [2]. However, only a few malignant tumor types could be completely cured at present due to the concealment and complexity of cancer occurrence and progression [3]. The application of targeted drugs has offered relatively good oncological outcomes in some tumors, but a considerable number of patients have innate drug resistance (DR) or develop DR after receiving treatment for a certain period [4, 5]. In recent years, immunotherapy has become an important means of cancer treatment. Immune checkpoint inhibitors bring hope to more patients [6, 7]. In the face of heterogeneity of cancer, target and immune therapy have limitation to control the progression of cancers once resistance or metastasis happens, leaving patients with few therapies to employ [8, 9]. Therefore, it is urgent to find new effective therapeutic targets.

CCNA2 (Cell cyclin A2) is located on the human chromosome 4, Q27 region, with a full length of 7489 bp, which is expressed in almost all tissues in the human body [10]. Generally, the protein coded by CCNA2 can activate cyclin-dependent kinase 2 (CDK2), thus promoting transition through G1/S and G2/M [11]; however, some studies have reported that

Disease summary for CCNA2 (mRNA)

Analysis type by cancer	Cancer vs. normal		Cancer vs. cancer			
			Cancer histology		Multi–cancer	
Bladder cancer	4		2	2	1	
Brain and CNS cancer	6	1	7	8		1
Breast cancer	19	2	7	8		
Cervical cancer	4		1	1	1	
Colorectal cancer	7		3	2	2	
Esophageal cancer	4		1	1	1	
Gastric cancer	5		4	2		
Head and neck cancer	10		1	1		2
Kidney cancer	2		3	1		1
Leukemia	3	8	7	6	7	
Liver cancer	5		1	1		
Lung cancer	19		7	8		
Lymphoma	6	1	7	7	7	
Melanoma						5
Myeloma		2				
Other cancer	6	1	4	2		
Ovarian cancer	3		6	6		
Pancreatic cancer	2					2
Prostant cancer	1		2	2		2
Sarcoma	13		10	13	1	2
Signficant unique analyses	117	15	70	71	18	14
Total unique analyses	373		639		188	

(a)

Figure 1: Continued.

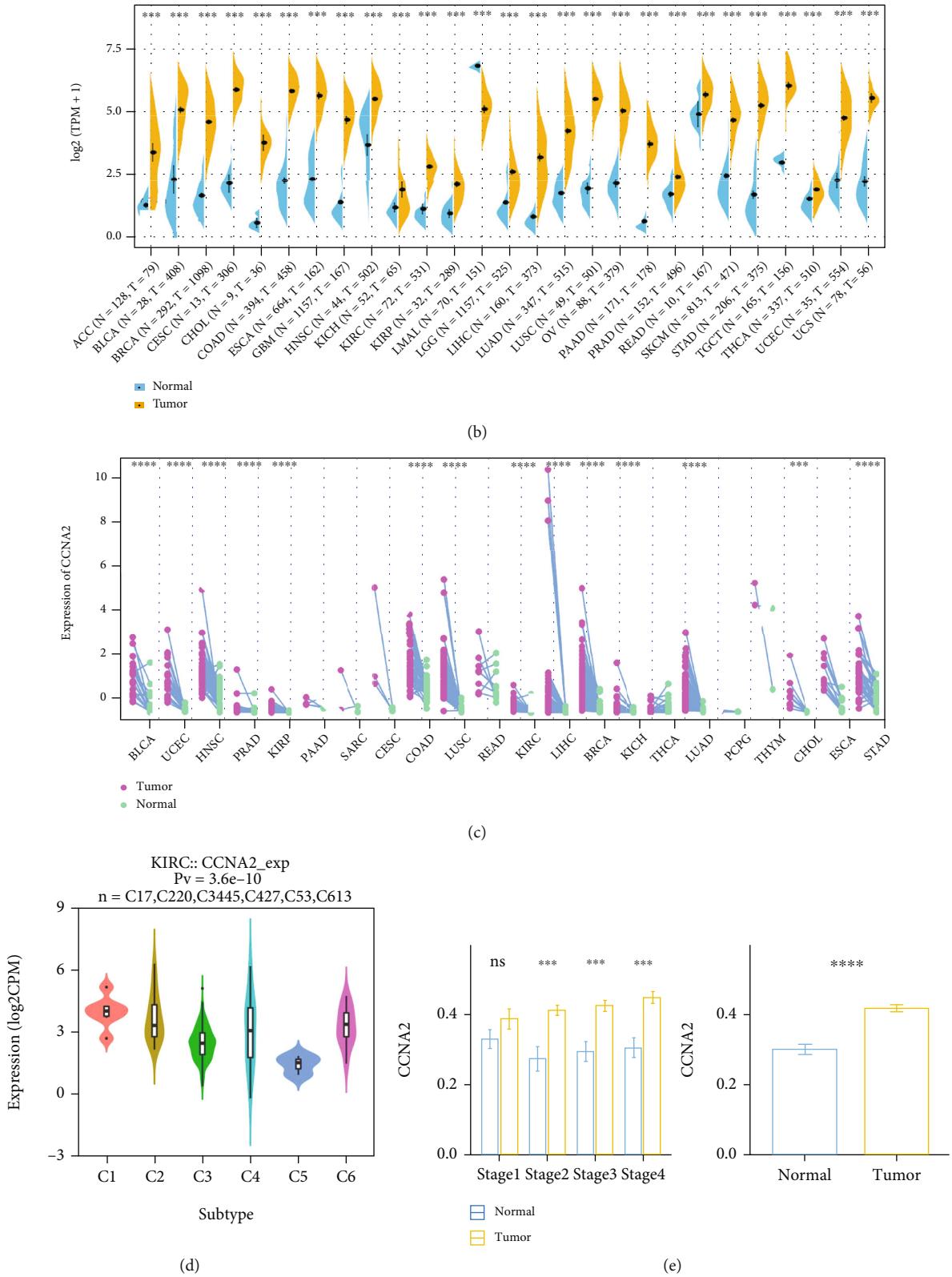

Figure 1: CCNA2 expression level in pancancer. (a) CCNA2 was increased in tumor tissues vs. normal tissues in Oncomine database. (b) Comparison of CCNA2 expression between tumor and normal tissues in TCGA database, $^{*}p < 0.05$, $^{**}p < 0.01$, $^{***}p < 0.001$, and $^{****}p < 0.0001$. (c) The expression level of CCNA2 was different in paired tumor and normal tissues of 22 cancer types from TCGA database, $^{*}p < 0.05$, $^{**}p < 0.01$, $^{***}p < 0.001$, and $^{****}p < 0.0001$. (d) CCNA2 expression was different in 6 ccRCC immune types: C1 (wound healing), C2 (IFN-gamma dominant), C3 (inflammatory), C4 (lymphocyte depleted), C5 (immunologically quiet), and C6 (TGF-b dominant)). (e) RT-PCR results of CCNA2 expression in the samples from SMMU cohort, $n = 32$.

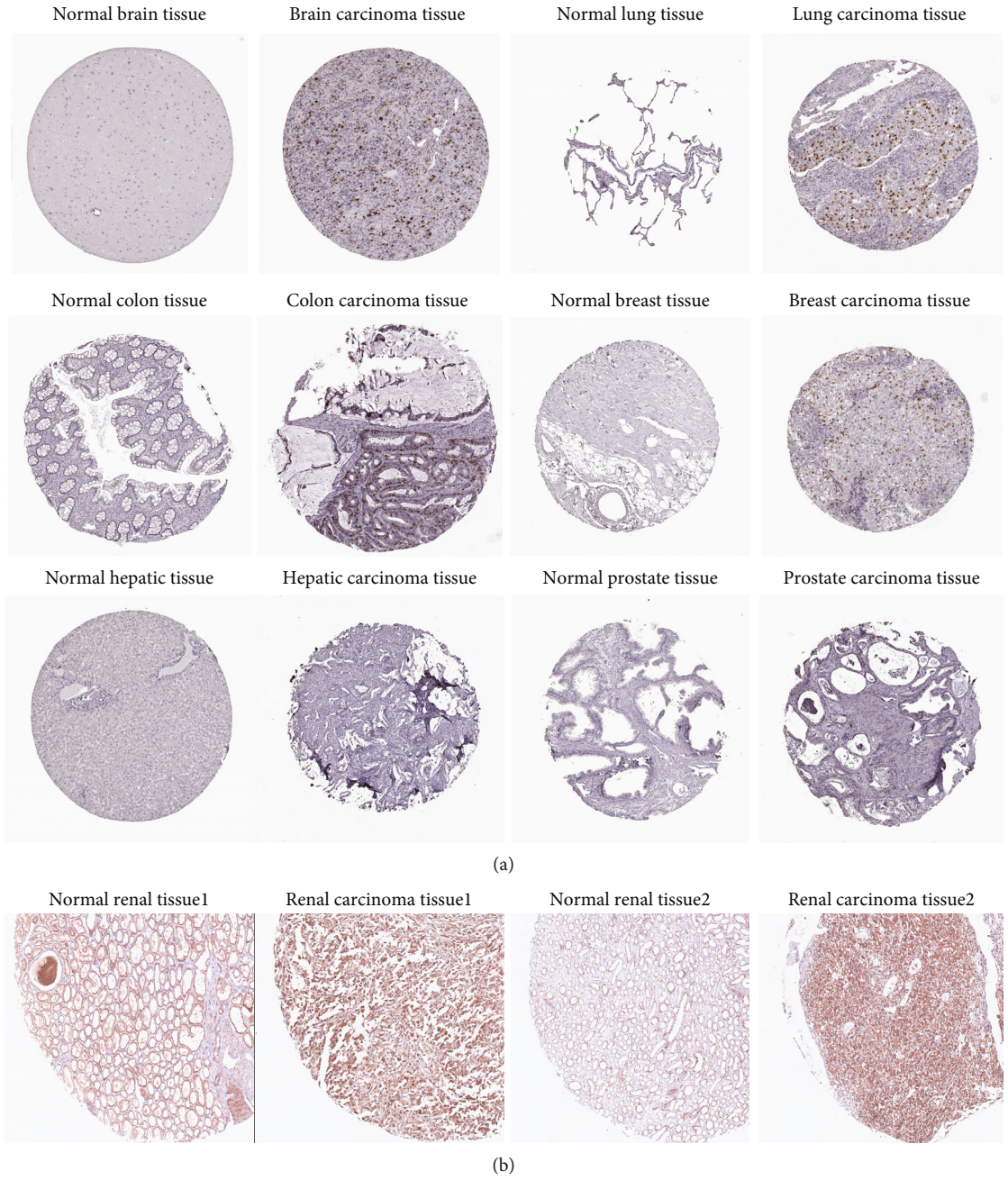

Figure 2: CCNA2 protein is highly expressed in tumor tissues vs. normal tissues. (a) Representative IHC images of CCNA2 expression retrieved from HPA database. (b) Representative immunohistochemical images of CCNA2 expression in ccRCC and adjacent tissues, scale bar = 50 μm.

CCNA2 might participate in the occurrence and progression of multiple tumors via affecting epithelial-mesenchymal transformation (EMT) and metastasis [12]. Recently, several studies have identified that CCNA2 might enhance cancer aggressive behavior, relapse, metastasis, and chemoresistance [13]. However, there is still no pancancer level analysis of the role of CCNA2 in various cancers, and the exact role of CCNA2 in tumorigenesis remains incompletely understood.

The aim of the present study was to explore the potential role of CCNA2 in tumor proliferation and analyze its correlation with the immune microenvironment in pancancer settings, especially in clear cell renal cell carcinoma (ccRCC) by conducting a comprehensive analysis of CCNA2 using several publicly available databases and inhouse datasets via bioinformatics and experiments.

2. Materials and Methods

2.1. Public Dataset Collection. The Cancer Genome Atlas (*TCGA*) database(http://cancergenome.nih.gov) is a comprehensive dataset containing multiple omics data of various cancers [14, 15]. TCGA database was utilized to download

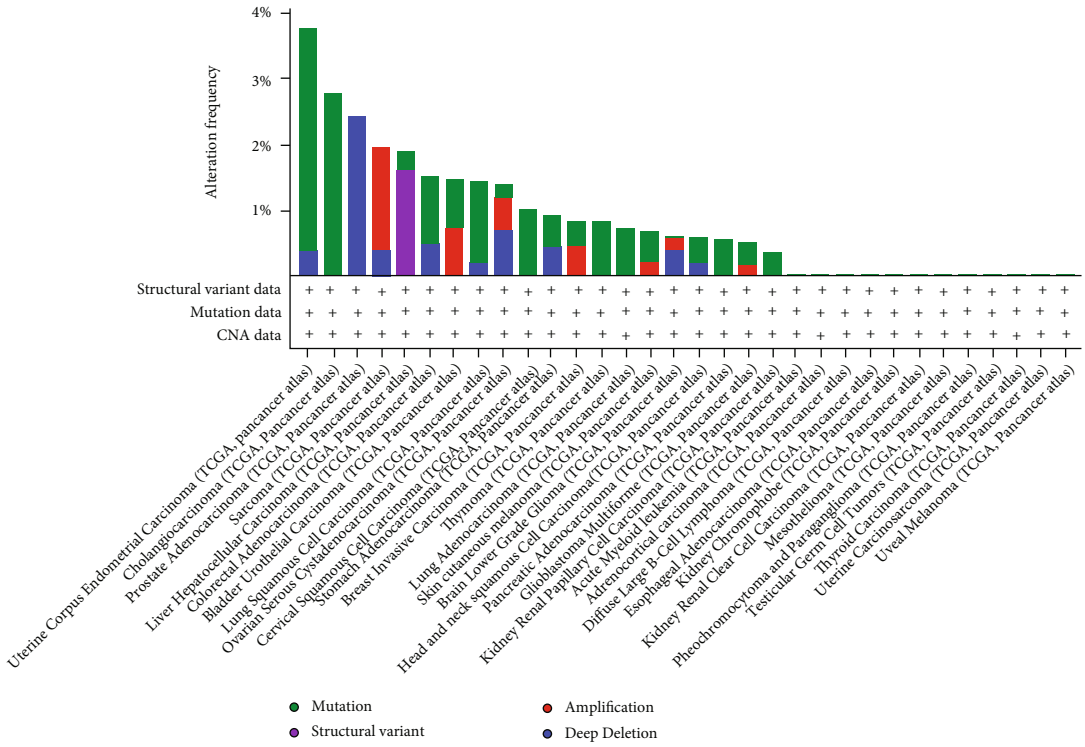

(a)

Figure 3: Continued.

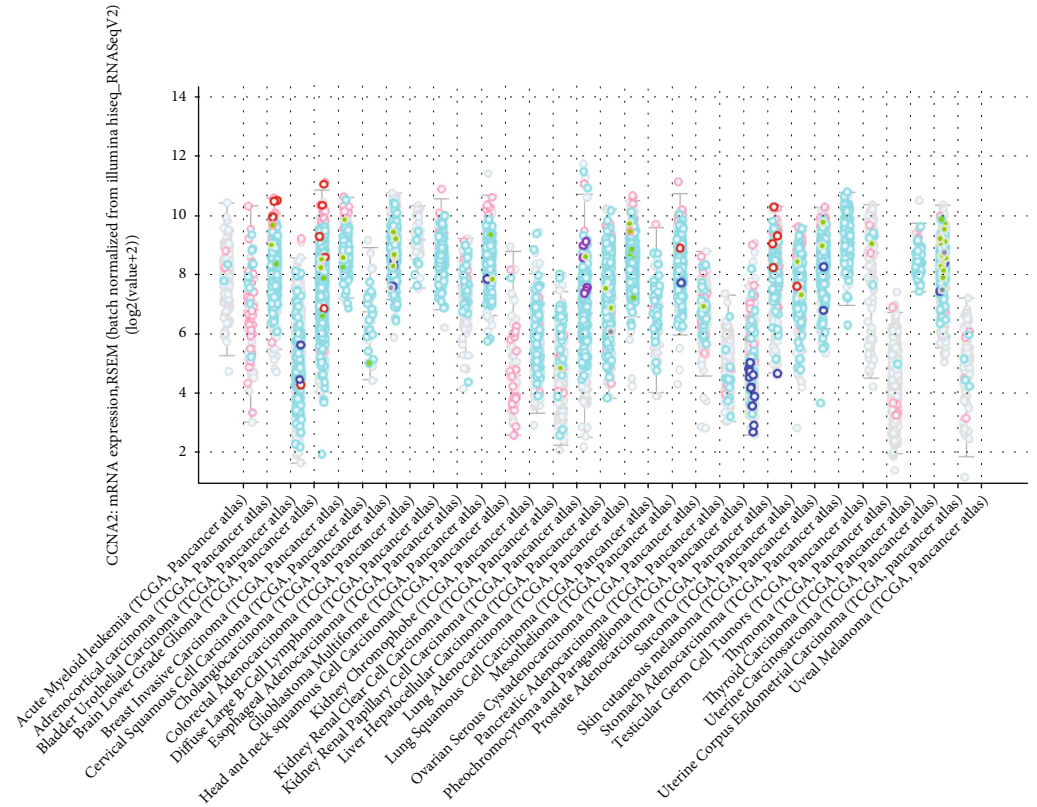

(b)

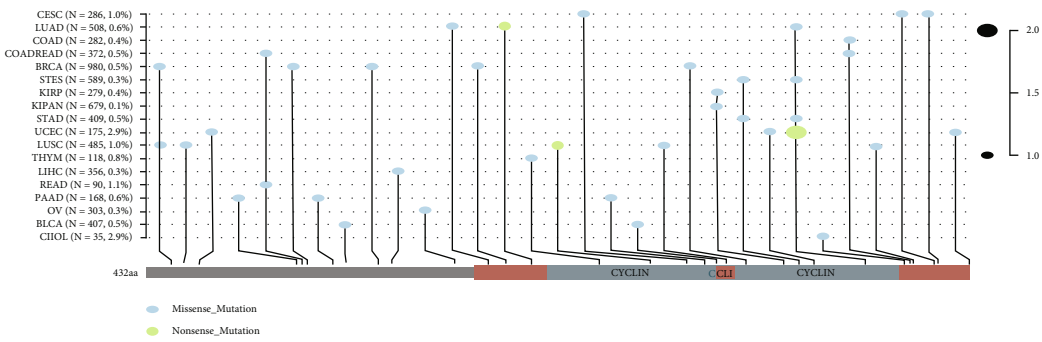

(c)

Figure 3: Continued.

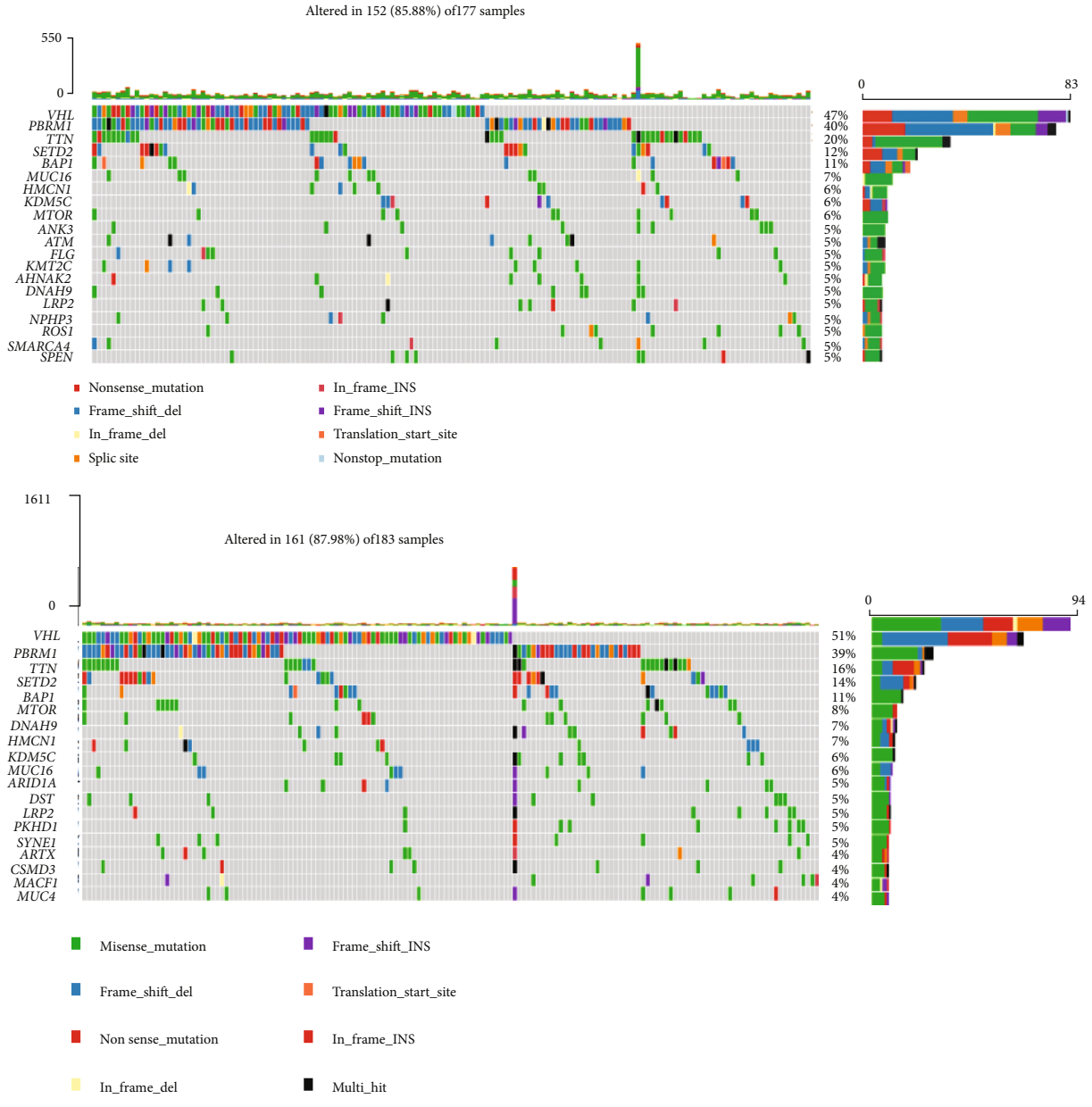

(d)

Figure 3: CCNA2 mutation landscape. (a and b) The mutation frequency and mutation count of CCNA2 in pancancer by cBioPortal database. (c) Mutation diagram of CCNA2 in different cancer types across protein domains. (d) The different mutation landscape in CCNA2 high- and low-expression groups in ccRCC.

expression profiles, clinical information, mutation data, tumor mutation burden (TMB), and microsatellite instability (MSI) data of 33 cancer types. Oncomine (https://www.oncomine.org/resource/login.html) is a web-based data mining platform that assembles 86,733 samples and 715 gene expression datasets together [16]. In this study, it was employed to detect the expression level of CCNA2 in pancancer in this study. HPA (http://www.proteinatlas.org/) database was used to evaluate differences in CCNA2 expression at the protein level in pancancer. cBioPortal database (http://www.cbioportal.org) was applied to investigate the copy number alteration and mutation landscape of CCNA2 in pancancer. Patients were excluded if they (1) did not have prognostic information and (2) died within 30 days.

2.2. Differential Expression of CCNA2 in TCGA and SMMU Cohorts. Analysis of CCNA2 expression in multiple cancers was performed in Oncomine and TCGA databases, using p value < 0.05 and absolute fold change > 1.5 as the threshold. The above obtained results were validated by quantitative real-time PCR (RT-qPCR) and immunohistochemical (IHC) staining to compare differences in mRNA and protein expressions. Informed consent about the tissue sample use was obtained from each patient before initiation of the

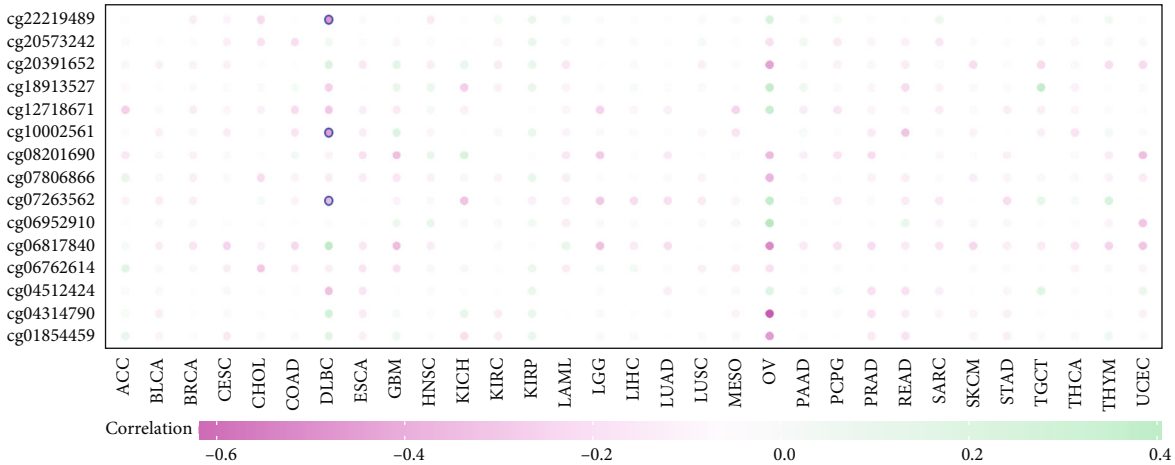

(a)

Figure 4: Continued.

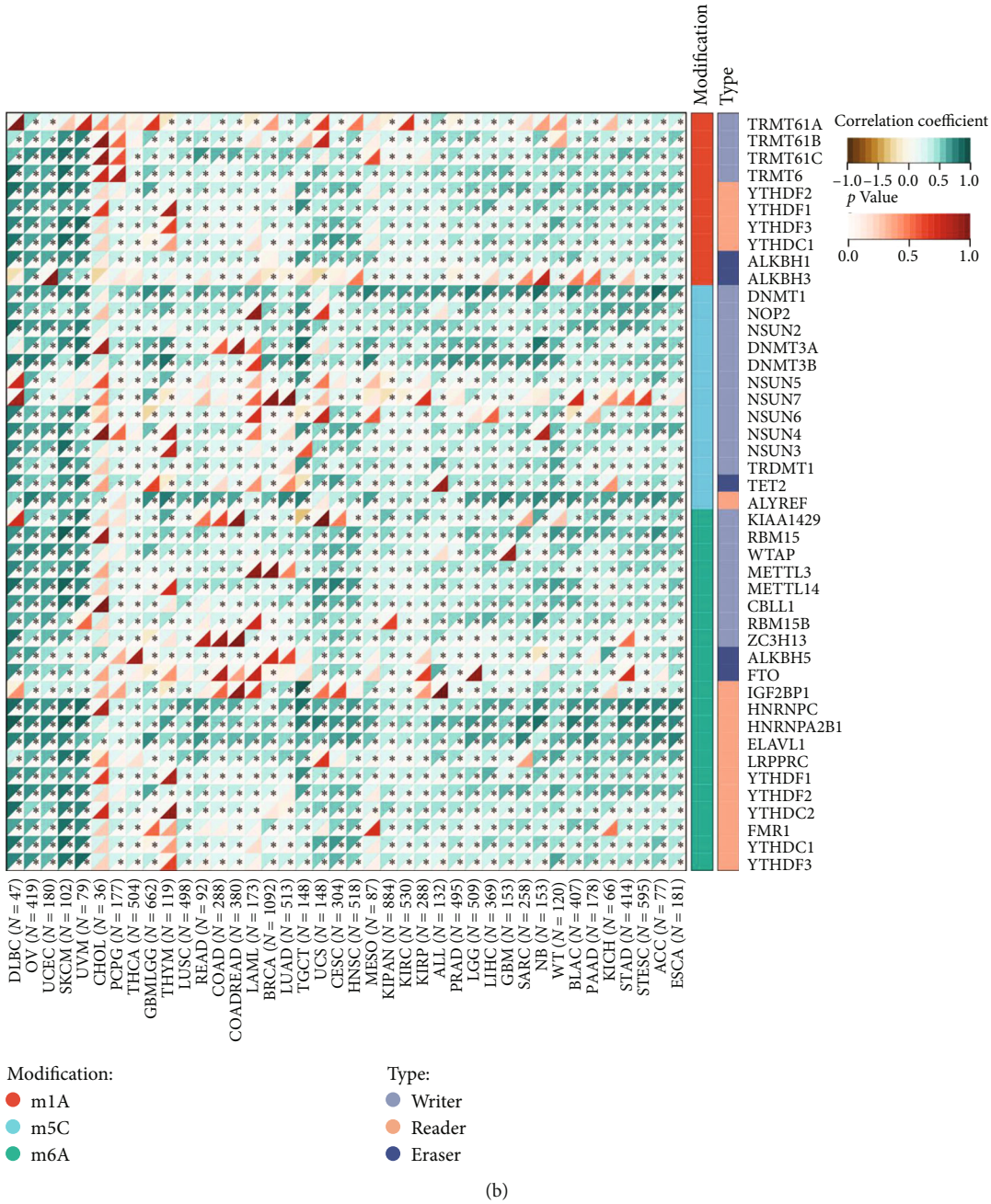

(b)

Figure 4: DNA methylation and RNA modification in CCNA2. (a) The correlation of CCNA2 expression and methylation degree in pancancer. (c) The correlation of CCNA2 expression and RNA modification regulator expression in pancancer.

research, and the study protocol was approved by the Institutional Review Board of the Second Military Medical University (Shanghai, China) Cancer Center. Altogether, 32 paired tumor and normal tissues were collected to perform a validation experiment. The primer sequences of CCNA2 are as follows: CGCTGGCGGTACTGAAGTC (forward primer) and GAGGAACGGTGACATGCTCAT (reverse primer). Antibodies for detecting CCNA2 expression were purchased from Abcam Company (CCNA2: ab181591).

2.3. Prognosis Analysis of CCNA2 in TCGA Cohort. The survival information of pancancer including overall survival (OS), progression-free interval (PFI), disease-free interval (DFI), and disease-free survival (DSS) was downloaded from TCGA database for evaluating the prognostic significance of CCNA2. Additionally, ccRCC patients were divided into CCNA2-high and CCNA2-low groups based on the median expression level of CCNA2. R packages "survival" and "survminer" were used, and the Cox analysis was applied to analyze the relationship between the expression of CCNA2 and patient prognosis.

2.4. Enrichment Analysis of CCNA2. Based on the guilt of association of a single gene in tumors, Pearson's correlation of expression between CCNA2 and other mRNAs retrieved from TCGA transcriptome data was analyzed. Sorted by

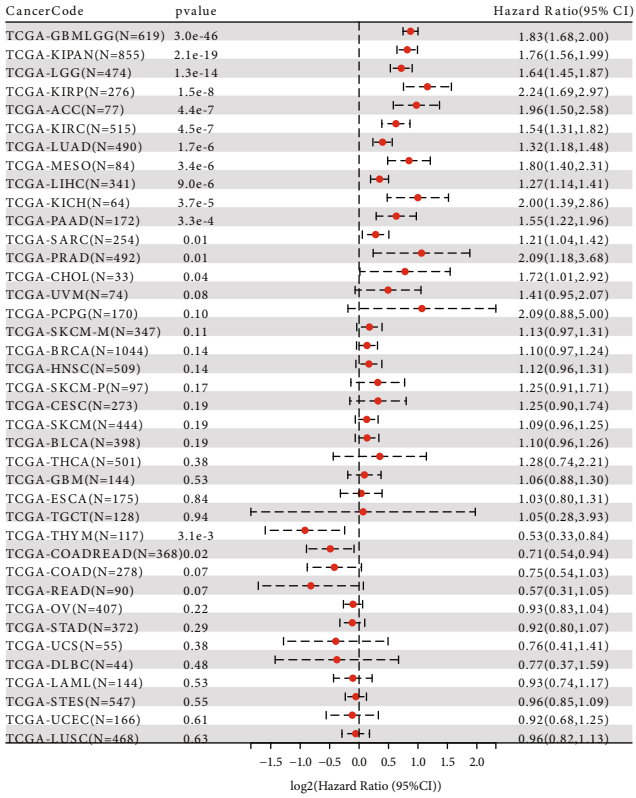

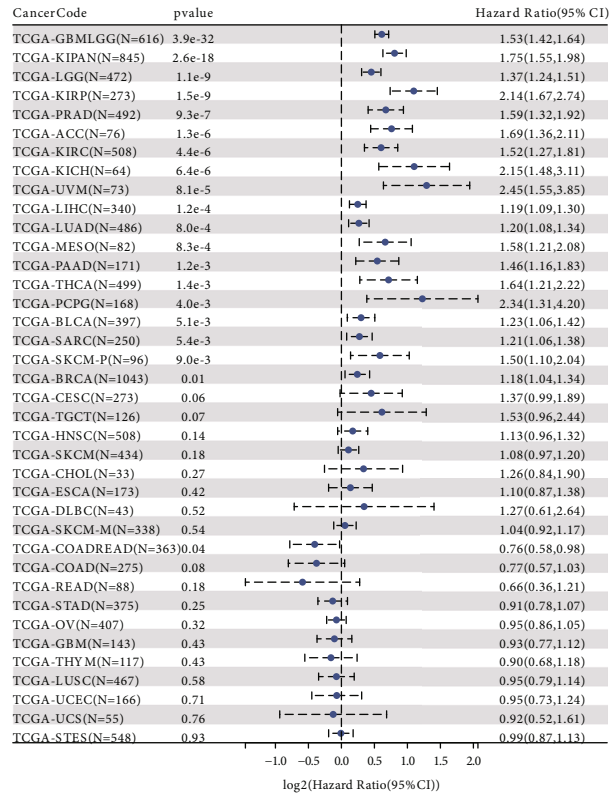

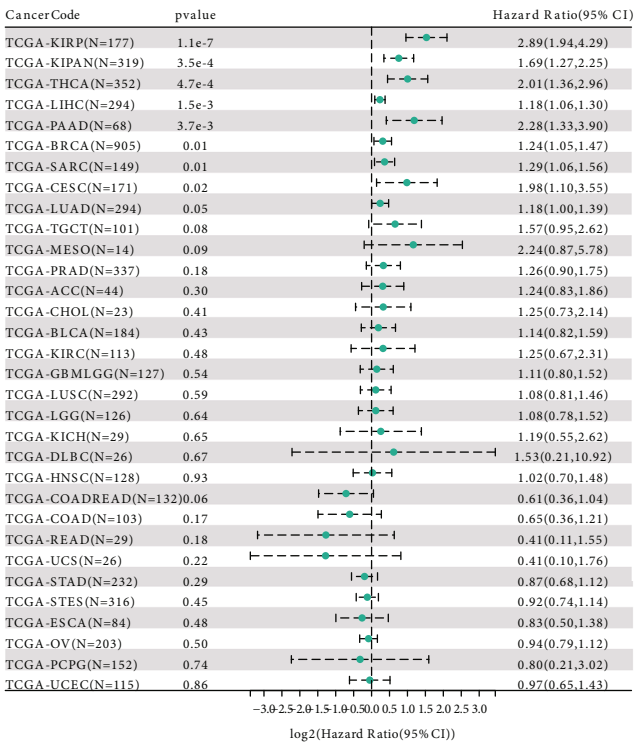

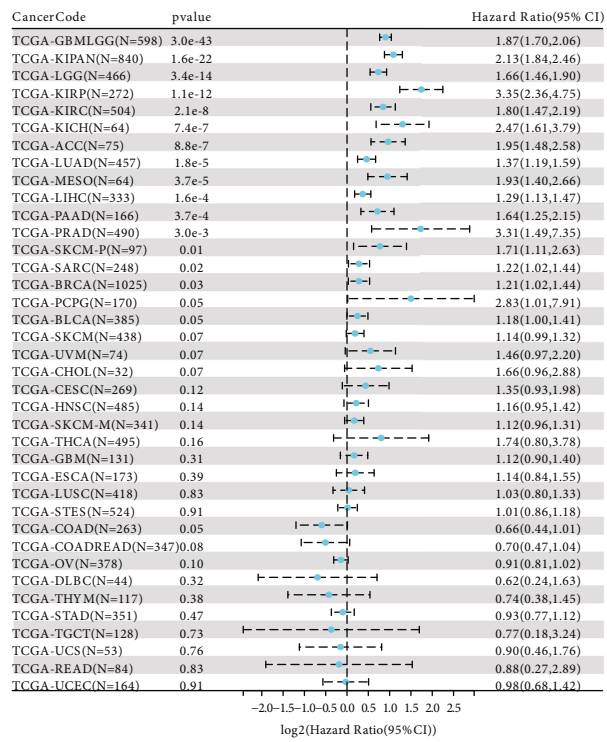

(a)

Figure 5: Continued.

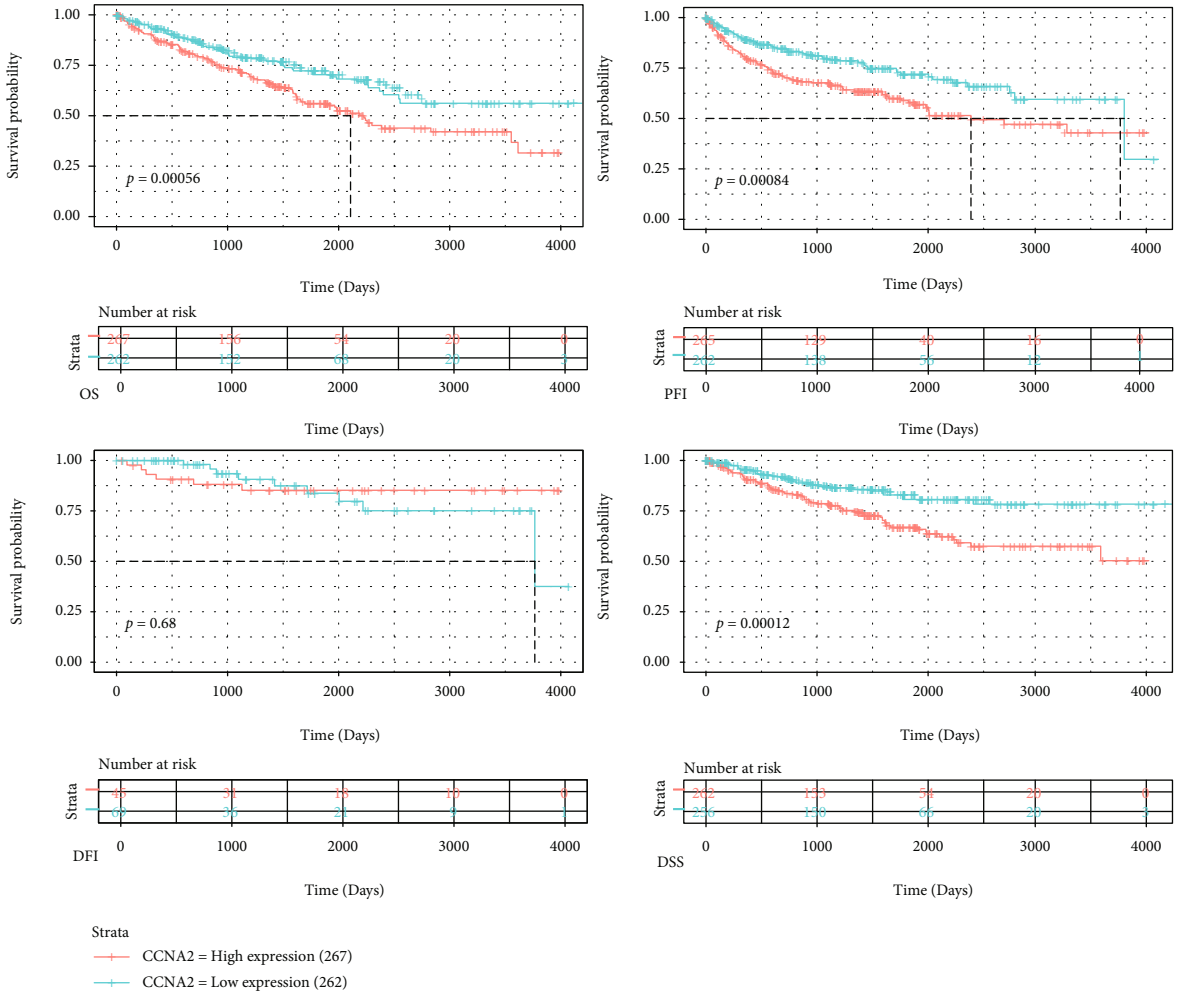

(b)

Figure 5: The prognostic significance of CCNA2 in various cancer types. (a) The impact of CCNA2 on OS, PFI, DFI, and DSS in pancancer using the Cox proportional hazard models. (b) The impact of CCNA2 on OS, PFI, DFI, and DSS in ccRCC using the Kaplan-Meier analysis.

the level of the association index between genes and CCNA2, those genes most related to CCNA2 expression were selected for enrichment analysis. R package "clusterProfiler" was used to perform Gene Ontology (GO) analysis, Kyoto Encyclopedia of Genes and Genomes (KEGG) analysis, and Gene Set Enrichment Analysis (GSEA) [17].

2.5. Assessment of Clinical Significance of CCNA2 Expression. Clinical characteristics including the tumor stage and drug sensitivity were introduced, and the relationship between CCNA2 expression and clinical characteristics was analyzed. The datasets including IC50 (half maximal inhibitory concentration) and gene expression of cancer cell lines were downloaded from CellMiner database (https://discover.nci.nih.gov/cellminer/home.do) and GDSC (https://www.cancerrxgene.org/) database [18].

2.6. Differences in the Tumor Microenvironment (TME) and Therapy Response. R package "ESTIMATE" was introduced to evaluate the relationship between the degree of immune and stromal cell infiltration and the expression of CCNA2 in pancancer. Coexpression analysis of immune-related genes and CCNA2 was performed via R package "ggpubr" and "ggcor." R package "CIBERSORT" was used to quantify the immune cell infiltration scores in pancancer, and then the correlation of the degree of immune cell infiltration and CCNA2 expression was calculated [19]. In addition, correlations between the neoantigen count, TMB, MSI and expression of T cell exhaustion marker genes, DNA mismatch repair (MMR) system genes (including MLH1, MSH2, MSH6, PMS2, and EPCAM), DNA methyltransferase (including DNMT1, DNMT2, DNMT3A, and DNMT3), ESTIMATE scores, and CCNA2 expression were analyzed. The immune infiltration scores were also calculated using the ssGSEA algorithm, and the correlation and difference between the immune cell infiltration and CCNA2 expression in ccRCC were analyzed. The impact of CCNA2 mutation on immune cell infiltration in ccRCC was analyzed by TIMER website (http://timer.cistrome.org/) [20]. CellMiner database (https://discover.nci.nih.gov/cellminer/home.do) and CCLE database (https://portals.broadinstitute.org/ccle) were implied to investigate the role of CCNA2 expression in therapy response [21, 22].

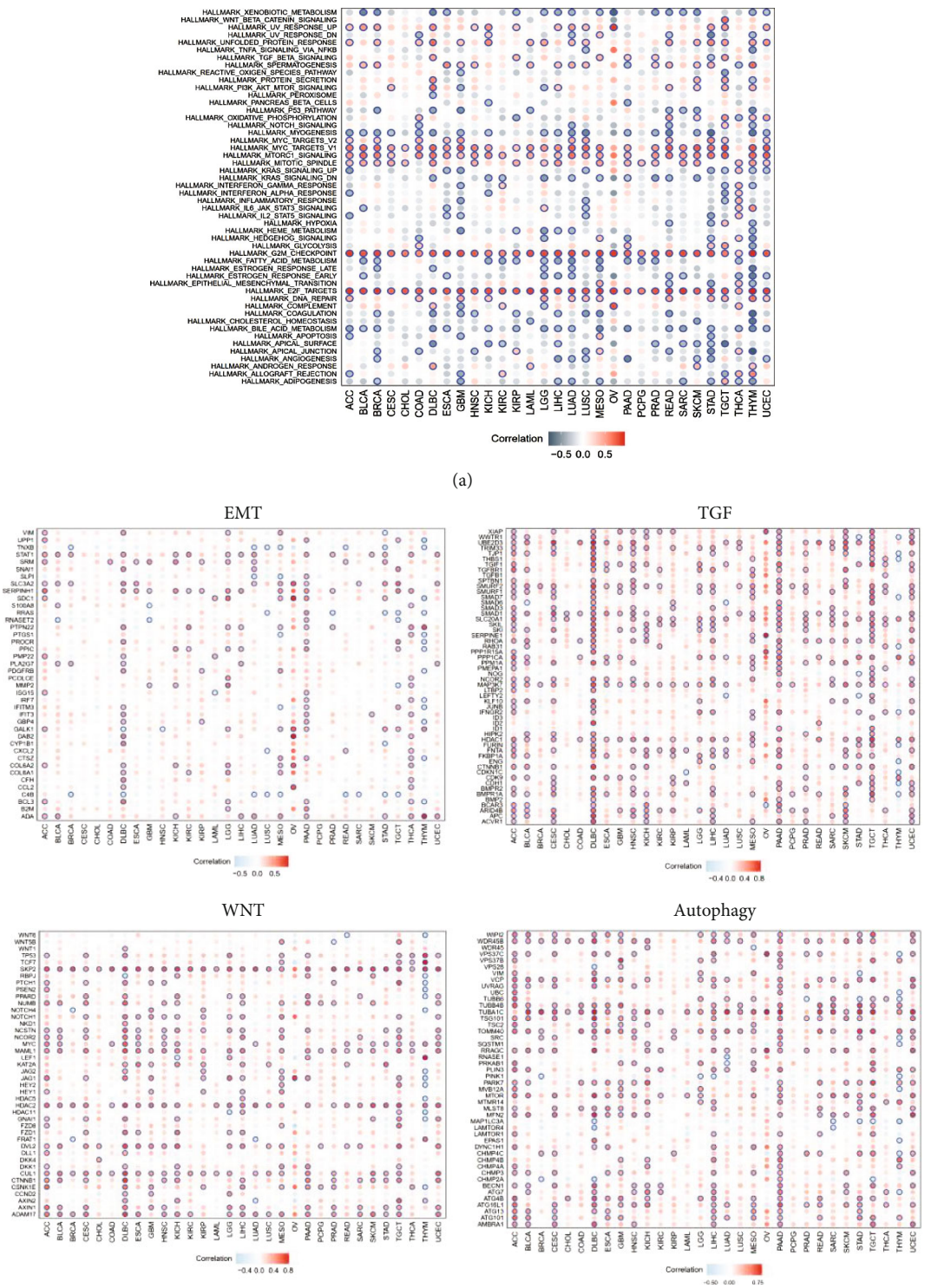

Figure 6: Association between CCNA2 and hallmarks in pancancer. (a) Correlations of CCNA2 expression with HALLMARKS enrichment score in 33 cancer types. (b) Correlation between CCNA2 expression and EMT, TGF, WNT, and autophagy pathway in pancancer.

2.7. Statistical Analysis. Differences in CCNA2 expression in the public datasets were compared by one-way ANOVA, and differences in clinical information and response to immune checkpoint inhibitors between the two different subgroups were compared by the chi-square test. Differences in OS and PFI between the CCNA2 high-expression and low-expression groups in ccRCC patients were compared by the Kaplan-Meier method and log-rank rest. The hazard ratios (HRs) were calculated by the univariate Cox regression and multiple Cox regression analysis. All p values were

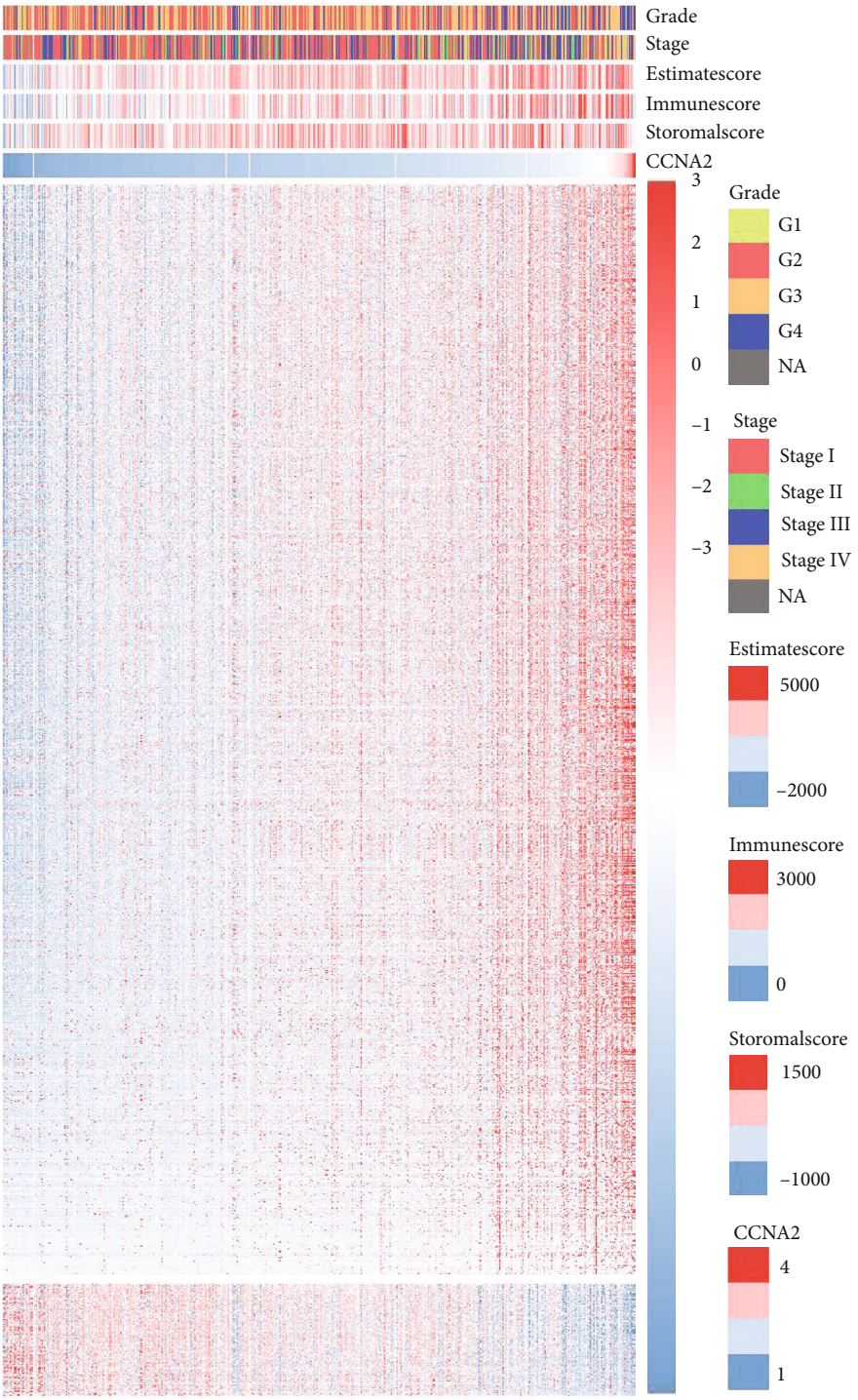

(a)

Figure 7: Continued.

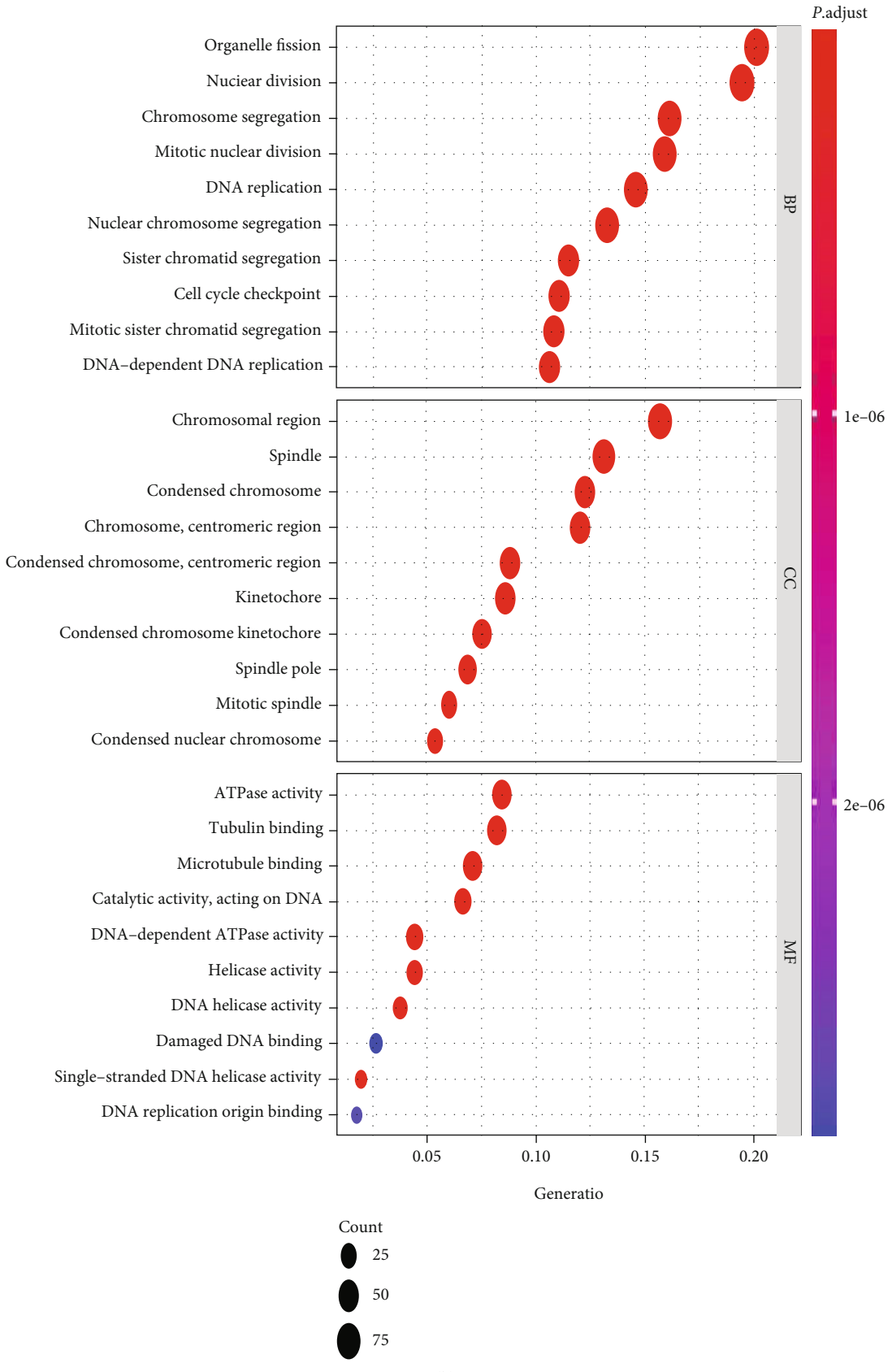

(b)

Figure 7: Continued.

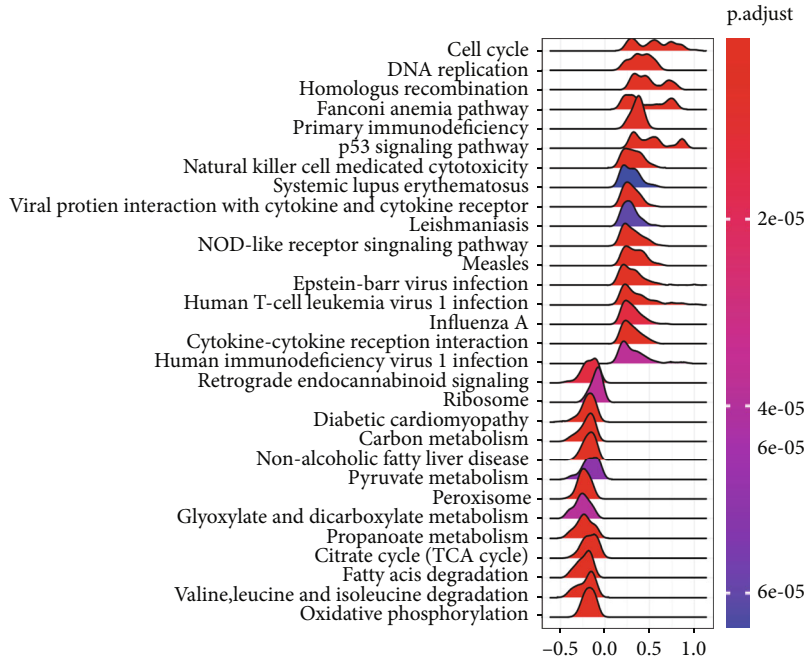

(c)

Figure 7: Continued.

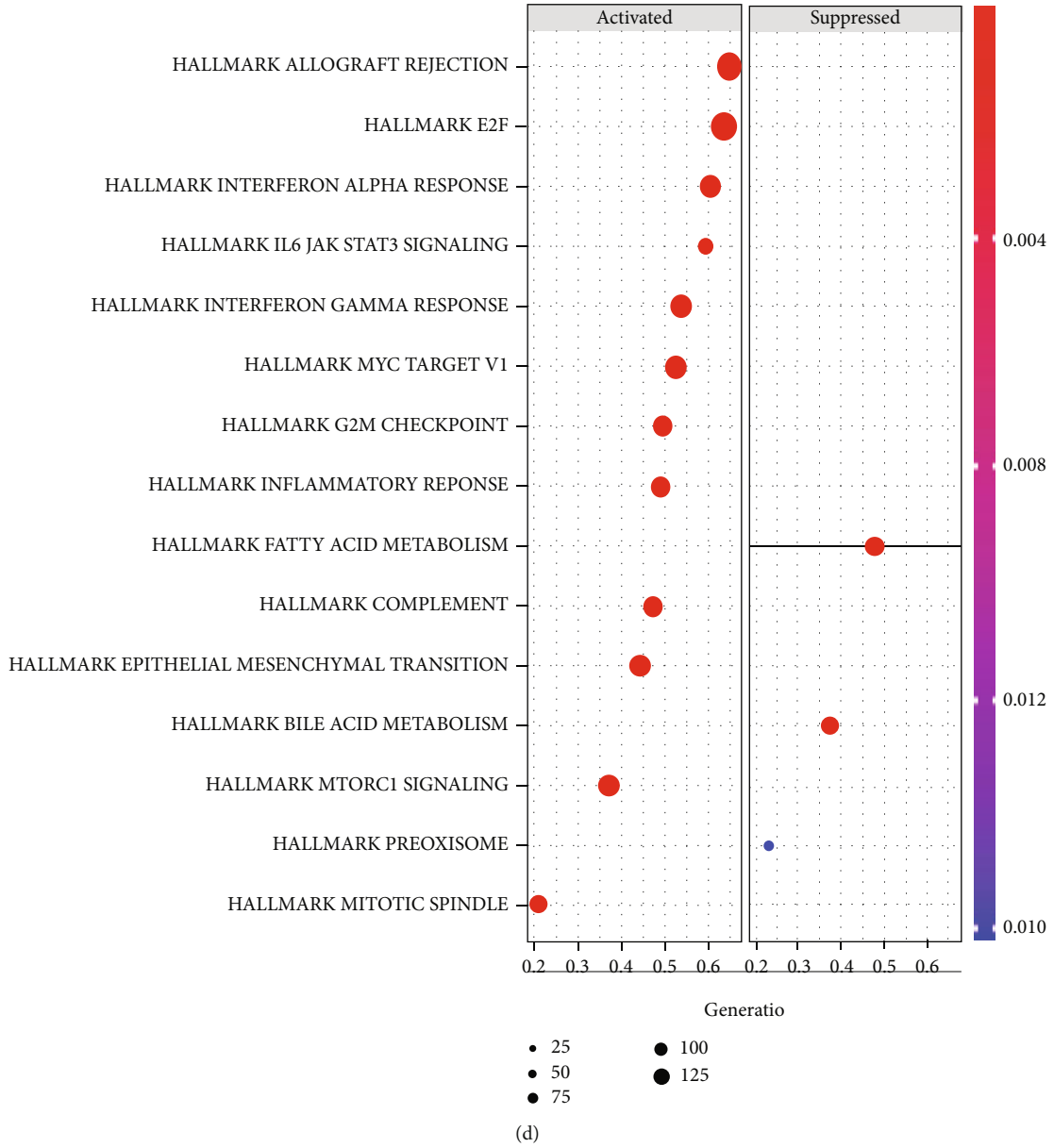

Figure 7: The biological function of CCNA2 in ccRCC. (a) Heatmap of association between estimated scores and DDX39 in TCGA ccRCC patients. (b–d) GO, KEGG, and GSEA analysis of CCNA2 in ccRCC.

two-sided, with $p < 0.05$ as statistically significant. Adjusted P value was obtained by the Benjamini-Hochberg (BH) multiple test correction. All data processing, statistical analysis, and plotting were conducted using R 4.0.4 software.

3. Results

3.1. CCNA2 mRNA Is Widely Upregulated in Cancers. The expression level of *CCNA2* in pancancer and normal tissues was analyzed firstly in Oncomine database. As shown in Figure 1(a), CCNA2 was differently expressed in most tumor and normal tissues. We next examined the differential expression of CCNA2 in TCGA database. Compared with the mRNA level in normal tissues, CCNA2 mRNA level was increased prominently in adrenocortical carcinoma (ACC), bladder urothelial carcinoma (BLCA), breast invasive carcinoma (BRCA), cervical squamous cell carcinoma and endocervical adenocarcinoma (CESC), cholangiocarcinoma (CAC), colon adenocarcinoma (COAD), esophageal carcinoma (ESCA), glioblastoma multiforme (GBM), head and neck squamous cell carcinoma (HNSC), kidney chromophobe (KICH), kidney renal clear cell carcinoma (KIRC), kidney renal papillary cell carcinoma (KIRP), brain lower grade glioma (LGG), liver hepatocellular carcinoma (LIHC), lung adenocarcinoma (LUAD), lung squamous cell carcinoma (LUSC), ovarian serous cystadenocarcinoma (OV), pancreatic adenocarcinoma (PAAD), prostate adenocarcinoma (PRAD), rectum adenocarcinoma (READ), skin cutaneous melanoma (SKCM), stomach adenocarcinoma (STAD), testicular germ cell tumor (TGCT), thyroid

(a)

Figure 8: Continued.

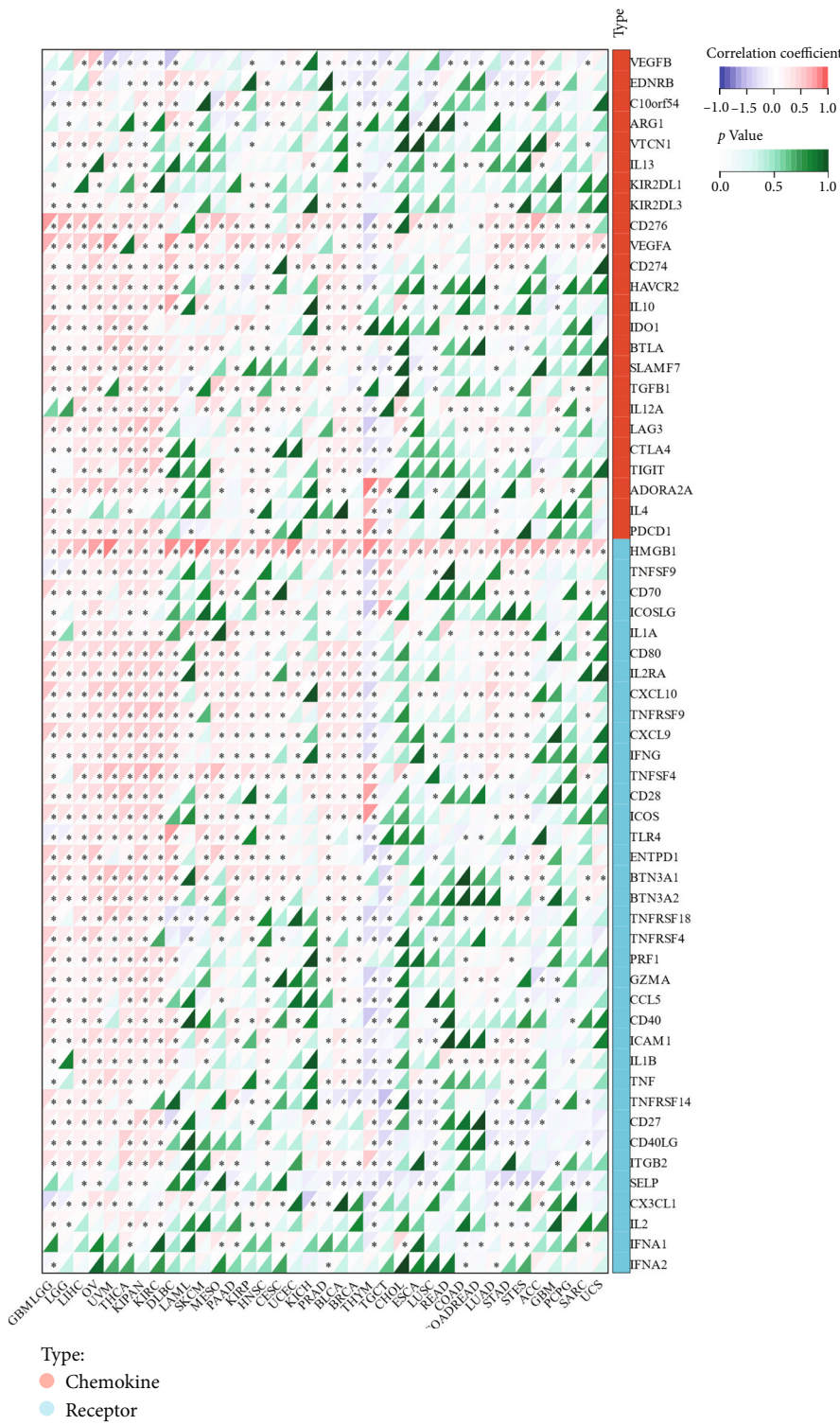

(b)

Figure 8: Continued.

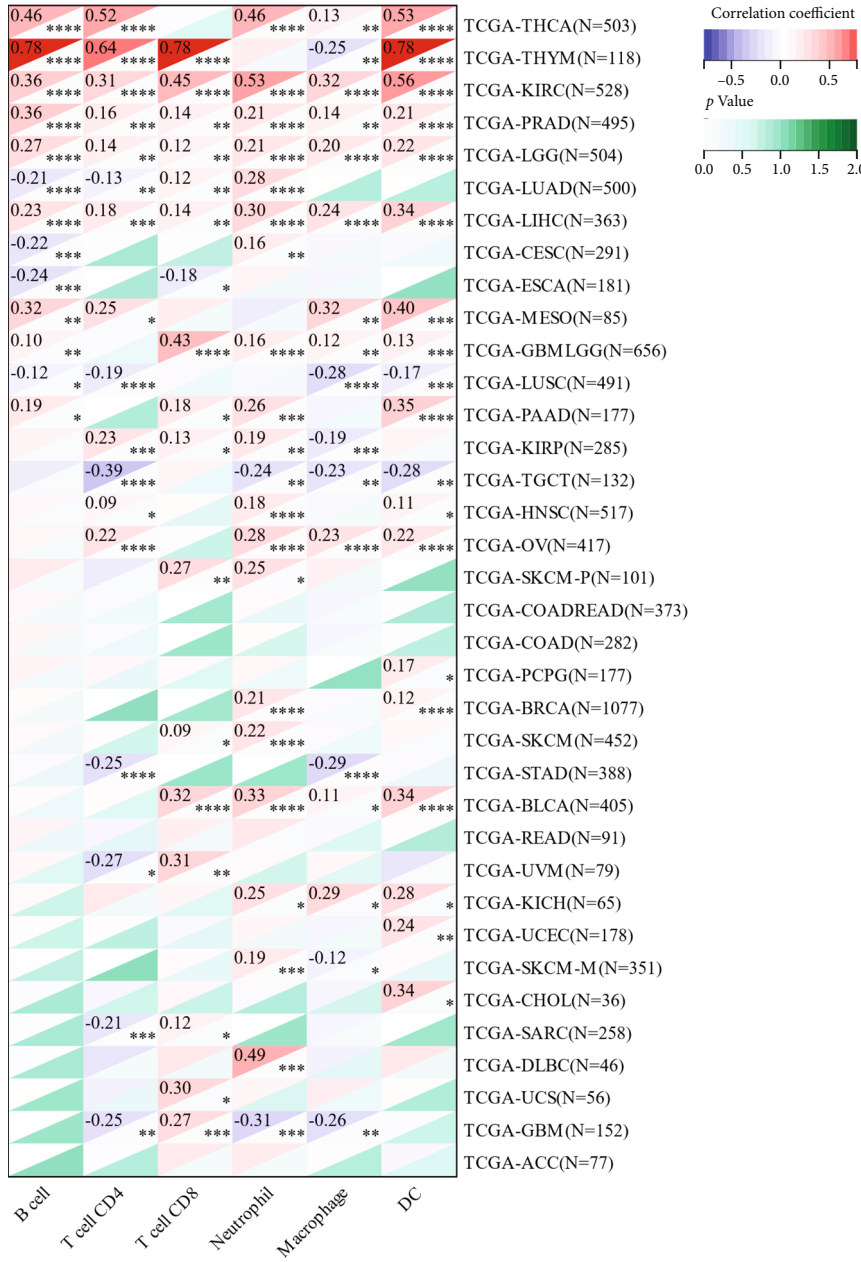

(c)

Figure 8: Continued.

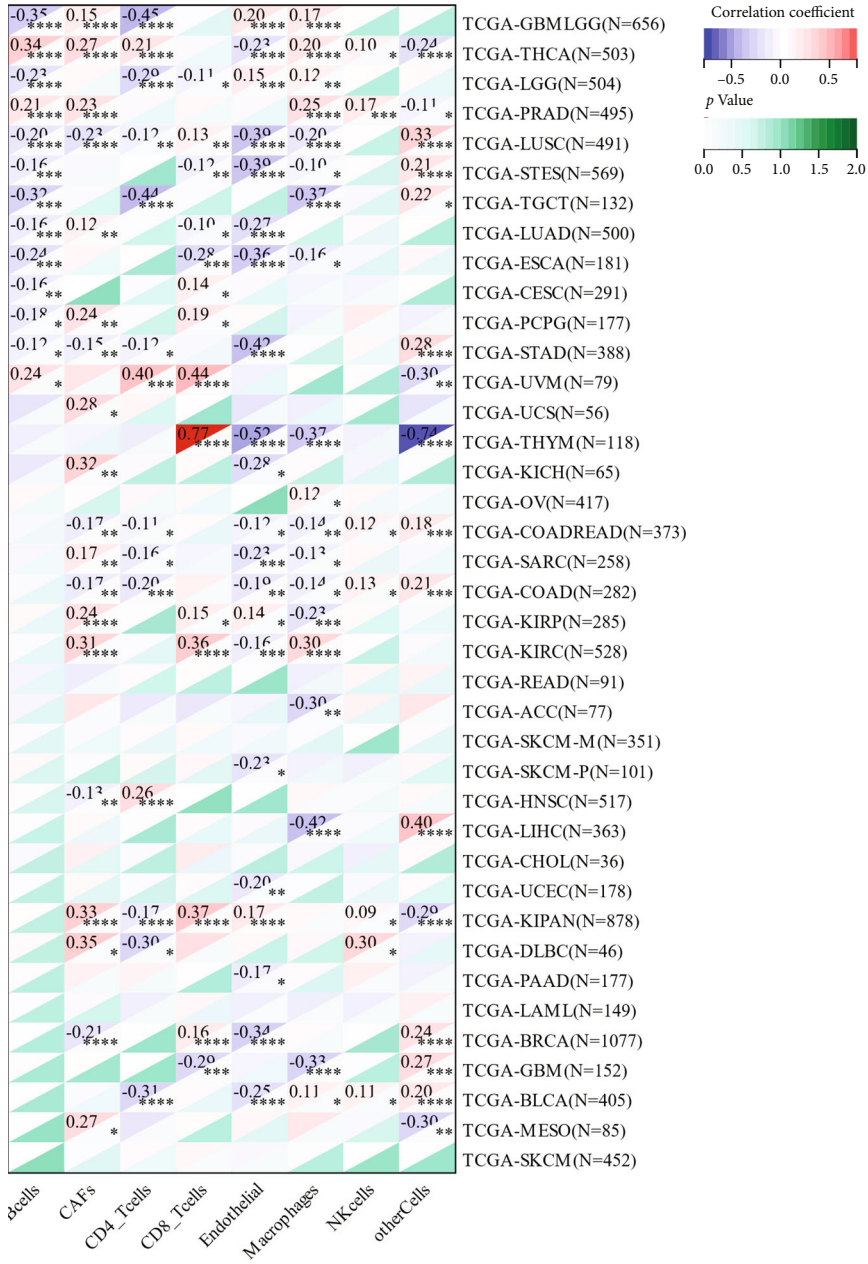

(d)

Figure 8: Continued.

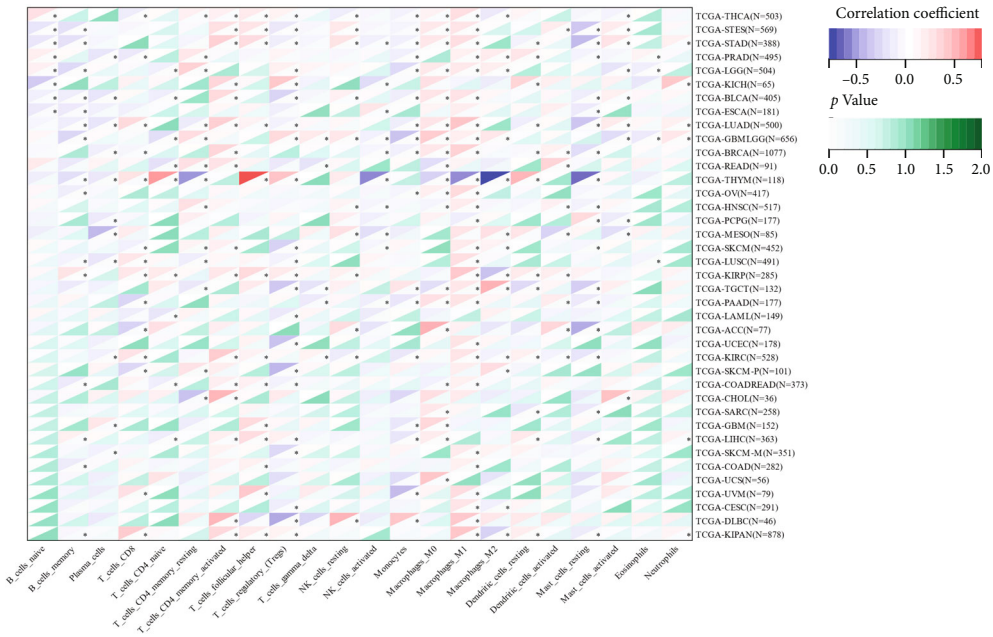

(e)

Figure 8: Association between CCNA2 and tumor immunity in pancancer. (a and b) Correlations of CCNA2 expression with immune moderator genes and immune checkpoint-related genes in 33 cancer types. (c, d, and e) Correlation between CCNA2 expression and immune cell infiltration via TIMER, EPIC, and CIBERSORT algorithms.

carcinoma (THCA), uterine corpus endometrial carcinoma (UCEC), and uterine carcinosarcoma (UCS), while it was decreased in acute myeloid leukemia (LAML) (Figure 1(b)). To make the result more creditable, the paired tumor and normal tissues in TCGA were further analyzed. As illustrated in Figure 1(c), CCNA2 was widely overexpressed in tumor tissues. In addition, the expression level of CCNA2 was significantly different in the five classic immune subtypes of ccRCC, of which C5 (immunologically quiet) was the lowest subgroup (Figure 1(d)). Through ccRCC and normal tissue from Changzheng Hospital, CCNA2 was highly expressed in tumor compared to normal tissues, which validated the above results (Figure 1(e)). To assess whether CCNA2 was expressed at different levels in various cancer stages, different pathological stages (I, II, III, and IV) of pancancer were collected. The results showed that the expression level of CCNA2 was significantly different in different stages of ACC, BRCA, COAD, KICH, KIRC, KIRP, LUAD, SKCM, TGCT, and THCA (Figure S1), suggesting that CCNA2 may play an important role in progression of various carcinomas.

3.2. Validation of Different Expression Levels of CCNA2 Protein. To assess CCNA2 protein expression, the IHC results from the HPA database and inhouse cohort were analyzed and compared. As shown in Figure 2(a), the protein expression levels of CCNA2 were highly consistent with mRNA expression above. IHC staining showed that the expression levels of CCNA2 mRNA and protein were low in the normal brain, lung, colon, breast, liver, and prostate but high in tumor tissues. These expression differences were also validated by the paired renal tissues from SMMU cohort indicating that the expression level of CCNA2 protein in ccRCC tissues was higher than normal tissues (Figure 2(b)).

3.3. The Landscape of CCNA2 Mutation Profile in Various Cancers. The genetic alteration and DNA methylation status of CCNA2 in different tumor samples of TCGA cohorts were observed, and the result is shown in Figures 3(a) and 3(b). As shown in Figure 3(a), the highest alteration frequency of CCNA2 (>3%) appeared in UCEC patients with "mutations" as the primary type. In addition, all PRAD cases with genetic alteration (~2.5% frequency) had copy number deletion of CCNA2 (Figure 3(b)). We further analyzed the type, site, and case number of the CCNA2 genetic alteration. As shown Figure 3(c), missense mutation of CCNA2 was the main type of genetic alteration. Then, we analyzed the mutation difference between CCNA2-high and CCNA2-low subgroups in ccRCC and found that the mutation rate of PBRM1 in CCNA2-high subgroup was higher than that in CCNA2-low subgroup. These two subgroups contained different mutation profiles: MTOR, ANK3, ATM, FLG, KMT2C, AHNAK2, NPHP3, ROS1, SMARCA4, and SPEN in CCNA2-high subgroup vs. DNAH9, ARID1A, DST, PKHD1, SYNE1, ATRX, CSDM3, MACF1, MUC4, and SPTA1 in CCNA2-low subgroup (Figure 3(d)).

3.4. Correlation of TREM2 Expression with DNA Methylation and RNA Modification. To further analyze the potential regulation effect of DNA methylation and RNA modification in CCNA2 expression, firstly, we systematically explored the correlation of DNA methylation level and CCNA2 expression, which indicated that DNA methylation could negatively regulated CCNA2 expression in BLCA via

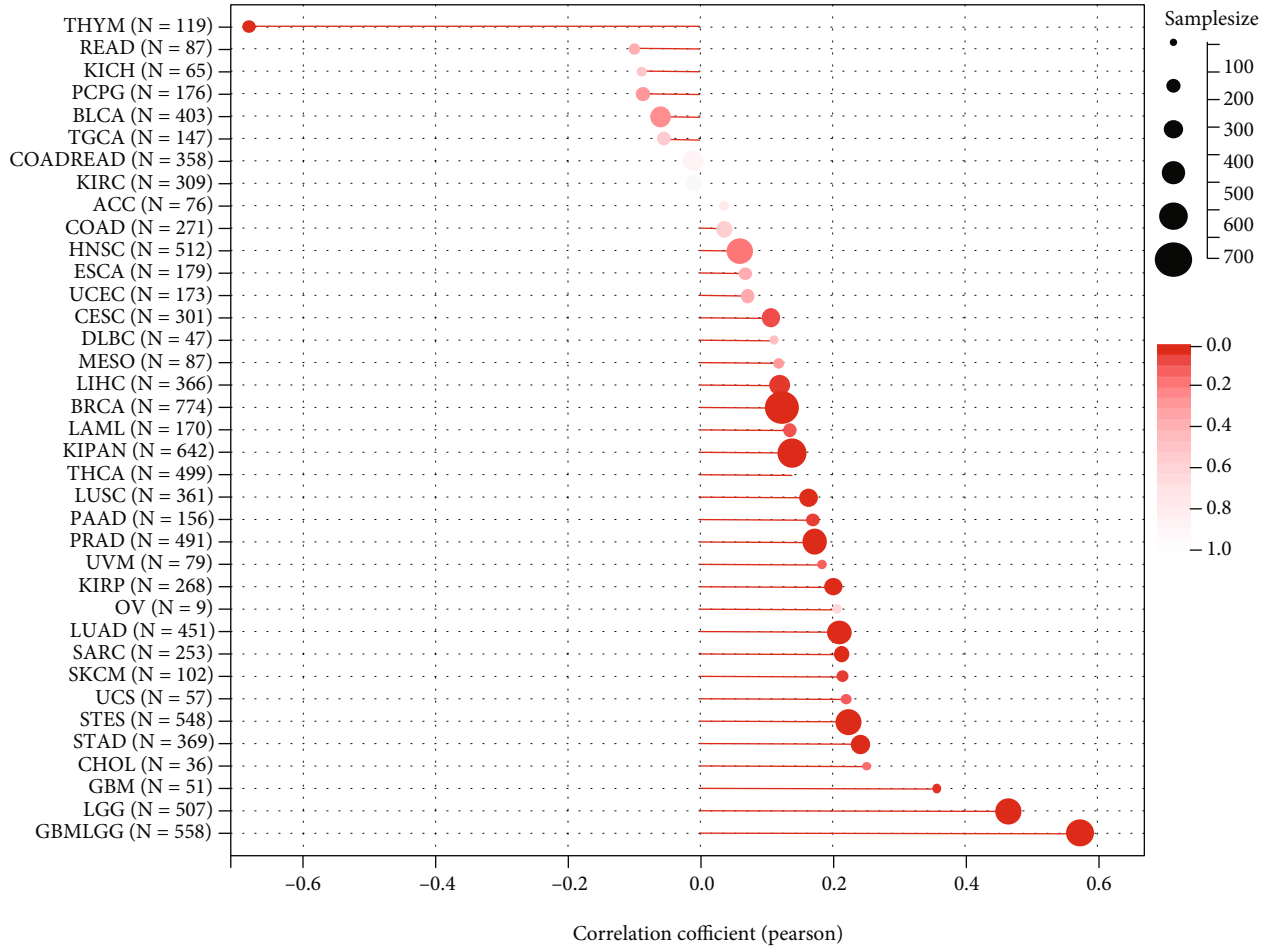

(a)

Figure 9: Continued.

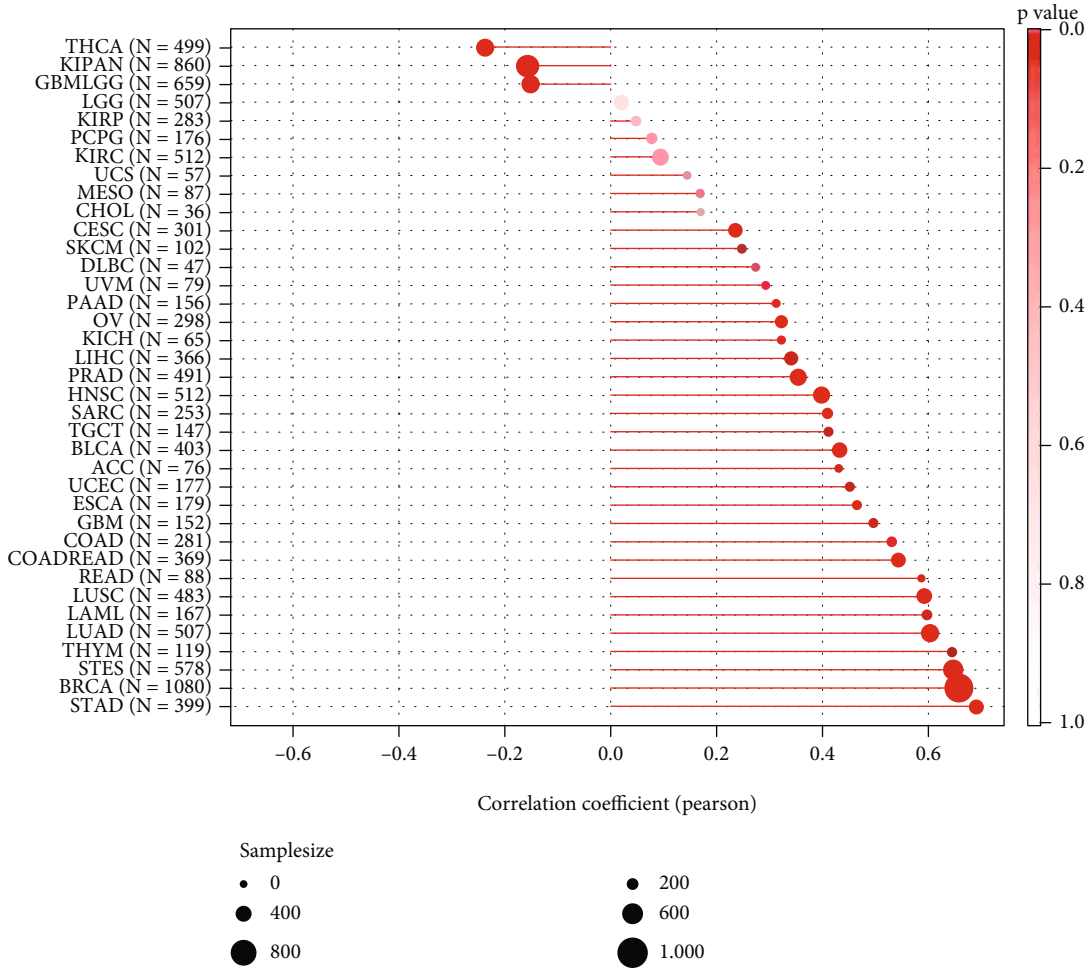

(b)

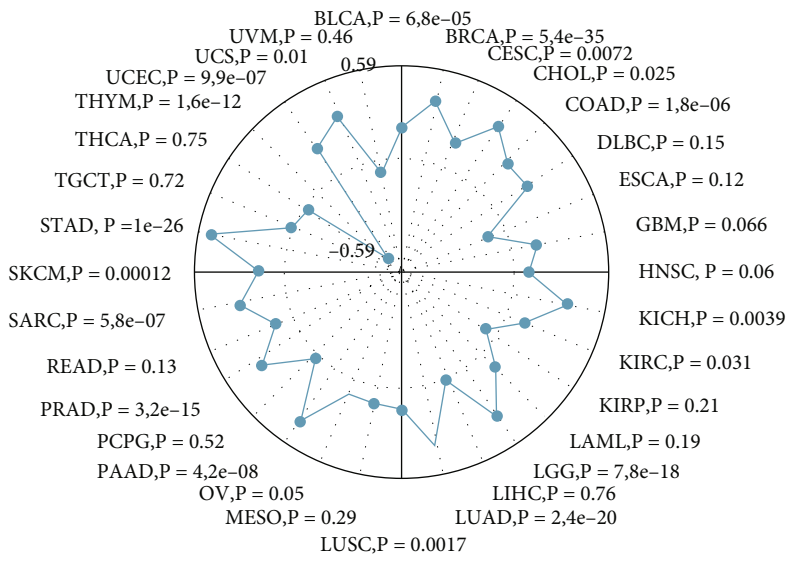

(c)

Figure 9: Continued.

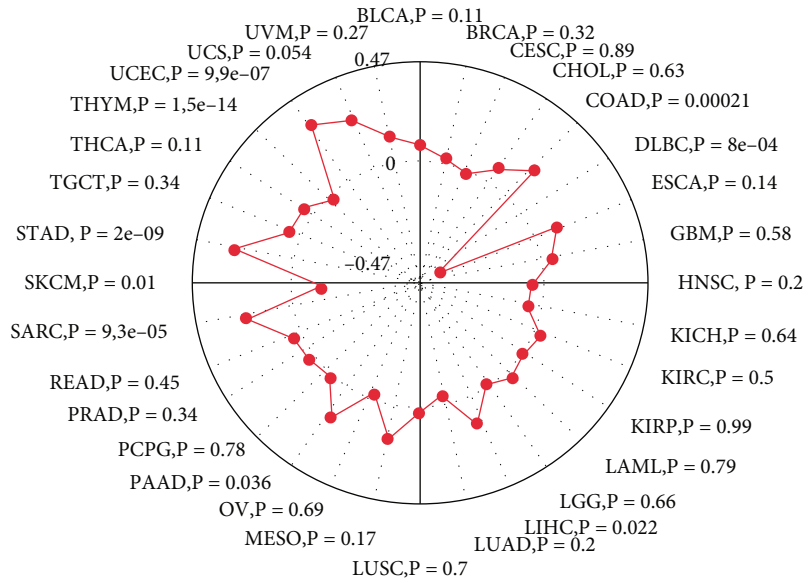

(d)

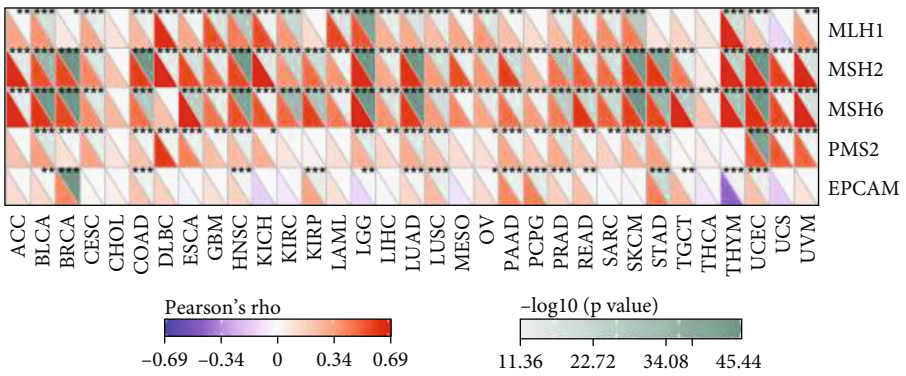

(e)

Figure 9: Continued.

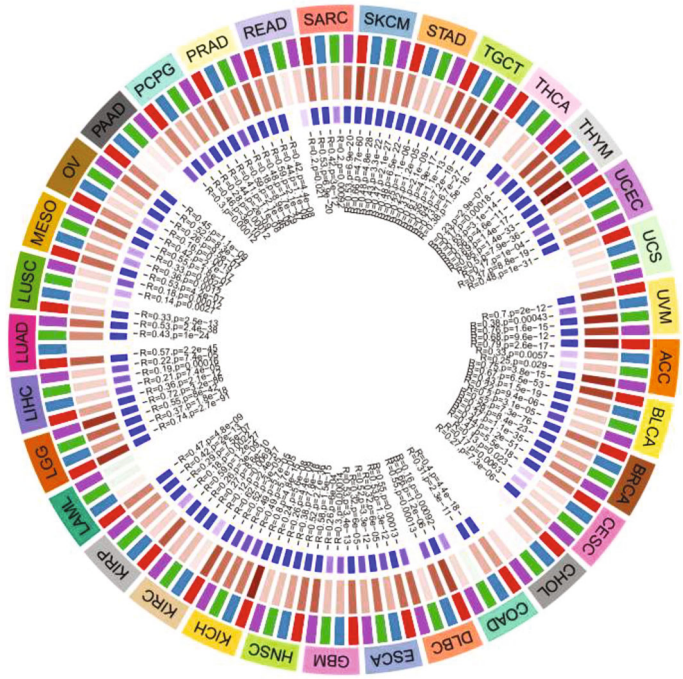

(f)

Figure 9: Correlations of CCNA2 with Stemness index, TMB, MSI, MMR, and DNA methyltransferases in pancancer. (a and b) Correlations of CCNA2 expression with DNAss and RNAss index in 33 cancer types. (c) Correlations of CCNA2 expression with TMB in 33 cancer types. (d) Correlations of CCNA2 expression with MSI in 33 cancer types. (e) Correlations of CCNA2 expression with expression levels of five MMR genes in 33 cancer types. (f) Correlations of CCNA2 expression with four DNA methyltransferases in 33 cancer types.

cg22219489, cg10002561, and cg07263562(Figure 4(a)); and RNA modification-related genes (including m1A, m5C, and m6A) were also significantly positive correlated with CCNA2 expression (Figure 4(b)). All those results indicated that CCNA2 expression might mainly regulated via RNA posttranscriptional modification.

3.5. The Association between CCNA2 mRNA Expression and Clinical Outcomes in Cancers. The association of CCNA2 expression with OS, PFI, DFI, and DSS in 33 cancer types in TCGA is shown in Figure 5(a), demonstrating a significant relationship between CCNA2 expression and prognosis in ACC, COAD, KICH, KIRC, KIRP, LGG, LIHC, LUAD, MESO, PAAD, PRAD, SARC, THYM, and UVM. Among them, the expression of CCNA2 was most significantly associated with the prognosis of KIRC. As shown in Figure 5(b), KIRC patients with high CCNA2 expression had a worse prognosis.

3.6. The Correlation of CCNA2 Expression and Canonical Tumorous Hallmarks. To explore the biological function of CCNA2 in different cancer types, we firstly utilized the GSVA to calculate the enrichment scores of 50 canonical tumor associated pathways in pancancer level; then, the correlation of those enrichment scores and CCNA2 expression was estimated. The results indicated that CCNA2 mainly positively regulated Myc, G2M checkpoint, and E2F_target pathways while negatively regulated xenobiotic metabolism, myogenesis, fatty acid metabolism, and bile acid metabolism in most cancer types (Figure 6(a)). In addition, CCNA2 participate nearly all the canonical hallmarks in THYM, which indicated that CCNA2 hold a leading role in the occurrence and development of THYM and could be treated as a promising treatment target. We also explored other aetiological pathways determining the clinical outcomes, including EMT, TGF, WNT, and autophagy pathways (Figure 6(b)). Interestingly, CCNA2 could activate those signals in most cancer types. CCNA2 might significantly activate EMT pathways in ACC, DLBC, LGG, MESO, PAAD, and THCA while inhibit EMT in THYM. Among TGF signal, CCNA2 could activate such a pathway in ACC, BLCA, CESC, DLBC, HNSC, KICH, LGG, LIHC, MESO, PAAD, SKCM, TGCT, and UCEC. In WNT signal, CCNA2 also stimulate this pathway in ACC, BLCA, CESC, DLBC, ESCA, KICH, LGG, LIHC, MESO, PAAD, TGCT, and UCEC. And CCNA2 might also participate in autophagy pathway especially in ACC, BLCA, CESC, DLBC, ESCA, GBM, HNSC, KICH, LIHC, MESO, PAAD, READ, TGCT, and UCEC.

3.7. The Biological Function of CCNA2 in ccRCC. Based on the character of "guilt of association" in the controlling networks in tumor, we use the transcriptome data collected from TCGA database, and the top 500 mRNAs mostly related to CCNA2 were retrieved via Spearman's correlation analysis. The correlation of those genes was presented in Figure 7(a). The enrichment function was performed based

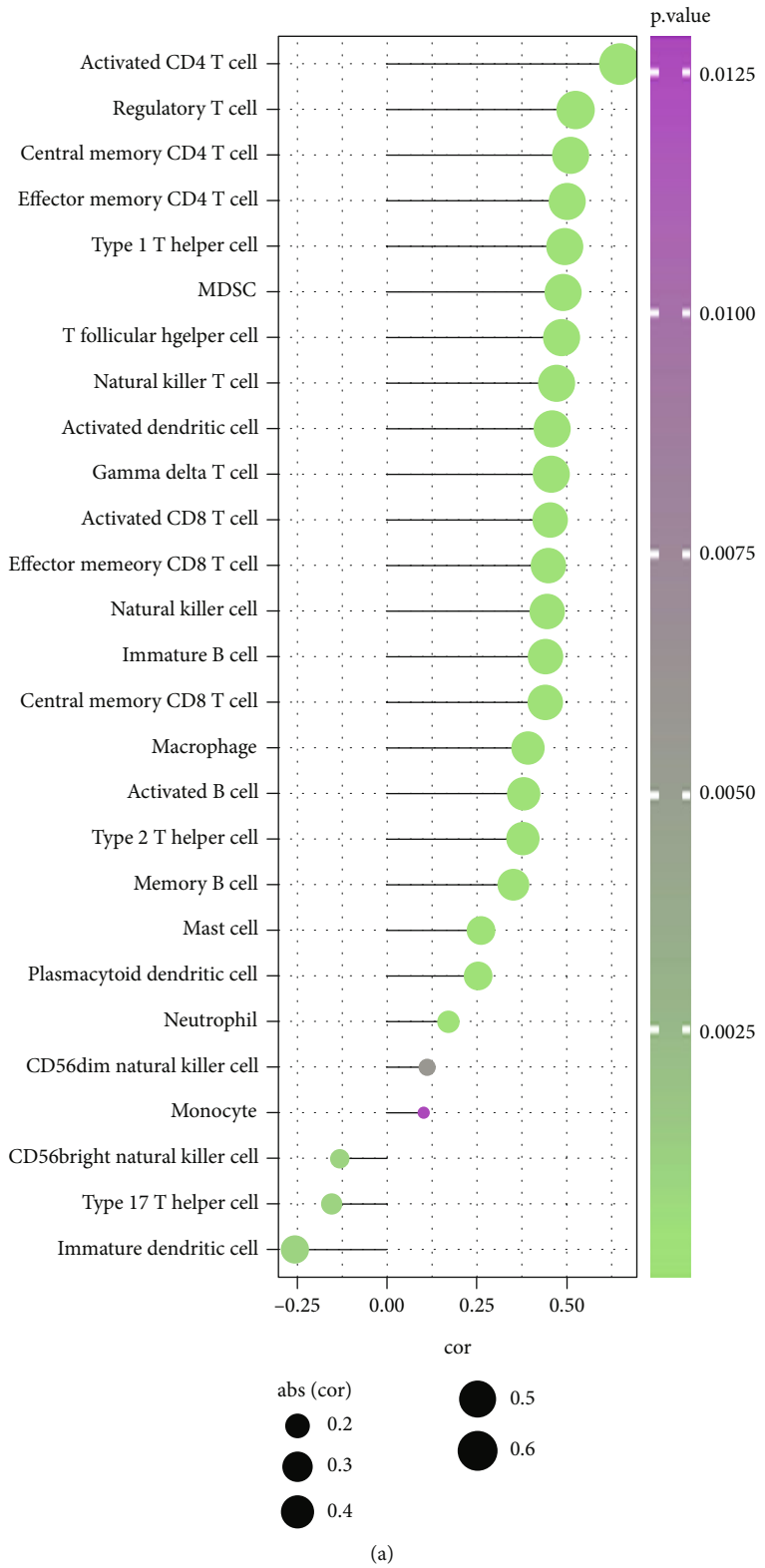

Figure 10: Continued.

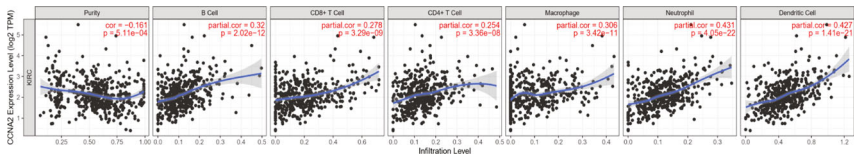

(b)

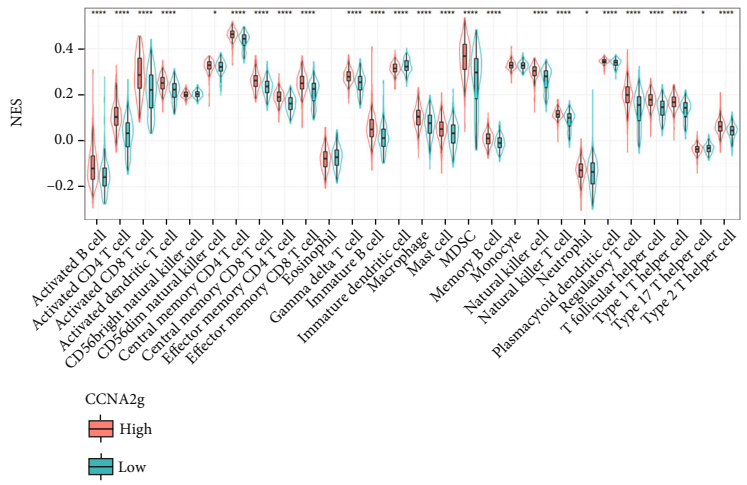

(c)

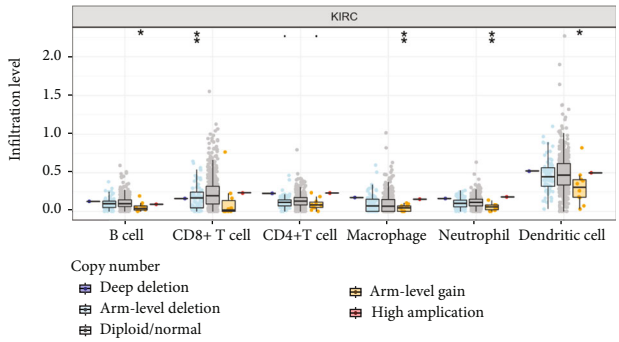

(d)

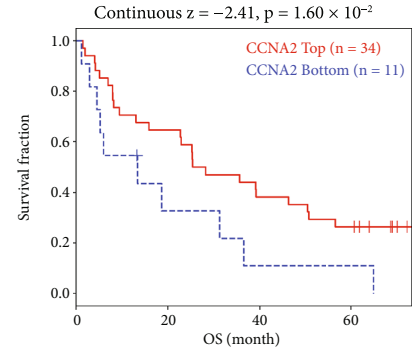

(e)

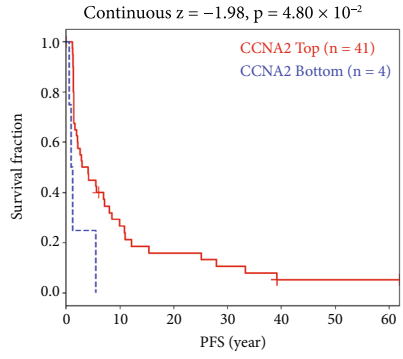

(f)

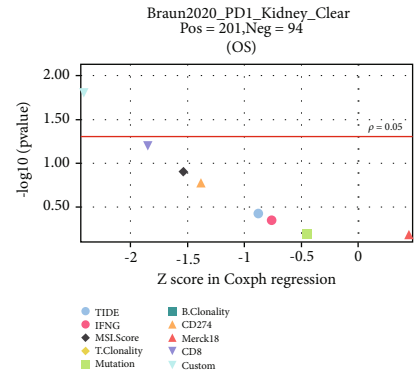

(g)

Figure 10: CCNA2 expression and mutation are related with immune infiltration in ccRCC. (a) Association between CCNA2 and NES of immune cells in ccRCC. (b) CCNA2 is correlated with multiple immune cell infiltration in TIMER database. (c) The different immune infiltration degrees in CCNA2 high- and CCNA2 low-expression groups in ccRCC. (d) Impact of CCNA2 mutation on immune cell infiltration. (e and f) Kaplan-Meier curves of survival ratios, OS, and PFS, as a measure of the immunotherapeutic response between ccRCC cohort with high- and low-expression level of CCNA2. (g) Difference of prognostic value including CCNA2 and other biomarkers or indexes. ∗ indicates $p < 0.05$, ∗∗ indicates $p < 0.01$, and ∗∗∗ indicates $p < 0.001$.

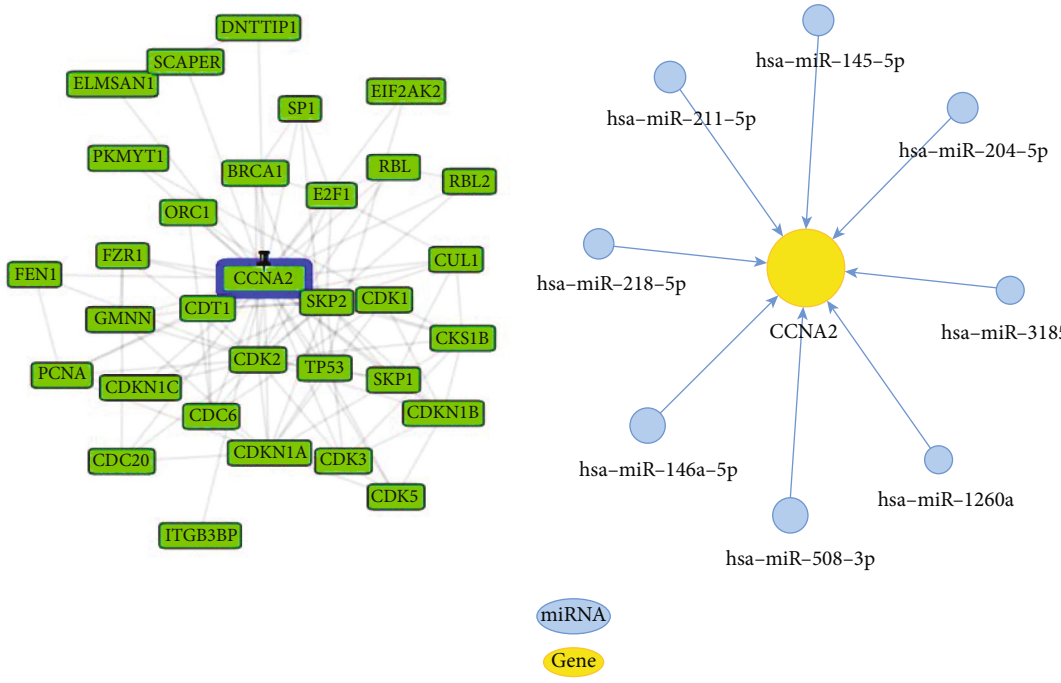

Figure 11: Continued.

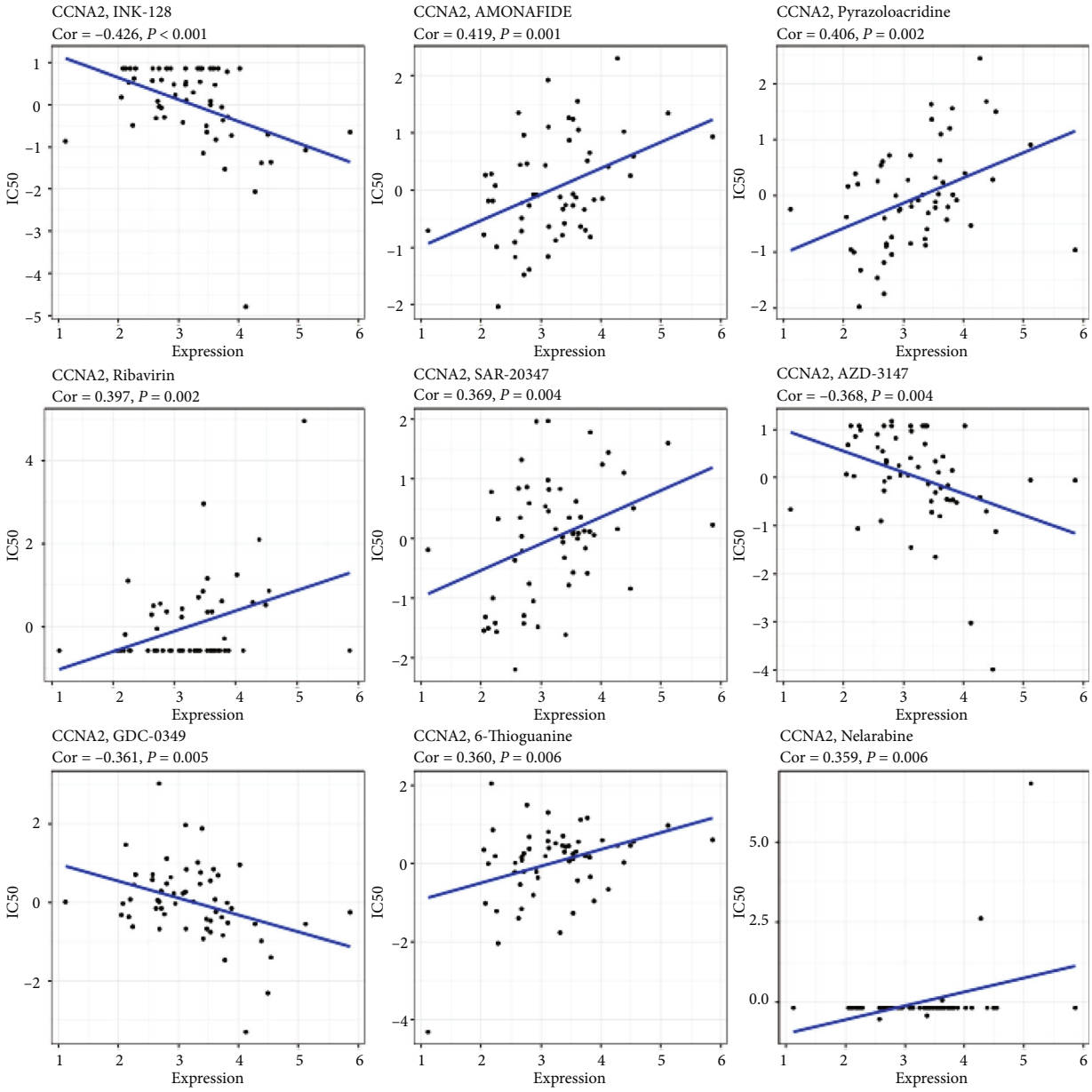

(c)

Figure 11: Continued.

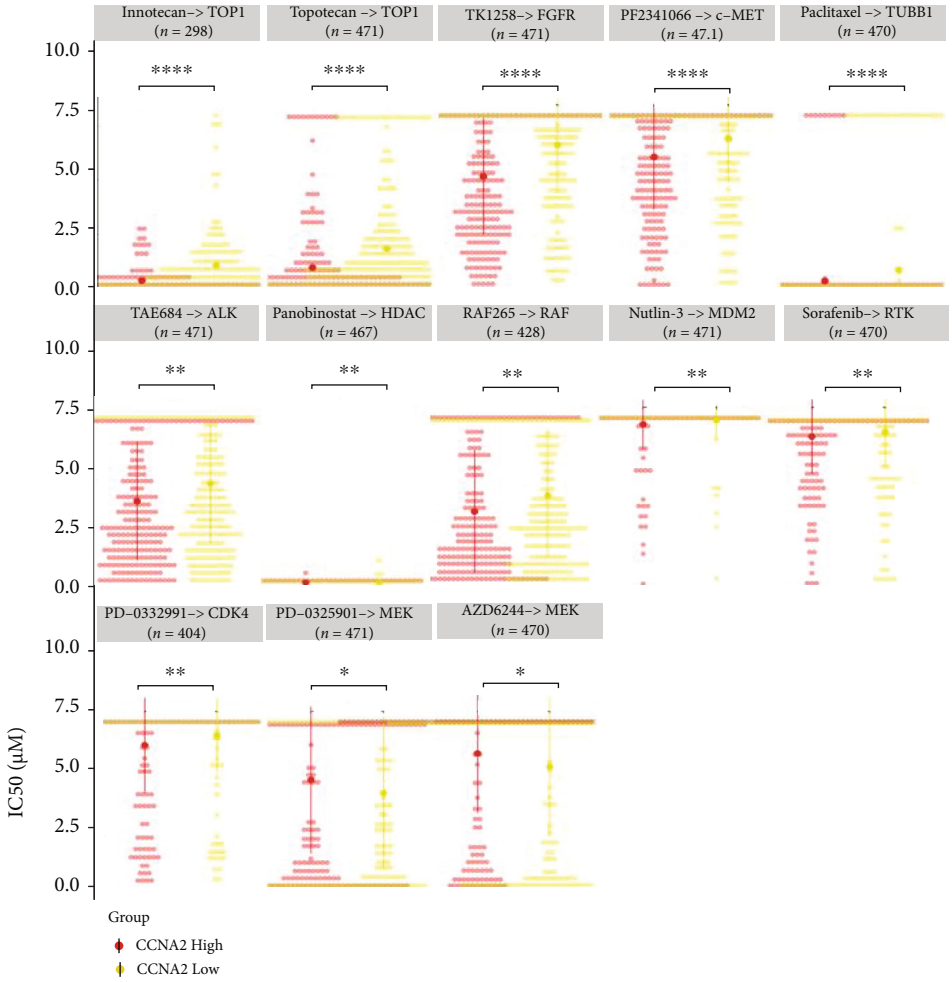

(d)

Figure 11: Correlation analysis between CCNA2 expression and drug sensitivity. (a) Network of functional gene partners of CCNA2 and mRNAs. (b) The ceRNA network of CCNA2 in cancers. (c) Correlation between CCNA2 and sensitivity of the top 9 anticancer drugs in CellMiner database. (d) Difference of drug sensitivity between CCNA2 high- and low-expression groups in GDSC database.

on those significantly related genes. GO analysis indicated that biological process module mainly enriched in organelle fission, nuclear division, chromosome segregation, mitotic nuclear division, and nuclear chromosome segregation; and the cellular component mainly involved in chromosomal region, spindle, and condensed chromosome; and molecular function centered on ATPase activity, tubulin binding, and microtubule binding (Figure 7(b)). KEGG results indicated that series of pathways related to CCNA2 in ccRCC, including cell cycle, DNA replication, homologous recombination, primary immunodeficiency, p53 signaling pathways, and natural killer cell-mediated cytotoxicity pathways (Figure 7(c)). GSEA further validated that CCNA2 could activate E2F targets, interferon alpha response, IL6-JAK-STAT signaling, interferon gamma response, Myc targets, G2M checkpoint, and inflammatory response while inhibit fatty acid metabolism and bile acid metabolism pathways in ccRCC (Figure 7(d)).

3.8. CCNA2 Is Associated with Tumor Evasion via Different Mechanisms by Infiltration Immune Cells. To explore the immune function of CCNA2 in pancancer types, the correlation between immune-regulated genes, immune checkpoint inhibitor genes, and CCNA2 expression was calculated firstly (Figures 8(a) and 8(b)). CCNA2 could positively regulate chemokine, chemokine receptors, MHC, immunoinhibitor, and immunostimulator in UVM, OV, THCA, KIPAN, KIRC, PAAD, GBM, LGG, DLBC, LIHC, PARD, BLCA, MESO, KIRP, and KICH while negatively regulate in THYM and TGCT. In addition, CCNA2 could positively regulate TAP1, TAP2, CD276, MICB, PVR, and ULBP1 in almost all the cancer types. We also found that CCNA2 could significantly regulate most immunomodulators in various cancer types, which indicated that CCNA2 could determine immunotherapy benefit of those cancer types. To detect whether CCNA2 could influence the process of immune cell infiltration degree in pancancer, we utilized three algorithms to evaluate the immune infiltration degree and calculate the correlation index between CCNA2 expression and immune cell infiltration degree. As Figure 8(c) indicated, CCNA2 was most significantly related with B cell, CD4 T cell, CD8 T cell, and DC cell in THCA, THYM, and KIRC. In addition,

CCNA2 was also significantly correlated with endothelial cell and macrophage cell in various cancers, especially in THYM (Figure 8(d)). Finally, CIBERSORT was employed to evaluate the immune cell infiltration degree in pancancer, which illustrated that CCNA2 could determine M1 macrophage in nearly all the cancer type, which further validated the results above (Figure 8(e)). All those results indicated that CCNA2 could regulate immune cell infiltration via different mechanism under various tumor microenvironments, and further experiment needs to decipher the heterogeneous mechanisms.

3.9. Correlation of CCNA2 Expression and Stemness, TMB, MSI, MMR, and DNA Methyltransferases. Since tumor is composed of heterogeneous cell clusters holding various degrees of functional and genetic heterogeneity, cancer stem cells (CSCs) are capable to maintain tumor survival via genetic and epigenetic factors, accelerate tumor metastasis, resist drug, and maintain tumor microenvironment [23]. Herein, we explored the association of CCNA2 expression and stemness including DNAss and RNAss. CCNA2 expression was significantly positively correlated with DNAss in GBM ($r > 0.5$) while negatively correlated in THYM ($r < -0.6$). In addition, CCNA2 expression was positively related to STAD, BRCA, STES, and THYM in RNAss ($r > 0.6$) (Figures 9(a) and 9(b)). TMB has been extensively studied and is suggested to play a vital role in tumor-responsiveness to immune checkpoint blockade [24]. MSI refers to the change in microsatellite sequence length caused by insertion or deletion mutation during DNA replication, which is often caused by MMR defects [25]. The relationship between CCNA2 expression and TMB and MSI in pancancer was also analyzed and displayed as a radar chart. As shown in Figures 9(c) and 9(d), CCNA2 high expression was positively correlated with TMB in BLCA, BRCA, CESC, CHOL, COAD, KICH, KIRC, LGG, LUAD, LUSC, PAAD, PRAD, SARC, SKCM, STAD, UCEC, and UCS and negatively correlated with THYM. CCNA2 high expression was also positively correlated with MSI in COAD, LIHC, PAAD, SARC, STAD, and UCEC but negatively correlated with MSI in DLBC and SKCM. MMR is a repair method that restores the normal nucleotide sequence in DNA molecules containing mismatched bases [26]. It is mainly used to correct mismatched base pairs on DNA double helix. The correlation between CCNA2 expression and MLH1, MSH2, MSH6, PMS2, and EPCAM is illuminated in Figure 9(e), showing that CCNA2 expression was positively correlated with MLH1 in 26 cancer types, with MSH2 and MSH6 in 31 cancer types, with PMS2 in 24 cancer types, and with EPCAM in 15 cancer types. On the contrary, there was a negative correlation between CCNA2 expression and EPCAM in LGG and THYM. DNA methylation is one of the important mechanisms of gene epigenetics, which is involved in the process of regulating gene expression and cell differentiation [27]. The relationship between four methyltransferases was analyzed, and the results showed that the expression level of CCNA2 was positively correlated with all four methyltransferases in 23 cancer types (Figure 9(f)). Meanwhile, it was not correlated with any of the four methyltransferases in UCS and CHOL or with DNMT2 in LUAD, PAAD, and THCA, DNMT3A in DLBC, LAML, PAAD, and READ, and DNMT3B in LAML and PAAD.

3.10. Relationship between CCNA2 and Tumor Immune Microenvironment in ccRCC. Renal cell carcinoma (RCC) is one of the earliest tumor types to use immunotherapy. As early as in the 1980s, interferon was used for advanced RCC [28]. With the emergence of immune checkpoint inhibitors, immunotherapy has ushered in a new era in the treatment field of RCC [29]. In view of the above positive results of CCNA2 analysis in KIRC, we comprehensively analyzed the relationship between CCNA2 expression and KIRC immune cell infiltration using multiple databases and found that CCNA2 expression was positively correlated with the infiltration of various immune cells, especially with T cell cells, which includes activated CD4 T cell, regulatory T cell, central memory CD4 T cell, effector memory CD4 T cell, type 1 T helper cell, MDSC, and T follicular he (Figure 10(a)). TIMER dataset indicated that CCNA2 expression was negatively correlated with tumor purity, thus enhancing infiltration of several immune cell types in ccRCC, including B cell, $CD8^+$ T cell, CD4+ T cell, macrophage, neutrophil, and dendritic cell (Figure 10(b)). ssGSEA analysis also identified that multiple immune cell types infiltrated differently between CCNA2-high and CCNA2-low subgroups (Figure 10(c)). Figure 10(d) shows the effect of CCNA2 mutation on the degree of immune cell infiltration. There were significant differences in the degree of cell infiltration between diploid/normal and arm-level gain in B cell, macrophage, neutrophil, and dendritic cell and between arm-level deletion and diploid/normal in CD8+ T cell. In addition, CCNA2 was a protective factor for OS and PFS in ccRCC immune checkpoint inhibitor cohort (Figures 10(e) and 10(f)); CCNA2 performed better in immune response rate than any other signature (including TIDE, MSI score, mutation, CD274, CD8, IFNG, T-Clonality, B-Clonality, and Merck18) in ccRCC cohort (Figure 10(g)).

3.11. Correlation Analysis between CCNA2 Expression and Drug Sensitivity. To decipher the functional partners of CCNA2 in cancers, gene network interaction analysis was performed in Figures 11(a) and 11(b), and the most relevant mRNA and miRNA were detected. As shown in Figure 11(a), CCNA2 expression was positively correlated with resistance of INK-128, AZD-3147, and GDC-0349, as well as with sensitivity of amonafide, pyrazoloacridine, ribavirin, SAR-20347, 6-thioguanine, and nelarabine. According to GDSC database, we found that high expression of CCNA2 could make cancer more sensitive to irinotecan (target at TOP1), topetecan (target at TOP1), TKI258 (target at FGFR), PF2341066 (target at c-MET), paclitaxel (target at TUBB1), TAE684 (target at ALK), panobinostat (target at HDAC), RAF265 (target at RAF), nutlin-3 (target at MDM2), sorafenib (target at RTK), and PD-032991 (target at CDK4) and resistant to AZD6244 (target at MEK) (Figure 11(b)).

4. Discussion

Our results indicated that CCNA2 is significantly related to the occurrence and progresses of various cancer types. Prior studies also reported functional relation between CCNA2 and clinical diseases, especially tumors [30]. Whether CCNA2 involves in the tumor microenvironment and pathogenesis of different tumors through common or specific mechanisms remains unclear. Our study illustrated the correlation of expression level and genomic alternation of CCNA2 with tumor staging, progression, tumor immunity, and drug sensitivity across pancancer and subtypes, especially in ccRCC.

Based on the genomic data collected from a variety of cancer types and a profound understanding about the biology and pathology of pancancer, TCGA has developed a series of therapeutic strategies for the treatment of various cancer types [14]. CCNA2 is a cyclin present in mammals and promotes S-phase progression and G2-M phase transition by binding CDK in the mitotic cell cycle [31]. CCNA2 is located on chromosome 4 and is encoded by human CCNA2, belonging to the highly conserved cyclin family. It is reported to be correlated with cytoskeleton dynamics and cell motility [32]. It was found in our study that CCNA2 was involved in tumor proliferation, invasion, and differentiation, thus could be treated as a novel and promising diagnostic also therapeutic targets for cancers.

In this study, we first disclosed that the mRNA expression of CCNA2 was upregulated in ACC, BLCA, BRCA, CESC, CHOL, COAD, ESCA, GBM, HNSC, KICH, KIRC, KRIP, LGG, LIHC, LUAD, LUSC, OV, PAAD, PRAD, READ, SKCM, STAD, TGCT, THCA, UCEC, and UCS cancer tissues vs. normal tissues by using TCGA, which indicated that CCNA2 might be an oncogenic molecule in tumorigenesis. Based on the IHC results from HPA database and SMMU cohort, we validate that CCNA2 expression was more pronounced in the corresponding tumor tissues vs. normal kidney, intestine, liver, lung, breast, prostate, and brain tissues. Furthermore, based on survival curves, we demonstrated CCNA2 mRNA expression as a dependable diagnostic factor, implying that CCNA2 is a possibly promising biomarker for pancancer diagnosis. More importantly, CCNA2 mRNA expression was significantly correlated with the patient prognosis in ACC, COAD, KICH, KIRC, KIRP, LGG, LIHC, LUAD, MESO, PAAD, PRAD, SARC, THYM, and UVM, suggesting that CCNA2 plays an important role in the progression of pancancer, especially KIRC patients with high expression of CCNA2 holding a worse prognosis. Our results are consistent with previous studies and clinical trials, which concluded that CCNA2 was highly expressed in multiple cancers and patients with high CCNA2 expression owning high-risk features. Gao et al. reported that CCNA2 is highly expressed in breast cancer and could be treated as a power predicative marker in BLCA patients [33]. Gan et al. also found that CCNA2 is overexpressed and acts as a novel biomarker in regulating the growth and apoptosis in colorectal cancer [34].

To further decipher the biological role of CCNA2 in the cancers and ccRCC, several enrichment function algorithms were implied. KEGG pathway results were primarily enriched in oocyte meiosis, cell cycle, pyrimidine metabolism, asthma, alpha linolenic acid metabolism, arachidonic acid metabolism, and linoleic acid metabolism. Meanwhile, GSEA results suggested that CCNA2 may be correlated with coagulation, KRAS signaling, myogenesis, bile acid metabolism, mtorc1 signaling, E2F targets, and G2M checkpoint. Ruan et al. found that CCNA2 could facilitate epithelial-to-mesenchymal transition via integrin $\alpha v\beta 3$ signaling in non-small-cell lung carcinoma [35]. CCNA2 could also act as a significant downstream facilitating tumor progression. Chen et al. suggested that ROBO1 could promote the development of pancreatic cancer via CCNA2/CDK axis [36]. Interestingly, our study illustrated that CCNA2 could enhance the development of ccRCC via several immune-related signals, including immunodeficiency, natural killer cell-mediated cytotoxicity pathway, and IL6-JAK-STAT3 pathways. Further study is required to clarify the detailed mechanism underlying the role of CCNA2 in impacting those signaling pathways in cancers and ccRCC.

TMB, MSI, and neoantigen indexes are two widely studied biomarkers which may have a profound impact on the response to tumor immunotherapy and patient survival [37]. However, those indexes only performed well in several types of tumors and hold high test costs. Consequently, it is urgent to discover new and economic biomarker for predicting immune therapy response. The results of our study showed that upregulation of CCNA2 mRNA was significantly and positively correlated with TMB, MSI, and neoantigen indexes in BLCA, BRCA, CESC, CHOL, COAD, KICH, KIRC, LGG, LUAD, LUSC, PAAD, PRAD, SARC, SKCM, STAD, UCEC, and UCS. The levels of DNA methylation and MMR state in tumors have increasingly been recognized as a promising index for evaluating efficacy of target and immune therapy [26, 38]. The current study also found that CCNA2 expression was positively correlated with DNA methylation and MMR in most cancers, which suggested that CCNA2 might influence DNA methylation level or MMR state, thus determining the clinical outcomes of cancer patients [39]. Some other interesting and relevant discoveries include the significant correlation between CCNA2 expression and MLH1, MSH2, MSH6, PMS2, and EPCAM, suggesting that CCNA2 may be involved in tumor-related developmental processes including signaling, migration, and proliferation [40, 41]. Zhou et al. found that CCNA2 is a potential diagnostic and prognostic biomarker for LUAD, and CCNA2 expression positively correlated with immunity therapy efficiency in LUAD [42]. Chen et al. also confirmed that CCNA2 is involved in hypoxia signature affecting the clinical outcomes and immune microenvironment of ACC [43]. To date, only several studies assessed the immune role of CCNA2 in cancers. Our findings may shed lights on the molecular mechanisms underlying tumor progression and metastasis and provide useful clues for seeking strategies for the clinical treatment and prognostic prediction of cancers.

TME and tumor evasion are correlated with cancer prognoses and therapeutic [8]. There are two major mechanisms of immune evasion until now, which are consisted of

dysfunctional T cell phenotypes and T cell exclusion [7, 44]. However, considering the complex compositions and communication of TME, it is necessary to identify the key molecules in TME [9]. Our study indicated that CCNA2 expression was significantly and positively correlated with the level of CD 4 T+ cell memory cells and M0 and M1 macrophage infiltration across various cancer types. Interestingly, CCNA2 is found significantly positively correlated with immune therapy response in BLCA, BRCA, KIRC, LGG, LUAD, PRAD, and THCA while negatively correlated with ACC, GBM, and TGCT. Wang et al. found that CCNA2 functions as a potential immune therapy maker in BLCA [45]; Xu et al. also confirmed that CCNA2 could activate macrophages, thus enhancing tumor immunity [46]. Also, CCNA2 expression was positively correlated with ImmuneScore in THCA and KIRC and negatively correlated with ImmuneScore in BRCA, LUSC, and GBM. Additionally, we found that CCNA2 was significantly correlated with immune checkpoint-related genes in KICH, KIRC, and THCA. Considering with complex and heterogeneity of TME and lack of robust immune biomarkers in KICH, KIRC, and THCA, CCNA2 seemed to be new indicator for those cancers. In a word, all these findings suggest that CCNA2 might play a significant role in TME and could regulate several key immune cell functions, though further study is required to verify these conclusions.

With the rapid development of immunotherapy for ccRCC in recent years, resistance, increasing recurrence rates, and side effects have surfaced, and there are indications that new biomarkers or therapy target for predicting efficacy and prognosis are in urgent need of discovery [47]. Although ccRCC is deemed as immune cell infiltration-high tumor, it is also notorious for immune dysfunction and depletion [48–50]. It is urgent to comprehensively analyze the mechanism of this abrogated immunity phenomenon in ccRCC. We utilized correlation analysis to determine the influence of CCNA2 expression in a series of immune cells in ccRCC. Interestingly, our results found that CCNA2 expression significantly related most of immune cell infiltration in ccRCC, among which CCNA2 positively correlated with several T cell types including activated $CD4^+$ T cell, regulatory T cells, central memory $CD4^+$ T cells, and effector $CD4^+$ T cell while negatively correlated with immature dendritic cell and Type17 T cells. The results from TIMER database further validated those result. Datasets from Braun et al. research further proved that CCNA2 could indicate a robust prognosis in CCNA2 high-expressed group who received immune checkpoint inhibitors therapy and thus CCNA2 could work as well-performed indicator for ICB sensitivity compared with other reported makers or signatures [51]. All results remind us of that CCNA2 as a valid and reliable evaluation biomarker with the utility for easy application in ccRCC patient clinical management.

During the past decades, chemotherapy remains the mainline treatment choice for later stage patients, while drug resistance is responsible for over 80% deaths in cancer patients receiving chemotherapy or target dugs [4, 52]. Considering such phenomenon and the burden to develop new drugs, our study also systematically analyzed the correlation of CCNA2 expression and drug sensitivity to explore the potential drug target at CCNA2. We found that CCNA2 expression was positively related to amonafide, pyrazoloacridine, ribavirin, SAR-20347, and 6-thioguanine. Amonafide shows a potential therapeutic effect on breast cancer, acute myeloid leukemia, and melanoma [53–55]. Pyrazoloacridine holds significant antitumor effect on several cancer types including breast cancer, neuroblastoma, and glioma [56–58]. Hence, these candidate molecular drugs might also possess potential efficacy for CCNA2 highly expressed cancer types.

However, there are still some limitations in our study. Firstly, our study was mainly based on bioinformatics analysis, which implies that there were few experiments to confirm our statements, which need further systematic experiments to validate those results. Secondly, we only perform IHC and RT-qPCR to detect the different expression level on ccRCC patients, which is urgent to decipher the detailed role of CCNA2 in ccRCC patients.

5. Conclusion

To sum up, our results suggest that CCNA2 expression was upregulated in pancancer tissues including RCC vs. normal tissues. In addition, high CCNA2 expression was correlated with poor clinicopathological features in various cancers, especially for ccRCC. CCNA2 might play pivotal pathogenic roles in the immuneoncology context of the TME. The strong association of CCNA2 with tumor immunity suggests that CCNA2 may prove to be a promising therapeutic target for immunotherapy.

Data Availability

The data used to support the findings of this study have been deposited in the TCGA repository (https://portal.gdc.cancer.gov/).

Conflicts of Interest

The authors have declared that no competing interest exists.

Authors' Contributions

Aimin Jiang, Ye Zhou, Wenliang Gong, and Xiao Pan have contributed equally to this work. Xiao Fang, Le Qu, and Linhui Wang conceptualized and designed this study. Xinxin Gan, Zhenjie Wu, and Bing Liu wrote the first draft of the manuscript. All authors contributed to the article and approved the submitted version. Aimin Jiang, Ye Zhou, Wenliang Gong, and Xin Pan have contributed equally to this work and share first authorship.

Acknowledgments

We greatly appreciate the patients and investigators who participated in the corresponding medical project for providing data. We thank Dr. Jianming Zeng (University of Macau) and all the members of his bioinformatics team,

biotrainee and Sangerbox, for generously sharing their experience and codes. This study was funded by the National Natural Science Foundation of China (82072812 to LH.W and nos. 81772740 and 82173345 to L.Q.) and Foundation for Distinguished Youths of Jiangsu Province (no. BK20200006 to L.Q.).

Supplementary Materials

Association between CCNA2 expression and tumor stage in pancancer. *(Supplementary Materials)*

References

[1] H. Sung, J. Ferlay, R. L. Siegel et al., "Global cancer statistics 2020: GLOBOCAN estimates of incidence and mortality worldwide for 36 cancers in 185 countries," *CA: a Cancer Journal for Clinicians*, vol. 71, no. 3, pp. 209–249, 2021.

[2] M. A. Dawson and T. Kouzarides, "Cancer epigenetics: from mechanism to therapy," *Cell*, vol. 150, no. 1, pp. 12–27, 2012.

[3] R. L. Siegel, K. D. Miller, H. E. Fuchs, and A. Jemal, "Cancer statistics, 2021," *CA: a Cancer Journal for Clinicians*, vol. 71, no. 1, pp. 7–33, 2021.

[4] C. Holohan, S. van Schaeybroeck, D. B. Longley, and P. G. Johnston, "Cancer drug resistance: an evolving paradigm," *Nature Reviews. Cancer*, vol. 13, no. 10, pp. 714–726, 2013.

[5] A. R. Moore, S. C. Rosenberg, F. McCormick, and S. Malek, "RAS-targeted therapies: is the undruggable drugged?," *Nature Reviews. Drug Discovery*, vol. 19, no. 8, pp. 533–552, 2020.

[6] D. M. Pardoll, "The blockade of immune checkpoints in cancer immunotherapy," *Nature Reviews. Cancer*, vol. 12, no. 4, pp. 252–264, 2012.

[7] Y. Yang, "Cancer immunotherapy: harnessing the immune system to battle cancer," *The Journal of Clinical Investigation*, vol. 125, no. 9, pp. 3335–3337, 2015.

[8] Y. Jiang and H. Zhan, "Communication between EMT and PD-L1 signaling: new insights into tumor immune evasion," *Cancer Letters*, vol. 468, pp. 72–81, 2020.

[9] X. Lei, Y. Lei, J. K. Li et al., "Immune cells within the tumor microenvironment: biological functions and roles in cancer immunotherapy," *Cancer Letters*, vol. 470, pp. 126–133, 2020.

[10] J. Li, W.-P. Qian, and Q.-Y. Sun, "Cyclins regulating oocyte meiotic cell cycle progression†," *Biology of Reproduction*, vol. 101, no. 5, pp. 878–881, 2019.

[11] S. Zhang, T. Tischer, and D. Barford, "Cyclin A2 degradation during the spindle assembly checkpoint requires multiple binding modes to the APC/C," *Nature Communications*, vol. 10, no. 1, p. 3863, 2019.

[12] N. Bendris, N. Arsic, B. Lemmers, and J. M. Blanchard, "Cyclin A2, Rho GTPases and EMT," *Small GTPases*, vol. 3, no. 4, pp. 225–228, 2012.

[13] M. Fischer, M. Quaas, L. Steiner, and K. Engeland, "The p53-p21-DREAM-CDE/CHR pathway regulates G2/M cell cycle genes," *Nucleic Acids Research*, vol. 44, no. 1, pp. 164–174, 2016.

[14] K. Tomczak, P. Czerwińska, and M. Wiznerowicz, "The Cancer Genome Atlas (TCGA): an immeasurable source of knowledge," *Contemporary Oncology (Poznan, Poland)*, vol. 1A, no. 1A, pp. 68–77, 2015.

[15] A. Blum, P. Wang, and J. C. Zenklusen, "SnapShot: TCGA-analyzed tumors," *Cell*, vol. 173, no. 2, p. 530, 2018.

[16] D. R. Rhodes, J. Yu, K. Shanker et al., "ONCOMINE: A Cancer Microarray Database and Integrated Data-Mining Platform," *Neoplasia (New York, N.Y.)*, vol. 6, pp. 1–6, 2004.

[17] G. Yu, L. G. Wang, Y. Han, and Q. Y. He, "clusterProfiler: an R package for comparing biological themes among gene clusters," *Omics: A Journal of Integrative Biology*, vol. 16, no. 5, pp. 284–287, 2012.

[18] T. Cokelaer, E. Chen, F. Iorio et al., "GDSCTools for mining pharmacogenomic interactions in cancer," *Bioinformatics (Oxford, England)*, vol. 34, no. 7, pp. 1226–1228, 2018.

[19] B. Chen, M. S. Khodadoust, C. L. Liu, A. M. Newman, and A. A. Alizadeh, "Profiling tumor infiltrating immune cells with CIBERSORT," *Methods in Molecular Biology (Clifton, N.J.)*, vol. 1711, pp. 243–259, 2018.

[20] T. Li, J. Fan, B. Wang et al., "TIMER: a web server for comprehensive analysis of tumor-infiltrating immune cells," *Cancer Research*, vol. 77, no. 21, pp. e108–e110, 2017.

[21] A. Luna, F. Elloumi, S. Varma et al., "CellMiner Cross-Database (CellMinerCDB) version 1.2: exploration of patient-derived cancer cell line pharmacogenomics," *Nucleic Acids Research*, vol. 49, no. D1, pp. D1083–D1093, 2021.

[22] J. Barretina, G. Caponigro, N. Stransky et al., "The Cancer Cell Line Encyclopedia enables predictive modelling of anticancer drug sensitivity," *Nature*, vol. 483, no. 7391, pp. 603–607, 2012.

[23] C. Tang, B. T. Ang, and S. Pervaiz, "Cancer stem cell: target for anti-cancer therapy," *FASEB Journal*, vol. 21, no. 14, pp. 3777–3785, 2007.

[24] D.-W. Lee, S. W. Han, J. M. Bae et al., "Tumor mutation burden and prognosis in patients with colorectal cancer treated with adjuvant fluoropyrimidine and oxaliplatin," *Clinical Cancer Research*, vol. 25, no. 20, pp. 6141–6147, 2019.

[25] A. Rizzo, A. D. Ricci, and G. Brandi, "PD-L1, TMB, MSI, and other predictors of response to immune checkpoint inhibitors in biliary tract cancer," *Cancers*, vol. 13, no. 3, p. 558, 2021.

[26] M. Baretti and D. T. Le, "DNA mismatch repair in cancer," *Pharmacology & Therapeutics*, vol. 189, pp. 45–62, 2018.

[27] A. Koch, S. C. Joosten, Z. Feng et al., "Analysis of DNA methylation in cancer: location revisited," *Nature Reviews. Clinical Oncology*, vol. 15, no. 7, pp. 459–466, 2018.

[28] K. Geissler, P. Fornara, C. Lautenschläger, H. J. Holzhausen, B. Seliger, and D. Riemann, "Immune signature of tumor infiltrating immune cells in renal cancer," *Oncoimmunology*, vol. 4, no. 1, article e985082, 2015.

[29] U. Capitanio and F. Montorsi, "Renal cancer," *Lancet (London, England)*, vol. 387, no. 10021, pp. 894–906, 2016.

[30] Q. Bayard, L. Meunier, C. Peneau et al., "Cyclin A2/E1 activation defines a hepatocellular carcinoma subclass with a rearrangement signature of replication stress," *Nature Communications*, vol. 9, no. 1, p. 5235, 2018.

[31] J. Y. Chotiner, D. J. Wolgemuth, and P. J. Wang, "Functions of cyclins and CDKs in mammalian gametogenesis†," *Biology of Reproduction*, vol. 101, no. 3, pp. 591–601, 2019.

[32] N. Bendris, A. Loukil, C. Cheung et al., "Cyclin A2: a genuine cell cycle regulator?," *Biomolecular Concepts*, vol. 3, no. 6, pp. 535–543, 2012.

[33] T. Gao, Y. Han, L. Yu, S. Ao, Z. Li, and J. Ji, "CCNA2 is a prognostic biomarker for ER+ breast cancer and tamoxifen resistance," *PLoS One*, vol. 9, no. 3, article e91771, 2014.

[34] Y. Gan, Y. Li, T. Li, G. Shu, and G. Yin, "CCNA2 acts as a novel biomarker in regulating the growth and apoptosis of colorectal

cancer," *Cancer Management and Research*, vol. Volume 10, pp. 5113–5124, 2018.

[35] J. S. Ruan, H. Zhou, L. Yang, L. Wang, Z. S. Jiang, and S. M. Wang, "CCNA2 facilitates epithelial-to-mesenchymal transition via the integrin $\alpha v\beta 3$ signaling in NSCLC," *International Journal of Clinical and Experimental Pathology*, vol. 10, no. 8, pp. 8324–8333, 2017.

[36] Q. Chen, P. Shen, W. L. Ge et al., "Roundabout homolog 1 inhibits proliferation via the YY1-ROBO1-CCNA2-CDK2 axis in human pancreatic cancer," *Oncogene*, vol. 40, no. 15, pp. 2772–2784, 2021.

[37] C. Luchini, F. Bibeau, M. J. L. Ligtenberg et al., "ESMO recommendations on microsatellite instability testing for immunotherapy in cancer, and its relationship with PD-1/PD-L1 expression and tumour mutational burden: a systematic review-based approach," *Annals of Oncology: Official Journal of the European Society for Medical Oncology*, vol. 30, no. 8, pp. 1232–1243, 2019.

[38] Z. Li, A. H. Pearlman, and P. Hsieh, "DNA mismatch repair and the DNA damage response," *DNA Repair*, vol. 38, pp. 94–101, 2016.

[39] R. Ijsselsteijn, J. G. Jansen, and N. de Wind, "DNA mismatch repair-dependent DNA damage responses and cancer," *DNA Repair*, vol. 93, article 102923, 2020.

[40] L. Chen, G. Chen, X. Zheng, and Y. Chen, "Expression status of four mismatch repair proteins in patients with colorectal cancer: clinical significance in 1238 cases," *International Journal of Clinical and Experimental Pathology*, vol. 12, no. 10, pp. 3685–3699, 2019.

[41] L. Huang, Y. Yang, F. Yang et al., "Functions of EpCAM in physiological processes and diseases (review)," *International Journal of Molecular Medicine*, vol. 42, no. 4, pp. 1771–1785, 2018.

[42] C. Zhou, Y. Wang, L. Lei, M. H. Ji, J. J. Yang, and H. Xia, "Identifying common genes related to platelet and immunity for lung adenocarcinoma prognosis prediction," *Frontiers in Molecular Biosciences*, vol. 7, article 563142, 2020.

[43] X. Chen, L. Yan, Y. Lu et al., "A hypoxia signature for predicting prognosis and tumor immune microenvironment in adrenocortical carcinoma," *Journal of Oncology*, vol. 2021, Article ID 2298973, 11 pages, 2021.

[44] E. J. Wherry, "T cell exhaustion," *Nature Immunology*, vol. 12, no. 6, pp. 492–499, 2011.

[45] Y. Wang, Q. Zhong, Z. Li, Z. Lin, H. Chen, and P. Wang, "Integrated profiling identifies CCNA2 as a potential biomarker of immunotherapy in breast cancer," *Oncotargets and Therapy*, vol. Volume 14, pp. 2433–2448, 2021.

[46] Y. Xu, G. Wu, J. Li et al., "Screening and identification of key biomarkers for bladder cancer: a study based on TCGA and GEO data," *BioMed Research International*, vol. 2020, Article ID 8283401, 20 pages, 2020.

[47] N. Chowdhury and C. G. Drake, "Kidney cancer: an overview of current therapeutic approaches," *The Urologic Clinics of North America*, vol. 47, no. 4, pp. 419–431, 2020.

[48] P. C. Barata and B. I. Rini, "Treatment of renal cell carcinoma: current status and future directions," *CA: a Cancer Journal for Clinicians*, vol. 67, no. 6, pp. 507–524, 2017.

[49] A. Sánchez-Gastaldo, E. Kempf, A. González del Alba, and I. Duran, "Systemic treatment of renal cell cancer: a comprehensive review," *Cancer Treatment Reviews*, vol. 60, pp. 77–89, 2017.

[50] A. Jiang, J. Meng, W. Gong et al., "Elevated SNRPA1, as a promising predictor reflecting severe clinical outcome via effecting tumor immunity for ccRCC, is related to cell invasion, metastasis, and sunitinib sensitivity," *Frontiers in Immunology*, vol. 13, article 842069, 2022.

[51] D. A. Braun, Y. Hou, Z. Bakouny et al., "Interplay of somatic alterations and immune infiltration modulates response to PD-1 blockade in advanced clear cell renal cell carcinoma," *Nature Medicine*, vol. 26, no. 6, pp. 909–918, 2020.

[52] A. M. Tsimberidou, E. Fountzilas, M. Nikanjam, and R. Kurzrock, "Review of precision cancer medicine: evolution of the treatment paradigm," *Cancer Treatment Reviews*, vol. 86, article 102019, 2020.

[53] S. L. Allen and A. S. Lundberg, "Amonafide: a potential role in treating acute myeloid leukemia," *Expert Opinion on Investigational Drugs*, vol. 20, no. 7, pp. 995–1003, 2011.

[54] Y. Gilad, H. Tuchinsky, G. Ben-David et al., "Discovery of potent molecular chimera (CM358) to treat human metastatic melanoma," *European Journal of Medicinal Chemistry*, vol. 138, pp. 602–615, 2017.

[55] J. Zhao, M. Lu, H. Lai et al., "Delivery of amonafide from fructose-coated nanodiamonds by oxime ligation for the treatment of human breast cancer," *Biomacromolecules*, vol. 19, no. 2, pp. 481–489, 2018.

[56] N. Keshelava, D. Tsao-Wei, and C. P. Reynolds, "Pyrazoloacridine is active in multidrug-resistant neuroblastoma cell lines with nonfunctional p53," *Clinical Cancer Research: An Official Journal of the American Association for Cancer Research*, vol. 9, no. 9, pp. 3492–3502, 2003.

[57] E. Galanis, J. C. Buckner, M. J. Maurer et al., "Phase I/II trial of pyrazoloacridine and carboplatin in patients with recurrent glioma: a North Central Cancer Treatment Group trial," *Investigational New Drugs*, vol. 23, no. 5, pp. 495–503, 2005.

[58] B. Ramaswamy, E. Mrozek, J. P. Kuebler, T. Bekaii-Saab, and E. H. Kraut, "Phase II trial of pyrazoloacridine (NSC#366140) in patients with metastatic breast cancer," *Investigational New Drugs*, vol. 29, no. 2, pp. 347–351, 2011.

Hindawi
Oxidative Medicine and Cellular Longevity
Volume 2022, Article ID 1863098, 19 pages
https://doi.org/10.1155/2022/1863098

Research Article

Human Papillomavirus Type 16 Early Protein E7 Activates Autophagy through Inhibition of Dual-Specificity Phosphatase 5

Chunting Hua,[1] **Qiaoli Zheng**,[1] **Jiang Zhu**,[1] **Siji Chen**,[1] **Yinjing Song**,[1] **Stijn van der Veen**,[1,2] **and Hao Cheng**[1]

[1]*Department of Dermatology, Sir Run Run Shaw Hospital, School of Medicine, Zhejiang University, Hangzhou, China*
[2]*Department of Microbiology, Collaborative Innovation Center for Diagnosis and Treatment of Infectious Diseases, School of Medicine, Zhejiang University, Hangzhou, China*

Correspondence should be addressed to Stijn van der Veen; stijnvanderveen@zju.edu.cn and Hao Cheng; chenghao1@zju.edu.cn

Received 25 November 2021; Revised 30 January 2022; Accepted 16 February 2022; Published 10 March 2022

Academic Editor: Natalia Krasteva

Consistent high-risk human papillomavirus (HPV) infection leads to various malignant cancers. Autophagy can promote cancer progression by helping cancer cells survive under stress or induce oncogenic effects when mutations or abnormalities occur. Mitogen activated protein kinases (MAPKs) can transduce various external or intrinsic stimuli into cellular responses, including autophagy, and dual-specificity phosphates (DUSPs) contribute to the direct regulation of MAPK activities. Previously, we showed that expression of DUSP5 was repressed in HPV16 E7-expressing normal human epidermal keratinocytes (NHEKs). Here we show that clinical HPV16 E7-positive precancerous and cancerous tissues also demonstrate low DUSP5 levels compared with control tissues, indicating that the inverse correlation between HPV16 E7 and DUSP5 is clinically relevant. We furthermore investigated the autophagy response in both DUSP5-deficient and HPV16 E7-expressing NHEKs. Confocal microscopy and Western analysis showed induction of LC3-II levels, autophagosome formation and autophagy fluxes in DUSP5-deficient NHEKs. Furthermore, Western analysis demonstrated specific induction of phosphorylated ERK in DUSP5-deficient and HPV16 E7-expressing NHEKs, indicating that HPV16 E7-mediated repression of DUSP5 results in induced MAPK/ERK signaling. Finally, phosphorylated mTOR and ULK (S757) were reduced in DUSP5-deficient NHEKs, while phosphorylated ULK (S555) and AMPK were increased, thereby inducing canonical autophagy through the mTOR and AMPK pathways. In conclusion, our results demonstrate that HPV16 E7 expression reduces DUSP5 levels, which in turn results in active MAPK/ERK signaling and induction of canonical autophagy through mTOR and MAPK regulation. Given its demonstrated inverse correlation with clinical cancerous tissues, DUSP5 may serve as a potential therapeutic target for cervical cancer.

1. Introduction

Human papillomavirus (HPV) is a double-stranded DNA virus with a circular genome that contains three functional regions: the early transcription region, the late transcription region and the upstream regulation region. Based on the general outcome of HPV infections, HPV is divided into two groups: high-risk HPV (HR-HPV) and low-risk HPV (LR-HPV). HR-HPV is associated with malignancies such as oropharyngeal cancer and cervical cancer, and its genome frequently integrates into the host-cell chromosome during malignant progression. Although bivalent, quadrivalent and nonavalent vaccines preventing HPV-induced cervical cancer are becoming more widely available, there are currently still no therapeutics. Therefore, a better understanding of HPV biology is still essential. Some of the abnormally expressed proteins associated with HPV infection may serve as potential prognostic markers or therapeutic targets. The early transcription region encodes the early genes E1, E2, E4, E5, E6 and E7, which are essential for replication, transcription and transformation. Furthermore, oncogene E7 can also regulate other cellular proteins or interfere in their normal function [1], thereby impacting cellular proliferation and autophagic responses.

Autophagy, a dynamic cellular recycling system that accounts for removal, degradation, and recycling by lysosomal activity, plays a crucial role in cellular homeostasis at basal levels and adaptation to stress conditions such as aging and pathogen infections. Increased numbers of autophagic vesicles and LC3-positive puncta in virus infected cells indicates activation of autophagy and could be interpreted as viral targeting and degradation [2–5]. Also, the role of autophagy in enhanced innate recognition of viral pathogens [6], negative inflammatory regulation to avoid excess inflammation [7], and enhanced antigen presentation [8, 9] further clarify various virus-autophagy interactions.

Many viruses have evolved measures to suppress or exploit autophagy for the benefit of infection [10, 11]. Also, autophagy is a key driver of malignant transformation in virus-related tumor development, which is selectively triggered during viral replication to increase the ability to live in a high-energy-required environment [12–14]. For instance, previous studies showed that classical swine fever virus [15] and bovine ephemeral fever virus [16] induce autophagy during viral replication, while inhibition of virus-induced autophagy with aspirin suppressed viral replication. Similarly, HPV also exploits the autophagic machinery for infection and proliferation of infected epithelial cells, although the role of autophagy appears to be less clear-cut as it can act as both tumor suppressor and a promoter [17]. Furthermore, the relationship between HPV16 E7 and autophagy also seems contradictory. Expression of HPV16 E7 in normal human keratinocytes resulted in stronger LC3 staining and an increased incidence of LC3 puncta, which is evidence for induced autophagy-related fluxes [18]. Furthermore, HPV16 E6/E7 played a positive role in autophagy activity in cervical cancer cells via accelerating autophagosome formation and degradation [19]. In contrast, depletion of HPV16 E7 from the W12 and CaSki cervical carcinogenesis models induced conversion of LC3B-I to LC3B-II and reduced the levels of p62, which similarly showed activation of autophagy fluxes [20]. HPV E6/E7-positive keratinocytes generate strong replicative and oxidative stresses, which are counteracted by autophagy activity [21]. Therefore, expression of oncogenes may promote aberrant cell proliferation and trigger metabolic stresses that increase energy requirements, which need to be tightly balanced by autophagy-related processes.

In our previous study, we showed that dual-specificity phosphatase 5 (DUSP5) is downregulated in HPV16 E7-expressing human keratinocytes [22]. DUSPs belong to a heterogeneous family of protein tyrosine phosphatases, which serve as major modulators of the mitogen activated protein kinase (MAPK) signaling pathway through specific dephosporylation of various MAPKs, such as extracellular signal regulated kinase (ERK), c-Jun N-terminal kinase (JNK) and p38 [23, 24]. MAPKs are serine/threonine-specific kinases that have evolved to communicate environmental and developmental signals from the membrane into adaptive and programmed responses in the nucleus [25, 26]. Different members of the DUSP family show distinct substrate specificities, tissue distribution and subcellular localization, and different modes of inducibility by extracellular stimuli [27].

Autophagy, which serves as the quick responsor to metabolic stress and nutrient status, is regulated by various kinases, such as mammalian target of rapamycin complex 1 (mTORC1) and MAPK. Several studies have shown that inhibition of DUSP1 activates autophagy [28–30], and it seems therefore that regulation of the expression or activity of DUSPs can be a promising alternative strategy to modulate autophagy. For instance, it was shown that during a *Mycobacterium bovis* Bacillus Calmette-Guerin (BCG) infection, DUSP5 inhibited the formation of autophagosomes by suppressing phosphorylation of signaling molecules in the ERK1/2 signaling cascade [31].

DUSP5, which is expressed at very low levels in cervical cancer cells, has been verified to be negatively modulated by lncRNA ARAP1 antisense RNA 1 and to contribute to cell proliferation and migration [32]. In our current study, we consistently found a negative correlation between DUSP5 and HPV16 E7 expression levels and DUSP5 deficiency resulted in induced autophagy fluxes. Modulation of DUSP5 may therefore serve as a novel strategy for autophagy regulation.

2. Materials and Methods

2.1. Clinical Samples of Patients and Ethical Statements. This study has been approved by the ethics committee of the Sir Run Run Shaw Hospital (Approval no. 20210330-39) and is in accordance with the Declaration of Helsinki. Briefly, samples were randomly picked after clinical diagnosis of cervicitis, cervical intraepithelial neoplasia or cervical cancer. Paraffin-embedded specimens of HPV16-negative or -positive cervical tissues were classified after DNA extraction and nested PCR verification for HPV detection.

2.2. DNA Extraction and Nested PCR. DNA from formalin-fixed and paraffin-embedded (FFPE) patient tissues was extracted using the FFPE Tissue Kit (QIAamp, Germany) following manufacturer's instructions. Briefly, tissue sections were collected in sterile tubes and xylene was used to remove paraffin. Tissues were subsequently lysed under denaturing conditions with proteinase K and incubated at 90°C to reverse formalin crosslinking. Nested PCR was performed using primer pairs MY09 (CGTCCMARRGGAWACTG ATCa)/MY11 (GCMCAGGGWCATAAYAATGGa) and G P5 + (TTTGTTACTGTGGTAGATACTAC)/GP6 + (GAAAA ATAAACTGTAAATCATATTC) for the first and second PCR reactions, respectively. PCR reactions were performed in a 25 μL volume using Taq enzyme (CWBIO, China). The reaction mixture was first heated to 95°C for 5 min, followed by 35 cycles of 30s denaturation at 95°C, 30s annealing at 57°C and 45 s extension at 72°C, with a final extension step at 72°C for 10 min. The second reaction was identical, except annealing was performed at 58°C. PCR products were run on a 2% agarose gel for visualization (Supplementary Figure 1).

2.3. Immunohistochemistry Staining. Paraffin-embedded tissue slides (3 μm thick) were heated at 65°C for 30 min and deparaffinized in xylene. After rehydration in a graded series of ethanol solutions, slides were immersed in 0.01 M sodium citrate buffer (pH 6.0) inside a pressure-cooker for 15 min to

achieve heat-induced antigen retrieval. Tissues were then incubated with 3% hydrogen peroxide for 30 min, rinsed with PBS, and incubated with 5% nonimmune goat serum for 30 min inside a moist chamber. Tissues were subsequently incubated overnight with anti-DUSP5 (ab200708, 1 : 500; Abcam) or anti-HPV16 E7 (1 : 500) at 4°C. Finally, the tissues were washed and incubated with secondary anti-rabbit IgG (Gene Tech, China) for 30 min, followed by staining with diaminobenzidine (DAB, Gene Tech) and hematoxylin. Images were obtained with a KFBIO Digital Slide Viewer.

2.4. Production of HPV16 E7 Polyclonal Antibody. HPV16 E7 was amplified from HPV16 whole virus plasmids and cloned into the plasmid pGEX4T-2 to obtain plasmid pGEX-4 T-2-HPV16 E7. HPV16 E7 expression was induced in *Escherichia coli* DH5α grown in Luria-Bertani (Beyotime, China) medium supplemented with 100 mg/L ampicillin (Beyotime, China) using 0.2 mM isopropyl β-D thiogalactopyranoside (Biosharp, China), followed by incubation at 26°C for 3 h. Cells were lysed by ultrasonication (Scientzbio, China) on ice at 200 W for 3 min (5 s on and 10s off). The lysates were centrifuged and supernatants were incubated with Glutaphione Sepharose 4B beads (GE Healthcare, USA) at 4°C for 4 h to capture the GST tag-containing proteins. The GST tag was subsequently removed with Thrombin (GE Healthcare, USA; Supplementary Figure 2). Purified HPV16 E7 was used for subcutaneous immunization of female New Zealand white rabbits (3 months old, approximately 2.5 kg). Blood was collected by cardiocentesis and serum was separated for isolation of IgG antibodies with rProteinG Agarose (Invitrogen, USA). The purified polyclonal antibodies were stored in sterile glycerol (50%) at -20°C. The titer and specificity of the antibodies were verified by Western blot analysis.

2.5. Cell Culture and Transfection. Normal human epidermal keratinocytes (NHEKs) were cultured in EpiLife culture medium (Gibco, USA) with 10% fetal bovine serum (Gibco, USA) and Human Keratinocyte Growth Supplement (Gibco, USA). Siha cells were cultured in DMEM (Gibco, USA) containing 10% fetal bovine serum (Gibco, USA). C33A cells were cultured in MEM (Gibco, USA) with 10% fetal bovine serum (Gibco, USA) and 1% Penicillin-Streptomycin Solution (Gibco, USA). All cells were cultured at 37°C in the presence of 5% CO2. Cells at 80% confluence were transfected with GFP-LC3 or mCherry-GFP-LC3 plasmid using Lipofectamine 3000 reagent (Invitrogen, USA). The culture medium was replaced 6 h after transfection and the cells were cultured for another 48 h before analysis.

2.6. Construction of HPV16 E7-NHEK Cell Line. The HPV16 E7-expressing NHEK cell lines were constructed by lentivirus infection. The HPV16 E7 gene was cloned into a p23 lentivirus-expression vector and transfected to 293 T cells. The coding sequence of HPV16 E7 is ATGCATGGAGATA CACCTACATTGCATGAATATATGTTAGATTTGCAAC CAGAGACAACTGATCTCTACTGTTATGAGCAATTAA ATGACAGCTCAGAGGAGGAGGATGAAATAGATGGT CCAGCTGGACAAGCAGAACCGGACAGAGCCCATTA CAATATTGTAACCTTTTGTTGCAAGTGTGACTCTACG CTTCGGTTGTGCGTACAAAGCACACACGTAGACATT CGTACTTTGGAAGACCTGTTAATGGGCACACTAGGA ATTGTGTGCCCCATCTGTTCTCAGAAACCATAA, which was amplified with the forward primer GGCGCGGCCGC ATGCATGGAGATACACCTAC and the reverse primer CTAGTCTAGACTCACTTGTCATCGTCGTCCTTGTAGT CTGGTTTCTGAGAACAGATGG, containing a FLAG-tag and XbaI restriction enzyme site. After 48 h, supernatant was collected and centrifuged to get the lentiviral particles. NHEKs were incubated with appropriate lentiviral particles in 12-well plates at a cell density of 1×10^5 with 10 μg/ml polybrene transfection reagent (#TR-1003-G, Merck Millipore) for 8 h, after which the supernatant was replaced with fresh culture medium. Subsequently, the cells were cultured for another 48 h before transfection efficiency was observed by microscopy and flowcytometry. New stable cell lines were established with further flowcytometry sorting. The RNA and protein levels of HPV16 E7 were tested by quantitative real-time PCR and western blot, respectively (Supplementary Figure 3).

2.7. Knock-down of DUSP5 and HPV16 E7. NHEKs and Siha were seeded in 6-well plates and incubated for 24 h before transfection with short interfering RNAs (siRNAs). siRNAs targeting three different regions of the DUSP5 or HPV16 E7 gene (siDUSP5 or si-HPV16 E7) and negative control siRNA were synthesized by GenePharma (Shanghai, China). The target sequences for the negative control were UUCU CCGAACHUGUCACGUTT and ACGUGACACGUUCG GAGAATT, while the three pairs of target sequences for DUSP5 were GCUCUUCACUGAUAGGCCATT and UG GCCUAUCAGUGAAGAGCTT,CCAUCUGCAUGGCUU ACCUTT and AGGUAAGCCAUGCAGAUGGTT, and G CUCCUGCAGUACGAAUCUTT and AGAUUCGUACU GCAGGAGCTT. Furthermore, three pairs of target sequences for HPV16 E7 were GCAACCAGAGACAACU GAUTT and AUCAGUUGUCUCUGGUUGCTT, GGAC AGAGCCCAUUACAAUTT and AUUGUAAUGGGCUC UGUCCTT, and GCUUCGGUUGUGCGUACAATT and UUGUACGCACAACCGAAGCTT. Transfection was performed using Lipofectamine RNAiMAX (Invitrogen, USA) at 70% confluence according to manufacturer's guidelines. 6 h after transfection, the medium was replaced with fresh culture medium. Cells were analyzed at 48 h post transfection for protein expression by Western blotting and quantitative real-time PCR to assess siRNA silencing efficiency.

2.8. Western Blotting and Quantitative Real-Time PCR. Experiments were performed as previously described [22]. Antibodies specific for ERK (#4695), JNK (#9252), p38 (#9212), phospho-ERK (Thr202/Tyr204) (#4370), phospho-JNK (Thr183/Tyr185) (#4668), phospho-p38 (Thr180/Tyr182) (#9211), LC3B (#2775S), mTOR (#2983), phospho-mTOR (Ser2448) (#2971), ULK1 (#8054), phospho-ULK1 (Ser555) (#5869), phospho-ULK1 (Ser757) (#14202), phospho-70S6 kinase (Thr389) (#9234), 70S6 kinase(#2708), phospho-4E-BP1 (Thr37/46) (#2855), 4E-BP1 (#9452), AMPK (#2603) and phospho-AMPK (Thr172) (#2531) were

purchased from Cell Signaling Technology (Danvers, MA). Antibodies against DUSP5 (#ab200708) were from Abcam (Cambridge, MA) and antibodies against p62 (#PM045) were from MBL Life science. Specific inhibitors U0126 (#HY-12031A), SB203580 (#HY-10256), SP600125 (#HY-12041) and bafilomycin A1 (#HY-100558) were obtained from MCE. Rapamycin (#V900930-1MG) and rose bengal (#330000) were from Sigma. U0216 (10 μM, 24 h), SB203580 (20 μM, 24 h), SP600125 (15 μM, 24 h), bafilomycin A1 (25 nM, 6 h) and rapamycin (100 nM, 12 h) were added to the cell cultures as described in different experiments. The primers for DUSP5 were TGTCGTCCTCACCTCGCTA and GGGCTCTCTCACTCTCAATCTTC.

2.9. Immunofluorescence and Confocal Microscopy. Cells were washed with PBS and fixed with 4% paraformaldehyde (Solarbio, China) for 20 min at room temperature. The fixed cells were permeabilized with 0.5% (v/v) Triton X-100 (Solarbio, China) for 10 min, and blocked with 10% goat serum in 1% bovine serum albumin for 1 h at room temperature. HPV16 E7-expressing NHEKs were immunostained with DUSP5 (Absin, #ab200708) while DUSP5-deficient NHEKs were immunostained with LC3B (CST, #2775S) antibodies overnight at 4°C. Subsequently, cells were incubated with Alexa Fluor 594 donkey anti-rabbit IgG (Yeasen, China) for 1 h at 37°C and then stained with 4,6-diamidino-2-phenylindole (DAPI, 1 : 1000 dilution, Abcam) for 10 min at room temperature in the dark. Images were obtained using a Nikon A1 confocal microscope.

2.10. GEO Data Mining. Clinical data was retrieved from the Gene Expression Omnibus (GEO) public database. 24 normal cervix and 19 HPV16 positive cervical cancer tissues from the dataset GSE9750 [33], which aimed to identify gene expression profiles in cervical cancer and the role of specific genes in cervical carcinogenesis, were selected. The expression data for DUSP5 in different samples was extracted and analyzed with GEO2R. GEO2R is an open, public and interactive web tool which helps identify gene expression under experimental conditions. See detailed information of each sample in Supplementary Table 1.

2.11. Statistical Analysis. For all experiments, at least three biologically independent replicates were performed and the results were analyzed using ImageJ and GraphPad prism7. Splitting the color channel, setting the threshold and size of particles, and analyzing were the main steps for quantification of confocal results. The data are presented as the means ± SEM (standard error of the mean). Statistical analyses include the paired *t*-test or 2-way ANOVA with Dunnett's multiple comparison test. Differences between groups were assessed by Student's *t*-test and $p < 0.05$ was considered statistically significant. $*$, $p < 0.05$; $**$, $p < 0.01$; $***$, $p < 0.005$; $****$, $p < 0.001$.

3. Results

3.1. Inverse Correlation between HPV16 E7 and DUSP5 Expression. In our previous study we transfected a HPV16 E7-expression vector into NHEKs and analyzed its effect on global transcriptional profiles. Pathway analysis showed differential gene expression of clusters associated with MAPK signaling, with specific downregulation of DUSP5 in HPV16 E7-positive NHEKs. To investigate the correlation between HPV16 E7 and DUSP5 gene expression in human clinical samples, the GSE9750 dataset available in GEO, which contains expression data of HPV16-positive human cervical cancer and control tissues, was analyzed. Indeed, gene expression levels of DUSP5 were significantly lower in HPV16 single positive cervical cancer tissues compared with normal cervical control tissues (Figure 1(a) and Supplementary Table 1), indicating a possible inverse correlation between HPV16 E7 and DUSP5. To further validate an inverse correlation between HPV16 E7 and DUSP5 at both mRNA and the protein levels, we used a lentivirus expression system for stable expression of E7 in NHEKs. Subsequent analysis of DUSP5 in E7-expressing NHEKs showed a significant reduction in DUSP5 protein and gene expression levels compared with control NHEKs (Figure 1(b)). Importantly, the inverse correlation between HPV16 E7 and DUSP5 was also observed in human cervical tissues. While HPV16 E7-negative cervicitis tissues showed high DUSP5 levels, HPV16 E7-positive cervical intraepithelial neoplasia (CIN) and cervical cancer tissues showed low DUSP5 expression levels (Figure 1(c)), indicating that DUSP5 plays an important role in disease progression. Finally, immunostained DUSP5 was detected by confocal microscopy in HPV16 E7-expressing NHEKs (Figure 1(d)). Compared with NHEK control cells, DUSP5 expression was significantly lower in both the nucleus and cytoplasm of HPV16 E7-positive NHEKs (Figure 1(e)). Overall, these results indicate that HPV16 E7 reduces DUSP5 expression levels.

3.2. HPV16 E7-Mediated DUSP5 Deficiency Induces Autophagy Flux and Autophagosome Formation. Given the role of DUSPs in regulation of MAPK signaling and consequently autophagy activity, we investigated whether HPV16 E7-mediated DUSP5 deficiency activates autophagy. We incubated NHEKs with increasing concentrations of rose bengal, which is an FDA-approved compound with strong potency against DUSP5 [34], and showed by Western analysis that DUSP5 protein levels were indeed decreased in a rose bengal concentration-dependent manner (Figures 2(a) and 2(b)). We furthermore investigated its impact on the autophagy activity marker proteins LC3 and p62. The expression levels of LC3-II, which is an essential component of the phagophore, were significantly higher after rose bengal treatment, while the levels of p62, which is a receptor for autophagy cargos, were significantly lower at higher doses. Similarly, rose bengal treatment of NHEKs transfected with a plasmid expressing GFP-LC3 showed a significant increase in LC3 puncta compared with control cells (Figures 2(c) and 2(d). Interestingly, while expression of HPV16 E7 in NHEKs resulted similarly in an elevation of LC3-II levels and reduction of p62 levels as observed after rose bengal treatment, combining rose bengal treatment with HPV16 E7 expression appears to provide additive autophagy responses, given that LC3-II levels were further

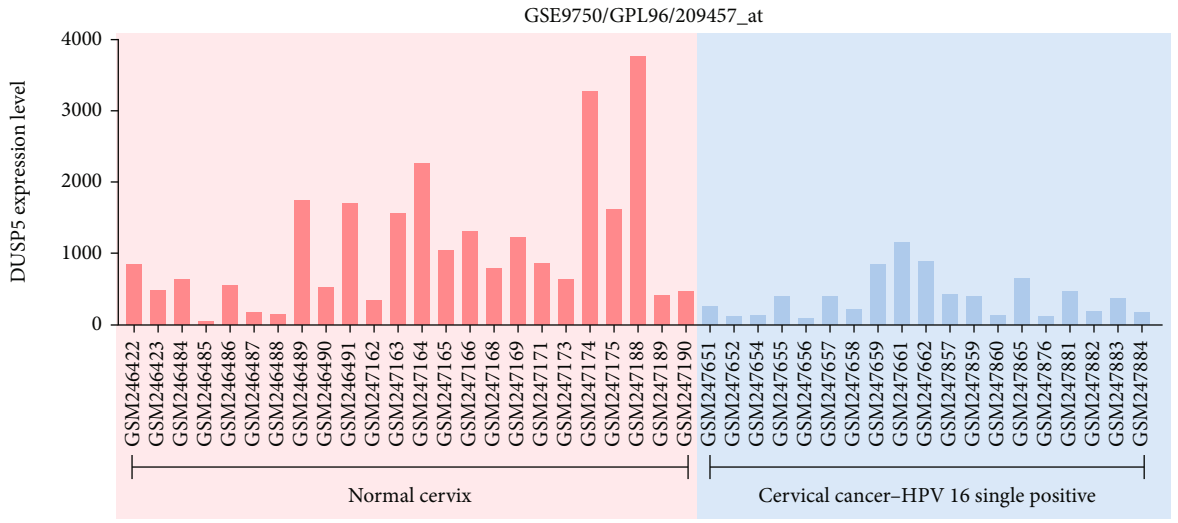

(a)

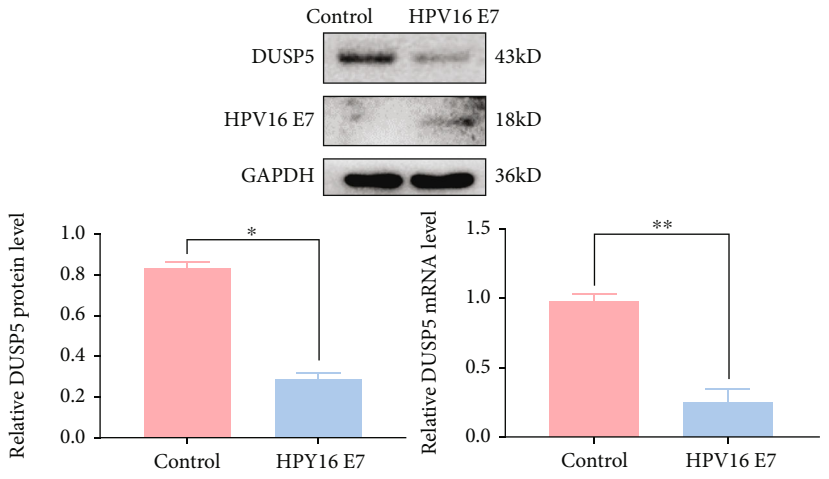

(b)

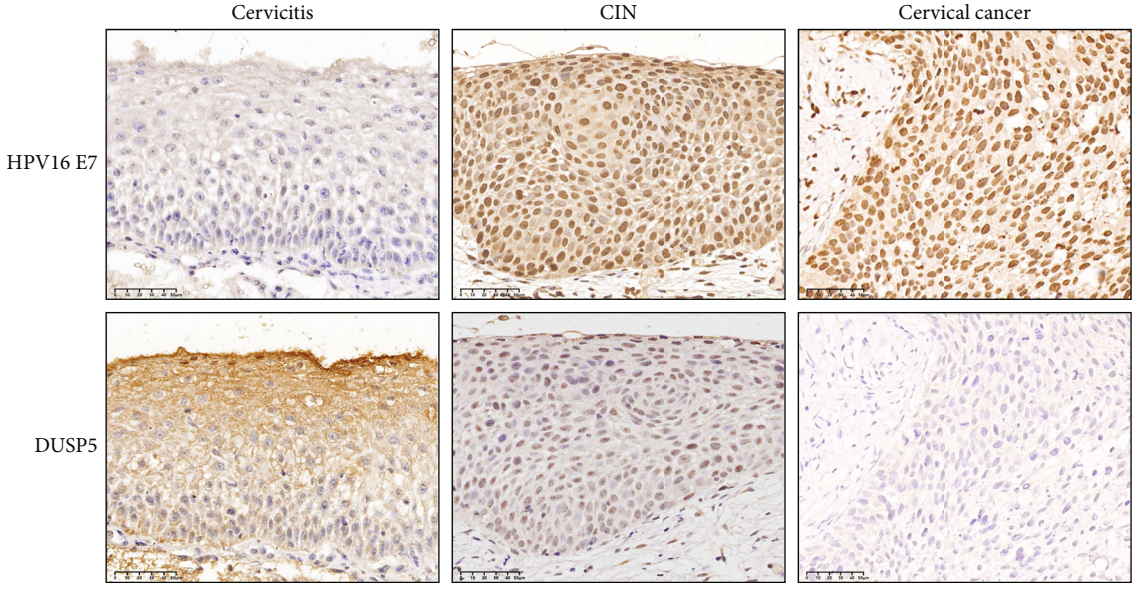

(c)

Figure 1: Continued.

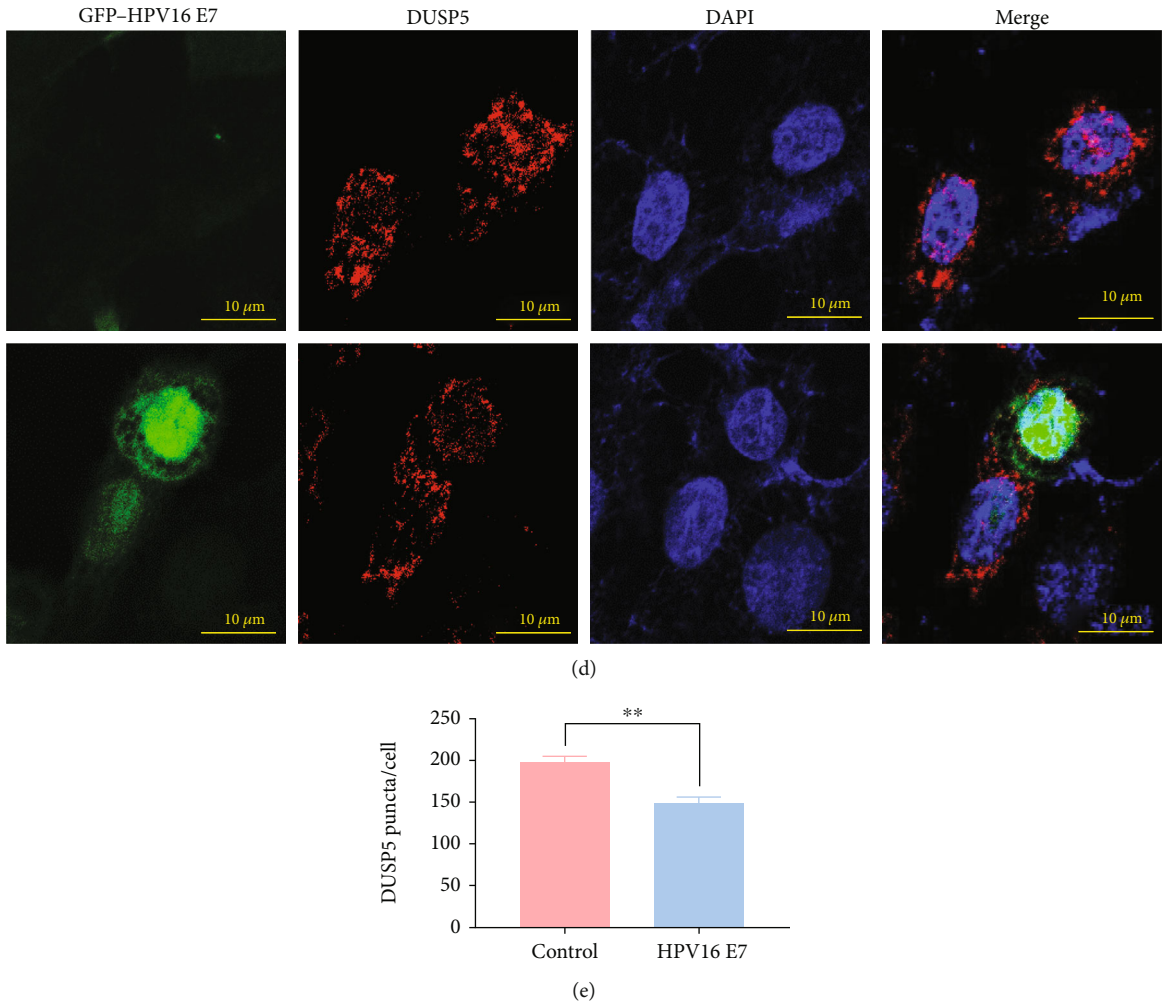

Figure 1: Inverse correlation between HPV16 E7 and DUSP5. (a) Expression levels of DUSP5 (GEO dataset GSE9750) in normal cervical epithelium and HPV16 single positive cervical cancer tissues. (b) Western analysis and quantitative real-time PCR analysis of DUSP5 in control and HPV16 E7-expressing NHEKs. (c) Immunohistochemical staining of HPV16 E7 and DUSP5 in cervicitis, cervical intraepithelial neoplasia (CIN) and cervical cancer tissues. (d) Confocal microscopy analysis of HPV16 E7 (Green) and DUSP5 (Red) in HPV16 E7-expressing NHEKs. (e) Quantification of DUSP5 puncta from confocal microscopy images. The graph represents the mean and standard deviation from three biological independent repeats, and at least 10 cells were analyzed per repeat. ImageJ was used for quantification. Significant differences were identified by Student's *t*-test. ∗, $P < 0.05$. ∗∗, $p < 0.01$.

increased in the combined treatment and p62 levels further reduced (Figures 2(e) and 2(f)). To validate the impact of HPV16 E7 on DUSP5 expression and autophagy in other cell models, E7 was knock-down in HPV16-positive Siha cells or expressed in the HPV-negative C33A cells. Subsequent Western analysis showed an increase in DUSP5 levels and decrease of LC3-II levels after E7 knock-down in Siha cells, while DUSP5 was decreased and LC3-II increased after expression of HPV16 E7 in C33A cells (Figures 2(g) and 2(g)).

To elaborate on these results, we knocked-down DUSP5 in NHEKs using siRNA transfection and again investigated LC3-II and p62 levels. The expression levels of LC3-II were significantly higher after knock-down of DUSP5, while the levels of p62 were significantly lower (Figures 3(a) and 3(b)). Furthermore, confocal microscopy analysis of immunostained LC3 showed higher numbers of LC3 puncta per cell, a hallmark of autophagosome biogenesis, in DUSP5 knock-down cells compared with control cells (Figures 3(c) and 3(d)). Therefore, these results indicate that DUSP5-deficient NHEKs display increased numbers of autophagosomes that are able to sequester p62-loaded cargos. To further investigate whether the increase in autophagosomes in DUSP5-deficient NHEKs was the result of increased autophagy activity or inhibited recycling, autophagy flux was analyzed using the canonical autophagy activator rapamycin and the V-ATPase inhibitor bafilomycin A1 (BafA1), which inhibits autophagosome-lysosome fusion. Addition of rapamycin, BafA1 or a combination of these increased the levels of LC3-II, with higher levels observed in DUSP5 knock-down NHEKs compared with control cells (Figures 3(e) and 3(f)). Furthermore, addition of rapamycin resulted in a decrease in p62 levels in both control and knock-down cells, which was prevented by addition of BafA1. Finally, autophagosome

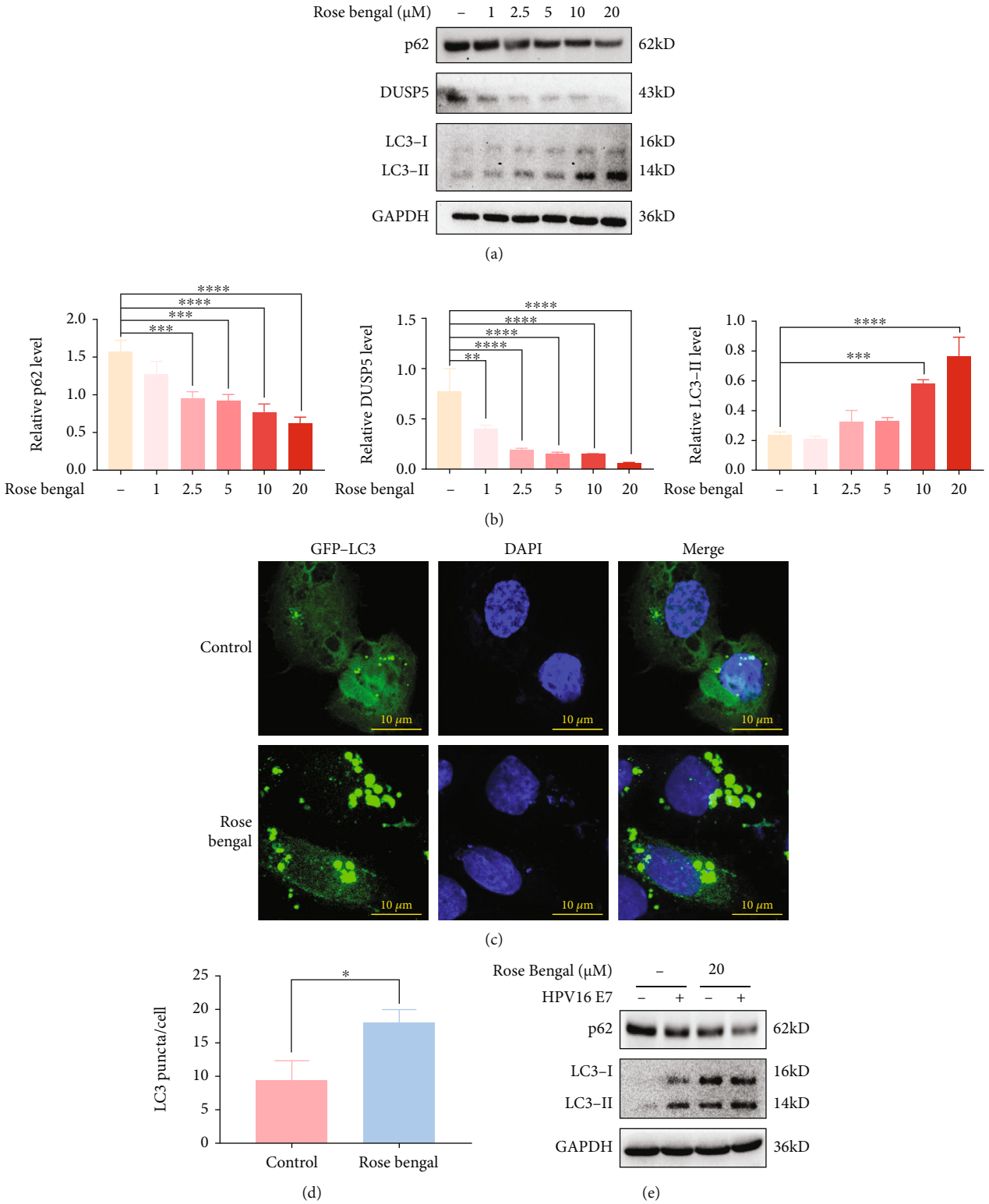

Figure 2: Continued.

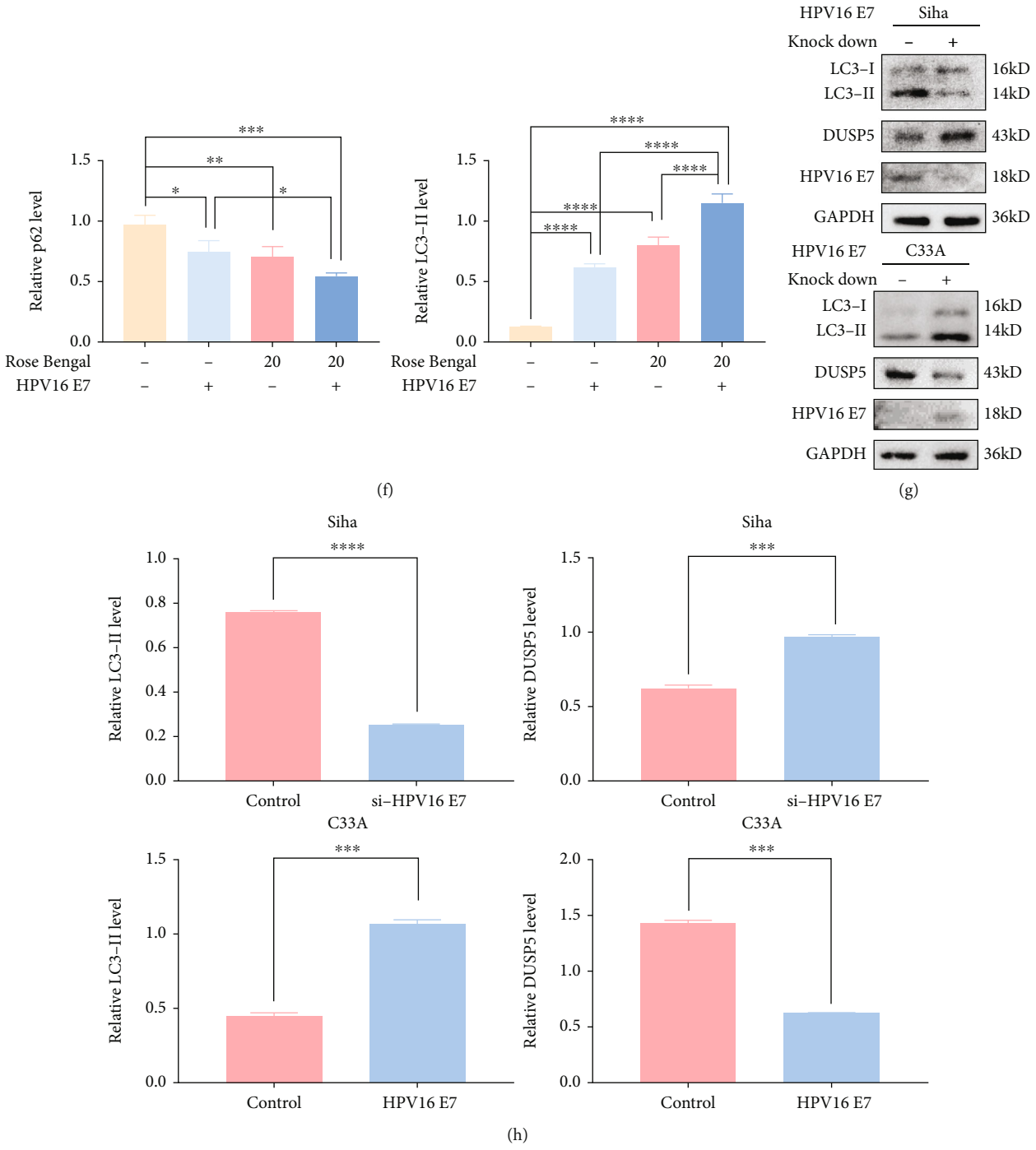

Figure 2: HPV16 E7-mediated DUSP5-deficiency induces autophagy. (a) Western analysis of p62, DUSP5 and LC3 levels in NHEKs after incubation with increasing concentrations of rose bengal (0 to 20 μM) for 48 h. (b) Quantification of p62, DUSP5 and LC3-II levels from panel a, using GAPDH for normalization. (c) Representative confocal microscopy images of NHEKs expressing GFP-LC3 with or without treatment with 20 μM rose bengal. (d) Quantification of LC3 puncta per cell from confocal microscopy images in panel c. The graph represents the mean and standard deviation from three biological independent repeats, and at least 10 cells were analyzed per repeat. (e) Western analysis of p62 and LC3 levels in HPV16 E7-expressing or control NHEKs after rose bengal treatment (0 or 20 μM, 8 h). (f) Quantification of p62 and LC3-II levels from panel e, using GAPDH for normalization. (g) Western analysis of LC3, DUSP5 and HPV16 E7 levels in HPV16-expressing Siha cells after knock-down of E7 and in C33A cells after expression of HPV16 E7. (h) Quantification of LC3-II and DUSP5 levels from panel g, using GAPDH for normalization. ImageJ was used for quantification. Significant differences were identified by Student's *t*-test. ∗, $p < 0.05$; ∗∗, $p < 0.01$; ∗∗∗, $p < 0.005$; ∗∗∗∗, $p < 0.001$.

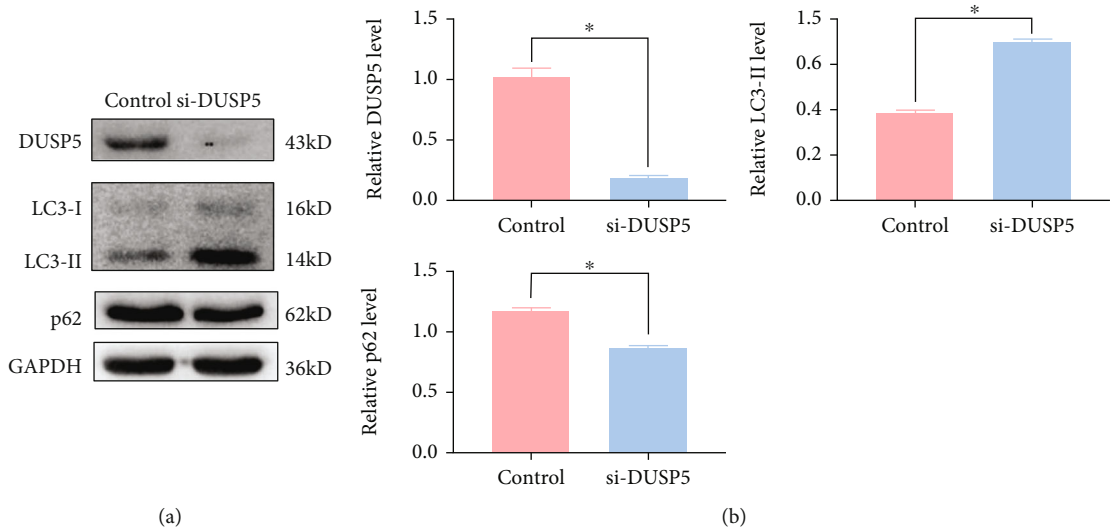

(a) (b)

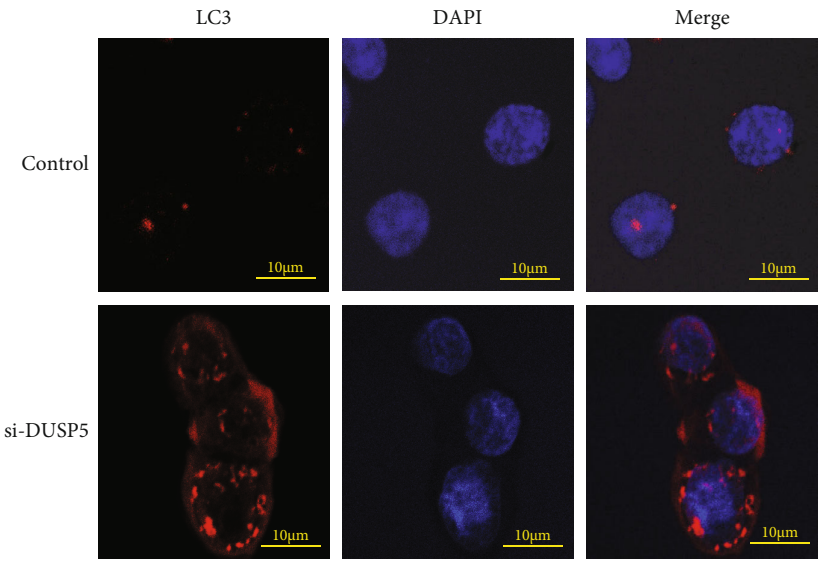

(c)

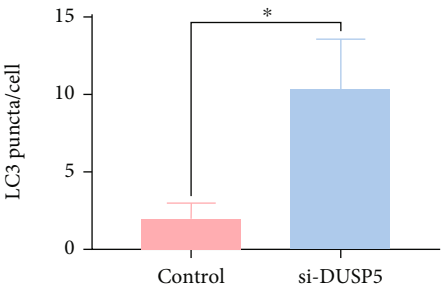

(d)

Figure 3: Continued.

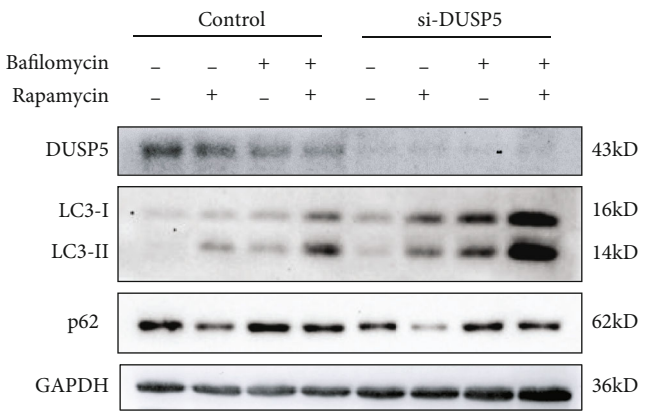

(e)

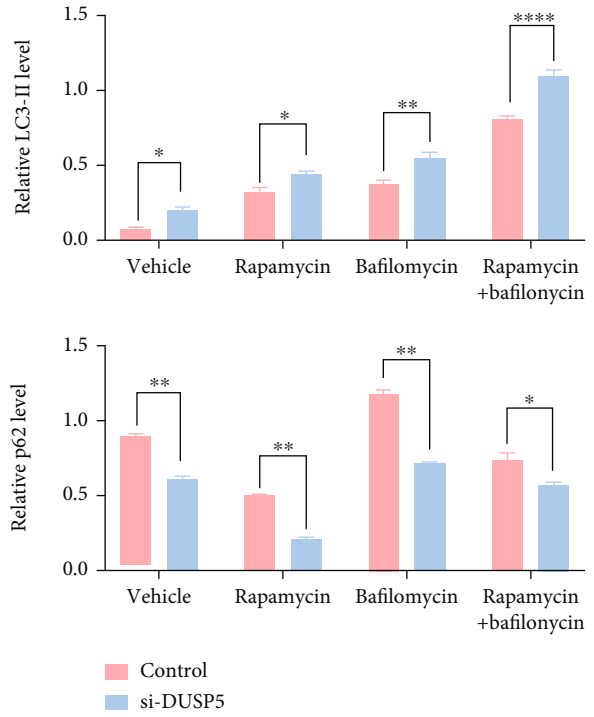

(f)

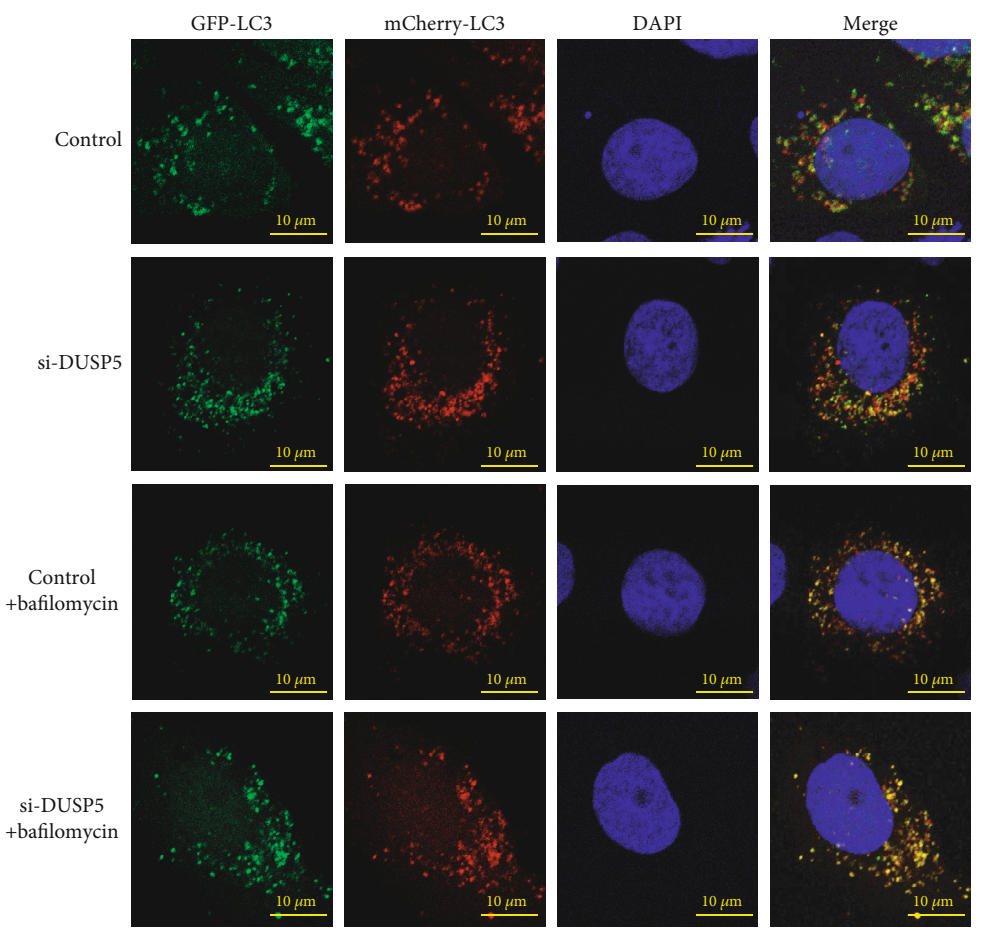

(g)

Figure 3: Continued.

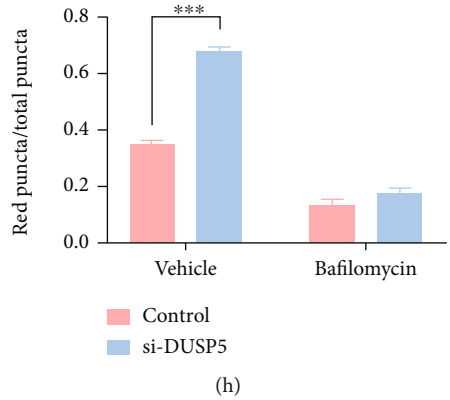

Figure 3: DUSP5 deficiency induces autophagy flux and autophagosome formation. Western analyses of DUSP5, LC3 and p62 levels in DUSP5-deficient and control NHEKs. (b) Quantification of DUSP5, LC3-II and p62 levels from panel a, using GAPDH for normalization. (c) Representative confocal microscopy images of endogenous immunostained LC3 puncta in DUSP5 deficient and control NHEKs. (d) Quantification of LC3 puncta per cell from panel c. (e) Western analysis of DUSP5, LC3 and p62 levels in DUSP5 deficient and control NHEKs after treatment with 100 nM rapamycin for 12 h or 25 nM bafilomycin A1 for 6 h. (f) Quantification of LC3-II and p62 levels from panel e, using GAPDH for normalization. (g) Representative confocal microscopy images of vehicle or BafA1 pretreated DUSP5 deficient and control NHEKs transfected with a vector expressing mCherry-GFP-LC3. (h) Quantification of the ratio of red LC3 puncta (autolysosomes) to all LC3 puncta (autophagosomes plus autolysosomes) from images represented in panel g. The graph represents the mean and standard deviation from three biological independent repeats, and at least 10 cells were analyzed per repeat. ImageJ was used for quantification. Significant differences were identified by Student's *t*-test. ∗, $p < 0.05$; ∗∗, $p < 0.01$; ∗∗∗, $p < 0.005$; ∗∗∗∗, $p < 0.001$.

maturation into autolysosomes was investigated after transfection with a plasmid expressing an mCherry-GFP-LC3 fusion protein. Since GFP is acid sensitive, its fluorescent activity is lost in the acidic environment of the autolysosome. Therefore, autophagosomes that mature into autolysosomes are visible as red puncta. Indeed, more red puncta were observed in DUSP5 deficient NHEKs than in control cells (Figures 3(g) and 3(h)), indicating that autophagosome maturation in DUSP5-deficient NHEKs was unaffected. As a control, cells were treated with BafA1, which inhibited autolysosome formation in both DUSP5-deficient NHEKs and control cells. Collectively, these data suggest that DUSP5 deficiency induces autophagy fluxes and does not interfere in autophagosome biogenesis and maturation processes.

3.3. DUSP5 Inhibits Autophagy via the MAPK/ERK Pathway. To explore the mechanism by which DUSP5 modulates autophagy activity, DUSP5-deficient and control NHEKs were investigated for the phosphorylation status of ERK, JNK and p38 in the presence and absence of inhibitors U0126 (p-ERK), SB203580 (p-p38) or SP600125 (p-JNK) after treatment for 24 h (Figures 4(a) and 4(b)). The levels of p-ERK were most significantly elevated in DUSP5-deficient NHEKs compared with control cells, while p-JNK showed a moderate but significant increase. Furthermore, addition of U0126 significantly reduced p-ERK levels in both DUSP5-deficient and control NHEKs, but a significant difference between these in p-ERK remained, which indicates that U0126 and DUSP5 do not interfere in each other's p-ERK-modulating activity. Importantly, only addition of U0126 and not addition of SB203580 or SP600125 resulted in a significant reduction in LC3-II levels, indicating that in NHEKs, DUSP5 deficiency activates autophagy fluxes by inducing the MAPK/ERK pathway. Interestingly, the p-JNK inhibitor seemed to elevate DUSP5 levels in the DUSP5 knock-down NHEKs, while the levels of p-JNK were most severely reduced in SP600125-treated DUSP5 knock-down cells. These results may be supported by the previously demonstrated feedback cross-regulation between JNK and ERK signaling cascades and DUSP5 [35]. Finally, the role of HPV16 E7 in DUSP5-deficiency-mediated increased p-ERK levels was validated. NHEKs expressing HPV16 E7 showed increased p-ERK levels compared with control cells (Figures 4(c) and 4(d)) and combining HPV16 E7 expression with DUSP5 siRNA was further cumulative for p-ERK levels.

3.4. DUSP5 Regulates Autophagy through mTOR Signaling. Mammalian target of rapamycin (mTOR) is activated as part of mTOR complex 1 (mTORC1) and suppresses canonical autophagy by phosphorylating ULK1 at serine 757, while phosphorylation of ULK1 at serine 555 by AMP activated protein kinase (AMPK) results in activation of autophagy [36]. In addition, activated mTORC1 phosphorylates its downstream substrates 4EBP1 and p70S6K, which are not related to autophagy. HPV16 E7 activates autophagy through mTOR signaling in NHEKs (Supplementary Figure 4). To further explore the mechanism by which DUSP5 deficiency promotes autophagy, the phosphorylation state of mTOR, ULK1, p70S6K, 4EBP1 and AMPK was analyzed in DUSP5-deficient and control NHEKs. Phosphorylation of mTOR, ULK1 (S757), p70S6K and 4EBP1 was significantly reduced in DUSP5-deficient NHEKs compared with control cells (Figures 5(a) and 5(d)). Addition of rapamycin further reduced phosphorylation levels. In contrast, phosphorylation of ULK1 (S555) and AMPK was promoted in DUSP5-deficient NHEKs (Figures 5(a), 5(b), 5(e) and 5(f)).

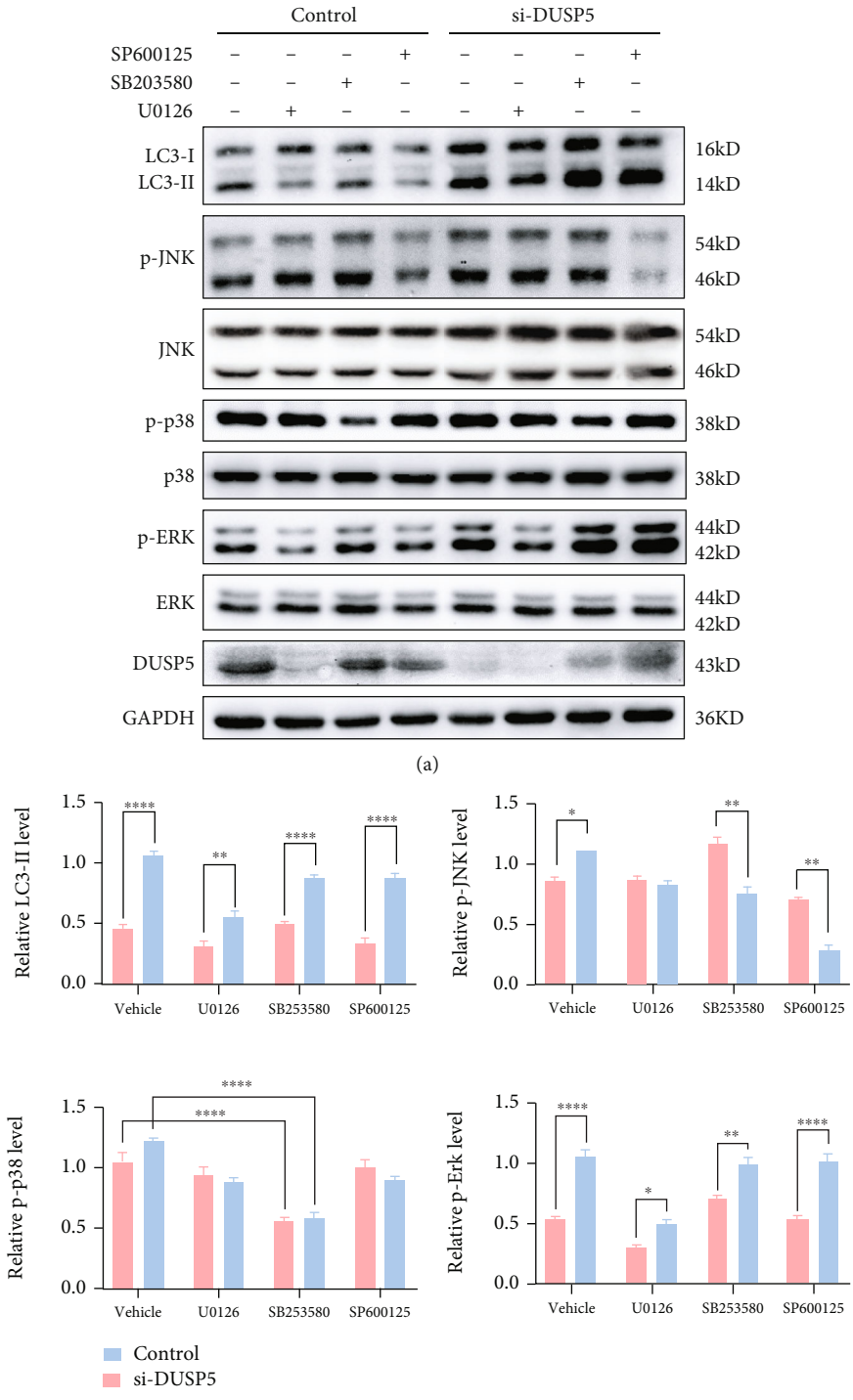

Figure 4: Continued.

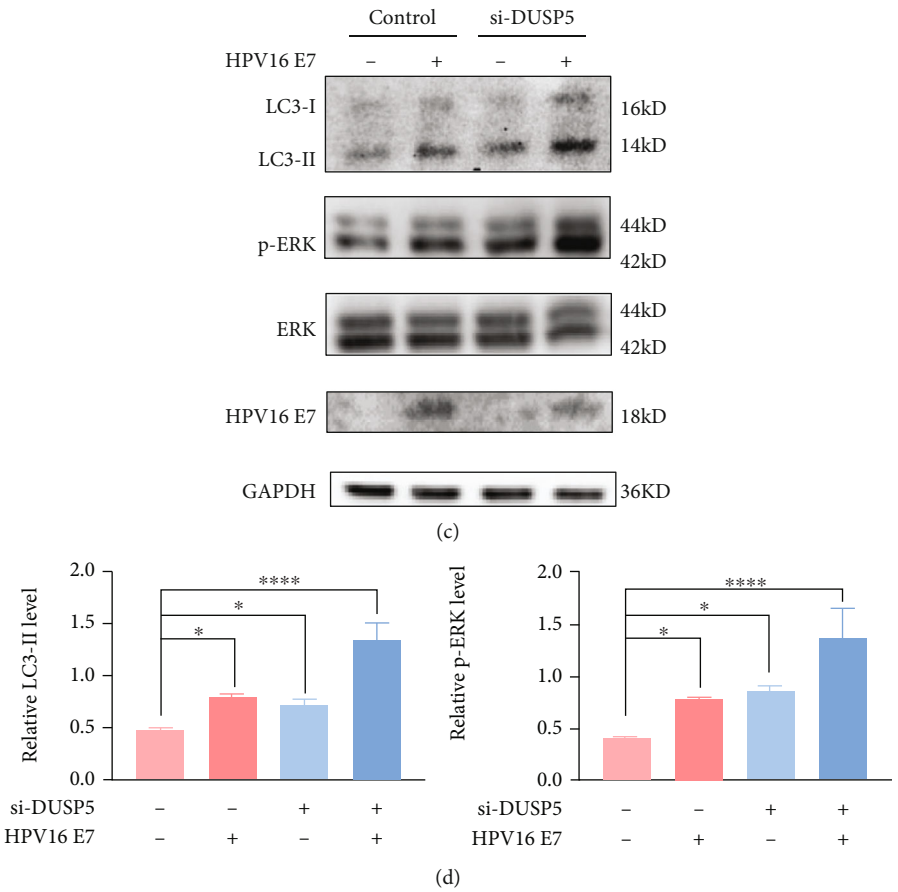

Figure 4: DUSP5 deficiency activates autophagy via the MAPK/ERK pathway. (a) Western analysis of phosphorylated and total JNK, p38, and ERK levels and DUSP5 and LC3 levels in DUSP5-deficient and control NHEKs. Cells were pretreated with U0126 (10 μM), SB203580 (20 μM), SP600125 (15 μM) or a vehicle control for 24 h. (b) Quantification of LC3-II and phosphorylated JNK, p38, and ERK levels from panel a, using GAPDH (LC3-II) or total JNK, p38, and ERK levels for normalization. (c) Western analysis of LC3, HPV16 E7, and phosphorylated and total ERK levels in HPV16 E7-expressing DUSP5-deficient NHEKs or control cells. (d) Quantification of LC3-II and phosphorylated ERK levels from panel c, using GAPDH (LC3-II) or total ERK levels for normalization. Significant differences were identified by Student's *t*-test. $*$, $p < 0.05$; $**$, $p < 0.01$; $***$, $p < 0.005$; $****$, $p < 0.001$.

Therefore, our results show that DUSP5 deficiency activates canonical autophagy through suppression of mTOR and activation of AMPK, resulting in activation of ULK1.

4. Discussion

Persistent HR-HPV infection is the leading cause of cervical cancer worldwide. The oncogenic effects of HPV are closely related to expression of oncoprotein E7, which is involved in the modulation of cell proliferation, apoptosis, and immortality. In response to metabolic stress, autophagy is crucial for survival and maintenance of cellular nutrient homeostasis. Previous research has shown that autophagy is inhibited at the early stages during cellular entry [37], but reactivated at the later stages of HPV-related anal cancer, as shown by detection of autophagy markers in low-grade and high-grade squamous intra-epithelial lesions [38, 39]. In our previous studies, we found that both LR-HPV type 11 pseudovirions and LR-HPV early protein E6 activate autophagy through ERK/mTOR and Akt/mTOR signaling [40, 41]. Although host cell-induced autophagy may target and eliminate invading viruses such as HPV, active autophagy fluxes are required to meet the tumorigenic potential and growing demand of cancer cell metabolism in advanced HPV infection stages. Therefore, tight regulation of autophagic activity is likely important during the HPV infection cycle and could be a specific target for treatment of cervical cancer and development of new prophylactic or therapeutic antiviral strategies.

In our previous study, we explored the cellular targets of the HPV16 E7 oncoprotein to better understand vital cellular signal transduction pathways in the modulation of cellular homeostasis and identified its repressive activity to DUSP5. Here, we now show that HR-HPV16 E7 promotes autophagy fluxes through DUSP5 repression, which promotes ERK/mTOR and AMPK signaling. Luo et al. also found an inverse correlation between HPV16 E7 and STING protein levels and loss of HPV16 E7 led to reduced autophagy. That study furthermore showed that HPV16 E7 promotes autophagy-dependent degradation of STING, which suppresses STING-dependent IFN-I responses [42]. Mattoscio et al. found enriched LC3 in autophagic structures and accumulation of p62 in HPV16 E6/E7-expressing primary

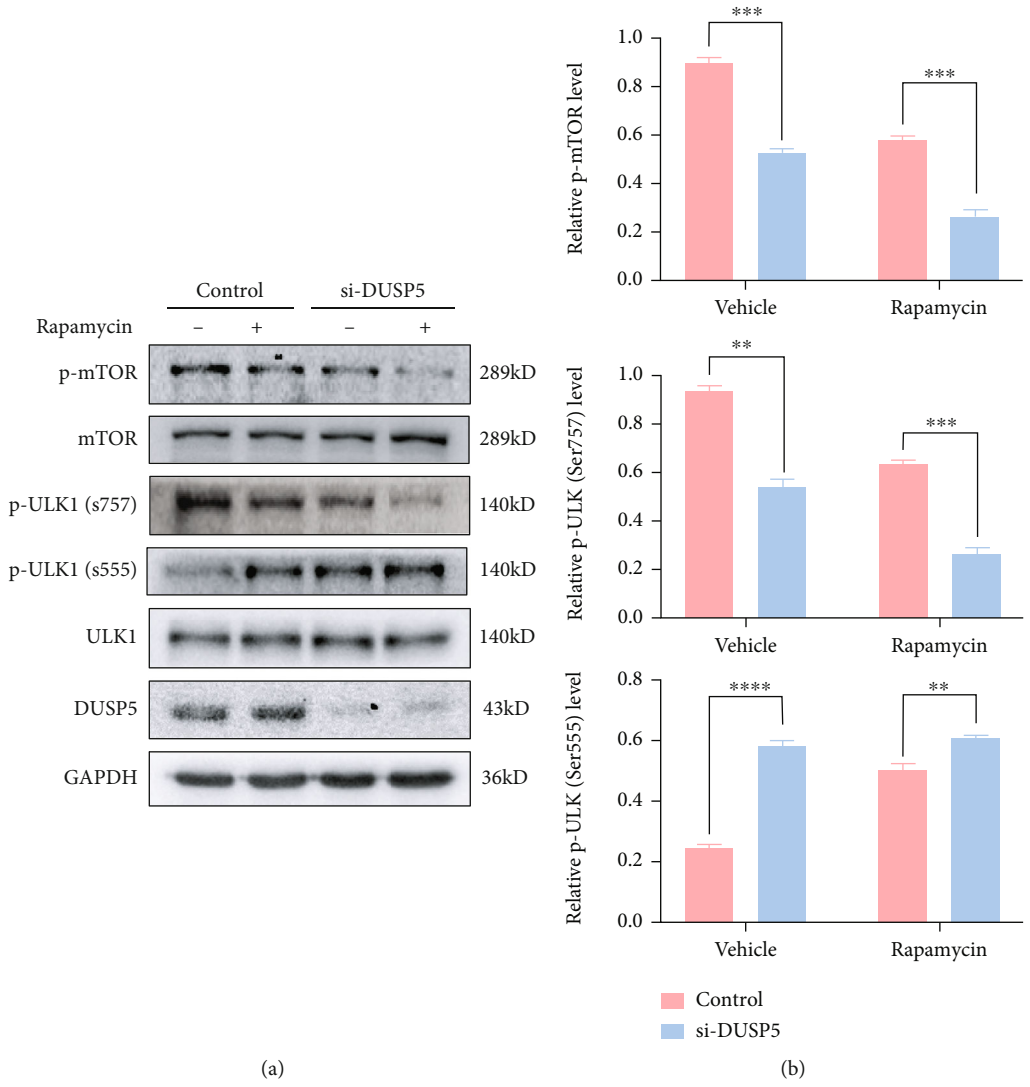

Figure 5: Continued.

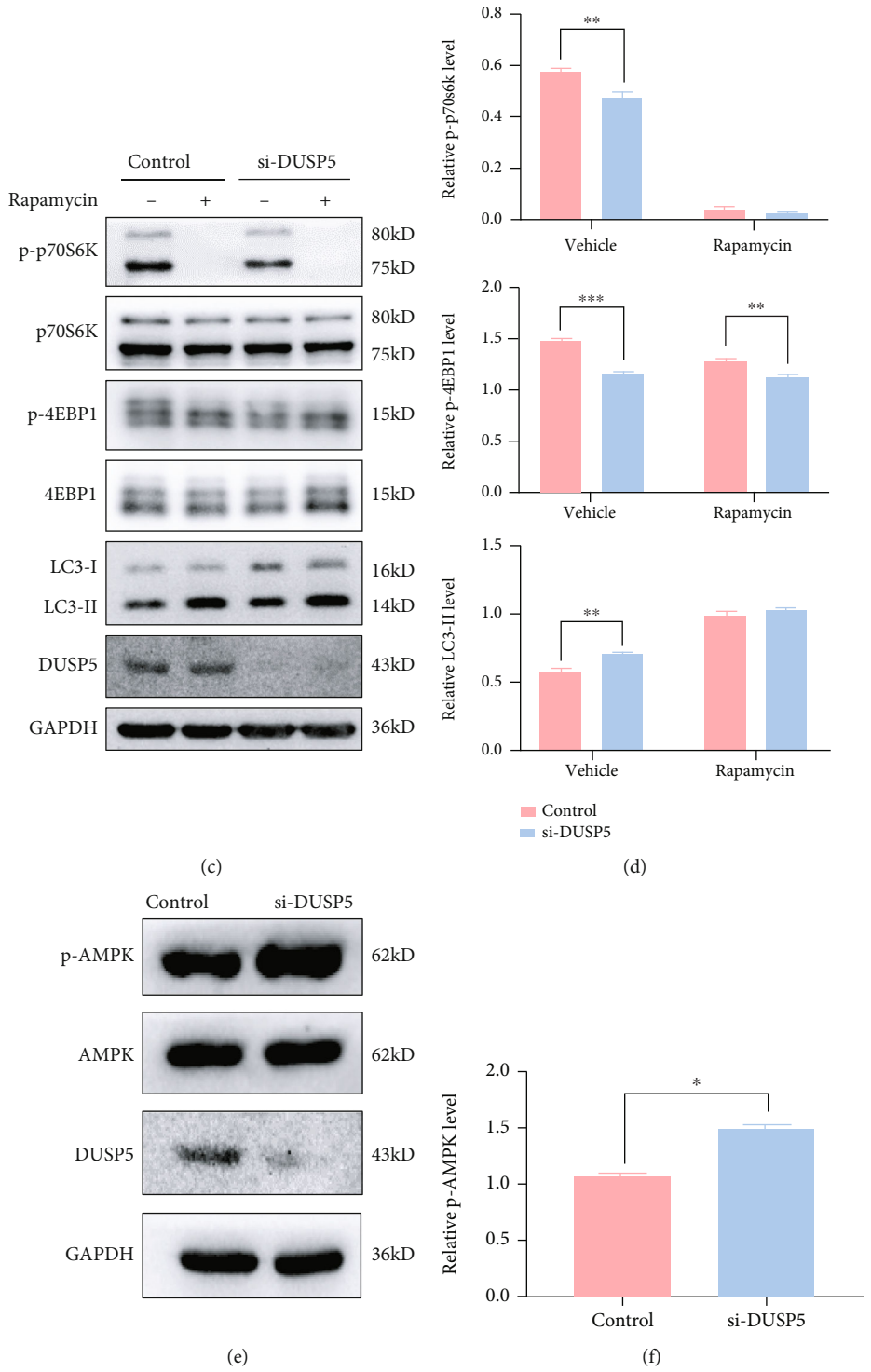

Figure 5: Effects of DUSP5 deficiency on mTOR signaling. (a) Western analysis of phosphorylated and total mTOR and ULK1 levels and DUSP5 levels inDUSP5-deficient and control NHEKs after pre-treatment with rapamycin or a vehicle control. (b) Quantification of phosphorylated mTOR and ULK1 levels from panel a, using total mTOR and ULK1 levels for normalization. (c) Western analysis of phosphorylated and total P70S6K and 4EBP1 levels and LC3 and DUSP5 levels in DUSP5-deficient and control NHEKs after pre-treatment with rapamycin or a vehicle control. (d) Quantification of phosphorylated P70S6K and 4EBP1 levels and LC3-II levels from panel c, using GAPDH (LC3-II) or total P70S6K and 4EBP1 levels for normalization. (e) Western analysis of phosphorylated and total AMPK levels and DUSP5 levels in DUSP5-deficient and control NHEKs. (f) Quantification of phosphorylated AMPK levels in panel e, suing total AMPK levels for normalization. Significant differences were identified by Student's *t*-test. ∗, $p < 0.05$; ∗∗, $p < 0.01$; ∗∗∗, $p < 0.005$; ∗∗∗∗, $p < 0.001$.

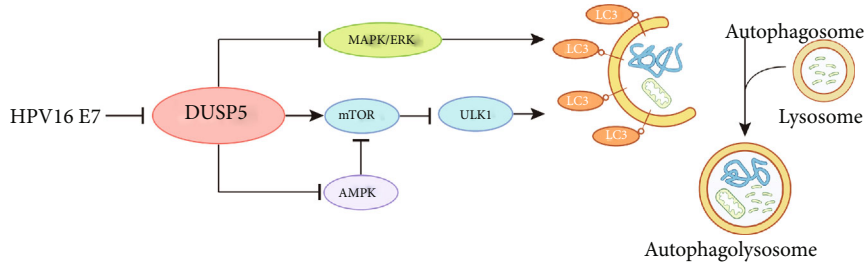

Figure 6: Schematic diagram showing that HPV16 E7 induces autophagy by inhibiting DUSP5 through the MAPK/ERK pathway and mTOR signaling.

human keratinocytes by transmission electron microscopy and Western blotting, suggesting that autophagosome-lysosome fusion was blocked. Furthermore, by comparing empty vector, E6, E7 and HPV16 E6/E7-transduced keratinocytes, they concluded that the blockage of late steps in basal autophagy was E6-dependent, because accumulation of p62 was already observed after transduction with HPV16 E6 alone [43]. Activated autophagy has been confirmed to correlate with poor prognosis in some cancer types, while targeting cancer cells with autophagosome inhibitor 3-methyl adenine induced apoptosis, pointing to a possible anticancer therapy [44].

Some studies have shown that activated MAPK/ERK signaling is involved in tumor growth and proliferation in cervical cancer [45, 46]. Therefore, targeting DUSPs, which are key regulators of MAPKs, is expected to be a suitable strategy for anticancer drug development. Our current study showed that expression of DUSP5 is severely repressed in cervical cancer tissues. Consistent with our results, DUSP5 expression in pre-eclampsia inhibits trophoblast proliferation, migration and invasion [47]. In addition, it has been shown that DUSP5-mediated ERK suppression can serve as a protective mechanism by blocking pulmonary vascular smooth muscle cell proliferation, by preventing pulmonary hypertension and right ventricular cardiac hypertrophy [48] and by inhibiting inflammation in adipocytes [35]. It has furthermore been shown that DUSP5 is critical for regulation of immunity and tolerance, since DUSP5-expressing mature T cells exhibit decreased IL-2-dependent proliferation and defective IL-2-mediated induction of genes [49]. Collectively, these studies suggest that DUSP5 has important functions in mammalian biology and may serve as a viable drug target.

Increased ERK phosphorylation was found in neural progenitor cells [50] and the rat fibroblast cell line 3Y1 [51], and human keratinocytes expressing HPV oncogene E7 or inhibitors of ERK signaling can reduce oncogene expression and inhibit a neoplastic phenotype through EGFR/MEK/ERK signaling [52] or K-Ras/ERK signaling [53, 54]. In a skin carcinogenesis mouse model, papilloma formation was found in mice lacking DUSP5 and its regulation of nuclear ERK activity also served DUSP5 as tumor suppressor in epidermis Ras modulation [55]. We consistently found DUSP5 deficiency increased ERK phosphorylation, similar as observed after HPV16 E7 expression. mTOR signaling was also found to be regulated by DUSP5, and based on their studies by Bermudez et al. on DUSP6 [56] and Benavides-Serrato et al. on DUSP10 and the mTORC2 pathway in glioblastoma [57], there might be crosstalk between the ERK and mTOR pathways. These studies and our result highlight the future potential of modulating ERK signaling for HPV neoplasia treatment.

5. Conclusions

In conclusion, understanding the role of autophagy during different stages of HPV-associated diseases provides an opportunity to generate novel autophagy-targeting treatment strategies. Our report sheds light on a novel molecular mechanism explaining how HPV16 E7 modulates host-cell autophagy, an important pathway for HPV-mediated malignant transformation and disease. We demonstrate that DUSP5 expression is inversely correlated with HPV16 E7 expression and that HPV16 E7-mediated repression of DUSP5 induces autophagy via phosphorylation of MAPK/ERK, mTOR and AMPK, resulting in activation of ULK1 (Figure 6).

Abbreviations

HPV: Human papillomavirus
NHEKs: Normal human epidermal keratinocytes.

Data Availability

The datasets used and analyzed during the current study are available from the corresponding author upon reasonable request.

Conflicts of Interest

The authors have declared that no competing interest exists.

Authors' Contributions

Chunting Hua carried out the experiments and wrote the original draft. Qiaoli Zheng, Jiang Zhu participated in formal data analysis. Siji Chen drew the graphical abstract. Yinjing Song assisted with data curation. Stijn van der veen and Hao Cheng contributed to supervision and manuscript proofreading. All authors have read and approved to submit the manuscript.

Acknowledgments

This study was supported by the Science and Technology Projects of Zhejiang Province (2018C04013), the Natural Science Foundation of Zhejiang Province (LQ19H190002), Young Scientists Fund of the National Natural Science Foundation of China (No. 81801992) and the Foundation from the Health Bureau of Zhejiang Province (2019PY037). The authors have declared that no competing interest exists. We would like to thank Sir Run Run Shaw Hospital and Collaborative Innovation Center for Diagnosis and Treatment of Infectious Diseases for supporting this study.

Supplementary Materials

Supplementary 1. Supplementary Figure 1: DNA Gel Electrophoresis of nested PCR products. M: DNA marker, Lane1: cervicitis tissue, Lane2: cervical intraepithelial neoplasia (CIN) tissue, Lane3: cervical cancer tissue.

Supplementary 2. Supplementary Figure 2: Verification of HPV16 E7 antibodies. Coomassie blue staining of different products during antibody preparation. M: protein marker, Lane1: supernatant of DH5α lysates after ultrasonication, Lane2: precipitation of DH5α lysates after ultrasonication, Lane3: supernatant of Lane1 lysates after incubation with Glutaphione-Sepharose 4B beads (GST fusion protein), Lane4: supernatant of Lane3 lysates after incubation with thrombin and cleavage of GST tag (HPV16 E7 protein), Lane5: precipitation of Lane4.

Supplementary 3. Supplementary Figure 3: Verification of HPV16 E7-expressing NHEKs. (a) Fluorescence microscopy observation of NHEKs carrying mock lentivirus and HPV16 E7. (b) Fluorescence activated cell sorting by flow cytometry of negative control, mock and HPV16 E7 lentivirus infected NHEKs. (c) Western analysis of HPV16 E7 in mock and HPV16 E7 lentivirus-infected NHEKs.

Supplementary 4. Supplementary Figure 4: HPV16 E7 activates autophagy through mTOR signaling. (a) Western analysis of phosphorylated and total mTOR, ULK1, P70S6K, and 4EBP1 and LC3 in HPV16 E7-expressing and control NHEKs. (b) Quantification of LC3-II, DUSP5 and phosphorylated mTOR, ULK1, P70S6K, and 4EBP1 levels from panel a, using GAPDH (LC3-II and DUSP5) or total mTOR, ULK1, P70S6K, and 4EBP1 levels for normalization. Significant differences were identified by Student's t-test. $*$, $p < 0.05$; $**$.

Supplementary 5. Supplementary Table 1: Accession, characteristics and value of DUSP5 of normal cervix or cervical cancer samples.

References

[1] C. A. Moody and L. A. Laimins, "Human papillomavirus oncoproteins: pathways to transformation," *Nature reviews. Cancer*, vol. 10, no. 8, pp. 550–560, 2010.

[2] D. Sir, W. L. Chen, J. Choi, T. Wakita, T. S. Yen, and J. H. Ou, "Induction of incomplete autophagic response by hepatitis C virus via the unfolded protein response," *Hepatology*, vol. 48, no. 4, pp. 1054–1061, 2008.

[3] M. Panyasrivanit, A. Khakpoor, N. Wikan, and D. R. Smith, "Linking dengue virus entry and translation/replication through amphisomes," *Autophagy*, vol. 5, no. 3, pp. 434-435, 2009.

[4] M. P. Taylor and K. Kirkegaard, "Modification of cellular autophagy protein LC3 by poliovirus," *Journal of Virology*, vol. 81, no. 22, pp. 12543–12553, 2007.

[5] M. N. Takahashi, W. Jackson, D. T. Laird et al., "Varicella-zoster virus infection induces autophagy in both cultured cells and human skin vesicles," *Journal of Virology*, vol. 83, no. 11, pp. 5466–5476, 2009.

[6] H. K. Lee, J. M. Lund, B. Ramanathan, N. Mizushima, and A. Iwasaki, "Autophagy-dependent viral recognition by plasmacytoid dendritic cells," *Science*, vol. 315, no. 5817, pp. 1398–1401, 2007.

[7] T. Prabakaran, C. Bodda, C. Krapp et al., "Attenuation of cGAS-STINGsignaling is mediated by a p62/SQSTM1-dependent autophagy pathway activated by TBK1," *The EMBO Journal*, vol. 37, no. 8, 2018.

[8] L. English, M. Chemali, J. Duron et al., "Autophagy enhances the presentation of endogenous viral antigens on MHC class I molecules during HSV-1 infection," *Nature Immunology*, vol. 10, no. 5, pp. 480–487, 2009.

[9] L. English, M. Chemali, and M. Desjardins, "Nuclear membrane-derived autophagy, a novel process that participates in the presentation of endogenous viral antigens during HSV-1 infection," *Autophagy*, vol. 5, no. 7, pp. 1026–1029, 2009.

[10] L. Ahmad, S. Mostowy, and V. Sancho-Shimizu, "Autophagy-Virus Interplay: From Cell Biology to Human Disease," *Frontiers in Cell and Developmental Biology*, vol. 6, p. 155, 2018.

[11] A. I. Chiramel, N. R. Brady, and R. Bartenschlager, "Divergent roles of autophagy in virus infection," *Cells*, vol. 2, no. 1, pp. 83–104, 2013.

[12] G. Randall, "Lipid Droplet Metabolism during Dengue Virus Infection," *Trends in Microbiology*, vol. 26, no. 8, pp. 640–642, 2018.

[13] W. C. Tang, R. J. Lin, C. L. Liao, and Y. L. Lin, "Rab18 facilitates dengue virus infection by targeting fatty acid synthase to sites of viral replication," *Journal of Virology*, vol. 88, no. 12, pp. 6793–6804, 2014.

[14] E. White, "The role for autophagy in cancer," *The Journal of Clinical Investigation*, vol. 125, no. 1, pp. 42–46, 2015.

[15] E. Zhu, H. Wu, W. Chen et al., "Classical swine fever virus employs the PERK- and IRE1-dependent autophagy for viral replication in cultured cells," *Virulence*, vol. 12, no. 1, pp. 130–149, 2021.

[16] H. H. Tseng, W. R. Huang, C. Y. Cheng et al., "Aspirin and 5-Aminoimidazole-4-carboxamide Riboside Attenuate Bovine Ephemeral Fever Virus Replication by Inhibiting BEFV-Induced Autophagy," *Frontiers in Immunology*, vol. 11, article 556838, p. 2999, 2020.

[17] A. K. Aranda-Rivera, A. Cruz-Gregorio, A. Briones-Herrera, and J. Pedraza-Chaverri, "Regulation of autophagy by high- and low-risk human papillomaviruses," *Reviews in Medical Virology*, vol. 31, no. 2, p. e2169, 2021.

[18] X. Zhou and K. Münger, "Expression of the human papillomavirus type 16 E7 oncoprotein induces an autophagy-related process and sensitizes normal human keratinocytes to cell death in response to growth factor deprivation," *Virology*, vol. 385, no. 1, pp. 192–197, 2009.

[19] C. Tingting, Y. Shizhou, Z. Songfa et al., "Human papillomavirus 16E6/E7 activates autophagy via Atg9B and LAMP1 in cervical cancer cells," *Cancer Medicine*, vol. 8, no. 9, pp. 4404–4416, 2019.

[20] J. E. Hanning, H. K. Saini, M. J. Murray et al., "Depletion of HPV16 early genes induces autophagy and senescence in a cervical carcinogenesis model, regardless of viral physical state," *The Journal of Pathology*, vol. 231, no. 3, pp. 354–366, 2013.

[21] E. Cararo-Lopes, M. H. Dias, M. S. da Silva et al., "Autophagy buffers Ras-induced genotoxic stress enabling malignant transformation in keratinocytes primed by human papillomavirus," *Cell Death & Disease*, vol. 12, no. 2, p. 194, 2021.

[22] C. Hua, J. Zhu, B. Zhang et al., "Digital RNA Sequencing of Human Epidermal Keratinocytes Carrying Human Papillomavirus Type 16 E7," *Frontiers in Genetics*, vol. 11, p. 819, 2020.

[23] K. L. Jeffrey, M. Camps, C. Rommel, and C. R. Mackay, "Targeting dual-specificity phosphatases: manipulating MAP kinase signalling and immune responses," *Nature Reviews. Drug Discovery*, vol. 6, no. 5, pp. 391–403, 2007.

[24] K. I. Patterson, T. Brummer, P. M. O'brien, and R. J. Daly, "Dual-specificity phosphatases: critical regulators with diverse cellular targets," *The Biochemical Journal*, vol. 418, no. 3, pp. 475–489, 2009.

[25] J. M. Kyriakis and J. Avruch, "Mammalian mitogen-activated protein kinase signal transduction pathways activated by stress and inflammation," *Physiological Reviews*, vol. 81, no. 2, pp. 807–869, 2001.

[26] W. Peti and R. Page, "Molecular basis of MAP kinase regulation," *Protein Science: a Publication of the Protein Society*, vol. 22, no. 12, pp. 1698–1710, 2013.

[27] K. Aoyama, M. Nagata, K. Oshima, T. Matsuda, and N. Aoki, "Retraction: Molecular cloning and characterization of a novel dual specificity phosphatase, LMW-DSP2, that lacks the Cdc25 homology domain.," *The Journal of Biological Chemistry*, vol. 288, no. 35, pp. 25658–27583, 2013.

[28] X. H. Fu, C. Z. Chen, S. Li et al., "Dual-specificity phosphatase 1 regulates cell cycle progression and apoptosis in cumulus cells by affecting mitochondrial function, oxidative stress, and autophagy," *American Journal of Physiology. Cell Physiology*, vol. 317, no. 6, pp. C1183–C1193, 2019.

[29] H. Huang, H. Liu, J. Tang et al., "M2 macrophage-derived exosomal miR-25-3p improves high glucose-induced podocytes injury through activation autophagy via inhibiting DUSP1 expression," *IUBMB life*, vol. 72, no. 12, pp. 2651–2662, 2020.

[30] J. Wang, J. Y. Zhou, D. Kho, J. J. Reiners Jr., and G. S. Wu, "Role for DUSP1 (dual-specificity protein phosphatase 1) in the regulation of autophagy," *Autophagy*, vol. 12, no. 10, pp. 1791–1803, 2016.

[31] J. Luo, D. Xue, F. Song, X. Liu, W. Li, and Y. Wang, "DUSP5 (dual-specificity protein phosphatase 5) suppresses BCG-induced autophagy via ERK 1/2 signaling pathway," *Molecular Immunology*, vol. 126, pp. 101–109, 2020.

[32] H. Min and W. He, "Long non-coding RNA ARAP1-AS1 promotes the proliferation and migration in cervical cancer through epigenetic regulation of DUSP5," *Cancer Biology & Therapy*, vol. 21, no. 10, pp. 907–914, 2020.

[33] L. Scotto, G. Narayan, S. V. Nandula et al., "Identification of copy number gain and overexpressed genes on chromosome arm 20q by an integrative genomic approach in cervical cancer: potential role in progression," *Genes, Chromosomes & Cancer*, vol. 47, no. 9, pp. 755–765, 2008.

[34] R. D. Bongard, M. Lepley, A. Gastonguay et al., "Discovery and Characterization of Halogenated Xanthene Inhibitors of DUSP5 as Potential Photodynamic Therapeutics," *Journal of Photochemistry and Photobiology A: Chemistry*, vol. 375, pp. 114–131, 2019.

[35] J. S. Habibian, M. Jefic, R. A. Bagchi et al., "DUSP5 functions as a feedback regulator of TNFα-induced ERK1/2 dephosphorylation and inflammatory gene expression in adipocytes," *Scientific Reports*, vol. 7, no. 1, pp. 1–11, 2017.

[36] P. Chen, Y. Wang, L. Chen, N. Song, and J. Xie, "Apelin-13 Protects Dopaminergic Neurons against Rotenone-Induced Neurotoxicity through the AMPK/mTOR/ULK-1 Mediated Autophagy Activation," *International Journal of Molecular Sciences*, vol. 21, no. 21, p. 8376, 2020.

[37] Z. Surviladze, R. T. Sterk, S. A. DeHaro, and M. A. Ozbun, "Cellular entry of human papillomavirus type 16 involves activation of the phosphatidylinositol 3-kinase/Akt/mTOR pathway and inhibition of autophagy," *Journal of Virology*, vol. 87, no. 5, pp. 2508–2517, 2013.

[38] H. Y. Wang, G. F. Yang, Y. H. Huang et al., "Reduced expression of autophagy markers correlates with high-risk human papillomavirus infection in human cervical squamous cell carcinoma," *Oncology Letters*, vol. 8, no. 4, pp. 1492–1498, 2014.

[39] W. Zhu, X. Pan, F. Li, Y. Zhang, and X. Lu, "Expression of Beclin 1 and LC3 in FIGO stage I-II cervical squamous cell carcinoma and relationship to survival," *Tumour Biology*, vol. 33, no. 5, pp. 1653–1659, 2012.

[40] R. Han, C. Hua, S. Sun et al., "Autophagy is induced in human keratinocytes during human papillomavirus 11 pseudovirion entry," *Aging*, vol. 12, no. 22, pp. 23017–23028, 2020.

[41] B. Zhang, Y. Song, S. Sun et al., "Human Papillomavirus 11 Early Protein E6 Activates Autophagy by Repressing AKT/mTOR and Erk/mTOR," *Journal of Virology*, vol. 93, no. 12, 2019.

[42] X. Luo, C. R. Donnelly, W. Gong et al., "HPV16 drives cancer immune escape via NLRX1-mediated degradation of STING," *The Journal of Clinical Investigation*, vol. 130, no. 4, pp. 1635–1652, 2020.

[43] D. Mattoscio, C. Casadio, C. Miccolo et al., "Autophagy regulates UBC9 levels during viral-mediated tumorigenesis," *PLoS Pathogens*, vol. 13, no. 3, p. e1006262, 2017.

[44] S. Fujii, S. Mitsunaga, M. Yamazaki et al., "Autophagy is activated in pancreatic cancer cells and correlates with poor patient outcome," *Cancer Science*, vol. 99, no. 9, pp. 1813–1819, 2008.

[45] Y. Che, Y. Li, F. Zheng et al., "TRIP4 promotes tumor growth and metastasis and regulates radiosensitivity of cervical cancer by activating MAPK, PI3K/AKT, and hTERT signaling," *Cancer Letters*, vol. 452, pp. 1–13, 2019.

[46] S. Li, Y. M. Ma, P. S. Zheng, and P. Zhang, "GDF15 promotes the proliferation of cervical cancer cells by phosphorylating AKT1 and Erk1/2 through the receptor ErbB2," *Journal of Experimental & Clinical Cancer Research*, vol. 37, no. 1, pp. 1–14, 2018.

[47] S. Zhang, Y. Zou, X. Tang et al., "Silencing of AFAP1-AS1 lncRNA impairs cell proliferation and migration by epigenetically promoting DUSP5 expression in pre-eclampsia," *Journal of Cellular Biochemistry*, vol. 122, no. 10, pp. 1506–1516, 2021.

[48] B. S. Ferguson, S. A. Wennersten, K. M. Demos-Davies et al., "DUSP5-mediated inhibition of smooth muscle cell proliferation suppresses pulmonary hypertension and right ventricular

hypertrophy," *American Journal of Physiology. Heart and Circulatory Physiology*, vol. 321, no. 2, pp. H382–H389, 2021.

[49] P. E. Kovanen, J. Bernard, A. Al-Shami et al., "T-cell Development and Function Are Modulated by Dual Specificity Phosphatase DUSP5*," *Journal of Biological Chemistry*, vol. 283, no. 25, pp. 17362–17369, 2008.

[50] K. Piltti, L. Kerosuo, J. Hakanen et al., "E6/E7 oncogenes increase and tumor suppressors decrease the proportion of self-renewing neural progenitor cells," *Oncogene*, vol. 25, no. 35, pp. 4880–4889, 2006.

[51] H. Yuan, S. Ito, T. Senga et al., "Human papillomavirus type 16 oncoprotein E7 suppresses cadherin-mediated cell adhesion via ERK and AP-1 signaling," *International Journal of Oncology*, vol. 35, no. 2, pp. 309–314, 2009.

[52] A. J. Luna, R. T. Sterk, A. M. Griego-Fisher et al., "MEK/ERK signaling is a critical regulator of high-risk human papillomavirus oncogene expression revealing therapeutic targets for HPV-induced tumors," *PLoS Pathogens*, vol. 17, no. 1, p. e1009216, 2021.

[53] S. S. Boon, C. Xia, J. Y. Lim et al., "Human Papillomavirus 58 E7 T20I/G63S Variant Isolated from an East Asian Population Possesses High Oncogenicity," *Journal of Virology*, vol. 94, no. 8, 2020.

[54] P. M. Campbell, A. L. Groehler, K. M. Lee, M. M. Ouellette, V. Khazak, and C. J. Der, "K-Ras promotes growth transformation and invasion of immortalized human pancreatic cells by Raf and phosphatidylinositol 3-kinase signaling," *Cancer Research*, vol. 67, no. 5, pp. 2098–2106, 2007.

[55] L. K. Rushworth, A. M. Kidger, L. Delavaine et al., "Dual-specificity phosphatase 5 regulates nuclear ERK activity and suppresses skin cancer by inhibiting mutant Harvey-Ras HRasQ61L-driven SerpinB2 expression," *Proceedings of the National Academy of Sciences of the United States of America*, vol. 111, no. 51, pp. 18267–18272, 2014.

[56] O. Bermudez, S. Marchetti, G. Pagès, and C. Gimond, "Post-translational regulation of the ERK phosphatase DUSP6/MKP3 by the mTOR pathway," *Oncogene*, vol. 27, no. 26, pp. 3685–3691, 2008.

[57] A. Benavides-Serrato, L. Anderson, B. Holmes et al., "mTORC2 modulates feedback regulation of p38 MAPK activity via DUSP10/MKP5 to confer differential responses to PP242 in glioblastoma," *Genes & Cancer*, vol. 5, no. 11-12, pp. 393–406, 2014.

Hindawi
Oxidative Medicine and Cellular Longevity
Volume 2022, Article ID 5503575, 15 pages
https://doi.org/10.1155/2022/5503575

Research Article

CBX4 Regulates Replicative Senescence of WI-38 Fibroblasts

Yu-Hsiu Chen,[1,2,3] **Xin Zhang**,[1,4] **Kuei-Yueh Ko**,[5] **Ming-Feng Hsueh**,[1,4] **and Virginia Byers Kraus**[1,3,4,6]

[1]*Duke Molecular Physiology Institute, Duke University, Durham, NC, USA*
[2]*Division of Rheumatology/Immunology/Allergy, Department of Internal Medicine, Tri-Service General Hospital, National Defense Medical Center, Taiwan*
[3]*Department of Pathology, Duke University Medical Center, Durham, NC, USA*
[4]*Department of Orthopaedic Surgery, Duke University, Durham, NC, USA*
[5]*Department of Biostatistics & Bioinformatics, Duke University, Durham, NC, USA*
[6]*Department of Medicine, Duke University School of Medicine, Durham, NC, USA*

Correspondence should be addressed to Virginia Byers Kraus; kraus004@duke.edu

Received 20 December 2021; Accepted 26 January 2022; Published 23 February 2022

Academic Editor: Milena Georgieva

Cellular senescence is characterized by cell cycle arrest and senescence-associated secretory phenotypes. Cellular senescence can be caused by various stress stimuli such as DNA damage, oxidative stress, and telomere attrition and is related to several chronic diseases, including atherosclerosis, Alzheimer's disease, and osteoarthritis. Chromobox homolog 4 (CBX4) has been shown to alleviate cellular senescence in human mesenchymal stem cells and is considered a possible target for senomorphic treatment. Here, we explored whether CBX4 expression is associated with replicative senescence in WI-38 fibroblasts, a classic human senescence model system. We also examined whether and how regulation of CBX4 modifies the senescence phenotype and functions as an antisenescence target in WI-38. During the serial culture of the WI-38 primary fibroblast cell line to a senescent state, we found increased expression of senescence markers, including senescence β-galactosidase (SA-βgal) activity, protein expression of p16, p21, and DPP4, and decreased proliferation marker EdU; moreover, CBX4 protein expression declined. With knockdown of CBX4, SA-βgal activity and p16 protein expression increased, and EdU decreased. With the activation of CBX4, SA-βgal activity, p16, and DPP4 protein decreased. In addition, CBX4 knockdown increased, while CBX4 activation decreased, gene expression of both CDKN2A (encoding the p16 protein) and DPP4. Genes related to DNA damage and cell cycle pathways were regulated by CBX4. These results demonstrate that CBX4 can regulate replicative senescence in a manner consistent with a senomorphic agent.

1. Introduction

Cellular senescence is a state of permanent cell cycle arrest related to telomere attrition, DNA damage, chronic inflammation, mitochondrial dysfunction, or other causes [1]. Cellular senescence has long been proposed as an anticancer mechanism since it can prevent the proliferation of cells with genomic instability [2]. It has also been linked to the pathogenesis of several chronic diseases, including atherosclerosis, Alzheimer's disease, and osteoarthritis (OA) [1, 3],. Cellular senescence was first described by Hayflick and Moorhead in 1961 as the phenomenon of cessation of cell division of human WI-38 fibroblasts after a maximum of 50 cell cycles [4]. The WI-38 primary cell line, originating from fetal lung tissue, has been widely used in vaccine development [5] and the study of senescence [6].

Senescent cells are characterized by decreasing proliferation and increasing cell granularity, cell size, lysosome content, and senescence-associated secretory phenotypes (SASPs). The accumulation of senescent cells and their secretion of SASPs are considered risk factors for age-related diseases. Several markers have been associated with cellular senescence, including increased senescence β-galactosidase (SA-β-gal) activity [6], and increased expression of

p16 protein (gene CDKN2A), p21 protein (gene CDKN1A) [7], DPP4 protein (also known as CD26) [8], and decreased Lamin B1 protein (gene LMNB1) [9] and proliferation marker EdU [10]. These markers are generally used to identify cellular senescence and could be used to monitor the effects of senolytic agents to eliminate senescent cells and/or senomorphics to modify senescence phenotypes.

Targeted senomorphic strategies that preserve senescent cells but eliminate their detrimental effects might preserve tissue function and reserve better than senolytic strategies. For this reason, our goal was to investigate one possible agent, chromobox homolog 4 (CBX4), for senomorphic characteristics. CBX4 is a nuclear protein detected in all cells. CBX4 has been shown to alleviate cellular senescence in human mesenchymal stem cells (hMSCs) and to attenuate OA upon local overexpression in an experimental posttraumatic OA mouse model [11]. CBX4, a polycomb repressive complex (PRC1) associated protein and an E3 small ubiquitin-related modifier-protein(SUMO) ligase [12], has been discovered to regulate protein activity involved in DNA damage repair [13]. Higher expression of CBX4 has been implicated in the progression of hepatocellular cancer, breast cancer, and osteosarcoma [14], [15], [16] but has a protective effect in colon cancer [17]. CBX4 has also been shown to regulate cell proliferation, differentiation, and self-renewal in hematopoietic stem cells and epidermal stem cells [18, 19]. However, CBX4 expression and its role in cellular senescence in a terminally differentiated cell, such as WI-38 fibroblasts, have not been thoroughly investigated. To fill this knowledge gap, we investigated the role of CBX4 in replicative senescence in WI-38 human diploid lung fibroblasts. We hypothesized that CBX4 could regulate WI-38 replicative senescence, preserve tissue integrity by reducing inflammation and maintaining cell viability, and thereby function as a senomorphic agent. We confirmed the senomorphic capability of CBX4 through modification of WI-38 senescence phenotypes with gain and loss of CBX4 expression *in vitro*.

2. Materials and Methods

2.1. Cell Line Culture. The human diploid fibroblast WI-38 cell line (American Type Culture Collection, ATCC® CCL75™) was cultured in Minimum Essential Medium Eagle (Sigma-Aldrich, M4655) containing 10% FBS (Sigma-Aldrich, F2442), 1× Non-Essential Amino Acids Solution (Gibco, 11140050), 1 : 100 L-Glutamine–Penicillin–Streptomycin solution (Sigma-Aldrich, G6784), and maintained in a 37°C, 5% CO2 incubator. WI-38 fibroblasts were cultured from a cumulative population doubling (CPD) level of 37 representing a proliferative state based on Sidler et al. [20, 21], to a senescent state defined by a failure to double after one week (CPD 56-60) [6]. Serial culture of WI-38 was performed by seeding cells at a density of 7000 cells/cm^2 and trypsinization with 0.25% (weight/volume) Trypsin-0.53 mM EDTA solution every 3-4 days until senescent status was reached. Cell numbers were recorded for estimated CPD and doubling time. Doubling time was calculated as follows: Doubling time = duration $*$ $\log_2(2)/\log_2$ (Final Cell Concentration) – $\log_2$ (Initial Cell Concentration) [22].

2.2. Lentiviral Transduction of CBX4. Lentiviral transduction was done without adding polybrene, which could induce cellular senescence [23]. GFP expressing lentiviral particles (copGFP, Santa Cruz Bio, sc-108084) were used as a control to monitor and optimize transduction efficiency. The copGFP control lentiviral particles added at MOI 0.5-8 to WI-38 with puromycin selection for 4 days were able to achieve >90% stable GFP expression (Figure S1). As our outcomes of interest related to senescence can be induced by stress, our goal was to maximize transduction efficiency with a minimum of stress. For this reason, for these studies, we elected to avoid the use of polybrene that we observed caused some cytotoxicity in this model system. CBX4 knockdown (KD) experiments were performed with CBX4 shRNA and control shRNA lentiviral particles (Santa Cruz Bio, sc-38193-V, sc108080). CBX4 shRNA and control lentiviral particles were added to presenescent WI-38 (CPD47-50) at a multiplicity of infection (MOI) of 0.5, 1, and 2. Culture media were changed 24 hours after transduction. 3 days later, transduced cells were trypsinized and reseeded at a density of 7000/cm^2 in 24-well plates. Puromycin 0.5 μg/ml was added to the culture medium to select stably transduced cells. After 3-4 days of selection, CBX4 KD cells were collected for further assays. CBX4 activation (ACT) experiments were performed with a CBX4 CRISPR/Cas9 Synergistic Activation Mediator (SAM) system and control particles (Santa Cruz Bio.sc-403903-LAC, sc-437282). CBX4 activation and control lentiviral particles were added to presenescent WI-38 (CPD47-50) at a MOI 6. Culture media were changed 24 hours after transduction. 3 days later, transduced cells were trypsinized and reseeded at a density of 7000 cells/cm^2 in 24-well plates. Antibiotics (puromycin 0.5 μg/ml, blasticidin 1 μg/ml, and hygromycin 50 μg/ml) were added sequentially to select stably transduced cells. After blasticidin selection, cells were detached and reseeded at a density of 7000 cells/cm^2 in 24-well plates and cultures continued with hygromycin selection. After 15-17 days of antibiotics selection, CBX4 ACT cells were collected for further assays.

2.3. Senescence β-Galactosidase (SA-β-gal). CellEvent Senescence Green Flow Cytometry Assay Kit (Thermo Fisher, C10840) was used to quantify SA-β-gal [24] activity. Following cell collection, $1 - 2 \times 10^4$ cells were fixed with 100 μl 4% paraformaldehyde (PFA, Thermo Fisher 50980487) for 15 minutes, washed twice with phosphate-buffered saline (PBS) containing 1% bovine serum albumin (BSA, Sigma A3294), and incubated with senescence green working solution, 100 μl at 37°C for 2 hours. Next, cells were washed twice with PBS containing 1% BSA, with detection using an Attune NxT flow cytometer (Thermo Fisher) or followed by permeabilization for costaining with EdU or p16. Unstained cells were used to determine the fluorescence background.

2.4. EdU Cell Proliferation Assays. EdU [10] (5-ethynyl-2′-deoxyuridine) (EMD Millipore, 1710525; Thermo Fisher, C10424) at a concentration of 10 μM was added to the WI-38 cell culture media for 24 hours. Cells were harvested and counted; $1-2\times10^4$ cells were fixed with 4% PFA and permeabilized with permeabilization buffer (Thermo Fisher, 00-8333-56), then incubated with Click working solution for 30 minutes. Finally, cells were washed twice with permeabilization buffer, followed by detection with an Attune NxT for flow cytometer. Unstained cells were used to determine the fluorescence background.

2.5. Flow Cytometry. The staining method for flow cytometry was done as previously described [25]. Following cell collection, $1-2\times10^4$ cells were resuspended in 100 μl PBS containing 1% BSA. PE-conjugated anti-DPP4 mAb (2 : 100, Thermo Fisher, 12-0269-42) was added for 30 mins at room temperature. After surface staining, the cells were washed, followed by flow cytometry acquisition or fixation and permeabilization for intracellular staining. For p21 staining, WI-38 cells were incubated with AF488-conjugated anti-p21 mAbs (1 : 100, CST, 5487). Unstained cells were used to determine the fluorescence background. For p16 staining, WI-38 cells were stained with unconjugated anti-p16 mAbs or a control antibody (20 : 100, both from Roche CINtec kit 9517) for 30 mins; then followed by AF647-conjugated anti-mouse IgG2a secondary antibody (1 : 1000, Jackson, 115607186). The stained cells were analyzed using an Attune NxT flow cytometer. Data were analyzed using FlowJo V10.8 software (BD Life Sciences) and were presented as gated percentage.

2.6. Western Blot. WI-38 cells were lysed using RIPA lysis buffer (Sigma-Aldrich, R0278) or a PARIS™ Kit (Thermo Fisher, AM1921) with a protease inhibitor cocktail (Sigma-Aldrich, P8340). PARIS™ Kit was used in lentiviral transduced samples to enable the use of cell lysates for both RNA and protein detection. A total of 5-10 μg extracted protein, determined by the DC protein assay (Bio-Rad, 5000112), was mixed with 4× Laemmli sample buffer (Bio-Rad, 1610747), heated to 95°C for 5 minutes, and electrophoresed (100 V for 2 hours) on 10% Mini-PROTEAN® TGX Stain-Free™ Protein Gels (Bio-Rad, 4568033). Proteins were transferred onto polyvinylidene fluoride (PVDF) membranes using the Trans-blot turbo system (Bio-Rad, 1704274), using a standard SD protocol: up to 1.0 A; 25 V for 30 minutes followed by blocking with Tris-buffered saline Tween 20 buffer (TBST, Thermo Fisher, 28360) containing 5% fat-free milk (CST, 9999 s) for 1 hour at room temperature. Membranes were washed three times with TBST and then incubated with primary antibodies, anti-CBX4 mAb (1 : 1000, CST, 30559), and reference control anti-β-actin-HRP mAb (1 : 2000, Santa Cruz Bio, sc-47778 HRP) and made in TBST containing 5% BSA with incubation overnight at 4°C. Membranes were washed three times with TBST, incubated with anti-rabbit IgG-HRP (1 : 500, Thermo Fisher, 32460) at room temperature for 1 hour, and then washed three times using TBST. β-Actin protein bands were visualized using Clarity™ Western ECL Substrate (Bio-Rad, 1705060); CBX4 protein bands were visualized using SuperSignal™ West Pico PLUS Chemiluminescent Substrate (Thermo Fishers, 34579). Membrane images were acquired with the ChemiDoc XRS system (Bio-Rad). Grey band density values were analyzed and calculated using Image lab (version 6.0, Bio-Rad).

2.7. Quantitative Real-Time Polymerase Chain Reaction (qRT-PCR). RNA was extracted using an Aurum™ Total RNA Mini Kit (Bio-Rad, 7326820) or PARIS™ Kit (Thermo Fisher, AM1921). cDNA was synthesized using the iScript™ cDNA Synthesis Kit (Bio-Rad, 1708891). Subsequently, qRT-PCR was performed using a SYBR green master mix (Applied Biosystems, 4309155) with a QuantStudio 6 Flex Real-Time PCR System (Applied Biosystems). Gene expression of *CDKN1A*, *CDKN2A*, *DPP4*, *LMNB1*, and *CBX4* was measured with *YWHAZ* as an internal reference control gene (see Table S1 for a list of primers).

2.8. qPCR Array. A custom RT2 Profiler PCR Array (Qiagen, 330171) was used to profile a total of 42 genes related to cellular senescence and/or CBX4 [1, 13, 26], along with 3 house-keeping genes, 1 genomic DNA control, 1 reverse transcription control, and 1 positive PCR control (Table S2). cDNA was synthesized using an RT^2 First Strand Kit (Qiagen, 330404). Subsequently, qRT-PCR was performed using a RT^2 SYBR Green ROX qPCR Mastermix (Qiagen, 330522) with the QuantStudio 6 Flex Real-Time PCR System (Applied Biosystems). The CT value of each gene was normalized with reference gene YWHAZ, $\Delta\mathrm{CT} = \mathrm{CT}(\text{target gene}) - \mathrm{CT}(\mathrm{YWHAZ})$, and relative gene expression change in serial culture was calculated relative to the earliest passage (CPD earliest) from each serial culture experiment, $\Delta\Delta\mathrm{CT} = \Delta\mathrm{CT}(\text{a target sample}) - \Delta\mathrm{CT}(\text{CPD earliest})$; $\text{fold change (FC)} = 2^{-\Delta\Delta\mathrm{CT}}$ was expressed using Log2 FC.

2.9. Statistical Analysis. Data are presented as mean ± standard error of the mean (SEM). Analyses were performed using GraphPad Prism 9 (GraphPad software) and R Statistical Software (manufacturer). To test the correlation coefficient between senescence markers and gene expression across the range of CPD from the serial culture and from the biological replicates, we used repeated measures correlation (Rmcorr) [27]; the repeated measures correlation coefficients (r_{rm}) are presented with a 95% confidence interval (CI). In addition, paired *t*-tests were used to compare data from control vs. knockdown or activation of CBX4. A mixed-effects model was used to compare the knockdown effects of CBX4 shRNA with MOI 0.5, 1, and 2. $p < 0.05$ was considered statistically significant.

2.10. Protein-Protein Interaction Network. STRING (Search Tool for the Retrieval of Interacting Genes/Proteins) V11.5 [28] was used to evaluate the known and predicted biological relationships of the qPCR array genes and corresponding proteins interactions; interactions with high confidence (score > 0.7) are reported. Gene Ontology (GO) enrichment analysis was performed.

2.11. Ingenuity Pathway Analysis (QIAGEN IPA). Gene expression of CBX4 ACT and CBX4 KD was normalized to the corresponding controls and analyzed by the QIAGEN IPA platform (QIAGEN Inc., https://digitalinsights.qiagen.com/IPA). IPA core analysis was used to assess canonical pathway enrichment for CBX4 ACT and KD separately. Biofunctional pathways regulated by CBX4 ACT and CBX4 KD were compared in a clustered hierarchical heat map.

3. Results

3.1. Senescence Markers Were Upregulated in the Senescent WI-38 Cells. Five independent serial cultures of WI-38 fibroblasts were performed from CPD 37 through CPD 60 when senescent status was attained (Figure 1(a)). The culture period from seeding (CPD 37) to senescent status (a failure to double after one week) was 54.80 ± 3.44 days; the average CPD corresponding to WI-38 senescence was 58.04 ± 0.78 CPD. We observed increased doubling time during the serial culture (Figure 1(a)). Flow cytometry was used to quantify SA-β-gal activity, protein expression of p21, p16, and DPP4 (CD26), and the proliferation marker, EdU. Compared to proliferating WI-38 (CPD 40-42), senescent WI-38 (CPD 55-60) expressed higher SA-β-gal activity and protein expression of p21, p16, DPP4, and lower proliferation marker EdU (Figure 1(b)). The p16 protein was coexpressed with SA-β-gal activity and DPP4 in senescent WI-38 cells (Figure 1(c)). As expected, EdU reflecting cell proliferation was greater in proliferating WI-38 than in senescent WI-38 and negatively correlated with SA-β-gal activity. During serial culture, SA-β-gal activity, and protein expression of p21, p16 and DPP4 increased, while EdU proliferation decreased (Figure 1(d)). CPD was positively correlated with SA-β-gal activity, protein expression of p21, p16, DPP4, and negatively correlated with EdU (Figure 1(e)). Interestingly, some markers changed relatively early in the course of the serial culture, such as p21 protein that increased from around CPD 40 and DPP4 protein that increased from CPD 45. Other markers changed later, such as p16 protein and SA-β-gal activity (all increased), and EdU proliferation (decreased) at around CPD 50 (Figures 1(a) and 1(d)). Gene expression with serial culture was consistent with protein level changes with an increase in senescence markers CDKN2A (p16), CDKN1A (p21), DPP4 (CD26), and a decrease in LMNB1 (Lamin B1), a gene expression measure of cell proliferation known to be decreased with senescence development [29] (Figure 1(f)). Similar to protein level changes with serial culture, CPD was positively correlated with gene expression of CDKN2A, CDKN1A, and DPP4 and negatively correlated with LMNB1 (Figure 1(g)).

3.2. CBX4 Decreased during WI-38 Serial Culture and Knockdown of CBX4 Increased Senescence. Given the reported role of CBX4 in regulating cellular senescence [11, 18], we next evaluated CBX4 protein expression and gene expression from proliferating through senescence status in the WI-38 cells. As shown in Figures 2(a)–2(c), CBX4 protein expression decreased significantly with serial passage ($r_{rm} = 0.877$, $p < 0.001$); in contrast, CBX4 gene expression increased with serial passage ($r_{rm} = 0.555$, $p < 0.001$). Moreover, compared to proliferating WI-38 (CPD 41), CBX4 protein decreased around 50% at CPD 50 (Figure 2(b)), when p16 and SA-β-gal activity started to increase and EdU proliferation decreased (Figure 1(d)). These results suggest that change in CBX4 protein may be involved in regulating replicative senescence.

We next evaluated the effect of CBX4 knockdown in presenescent WI-38 passages (CPD 47-50). Compared to the control group, cell numbers were significantly lower in the CBX4 knockdown group (Figures S2A and B). Overall CBX4 protein and gene expression were significantly decreased in the CBX4 knockdown group: mean difference of protein expression ratio -0.577 ± 0.059; and mean difference of gene expression ratio -0.302 ± 0.041 (Figures 3(a) and 3(b), all $p < 0.001$). Similar levels of knockdown in CBX4 protein and gene expression were achieved with MOI 0.5, 1, and 2 (Figure S3A). After CBX4 knockdown, SA-β-gal activity increased $21.26\% \pm 2.60\%$, p16 protein increased $22.89\% \pm 1.81\%$, and EdU proliferation decreased $13.76\% \pm 1.88\%$, all significantly (Figures 2(c) and 2(d), all $p < 0.001$). Similar degrees of change in senescence markers were achieved with MOI 0.5, 1, and 2 (Figure S3B). Our findings suggest that a mean 57% knockdown of CBX4 protein was sufficient to cause a cellular senescent phenotype in WI-38. This result is consistent with our observation in serial cultures that most senescence markers developed at 50% reduction of CBX4 protein.

3.3. CBX4 Activation Decreased Senescence in WI-38. Based on these results, we hypothesized that activation of CBX4 would be senomorphic and decrease senescence in the WI-38 cells. We activated endogenous CBX4 expression using the CRISPR/Cas9 Synergistic Activation Mediator (SAM) system. Compared to control, cell numbers were not significantly different in the CBX4 activation group (Figures S2C and D). With this activation system, both increased CBX4 protein and gene expression were achieved: protein mean difference ratio $+0.901 \pm 0.214$, $p = 0.0084$; and gene mean difference ratio $+1.894 \pm 0.310$, $p = 0.0036$ (Figures 4(a) and 4(b)). In association with CBX4 activation, p16 and DPP4 protein expression and SA-β-gal activity were decreased as profiled by flow cytometry: p16 $-9.25\% \pm 2.41\%$, $p = 0.0085$; DPP4 $-12.24\% \pm 3.24\%$, $p = 0.0092$; and SA $-\beta-$ gal activity $-9.27\% \pm 2.47\%$, $p = 0.0095$ (Figures 4(c) and 4(d)). However, the mean percentage of EdU positive cells was not significantly increased: $+7.11\% \pm 3.87\%$, $p = 0.116$. Our results are consistent with a senomorphic effect of CBX4 in WI-38 cells.

3.4. Senescence-Related Genes and Pathways Regulated by CBX4. We examined the gene changes during WI-38 cell serial culture from proliferating to senescent cell state (11 time points) by qPCR array. A total of 37 out of 42 selected genes were detected; DAO, TP63, TNF, LY6D, and SOX2 were unable to be detected. Relative gene expression results were ordered in a heat map based on correlation with CPD values (Figures 5(a) and 5(b)). With serial culture, expression of several genes (such as CDK1, E2F1, DNMT1, PCNA,

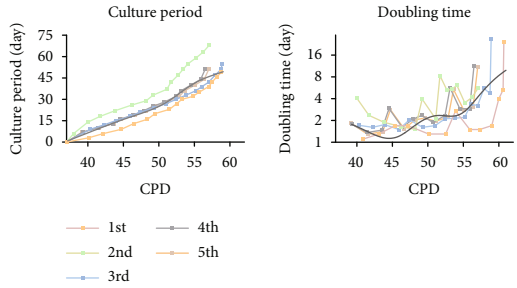

(a)

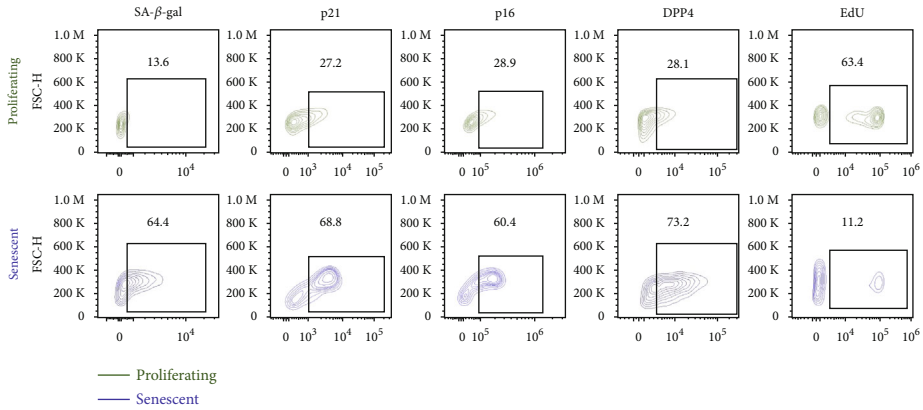

(b) Representative staining of single senescent marker in WI-38

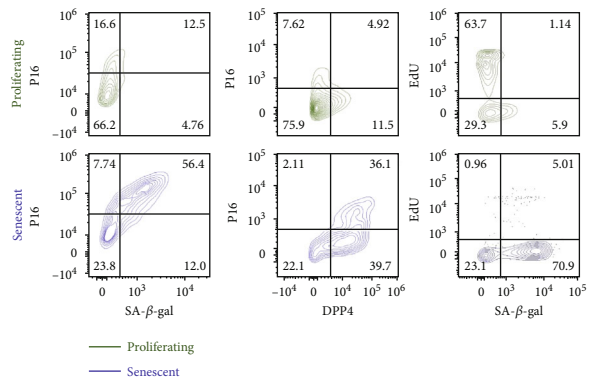

(c) Representative staining of costaining senescent markers in WI-38

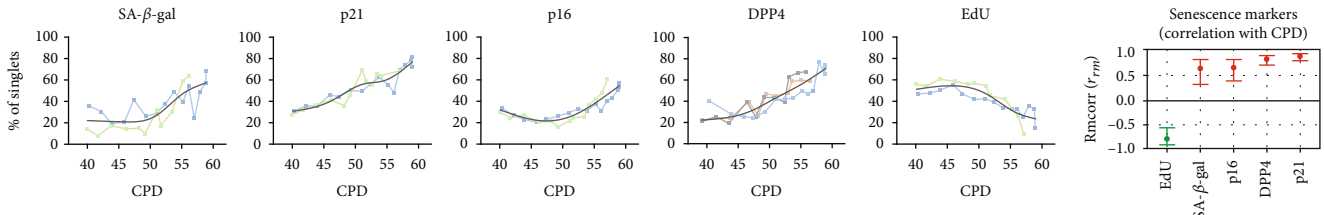

(d) Timecourse of senescence marker development by flow cytometry

(e)

Figure 1: Continued.

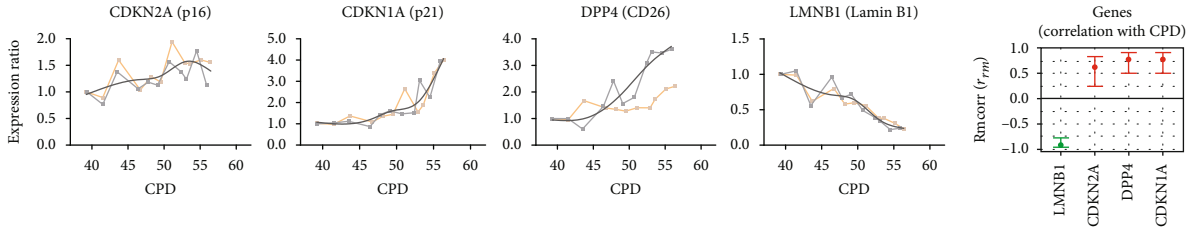

(f) Timecourse of senescence marker development by gene expression (g)

Figure 1: The timecourse of senescence marker expression with the serial culture of the WI-38 replicative senescence cell model system. Human diploid fibroblast WI-38 cells were profiled for senescence markers by flow cytometry and qPCR. Each serial culture is represented in a different color; the trend-line for expression of each marker was created by a smoothing spline function with 5 knots. (a) Serial culture of WI-38 was performed from CPD 37 to senescent status (CPD 56–60) for a total of 5 times. Doubling time increased during the serial culture. (b) and (c) SA-β-gal activity, protein expression of p21, p16, DPP4, and EdU proliferation markers detected by flow cytometry in proliferating (CPD 40-42, dark green) and senescent (CPD 56-60, blue) WI-38, both individually as single markers (b) or combined (c). Compared to proliferating WI-38, senescent WI-38 expressed higher SA-β-gal activity, p21, p16, DPP4 protein, and lower EdU (b). In the senescent WI-38, p16 protein was positively co-expressed with SA-β-gal activity and DPP4; SA-β-gal activity was negatively correlated with the proliferation marker EdU (c). (d) and (f) Serial culture of WI-38 from proliferating to senescent status was done repeatedly to characterize the timecourse of senescence marker development by flow cytometry and qPCR. There are no qPCR equivalents for SA-β-gal activity or EdU; however, Lamin B1 (LMNB1) was quantified by qPCR to provide a gene expression representation of cell proliferation and senescence. (e) and (g) The associations of senescence markers and genes with CPD were evaluated by repeated measures correlation (Rmcorr). The Rmcorr correlation efficient (r_{rm}) of CPD with senescence markers (% of total cells) and genes (expression ratio) is depicted for analyses adjusted for repeated measurements. Green: negative correlation. Red: positive correlation.

and BCL2) decreased, while other genes (such as CDKN1A, DPP4, FAS, and MDM2) increased. A total of 20 of the 37 detected genes were significantly correlated with CPD (Figure 5(c)). Pairwise correlations among the genes revealed that two groups of genes strongly clustered together (Figure 5(d)). The first group consisted of STAT1, BAX, SLC52A1, STAT3, FAS, CDKN1A, DPP4, and MDM2 whose expression increased with increasing CPD of serial culture. In contrast, the second group consisted of DNMT1, E2F1, CDK1, PARP1, and PCNA whose expression decreased during serial culture. Subsequently, we examined changes in gene expression in response to knockdown and activation of CBX4 compared to their paired control. Knockdown of CBX4 decreased expression of CXCL8, PCNA, DNMT1, E2F1, and PARP1 and increased expression of DPP4, SLC52A1, and CDKN2A (Figure 5(e)). Activation of CBX4 in presenescent cells increased expression of SIRT1 and MDM4 and decreased expression of DPP4, HDAC1, and CDKN2A (Figure 5(f)). Interestingly, CBX4 knockdown increased, while CBX4 activation decreased, gene expression of both CDKN2A and DPP4, suggesting that these genes may be direct targets and mediators of CBX4 regulation of senescence.

The protein-protein interactions (PPI) of the 37 proteins corresponding to the 37 detected genes were analyzed with STRING. STRING identified 37 nodes, 160 edges, 8.65 average node degrees, an average local clustering coefficient of 0.604, and PPI enrichment p value < 1.0e-16; taken together, this indicates our selected panel represented a highly interactive network. The Gene Ontology (GO) showed our detected panel associated with several senescence-related pathways such as DNA damage repair, cell cycle, apoptosis, and replicative senescence (Figure 6(a)). IPA core analysis identified several canonical pathways related to CBX4 regulation including DNA damage repair, cell cycle regulation, and p53 signaling pathway; each of these senescence-related pathways was involved in CBX4 knockdown and activation (Figure 6(b)). Hierarchical cluster heatmaps based on biofunctional pathways demonstrated that cellular proliferation and cell viability were higher, and apoptosis, transcription of RNA and DNA were lower with CBX4 ACT compared with CBX4 KD (Figure 6(c)).

4. Discussion

In this study, we investigated the role of CBX4 in replicative senescence using the human primary diploid fibroblast WI-38 model system. We characterized the senescence phenotype using multiple senescence markers, including population doubling time, p21, p16, SA-β-gal activity, DPP4, and proliferation marker EdU in serial culture. CBX4 protein expression decreased significantly during the serial culture of WI-38. By knockdown, we achieved a 57% reduction of CBX4 expression in presenescent WI-38, analogous to increasing the senescence phenotype ~5 CPD (estimation based on SA-β-gal activity and p16 protein expression); by activation, we achieved a 90% elevation of CBX4 expression analogous to reducing senescence ~2 CPD. Specifically, at the molecular level, knockdown of CBX4 increased gene expression of CDKN2A and DPP4 and decreased CXCL8, PCNA, DNMT1, E2F1, and PARP1; activation of CBX4 increased gene expression of SIRT1 and MDM4 and decreased DPP4, HDAC1, and CDKN2A. Taken together, our results demonstrate that CBX4 regulates replicative senescence in WI-38 cells.

We showed that DPP4 is highly correlated with WI-38 replicative senescence and could be useful as a senescence treatment target and as a senescence biomarker. The protein

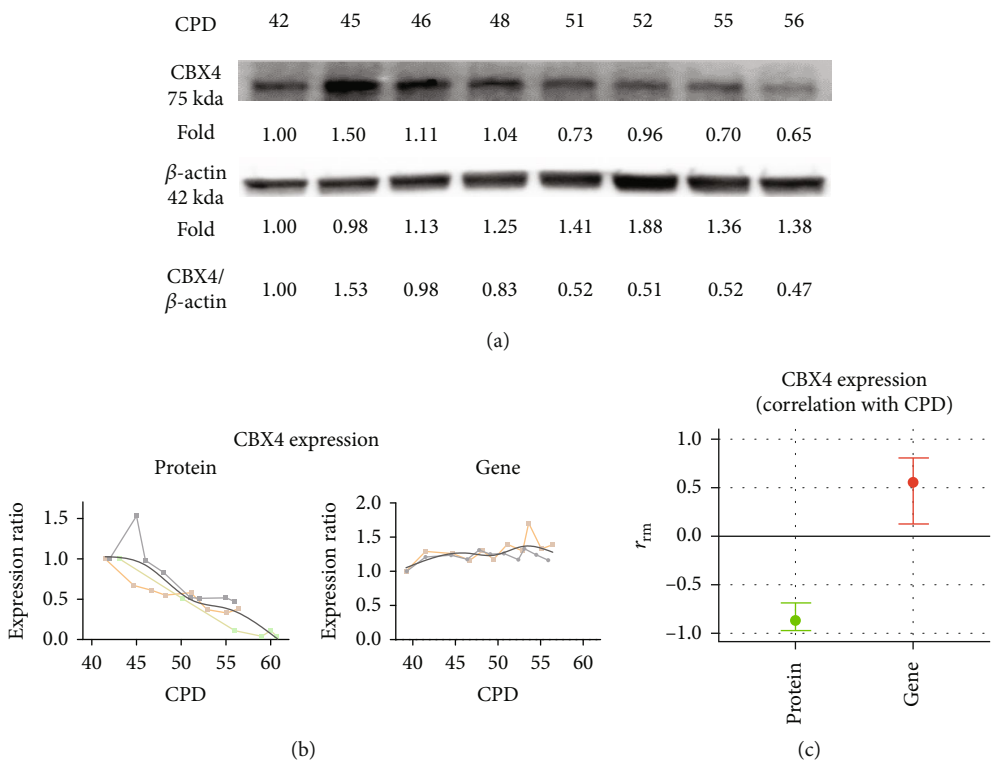

Figure 2: CBX4 decreased with WI-38 serial culture. CBX4 protein and gene expression were investigated in each generation of the WI-38 serial culture. Protein expression was examined by Western blot and normalized with β-actin. Gene expression was analyzed by qPCR and normalized with YWHAZ. Decreased CBX4 protein expression with serial culture is shown in a representative Western blot (a). CBX4 protein expression ($n = 3$) and gene expression ($n = 2$) in serial culture were normalized to controls and depicted as an expression ratio relative to CPD 41 ((b) left, protein) and CPD 39 ((b) right, gene). The Rmcorr correlation coefficient (rrm) and confidence interval of CPD with CBX4 protein and gene expression are depicted (c) for repeated measurements. Green: negative correlation. Red: positive correlation.

and gene expressions of DPP4 were both significantly positively correlated with CPD. Also, DPP4 expression was regulated up and down by CBX4 knockdown and activation, respectively. DPP4 is a transmembrane glycoprotein that can also circulate in a soluble form in plasma. DPP4 has been known to regulate glucose metabolism by inactivation of GIP; both GLP-1 and DPP4 inhibitors have been used for type 2 diabetes mellitus (DM) treatment [8]. DPP4 was recently identified as a surface marker on senescent human WI-38 primary fibroblasts and found to be more highly expressed on the surface human peripheral blood mononuclear cells isolated from individuals aged 78 to 88 yrs old compared to individuals aged 27 to 36 yrs old [8]. The cell surface expression of DPP4 makes it a promising candidate for targeted treatment of senescent cells through antibody-dependent cell-mediated cytotoxicity [8]. Treatment of senescence-related chronic disease, as shown by recent studies with DPP4 inhibitors that ameliorated atherosclerosis in type 2 DM patients [30, 31], prevented vascular aging [32] and protected chondrocytes from TNF-α-induced senescence [33]. We noticed increased SIRT1 in association with DPP4 reduction upon CBX4 activation of WI-38 cells. These results are consistent with a recent study showing that DPP4 inhibition reduced endothelial senescence by activating the AMPK/SIRT1/Nrf2 pathway [34]. Nevertheless, a complete understanding of the interrelationship of CBX4 and DPP4 remains to be elucidated.

We observed increased SA-β-gal activity, protein expression of p16 and p21, and decreased EdU proliferation with WI-38 serial culture. Although these results are consistent with previous studies in the WI-38 senescent model system [6, 8, 35], there was an interesting discordance in the temporal patterns of expression of the various senescence markers. For instance, we observed that decreased CBX4 protein expression in WI-38 serial cultures preceded the appearance of many senescence markers; thus, CBX4 could be a factor regulating WI-38 replicative senescence. This hypothesis is supported by the ability of CBX4 knockdown and activation to regulate the expression of many senescence-related genes, including HDAC1 shown to mediate the transition to a senescent phenotype [36]. This hypothesis is also supported by recent data from hMSCs showing that CBX4 deficiency leads to characteristics associated with premature cellular senescence, while CBX4 overexpression reduced these senescent markers including SA-β-gal activity, p21, and p16 [11]. In addition, we observed that serial cell passage of WI-38 led to increased expression of p21 earlier than p16. This observation is consistent with a prior study showing early regulation of p21 in a senescent fibroblast model [37]. It has therefore been suggested that p16, whose expression

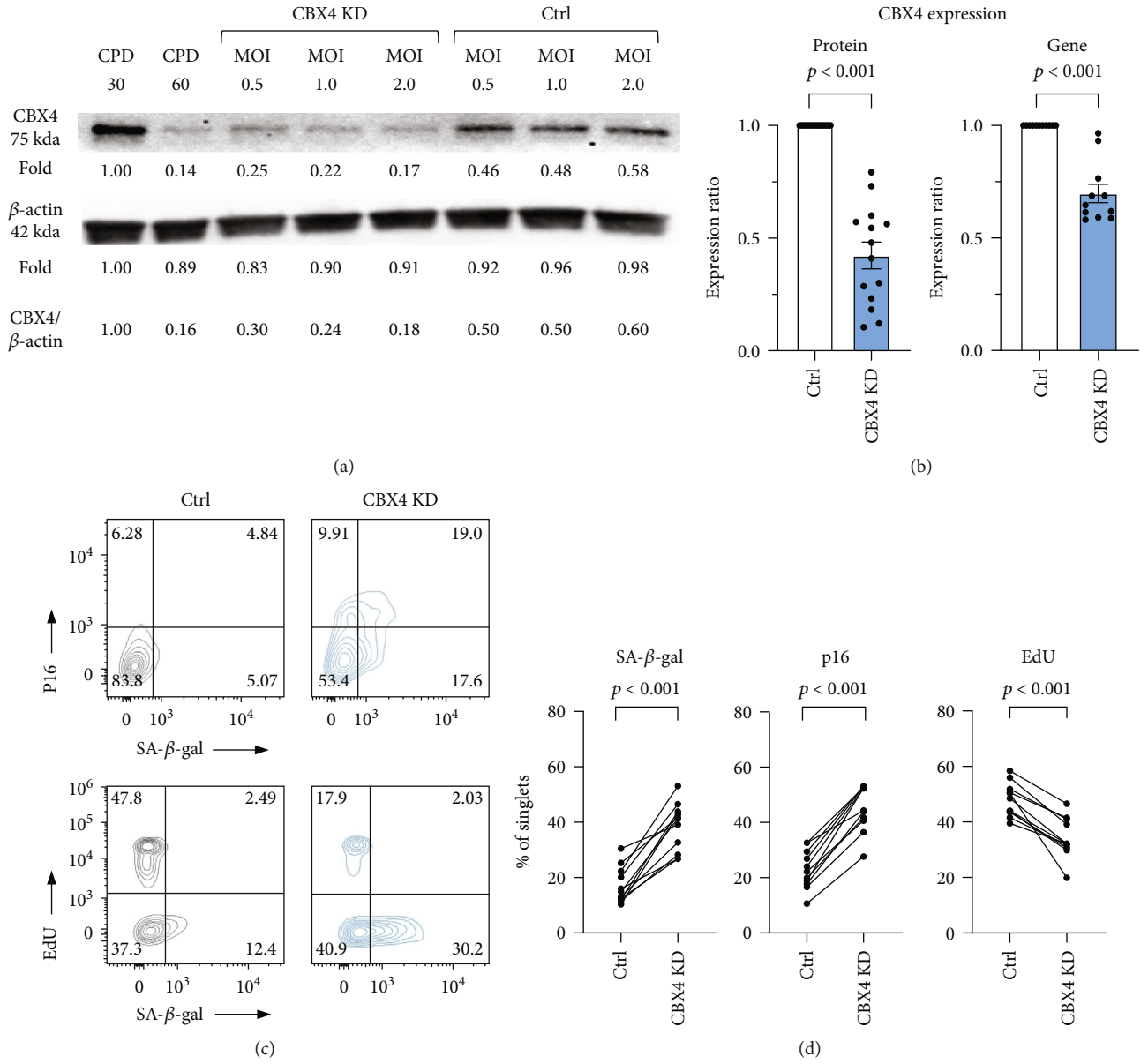

Figure 3: Knockdown of CBX4 increased senescence markers in WI-38 cells. Knockdown (KD) of CBX4 was performed with CBX4 shRNA carried by lentiviral particles with different multiplicity of infection (MOI) 0.5, 1, and 2. (a) Representative Western blot of CBX4 protein expression in proliferating (positive control CPD30) and senescent (negative control CPD60) WI-38, in CBX4 KD and lentiviral control (Ctrl) at three MOI. (b) Overall significant reduction of CBX4 protein ($n = 14$) and gene expression ($n = 11$) due to lentiviral KD (control grey, CBX4 KD light blue). (c) and (d) SA-β-gal activity, p16 and EdU proliferation expression in control and CBX4 KD in representative flow cytometry (C), and overall demonstrating increased protein expression of senescence markers SA-β-gal activity and p16, and decreased proliferation marker EdU after knockdown of CBX4 ((d), $n = 11$).

increases later than p21, may be critical in maintaining senescence status [37]. In contrast, p21 was recently shown to be related to immunosurveillance of senescent cells, mediated by p21 binding to pRB leading to cell cycle arrest and CXCL14 expression; clearance of the stressed cells by immune cells ensued if the p21 levels did not recuperate [38]. The fact that CBX4 knockdown and activation were not mirror-images of each other is also likely a result of a different CPD starting point for each of these manipulations since, as noted here, development of senescence in the WI-38 was not a linear process but rather a staged process with different markers having different inflection points in the process. Taken together, these data suggest that different senescence markers may predominate at different biological ages and that optimal monitoring of antisenescence treatment effects requires the use of markers appropriate to the stage of senescence being treated.

CBX4 is a member of the polycomb chromobox (CBX) family. CBX proteins, including CBX1/2/3/4/5/6/7/8, are major regulators of histone methylation, which can function as epigenetic modulators, maintaining heterochromatin organization and reducing related gene expression [39].

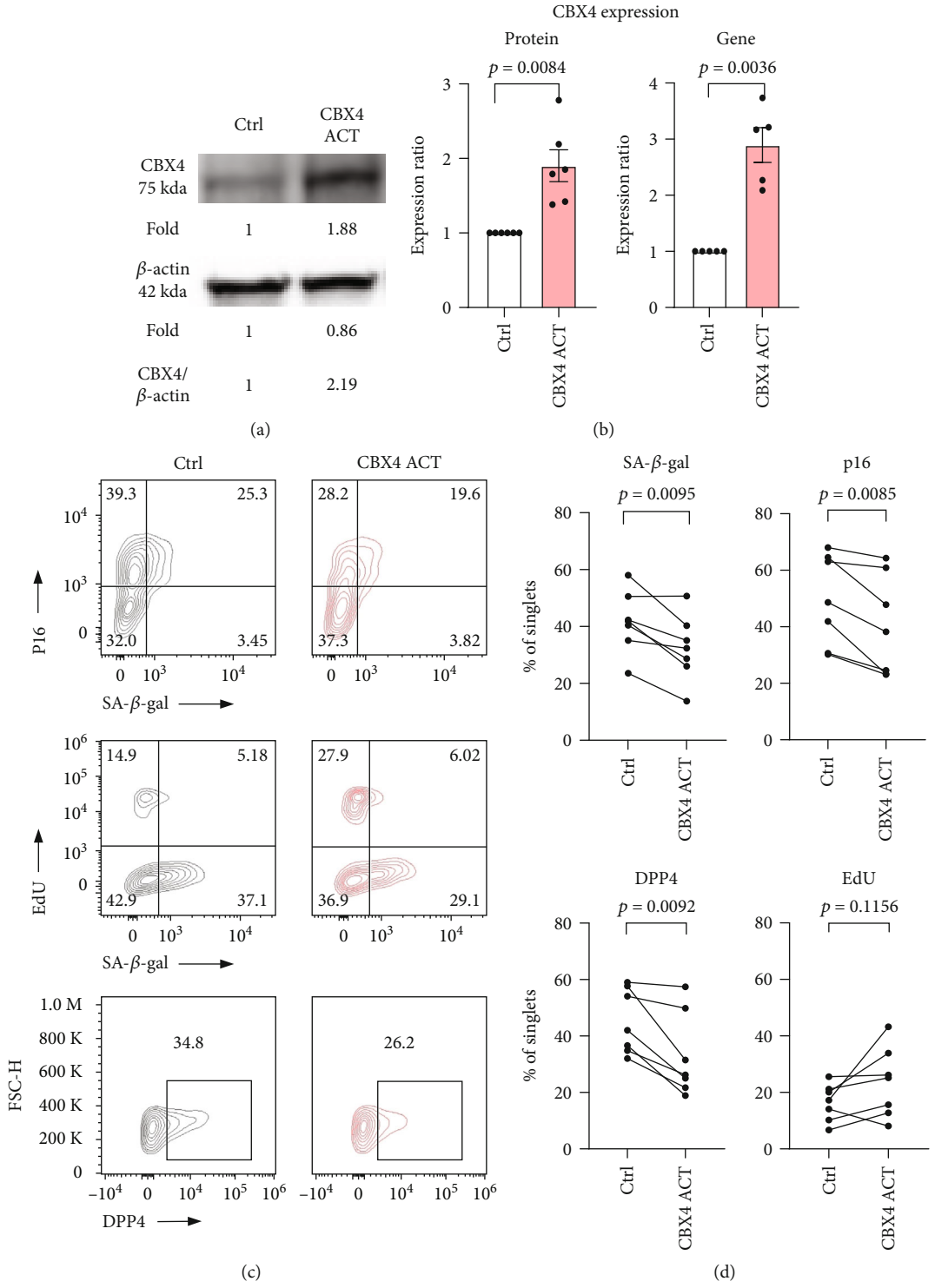

Figure 4: Activation of CBX4 reduced cellular senescence markers in WI-38. CBX4 was activated using the CRISPR/Cas9 Synergistic Activation Mediator (SAM) lentiviral particle system in presenescent WI-38 (CPD47-50). (a) Representative Western blot of CBX4 protein expression in CBX4 activation (ACT) and lentiviral control (Ctrl). (c) CBX4 protein ($n = 6$) and gene expression ($n = 5$) both increased in response to CBX4 ACT compared with Ctrl (Ctrl: white, CBX4 ACT: light red). (c) SA-βgal, p16, and EdU proliferation expression in Ctrl and CBX4 ACT in representative flow cytometry. (d) By flow cytometry, CBX4 activation resulted in decreased protein expression of senescence markers SA-βgal, p16, and DPP4 and nonsignificantly increased EdU ($n = 7$).

CBX proteins are known to be essential for cell proliferation, maintenance of adult stem cell populations, and regulation of stem cell self-renewal [39, 40]. Loss of CBX2 causes senescence-associated chromosomal rearrangements in mouse embryonic fibroblasts [41]. CBX7 regulates replicative senescence [42] and maintains pluripotency in embryonic

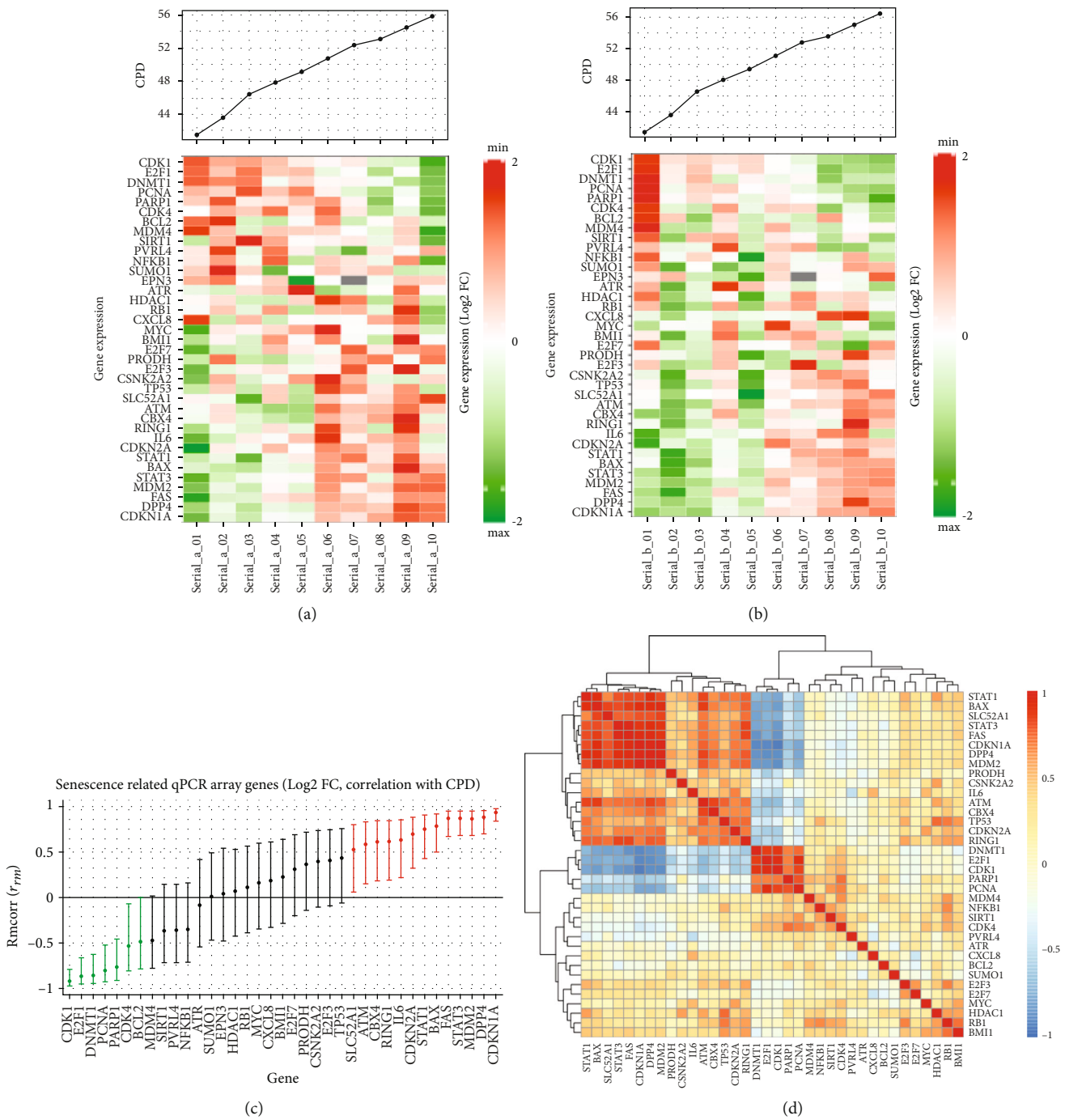

Figure 5: Continued.

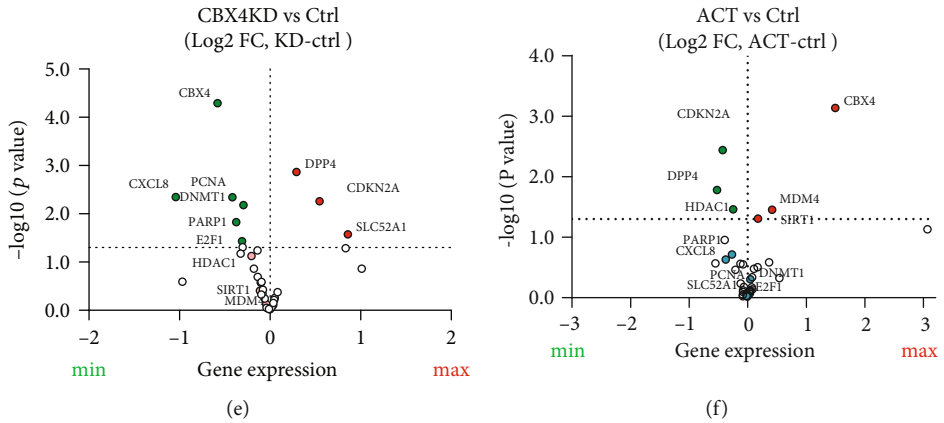

Figure 5: Regulation of senescence-related genes by CBX4. A selected panel of senescence-related genes was analyzed by qPCR microarray. Two serial culture experiments were performed, and the resulting Log2FC values were computed (normalized with YWHAZ and calculated relative to the earliest CPD of serial culture). (a) and (b) Heatmaps of standardized gene expression at 10 time points of WI-38 serial culture performed in two biological replicates. (c) the Rmcorr correlation (and 95% confidence intervals) of CPD with expression (Log2 FC) of 37 senescence-related genes from serial culture. Green: positive correlation of gene expression with CPD. Red: negative correlation gene expression with CPD. Black: insignificant correlation of gene expression with CPD. (d) Heatmap of pairwise Spearman correlations of genes measured in the serial culture experiment. Based on expression pattern and consistent with (a) and (b), two groups of genes were highly clustered. (e) Volcano plot of gene expression changes in response to CBX4 KD vs. Ctrl showing increased expression of DPP4, CDKN2A, and SLC52A1 and decreased expression of CXCL8, PCNA, DNMT1, E2F1, and PARP1. (f) Volcano plot of gene expression changes in response to CBX4 ACT vs. Ctrl showing decreased expression of DPP4, CDKN2A, and HDAC1 and increased expression of CBX4, SIRT1, and MDM4. Red: increased expression, green: decreased expression.

stem cells and hematopoietic stem cells [19, 43]. CBX2/4/6/7/8 is involved in PRC-mediated inhibition of p16 expression [44]. Based on our data, a variety of mechanisms mediated by CBX4 may be involved in its senomorphic activities. For instance, the function of CBX4 SUMO E3 ligase activity has been shown to be associated with DNA damage repair mediated by CBX4 SUMOylation of BMI1 that stabilizes BMI1 on the DNA damage site and thereby facilitates DNA damage repair [13]. Also, CBX4 is a PRC1-associated protein; PRC1 has been shown to regulate cell cycle and gene transcription by chromatin modification [45, 46]. PRC1 was shown to bind the *p16* promoter and repress p16 expression in young cells [45]. This function is consistent with the increased p16 expression we observed upon CBX4 knockdown. Moreover, Ren et al. showed that CBX4 alleviates senescence in hMSCs, in part at least, by maintaining nucleolar homeostasis through repression of rRNA transcription. In our IPA analysis, we also found CBX4 activation decreased transcription of RNA pathways compared to CBX4 knockdown. Therefore, transcriptional repression by CBX4 may also contribute to the senomorphic effect.

Interestingly, activation of CBX4 led to a decrease in senescence markers and an increase in *SIRT1*, an important antagonist of the oxidative stress pathway; it surprisingly did not lead to a significant increase in cell proliferation. This may be due to the fact that CBX4 activation also leads to a decrease in HDAC1. HDAC1 inhibition was previously shown to increase p21 and decrease proliferation of WI-38 [47]. So, effects on HDAC1 may be counteracting possible oncogenic, pro-proliferative responses of WI-38 to CBX4. This interpretation is consistent with data showing that CBX4 interacted with HDAC1 to repress the tumor suppressor KLF6 in clear cell renal carcinoma while knockdown of HDAC1 restored KLF6 function [48]. These results may explain why activation of CBX4 did not significantly increase WI-38 proliferation in our study. Not surprisingly, one of the potential concerns related to CBX4 treatment is its oncogenic properties in hepatic cancer and breast cancer [14, 15]. However, activation of CBX4 in the terminal differentiated presenescent WI-38 fibroblast did not increase the proliferation of the cells, which may make CBX4 a good senomorphic target for aging, particularly if administered judiciously and with appropriate monitoring.

Although CBX4 gene and downstream protein expression were readily modulated at a transcriptional level in our knockdown and activation experiments with shRNA and the dCas9 system, respectively, we were surprised to observe a discordance between CBX4 gene (increase 1.5 times) and protein (significantly decreased) expression in the serial culture system. This might be explained by translational level regulatory mechanisms. Like many other transcriptional regulatory factors, CBX4 can be modulated by posttranslational modifications including conjugation to ubiquitin and ubiquitin-like proteins such as SUMO, that target CBX4 for degradation through the ubiquitin proteosome system [49] and by phosphorylation, methylation, and demethylation [50]. CBX4 itself is a SUMO E3 ligase so it is both sumoylated and sumoylates other proteins. In addition, SALL1 has been noted to enhance the stability of CBX4 protein by modulating its ubiquitination thereby avoiding its degradation via the proteasome [49]. Future analysis of SALL1 in the WI-38 model system might inform an understanding of the discordance in gene and protein expression of CBX4 with serial culture. Nevertheless, the dramatic decline in CBX4 protein and associated changes in WI-38 senescence cell phenotype with serial culture are

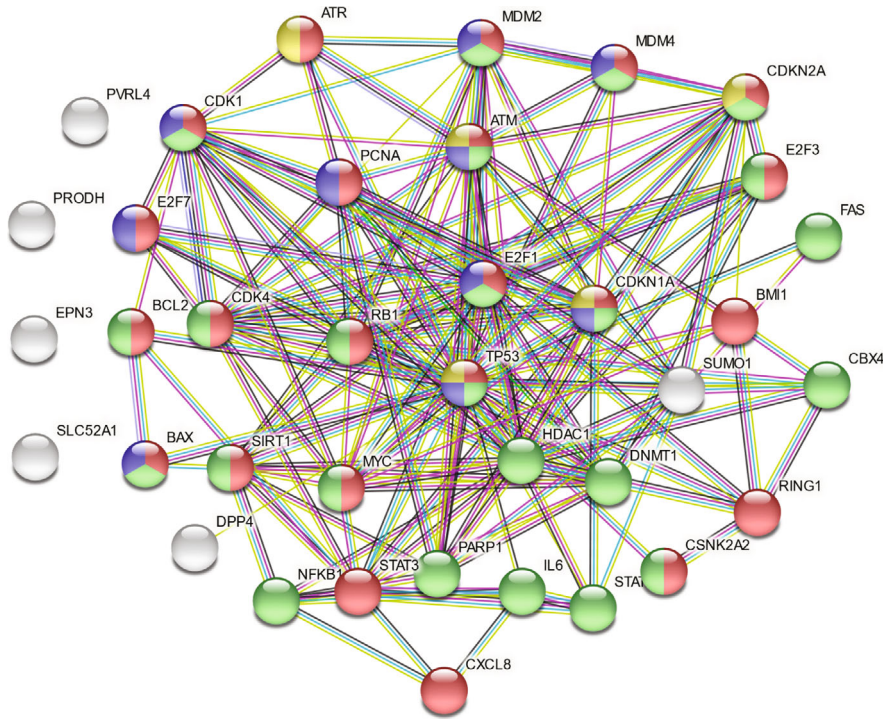

(a) STRING analysis of interactions of proteins corresponding to the 37 analyzed and detected genes

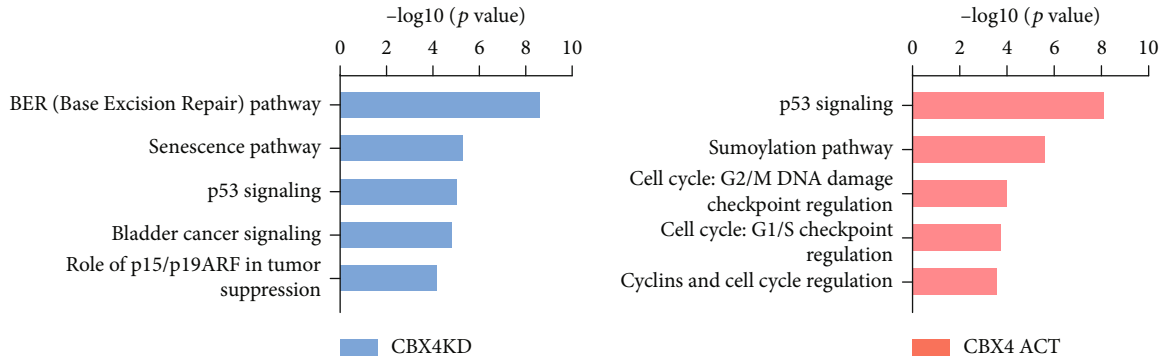

(b) Canonical pathway analysis of CBX4 knockdown (KD) and activation (ACT)

Figure 6: Continued.

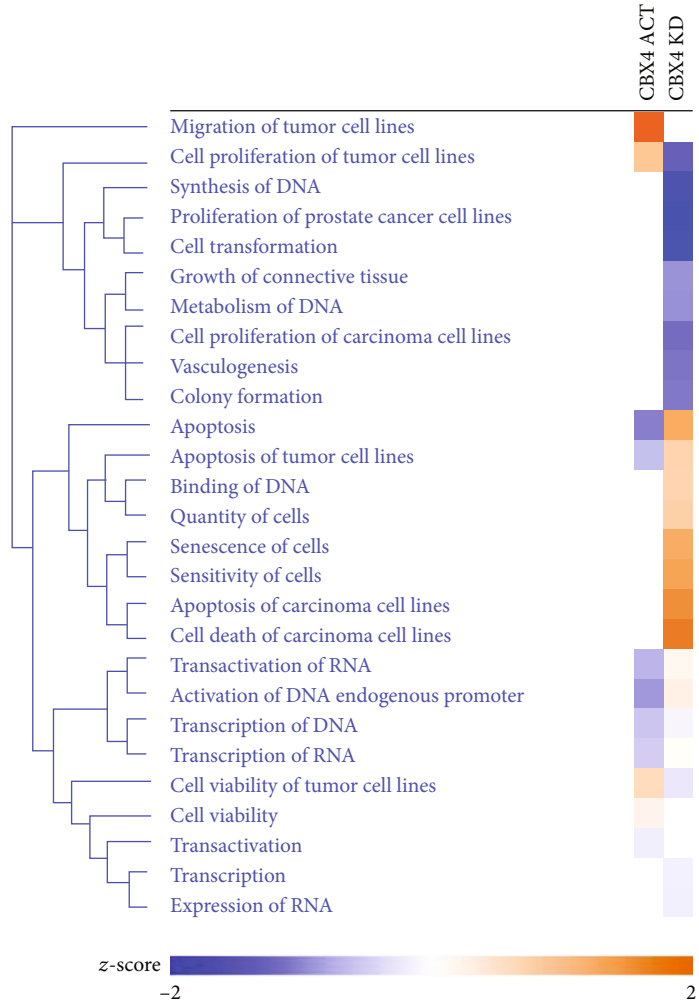

(c) Biofunction pathway analysis comparison of CBX4 knockdown and activation

FIGURE 6: String network and IPA pathway analysis of CBX4 activation and knockdown in senescence. (a) STRING analysis of interactions of proteins corresponding to the 37 analyzed and detected genes. Red: genes related to regulation of cell cycle (GO: 0051726, strength: 1.0, FDR: 1.57e-15); green: genes related to regulation of apoptotic process (GO: 0042981, strength: 0.91, FDR: 8.16e-15); purple: genes related to DNA damage response, signal transduction by p53 class mediator resulting in cell cycle arrest (GO: 0006977, strength: 1.95, FDR: 4.18e-14); yellow: proteins related to replicative senescence (GO: 0090399, strength: 2.31, FDR: 2.15e-08). (b) and (c) CBX4 knockdown (KD, light blue) and activation (ACT, light red) were normalized with the control for the gene expression and analyzed for canonical pathways (b) and compared using biofunction pathway analysis and presented in the heat map ((c), orange: increase; blue: decrease).

fully consistent with results obtained with lentiviral modulation (repression and activation) of CBX4.

There were several limitations of this study. We were limited to evaluating WI-38 from CPD40 due to the lack of availability of very early passage numbers (<CPD30) from the ATCC. At the start of the serial cultures, there appeared to be a slight increase then decrease of senescence markers in cells immediately after thaw and culture; we attribute these perturbations to stress then recovery responses. We limited our study to replicative senescence, so results may not be applicable to other causes of senescence. We identified only 20 out of 42 genes correlated with CPD in the serial culture of WI-38. Additional genes associated with CPD might have been identified with a greater number of independent serial culture samples than the two we evaluated (corresponding to 22 total samples). In addition, Rmcorr analysis captures the linear relationship of gene expression and CPD; therefore, nonlinear dynamics of gene expression might not have been detected with this method. A strength of our study was the flow cytometry-based measurement that profiled senescence makers at the single cell level and discerned the associations of different senescence markers by their coexpression patterns. Another strength of this study was the use of the classic WI-38 model system, the first in which senescence was described [4], to explore the role of CBX4 in replicative senescence.

In summary, CBX4 protein expression decreased with serial culture of WI-38 cells. Knockdown of CBX4 increased cellular senescence, whereas activation of CBX4 decreased senescence. Notably, CBX4 activation was senomorphic; it was able to achieve a reduction in the senescence phenotype without cell killing or a marked increase in cell proliferation

that might increase the risk of cancer. Based on the change in patterns of gene expression with CBX4 modulation, the mechanisms by which CBX4 may regulate senescence in WI-38 appear to be mostly related to the DNA damage repair pathway and PRC1-related cell cycle and transcriptional regulation. Taken together, our results demonstrate that CBX4 regulates replicative senescence in WI-38 cells therefore functions as a senomorphic and potential antisenescence target.

Data Availability

All data generated or analyzed during this study are included in the published article.

Conflicts of Interest

All authors declare that there are no conflicts of interest associated with this study.

Authors' Contributions

Yu-Hsiu Chen, Xin Zhang, Ming-Feng Hsueh, and Virginia Byers Kraus conceived and designed the experiments. Yu-Hsiu Chen performed the experiments. Yu-Hsiu Chen and Kuei-Yueh Ko analyzed the data. Yu-Hsiu Chen and Virginia Byers Kraus drafted and revised the manuscript. All authors reviewed, edited, and approved the final version of the manuscript.

Acknowledgments

This study is funded in part by a student grant from the government of Taiwan (Y-HC), NIH/NIA P30-AG028716 (M-FH and VBK), and NIH/NIA R01AG070146 (VBK and XZ).

Supplementary Materials

All supplementary material is provided in the supplementary file. Table S1: primers used for RT-PCR detection of senescence target genes. Table S2: qPCR custom microarray panel (Qiagen, 330171). Figure S1: transduction efficiency of copGFP control lentiviral particles with different MOI and with/without adding polybrene. Figure S2: number of WI-38 cells in response to CBX4 knockdown (KD) or activation (ACT) compared to control (Ctrl). Figure S3: effect of CBX4 knockdown on senescence outcomes in WI-38 cells. *(Supplementary Materials)*

References

[1] D. McHugh and J. Gil, "Senescence and aging: causes, consequences, and therapeutic avenues," *The Journal of Cell Biology*, vol. 217, pp. 65–77, 2018.

[2] J. Bartkova, N. Rezaei, M. Liontos et al., "Oncogene-induced senescence is part of the tumorigenesis barrier imposed by DNA damage checkpoints," *Nature*, vol. 444, no. 7119, pp. 633–637, 2006.

[3] C. Martínez-Cué and N. Rueda, "Cellular senescence in neurodegenerative diseases," *Frontiers in Cellular Neuroscience*, vol. 14, 2020.

[4] L. Hayflick and P. S. Moorhead, "The serial cultivation of human diploid cell strains," *Experimental Cell Research*, vol. 25, pp. 585–621, 1961.

[5] S. J. Olshansky and L. Hayflick, "The role of the WI-38 cell strain in saving lives and reducing morbidity," *AIMS Public Health*, vol. 4, no. 2, pp. 127–138, 2017.

[6] H. Chen, Y. Li, and T. O. Tollefsbol, "Cell senescence culturing methods," *Methods in Molecular Biology*, vol. 1048, pp. 1–10, 2013.

[7] D. A. Alcorta, Y. Xiong, D. Phelps, G. Hannon, D. Beach, and J. C. Barrett, "Involvement of the cyclin-dependent kinase inhibitor p 16 (INK4a) in replicative senescence of normal human fibroblasts," *Proceedings of the National Academy of Sciences*, vol. 93, p. 13742, 1996.

[8] K. M. Kim, J. H. Noh, M. Bodogai et al., "Identification of senescent cell surface targetable protein DPP4," *Genes & Development*, vol. 31, pp. 1529–1534, 2017.

[9] A. Freund, R.-M. Laberge, M. Demaria, and J. Campisi, "Lamin B1 loss is a senescence-associated biomarker," *Molecular Biology of the Cell*, vol. 23, pp. 2066–2075, 2012.

[10] T. J. Mead and V. Lefebvre, "Proliferation assays (BrdU and EdU) on skeletal tissue sections," *Methods in molecular biology (Clifton, NJ)*, vol. 1130, pp. 233–243, 2014.

[11] X. Ren, B. Hu, M. Song et al., "Maintenance of nucleolar homeostasis by CBX4 alleviates senescence and osteoarthritis," *Cell Reports*, vol. 26, 2019.

[12] J. C. Merrill, T. A. Melhuish, M. H. Kagey, S.-H. Yang, A. D. Sharrocks, and D. Wotton, "A role for non-covalent SUMO interaction motifs in Pc2/CBX4 E3 activity," *PLoS One*, vol. 5, article e8794, 2010.

[13] I. H. Ismail, J.-P. Gagné, M.-C. Caron et al., "CBX4-mediated SUMO modification regulates BMI1 recruitment at sites of DNA damage," *Nucleic Acids Research*, vol. 40, pp. 5497–5510, 2012.

[14] J. Li, Y. Xu, X.-D. Long et al., "Cbx4 governs HIF-1α to potentiate angiogenesis of hepatocellular carcinoma by its SUMO E3 ligase activity," *Cancer Cell*, vol. 25, pp. 118–131, 2014.

[15] J. S. Zeng, Z. D. Zhang, L. Pei et al., "CBX4 exhibits oncogenic activities in breast cancer via Notch1 signaling," *The International Journal of Biochemistry & Cell Biology*, vol. 95, pp. 1–8, 2018.

[16] X. Wang, G. Qin, X. Liang et al., "Targeting the CK1α/CBX4 axis for metastasis in osteosarcoma," *Nature Communications*, vol. 11, no. 1, 2020.

[17] X. Wang, L. Li, Y. Wu et al., "CBX4 suppresses metastasis via recruitment of HDAC3 to the Runx2 promoter in colorectal carcinoma," *Cancer Research*, vol. 76, pp. 7277–7289, 2016.

[18] M. Luis Nuno, L. Morey, S. Mejetta et al., "Regulation of Human Epidermal Stem Cell Proliferation and Senescence Requires Polycomb- Dependent and -Independent Functions of Cbx4," *Cell Stem Cell*, vol. 9, no. 3, pp. 233–246, 2011.

[19] K. Klauke, V. Radulović, M. Broekhuis et al., "Polycomb Cbx family members mediate the balance between haematopoietic stem cell self-renewal and differentiation," *Nature Cell Biology*, vol. 15, pp. 353–362, 2013.

[20] C. Sidler, R. Woycicki, I. Kovalchuk, and O. Kovalchuk, "WI-38 senescence is associated with global and site-specific hypomethylation," *Aging (Albany NY)*, vol. 6, pp. 564–574, 2014.

[21] C. Sidler, R. Woycicki, D. Li, B. Wang, I. Kovalchuk, and O. Kovalchuk, "A role for SUV39H1-mediated H3K9 trimethylation in the control of genome stability and senescence in WI38 human diploid lung fibroblasts," *Aging (Albany NY)*, vol. 6, pp. 545–563, 2014.

[22] V. Roth, *Doubling Time Computing*, 2006, http://wwwdoubling-timecom/computephp.

[23] A. Griukova, P. Deryabin, M. Sirotkina, A. Shatrova, N. Nikolsky, and A. Borodkina, "P38 MAPK inhibition prevents polybrene-induced senescence of human mesenchymal stem cells during viral transduction," *PLoS One*, vol. 13, no. 12, 2018.

[24] L.-Z. Liao, Z.-C. Chen, S.-S. Wang, W.-B. Liu, C.-L. Zhao, and X.-D. Zhuang, "NLRP3 inflammasome activation contributes to the pathogenesis of cardiocytes aging," *Aging*, vol. 13, pp. 20534–20551, 2021.

[25] M.-F. Hsueh, X. Zhang, S. S. Wellman, M. P. Bolognesi, and V. B. Kraus, "Synergistic roles of macrophages and neutrophils in osteoarthritis progression," *Arthritis & Rheumatology*, vol. 73, pp. 89–99, 2021.

[26] T. Nagano, M. Nakano, A. Nakashima et al., "Identification of cellular senescence-specific genes by comparative transcriptomics," *Scientific Reports*, vol. 6, no. 1, 2016.

[27] J. Z. Bakdash and L. R. Marusich, "Repeated measures correlation," *Frontiers in Psychology*, vol. 8, 2017.

[28] D. Szklarczyk, A. L. Gable, D. Lyon et al., "STRING v11: protein–protein association networks with increased coverage, supporting functional discovery in genome-wide experimental datasets," *Nucleic Acids Research*, vol. 47, no. D1, pp. D607–D613, 2019.

[29] T. Shimi, V. Butin-Israeli, S. A. Adam et al., "The role of nuclear lamin B1 in cell proliferation and senescence," *Genes & Development*, vol. 25, pp. 2579–2593, 2011.

[30] T. Mita, N. Katakami, T. Shiraiwa et al., "Sitagliptin attenuates the progression of carotid intima-media thickening in insulin-treated patients with type 2 diabetes: the sitagliptin preventive study of intima-media thickness evaluation (SPIKE)," *Diabetes Care*, vol. 39, no. 3, pp. 455–464, 2016.

[31] F. Cao, K. Wu, Y.-Z. Zhu, and Z.-W. Bao, "Roles and mechanisms of dipeptidyl peptidase 4 inhibitors in vascular aging," *Frontiers in Endocrinology*, vol. 12, 2021.

[32] M. Xin, X. Jin, X. Cui et al., "Dipeptidyl peptidase-4 inhibition prevents vascular aging in mice under chronic stress: modulation of oxidative stress and inflammation," *Chemico-Biological Interactions*, vol. 314, article 108842, 2019.

[33] J. Bi, W. Cai, T. Ma et al., "Protective effect of vildagliptin on TNF-α-induced chondrocyte senescence," *IUBMB Life*, vol. 71, pp. 978–985, 2019.

[34] Z. Chen, J. Yu, M. Fu et al., "Dipeptidyl peptidase-4 inhibition improves endothelial senescence by activating AMPK/SIRT1/Nrf2 signaling pathway," *Biochemical Pharmacology*, vol. 177, article 113951, 2020.

[35] A. Hernandez-Segura, J. Nehme, and M. Demaria, "Hallmarks of cellular senescence," *Trends in Cell Biology*, vol. 28, pp. 436–453, 2018.

[36] D. Willis-Martinez, H. W. Richards, N. A. Timchenko, and E. E. Medrano, "Role of HDAC1 in senescence, aging, and cancer," *Experimental Gerontology*, vol. 45, pp. 279–285, 2010.

[37] G. H. Stein, L. F. Drullinger, A. Soulard, and V. Dulić, "Differential roles for cyclin-dependent kinase inhibitors p21 and p16 in the mechanisms of senescence and differentiation in human fibroblasts," *Molecular and Cellular Biology*, vol. 19, pp. 2109–2117, 1999.

[38] I. Sturmlechner, C. Zhang, C. C. Sine et al., "p21 produces a bioactive secretome that places stressed cells under immunosurveillance," *Science*, vol. 374, no. 6567, p. eabb3420, 2021.

[39] A. J. van Wijnen, L. Bagheri, A. A. Badreldin et al., "Biological functions of chromobox (CBX) proteins in stem cell self-renewal, lineage-commitment, cancer and development," *Bone*, vol. 143, article 115659, 2021.

[40] L. Morey, G. Pascual, L. Cozzuto et al., "Nonoverlapping functions of the polycomb group Cbx family of proteins in embryonic stem cells," *Cell Stem Cell*, vol. 10, no. 1, pp. 47–62, 2012.

[41] C. Baumann, X. Zhang, and R. De La Fuente, "Loss of CBX2 induces genome instability and senescence-associated chromosomal rearrangements," *Journal of Cell Biology*, vol. 219, 2020.

[42] J. Gil, D. Bernard, D. Martínez, and D. Beach, "Polycomb CBX7 has a unifying role in cellular lifespan," *Nature Cell Biology*, vol. 6, pp. 67–72, 2004.

[43] A. O'Loghlen, A. M. Muñoz-Cabello, A. Gaspar-Maia et al., "MicroRNA Regulation of Cbx7 Mediates a Switch of Polycomb Orthologs during ESC Differentiation," *Cell Stem Cell*, vol. 10, no. 1, pp. 33–46, 2012.

[44] H. Rayess, M. B. Wang, and E. S. Srivatsan, "Cellular senescence and tumor suppressor gene p16," *International Journal of Cancer*, vol. 130, pp. 1715–1725, 2012.

[45] K. M. LaPak and C. E. Burd, "The molecular balancing act of p16INK4ain cancer and aging," *Molecular Cancer Research*, vol. 12, no. 2, pp. 167–183, 2014.

[46] L. Morey and K. Helin, "Polycomb group protein-mediated repression of transcription," *Trends in Biochemical Sciences*, vol. 35, pp. 323–332, 2010.

[47] R. F. Place, E. J. Noonan, and C. Giardina, "HDACs and the senescent phenotype of WI-38 cells," *BMC Cell Biology*, vol. 6, no. 1, p. 37-, 2005.

[48] N. Jiang, G. Niu, Y. H. Pan et al., "CBX4 transcriptionally suppresses KLF6 via interaction with HDAC1 to exert oncogenic activities in clear cell renal cell carcinoma," *eBioMedicine*, vol. 53, article 102692, 2020.

[49] I. Giordano, L. Pirone, V. Muratore et al., "SALL1 modulates CBX4 Stability, Nuclear Bodies, and Regulation of Target Genes, nuclear bodies, and regulation of target genes," *Frontiers in Cell and Developmental Biology*, vol. 9, 2021.

[50] R. G. Ma, Y. Zhang, T. T. Sun, and B. Cheng, "Epigenetic regulation by polycomb group complexes: focus on roles of CBX proteins," *Journal of Zhejiang University. Science. B*, vol. 15, pp. 412–428, 2014.

Hindawi
Oxidative Medicine and Cellular Longevity
Volume 2022, Article ID 3920664, 15 pages
https://doi.org/10.1155/2022/3920664

Research Article

Ferritinophagy-Mediated Ferroptosis and Activation of Keap1/Nrf2/HO-1 Pathway Were Conducive to EMT Inhibition of Gastric Cancer Cells in Action of 2,2′-Di-pyridineketone Hydrazone Dithiocarbamate Butyric Acid Ester

Deng Guan,[1,2,3] Wei Zhou,[2] Huiping Wei,[2] Ting Wang,[4] Kangwei Zheng,[1] Chunjie Yang,[1] Rui Feng,[4] Ruifang Xu,[4] Yun Fu,[3] Cuiping Li,[3] Yongli Li,[2] and Changzheng Li[1,3,4]

[1]*College of Pharmacy, Sanquan College of Xinxiang Medical University, Xinxiang, Henan, China*
[2]*College of Basic Medical Science, Sanquan College of Xinxiang Medical University, Xinxiang, Henan, China*
[3]*College of Basic Medical Science, Xinxiang Medical University, Xinxiang, Henan, China 453003*
[4]*Experimental Teaching Center of Biology and Basic Medical Sciences, Sanquan College of Xinxiang Medical University, Xinxiang, Henan, China*

Correspondence should be addressed to Yongli Li; liyongli@sqmc.edu.cn and Changzheng Li; changzhenl@yahoo.com

Received 31 December 2021; Accepted 31 January 2022; Published 21 February 2022

Academic Editor: Milena Georgieva

In metastasis of cancer cells, the epithelial-mesenchymal transition (EMT) is prerequired. Ferroptosis is an iron-mediated cellular death process, but whether it involves EMT regulation remains elusive. In addition, how stress responders (Nrf2) respond to the redox alteration and cross-talking between them needs to be determined. Our data revealed that DpdtbA (2,2′-di-pyridineketone hydrazone dithiocarbamate butyric acid ester) resisted TGF-β1-induced EMT in gastric cancer lines (SGC-7901 and MGC-823) through ferritinophagy-mediated ROS production. Furthermore, the depletion of Gpx4 and xCT as well as enhanced lipid peroxidation indicated that DpdtbA acted as Erastin did in ferroptosis induction, which thus provided chance to explore the causal relationship between ferroptosis and EMT. Our data illustrated that ferritinophagy-mediated ferroptosis promoted the EMT inhibition. In addition, activated Nrf2 involved the regulation on both ferroptosis and EMT in response to the alteration in the cellular redox environment. In brief, ferritinophagy-mediated ferroptosis and activation of the Keap1/Nrf2/HO-1 pathway were conducive to the EMT inhibition.

1. Introduction

The uncontrollable propagation and migration to the nearby organs are one of the features of cancerous cells [1], while the undergoing epithelial-mesenchymal transition (EMT) is a prerequisite. During EMT, the tumor cells lose cell-cell adhesion and gain the traits of migration and invasion. At the molecular level, epithelial markers, such as ZO-1 and E-cadherin, are weakened, while vimentin and N-cadherin are increased correspondingly [2–4]. In addition, the transforming growth factor (TGF), cytokine, nuclear receptor, receptor tyrosine kinase (RTK), and reactive oxygen species (ROS) are shown to play a role in the EMT regulation [5–7]. In addition to the abovementioned, EMT in fact is in a hybrid E/M phenotype for cancer cells, and "phenotypic stability factors" (PSFs, GRHL2, OVOL2, ΔNp63α, and NUMB) can maintain the hybrid E/M phenotype [8–11], indicating that the EMT process is quite complex. Finally, EMT not only enables the multistep process leading to the colonization of distant anatomical sites but also endows malignant cells with an accrued resistance to a variety of therapeutic regimens [12].

Ferroptosis is an iron-dependent cell death, distinct from apoptosis. In ferroptosis, cell death is executed by reactive oxygen species- (ROS-) mediated peroxidation of polyunsaturated fatty acids (PUFAs), which can be reduced by

glutathione peroxidase 4- (Gpx4-) mediated glutathione (GSH) [13]. Cysteine deriving from cystine reduction is used for GSH synthesis, while cystine transportation into the cell was through the system Xc-transporter SLC7A11 subunit; therefore, depletion of cysteine resulted in ferroptosis. Interestingly, Viswanathan et al. found that therapy-resistant cancer cells cross EMT and were sensitive to ferroptosis, which meant that ferroptosis inducers may be used to inhibit the EMT of cancer cells [14, 15]. In addition, NCOA4-mediated ferritin degradation in lysosomes triggered to ferroptosis induction [16], which was due to Fenton reaction-mediated ROS production. Some iron chelators were able to induce ferritinophagy in previous reports [17, 18]; however, the relationship between ferritinophagy, EMT, and ferroptosis remains unclear.

Nuclear factor erythroid 2-related factor 2 (Nrf2) is the master regulator of antioxidant and cytoprotective systems [19] and is located in the cytoplasm under normal circumstances. During oxidative stress insulting, Nrf2 is translocated to the nucleus, where it binds to the antioxidant response elements and activates its downstream target genes [20], including glutathione (GSH) synthesis, chemoresistance, and cytoprotection [21]. The homeostasis of Nrf2 is controlled by Kelch-like ECH-associated protein 1 (Keap1) to proteasomal degradation [22]. The accumulating evidence reveals that the Nrf2 plays a role in tumorigenesis [23]. In addition, reactive oxygen species (ROS) are recognized as actors in the adaptation of cancer cells to therapy, which is important in cancer cell drug resistance [22]. On the other hand, emerging evidence suggests the involvement of Nrf2 in transforming growth factor β1- (TGF-β1-) stimulated EMT in rat renal tubular cells and AECs [24]. However, the function of Nrf2 in EMT modulation remains to be determined.

Our previous work showed that "ferritinophagic flux" (NCOA4/ferritin) was a dominant driving force in determination of status of EMT in the CT26 cell line and gastric cancer cell lines in normal oxygenation [25–27]; however, cancer cells almost grow in hypoxia environment. The recent research revealed that 2,2′-di-pyridylketone hydrazone dithiocarbamate butyric acid (DpdtbA) also induced EMT inhibition in the hypoxia environment, which was related to activation of the p53 and PHD2/hif-1α pathway [28]. Since that "ferritinophagic flux" (NCOA4/ferritin) played a crucial role in determination of the status of EMT, the cellular redox response may occur. In this study, we found that DpdtbA treatment also resulted in depletion of Gpx4 and xCT and increase in lipid peroxidation, hinting there was an occurrence of ferroptosis; thus, the causal relationship between EMT and ferroptosis was explored. Our data revealed that ferroptosis induction was conducive to EMT inhibition. In addition, in response to ferritinophagy-mediated ferroptosis, the Nrf2 activation may be triggered. Interestingly, knockdown of Nrf2 by siRNA resulted in attenuation in ferroptosis induction and EMT promotion, hinting there was cross-talk between redox responder (Nrf2) and the induced cellular events. Our data strongly suggested that the ferroptosis induction and activation of the Keap1/Nrf2/HO-1 pathway were advantageous to the EMT inhibition, which highly depended on the strength of ferritinophagic flux (ROS production).

2. Materials and Methods

2.1. Materials. 3-Methyladenine (3-MA), dichlorofluorescein (H_2DCF-DA), ferrostatin-1, 4′,6-diamidino-2-phenylindole (DAPI), TGF-β1, N-acetyl-L-cysteine (NAC), Roswell Park Memorial Institute- (RPMI-) 1640, and other chemicals were purchased from Sigma-Aldrich (USA). Erastin was from MedChemExpress. Antibodies of vimentin, NCOA4, Nrf2, Keap1, HO-1, and gapdh for Western blotting were obtained from Proteintech Group Inc. (Wuhan, China). Antibodies of E-cadherin and ferritin (H chain) and secondary antibodies (fluorescence labeled for immunofluorescence) were purchased from Cell Signaling Technology (USA). Ferritin antibody for immunofluorescence was obtained from Santa Cruz Biotechnology (USA, Santa Cruz). NCOA4 antibody for immunofluorescence was purchased from Atlas Antibody (Sweden). Secondary antibodies for Western blotting were obtained from EarthOx, LLC (San Francisco, USA).

2.2. Cell Treatment. The cells (SGC-7901 and MGC-803, Yuchi Cell Biological Technology Co. Ltd.) in the exponential phase were cultured in RPMI-1640 medium supplemented with 10% fetal calf serum (FCS) and antibiotics as described previously [25]. The DpdtbA in 70% DMSO was used for cell treatment at a ratio of 1 : 100 (cell culture) in order to minimize toxicity of the solvent (DMSO final concentration $\leq$ 0.7%) [29]. In parallel, 70% DMSO was added to counteract the effect of the solvent when performing intergroup analysis.

2.3. Assay of Cellular ROS. MGC-803 (or SGC-7901) cells were treated by DpdtbA (5.0 μM) or inhibitor (at indicated concentration) for 24 h. After trypsin digestion, the cells were collected by centrifugation, then resuspended in H_2DCF-DA containing serum-free culture medium for 30 min. A flow cytometer (Becton-Dickinson, USA) was used to perform the intracellular ROS assay [25].

2.4. Knockdown of NCOA4 and Nrf2. Genetic knockdown of NCOA4 (or Nrf2) was performed based on the procedure as described previously [25]. The small-interfering RNA (siRNA-mate (siN0000001-1-5) and siRNA (siG000008031A-1-5 and siG000008031B-1-5 for NCOA4; siB160506092821-1-5 and siB160729033042-1-5 for Nrf2)) were obtained from Ribobio, China. Briefly, the MGC-803 cells (1×10^6) were transfected with 100 pmol of siRNA using Lipofectamine™ Stem Transfection Reagent (Invitrogen, USA) for 12 h. For immunofluorescence, confocal analysis of the MGC-803 cells was performed as described above except culturing the cells firstly in 24-well plates with cover glass.

2.5. Immunofluorescence Analysis. An immunofluorescence confocal analysis was conducted to investigate the changes of either EMT-related or ferritinophagy-related proteins [25]. Briefly, the MGC-803 (SGC-7901) cells on the cover glass were treated in the following steps: fixation with 4% paraformaldehyde, permeation in 0.5% Triton X-100

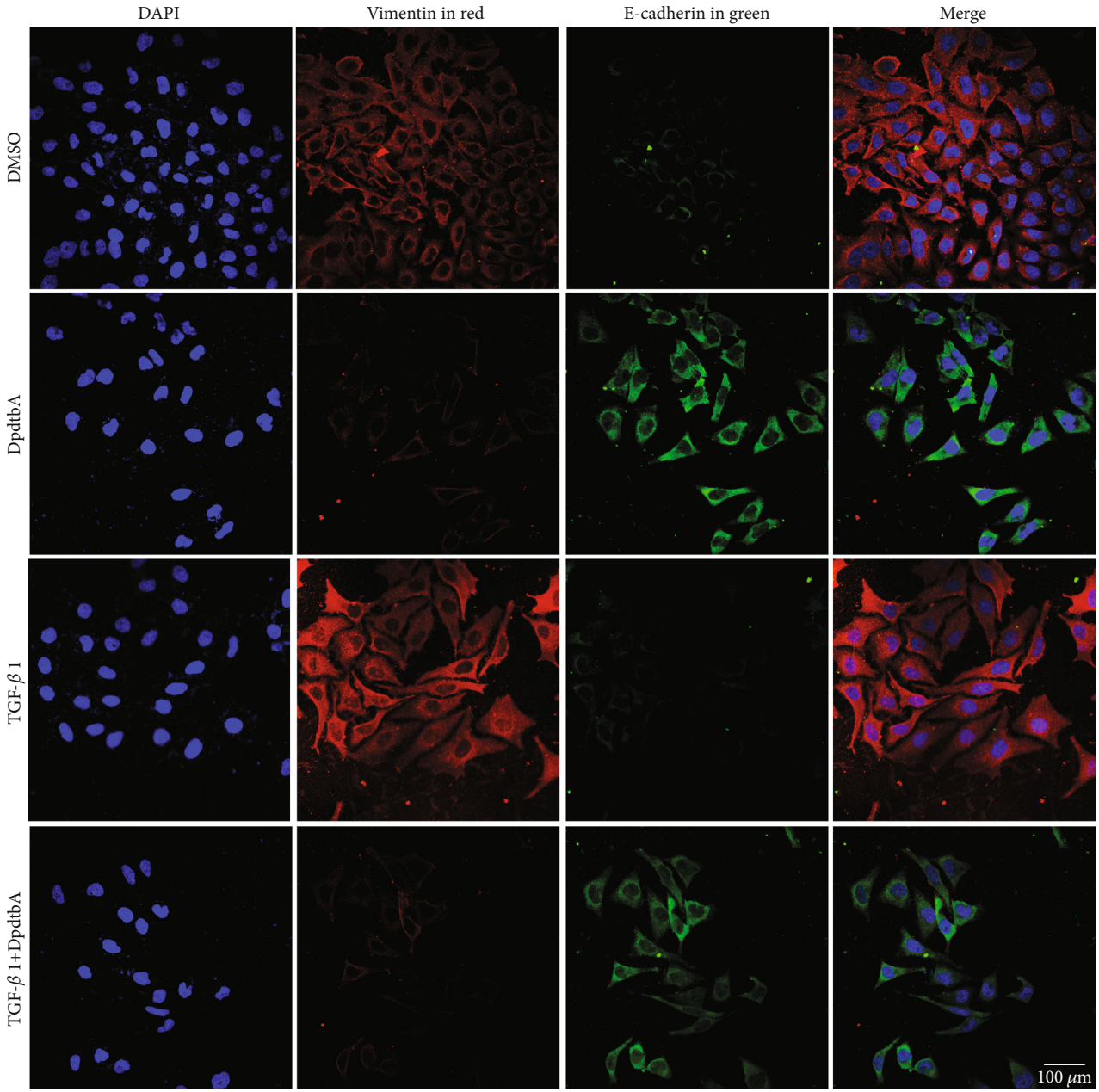

Figure 1: DpdtbA treatment resulted in alteration in level of EMT-related proteins in MGC-803 cell line. Objective size: 40 × 10; scale bar: 100 μm.

(30 min), and blockage in 1% BSA (1 h). Next, the cells were treated with investigated primary antibody (ferritin and H chain (Santa Cruz Biotechnology), NCOA4 (Atlas Antibodies), and vimentin and E-cadherin (Cell Signaling Technology)) at 4°C for overnight. Then, the fluorescence-labeled secondary antibody was used to associate with primary antibody. Finally, the cells were counterstained further with DAPI. The representative cells were recorded on a confocal laser scanning microscope (Nikon Eclipse Ts2, Japan) at a magnification of 400x.

2.6. Western Blotting Analysis. The procedure for Western blotting was as described previously [25]. The cells (MGC-803 or SGC-7901) treated by indicated agents were scraped in 200 μl lysis buffer and lysed on ice for 30 min. The supernatant was collected by centrifugation. The protein concentration of the supernatant was determined by using enhanced BCA protein assay kit (Beyotime, China). Equal amounts of denatured proteins were loaded on 13~15% sodium dodecyl sulfate-polyacrylamide gels for electrophorese analysis. Next, the separated proteins on the gel were transferred to a polyvinylidene difluoride membrane (Millipore, Billerica, MA). The membrane was incubated with an appropriate primary antibody after blockage by nonfat milk at 4°C for overnight; then, the secondary antibody was added to associate the primary antibody. The protein band was visualized by using a supersensitive ECL solution (Boster Biological Technology Co. Ltd.) on a Syngene G: BOX imager (Cambridge, United

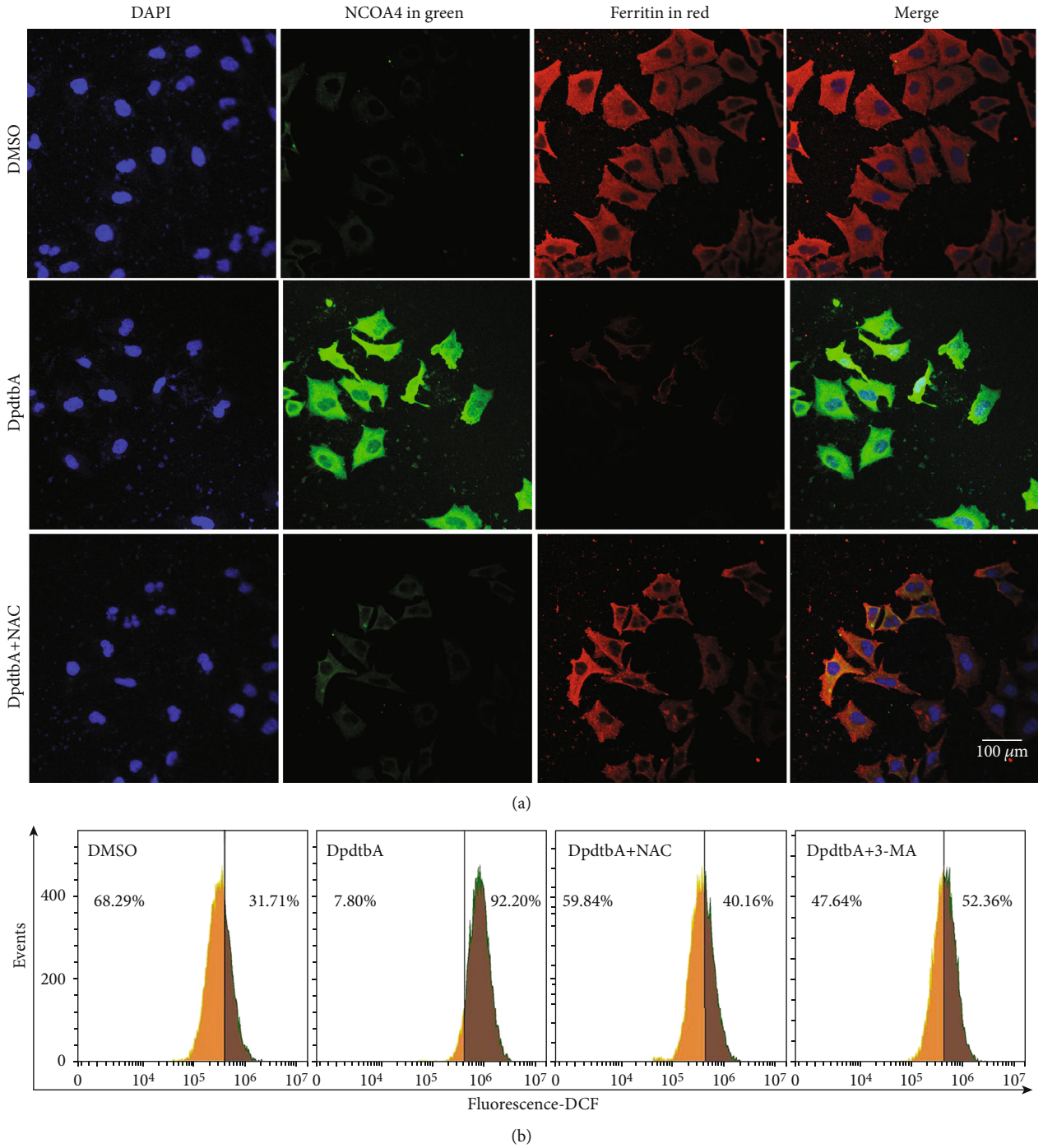

Figure 2: DpdtbA-induced ferritinophagy correlated with the ROS production. (a) DpdtbA-induced ferritinophagy was redox active; objective size: 40 × 10; scale bar: 100 μm. (b) DpdtbA-induced ROS production involved autophagy.

Kingdom). Quantification analysis of fluorescence intensity of the protein band was performed using ImageJ software.

2.7. Statistical Analysis. Results are presented as the mean ± SEM. Comparisons between multiple groups were performed by one-way ANOVA with Dunnett's post hoc correction. A p value < 0.05 was considered statistically significant.

3. Results

3.1. DpdtbA Treatment Resulting in Alteration in EMT-Related Proteins in Gastric Cancer Cell Line-Involved ROS Production. DpdtbA (2,2′-di-pyridineketone hydrazone dithiocarbamate butyric acid ester) exhibited significant antitumor activity [30, 31]. In addition, DpdtbA treatment led to suppression of EMT-related markers under normoxia

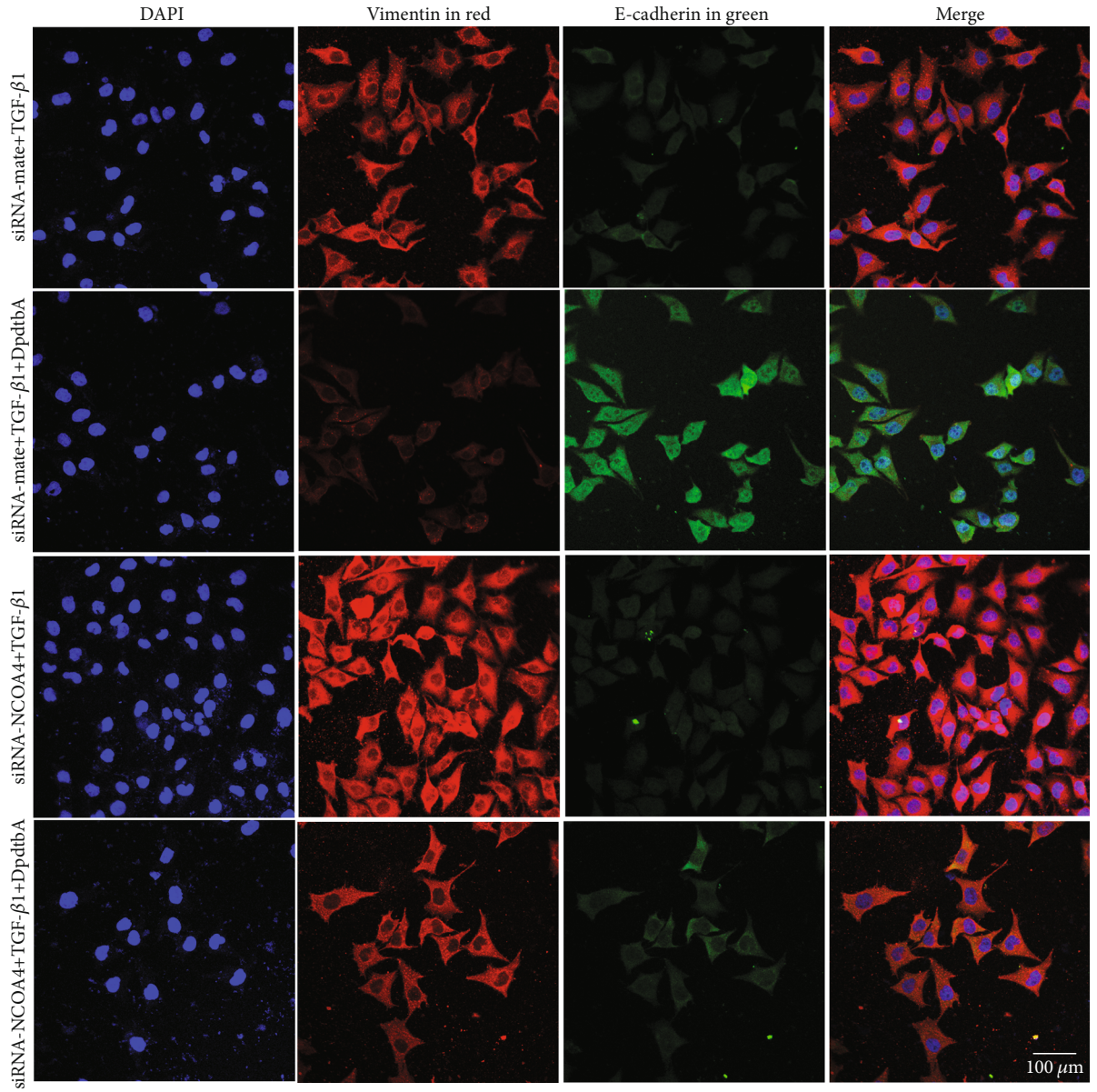

Figure 3: TGF-β1-induced EMT involved NCOA4 regulation in MGC-803 cell. Objective size: 40 × 10; scale bar: 100 μm.

and hypoxia conditions [28]; however, the detail of inhibition of mechanism was not fully determined. To this end, a model of EMT was first established through TGF-β1 induction. As shown in Figure 1, TGF-β1 treatment resulted in the cells in stretched and fibroblast-like shape, supporting the cells undergoing EMT [30], but the addition of DpdtbA led to retraction of the cells in shape. Importantly, the EMT-related proteins were faded in red fluorescence (vimentin) and enhanced in green (E-cadherin) even in the presence of TGF-β1. Similar observation was in the SGC-7901 cell line (Fig. S1). Those indicated that DpdtbA was able to inhibit EMT transformation in gastric cancer lines.

ROS production was observed in EMT induction [31], but whether the EMT inhibition is also associated with the ROS production has not been fully determined. For this purpose, the alteration of cellular redox status was further determined. Thus, a ROS scavenger, N-acetyl-L-cysteine (NAC), was used to determine whether there was ROS involvement in the action of mechanism of DpdtbA. Fig. S2 shows that addition of NAC almost neutralized the effect of DpdtbA on the regulation of EMT-related proteins, hinting that the EMT inhibition was involved in ROS production.

3.2. Ferritinophagy-Mediated ROS Production Played a Role in DpdtbA-Induced EMT Inhibition. Our previous study revealed that ferritinophagy was an important contributor in ROS production [18]. DpdtbA may have similar action in ferritinophagy induction. Figure 2 shows that DpdtbA treatment caused an enhancement in green fluorescence of NCOA4, fading in red fluorescence of ferritin compared to DMSO in MGC-803 cells, indicating that a ferritinophagy occurred. Furthermore, although ferritinophagy is related

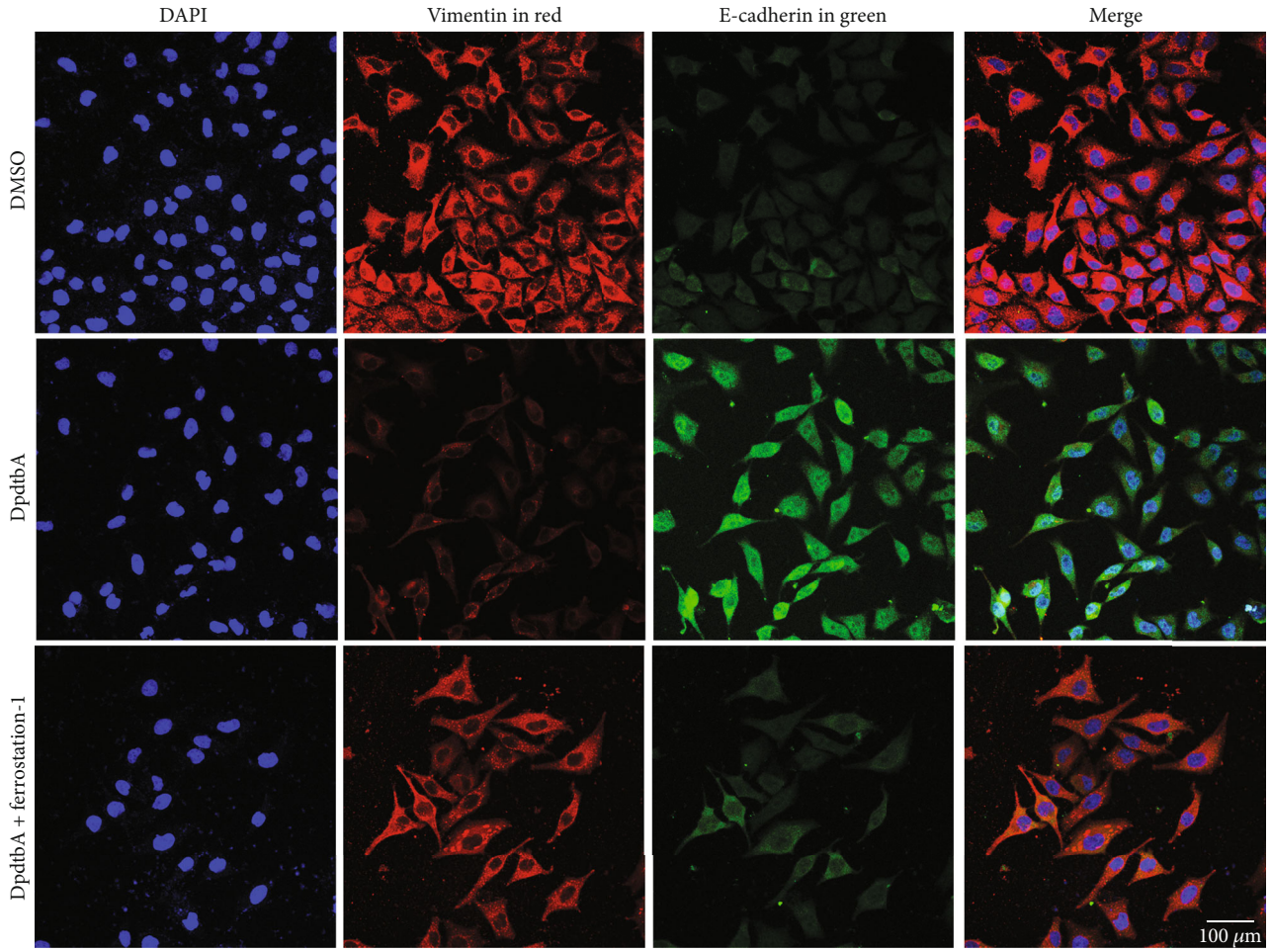

(a)

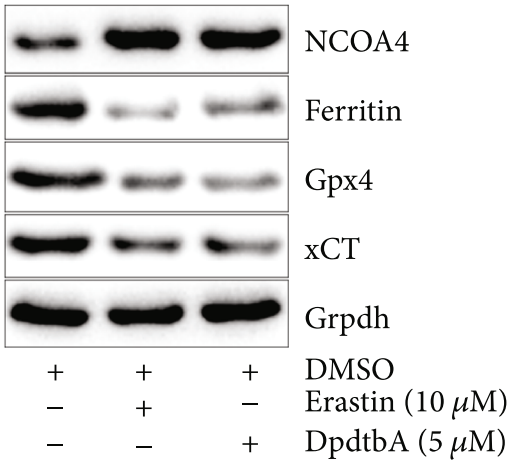

(b)

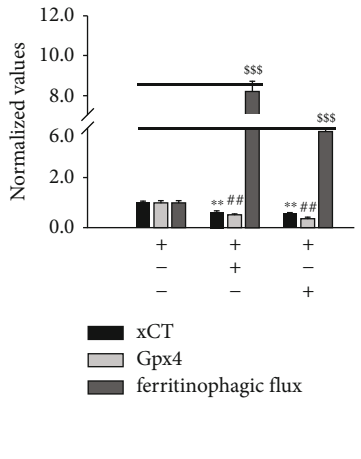

(c)

Figure 4: Continued.

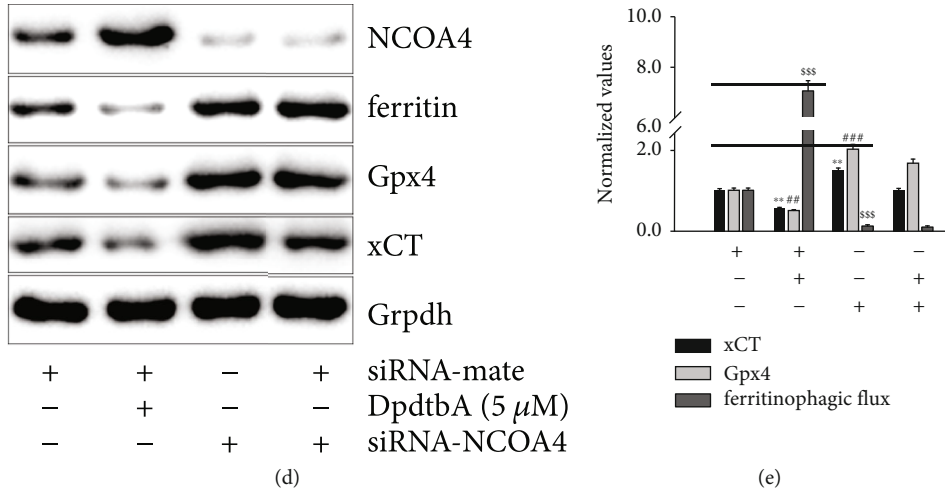

Figure 4: DpdtbA-induced EMT inhibition involved ferroptosis. (a) Ferrostatin-1 could attenuate the regulatory effect of DpdtbA on EMT-related proteins in MGC-803. The concentrations of Erastin and DpdtbA were as indicated, all the same, unless otherwise specified. Objective size: 40 × 10; scale bar: 100 μm. (b) Both DpdtbA and Erastin treatment resulted in ferritinophagy (NCOA4-mediated ferritin degradation) and depletion of Gpx4 and xCT; (c) quantitative analysis derived from (b) indicated that the ferroptosis induction of those agents correlated with the enhanced ferritinophagic flux; (d) knockdown of NCOA4 weakened the regulatory effect of DpdtbA on ferroptosis-related proteins in MGC-803 cell; (e) quantitative analysis derived from (c). $^{**,\#\#}p < 0.05$ vs. control, $^{***,\#\#\#}p < 0.01$ vs. control, one-way ANOVA with Dunnett's post hoc correction.

to ROS production, it is not necessary in fact. DFO is a ferritinophagy inducer, but it is used as a ROS scavenger. Therefore, the redox characteristic of the induced ferritinophagy needed to be determined. For this purpose, the ROS assay was conducted via flow cytometry after the cells were stained by H_2DCF-DA. As shown in Figure 2(b), DpdtbA treatment resulted in significant increase of ROS compared to DMSO, but addition of NAC abated markedly the inductive effect of DpdtbA on ROS induction. Similarly, addition of 3-methyladenine (3-MA), an autophagy inhibitor, also weakened the ROS production, indicating that DpdtbA-induced ROS production correlated with the occurrence of ferritinophagy. Similarly, this scene also occurred in SGC-7901 cells (Fig. S3).

To further determine the contribution of ferritinophagy to the EMT inhibition, the genetic knockdown of NCOA4 was performed. As shown in Figure 3, the intensity of red fluorescence of vimentin was decreased, while the intensity of green fluorescence of E-cadherin was accordingly increased once there was DpdtbA treatment in the presence of TGF-β1. Interestingly, knockdown of NCOA4 gave rise to slight enhancement of vimentin in red fluorescence, prompting that NCOA4 may involve the regulation of EMT-related proteins. As a result, knockdown of NCOA4 would significantly attenuate the regulatory effect of DpdtbA on EMT-related proteins. Those indicated that NCOA4-mediated ferritinophagy contributed to the EMT inhibition, which was in accordance with our previous observations [30].

3.3. DpdtbA-Induced EMT Inhibition Involved Ferritinophagy-Mediated Ferroptosis. Ferroptosis induction involved ROS production, while ferritinophagy-mediated ROS production contributed to the EMT inhibition, which promoted us to consider whether ferroptosis was involved in the EMT process. Thus, a ferroptosis-specific inhibitor, ferrostatin-1 (fer-1), was used to determine if this was true. As expected, the ferroptosis inhibitor indeed neutralized the regulatory effect of DpdtbA on vimentin and E-cadherin (Figure 4(a)), implying that the EMT inhibition may involve ferroptosis induction. In addition, the depletions of either selenoenzyme glutathione peroxidase 4 (Gpx4) or solute carrier family 7 member 11 (xCT) may trigger ferroptosis [32, 33]; then, their abundances were investigated. Fig. S4A shows that DpdtbA treatment caused downregulation of both Gpx4 and xCT, but addition of ferrostatin-1 markedly stopped them from decrease induced by the agent. This situation was also observed in the SGC-7901 cell (Fig. S4C). In addition to the abovementioned, lipid peroxidation and depletion of GSH were critical characteristics for ferroptosis induction [34, 35]; DpdtbA could achieve similar consequence as Erastin, a ferroptosis inducer did; and such action could be abated by the addition of ferrostatin-1 (or NAC) in Fig. S5; this further supported that the agent was able to induce ferroptosis.

As mentioned above, DpdtbA induced ferroptosis as Erastin did; the causal relation between ferritinophagy and ferroptosis needs to be determined. As shown in Figure 4(b), DpdtbA and Erastin treatment produced depletion of ferritin and upregulation of NCOA4 along with depletions of Dpx4 and xCT, clearly indicating that ferritinophagy caused ferroptosis. To reinforce the role of ferritinophagy, we used the term of ferritinophagic flux (NCOA4/ferritin). Figure 4(c) shows that the depletions of Gpx4 and xCT correlated with enhanced ferritinophagic flux, implying that ferritinophagic flux determined the fate of ferroptosis. To corroborate the above speculation, the

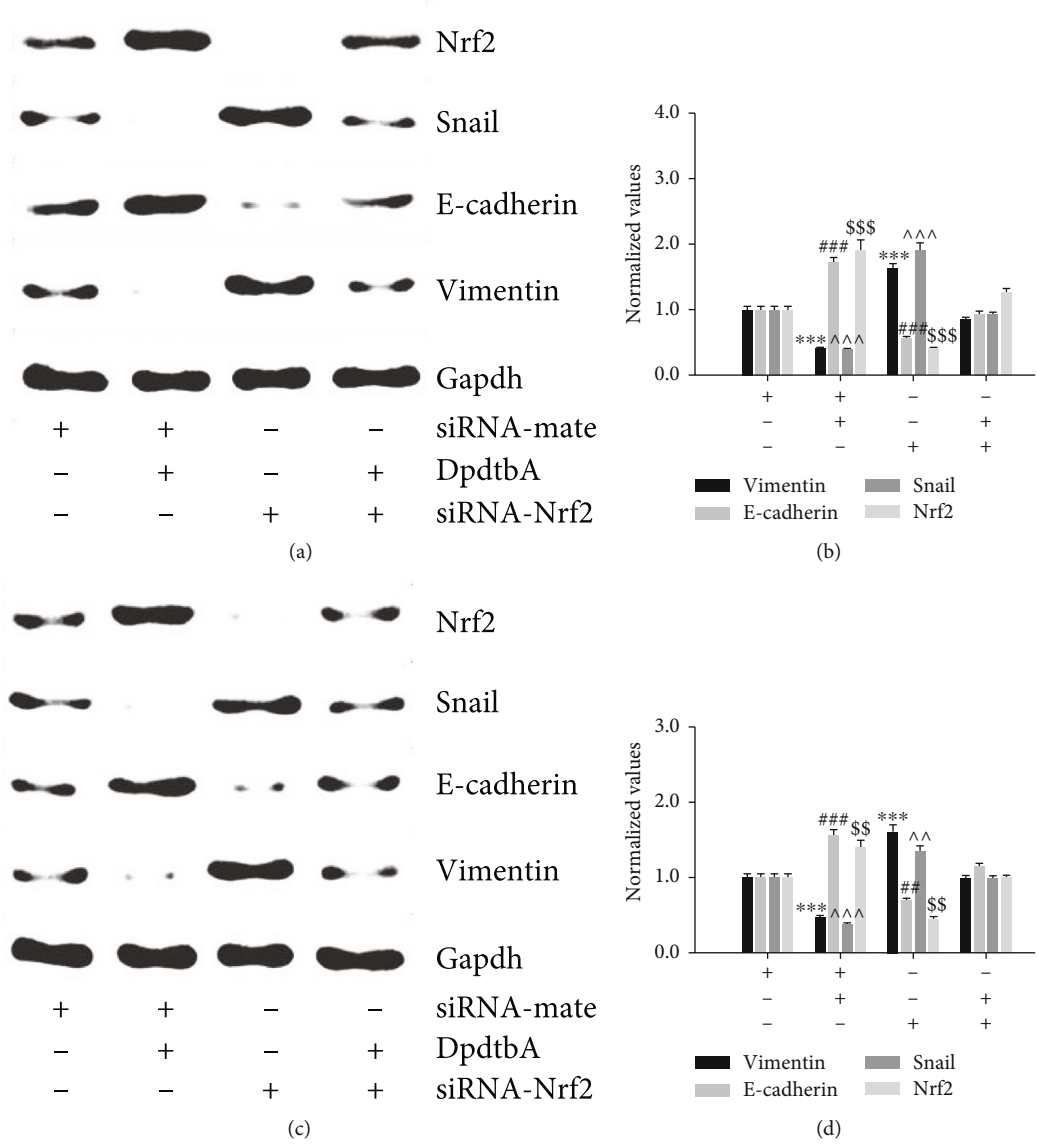

Figure 5: Nrf2 had a role in DpdtbA-induced EMT inhibition. (a) The EMT inhibition induced by DpdtbA was related to activation of Nrf2 in MGC-803 cells. (b) Quantitative analysis derived from (a) after normalization. (c) DpdtbA-induced EMT inhibition was achieved through activation of Nrf2 in SGC-7901 cells. (d) Quantitative analysis derived from (c) after normalization. $^{**,\#\#}p < 0.05$; $^{***,\#\#\#,\$\$\$}p < 0.01$ vs. control, one-way ANOVA with Dunnett's post hoc correction.

effect of NCOA4 on ferroptosis induction was conducted. Figure 4(d) reveals that knockdown of NCOA4 led to upregulations of xCT, Gpx4, and ferritin; therefore, it can be imaged that such an action would chip away the regulative effect of DpdtbA on ferroptosis-related proteins. Surely either concentration of DpdtbA or efficiency of NCOA4 knockdown determined the abundance of those proteins. The quantitative analysis of the related proteins is presented in Figure 4(e) after normalization. Clearly, the data further supported the above conclusion that ferroptosis induction depended on the strength of the ferritinophagic flux.

3.4. DpdtbA-Induced EMT Involved Nrf2 Activation. Since DpdtbA-induced EMT inhibition was achieved through ferritinophagy-mediated ferroptosis induction, the cellular redox environment would be changed accordingly. Nrf2, which is one of the master transcription factors, may respond to the redox change. Fig. S6 shows that the Nrf2 was upregulated when the cell was exposed to DpdtbA, implying that Nrf2 might involve the EMT regulation. To this end, the Nrf2 was knocked down to assay its effect on EMT regulation. As shown in Figure 5(a), knockdown of Nrf2 led to obvious increases of abundance of snail and vimentin, while DpdtbA treatment caused those proteins to be downregulated; therefore, a rescued result would be expected in the combination treatment of Nrf2 knockdown with DpdtbA. Those data clearly supported that Nrf2 also involved EMT regulation in the MGC-803 cell. The quantitative analysis derived from Figure 5(a) is presented in Figure 5(b) after normalization. Clearly, the changes for the indicated proteins in Figure 5(b) were significant in individual treatment, not in combination

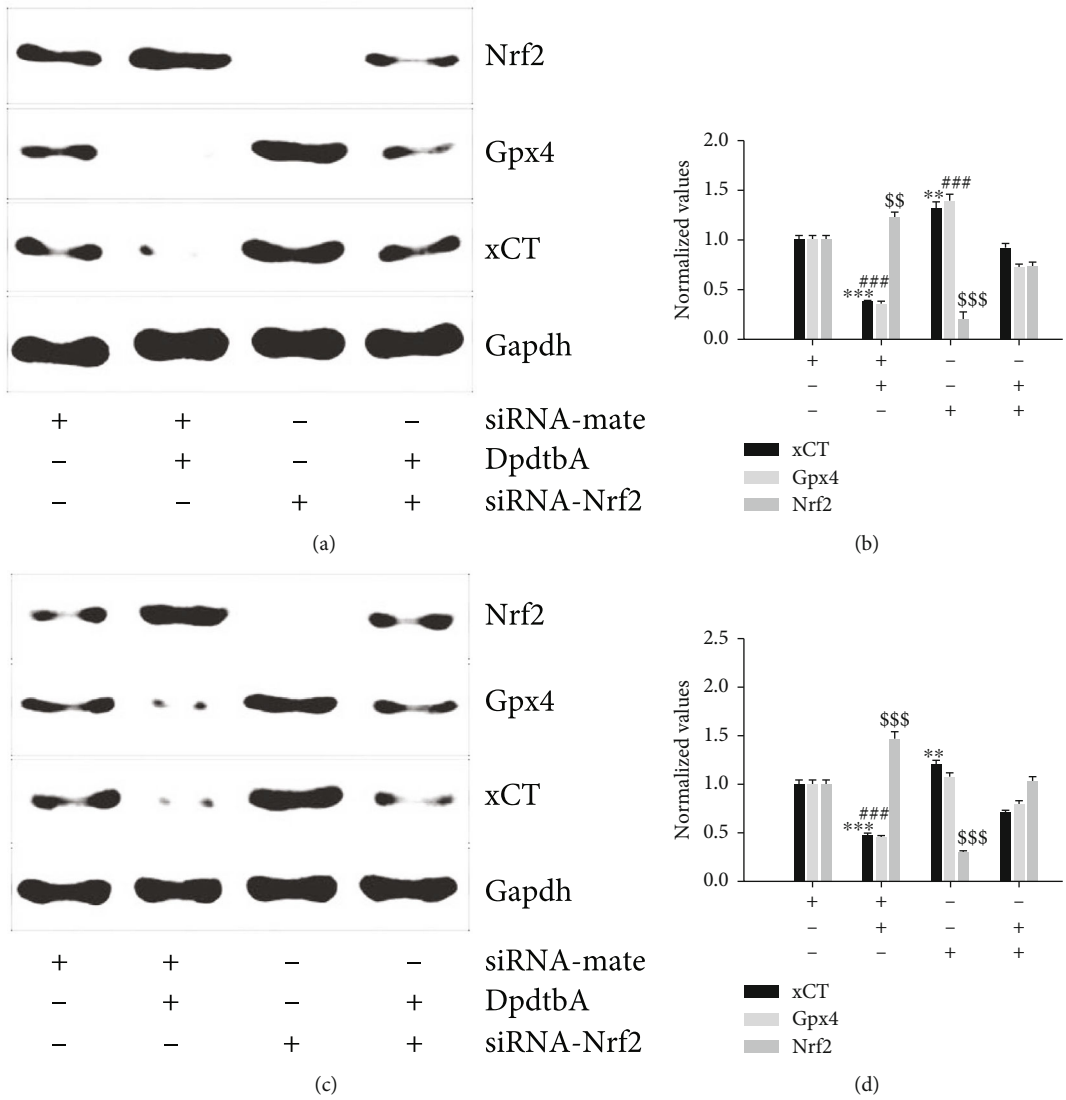

Figure 6: DpdtbA-induced ferroptosis involved Nrf2 activation. (a) The downregulation of Gpx4 and xCT correlated with activation of Nrf2 in MGC-803 cells; (b) quantitative analysis derived from (a) after normalization; (c) the downregulation of Gpx4 and xCT correlated with activation of Nrf2 in SGC-7901 cells; (d) quantitative analysis derived from (c) after normalization. $^{**,\#\#}p < 0.05$; $^{***,\#\#\#,\$\$\$}p < 0.01$ vs. control, one-way ANOVA with Dunnett's post hoc correction.

treatment. A similar situation occurred in the SGC-7901 cell (Figures 5(c) and 5(d)). Those suggested that the activation of Nrf2 was conducive to the inhibition of EMT, inconsistent with what was reported previously [36].

3.5. Nrf2 Activation Was Related to Ferroptosis Induction. It has been demonstrated that activation of Nrf2 induces the expression of multiple defensive genes in transcription, including xCT that serves to cope with ferroptosis [34]. Similarly, Gpx4 is responsible for reduction of peroxidation of polyunsaturated fatty acids, and its expression was regulated by chaperone-mediated autophagy [37]. The depletion of either xCT or Gpx4 triggers to ferroptosis. Thus, the correlation of activation of Nrf2 with Gpx4 and xCT was further investigated. Figure 6 shows that DpdtbA treatment resulted in depletions of Gpx4 and xCT and activation of Nrf2; nevertheless, Nrf2 knockdown significantly attenuated the regulatory effect of DpdtbA on ferroptosis-related proteins in MGC-803 cells, indicating that Nrf2 also involved the regulation of ferroptosis (Figure 6(a)). The comparative analysis was performed after normalization (Figure 6(b)). Similar observation occurred in SGC-7901 cells (Figures 6(c) and 6(d)). Those all indicated that Nrf2 as a redox-sensitive transcriptional factor was implicated in ferroptosis induction. Next, the degradation manner of Gpx4 and xCT was further investigated because either ubiquitin-proteasome system (UPS) or autophagy controls their stability. Fig. S6 shows that the addition of 3-MA could attenuate the regulatory effect of DpdtbA on Gpx4 and xCT, implying that DpdtbA-induced autophagy was in charge of the dynamic equilibrium of Gpx4 and xCT.

3.6. Ferritinophagy-Mediated ROS Production Was Responsible for Activation of Keap1/Nrf2/HO-1 Pathway.

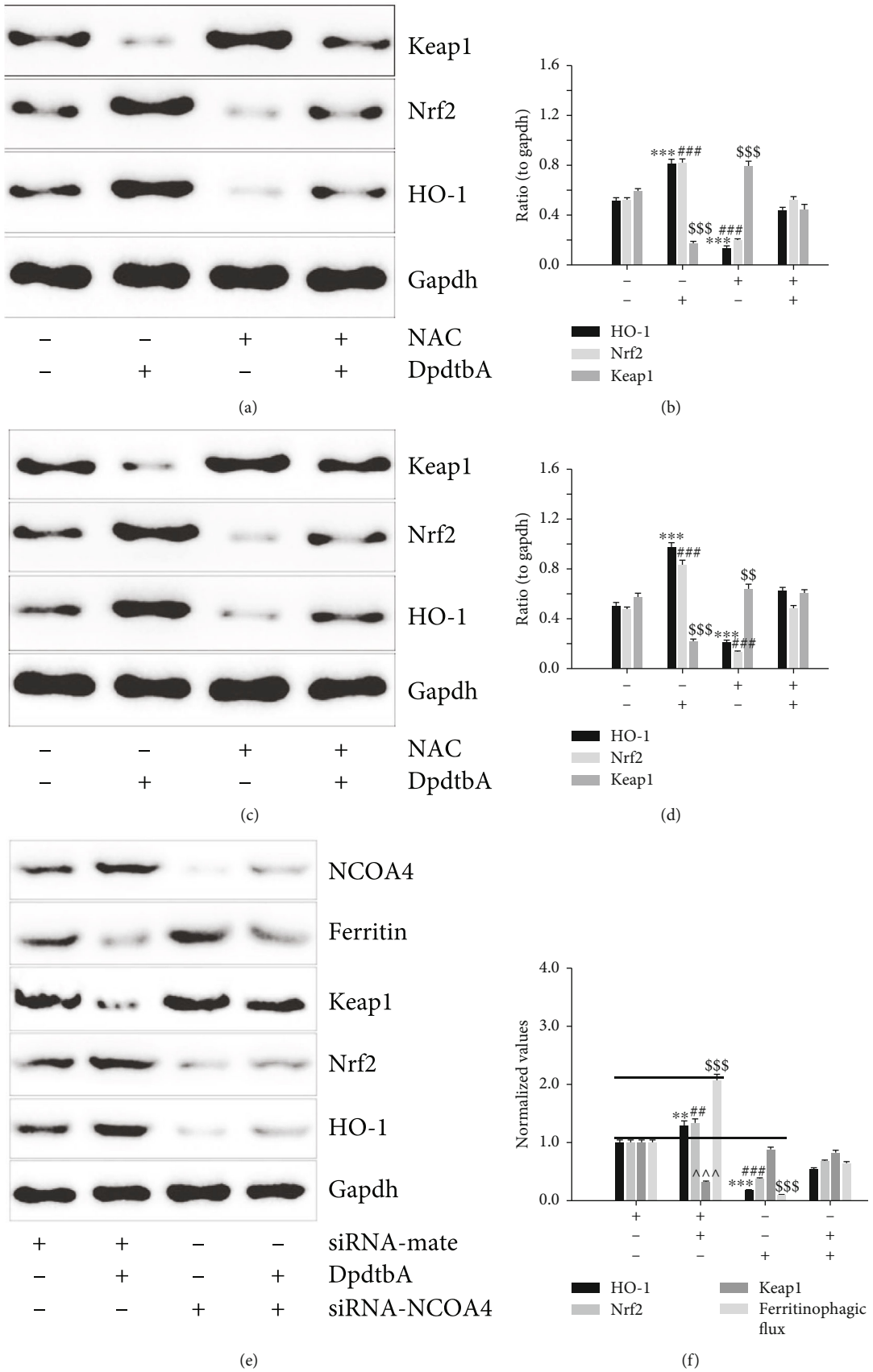

Figure 7: Continued.

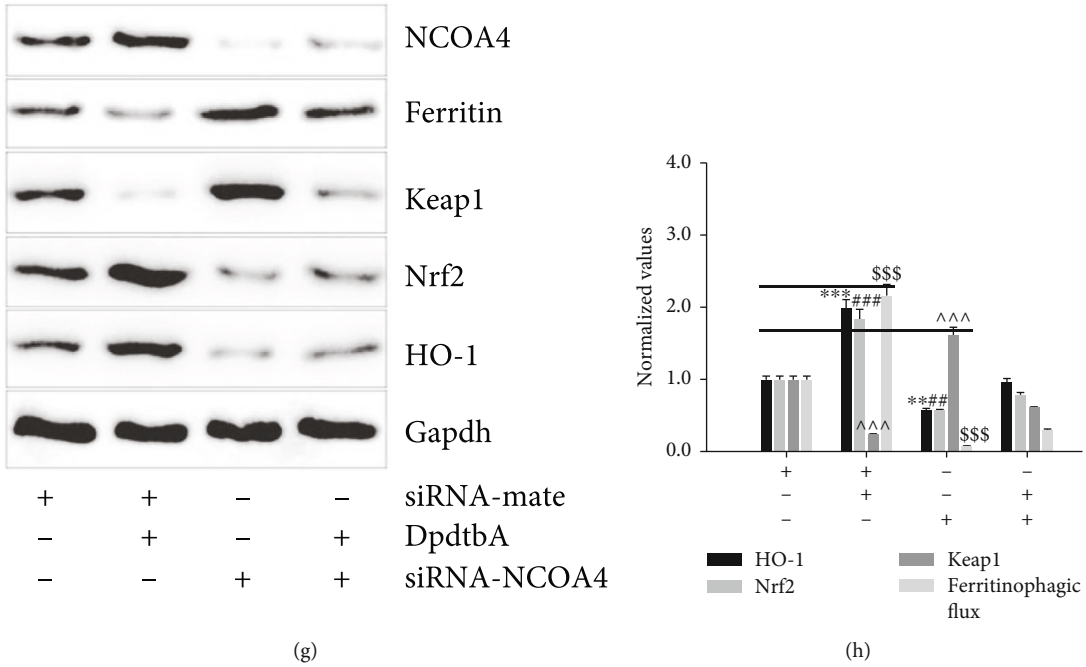

Figure 7: Ferritinophagy-mediated ROS production triggered the activation of Keap1/Nrf2/HO-1 pathway. (a) Keap1 downregulation resulted in activation of Nrf2 and its downstream target gene in MGC-803 cells; (b) quantitative analysis derived from (a) after normalization; (c) Keap1 downregulation resulted in activation of Nrf2 and its downstream target gene in SGC-7901 cells; (d) quantitative analysis derived from (c) after normalization; (e) the enhanced ferritinophagic flux correlated with activation of Keap1/Nrf2/HO-1 pathway in MGC-803; (f) quantitative analysis derived from (e); (g) the enhanced ferritinophagic flux correlated with activation of Keap1/Nrf2/HO-1 pathway in SGC-7901; (h) quantitative analysis derived from (g). $^{**,\$\$,\#\#}p < 0.05$; $^{***,\#\#\#,\$\$\$}p < 0.01$ vs. control, one-way ANOVA with Dunnett's post hoc correction.

Since Nrf2 activation involved the EMT inhibition and ferroptosis induction, the underlying mechanism of Nrf2 activation needed to be determined. It has been demonstrated that the homeostasis of Nrf2 is controlled by Keap1 through proteasomal degradation [22]. For this reason, the level of Keap1 was determined by Western blotting. Figure 7(a) shows that Keap1 was significantly downregulated upon DpdtbA treatment, implying that the activation of Nrf2 was due to degradation of Keap1. Next, we determined the manner of Keap1 degradation. Fig. S7 shows that addition of 3-MA or ferrostatin-1 could neutralize the regulatory effect of DpdtbA on Keap1, supporting that autophagy controlled the homeostasis of Keap1. HO-1 is a downstream gene of Nrf2, and the Nrf2 activation was accompanied by upregulation of HO-1 (Figure 7(a)). A quantitative comparison is shown in Figure 7(b). In addition, addition of NAC could attenuate the regulatory effect of DpdtbA on Keap1/Nrf2/HO-1, indicating that the cellular redox alteration caused the activation of the pathway (Figure 7(a)). Similar results were observed in SGC-7901 cells (Figures 7(c) and 7(d)). To illustrate that the ferritinophagy induction was responsible for the activation of Keap1/Nrf2/HO-1, the effect of the NCOA4 knockdown on the pathway was further investigated. As shown in Figures 7(e) and 7(g), knockdown of NCOA4 markedly attenuated the regulatory effect of DpdtbA on the proteins in the pathway, supporting that activation of keap1/Nrf2/HO-1 highly depended on the strength of the ferritinophagic flux (Figures 7(f) and 7(h)).

4. Discussion

Now that epithelial-mesenchymal transition (EMT) is a necessary step for metastasis of cancer cells [38, 39], the new-type EMT inhibitor needed to be developed. Dithiocarbamate derivatives exhibited significant regulatory effect on EMT-related proteins in our previous studies [28, 31, 40], but the details in the molecular level remained unclear. During EMT transformation, upregulation of vimentin and downregulation of E-cadherin were normally observed with morphological change [41, 42]; therefore, the opposite trend achieved would be good for metastasis inhibition. DpdtbA exhibited EMT inhibition like other dithiocarbamate derivatives through influencing the expression of vimentin and E-cadherin (Figure 1). In addition, ROS production was reported in EMT development [7]; however, the role of ROS in EMT inhibition was payed little attention; we reported that 2,2′-di-pyridine ketone hydrazone dithiocarbamatic acid (DpdtC) inhibited EMT via through massive ROS production, i.e., a manner of "attacking poison with poison" [28]. As an analog of DpdtC, DpdtbA-inhibited EMT may be through a similar way. Thus, the redox state of the cells before and after treatment was investigated. As expected, DpdtbA treatment caused massive ROS production. Next, the origin of ROS production was further determined. As we know, mitochondria-derived ROS is in first place, but degradation of iron-containing proteins in lysosomes (or proteasomes) is also an additional ROS source.

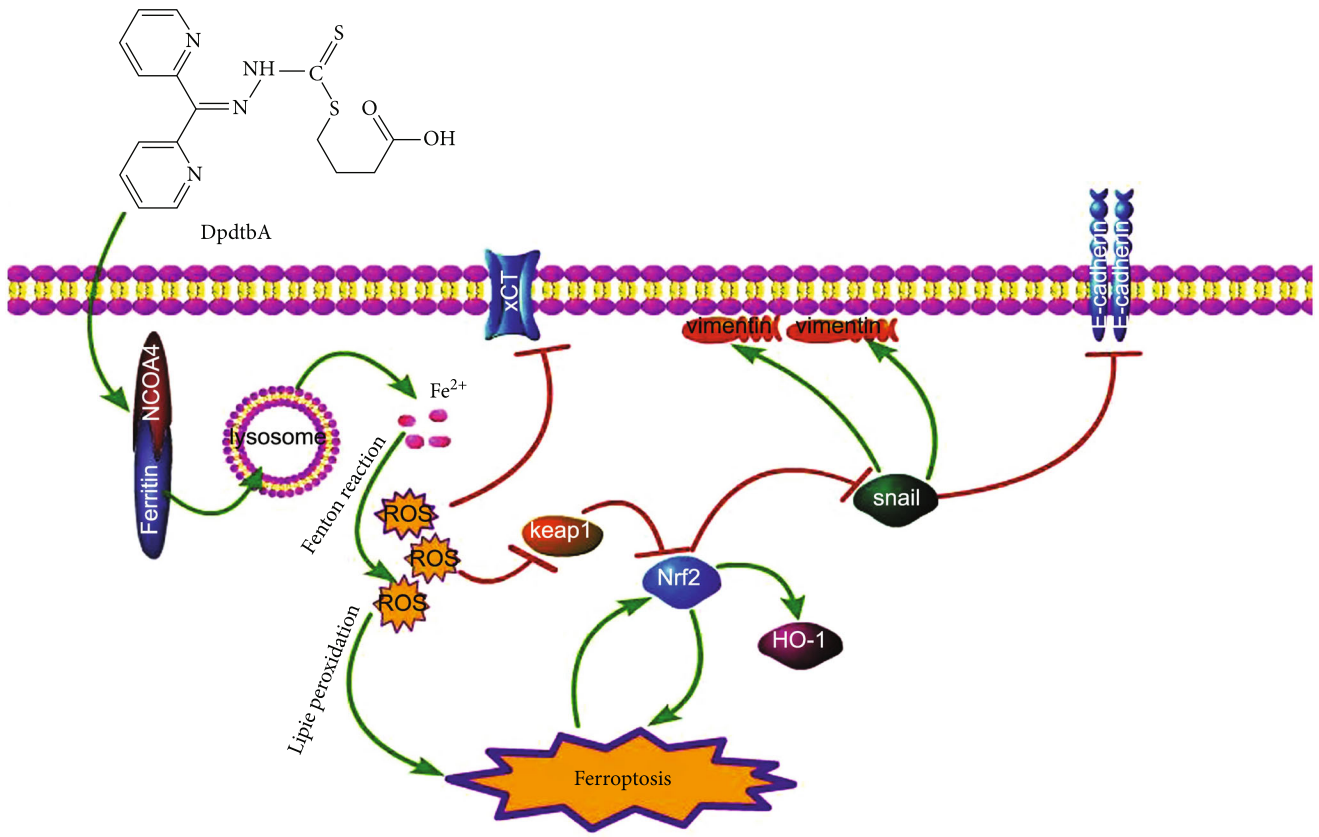

Figure 8: Ferritinophagy-mediated ferroptosis induction contributed to the EMT inhibition was through activation of Nrf2 in action of mechanism of DpdtbA. Ferritinophagy induction caused ROS production, accordingly triggered to ferroptosis and Nrf2 response. The activation of Nrf2 led to downregulation of snail, ultimately achieving the EMT inhibition.

The present study revealed that DpdtbA treatment led to an occurrence of ferritinophagy, which was responsible for the ROS production (Figure 2). NCOA4 knockdown cancelled out the regulatory effect of DpdtbA on EMT, further supporting that NCOA4-mediated ferritinophagy contributed to the EMT inhibition (Figure 3). Those indicated that EMT inhibition could be achieved through generating massive ROS, similar to that reported previously [28]. This again supported the hypothesis that the strength of the ferritinophagic flux may determine the status of EMT.

Iron-mediated reactive oxygen species (ROS) production leads to lipid peroxidation and cell death in Erastin-induced ferroptosis [32, 33, 43]. To deal with the increased lipid peroxides, GSH peroxidase 4 (Gpx4) catalyzes the GSH-dependent reduction of membrane lipid peroxides [44]; thus, Gpx4 downregulation (deletion) activates the ferroptotic cascade. The depletions of Gpx4, xCT, and GSH as well as enhanced lipid peroxidation in the present study suggested that there was an occurrence of ferroptosis in the action of mechanism of DpdtbA [44]. Recently, the relationship between ferroptosis and EMT has received widespread attention; however, it is far from clear for the contrary observations [45–47]. Our results demonstrated that ferroptosis induction favored EMT inhibition in gastric cancer cells (Figure 4), or this was related to ferritinophagy-mediated ROS production. This discrepancy in the effect of ferroptosis on EMT may be related to ROS sources and the cell line specificity.

Nuclear factor E2-related factor 2 (Nrf2) is the key regulatory factor required for cells to maintain an oxidative steady state [48]. DpdtbA induced EMT inhibition along with Nrf2 accumulation and depletion of snail, hinting that Nrf2 influenced the transcription factor of EMT transformation, and this concept is reinforced with knockdown of Nrf2 (Figure 5). This indicated that Nrf2 activation involved the EMT inhibition, in accordance with what were reported previously [49, 50]. However, the contrary effect of Nrf2 activation on EMT in hepatocellular carcinoma cells was observed [51]; this may reflect the yin/yang aspect of Nrf2 signaling [52]. In addition, Nrf2 also plays a role in ferroptosis regulation. Many of the key iron storage, metabolism, and transport proteins are regulated by Nrf2 [53], while the bulk of the iron-related Nrf2 target genes serve antiferroptotic functions; therefore, Nrf2 can mitigate lipid peroxidation and ferroptosis [54]. But there is some evidence in the literature of Nrf2 downstream targets that promote the ferroptotic cascade [55], including our observation (Figure 6). This double-edged (yin/yang of aspects) Nrf2 may lie in its regulation of not only iron processing but also autophagy activation proteins needed for ferritinophagy occurrence. Nrf2 plays a crucial role in mediating ferritinophagy-dependent activation of ferroptosis [54]. Cytosolic repressor protein Keap1 is known to be in charge of the level of Nrf2 through formation of the Nrf2-Keap1 complex for ubiquitination degradation of Nrf2 [56]. Nrf2 has several target genes, including intracellular

redox-balancing proteins like heme oxygenase-1 (HO-1), glutathione peroxidases (GPX), and SLC7A11 [57, 58]. Heme oxygenase-1 (HO-1) induction by Nrf2 protects against the cytotoxicity of various oxidative stresses and inflammatory response, and HO-1 is regulated by the Keap1/Nrf2/HO-1 pathway [59]. The current study showed that DpdtbA-induced activation of Nrf2 was due to autophagic degradation of keap1 (Figure 7) [60, 61]. On the other hand, human Keap1 contains 27 cysteines, and the unique structure (composition) makes it more vulnerable to electrophilic modification and redox sensitive, which leads to escape of Nrf2 from their complex [62]. The ferritinophagy-mediated ROS production did not only cause ferroptosis and protein modification; therefore, activation of Nrf2 derived from Keap1 modification cannot be excluded. Nrf2 may play a crucial role in mediating ferritinophagy-dependent activation of ferroptosis [55]. The current study showed that occurrence of ferroptosis was derived from ferritinophagy induction, whereas Nrf2 activation led to upregulation of HO-1, being advantageous to ferroptosis induction [63]. Together, the action of the mechanism of DpdtbA in EMT inhibition could be proposed based on the presented data (Figure 8). Surely, Nrf2 serving either an anti- or proferroptotic role may also depend on the cell lines used. To solve the mystery on Nrf2 requires more studies.

Taken together, DpdtbA-induced EMT inhibition involved ferritinophagy-mediated ROS production and ferroptosis induction. Equally, along with those cellular events, Nrf2 was activated in response to the alteration in cellular redox environment; conversely, Keap1/Nrf2/HO-1 signaling also regulated EMT and ferroptosis. In brief, our data strongly suggested that the fate of ferroptosis, EMT status, and activation of the Keap1/Nrf2/HO-1 pathway highly depended on the strength of ferritinophagic flux (or ferritinophagy-mediated ROS production).

Abbreviations

EMT: Epithelial-mesenchymal transition
ROS: Reactive oxygen species
Nrf2: Nuclear factor erythroid 2-related factor 2
DpdtbA: 2,2′-Di-pyridine ketone hydrazone dithiocarbamate butyric acid
NAC: N-Acetyl-L-cysteine
NCOA4: Nuclear receptor coactivator 4.

Data Availability

All data are available in the manuscript.

Conflicts of Interest

The authors declare no conflict of interest.

Authors' Contributions

Geng Guan, Wei Zhou, and Huiping Wei performed the experiments, and they contributed equally to this work. Yongli Li and Changzheng Li conceived and designed the experiments. Ting Wang, Rui Feng, and Ruifang Xu performed some immunofluorescence experiments. Kangwei Zheng and Chunjie Yang performed data analysis. Changzheng Li prepared and wrote the paper. Cuiping Li and Yun Fu worked on English proofreading of the manuscript. Deng Guan, Wei Zhou, and Huiping Wei contributed equally to this work.

Acknowledgments

The present study was supported by grants awarded by the National Natural Science Foundation of China (No. 21571153); the Key Science and Technology Projects of the Henan Provincial Department of Science and Technology (202102310770); the Key Research Project Funding Program of Higher Educational Institutions of Henan Province (19A310021 and 21A310017), and the Innovation Team awarded by Sanquan College of Xinxiang Medical University (SQTD201802).

Supplementary Materials

Fig. S1: DpdtbA could reverse TGF-β1-induced EMT in SGC-7901 cell line. Objective size: 40×10; scale bar: 100 μm. Fig. S2: NAC could significantly attenuate DpdtbA-induced EMT inhibition in MGC-803 cell. Objective size: 40×10; scale bar: 100 μm. Fig. S3: NAC could markedly neutralize DpdtbA-induced ferritinophagy in SGC-7901 cells. Objective size: 40×10; scale bar: 100 μm. Fig. S4: DpdtbA treatment resulted in downregulation of ferroptosis-related proteins. (A) Addition of ferrostatin-1 attenuated the regulatory effect of DpdtbA on ferroptosis-related proteins in MGC-803 cell; (B) quantitative analysis derived from (A); (C) addition of ferrostatin-1 attenuated the regulatory effect of DpdtbA on ferroptosis-related proteins in SGC-7901 cell; (D) quantitative analysis derived from (C). $^{***,\#\#\#}p < 0.01$ vs. control, one-way ANOVA with Dunnett's post hoc correction. Fig. S5: DpdtbA treatment resulted in depletion of GSH and enhanced lipid peroxidation. (A) Changes of GSH when the cells are exposed to the agents; (B) the abundance of lipid peroxidation in absorbance was caused by the indicated agents. $^{***,\#\#\#}p < 0.01$ vs. control, one-way ANOVA with Dunnett's post hoc correction. Fig. S6: DpdtbA treatment led to autophagic degradation of Gpx4 and xCT. (A) Western blot analysis; (B) quantitative analysis derived from (A). $^{**,\#\#}p < 0.05$ vs. control, one-way ANOVA with Dunnett's post hoc correction. Fig. S7: autophagic degradation of keap1 was responsible for activation of Nrf2. (A) Western blot analysis; (B) quantitative analysis derived from (A). $^{**,\#\#}p < 0.05$ vs. control, one-way ANOVA with Dunnett's post hoc correction. *(Supplementary Materials)*

References

[1] D. Hanahan and R. A. Weinberg, "Hallmarks of cancer: the next generation," *Cell*, vol. 144, no. 5, pp. 646–674, 2011.

[2] J. H. Tsai, J. L. Donaher, D. A. Murphy, S. Chau, and J. Yang, "Spatiotemporal regulation of epithelial-mesenchymal

transition is essential for squamous cell carcinoma metastasis," *Cancer Cell*, vol. 22, no. 6, pp. 725–736, 2012.

[3] S. Lamouille, J. Xu, and R. Derynck, "Molecular mechanisms of epithelial-mesenchymal transition," *Nature Reviews Molecular Cell Biology*, vol. 15, no. 3, pp. 178–196, 2014.

[4] A. Sioutas, L. K. Vainikka, M. Kentson et al., "Oxidant-induced autophagy and ferritin degradation contribute to epithelial–mesenchymal transition through lysosomal iron," *Journal of Inflammation Research*, vol. Volume 10, pp. 29–39, 2017.

[5] J. Massague, E. Batlle, and R. R. Gomis, "Understanding the molecular mechanisms driving metastasis," *Molecular Oncology*, vol. 11, no. 1, pp. 3-4, 2017.

[6] C. Y. Loh, J. Y. Chai, T. F. Tang et al., "The E-cadherin and N-cadherin switch in epithelial-to-mesenchymal transition: signaling, therapeutic implications, and challenges," *Cell*, vol. 8, no. 10, p. 1118, 2019.

[7] Q. H. Xu, Y. Xiao, X. Q. Li et al., "Resveratrol counteracts hypoxia-induced gastric cancer invasion and EMT through hedgehog pathway suppression," *Anti-Cancer Agents in Medicinal Chemistry*, vol. 20, no. 9, pp. 1105–1114, 2020.

[8] M. K. Jolly, S. C. Tripathi, D. Jia et al., "Stability of the hybrid epithelial/mesenchymal phenotype," *Oncotarget*, vol. 7, no. 19, pp. 27067–27084, 2016.

[9] T. T. Dang, M. A. Esparza, E. A. Maine, J. M. Westcott, and G. W. Pearson, "ΔNp63α promotes breast cancer cell motility through the selective activation of components of the epithelial-to-mesenchymal transition program," *Cancer Research*, vol. 75, no. 18, pp. 3925–3935, 2015.

[10] F. Bocci, M. K. Jolly, S. C. Tripathi et al., "Numb prevents a complete epithelial–mesenchymal transition by modulating notch signalling," *Interface*, vol. 14, no. 136, article 20170512, 2017.

[11] T. Hong, K. Watanabe, C. H. Ta, A. Villarreal-Ponce, Q. Nie, and X. Dai, "An Ovol2-Zeb1 mutual inhibitory circuit governs bidirectional and multi-step transition between epithelial and mesenchymal states," *PLoS Computational Biology*, vol. 11, no. 11, article e1004569, 2015.

[12] J. J. Chen and L. Galluzzi, "Fighting resilient cancers with iron," *Trends in Cell Biology*, vol. 28, no. 2, pp. 77-78, 2018.

[13] T. Hirschhorn and B. R. Stockwell, "The development of the concept of ferroptosis," *Free Radical Biology & Medicine*, vol. 133, pp. 130–143, 2019.

[14] V. S. Viswanathan, M. J. Ryan, H. D. Dhruv et al., "Dependency of a therapy-resistant state of cancer cells on a lipid peroxidase pathway," *Nature*, vol. 547, no. 7664, pp. 453–457, 2017.

[15] M. Sang, R. Luo, Y. Bai et al., "Mitochondrial membrane anchored photosensitive nano-device for lipid hydroperoxides burst and inducing ferroptosis to surmount therapy-resistant cancer," *Theranostics*, vol. 9, no. 21, pp. 6209–6223, 2019.

[16] M. Tang, Z. Chen, D. Wu, and L. Chen, "Ferritinophagy/ferroptosis: iron-related newcomers in human diseases," *Journal of Cellular Physiology*, vol. 233, no. 12, pp. 9179–9190, 2018.

[17] J. D. Mancias, X. Wang, S. P. Gygi, J. W. Harper, and A. C. Kimmelman, "Quantitative proteomics identifies NCOA4 as the cargo receptor mediating ferritinophagy," *Nature*, vol. 509, no. 7498, pp. 105–109, 2014.

[18] T. F. Huang, Y. J. Sun, Y. L. Li et al., "Growth inhibition of a novel iron chelator, DpdtC, against hepatoma carcinoma cell lines partly attributed to ferritinophagy-mediated lysosomal ROS generation," *Oxidative Medicine and Cellular Longevity*, vol. 2018, Article ID 4928703, 13 pages, 2018.

[19] G. O. Latunde-Dada, "Ferroptosis: role of lipid peroxidation, iron and ferritinophagy," *Biochimica et Biophysica Acta, General Subjects*, vol. 1861, no. 8, pp. 1893–1900, 2017.

[20] W. Hou, Y. Xie, X. Song et al., "Autophagy promotes ferroptosis by degradation of ferritin," *Autophagy*, vol. 12, no. 8, pp. 1425–1428, 2016.

[21] J. C. Lee, C. K. Tseng, K. C. Young et al., "Andrographolide exerts anti-hepatitis C virus activity by up-regulating haeme oxygenase-1 via the p38 MAPK/Nrf2 pathway in human hepatoma cells," *British Journal of Pharmacology*, vol. 171, no. 1, pp. 237–252, 2014.

[22] A. Raghunath, K. Sundarraj, R. Nagarajan et al., "Antioxidant response elements: discovery, classes, regulation and potential applications," *Redox Biology*, vol. 17, pp. 297–314, 2018.

[23] I. Bellezza, I. Giambanco, A. Minelli, and R. Donato, "Nrf2-Keap1 signaling in oxidative and reductive stress," *Biochimica et Biophysica Acta (BBA) - Molecular Cell Research*, vol. 1865, no. 5, pp. 721–733, 2018.

[24] H. S. Zhang, Z. G. Zhang, S. H. L. Du GY et al., "Nrf2 promotes breast cancer cell migration via up-regulation of G6PD/HIF-1α/Notch1 axis," *Journal of Cellular and Molecular Medicine*, vol. 23, no. 5, pp. 3451–3463, 2019.

[25] Y. J. Sun, C. P. Li, J. K. Feng et al., "Ferritinophagic flux activation in CT26 cells contributed to EMT inhibition induced by a novel iron chelator, DpdtpA," *Oxidative Medicine and Cellular Longevity*, vol. 2019, 8753414 pages, 2019.

[26] J. K. Feng, C. P. Li, R. F. Xu et al., "DpdtC-induced EMT inhibition in MGC-803 cells was partly through ferritinophagy-mediated ROS/p53 pathway," *Oxidative Medicine and Cellular Longevity*, vol. 2020, 9762314 pages, 2020.

[27] Z. J. Xu, J. K. Feng, Y. L. Li et al., "The vicious cycle between ferritinophagy and ROS production triggered EMT inhibition of gastric cancer cells was through p53/AKT/mTor pathway," *Chemico-Biological Interactions*, vol. 328, article 109196, 2020.

[28] D. Guan, C. P. Li, Y. L. Li et al., "The DpdtbA induced EMT inhibition in gastric cancer cell lines was through ferritinophagy-mediated activation of p53 and PHD2/hif-1α pathway," *Journal of Inorganic Biochemistry*, vol. 218, article 111413, 2021.

[29] P. V. Dludla, B. Jack, A. Viraragavan et al., "A dose-dependent effect of dimethyl sulfoxide on lipid content, cell viability and oxidative stress in 3T3-L1 adipocytes," *Toxicology Reports*, vol. 5, pp. 1014–1020, 2018.

[30] M. Saitoh, "Involvement of partial EMT in cancer progression," *Journal of Biochemistry*, vol. 164, no. 4, pp. 257–264, 2018.

[31] R. Chatterjee and C. Jyotirmoy, "ROS and oncogenesis with special reference to EMT and stemness," *European Journal of Cell Biology*, vol. 99, no. 2-3, article 151073, 2020.

[32] W. S. Yang, R. SriRamaratnam, M. E. Welsch et al., "Regulation of ferroptotic cancer cell death by GPX4," *Cell*, vol. 156, no. 1-2, pp. 317–331, 2014.

[33] S. Doll and C. Marcus, "Iron and ferroptosis: a still ill-defined liaison," *IUBMB Life*, vol. 69, no. 6, pp. 423–434, 2017.

[34] J. Fujii, T. Homma, and S. Kobayashi, "Ferroptosis caused by cysteine insufficiency and oxidative insult," *Free Radical Research*, vol. 54, no. 11-12, pp. 969–980, 2020.

[35] M. Conrad and H. Sato, "The oxidative stress-inducible cystine/glutamate antiporter, system x (c) (−) : cystine supplier and beyond," *Amino Acids*, vol. 42, no. 1, pp. 231–246, 2012.

[36] Z. Zhang, J. Qu, C. Zheng et al., "Nrf2 antioxidant pathway suppresses numb-mediated epithelial-mesenchymal transition during pulmonary fibrosis," *Cell Death & Disease*, vol. 9, no. 2, p. 83, 2018.

[37] Z. Wu, Y. Geng, X. Lu et al., "Chaperone-mediated autophagy is involved in the execution of ferroptosis," *Proceedings of the National Academy of Sciences of the United States of America*, vol. 116, no. 8, pp. 2996–3005, 2019.

[38] N. Gavert and A. Ben-Ze'ev, "Epithelial–mesenchymal transition and the invasive potential of tumors," *Trends in Molecular Medicine*, vol. 14, no. 5, pp. 199–209, 2008.

[39] B. Du and J. S. Shim, "Targeting epithelial-mesenchymal transition (EMT) to overcome drug resistance in cancer," *Molecules*, vol. 21, no. 7, p. 965, 2016.

[40] Z. Wang, C. P. Li, Y. L. Li et al., "DpdtbA-induced growth inhibition in human esophageal cancer cells involved inactivation of the p53/EGFR/AKT pathway," *Oxidative Medicine and Cellular Longevity*, vol. 2019, 5414614 pages, 2019.

[41] T. R. Samatov, A. G. Tonevitsky, and U. Schumacher, "Epithelial-mesenchymal transition: focus on metastatic cascade, alternative splicing, non-coding RNAs and modulating compounds," *Molecular Cancer*, vol. 12, no. 1, p. 107, 2013.

[42] A. Dongre and R. A. Weinberg, "New insights into the mechanisms of epithelial-mesenchymal transition and implications for cancer," *Nature reviews. Molecular cell biology*, vol. 20, no. 2, pp. 69–84, 2019.

[43] S. J. Dixon, K. M. Lemberg, M. R. Lamprecht et al., "Ferroptosis: an iron-dependent form of nonapoptotic cell death," *Cell*, vol. 149, no. 5, pp. 1060–1072, 2012.

[44] A. Anandhan, M. Dodson, C. J. Schmidlin, P. Liu, and D. D. Zhang, "Breakdown of an ironclad defense system: the critical role of Nrf2 in mediating ferroptosis," *Cell Chemical Biology*, vol. 27, no. 4, pp. 436–447, 2020.

[45] M. Wang, S. Li, Y. Wang, H. Cheng, J. Su, and Q. Li, "Gambogenic acid induces ferroptosis in melanoma cells undergoing epithelial-to-mesenchymal transition," *Toxicology and Applied Pharmacology*, vol. 401, article 115110, 2020.

[46] L. Sun, H. Dong, W. Zhang et al., "Lipid peroxidation, GSH depletion, and SLC7A11 inhibition are common causes of EMT and ferroptosis in A549 cells, but different in specific mechanisms," *DNA and Cell Biology*, vol. 40, no. 2, pp. 172–183, 2021.

[47] J. Lee, J. H. You, M. S. Kim, and J. L. Roh, "Epigenetic reprogramming of epithelial-mesenchymal transition promotes ferroptosis of head and neck cancer," *Redox Biology*, vol. 37, article 101697, 2020.

[48] A. T. Dinkova-Kostova, R. V. Kostov, and A. G. Kazantsev, "The role of Nrf2 signaling in counteracting neurodegenerative diseases," *The FEBS Journal*, vol. 285, no. 19, pp. 3576–3590, 2018.

[49] J. Wang, H. Zhu, L. Huang et al., "Nrf2 signaling attenuates epithelial-to-mesenchymal transition and renal interstitial fibrosis via PI3K/Akt signaling pathways," *Experimental and Molecular Pathology*, vol. 111, article 104296, 2019.

[50] F. Feng, P. Cheng, S. Xu et al., "Tanshinone IIA attenuates silica-induced pulmonary fibrosis via Nrf2-mediated inhibition of EMT and TGF-β1/Smad signaling," *Chemico-Biological Interactions*, vol. 319, article 109024, 2020.

[51] R. Feng, Y. Morine, T. Ikemoto et al., "Nrf2 activation drive macrophages polarization and cancer cell epithelial-mesenchymal transition during interaction," *Cell Communication and Signaling: CCS*, vol. 16, no. 1, p. 54, 2018.

[52] X. J. Wang, Z. Sun, N. F. Villeneuve et al., "Nrf2 enhances resistance of cancer cells to chemotherapeutic drugs, the dark side of Nrf2," *Carcinogenesis*, vol. 29, no. 6, pp. 1235–1243, 2008.

[53] M. J. Kerins, J. Milligan, J. A. Wohlschlegel, and A. Ooi, "Fumarate hydratase inactivation in hereditary leiomyomatosis and renal cell cancer is synthetic lethal with ferroptosis induction," *Cancer Science*, vol. 109, no. 9, pp. 2757–2766, 2018.

[54] M. Dodson, R. Castro-Portuguez, and D. D. Zhang, "NRF2 plays a critical role in mitigating lipid peroxidation and ferroptosis," *Redox Biology*, vol. 23, article 101107, 2019.

[55] C. C. Gai, M. Y. Yu, Z. Li et al., "Acetaminophen sensitizing erastin-induced ferroptosis via modulation of Nrf2/heme oxygenase-1 signaling pathway in non-small-cell lung cancer," *Journal of cellular physiology*, vol. 235, no. 4, pp. 3329–3339, 2020.

[56] Z. Fan, A. K. Wirth, D. Chen et al., "Nrf2-Keap1 pathway promotes cell proliferation and diminishes ferroptosis," *Oncogene*, vol. 6, no. 8, article e371, 2017.

[57] I. Gañán-Gómez, Y. Wei, H. Yang, M. C. Boyano-Adánez, and G. García-Manero, "Oncogenic functions of the transcription factor Nrf2," *Free Radical Biology & Medicine*, vol. 65, pp. 750–764, 2013.

[58] X. Sun, Z. Ou, R. Chen et al., "Activation of the p62-Keap1-NRF2 pathway protects against ferroptosis in hepatocellular carcinoma cells," *Hepatology*, vol. 63, no. 1, pp. 173–184, 2016.

[59] K. C. Wu, S. S. Huang, Y. H. Kuo et al., "A Helminthostachys zeylanica constituent, prevents LPS-induced acute lung injury through TLR4-mediated MAPK and NF-κB signaling pathways," *Molecules*, vol. 22, no. 4, p. 573, 2017.

[60] K. Taguchi, N. Fujikawa, M. Komatsu et al., "Keap1 degradation by autophagy for the maintenance of redox homeostasis," *Proceedings of the National Academy of Sciences of the United States of America*, vol. 109, no. 34, pp. 13561–13566, 2012.

[61] W. Fan, Z. Tang, D. Chen et al., "Keap1 facilitates p62-mediated ubiquitin aggregate clearance via autophagy," *Autophagy*, vol. 6, no. 5, pp. 614–621, 2010.

[62] A. Kopacz, D. Kloska, H. J. Forman, A. Jozkowicz, and A. Grochot-Przeczek, "Beyond repression of Nrf2: an update on Keap1," *Free Radical Biology & Medicine*, vol. 157, pp. 63–74, 2020.

[63] L. C. Chang, S. K. Chiang, S. E. Chen, Y. L. Yu, R. H. Chou, and W. C. Chang, "Heme oxygenase-1 mediates BAY 11-7085 induced ferroptosis," *Cancer Letters*, vol. 416, pp. 124–137, 2018.

Hindawi
Oxidative Medicine and Cellular Longevity
Volume 2022, Article ID 4107433, 16 pages
https://doi.org/10.1155/2022/4107433

Review Article

CGRP: A New Endogenous Cell Stemness Maintenance Molecule

Xiaoting Lv,[1] **Qingquan Chen**,[2] **Shuyu Zhang**,[3] **Feng Gao**,[4] **and Qicai Liu**[5]

[1]*Department of Respiratory and Critical Care Medicine, Research Laboratory of the Respiratory System Diseases, 1st Affiliated Hospital, Fujian Medical University, Fuzhou, Fujian 350005, China*
[2]*Department of Laboratory Medicine, School of Medical Technology and Engineering, Fujian Medical University, Fuzhou, Fujian 350004, China*
[3]*Clinical Laboratory, Fujian Maternity and Child Health Hospital, Affiliated Hospital of Fujian Medical University, Fuzhou, Fujian 350005, China*
[4]*Department of Pathology, 1st Affiliated Hospital, Fujian Medical University, Fuzhou, Fujian, 350005, China*
[5]*Department of Reproductive Medicine Centre, 1st Affiliated Hospital, Fujian Medical University, Fuzhou, Fujian 350005, China*

Correspondence should be addressed to Feng Gao; fengfang77777@163.com and Qicai Liu; lqc673673673@163.com

Received 18 November 2021; Accepted 11 January 2022; Published 29 January 2022

Academic Editor: Milena Georgieva

Stem cells have the ability of self-replication and multidirectional differentiation, but the mechanism of how stem cells "maintain" this ability and how to "decide" to give up this state and differentiate into cells with specific functions is still unknown. The Nobel Prize in physiology and medicine in 2021 was awarded to "temperature and tactile receptor," which made the pain receptor TRPV1-calcitonin gene-related peptide (CGRP) pathway active again. The activation and blocking technology of CGRP has been applied to many clinical diseases. CGRP gene has complex structure and transcription process, with multiple methylation and other modification sites. It has been considered as a research hotspot and difficulty since its discovery. Drug manipulation of TRPV1 and inhibition of CGRP might improve metabolism and prolong longevity. However, whether the TRPV1-neuropeptide-CGRP pathway is directly or indirectly involved in stem cell self-replication and multidirectional differentiation is unclear. Recent studies have found that CGRP is closely related to the migration and differentiation of tumor stem cells, which may be realized by turning off or turning on the CGRP gene expression in stem cells and activating a variety of ways to regulate stem cell niches. In this study, we reviewed the advances in researches concentrated on the biological effects of CGRP as a new endogenous switching of cell stemness.

1. Introduction

Stem cells are a kind of cells with the ability of self-replication and multidirectional differentiation, which can differentiate into any cells in the body. However, how stem cells preserve this ability and "decide" to give up this state and transform into specific cells are two questions perplexing scientists. Successfully answering these two questions will greatly expand our ability to use stem cells to treat diseases. There are many specific open DNA regions in stem cells, which help stem cells produce many proteins to prevent stem cells from self-differentiation. Once stem cells begin to differentiate into a specific type of cells, these specific open DNA region fragments will be closed due to a variety of regulatory mechanisms, such as methylation, transcription factors, enhancers, and silencers [1–3], the pattern that stem cells begin to differentiate only by reading specific DNA regions. The regulation mechanism of the "selective silencing" process needs to be deeply studied, and the molecular switch of cell stemness is the mainstream direction in the current research. In the past, transcription factors of OCT4, SOX2, and NANOG were considered to be the stemness-related molecular switches for embryonic stem cells. That is, as the expression of OCT4, SOX2, and NANOG was increased, self-renewal genes were turned on and differentiation genes were turned off. When OCT4, SOX2, and NANOG express, self-replication genes were turned on while differentiation genes were turned off. These three transcription factors could interact to regulate the downstream target genes for maintenance and self-

differentiation of embryonic stem cells, which allowed stem cells to renew themselves without input signals [4–6]. In addition, OCT4, SOX2, and NANOG transcription factors have been hotspots in recent research of tumor stem cells [7, 8], yet their research in other stem cell differentiation fields is extremely limited, which is still far from clinical application. Therefore, it is necessary to explore other potential cell stemness switching molecules.

Calcitonin gene-related peptide (CGRP) is a bioactive peptide composed of 37 amino acids, which is mainly distributed in C and Aδ sensory fibers of the peripheral and central nervous system (CNS) and closely connected with peripheral blood vessels [9–12]. As an important member of the neuropeptide family, CGRP is expressed in a variety of body fluids, such as plasma [13, 14], saliva [15], tears [16], knee synovial fluid [17], and cerebrospinal fluid [18, 19]. CGRP in the human body mainly includes two isomers: α-CGRP and β-CGRP, which are encoded by CALCA and CALCB, respectively [20]. Among them, α-CGRP is mainly distributed in the central and peripheral nervous systems [21, 22], while β-CGRP is mainly distributed in the brain, intestine, and thyroid [23]. The consistency between α-CGRP and β-CGRP sequences is more than 90%, and there is only one amino acid difference between these two isomers [24].

The posttranscriptional process and shearing process of CGRP gene are diverse and complex, which is strictly controlled in a specific way. CGRP gene transcription was activated or inhibited by different tissue-specific factors. CALCA transcripts are expressed differently in different tissues, such as calcitonin transcripts in thyroid C cells and α-CGRP transcripts in nerve cells, and CALCB transcripts were also expressed only in specific cell lines [23]. CALCA is transcribed into a primary transcript mRNA precursor containing six exons and then cut into three different secondary transcripts (Figure 1(a)): (1) α-CGRP: mature CGRP mRNA is formed by cutting special introns containing exons 1, 2, 3, 5, and 6. Among them, exons 1 and 6 are noncoding RNA, and exons 2, 3, and 5 are the gene basis of α-CGRP polypeptide precursor in translation. The macromolecular polypeptide precursor is hydrolyzed by protease: signal peptide related to exon 2 is further cleaved. The N-terminal polypeptide related to exon 3 and CGRP related to exon 5 mainly are produced in nerve cells. (2) Calcitonin (CT): it is cut into mature CT mRNA composed of exons 1, 2, 3, and 4. During translation mainly occurring in thyroid cells, CT precursor protein is hydrolyzed by protease into the following peptides: signal peptide, N-terminal polypeptide, and C-terminal polypeptide, which is called carboxyl terminal polypeptide 1 (ccp-1). The α-CGRP and CT transcripts had three common exons, but contained different 3′ ends. (3) Recently, a third mode of CT/CGRP mRNA formation has been found. This mature CT mRNA II contains 6 exons. During translation mainly occurring in B cells, the CT precursor protein with different amino acid sequence from CT precursor protein is formed, which is hydrolyzed by protease to release CCP-1. In addition, the increased concentration of N-terminal and C-terminal regulatory peptides could negatively inhibit the expression of CT/CGRP gene. b-CGRP encodes only one transcript, but contains a potential 3′ splice site and a fragment similar to calcitonin exon, called "degenerate exon." Although the splicing of this "residual" exon has never been observed, the Bgl I1 site in this fragment can be inserted into different fragments of CGRP gene to construct CALCA gene and CALCB gene chimera (Figure 1(b)) [23].

In addition to the known biological functions of relaxing blood vessels and relieving pain, CGRP is also involved in the regulation of immune response and cell proliferation and apoptosis after tissue injury [9, 12, 25, 26]. What is more, CGRP has been proven to be an important neuroendocrine regulator of human longevity. It is known that the antagonistic effect of transient receptor potential cation channel subfamily V member 1 (TRPV1)+ neurons on the insulin secretion of pancreatic B cells and the negative impact on metabolism may be achieved by stimulating the sustained high level of CGRP, and the CGRP homeostasis is destroyed with aging, resulting in the decline of metabolism [27]. More importantly, CALCA and CALCB, which were highly expressed in undifferentiated pluripotent stem cells, have been proven to play a regulatory role in stem cell differentiation as immune privilege genes [28]. During the physiological process of tissue injury repair, it was found that CGRP+ sensory nerve fibers were reinnervated. High expression of CGRP could not only promote the migration of mesenchymal stem cells (MSCs) to damaged tissues [29] but also promote stem cell differentiation [30, 31]. CGRP is also considered as a tumor growth factor to induce the occurrence and development of malignant tumors [32, 33]. Therefore, the abnormal expression of CGRP gene can regulate the ability of differentiation and self-renewal in stem cells.

The expression of CGRP gene can be regulated at the transcriptional level. DNA methylation is the most widely studied content of epigenetics. It mainly studies the regulation of gene expression at the transcriptional level without DNA sequence change, and this change can exist and inherit stably during DNA replication. Cytosine residue methylation is the most widely studied epigenetic modification, which mostly exists in CG sequence [34]. Different elements such as promoter, gene ontology, enhancer, silencer, and transposon in genome can be methylated and affect gene expression [35]. About half of the genes in vertebrates are enriched in CpG sequences on the promoter, which is called CpG island. The DNA methylation level of the promoter with CpG island can be closely related to the transcriptional activity of the gene by binding to transcription factors or changing chromatin structure [36]. It also reflects species specificity [37]. CALCA has a 5′ flanking sequence of more than 1.8 kb. A large area of CpG island has been found in the 5′ end promoter (Figure 1(a)). It is rich in CpG, has high content of G+C, and contains several rare restriction endonuclease digestion sites and two different CpG-rich regions, one around exon 1 and another in about 1.5 kb upstream in a nonmethylated state generally [38]. DNA methylation regulates cell proliferation, apoptosis, and gene expression, which is closely related to tumor [33, 39]. Abnormal methylation levels of CALCA promoter and exon can change cell stemness [35, 40]. Methylation of CALCA promoter in bone marrow cells is often observed in patients with myelodysplastic syndrome (MDS) so demethylated drugs can delay

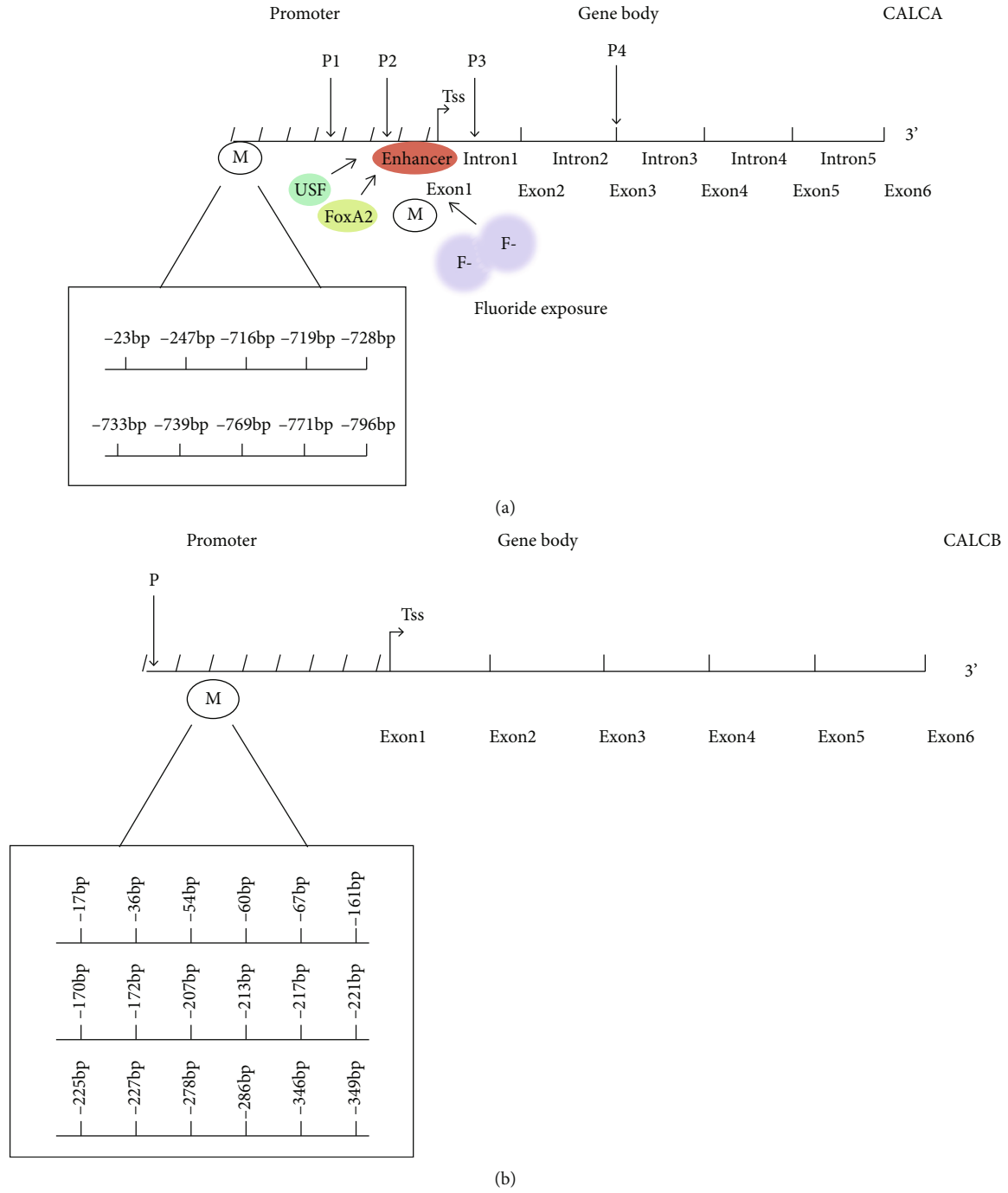

Figure 1: Diagram of the structures for both the CALCA and CALCB genes. Both the CALCA and CALCB genes contain all six exons, with multiple methylation and other modification sites. (a) Multiple methylation sites of CALCA promoter with a large area of CpG in the 5′ end were found in different types of bacterial preterm sepsis (-716 bp, -719 bp, -728 bp, -733 bp, -739 bp, -769 bp, -771 bp, and -796 bp) and pancreatic ductal adenocarcinoma and its paracancer (-23 bp, -247 bp), and the methylation of CALCA exon 1 was related to fluoride exposure. CALCA enhancer could also be activated by upstream stimulating factor (USF) and forkhead protein Foxa2. Four novel polymorphic alleles were found in neurological or psychiatric disease: two (g.979G>A and g.4218T>C) represented single nucleotide polymorphisms (SNPs), one consisted of two coupled SNPs in close vicinity to each other (g.1210T>C and g.1214C>G), and one was an intronic 16 bp microdeletion (2919-2934del16). One of the SNPs (g.4218T>C) causes a nonsynonymous amino acid change (Leu66Pro) in the third exon, an exon common to both procalcitonin and pro-a-CGRP. (b) Multiple methylation sites of CALCB promoter with a large area of CpG in the 5′ end were found in pancreatic ductal adenocarcinoma and its paracancer (-17 bp, -36 bp, -54 bp, -60 bp, -67 bp, -161 bp, -170 bp, -172 bp, -213 bp, -217 bp, -221 bp, -225 bp, -227 bp, -247 bp, -278 bp, -286 bp, -346 bp, and -349 bp). Promoter polymorphisms of CALCB gene (rs11603873 T/C and rs79501047 A/G) are common in the Han population, and the rs11603873 C genotype has a high risk of salivary adenoid cystic carcinoma compared with the rs11603873 T genotype.

the progression of MDS [41]. In addition, DNA methylation is one of the regulatory mechanisms on gene tissue-specific expression [42]. The degree of DNA methylation is regulated by microenvironment, which is also called stem cell niches [43, 44]. Both CALCA and CALCB have multiple methylation sites (Figure 1). So the promoter region of CALCA gene in different subtypes of the same disease could have methylation changes at different sites [45]. Thus, the methylation level of CGRP gene could be used as a biomarker for diagnosis and treatment in many clinical diseases. The use of demethylated drugs in the microenvironment of stem cells might also benefit patients.

At present, the function of CGRP in stemness-related fields is not clear. The goal of this review is to provide an overview about regulation mechanism of CGRP pathophysiology, with an emphasis on the biological effects on cell stemness in different tissues.

2. CGRP and Lung Stem Cells

2.1. CGRP and Lung Stem Cells and Their Microenvironment. Lung epithelial stem cells are considered to be facultative stem cells. Namely, it is in a resting state and participates in the process of lung breathing, secreting proteins that are crucial to gas exchange normally. However, they will become transient expansion cells and differentiate into one or more highly differentiated cells quickly in regeneration and repair after injury [46]. Lung epithelial stem cells include basal cells (BCS) (basal stem cells (BSCs) and basal lumen progenitor cells (BLPCs)) of proximal airway (trachea bronchus), ductal cells, Clara cells of bronchioles and pulmonary neuroendocrine cells (PNECs), distal airway stem cells (DASCs), and alveolar epithelial stem cells such as type II alveolar cells (AT II). In the early embryo (embryonic stage 13-15 days (E13-E15)), CGRP is positive by immunostaining in all epithelial cells of the distal airway, but it is limited to different cell lines such as PNECs at the late embryonic stage [47]. The transient expression of CGRP in different differentiated cell types in stem cells indicates that CGRP may modulate the activity of stem cells.

Stem cell niches, composed of different types of cells, extracellular matrix proteins, and growth factors, are specialized microenvironments that promote the maintenance of stem cells and regulate their function [48]. Stem cell niches play a key role in determining the function and differentiation efficiency of stem cells [44, 49]. For example, tracheal submucosal secretory glands (SMGs) provide a survival microenvironment for airway stem cells, and the mucus secreted by niches is not only related to congenital immunomodulation but also contains the substances which can maintain the pluripotency of epithelial stem cells and provide local environmental signals to maintain and mobilize stem cells [50]. Thus, the occurrence of a variety of hypersecretive lung diseases such as chronic bronchitis, asthma, and cystic fibrosis may be related to the abnormal proliferation and differentiation of stem cells in SMGs [50].

The function of SMGs was regulated by sympathetic or parasympathetic nerves. There are abundant parasympathetic neurons with transient receptor potential vanilloid 1 (TRPV1) membrane protein in the tracheal mucosal layer, and the CGRP released by TRPV1+ neurons is the main source of CGRP [51, 52]. In stable conditions, CGRP expression maintained a low level and is increased after lung injury. Only high secretion of CGRP was detected in patients with hereditary cystic fibrosis in the submucosal secretory gland of the trachea, while the levels of other neurotransmitters such as VIP and SP did not change significantly, which confirmed that CGRP was the main neurotransmitter [52]. Although the elevated CGRP level can stimulate the proliferation of mouse SMG progenitor cells [52], it is speculated that CGRP has limited effect on slow circulating stem cells due to the short expression of CGRP [51]. Therefore, CGRP secreted by TRPV1 neurons in the stem cell niches may take effect on lung pluripotent stem cells through downstream pathways to induce the proliferation and differentiation of stem cells [53–56] (Figure 2).

2.2. The Downstream Pathway of Lung Stem Cells Regulated by CGRP

2.2.1. Sonic Hedgehog Signaling Pathway. Sonic hedgehog (SHH) signaling pathway is a major regulator of cell proliferation, cell differentiation, and tissue polarity [57]. In multiple adult tissues, it becomes active during differentiation, proliferation, and maintenance by regulating cell stemness in the process of embryonic development [58, 59]. Abnormal expression of the SHH pathway may cause severe lung dysplasia [60, 61].

Pulmonary fibrosis is characterized by epithelial mesenchymal transition (EMT) in epithelial lesions. Highly differentiated AT I cells with limited repair ability cover more than 95% of the alveolar surface, meaning that it is more vulnerable to be damaged [62–64]. Adamson et al. found that alveolar stem cells (AT II cells) could migrate and proliferate to the alveolar surface after mild alveolar injury [62, 65, 66]. At the same time, it promoted the transformation of activated fibroblasts into quiescent state and inhibited TGF-β thus limiting lung fibrosis [67]. However, if the alveolar epithelium was damaged more seriously or the ability of proliferation of AT II cells was impaired, it will lead to lung fibrosis [68, 69]. It was found that the expression of SHH, smoothened (Smo), patched (Ptch), and Gli1 pathway proteins was increased significantly in idiopathic pulmonary fibrosis (IPF), suggesting that the SHH pathway may accelerate pulmonary fibrosis via alteration of self-renewal and differentiation of lung stem cells [70–72]. It was shown that CGRP could protect AT II cells from hyperoxia-induced damage through the SHH signaling pathway [73] (Figure 2). Further study will focus on the relationship of CGRP and SHH pathway on the proliferation and differentiation of lung stem cells in pulmonary fibrosis.

2.2.2. Wnt Signaling Pathway. The Wnt signaling pathway is also considered to be one of the key cascades that regulate development and stem cells and closely related to maintenance, metastasis, and immunity in the tumor stem cells [74]. After alveolar injury, AT II cells clonally proliferated as alveolar stem cells and then transdifferentiated into AT I cells [75]. It was found that the Wnt7b/β-catenin signaling

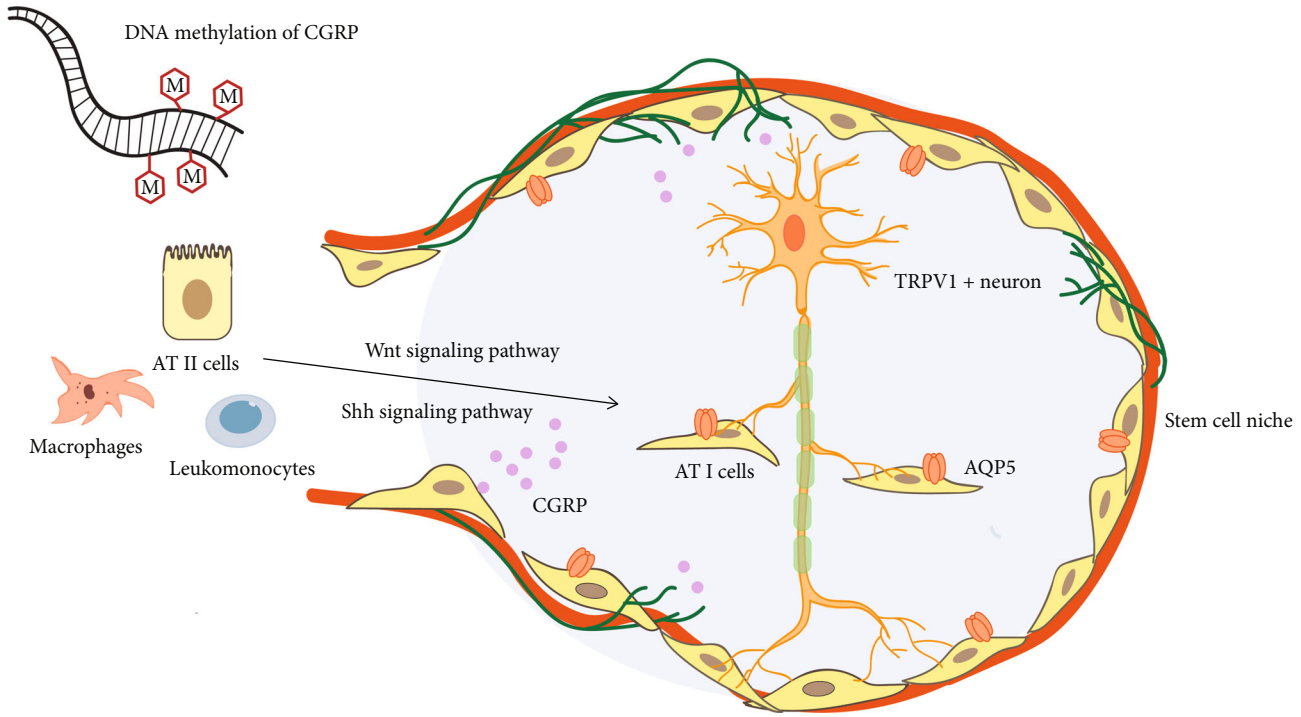

Figure 2: CGRP secreted by TRPV1 neurons in the stem cell niches promotes the proliferation and differentiation of AT II cells. Stem cell niches are specialized microenvironment composed of different types of cells, extracellular matrix proteins, and growth factors. Promoter DNA methylation regulates CGRP expression. CGRP secreted by TRPV1 neurons in the stem cell niches takes effect on lung pluripotent stem cells to induce the proliferation and differentiation of AT II cells through downstream pathways, such as Sonic hedgehog signaling pathway and Wnt signaling pathway.

pathway was involved in the protective action of CGRP on hyperoxia-induced lung injury and CGRP inhibitor CGRP8-37-induced obvious inflammation with damaged AT II cells and alveolar structural remodeling in lung tissue [76].

The transdifferentiation of AT II cells may be regulated by CGRP and Wnt signaling pathway in pulmonary fibrosis. Recently, it has been found that the imbalance of water and sodium in alveolar epithelial cells could promote apoptosis and enhance epithelial mesenchymal transformation. That is to change ATII cell stemness and promote pulmonary fibrosis [77]. Aquaporin 5 (AQP5), located in the membrane of alveolar epithelial cells, is a member of the AQP family which participates in maintaining water electrolyte balance. Usually, AQP5 is considered as the differentiation marker of AT I cells [77, 78]. In acute lung injury, it was confirmed that the level of AQP5 in the early stage of inflammation was negatively correlated with the apoptosis of AT I [78, 79]. Our research has found that alveolar epithelial cells were widely apoptotic and the transdifferentiation ability of alveolar stem cells AT II was impaired in the process of pulmonary fiber. At the same time, the imbalance of β-CGRP/α-CGRP regulated AQP5 expression and promoted transition of alveolar epithelial cell apoptosis via the TGF-β/P-smad1/Smad4 pathway leading to a decreased AQP5 expression in pulmonary fibrosis [80]. In vitro experiments also confirmed that Wnt7a was a ligand of AQP5, the differentiation marker of AT I cells, and the Wnt pathway can affect the transdifferentiation of AT II cells to AT I cells by regulating the expression of AQP5 [75]. Therefore, treatment with AT II cells can accelerate the repair of alveolar epithelium, which may be expected to be used to repair lung injury such as lung fibrosis [81].

2.3. Promoter DNA Methylation Regulates CGRP Expression. CGRP can possess multiple methylation sites via complex processing procedures. In different types of bacterial preterm septicemia, CpG sites in the promoter region of CALCA gene can have four different DNA methylation patterns, such as -769 bp, -771 bp, and -778 bp CpG mutation (Figure 1(a)). Different DNA methylation sites in different infection types lead to different expression levels of CGRP, suggesting its potential role as epigenetic biomarkers and demethylation therapy [45].

3. CGRP and Bone Stem Cells

3.1. CGRP and Hematopoietic Stem Cells. Stem cell regulation and classification of human bone stem cells remain largely unexplored [82]. The most well-characterized stem cells in the skeleton is the hematopoietic stem cell (HSC), defined by its functional ability to form colonies in vitro and serially reconstitute long-term hematopoiesis in conditioned hosts [83].

CGRP treatment in mice can reduce the number of IL-7-reactive B cell progenitor cells in the bone marrow. The reduction is dose-dependent and can be blocked by CGRP receptor antagonist CGRP8-37. Even a single injection of CGRP still has a long-term effect on B cell development

[84]. The stem cells niche in which HSCs are located could also be affected by CGRP. Studies have shown that CGRP+ nociceptive nerves were necessary for HSC mobilization, induced by CGRP driving granulocyte colony-stimulating factor (G-CSF), suggesting that CGRP+ nociceptive nerves were interacted with sympathetic nerves to regulate HSC niches and maintain the function of HSC in the bone marrow [85–89]. Unlike the sympathetic nerves that regulate HSC through niches indirectly [85, 86, 88], parasympathetic nerves act on HSC through RAMP1 and calcitonin receptor-like receptor (CALCRL) directly and promote CGRP excretion by activating the Gas/adenylate cyclase/cAMP pathway (Gas/AC/cAMP pathway). And then capsaicin, a natural component of pepper, can trigger the activation nociceptive neurons to enhance the HSC mobilization in mice via releasing CGRP [89].

3.2. CGRP and Mesenchymal Stem Cells. Mesenchymal stem cells (MSCs), the nonhematopoietic lineages in skeletal tissue, are a kind of mesodermal pluripotent stem cells, which mainly exist in the bone marrow [82]. Recent studies have shown that the CGRP gene can be stably expressed in MSC after transfection with recombinant CGRP lentivirus. And CGRP recombinant lentivirus transfection has little effect on the proliferation and aging of bone marrow mesenchymal stem cells [90]. The bone MSCs of rats modified by CGRP might inhibit the proliferation and migration of rat vascular smooth muscle cells (VSMCs) [90]. These results lay a foundation for the application of CGRP-modified bone marrow mesenchymal stem cells in the treatment of vascular restenosis.

CGRP could induce osteogenic differentiation of bone marrow MSCs after skull defect [91]. The number of MSCs in knee synovial fluid was increased after traumatic meniscus injury, while MSCs were scarcely discovered in degenerative meniscus injury. So CGRP in synovial fluid after trauma were speculated that it could also induce MSCs to enter synovial fluid from the synovium [29]. The sensory neurons (SNs) that could release CGRP in the early to middle stage of bone integration could remodel endothelial cell extracellular matrix, enhance angiogenesis, and induce bone mesenchymal stem cells to differentiate into osteoblasts [92, 93]. It was suggested that before periosteal vascularization, ossification, and mineralization of ulna fracture, the proliferation and dendrization of CGRP+ TrkA+ sensory nerve fibers in reactive periosteum were obvious in the cell domain with a variety of nerve growth factor (NGF), meaning that reinnervation of CGRP+ sensory nerve fibers could promote bone stem cell differentiation [30]. The CGRP level in the blood of patients with fracture was increased significantly, and the CGRP-positive nerve fibers were also been found clearly at the fracture sites in the early stages of fracture [94, 95]. α-CGRP is closely related to the osteogenic differentiation of stem cells. Bone remodeling in CALCA knockout mice appeared to be a significant problem, while mice lacking β-CGRP have been shown to display only a mild and temporary problem [22, 95, 96].

The mechanism of CGRP promoting osteogenic differentiation in stem cells could be demonstrated by the following four aspects. Firstly, α-CGRP enhanced osteogenic differentiation of stem cells by inducing calmodulin- and RAMP1-dependent activation of cAMP response element-binding protein 1 (CREB1) and Sp7 (also known as osterix) [97]. RAMP1 could also promote CGRP-induced osteogenic differentiation of BMSCs by regulating the Hippo/Yap pathway [98–101]. Moreover, magnesium ion can help CGRP mediate osteogenic differentiation of stem cells in newborn bone [97]. Magnesium ion can induce the formation of new bone, and magnesium deficiency will lead to osteoporosis. Magnesium ion can stimulate the release of α-CGRP, promoting the osteogenic differentiation of stem cells in the periosteum. If sensory nerves were destroyed or periosteum with a large number of sensory nerves was removed, magnesium-induced bone formation is greatly reduced [97, 102]. Thirdly, it was demonstrated that CGRP administration not only stimulated osteoblast differentiation but also inhibited OPG/RANKL-regulated osteoclastogenesis [103]. Finally, after distraction osteogenesis (DO), CGRP significantly increased the proportion of endothelial progenitor cells (EPCs) and capillary density. In addition, the endothelial differentiation of MSCs was induced and the number of endothelial progenitor cells (EPCs) by activating the PI3K/Akt signaling pathway was increased in defected bone area [104]. CGRP may act as a modulator of bone metabolism through osteoblast- and osteoclast-associated mechanisms, which result in osteoblast formation with subsequent activation of bone formation.

3.3. Abnormal Methylation Levels of CALCA Promoter and Exon Change Function of Stem Cells. It is known that excessive exposure to fluoride affected bone mineral density (BMD). Fluoride exposure can upregulate the methylation level of CALCA exon 1 and inhibit the expression of CT in Chinese women, resulting in the decrease of bone mineral density [40]. After alveolar bone destruction caused by periodontitis, CGRP can promote bone tissue repair, growth, and metabolism to realize bone tissue regeneration (Figure 1(a)) [105], which may be achieved by affecting the function of dental pulp stem cells (DPSCs). As Chinese toothpaste products generally contain fluoride, we speculate that fluoride may reduce bone mineral density by the CALCA methylation, causing alveolar bone destruction and blocking the regeneration process of periodontal alveolar bone.

Studies showed that adipose-derived stem cells (ASCs) in patients with type 2 diabetes mellitus (T2DM) caused upregulation of methylation level in promoter region of CALCA target fragment, resulting in a significant reduction in the osteogenic function of stem cells [35]. The above studies indicated that the abnormal methylation level of CALCA segments in stem cells may change the cell stemness on bone stem cells.

4. CGRP and Skeletal Muscle Repair

CGRP signal can regulate the differentiation of muscle MSCs and muscle repair. Interleukin- (IL-) 33 produced by local MSCs in injured muscle stimulates Foxp3+CD4+ regulatory T (Treg) cells to promote the repair of acute or chronic

injured skeletal muscle [106, 107]. IL-33+ muscle MSCs are surprisingly close to large fiber nerve bundles and small fiber sensory neurons, which can transcribe a series of genes of encoding neuropeptides, neuropeptide receptors, and other nerve-related proteins, including muscle MSC subtypes that simultaneously express IL-33 and CGRP receptors; CGRP signal can regulate the production of IL-33 by muscle MSCs and the subsequent accumulation of muscle dendrites [108]. In the early stage of acute skeletal muscle injury, a single injection of CGRP can induce bone marrow mesenchymal stem cells to produce a large number of genetic programs [108].

5. CGRP and Skin Stem Cells

Skin is a complex and highly regenerative tissue. There are many different types of stem cells, including epidermal stem cells, mesenchymal stem cells, endothelial and hematopoietic precursor cells, and neural crest-derived precursor cells. In vitro experiments confirmed that nearly 100% of induced pluripotent stem cells (iPSC) produced by human skin fibroblasts expressed neuronal markers, such as BRN3A and β3-tubulin. Its TRPV1 and neurofilament M were positive [109]. More importantly, CGRP could be released by IPSC-derived neurons when stimulated with molecules that induce neuropeptide release, suggesting that innervation plays a central role in many human skin diseases, such as psoriasis and atopic dermatitis [109]. Skin-derived precursor cells (SKPs) were induced to differentiate into sensory neurons (SNs) in vitro which expressed TRPV1, CGRP, PAR2, TRPA1, substance P, etc., meaning that CGRP is closely related to SKP differentiation [110]. In addition, the epidermal stem cells have been reported to be related to epidermal hyperproliferative diseases and skin tumors. Epidermal stem cells can not only maintain the stability of the homeostasis but also participate in tissue regeneration and repair. It is confirmed that CGRP promoted epidermal stem cells to enter S phase, stimulated epidermal stem cells to leave their niches, broke the static state, and induced differentiation [111].

On the other hand, the high level of plasma α-CGRP and β-CGRP and CGRP gene polymorphism has been found in patients of psoriasis and CALCA T-692C polymorphism TT genotype is a susceptible factor in patients with psoriasis vulgaris (Figure 1(a)) [112].

6. CGRP and Nervous System Diseases

6.1. CGRP and the Stem Cell Repair Process of Neurovascular Inflammation. CGRP triggered antiapoptotic signaling and released a number of neurotrophins (including insulin-like growth factor-1 (IGF-1), basic fibroblast growth factor (bFGF), and nerve growth factor (NGF)), increasing antioxidant defenses. It also upregulated the growth factor signals from endothelial cells to brain parenchyma, enhanced the blood-brain barrier, promoted stem cell niche neurogenesis and angiogenesis, and stimulated neurogenesis. Therefore, CGRP is involved in neuroprotective activation after extensive ischemia injury, hyperthermia, and seizure and activates neuroprotective processes [113]. Carriers of at least one C allele at the polymorphic site CALCA T-692C showed increased risk for hypertension [114]. The CALCB gene polymorphism rs16930880 was also confirmed to be associated with vasospasm of Reynolds phenomenon [115]. As the mice grew older, the aging lumbar dorsal root ganglia (DRGs) showed peripheral sensitization, inflammatory reaction, and high expression of neurotransmitter CALCA mRNA [116]. The high expression of CGRP is involved in the stem cell repair process of neurovascular inflammation. Therefore, it is speculated that the stem cell niches are related to the survival, proliferation, migration, and differentiation of stem cells, which may be beneficial for natural or therapeutic CGRP nerve regeneration.

6.2. CGRP Methylation and Migraine. CGRP is known as the strongest vasodilator. In the pathophysiology of migraine, it was related to neurogenic inflammation and cerebral vasodilation [117], neuropeptide CGRP, abundant in trigeminal ganglion neurons, released from peripheral and central nerve. It was interacted with adjacent neurons and satellite glial cells in trigeminal ganglion endocrine, making peripheral sensitization permanent, and it could drive central sensitization of secondary neurons, which may promote the progression of paroxysmal migraine to chronic migraine [118, 119].

There is a strong correlation between DNA methylation of migraine-related genes in migraine patients [120]. On the one hand, it was reported that CpG island methylation around the 18 bp enhancer was a key determinant for the specific expression of CALCA gene in trigeminal neurons [121, 122]. The enhancer of CALCA gene is located about 1 KB upstream in the transcription initiation site, and its methylation on the flank of the enhancer could induce trigeminal ganglion glial cells to activate and produce pro-CT and CGRP in vitro [123]. Upstream stimulating factor (USF) 1 and USF2 could combine with CGRP enhancer, inducing CALCA promoter activity in trigeminal neurons (Figure 1(a)) [122]. CALCA enhancer could also be activated by USF and forkhead protein Foxa2 [124]. On the other hand, transcriptional memory allows certain genes to respond to previously experienced signals more robust. Interestingly, it is proved that cytokine TNF-α transcriptional memory is related to methyl-labeled genes [125]. Also, coding as a therapeutic target for migraine, CALCB has high initial methylation level and CpG density around NF-κB sites, which are correlated with the functional potential of transcriptional memory modules. TNF-α-mediated transcriptional memory is governed by active DNA demethylation of CALCB which makes memory genes extremely sensitive to many low-dose inflammatory signals [126].

The rs3781719 (T>C) single nucleotide polymorphism of 5-UTR in the promoter region of CALCA gene can also affect the expression of CGRP in the process of migraine [127]. The polymorphism of CALCA gene can affect the therapeutic effect of neuroblocker on a botulinum toxin A by changing the expression of CALCA gene [128]. Therefore, the treatment of interfering with the CGRP function of peripheral trigeminal nervous system is effective for

migraine. Blocking the sensitization of trigeminal nerve by reducing the activity and level of peripheral CGRP may be effective to block the attack of migraine.

6.3. CGRP Gene Polymorphism and Other Neurological Diseases. Multiple polymorphisms of CALCA gene include two (g.979G>A and g.4218T>C) that represented single nucleotide polymorphisms (SNPs), one consisted of two coupled SNPs in close vicinity to each other (g.1210T>C and g.1214C>G), and one was an intronic 16 bp microdeletion (2919-2934del16). One of the SNPs (g.4218T>C) causes a nonsynonymous amino acid change (Leu66Pro) in the third exon, an exon common to both procalcitonin and pro-a-CGRP, which have been identified to be related to Parkinson's disease, schizophrenia, depression, and mania [129] (Figure 1(a)). The seemingly nonfunctional intron polymorphism could also disrupt normal RNA processing or introduce splicing sites into transcripts. It is reported that the 16 bp deletion in the first intron of CALCA gene matched the binding site of transcription factor AP-2 strongly expressed in neural crest-derived cells, and the deletion also eliminated the intron splicing enhancer (ISE) which might induce exon skipping [130].

7. CGRP and Tumor Stem Cells

When cancer cells undergo the EMT, they partially and transiently dedifferentiate. This transition provides an opportunity to adjust cellular gene expression and acquire a stem cell phenotype for self-perpetuation and propagation [131]. Some "negative" tissues and cell lines (such as malignant tumors) traditionally considered negative actually highly express CGRP, and some enzymes used for restricted CGRP expression could recognize CpG sites of some tumor cells [123, 132]. The possible mechanisms of obtaining cancer cell stemness by CGRP expression are as follows.

7.1. CGRP Regulates the Proliferation and Differentiation of Lung Tumor Stem Cells through the SHH Signaling Pathway. CGRP could regulate cell proliferation and apoptosis as a tumor growth factor by blocking the G0/G1 phase of the cell cycle to S phase and protect tumor cells from drug-induced apoptosis [133–135]. The SHH signal pathway plays a key role in the process of carcinogenesis and development, and its abnormal activation is closely related to the proliferation and differentiation of lung cancer stem cells (CSCs). Further studies show that the SHH signal pathway may be regulated by CGRP on the proliferation and differentiation of lung cancer cells [61, 136]. Pancreatic cancer cells could activate the SHH signaling pathway which increased the expression of CGRP and TRPV1 in the dorsal root ganglion in a concentration- and time-dependent manner, resulting in the pain of pancreatic cancer [137, 138]. In a word, whether CGRP regulates cell stemness through the SHH signaling pathway needs further study.

7.2. PNECs Regulate ILC2s through CGRP in Small Cell Lung Cancer. PNECs are rare cells with many neuronal characteristics in the body, having the secretory vesicles and the ability to sense environmental stimuli, and stem cells which can sense hypoxia and respond by differentiating into solitary NE cells secrete a protective peptide that mitigates hypoxic injury [139]. PNECs are considered as both progenitor cells and progenitor cell niches after airway epithelial injury [140]. In lung tissues, basal stem cells can directly differentiate into isolated PNECs triggered by hypoxia. Resection of these isolated PNECs could enhance epithelial damage, and administration of CGRP can save this excessive damage [139]. Thus, lung stem cells can reduce hypoxia damage by differentiating into PNECs which secrete CGRP under hypoxia condition.

Tumorigenesis is a complex process, which involves the interaction between cancerous cells and a variety of normal cells. Tumor is considered to be closely related to immunity. Small cell lung cancer (SCLC) is the most invasive type of lung cancer, characterized by poor prognosis and rapid resistance to treatments. The SCLC-like tumors growing subcutaneously in immunodeficient mice seemed to have low tumor potential (slow growth and noninvasive) [141]. PNECs are located near group 2 intrinsic lymphoid cells (ILC2s) near the airway branch point, and the function is still unclear [142]. CGRP is known to inhibit type 2 immune response in lung infection by inhibiting the production of type 2 cytokines in ILC2s in the lung [26]. CGRP released by PNECs can stimulate ILC2s and trigger downstream immune responses in bronchial asthma models [142]. Therefore, different microenvironment factors affect the neuroimmune function of PNECs, which may be related to tumor immune disorder.

High expression of CGRP promotes the malignant transformation of small cell lung cancer target cell PNECs (Figure 3). Lineage tracing experiment shows that CGRP+ PNECs can not only self-renew in steady state but also differentiate into Clara cells and ciliary cells after lung injury [31]. SCLC is likely to originate from CGRP+ PNECs in neuroendocrine cells, consistent with their morphology and the neuroendocrine markers [143–146]. Inhibition of Notch signal can induce up to 10% of lung progenitor cells derived from human embryonic stem cells (hESCs) to produce PNEC and form early tumors similar to SCLC [141]. The expression of CGRP increased significantly during the carcinogenesis of PNECs [147, 148]. Therefore, it is of great significance to explore the mechanism of high CGRP expression promoting the malignant transformation of PNECs, and it also lays a foundation for the research of tumor therapy.

7.3. Trypsin Overexpression Induced Abnormal Splicing of CGRP in Pancreatic Cancer Stem Cells. The change of cell cycle is the driving force of tumor biological behavior [149], but whether it is unique in the role of cell cycle disorder in the occurrence of pancreatic cancer is still unknown. CGRP can induce G2/M phase arrest by regulating G2/M phase-related proteins [150]. Moreover, it is found that CGRP can arrest the cell cycle of pancreatic cancer stem cells in the G0/G1 stage [151]. Trypsin overexpression induced abnormal splicing of CGRP in pancreatic cancer stem cells, driving cell cycle disorder [152].

However, CGRP does not complete the malignant cell transformation independently as Ras/Notch and other

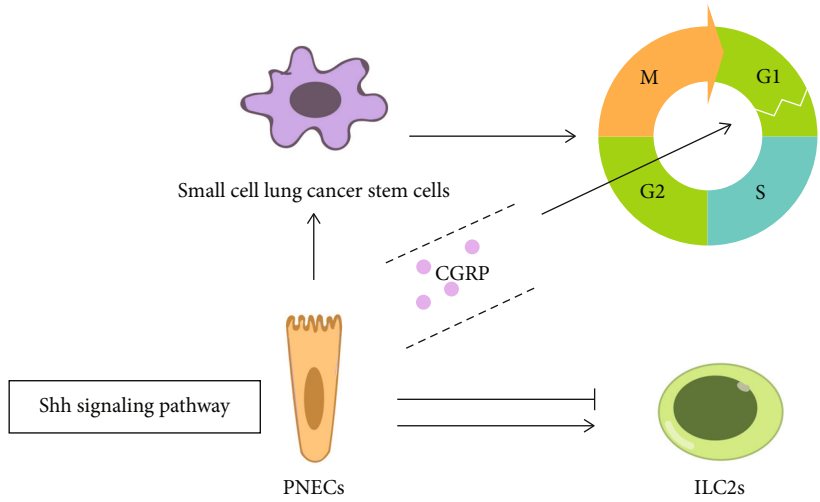

Figure 3: High CGRP expression promotes the malignant transformation of PNECs through the SHH signaling pathway. PNECs regulate group 2 innate lymphoid cells (ILC2s) through CGRP in small cell lung cancer which may affect the immune status of the tumor microenvironment. Moreover, CGRP protects stem cells from apoptosis by blocking the G0/G1 phase of the cell cycle to S phase through the SHH signaling pathway.

oncogenes in this process. The helicase Prp2 (blue) and the coactivator Spp2 (purple) combine stably with the anchor molecules on the spliceosome, so as to binding Prp2 to the activated spliceosome and allowing a greater role for Prp2. CGRP pre-mRNA (red) is loaded into the characteristic channel between the N- and C-halves of Prp2. The process of ATP binding and hydrolyzation or trypsin (green, specific high expression in the pancreas) triggers Prp2 to move into sensitive binding site of trypsin, driving pre-mRNA to move unidirectionally and gradually towards its $3'$ end. By CGRP disturbing cell cycle, abnormal shearing breaks the genetic stability and amplifies oncogenic signals, whose function is similar to that of an essential translator and amplifier in the carcinogenic pathway [153–156]. Therefore, oncogenic signals are closely related to cell proliferation and transformation, which eventually leads to tumor production (Figure 4) [132].

7.4. Abnormal CGRP Target Gene Fragments Regulate Cell Stemness. Elevated promoter methylation level may be one of the most obvious characteristics for malignant tumors [157]. Many studies have showed that there are tumor-specific changes of DNA fragments in patients' serum with various malignant tumors, such as abnormal promoter methylation [158]. By real-time quantitative methylation-specific polymerase chain reaction (QMSP), it was found that the level of CALCA methylation in patients with lung cancer was significantly higher than that in benign lung lesions [157]. The high frequency of promoter methylation of CALCA gene has been found in cervical cancer and bladder cancer [159, 160]. Similarly, the previous study of our research group also found that the CpG island methylation of CALCA and CALCB in pancreatic ductal adenocarcinoma was significantly higher than that in adjacent tissues and CGRP participated in cell proliferation, apoptosis, differentiation, and survival through the AKT/CREB signaling pathway and finally promoted the occurrence and development of tumors [33]. CpG island hypermethylation of CALCA occurs in juvenile mononuclear leukemia (JMML), regaining the hypermethylated phenotype upon relapse after treatment [161]. Thus, the abnormal methylation level of CALCA fragment in the promoter region of stem cells is an important reason for the change of cell stemness [35], and high-methylation phenotype is also an important biomarker in the process of tumor diagnosis and treatment.

7.5. Transcription Factors Combined with GGAA Microsatellite Sequence Control CGRP Expression. Studies also confirmed that CALCB was a specific secretory peptide in Ewing's sarcoma (EWS). Silencing CALCB inhibited the growth of EWS cells, and the transcription factor ewsr1-fli1 combined with GGAA microsatellite sequence could regulate the expression of CALCB by improving enhancer activity, leading to the differentiation and proliferation of stem cells [132].

7.6. CGRP Gene Polymorphisms Increase Tumor Risk. CGRP has multiple gene polymorphic loci in tumors, and gene polymorphisms increase the risk of malignancy. It is known that extracellular calcium upregulates the proliferation of ovarian surface epithelial cells, which is very important for malignant transformation into ovarian cancer [162]. The CALCA gene codes for calcitonin, an important regulator of bone calcium metabolism. It was also reported that the T → C transition in base pairs upstream (-624) of the translation initiation codon of the CALCA gene increased risk of ovarian malignancy among Japanese (Figure 1(a)) [163].

Our previous study showed that promoter polymorphisms of CALCB gene (rs11603873 T/C and rs79501047 A/G) are common in the Han population, and the rs11603873 C genotype has a high risk of salivary adenoid cystic carcinoma compared with the rs11603873 T genotype, 2.27 times, and the rs79501047 G genotype was 3.76 times than that of the rs79501047 A genotype [164]. In a word, the polymorphism of βCGRP gene is related with genetic

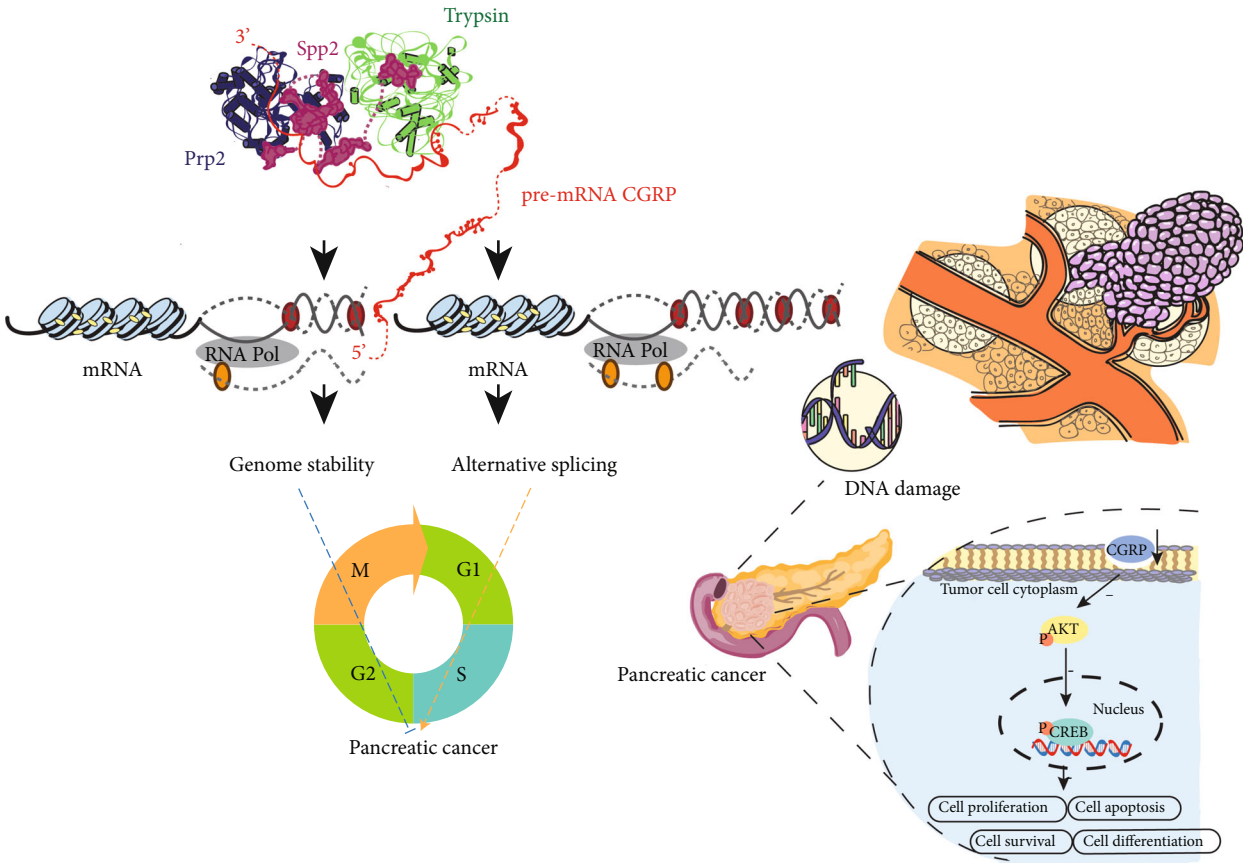

Figure 4: Abnormal CGRP expression promotes cell cycle disorder and promotes the occurrence of pancreatic cancer. The helicase Prp2 (blue) and the coactivator Spp2 (purple) combine stably with the anchor molecules on the spliceosome, so as to binding Prp2 to the activated spliceosome and allowing a greater role for Prp2. CGRP pre-mRNA (red) is loaded into the characteristic channel between the N- and C-halves of Prp2. The process of ATP binding and hydrolyzation or trypsin (green, specific high expression in the pancreas) triggers Prp2 to move into sensitive binding site of trypsin, driving pre-mRNA to move unidirectionally and gradually towards its 3′ end. By CGRP disturbing cell cycle, abnormal shearing breaks the genetic stability and amplifies oncogenic signals, whose function is similar to that of an essential translator and amplifier in the carcinogenic pathway.

susceptibility to salivary adenoid cystic carcinoma, and serum CGRP and βCGRP can be used as new markers of salivary adenoid cystic carcinoma.

8. Summary

The 2021 Nobel Prize in physiology and medicine "temperature and tactile receptors" helps us perceive the world, feel temperature and pressure. CGRP has complex biological functions, and it is regulated by multiple cells and factors. Meanwhile, CGRP reacts on cells and other factors and helps maintain the stability of the body in the inflammatory state. Its complex shear mechanism provides the possibility for the different functional states in different tissues, and the adaptation is produced by organisms facing different environments during evolution. CGRP could regulate cell stemness during body damage repair and promote stem cell proliferation and differentiation, which has great potential application value in gene therapy. "New discoveries make life better," manipulating CGRP may be able to controllably regulate stem cell differentiation, so as to realize the ultimate human dream of health and longevity.

Data Availability

The data used to support the findings of this study are currently under embargo while the research findings are commercialized. Requests for data, 12 months after publication of this article, will be considered by the corresponding authors.

Conflicts of Interest

The authors have no competing interests to declare.

Authors' Contributions

Q.-C.L., F.G., and X.-T.L. planned the project. Q.-C. L. and F.G. conceived and designed the study. Q.-C.L., Q.-Q.C., and S.-Y.Z. analyzed the data and drafted the manuscript. All authors reviewed the manuscript and approved the final version.

Acknowledgments

We would like to thank the students (Yuxin Liu) from the Department of Medical Laboratory of Fujian Medical

University for their support in language processing. This work was financially supported by the National Natural Science Foundation of China (No. 81800070 to Xiaoting Lv, No. 81871293 to Qicai Liu, and No. 82172953 to Feng Gao) and the Natural Science Foundation of Fujian Province (No. 2021J01222 to Xiaoting Lv and No. 2021J02036 to Qicai Liu).

References

[1] L. Li and F. Guo, "Single-cell multi-omics sequencing of human early embryos," *Nature Cell Biology*, vol. 20, pp. 847–858, 2018.

[2] J. Wu, J. Xu, B. Liu et al., "Chromatin analysis in human early development reveals epigenetic transition during ZGA," *Nature*, vol. 557, pp. 256–260, 2018.

[3] Z. Chen, F. Miao, B. H. Braffett et al., "DNA methylation mediates development of HbA1c-associated complications in type 1 diabetes," *Nature Metabolism*, vol. 2, pp. 744–762, 2020.

[4] V. Chickarmane, C. Troein, U. A. Nuber, H. M. Sauro, and C. Peterson, "Transcriptional dynamics of the embryonic stem cell switch," *PLoS Computational Biology*, vol. 2, article e123, 2006.

[5] J. Yu, M. A. Vodyanik, K. Smuga-Otto et al., "Induced pluripotent stem cell lines derived from human somatic cells," *Science*, vol. 318, pp. 1917–1920, 2007.

[6] L. A. Boyer, T. I. Lee, M. F. Cole et al., "Core transcriptional regulatory circuitry in human embryonic stem cells," *Cell*, vol. 122, pp. 947–956, 2005.

[7] K. Takahashi and S. Yamanaka, "Induction of pluripotent stem cells from mouse embryonic and adult fibroblast cultures by defined factors," *Cell*, vol. 126, pp. 663–676, 2006.

[8] B. van Schaijik, P. F. Davis, A. C. Wickremesekera, S. T. Tan, and T. Itinteang, "Subcellular localisation of the stem cell markers OCT4, SOX2, NANOG, KLF4 and c-MYC in cancer: a review," *Journal of Clinical Pathology*, vol. 71, pp. 88–91, 2018.

[9] F. A. Russell, R. King, S. J. Smillie, X. Kodji, and S. D. Brain, "Calcitonin gene-related peptide: physiology and pathophysiology," *Physiological Reviews*, vol. 94, pp. 1099–1142, 2014.

[10] C. A. Maggi, "Tachykinins and calcitonin gene-related peptide (CGRP) as co-transmitters released from peripheral endings of sensory nerves," *Progress in Neurobiology*, vol. 45, pp. 1–98, 1995.

[11] M. G. Rosenfeld, J. J. Mermod, S. G. Amara et al., "Production of a novel neuropeptide encoded by the calcitonin gene via tissue-specific RNA processing," *Nature*, vol. 304, pp. 129–135, 1983.

[12] W. S. Schou, S. Ashina, F. M. Amin, P. J. Goadsby, and M. Ashina, "Calcitonin gene-related peptide and pain: a systematic review," *The Journal of Headache and Pain*, vol. 18, p. 34, 2017.

[13] P. J. Goadsby and L. Edvinsson, "The trigeminovascular system and migraine: studies characterizing cerebrovascular and neuropeptide changes seen in humans and cats," *Annals of Neurology*, vol. 33, pp. 48–56, 1993.

[14] P. J. Goadsby, L. Edvinsson, and R. Ekman, "Vasoactive peptide release in the extracerebral circulation of humans during migraine headache," *Annals of Neurology*, vol. 28, pp. 183–187, 1990.

[15] R. K. Cady, C. V. Vause, T. W. Ho, M. E. Bigal, and P. L. Durham, "Elevated saliva calcitonin gene-related peptide levels during acute migraine predict therapeutic response to rizatriptan," *Headache*, vol. 49, pp. 1258–1266, 2009.

[16] K. Kamm, A. Straube, and R. Ruscheweyh, "Calcitonin gene-related peptide levels in tear fluid are elevated in migraine patients compared to healthy controls," *Cephalalgia*, vol. 39, pp. 1535–1543, 2019.

[17] J. Larsson, A. Ekblom, K. Henriksson, T. Lundeberg, and E. Theodorsson, "Concentration of substance P, neurokinin A, calcitonin gene-related peptide, neuropeptide Y and vasoactive intestinal polypeptide in synovial fluid from knee joints in patients suffering from rheumatoid arthritis," *Scandinavian Journal of Rheumatology*, vol. 20, pp. 326–335, 1991.

[18] R. M. van Dongen, R. Zielman, M. Noga et al., "Migraine biomarkers in cerebrospinal fluid: a systematic review and meta-analysis," *Cephalalgia*, vol. 37, pp. 49–63, 2017.

[19] A. S. Wattiez, L. P. Sowers, and A. F. Russo, "Calcitonin gene-related peptide (CGRP): role in migraine pathophysiology and therapeutic targeting," *Expert opinion on therapeutic targets*, vol. 24, pp. 91–100, 2020.

[20] A. F. Russo, C. Nelson, B. A. Roos, and M. G. Rosenfeld, "Differential regulation of the coexpressed calcitonin/alpha-CGRP and beta-CGRP neuroendocrine genes," *The Journal of Biological Chemistry*, vol. 263, pp. 5–8, 1988.

[21] Y. Singh and G. Gupta, "Calcitonin gene-related peptide (CGRP): a novel target for Alzheimer's disease," *CNS Neuroscience & Therapeutics*, vol. 23, pp. 457–461, 2017.

[22] A. K. Huebner, J. Keller, P. Catala-Lehnen et al., "The role of calcitonin and alpha-calcitonin gene-related peptide in bone formation," *Archives of Biochemistry and Biophysics*, vol. 473, pp. 210–217, 2008.

[23] M. M. Bennett and S. G. Amara, "Molecular mechanisms of cell-specific and regulated expression of the calcitonin/alpha-CGRP and beta-CGRP genes," *Annals of the New York Academy of Sciences*, vol. 657, pp. 36–49, 1992.

[24] P. K. Muddhrry, M. A. Ghatki, R. A. Spokks et al., "Differential expression of alpha-CGRP and beta-CGRP by primary sensory neurons and enteric autonomic neurons of the rat," *Neuroscience*, vol. 25, pp. 195–205, 1988.

[25] C. Schaeffer, D. Vandroux, L. Thomassin, P. Athias, L. Rochette, and J. L. Connat, "Calcitonin gene-related peptide partly protects cultured smooth muscle cells from apoptosis induced by an oxidative stress via activation of ERK1/2 MAPK," *Biochimica et Biophysica Acta (BBA) - Molecular Cell Research*, vol. 1643, no. 1-3, pp. 65–73, 2003.

[26] H. Nagashima, T. Mahlakõiv, H. Y. Shih et al., "Neuropeptide CGRP limits group 2 innate lymphoid cell responses and constrains type 2 inflammation," *Immunity*, vol. 51, pp. 682–695.e686, 2019.

[27] C. E. Riera, M. O. Huising, P. Follett et al., "TRPV1 pain receptors regulate longevity and metabolism by neuropeptide signaling," *Cell*, vol. 157, pp. 1023–1036, 2014.

[28] H. F. Chen, C. Y. Yu, M. J. Chen et al., "Characteristic expression of major histocompatibility complex and immune privilege genes in human pluripotent stem cells and their derivatives," *Cell Transplantation*, vol. 24, pp. 845–864, 2015.

[29] N. Watanabe, K. Endo, K. Komori et al., "Mesenchymal stem cells in synovial fluid increase in knees with degenerative meniscus injury after arthroscopic procedures through the

endogenous effects of CGRP and HGF," *Stem Cell Reviews and Reports*, vol. 16, pp. 1305–1315, 2020.

[30] Z. Li, C. A. Meyers, L. Chang et al., "Fracture repair requires TrkA signaling by skeletal sensory nerves," *The Journal of Clinical Investigation*, vol. 129, pp. 5137–5150, 2019.

[31] H. Song, E. Yao, C. Lin, R. Gacayan, M. H. Chen, and P. T. Chuang, "Functional characterization of pulmonary neuroendocrine cells in lung development, injury, and tumorigenesis," *Proceedings of the National Academy of Sciences of the United States of America*, vol. 109, pp. 17531–17536, 2012.

[32] L. Schneider, W. Hartwig, T. Flemming et al., "Protective effects and anti-inflammatory pathways of exogenous calcitonin gene-related peptide in severe necrotizing pancreatitis," *Pancreatology*, vol. 9, pp. 662–669, 2009.

[33] F. Gao, G. Liu, J. Wang et al., "Methylation of CALCA and CALCB in pancreatic ductal adenocarcinoma," *Oxidative Medicine and Cellular Longevity*, vol. 2021, Article ID 2088345, 13 pages, 2021.

[34] S. J. Cokus, S. Feng, X. Zhang et al., "Shotgun bisulphite sequencing of the Arabidopsis genome reveals DNA methylation patterning," *Nature*, vol. 452, pp. 215–219, 2008.

[35] L. Wang, F. Ding, S. Shi, X. Wang, S. Zhang, and Y. Song, "Hypermethylation in Calca promoter inhibited ASC osteogenic differentiation in rats with type 2 diabetic mellitus," *Stem Cells International*, vol. 2020, Article ID 5245294, 11 pages, 2020.

[36] R. A. Tahir, D. A. Zheng, A. Nazir, and H. Qing, "A review of computational algorithms for CpG islands detection," *Journal of Biosciences*, vol. 44, 2019.

[37] L. Shi, Q. Lin, and B. Su, "Human-specific hypomethylation of CENPJ, a key brain size regulator," *Molecular Biology and Evolution*, vol. 31, pp. 594–604, 2014.

[38] P. M. Broad, A. J. Symes, R. V. Thakker, and R. K. Craig, "Structure and methylation of the human calcitonin/alpha-CGRP gene," *Nucleic Acids Research*, vol. 17, pp. 6999–7011, 1989.

[39] D. L. Hay, C. S. Walker, and D. R. Poyner, "Adrenomedullin and calcitonin gene-related peptide receptors in endocrine-related cancers: opportunities and challenges," *Endocrine-Related Cancer*, vol. 18, pp. C1–14, 2011.

[40] R. Sun, G. Zhou, L. Liu et al., "Fluoride exposure and CALCA methylation is associated with the bone mineral density of Chinese women," *Chemosphere*, vol. 253, article 126616, 2020.

[41] D. O. Vidal, V. A. Paixão, M. Brait et al., "Aberrant methylation in pediatric myelodysplastic syndrome," *Leukemia Research*, vol. 31, pp. 175–181, 2007.

[42] J. A. Hackett, J. P. Reddington, C. E. Nestor et al., "Promoter DNA methylation couples genome-defence mechanisms to epigenetic reprogramming in the mouse germline," *Development*, vol. 139, pp. 3623–3632, 2012.

[43] R. J. Klose and A. P. Bird, "Genomic DNA methylation: the mark and its mediators," *Trends in Biochemical Sciences*, vol. 31, pp. 89–97, 2006.

[44] T. Sugiyama, Y. Omatsu, and T. Nagasawa, "Niches for hematopoietic stem cells and immune cell progenitors," *International Immunology*, vol. 31, pp. 5–11, 2019.

[45] K. A. Tendl, S. M. Schulz, T. P. Mechtler et al., "DNA methylation pattern of CALCA in preterm neonates with bacterial sepsis as a putative epigenetic biomarker," *Epigenetics*, vol. 8, pp. 1261–1267, 2013.

[46] B. R. Stripp, "Hierarchical organization of lung progenitor cells: is there an adult lung tissue stem cell?," *Proceedings of the American Thoracic Society*, vol. 5, pp. 695–698, 2008.

[47] C. W. Wuenschell, M. E. Sunday, G. Singh, P. Minoo, H. C. Slavkin, and D. Warburton, "Embryonic mouse lung epithelial progenitor cells co-express immunohistochemical markers of diverse mature cell lineages," *The Journal of Histochemistry and Cytochemistry*, vol. 44, pp. 113–123, 1996.

[48] G. M. Crane, E. Jeffery, and S. J. Morrison, "Adult haematopoietic stem cell niches," *Nature Reviews. Immunology*, vol. 17, pp. 573–590, 2017.

[49] M. L. Donne, A. J. Lechner, and J. R. Rock, "Evidence for lung epithelial stem cell niches," *BMC Developmental Biology*, vol. 15, p. 32, 2015.

[50] J. Y. Choi, N. S. Joo, M. E. Krouse et al., "Synergistic airway gland mucus secretion in response to vasoactive intestinal peptide and carbachol is lost in cystic fibrosis," *The Journal of Clinical Investigation*, vol. 117, pp. 3118–3127, 2007.

[51] P. Baral, B. D. Umans, L. Li et al., "Nociceptor sensory neurons suppress neutrophil and $\gamma\delta$ T cell responses in bacterial lung infections and lethal pneumonia," *Nature Medicine*, vol. 24, pp. 417–426, 2018.

[52] W. Xie, J. T. Fisher, T. J. Lynch et al., "CGRP induction in cystic fibrosis airways alters the submucosal gland progenitor cell niche in mice," *The Journal of Clinical Investigation*, vol. 121, pp. 3144–3158, 2011.

[53] K. E. Fasanella, J. A. Christianson, R. S. Chanthaphavong, and B. M. Davis, "Distribution and neurochemical identification of pancreatic afferents in the mouse," *The Journal of Comparative Neurology*, vol. 509, pp. 42–52, 2008.

[54] J. Meng, S. V. Ovsepian, J. Wang et al., "Activation of TRPV1 mediates calcitonin gene-related peptide release, which excites trigeminal sensory neurons and is attenuated by a retargeted botulinum toxin with anti-nociceptive potential," *The Journal of Neuroscience*, vol. 29, pp. 4981–4992, 2009.

[55] M. Aita, T. Maeda, and K. Seo, "The effect of neonatal capsaicin treatment on the CGRP-immunoreaction in the trigeminal subnucleus caudalis of mice," *Biomedical Research*, vol. 29, pp. 33–42, 2008.

[56] D. X. Gram, B. Ahrén, I. Nagy et al., "Capsaicin-sensitive sensory fibers in the islets of Langerhans contribute to defective insulin secretion in Zucker diabetic rat, an animal model for some aspects of human type 2 diabetes," *The European Journal of Neuroscience*, vol. 25, pp. 213–223, 2007.

[57] W. Zhao, X. Pan, T. Li, C. Zhang, and N. Shi, "*Lycium barbarum* polysaccharides protect against trimethyltin chloride-induced apoptosis via sonic hedgehog and PI3K/Akt signaling pathways in mouse neuro-2a cells," *Oxidative Medicine and Cellular Longevity*, vol. 2016, Article ID 9826726, 18 pages, 2016.

[58] K. S. Jeng and C. F. Chang, "Sonic hedgehog signaling in organogenesis, tumors, and tumor microenvironments," *International Journal of Molecular Sciences*, vol. 21, 2020.

[59] M. Saqui-Salces and J. L. Merchant, "Hedgehog signaling and gastrointestinal cancer," *Biochimica et Biophysica Acta*, vol. 1803, pp. 786–795, 2010.

[60] G. B. Carballo, J. R. Honorato, G. P. F. de Lopes, and T. Spohr, "A highlight on Sonic hedgehog pathway," *Cell Communication and Signaling: CCS*, vol. 16, p. 11, 2018.

[61] E. Giroux-Leprieur, A. Costantini, V. W. Ding, and B. He, "Hedgehog signaling in lung cancer: from oncogenesis to

cancer treatment resistance," *International Journal of Molecular Sciences*, vol. 19, 2018.

[62] I. Y. Adamson and D. H. Bowden, "The type 2 cell as progenitor of alveolar epithelial regeneration. A cytodynamic study in mice after exposure to oxygen," *Laboratory Investigation*, vol. 30, pp. 35–42, 1974.

[63] I. Y. Adamson, C. Hedgecock, and D. H. Bowden, "Epithelial cell-fibroblast interactions in lung injury and repair," *The American Journal of Pathology*, vol. 137, pp. 385–392, 1990.

[64] J. F. Tomashefski Jr., "Pulmonary pathology of the adult respiratory distress syndrome," *Clinics in Chest Medicine*, vol. 11, pp. 593–619, 1990.

[65] M. J. Evans, L. J. Cabral-Anderson, and G. Freeman, "Effects of NO_2 on the lungs of aging rats: II. Cell proliferation," *Experimental and molecular pathology*, vol. 27, pp. 366–376, 1977.

[66] L. J. Cabral-Anderson, M. J. Evans, and G. Freeman, "Effects of NO_2 on the lungs of aging rats: I. Morphology," *Experimental and molecular pathology*, vol. 27, pp. 353–365, 1977.

[67] K. A. Correll, K. E. Edeen, R. L. Zemans et al., "Transitional human alveolar type II epithelial cells suppress extracellular matrix and growth factor gene expression in lung fibroblasts," *American Journal of Physiology. Lung Cellular and Molecular Physiology*, vol. 317, pp. L283–l294, 2019.

[68] W. M. Haschek and H. Witschi, "Pulmonary fibrosis–a possible mechanism," *Toxicology and Applied Pharmacology*, vol. 51, pp. 475–487, 1979.

[69] I. Y. Adamson, L. Young, and D. H. Bowden, "Relationship of alveolar epithelial injury and repair to the induction of pulmonary fibrosis," *The American Journal of Pathology*, vol. 130, pp. 377–383, 1988.

[70] N. Cigna, E. F. Moshai, S. Brayer et al., "The hedgehog system machinery controls transforming growth factor-β-dependent myofibroblastic differentiation in humans: involvement in idiopathic pulmonary fibrosis," *The American Journal of Pathology*, vol. 181, pp. 2126–2137, 2012.

[71] P. M. Fitch, S. E. Howie, and W. A. Wallace, "Oxidative damage and TGF-β differentially induce lung epithelial cell sonic hedgehog and tenascin-C expression: implications for the regulation of lung remodelling in idiopathic interstitial lung disease," *International Journal of Experimental Pathology*, vol. 92, pp. 8–17, 2011.

[72] A. L. Bolaños, C. M. Milla, J. C. Lira et al., "Role of Sonic Hedgehog in idiopathic pulmonary fibrosis," *American Journal of Physiology. Lung Cellular and Molecular Physiology*, vol. 303, pp. L978–L990, 2012.

[73] H. X. Dang, J. Li, C. Liu et al., "CGRP attenuates hyperoxia-induced oxidative stress-related injury to alveolar epithelial type II cells via the activation of the Sonic hedgehog pathway," *International Journal of Molecular Medicine*, vol. 40, pp. 209–216, 2017.

[74] T. Zhan, N. Rindtorff, and M. Boutros, "Wnt signaling in cancer," *Oncogene*, vol. 36, pp. 1461–1473, 2017.

[75] E. M. Abdelwahab, J. Rapp, D. Feller et al., "Wnt signaling regulates trans-differentiation of stem cell like type 2 alveolar epithelial cells to type 1 epithelial cells," *Respiratory Research*, vol. 20, p. 204, 2019.

[76] S. Wang, H. Dang, F. Xu, J. Deng, and X. Zheng, "The Wnt7b/β-catenin signaling pathway is involved in the protective action of calcitonin gene-related peptide on hyperoxia-induced lung injury in premature rats," *Cellular & Molecular Biology Letters*, vol. 23, p. 4, 2018.

[77] B. Li, X. Huang, X. Xu, W. Ning, H. Dai, and C. Wang, "The profibrotic effect of downregulated Na, K-ATPase β1 subunit in alveolar epithelial cells during lung fibrosis," *International Journal of Molecular Medicine*, vol. 44, pp. 273–280, 2019.

[78] D. C. Blaydon, L. K. Lind, V. Plagnol et al., "Mutations in AQP5, encoding a water-channel protein, cause autosomal-dominant diffuse nonepidermolytic palmoplantar keratoderma," *American Journal of Human Genetics*, vol. 93, pp. 330–335, 2013.

[79] X. Li, R. Li, Q. Fang et al., "Oxycodone attenuates vascular leak and lung inflammation in a clinically relevant two-hit rat model of acute lung injury," *Cytokine*, vol. 138, article 155346, 2021.

[80] X. Lv, F. Gao, S. Zhang et al., "Maladjustment of β-CGRP/α-CGRP regulation of AQP5 promotes transition of alveolar epithelial cell apoptosis to pulmonary fibrosis," *Journal of Interferon & Cytokine Research*, vol. 40, pp. 377–388, 2020.

[81] A. Jacob, M. Morley, F. Hawkins et al., "Differentiation of human pluripotent stem cells into functional lung alveolar epithelial cells," *Cell Stem Cell*, vol. 21, pp. 472–488.e410, 2017.

[82] C. K. Chan, G. S. Gulati, R. Sinha et al., "Identification of the human skeletal stem cell," *Cell*, vol. 175, pp. 43–56.e21, 2018.

[83] C. M. Baum, I. L. Weissman, A. S. Tsukamoto, A. M. Buckle, and B. Peault, "Isolation of a candidate human hematopoietic stem-cell population," *Proceedings of the National Academy of Sciences of the United States of America*, vol. 89, pp. 2804–2808, 1992.

[84] J. J. Schlomer, B. B. Storey, R. T. Ciornei, and J. P. McGillis, "Calcitonin gene-related peptide inhibits early B cell development in vivo," *Journal of Leukocyte Biology*, vol. 81, pp. 802–808, 2007.

[85] Y. Katayama, M. Battista, W. M. Kao et al., "Signals from the sympathetic nervous system regulate hematopoietic stem cell egress from bone marrow," *Cell*, vol. 124, pp. 407–421, 2006.

[86] D. Lucas, C. Scheiermann, A. Chow et al., "Chemotherapy-induced bone marrow nerve injury impairs hematopoietic regeneration," *Nature Medicine*, vol. 19, pp. 695–703, 2013.

[87] M. Maryanovich and A. H. Zahalka, "Adrenergic nerve degeneration in bone marrow drives aging of the hematopoietic stem cell niche," *Nature Medicine*, vol. 24, pp. 782–791, 2018.

[88] S. Méndez-Ferrer, T. V. Michurina, F. Ferraro et al., "Mesenchymal and haematopoietic stem cells form a unique bone marrow niche," *Nature*, vol. 466, pp. 829–834, 2010.

[89] X. Gao and D. Zhang, "Nociceptive nerves regulate haematopoietic stem cell mobilization," *Nature*, vol. 589, pp. 591–596, 2021.

[90] P. Chen, F. He, T. Liu, S. Ma, and B. Shi, "Construction of calcitonin gene-related peptide-modified mesenchymal stem cells and analysis of their effects on the migration and proliferation of vascular smooth muscle cells," *In Vitro Cellular & Developmental Biology. Animal*, vol. 56, pp. 181–191, 2020.

[91] X. Yu, S. Liu, X. Chen, Y. Du, X. Yin, and S. Li, "Calcitonin gene related peptide gene-modified rat bone mesenchymal stem cells are effective seed cells in tissue engineering to repair skull defects," *Histology and Histopathology*, vol. 34, pp. 1229–1241, 2019.

[92] A. Leroux, B. Paiva Dos Santos, J. Leng, H. Oliveira, and J. Amédée, "Sensory neurons from dorsal root ganglia regulate endothelial cell function in extracellular matrix remodelling," *Cell Communication and Signaling: CCS*, vol. 18, p. 162, 2020.

[93] Y. Guo, H. Chen, Y. Jiang et al., "CGRP regulates the dysfunction of peri-implant angiogenesis and osseointegration in streptozotocin-induced diabetic rats," *Bone*, vol. 139, article 115464, 2020.

[94] M. I. Hukkanen, Y. T. Konttinen, R. G. Rees, S. J. Gibson, S. E. Santavirta, and J. M. Polak, "Innervation of bone from healthy and arthritic rats by substance P and calcitonin gene related peptide containing sensory fibers," *The Journal of Rheumatology*, vol. 19, pp. 1252–1259, 1992.

[95] J. Appelt, A. Baranowsky, D. Jahn et al., "The neuropeptide calcitonin gene-related peptide alpha is essential for bone healing," *eBioMedicine*, vol. 59, article 102970, 2020.

[96] D. Naot, D. S. Musson, and J. Cornish, "The activity of peptides of the calcitonin family in bone," *Physiological Reviews*, vol. 99, pp. 781–805, 2019.

[97] Y. Zhang, J. Xu, Y. C. Ruan et al., "Implant-derived magnesium induces local neuronal production of CGRP to improve bone-fracture healing in rats," *Nature Medicine*, vol. 22, pp. 1160–1169, 2016.

[98] H. Karvonen, H. Barker, L. Kaleva, W. Niininen, and D. Ungureanu, "Molecular mechanisms associated with ROR1-mediated drug resistance: crosstalk with hippo-YAP/TAZ and BMI-1 pathways," *Cell*, vol. 8, 2019.

[99] J. A. Ajani, S. Song, H. S. Hochster, and I. B. Steinberg, "Cancer stem cells: the promise and the potential," *Seminars in Oncology*, vol. 42, Supplement 1, pp. S3–17, 2015.

[100] S. Patel, J. Tang, J. M. Overstreet et al., "Rac-GTPase promotes fibrotic TGF-β1 signaling and chronic kidney disease via EGFR, p 53, and Hippo/YAP/TAZ pathways," *The FASEB Journal*, vol. 33, pp. 9797–9810, 2019.

[101] Q. Zhang, Y. Guo, H. Yu et al., "Receptor activity-modifying protein 1 regulates the phenotypic expression of BMSCs via the Hippo/Yap pathway," *Journal of Cellular Physiology*, vol. 234, pp. 13969–13976, 2019.

[102] S. Castiglioni, A. Cazzaniga, W. Albisetti, and J. A. Maier, "Magnesium and osteoporosis: current state of knowledge and future research directions," *Nutrients*, vol. 5, pp. 3022–3033, 2013.

[103] H. He, J. Chai, S. Zhang et al., "CGRP may regulate bone metabolism through stimulating osteoblast differentiation and inhibiting osteoclast formation," *Molecular Medicine Reports*, vol. 13, pp. 3977–3984, 2016.

[104] J. Mi, J. Xu, H. Yao et al., "Calcitonin gene-related peptide enhances distraction osteogenesis by increasing angiogenesis," *Tissue Engineering. Part A*, vol. 27, pp. 87–102, 2021.

[105] X. Yu, L. Lv, J. Zhang, T. Zhang, C. Xiao, and S. Li, "Expression of neuropeptides and bone remodeling-related factors during periodontal tissue regeneration in denervated rats," *Journal of Molecular Histology*, vol. 46, pp. 195–203, 2015.

[106] W. Kuswanto, D. Burzyn, M. Panduro et al., "Poor repair of skeletal muscle in aging mice reflects a defect in local, interleukin-33-dependent accumulation of regulatory T cells," *Immunity*, vol. 44, pp. 355–367, 2016.

[107] J. E. Heredia, L. Mukundan, F. M. Chen et al., "Type 2 innate signals stimulate fibro/adipogenic progenitors to facilitate muscle regeneration," *Cell*, vol. 153, pp. 376–388, 2013.

[108] K. Wang, O. K. Yaghi, R. G. Spallanzani et al., "Neuronal, stromal, and T-regulatory cell crosstalk in murine skeletal muscle," *Proceedings of the National Academy of Sciences of the United States of America*, vol. 117, pp. 5402–5408, 2020.

[109] Q. Muller, M. J. Beaudet, T. De Serres-Bérard, S. Bellenfant, V. Flacher, and F. Berthod, "Development of an innervated tissue-engineered skin with human sensory neurons and Schwann cells differentiated from iPS cells," *Acta Biomaterialia*, vol. 82, pp. 93–101, 2018.

[110] A. Bataille, R. Leschiera, K. Hérondelle et al., "In vitro differentiation of human skin-derived cells into functional sensory neurons-like," *Cell*, vol. 9, p. 1000, 2020.

[111] J. Dong, Y. He, X. Zhang et al., "Calcitonin gene-related peptide regulates the growth of epidermal stem cells in vitro," *Peptides*, vol. 31, pp. 1860–1865, 2010.

[112] R. Guo, F. F. Li, M. L. Chen, M. Z. Yao, H. L. He, and D. Li, "The role of CGRP and CALCA T-692C single-nucleotide polymorphism in psoriasis vulgaris," *Die Pharmazie*, vol. 70, pp. 88–93, 2015.

[113] J. M. Borkum, "CGRP and brain functioning: cautions for migraine treatment," *Headache*, vol. 59, pp. 1339–1357, 2019.

[114] X. L. Luo, T. L. Yang, X. P. Chen, and Y. J. Li, "Association of CALCA genetic polymorphism with essential hypertension," *Chinese Medical Journal*, vol. 121, pp. 1407–1410, 2008.

[115] S. Munir, M. B. Freidin, S. Brain, and F. M. K. Williams, "Association of Raynaud's phenomenon with a polymorphism in the NOS1 gene," *PLoS One*, vol. 13, article e0196279, 2018.

[116] K. Vincent, C. P. G. Dona, T. J. Albert, and C. L. Dahia, "Age-related molecular changes in the lumbar dorsal root ganglia of mice: signs of sensitization, and inflammatory response," *JOR Spine*, vol. 3, article e1124, 2020.

[117] D. Scuteri, M. T. Corasaniti, P. Tonin, P. Nicotera, and G. Bagetta, "Role of CGRP pathway polymorphisms in migraine: a systematic review and impact on CGRP mAbs migraine therapy," *The Journal of Headache and Pain*, vol. 22, p. 87, 2021.

[118] S. Iyengar, K. W. Johnson, M. H. Ossipov, and S. K. Aurora, "CGRP and the trigeminal system in migraine," *Headache*, vol. 59, pp. 659–681, 2019.

[119] S. T. Chen and J. W. Wu, "A new era for migraine: the role of calcitonin gene-related peptide in the trigeminovascular system," *Progress in Brain Research*, vol. 255, pp. 123–142, 2020.

[120] D. Goel, K. Un Nisa, M. I. Reza, Z. Rahman, and S. Aamer, "Aberrant DNA methylation pattern may enhance susceptibility to migraine: a novel perspective," *CNS & Neurological Disorders Drug Targets*, vol. 18, pp. 504–515, 2019.

[121] P. L. Durham, P. X. Dong, K. T. Belasco et al., "Neuronal expression and regulation of CGRP promoter activity following viral gene transfer into cultured trigeminal ganglia neurons," *Brain Research*, vol. 997, pp. 103–110, 2004.

[122] K. Y. Park and A. F. Russo, "Control of the calcitonin gene-related peptide enhancer by upstream stimulatory factor in trigeminal ganglion neurons," *The Journal of Biological Chemistry*, vol. 283, pp. 5441–5451, 2008.

[123] K. Y. Park, J. R. Fletcher, A. C. Raddant, and A. F. Russo, "Epigenetic regulation of the calcitonin gene-related peptide gene in trigeminal glia," *Cephalalgia*, vol. 31, pp. 614–624, 2011.

[124] T. J. Viney, T. W. Schmidt, W. Gierasch et al., "Regulation of the cell-specific calcitonin/calcitonin gene-related peptide

enhancer by USF and the Foxa2 forkhead protein," *The Journal of Biological Chemistry*, vol. 279, pp. 49948–49955, 2004.

[125] Z. Zhao, M. Lan, J. Li et al., "The proinflammatory cytokine TNFα induces DNA demethylation-dependent and -independent activation of interleukin-32 expression," *The Journal of Biological Chemistry*, vol. 294, pp. 6785–6795, 2019.

[126] Z. Zhao, Z. Zhang, J. Li et al., "Sustained TNF-α stimulation leads to transcriptional memory that greatly enhances signal sensitivity and robustness," *eLife*, vol. 9, article e61965, 2020.

[127] L. H. Lassen, P. A. Haderslev, V. B. Jacobsen, H. K. Iversen, B. Sperling, and J. C. Olesen, "CGRP may play a causative role in migraine," *Cephalalgia*, vol. 22, pp. 54–61, 2002.

[128] R. Moreno-Mayordomo, M. Ruiz, J. Pascual et al., "CALCA and TRPV1 genes polymorphisms are related to a good outcome in female chronic migraine patients treated with onabotulinumtoxin A," *The Journal of Headache and Pain*, vol. 20, p. 39, 2019.

[129] S. Buervenich, F. Xiang, O. Sydow et al., "Identification of four novel polymorphisms in the calcitonin/alpha-CGRP (CALCA) gene and an investigation of their possible associations with Parkinson disease, schizophrenia, and manic depression," *Human Mutation*, vol. 17, pp. 435-436, 2001.

[130] S. Menon, J. Buteri, B. Roy et al., "Association study of calcitonin gene-related polypeptide-alpha (CALCA) gene polymorphism with migraine," *Brain Research*, vol. 1378, pp. 119–124, 2011.

[131] H. Wang and J. J. Unternaehrer, "Epithelial-mesenchymal transition and cancer stem cells: at the crossroads of differentiation and dedifferentiation," *Developmental Dynamics*, vol. 248, pp. 10–20, 2019.

[132] M. Dallmayer, J. Li, S. Ohmura et al., "Targeting the CALCB/RAMP1 axis inhibits growth of Ewing sarcoma," *Cell Death & Disease*, vol. 10, p. 116, 2019.

[133] Y. Haibe, M. Kreidieh, H. El Hajj et al., "Resistance mechanisms to anti-angiogenic therapies in cancer," *Frontiers in Oncology*, vol. 10, p. 221, 2020.

[134] Q. C. Liu, F. Chen, C. Y. Wu et al., "CALCB splice region pathogenic variants leading to plasma cell neurotropic enrichment in type 1 autoimmune pancreatitis," *Cell Death & Disease*, vol. 8, article e2591, 2017.

[135] T. Gluexam, A. M. Grandits, A. Schlerka et al., "CGRP signaling via CALCRL increases chemotherapy resistance and stem cell properties in acute myeloid leukemia," *International Journal of Molecular Sciences*, vol. 20, 2019.

[136] H. Fernandes-Silva, J. Correia-Pinto, and R. S. Moura, "Canonical sonic hedgehog signaling in early lung development," *Journal of developmental biology*, vol. 5, 2017.

[137] L. Han, J. Jiang, M. Xue et al., "Sonic hedgehog signaling pathway promotes pancreatic cancer pain via nerve growth factor," *Regional Anesthesia and Pain Medicine*, vol. 45, pp. 137–144, 2020.

[138] L. Han, J. Ma, W. Duan et al., "Pancreatic stellate cells contribute pancreatic cancer pain via activation of sHH signaling pathway," *Oncotarget*, vol. 7, pp. 18146–18158, 2016.

[139] M. Shivaraju, U. K. Chitta, R. M. Grange et al., "Airway stem cells sense hypoxia and differentiate into protective solitary neuroendocrine cells," *Science*, vol. 371, pp. 52–57, 2021.

[140] A. Garg, P. Sui, J. M. Verheyden, L. R. Young, and X. Sun, "Consider the lung as a sensory organ: a tip from pulmonary neuroendocrine cells," *Current Topics in Developmental Biology*, vol. 132, pp. 67–89, 2019.

[141] H. J. Chen, A. Poran, A. M. Unni et al., "Generation of pulmonary neuroendocrine cells and SCLC-like tumors from human embryonic stem cells," *The Journal of Experimental Medicine*, vol. 216, pp. 674–687, 2019.

[142] P. Sui, D. L. Wiesner, J. Xu et al., "Pulmonary neuroendocrine cells amplify allergic asthma responses," *Science*, vol. 360, p. -eaan8546, 2018.

[143] G. Ferone, J. Y. Song, O. Krijgsman et al., "FGFR1 oncogenic activation reveals an alternative cell of origin of SCLC in Rb1/p 53 mice," *Cell Reports*, vol. 30, pp. 3837–3850.e3833, 2020.

[144] K. S. Park, M. C. Liang, D. M. Raiser et al., "Characterization of the cell of origin for small cell lung cancer," *Cell Cycle*, vol. 10, pp. 2806–2815, 2011.

[145] K. D. Sutherland, N. Proost, I. Brouns, D. Adriaensen, J. Y. Song, and A. Berns, "Cell of origin of small cell lung cancer: inactivation of Trp53 and Rb1 in distinct cell types of adult mouse lung," *Cancer Cell*, vol. 19, pp. 754–764, 2011.

[146] J. R. Rock, C. E. Barkauskas, M. J. Cronce et al., "Multiple stromal populations contribute to pulmonary fibrosis without evidence for epithelial to mesenchymal transition," *Proceedings of the National Academy of Sciences of the United States of America*, vol. 108, pp. E1475–E1483, 2011.

[147] S. K. Liang, C. C. Hsu, H. L. Song et al., "FOXM1 is required for small cell lung cancer tumorigenesis and associated with poor clinical prognosis," *Oncogene*, vol. 40, pp. 4847–4858, 2021.

[148] M. Toda, T. Suzuki, K. Hosono et al., "Neuronal system-dependent facilitation of tumor angiogenesis and tumor growth by calcitonin gene-related peptide," *Proceedings of the National Academy of Sciences of the United States of America*, vol. 105, pp. 13550–13555, 2008.

[149] P. Dey, J. Baddour, F. Muller et al., "Genomic deletion of malic enzyme 2 confers collateral lethality in pancreatic cancer," *Nature*, vol. 542, pp. 119–123, 2017.

[150] Z. Du, H. Zhang, Q. Chen, Y. Gao, and B. Sun, "Intranasal calcitonin gene-related peptide protects against focal cerebral ischemic injury in rats through the Wnt/β-catenin pathway," *Medical Science Monitor*, vol. 24, pp. 8860–8869, 2018.

[151] Q. Liu, L. Guo, S. Zhang, J. Wang, X. Lin, and F. Gao, "PRSS1 mutation: a possible pathomechanism of pancreatic carcinogenesis and pancreatic cancer," *Molecular Medicine*, vol. 25, p. 44, 2019.

[152] Z. Tan, L. Gao, Y. Wang et al., "PRSS contributes to cetuximab resistance in colorectal cancer," *Science Advances*, vol. 6, p. eaax5576, 2020.

[153] A. Wallrapp, P. R. Burkett, S. J. Riesenfeld et al., "Calcitonin gene-related peptide negatively regulates alarmin-driven type 2 innate lymphoid cell responses," *Immunity*, vol. 51, pp. 709–723.e706, 2019.

[154] T. G. Phan and P. I. Croucher, "The dormant cancer cell life cycle," *Nature Reviews. Cancer*, vol. 20, pp. 398–411, 2020.

[155] S. Cherry and K. W. Lynch, "Alternative splicing and cancer: insights, opportunities, and challenges from an expanding view of the transcriptome," *Genes & Development*, vol. 34, pp. 1005–1016, 2020.

[156] R. Bai, R. Wan, C. Yan, Q. Jia, J. Lei, and Y. Shi, "Mechanism of spliceosome remodeling by the ATPase/helicase Prp2 and its coactivator Spp2," *Science*, vol. 371, 2021.

[157] Z. Yang, W. Qi, L. Sun, H. Zhou, B. Zhou, and Y. Hu, "DNA methylation analysis of selected genes for the detection of early-stage lung cancer using circulating cell-free DNA,"

Advances in Clinical and Experimental Medicine, vol. 28, pp. 355–360, 2019.

[158] A. Widschwendter, H. M. Müller, H. Fiegl et al., "DNA methylation in serum and tumors of cervical cancer patients," *Clinical Cancer Research*, vol. 10, pp. 565–571, 2004.

[159] N. Yang, E. R. Nijhuis, H. H. Volders et al., "Gene promoter methylation patterns throughout the process of cervical carcinogenesis," *Cellular Oncology*, vol. 32, pp. 131–143, 2010.

[160] M. Brait, S. Begum, A. L. Carvalho et al., "Aberrant promoter methylation of multiple genes during pathogenesis of bladder cancer," *Cancer Epidemiology, Biomarkers & Prevention*, vol. 17, pp. 2786–2794, 2008.

[161] C. Olk-Batz, A. R. Poetsch, P. Nöllke et al., "Aberrant DNA methylation characterizes juvenile myelomonocytic leukemia with poor outcome," *Blood*, vol. 117, pp. 4871–4880, 2011.

[162] S. A. Hobson, S. E. McNeil, F. Lee, and K. D. Rodland, "Signal transduction mechanisms linking increased extracellular calcium to proliferation in ovarian surface epithelial cells," *Experimental Cell Research*, vol. 258, pp. 1–11, 2000.

[163] M. T. Goodman, R. Ferrell, K. Mcduffie et al., "Calcitonin gene polymorphism *CALCA-624 (T/C)* and ovarian cancer," *Environmental and Molecular Mutagenesis*, vol. 46, pp. 53–58, 2005.

[164] C. Dai, B. Zhang, Y. Liao et al., "CALCB rs3829222 T/T genotype and low expression of CALCB are high-risk factors for adenoid cystic carcinoma of salivary gland," *Disease Markers*, vol. 2021, Article ID 5546858, 5 pages, 2021.

Hindawi
Oxidative Medicine and Cellular Longevity
Volume 2022, Article ID 3647744, 8 pages
https://doi.org/10.1155/2022/3647744

Research Article

Overexpression of miR-126 Protects Hypoxic-Reoxygenation-Exposed HUVEC Cellular Injury through Regulating LRP6 Expression

Md Sayed Ali Sheikh,[1] **A. Almaeen**,[2] **A. Alduraywish**,[1] **Basil Mohammed Alomair**,[1] **Umme Salma**,[3] **Li Fei**,[4] **and T. L. Yang**[4]

[1]*Department of Internal Medicine, College of Medicine, Jouf University, Sakaka, Saudi Arabia*
[2]*Department of Pathology, College of Medicine, Jouf University, Sakaka, Saudi Arabia*
[3]*Department of Gynecology and Obstetrics, College of Medicine, Jouf University, Sakaka, Saudi Arabia*
[4]*Department of Cardiology, Xiangya Hospital, Central South University, China*

Correspondence should be addressed to Md Sayed Ali Sheikh; drsheikh07@hotmail.com

Received 22 October 2021; Accepted 23 December 2021; Published 17 January 2022

Academic Editor: ChangHui Shen

The aim of the study was to explore the clinical impact of circulatory miR-126 as a candidate for novel biomarker in patients with coronary artery disease (CAD) and its protective role against hypoxia/reoxygenation- (H/R-) exposed HUVEC cellular injury. A total of 278 subjects, which included 153 subjects with angiographically confirmed CAD, 70 unstable angina subjects, and 55 healthy individuals, along with 18-hour HR-induced HUVECs were recruited in this study. Plasma miR-126 levels were significantly downregulated in stable and unstable CAD patients as well as 18-hour HR-exposed HUVECs as compared with controls. Stable and unstable CAD subjects were significantly differentiated from healthy individuals with a predictive value of AUC 0.903 and 0.923, respectively. Moreover, peripheral circulatory miR-126 expressions in elderly (71-90 years) stable and unstable CAD patients were comparatively lower than younger (30-50 years) subjects. The caspase-3 activity, intracellular ROS concentrations, and cellular viabilities were evidently increased in 18-hour HR-exposed HUVECs than in normal cells ($P < 0.001$). On the contrary, mimic expressions of miR-126 prominently reduced caspase-3 activity and intracellular ROS levels and markedly enhanced HUVEC cellular viabilities ($P < 0.001$). LRP6 expressions were significantly elevated in HR-induced HUVECs, whereas overexpression of miR-126 remarkably decreased LRP6 expressions ($P < 0.001$). Plasma miR-126 could be used as a novel biomarker for early prediction of CAD subjects. Overexpression of miR-126 significantly improved HUVEC cellular viabilities by downregulation of LRP6 protein expression, suggesting a potential therapeutic target for CAD patients.

1. Introduction

Ischemic coronary artery disease (CAD) is a predominant cause of high morbidity and mortality among all the races in both genders all over the world. The CAD incidence rate is amenable for increase by approximately 20% over the next nine years. Early detection of major risk factors, prompt diagnosis, and proper management can significantly decline morbidity and mortality [1]. Globally, invasive coronary angiogram (CAG) has been widely used to confirm the diagnosis of atherosclerotic ischemic coronary heart disease, but it has some limitations in its availability and unsuitability for extremely senescent patients and cases of end-stage renal failure. Therefore, noninvasive universal clinical biomarkers are required by clinicians to diagnose all types of CAD subjects. In the 20th century, advanced percutaneous transluminal coronary angioplasty (PTCA) has become the treatment of choice for the CAD patients, yet multivessel lesions and complex left main coronary occlusion are not manageable by such a treatment modality. As a result, it is necessary to

discover newer molecular targets for the management of CAD patients. Coronary artery disease occurs mainly due to progressive chronic atherosclerotic inflammation in the coronary arteries. Several research groups have demonstrated that different atherosclerotic linked microRNAs (miR-217, miR-200c, miR-146a, miR-34a, miR-221, and miR-19b) have an essential role in terms of development and progression of coronary atherosclerosis [2–4].

It was demonstrated that altered miR-126 is implicated in endothelial dysfunction, generation of stable atherosclerotic plaque and subsequently erosion, rupture of atherosclerotic plaque, and formation of thrombus within coronary artery that leads to acute coronary syndrome through several inflammatory signaling pathways including MAPK, PDGF, IGF1, and VCAM-1 [3–5].

In fact, low-density lipoprotein receptor-related protein 6 (LRP6) is one of the members of the low-density lipoprotein receptor (LDLR) family and significantly regulates lipid metabolism via several Wnt/β-catenin signaling pathways and is critically involved in various cardiovascular diseases including coronary artery disease [6]. Moreover, accumulating evidence showed that LRP6 expression levels were highly increased in human atherosclerotic coronary arteries and linked with platelet-derived growth factor receptor β [7]. Xu et al. reported mutations of LRP6 were genetically associated with early onset of coronary artery disease [8].

Several research groups have demonstrated that plasma miR-126 levels were remarkably deregulated in both single and complex CAD lesions as well as in acute coronary syndrome [9, 10]. Yang et al. explored the protective role of miR-126 against hypoxia/reoxygenation- (H/R-) induced injury on human cardiac microvascular endothelial cells (HCMECs) by inhibiting inflammatory response through regulating PI3K/Akt/eNOS signaling pathway [11]. Moreover, Matilde et al.'s research group demonstrated that miR-126 prevents age-related endothelial senescence by targeting hypoxia-inducible factor-1α (HIF-1α), suggesting a new therapeutic modulation of age-associated coronary artery disease [12].

However, the relationship between miR-126 and LRP6 associated with coronary artery diseases and HR-exposed HUVECs are not fully explored. Therefore, the current study investigated the clinical significance of circulating miR-126 in CAD patients, and its protective effects against hypoxia/reoxygenation- (H/R-) induced HUVEC cellular injury and the underlying molecular mechanism linked with LRP6.

2. Materials and Methods

2.1. Human Participants. 153 stable angina subjects, 75 unstable angina participants, and 55 healthy populations were selected from Cardiology Department and Health Center of Xiangya Hospital of Central South University between January 2016 and July 2017. CAD was confirmed by two coronary interventional experts through invasive coronary angiogram, at least one major coronary artery with fifty or more than fifty percent atherosclerotic stenosis in both male and female subjects. According to ACC/ESC clinical guidelines, CAD patients were subcategorized into either stable or unstable groups. Patients with cardiomyopathy, COPD with pulmonary hypertension, rheumatic valvular heart diseases, heart failure, cerebrovascular accident, and implanted coronary stent or coronary artery bypass graft (CABG) were not included in this study. Well-matched age and gender, healthy controls who were free from cardiovascular diseases, chronic kidney or liver diseases, chronic inflammatory conditions, and malignancy were recruited. This study was carried out by adhering to Declaration of Helsinki Human Research Protocols, from all the participants, written informed consents were obtained prior to study, and the Ethical Review Board of Xiangya Hospital approved this research. Peripheral 5 mL venous blood samples were obtained from all the study subjects in EDTA-coated tubes. Within 30 minutes, all the samples were centrifuged twice: at 3,000 revolutions for 15 min at 4°C and at 15,000 revolutions for 10 min at 4°C, respectively; then cell and debris-free pure plasma was transferred in EP tubes and afterward preserved at −80°C for RNA extraction.

2.2. Cell Culture, Establishment of Hypoxia/Reoxygenation (H/R), and Transfection of HUVEC. Human umbilical vein endothelial cells (HUVECs) were obtained from the Cell Institute of Chinese Academy of Health Sciences (Shanghai, China). The cells were cultured in 6-well plates with Dulbecco's Modified Eagle's Medium (DMEM) containing 10 percent (*v*/*v*) heat-inactivated fetal bovine serum (FBS) in a 95% air and 5% CO_2 constant incubator at 37°C. For generation of hypoxic model, the HUVECs were subjected to 1% O_2, 5% CO_2, and 95% N_2 in a modular incubator using glucose, sodium pyruvate, and serum-free DMEM for 12 hours. After that, the cells were placed to a normoxic incubator maintaining 5% CO_2, 37°C temperature, and 95% air for 6 hours to enhance hypoxia/reoxygenation-induced HUVEC cellular injury.

Lipofectamine 2000 reagents at 3 mg/mL concentrations were used for the transfections of HUVECs following the manufacturer's protocols. Mimic-miR-126 (50 nmol/L mimic) was used to regulate the mimic expression of miR-126 in HUVECs, and 50 nmol/L mimic-negative control (NC), that is similar in nature to mimic, was served as an inner control.

2.3. Luciferase Reporter Activity Assays. The target gene of miR-126 was confirmed by Luciferase reporter gene analysis. miR-126 was predicted with the complementary sequence of 3′-UTR of LRP6 by Target scan (http://www.targetscan.org/), and 24-well plate HUVECs were transfected with Lipofectamine 2000, mimic-miR-126, and NC-miR-126 for 18 hours. The luciferase activities were demonstrated through Dual-Luciferase Reporter Assay kits by following the company's instructions (Beyotime, Jiangsu, China), and the values were normalized to Renilla, and the data were measured by fluorescent activity.

2.4. Measurement of ROS, Caspase-3, and Cellular Proliferation. After proper hypoxia/reoxygenation treatment, 5 μM dichlorodihydrofluorescein diacetate (DCFH-DA) was added into 96-well black plate cultured HUVECs

and incubated for 30 minutes at 37°C [DCFH-DA, Molecular Probes, Eugene, USA]. After that, cells were washed twice by PBS, and finally, intracellular ROS levels were detected at 490 nm wavelengths through a SpectraMax microplate reader (Molecular Devices, Sunnyvale, CA).

Caspase-3 activities were demonstrated from healthy and treated HUVECs by adding 100 μL caspase-3 substrate (Ac-DEVD-pNA) (Beyotime, Shanghai, China) into 96-well plates, incubated for 2 hours at 37°C, and absorbance was measured at the 405 nm wavelength by microplate SpectraMax absorbance reader (Molecular Devices, Sunnyvale, CA).

CCK-8 reagents were used according to the manufacturer's protocols for the detection of cellular viabilities (Beyotime, Shanghai, China). The 10 μL CCK-8 solution was added into each 96-well culture plate's normoxic and HR-exposed HUVECs and inoculated for 2 hours at 37°C; then, cellular growths were assessed by a microplate absorbance reader at the wavelength of 450 nm (Molecular Devices, Sunnyvale, CA, USA).

2.5. Extraction of RNA and Analysis of miRNA Expressions. Total pure RNAs were isolated from human plasma and normoxic and treated HUVECs by using the TRIzol reagent (Invitrogen, CA, USA) following the company's guidelines. The primers of miR-126, mimic-miR-126, NC-miR-126, and inner control miR-156a were obtained from RiboBio (Guangzhou, China). LRP6 and endogenous control β-actin primers were collected from Sangon Biotech (Shanghai, China). Expression of miR-126 and LRP6 was determined through quantitative real-time polymerase chain reaction (qRT-PCR) technique by using Master Mix SYBR Green PCR reagents. In our previous studies, the measurement of miRNAs' expressions via qRT-PCR protocols was explained in details [13, 14].

2.6. Statistical Data Analysis. Statistical version 21 software (SPSS 21.0) was applied for the analysis of the data. For continuous variation, an independent-sample t -test, the Mann–Whitney, and one-way ANOVA were performed between groups. Among groups for categorical variation, the chi-square (χ^2) and Fischer's exact tests were used. The clinical impact of plasma miR-126 as a biomarker was evaluated with Receiver Operating Characteristic (ROC) curve. A value of $P < 0.05$ indicated statistically significant results.

3. Results

3.1. Baseline and Clinical Characteristics of the Study Groups. The demographic general characteristics of the healthy, stable, and unstable participants in this study are detailed in Table 1. Among 153 patients with stable angina cases, 85 were males and 68 were females and their ages ranged between 30 and 90 years (65.1 ± 12.4); within the 70 unstable angina patients, 43 were males and 27 were females, and their ages ranged from 30 to 90 years (68.5 ± 14.8), and 55 healthy volunteers (30 males and 25 females), aged between 30 and 90 years (57.2 ± 11.3), were enrolled in the study, as well. Family history of coronary heart disease and hs-CRP levels were evidently higher in CAD (either stable or unstable angina cases) than control healthy individuals ($P < 0.001$). However, other variables such lipid profiles, AST, ALT, blood pressure, heart rate, glucose concentrations, cardiac function, smoking status, essential hypertension, and creatinine levels among healthy, stable, and unstable participants were compared but appeared statistically insignificant.

3.2. Expression of Plasma miR-126 in Coronary Artery Disease Patients and Hypoxia/Reoxygenation HUVEC Cells. Plasma miR-126 expression levels were significantly downregulated in stable coronary artery disease and unstable coronary artery disease patients by 2.7 (0.822 ± 0.29) and 3.2 (0.695 ± 0.29) folds, respectively, as compared with healthy participants (2.22 ± 0.67) ($P < 0.001$) (Figure 1(a)). Circulating plasma miR-126 concentrations were lower in unstable CAD patients than in stable CAD patients but statistically insignificant. Moreover, expressions of miR-126 were prominently downregulated in 18-hour hypoxia/reoxygenation- (H/R-) exposed HUVECs by 2.5 (1.130 ± 0.10) folds than normally incubated HUVECs (0.45 ± 0.16) ($p < 0.001$) (Figure 1(b)).

3.3. Relationship of miR-126 Expression with Aging and Gender. Circulating miR-126 expressions in healthy male and female (71-90 yrs) subjects were comparatively lower than younger male and female healthy participants in the age groups of 30-50 yrs and 51-70 yrs ($P > 0.05$) (Figure 2(a)). In either stable or unstable CAD subjects of both genders, circulating miR-126 levels in the extremely aged group (71-90 yrs) were significantly lower compared to those in younger male and female (30-50 yrs and 51-70 yrs) subjects ($P < 0.001$) (Figures 2(b) and 2(c)). These results suggested that underexpression of circulating miR-126 has strong correlation with geriatric people. However, the miR-126 expressions among the 30-50 yrs and 51-70 yrs groups in stable and unstable CAD patients of either sex were not significantly different. It was noted that the expression levels of miR-126 were the lowest in unstable angina cases followed by stable and healthy subjects. Gender wise, no significant variation in plasma miR-126 concentrations across all study groups (i.e., healthy, stable, and unstable angina groups) was discernible ($P > 0.05$) (Figures 2(d)–2(f)).

3.4. Clinical Significance of Plasma miR-126 for CAD Patients. To investigate the clinical significance of circulatory miR-126 as a useful diagnostic biomarker of stable and unstable CAD, area under the Receiver Operating Characteristic (ROC) curve analyses were performed. ROC analysis showed that miR-126 strongly distinguished stable and unstable CAD subjects from healthy subjects with their high AUC predictive values were 0.903 (sensitivity 0.90%, specificity 0.95%) and 0.928 (sensitivity 0.92%, specificity 0.94%), respectively (highly significant with $P < 0.001$) (Figures 3(a) and 3(b)). Moreover, area under curve (AUC) values exhibited no significant correlation between stable and unstable CAD patients. These results indicated

Table 1: Clinical data of the study population.

Variables	Healthy volunteers (55)	Stable CAD group (153)	Unstable CAD group (70)	P_1	P_2	P_3
Age (years)	57.2 ± 11.3	65.1 ± 12.4	68.5 ± 14.8	0.186	0.157	0.319
Male/female	30/25	85/68	43/27	0.122	0.504	0.183
Current smoker	59% (32)	72% (110)	75% (52)	0.708	0.643	1.00
Essential hypertension	—	74% (113)	82% (57)	—	—	0.068
Hyperlipidemia	—	85% (130)	89% (62)	—	—	0.274
Family history	9% (5)	63% (96)	66% (46)	0.000	0.000	0.832
Diabetes mellitus	—	26% (40)	32% (22)	—	—	0.159
SBP (mmHg)	122.2 ± 10.3	129.4 ± 14.2	132.8 ± 12.7	0.085	0.066	0.114
DBP (mmHg)	74.6 ± 6.8	80.5 ± 7.3	82.1 ± 9.5	0.094	0.081	0.132
Heart rate (beats/min)	71.9 ± 8.6	75.2 ± 10.3	78.4 ± 11.2	0.407	0.375	0.729
Fasting glucose (mmol/L)	4.79 ± 0.5	5.06 ± 0.9	5.3 ± 1.2	0.073	0.069	0.251
Cr (μmol/L)	80.9 ± 18.1	82.5 ± 22.7	85.6 ± 24.8	0.073	0.069	0.148
hs-CRP (mg/L)	2.7 ± 1.68	11.3 ± 9.7	16.5 ± 11.4	0.000	0.000	0.091
Total cholesterol	4.2 ± 0.73	4.39 ± 0.75	4.56 ± 1.3	0.084	0.075	0.116
HDL-C (mmol/L)	1.1 ± 0.4	0.92 ± 0.6	0.83 ± 0.7	0.095	0.087	0.123
Triglyceride (mmol/L)	1.26 ± 0.5	1.39 ± 0.9	1.48 ± 0.7	0.099	0.095	0.104
LDL-C (mmol/L)	2.21 ± 1.3	2.44 ± 1.7	2.51 ± 1.6	0.219	0.157	0.289
Left ventricular ejection fraction (%)	61.7 ± 9.4	58.7 ± 10.3	54.2 ± 10.7	0.326	0.271	0.467
AST (U/L)	11 ± 7.6	13 ± 9.3	16 ± 7.1	0.794	0.592	0.813
ALT (U/L)	14 ± 5.6	18 ± 8.2	20 ± 7.6	0.203	0.177	0.369

CAD: coronary artery disease patients; SBP: systolic blood pressure; DBP: diastolic blood pressure; AST: aspartate aminotransferase; ALT: alanine aminotransferase; P_1: healthy participants and stable CAD; P_2: health control subject versus unstable CAD; P_3: stable CAD versus unstable CAD patients.

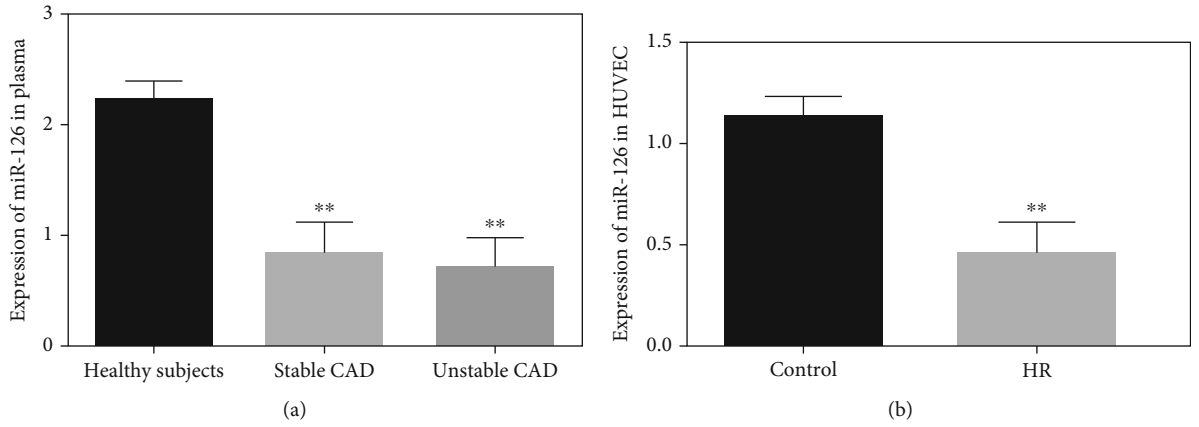

Figure 1: Circulatory miR-126 expression in CAD and HUVECs. (a) miR-126 concentrations between stable, unstable, and healthy individuals. (b) The expression levels of miR-126 within control and 18-hour hypoxia/reoxygenation HUVECs; miR-156a was used as an inner control. $^{**}P < 0.001$.

circulatory miR-126 may be considered a potential diagnostic biochemical marker for early prediction of CAD subjects.

3.5. Expression of miR-126 in HUVEC Cells and Luciferase Analysis. HUVECs were exposed to 12-hour hypoxic and 6-hour normoxic conditions. The miR-126 expression levels were remarkably downregulated in H/R-injured HUVECs compared with normal HUVECs ($P < 0.001$). Conversely, miR-126 concentrations were markedly upregulated in H/R-exposed HUVECs treated with mimic-miR-126. However, no obvious differences were observed in miR-126 expressions between the H/R and negative control (NC) groups (Figure 4(a)). Moreover, luciferase activity levels were significantly elevated by 2-folds in H/R-incubated HUVEC (1.804 ± 0.11) cells than controls (0.903 ± 0.08), and there was no significant effect in negative controls. The luciferase

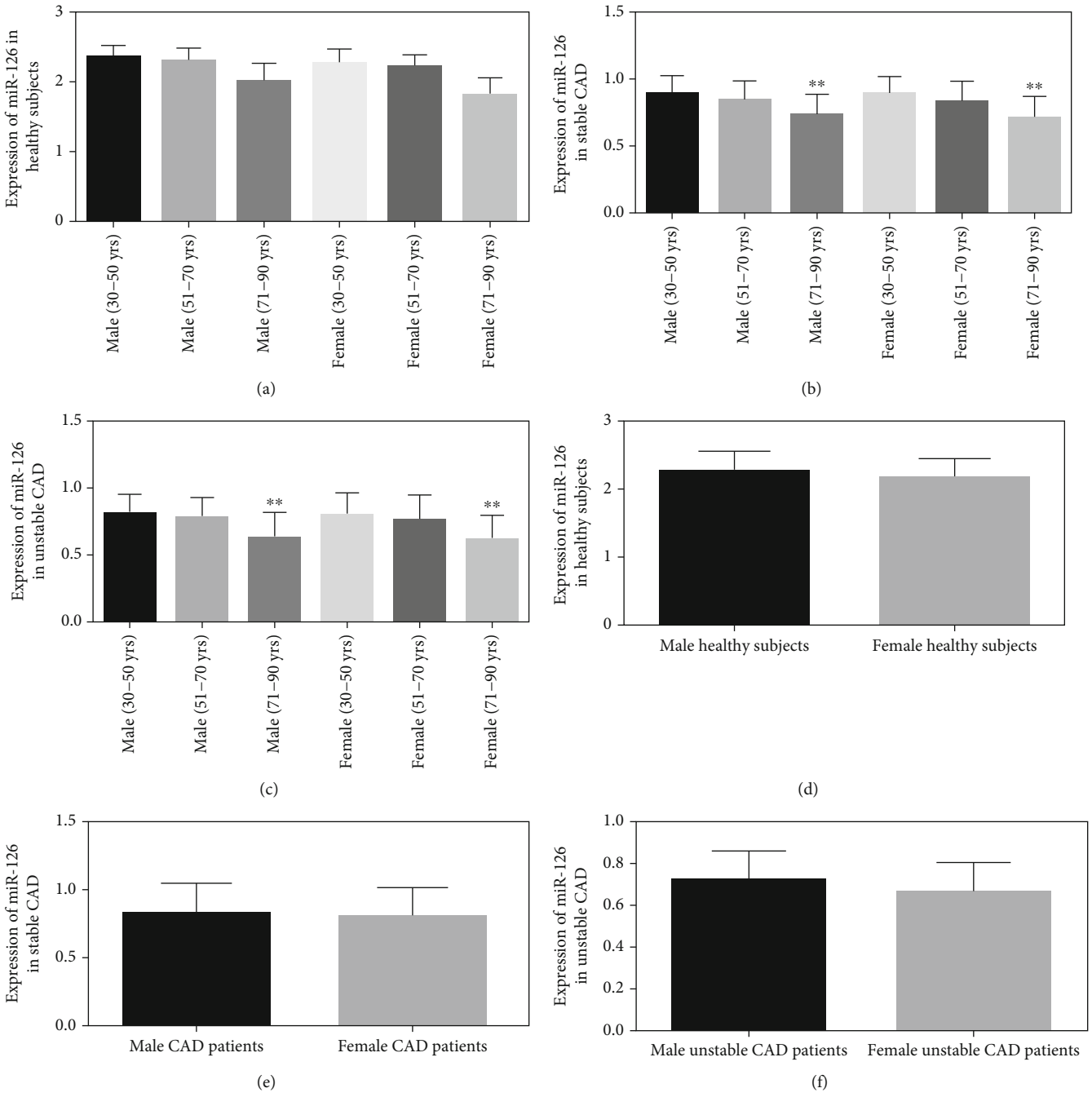

Figure 2: Expression patterns of circulatory miR-126 among different age groups in both male female subjects. (a) Plasma miR-126 expression among healthy subjects. (b) Circulatory miR-126 concentrations in stable CAD subjects. (c) Expression of plasma miR-126 in unstable angina patients. (d) Healthy male versus healthy female subjects' miR-126 levels. (e) Male versus female CAD subjects' plasma miR-126. (f) The level of miR-126 among unstable male and female CAD patients. $^{**}P < 0.001$.

expressions were remarkably regulated by the mimic-miR-126 in H/R-exposed HUVECs (Figure 4(b)).

3.6. Effects of Mimic-miR-126 on LRP6 and Cellular Viability in H/R-Exposed HUVEC Cells. Compared with normoxic cells, the LRP6 levels were prominently upregulated in hypoxia/reoxygenation- (H/R-) incubated HUVECs which amazingly reversed back near to those of the control group upon transfection with mimic-miR-126. There was no effect observed between the H/R and negative control (NC) groups, indicating that miR-126 significantly regulated LRP6 expression levels in healthy and H/R-injured HUVECs (Figure 5(a)). Similarly, caspase-3 activities were highly elevated in H/R-induced HUVECs compared with normally cultured cells but, again, markedly reduced by transfecting H/R-injured HUVECs with mimic-miR-126. Among the NC group, there was no effect on caspase-3 activities (Figure 5(b)). The aforementioned findings strongly

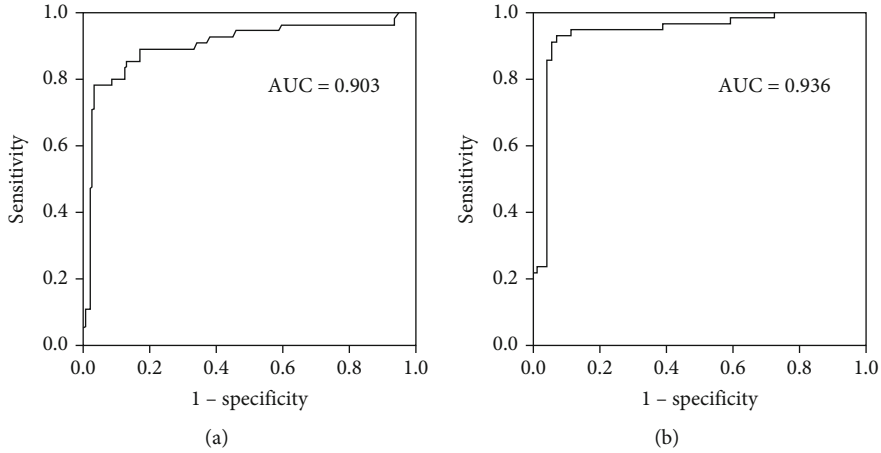

Figure 3: Diagnostic significance of plasma miR-126 for CAD subjects was evaluated by ROC curve analysis. (a) Healthy subjects versus stable CAD patients (AUC 0.903). (b) Healthy individuals versus unstable CAD subjects (AUC 0.936).

acknowledged that overexpression of miR-126 may exert a protective role against cellular damage in the H/R environment. The intracellular ROS concentrations were highly increased in H/R-induced HUVECs than those in controls. On the other hand, ROS levels in H/R-exposed HUVECs transfected with mimic-miR-126 were remarkably decreased compared with H/R groups, but ROS levels within NC and HR groups were not significantly changed, suggesting that mimic-miR-126 has major effects on preventing oxidative stress associated HUVEC cellular injuries during H/R conditions (Figure 5(c)). The HUVEC cellular viability was evidently reduced in H/R-exposed groups as compared with normal control groups. In contrast, overexpression of miR-126 by the mimic-miR-126 in H/R-cultured HUVEC group imparted a better outlook of cellular viability, while no clear changes were demonstrated in the HR and NC groups, suggesting that mimic-miR-126 may play an essential role in cellular protection against damage in H/R situations (Figure 5(d)).

4. Discussion

Atherosclerotic ischemic coronary heart disease is the single most important issue of premature death, and it imposes a major economic burden on the society across the world. Early identification and prompt appropriate management have a significant impact to reduce CAD mortality incidence. In the present study, we explored the clinical impact of miR-126 in CAD patients and its potential role to protect H/R-induced HUVECs cell damage. This study found that circulating miR-126 expression levels were evidently downregulated in stable and unstable CAD patients than healthy subjects, though miR-126 concentrations were comparatively lower in unstable angina groups than in stable groups, but the differences were not significant. Wang et al. demonstrated miR-126 expressions were obviously downregulated in the peripheral circulation of stable and unstable CAD patients compared with control subjects. Another study also reported expression of circulating miR-126 levels in single and multivessel CAD subjects was considerably lower than healthy subjects [9, 15].

The present research reported that miR-126 had significant correlation with CAD and aging. Circulating plasma miR-126 concentrations were evidently downregulated in geriatric (71-90 years) stable and unstable CAD patients of either sex as compared with comparatively younger age (30-50 years) patients. However, the expression patterns of peripheral circulatory miR-126 among healthy, stable, and unstable CAD groups did not show significant differences based on gender. Even among healthy volunteers, older male and female (71-90 years) participants had lower plasma miR-126 concentrations than the younger (30-50 years) did, but statistically nonsignificant. Very recently, Alessia et al. demonstrated miR-126 has linked with Fabry disease (FD) and premature aging [16]. Another study showed that in the middle age type-2 diabetic patients, senescence was associated with reduced miR-126 levels [17].

Diagnostic significance of circulatory miR-126 levels was determined through ROC curve analysis. The CAD patients, either stable or unstable, were strongly demarcated from healthy subjects with high sensitivity and specificity and AUC of 0.903 and 0.936, respectively, and that was highly significant statistically. However, utilization of circulatory miR-126 levels in differentiation between stable and unstable CAD groups was nonsignificant. These results indicated downregulated plasma miR-126 might serve as a useful noninvasive biomarker for early evaluation of CAD patients which is supported by other clinical studies [9, 15]. This study demonstrated hs-CRP concentrations being significantly higher in unstable and stable CAD patients in reference to the healthy participants. Our prior study also reported that elevated hs-CRP is linked with coronary artery disease and atherosclerosis which requires more molecular studies to discover the underlying mechanisms. Worth mentioning, family history was found to have a strong association with CAD [18].

It has been well known that mutation or dysregulation of LRP6 proteins is directly associated with oxidative stress, dyslipidemia, atherosclerosis, and coronary artery disease

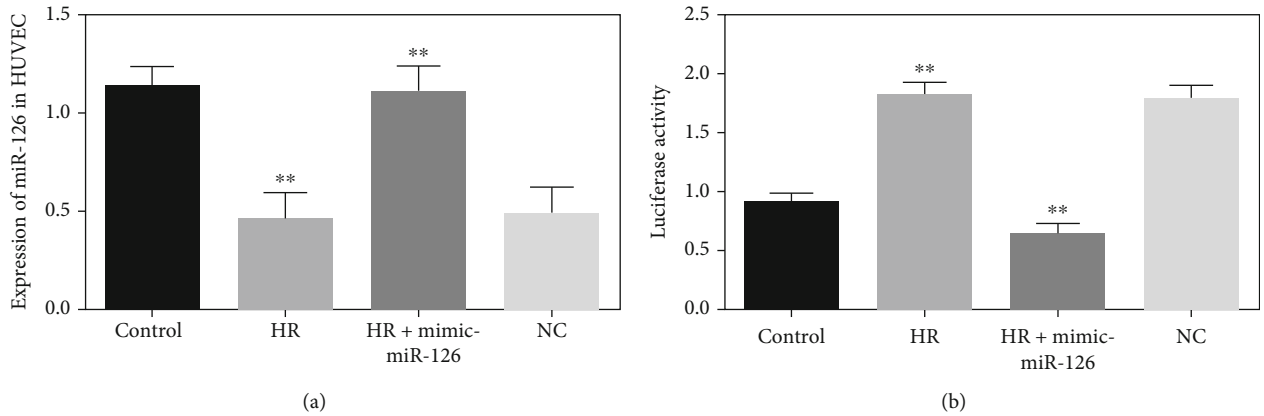

Figure 4: Expression of miR-126 in HUVECs and detection of the target gene. (a) Expression of miR-126 in normoxic, HR, HR transfected with mimic-miR-126, and negative control (NC) in HUVECs. (b) Luciferase reporter gene analysis among normal culture, HR, HR with mimic-miR-126, and NC groups in HUVECs and normalized against the expressions of Renilla reniformis. $^{**}P < 0.001$.

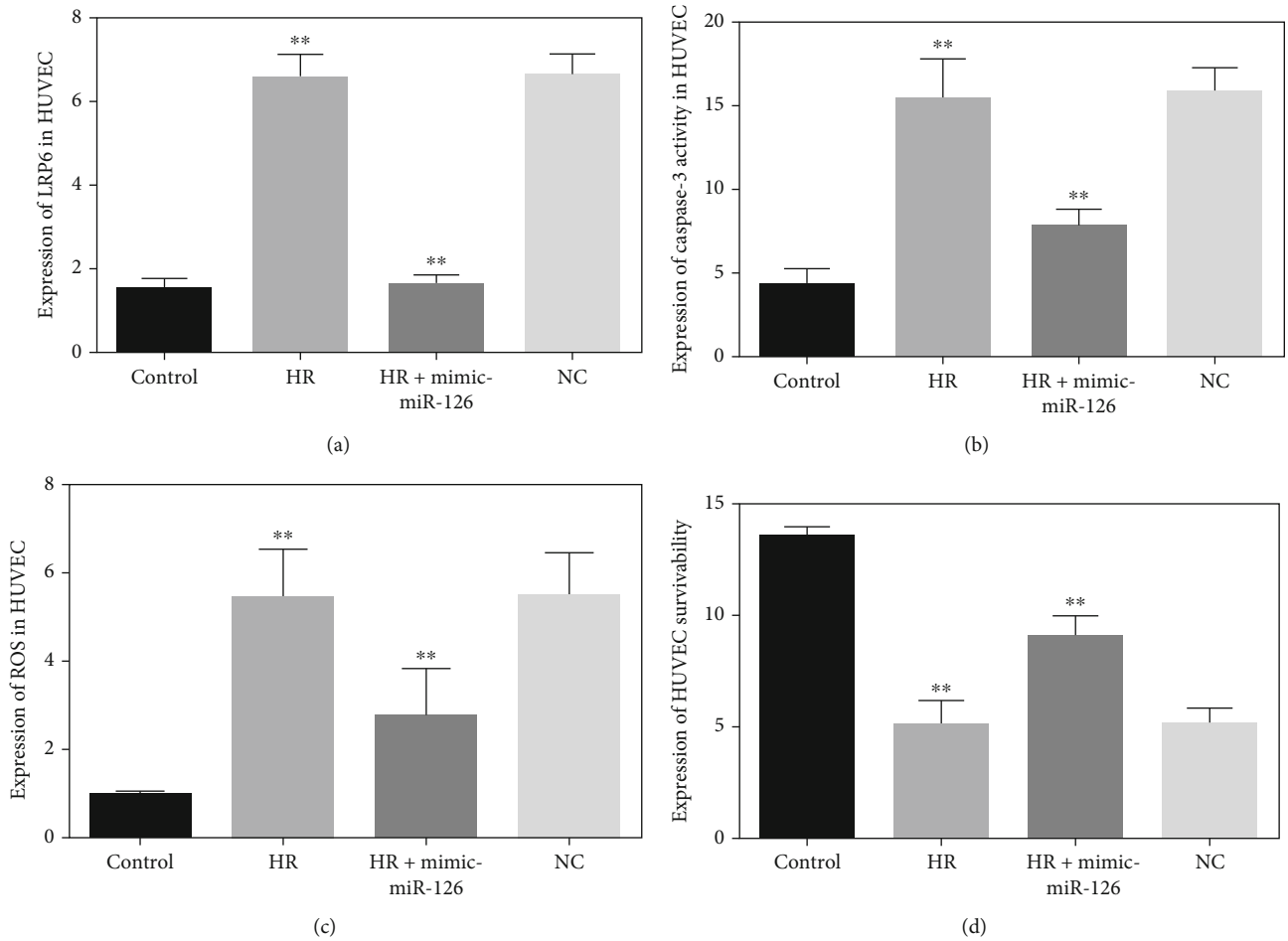

Figure 5: (a) LRP6 expression levels in normal, 18-hour HR, HR treated with mimic-miR-126, and NC groups in HUVECs. (b) Capase-3 expression between normal versus HR, HR versus HR plus mimic-miR-126, HR, and miR-126 NC groups in HUVECs. (c) Intracellular ROS concentrations in HUVECs between control and HR, HR, and HR transfected with mimic-miR-126, NC, and HR groups. $^{**}P < 0.001$.

[19–21]. Caspase-3 activities were enormously increased in 18-hour H/R-exposed HUVECs but remarkably reduced after transfection with mimic-126. Similarly, the intracellular ROS levels in H/R-stressed HUVECs were highly elevated, but markedly reduced after being incubated with mimic-miR-126. Furthermore, cellular viability noticeably decreased in H/R-HUVECs as compared with normal cells and exceptionally increased after transfection with mimic-

miR-126. These findings suggested that mimic-miR-126 protected against H/R-induced cellular injuries; hence, it could be a useful therapeutic target for atherosclerotic coronary artery disease. However, this is a single-center, tertiary-level hospital-based study with relatively small sample size. Therefore, multicentric larger clinical studies will be required to confirm the positive role miR-126 as a biomarker and promising therapeutic target in ischemic heart disease.

5. Conclusion

Downregulated plasma miR-126 levels may be able to serve as a new biomarker for early diagnosis of stable and unstable CAD patients, and mimic-miR-126 could be a potential therapeutic target in atherosclerotic coronary artery disease by inhibiting LRP6 protein expression.

Data Availability

From corresponding author upon reasonable request data will be available.

Conflicts of Interest

None of the authors have any conflicts of interest.

Acknowledgments

This work was funded by the Deanship of Scientific Research at Jouf University under grant no. DSR-2021-01-03159.

References

[1] S. S. Virani, A. Alonso, H. J. Aparicio et al., "Heart disease and stroke Statistics-2021 update: a report from the American Heart Association," *Circulation*, vol. 143, no. 8, pp. e254–e743, 2021.

[2] Y. Lu, T. Thavarajah, W. Gu, J. Cai, and Q. Xu, "Impact of miRNA in atherosclerosis," *Arteriosclerosis, Thrombosis, and Vascular Biology*, vol. 38, no. 9, pp. e159–e170, 2018.

[3] A. Churov, V. Summerhill, A. Grechko, V. Orekhova, and A. Orekhov, "MicroRNAs as potential biomarkers in atherosclerosis," *International Journal of Molecular Sciences*, vol. 20, no. 22, p. 5547, 2019.

[4] Y. Yan, D. Song, J. Wu, and J. Wang, "Long non-coding RNAs link oxidized low-density lipoprotein with the inflammatory response of macrophages in atherogenesis," *Frontiers in Immunology*, vol. 11, p. 24, 2020.

[5] X.-Z. Hao and H.-M. Fan, "Identification of miRNAs as atherosclerosis biomarkers and functional role of miR-126 in atherosclerosis progression through MAPK signalling pathway," *European Review for Medical and Pharmacological Sciences*, vol. 21, no. 11, pp. 2725–2733, 2017.

[6] S. Kang, "Low-density lipoprotein receptor-related protein 6-mediated signaling pathways and associated cardiovascular diseases: diagnostic and therapeutic opportunities," *Human Genetics*, vol. 139, no. 4, pp. 447–459, 2020.

[7] A. R. Keramati, R. Singh, A. Lin et al., "Wild-type LRP6 inhibits, whereas atherosclerosis-linked LRP6R611C increases PDGF-dependent vascular smooth muscle cell proliferation," *Proc Natl Acad Sci USA.*, vol. 108, no. 5, pp. 1914–1918, 2011.

[8] Y. Xu, W. Gong, J. Peng et al., "Functional analysis LRP6 novel mutations in patients with coronary artery disease," *PLoS One*, vol. 9, no. 1, article e84345, 2014.

[9] H.-Y. Li, X. Zhao, Y.-Z. Liu et al., "Plasma microRNA-126-5p is associated with the complexity and severity of coronary artery disease in patients with stable angina pectoris," *Cellular Physiology and Biochemistry*, vol. 39, no. 3, pp. 837–846, 2016.

[10] H. Ling, Z. Guo, Y. Shi, L. Zhang, and C. Song, "Serum exosomal microRNA-21, microRNA-126, and PTEN are novel biomarkers for diagnosis of acute coronary syndrome," *Frontiers in Physiology*, vol. 11, p. 654, 2020.

[11] H.-H. Yang, Y. Chen, C.-Y. Gao, Z.-T. Cui, and J.-M. Yao, "Protective effects of microRNA-126 on human cardiac microvascular endothelial cells against hypoxia/reoxygenation-induced injury and inflammatory response by activating PI3K/Akt/eNOS signaling pathway," *Cellular Physiology and Biochemistry*, vol. 42, no. 2, pp. 506–518, 2017.

[12] M. Alique, G. Bodega, C. Giannarelli, J. Carracedo, and R. Ramírez, "MicroRNA-126 regulates hypoxia-inducible factor-1α which inhibited migration, proliferation, and angiogenesis in replicative endothelial senescence," *Scientific Reports*, vol. 9, no. 1, p. 7381, 2019.

[13] M. S. A. Sheikh, "Diagnostic role of plasma microRNA-21 in stable and unstable angina patients and association with aging," *Cardiology Research and Practice*, vol. 2020, Article ID 9093151, 7 pages, 2020.

[14] M. S. Ali Sheikh, U. Salma, B. Zhang, J. Chen, J. Zhuang, and Z. Ping, "Diagnostic, prognostic, and therapeutic value of circulating miRNAs in heart failure patients associated with oxidative stress," *Oxidative Medicine and Cellular Longevity*, vol. 2016, Article ID 5893064, 13 pages, 2016.

[15] X. Wang, Y. Lian, X. Wen et al., "Expression of miR-126 and its potential function in coronary artery disease," *African Health Sciences*, vol. 17, no. 2, pp. 474–480, 2017.

[16] A. Lo Curto, S. Taverna, M. A. Costa et al., "Can be miR-126-3p a biomarker of premature aging? An ex vivo and in vitro study in Fabry disease," *Cell*, vol. 10, no. 2, p. 356, 2021.

[17] J. Banerjee, S. Roy, Y. Dhas, and N. Mishra, "Senescence-associated miR-34a and miR-126 in middle-aged Indians with type 2 diabetes," *Clinical and Experimental Medicine*, vol. 20, no. 1, pp. 149–158, 2020.

[18] M. S. A. Sheikh, "Role of plasma soluble lectin-like oxidized low-density lipoprotein receptor-1 and microRNA-98 in severity and risk of coronary artery disease," *Balkan Medical Journal*, vol. 38, no. 1, pp. 13–22, 2021.

[19] W. Jeong and E.-h. Jho, "Regulation of the low-density lipoprotein receptor-related protein LRP6 and its association with disease: Wnt/β-catenin signaling and beyond," *Frontiers in Cell and Development Biology*, vol. 9, p. 714330, 2021.

[20] H. A. Çakmak and M. Demir, "MicroRNA and cardiovascular diseases," *Balkan Medical Journal*, vol. 37, no. 2, pp. 60–71, 2020.

[21] F. Jansen, T. Stumpf, S. Proebsting et al., "Intercellular transfer of miR-126-3p by endothelial microparticles reduces vascular smooth muscle cell proliferation and limits neointima formation by inhibiting LRP6," *Journal of Molecular and Cellular Cardiology*, vol. 104, pp. 43–52, 2017.

Hindawi
Oxidative Medicine and Cellular Longevity
Volume 2022, Article ID 3334522, 30 pages
https://doi.org/10.1155/2022/3334522

Research Article

Identification of Aging-Related Genes Associated with Prognostic Value and Immune Microenvironment Characteristics in Diffuse Large B-Cell Lymphoma

Cancan Luo,[1,2] Han Nie,[3,4] and Li Yu[1,2]

[1]*Department of Hematology, The Second Affiliated Hospital of Nanchang University, Nanchang, China*
[2]*Institute of Hematology, Nanchang University, Nanchang, China*
[3]*Department of Stem Cell Biology, Atomic Bomb Diseases Institute, Nagasaki University, Japan*
[4]*Department of Stem Cell Biology, Nagasaki University Graduate School of Biomedical Sciences, 1-12-4 Sakamoto, Nagasaki 852-8523, Japan*

Correspondence should be addressed to Li Yu; iluyuliyl@163.com

Received 28 September 2021; Revised 11 December 2021; Accepted 24 December 2021; Published 13 January 2022

Academic Editor: Milena Georgieva

Diffuse large B-cell lymphoma (DLBCL) is a complex invasive tumour that occurs mainly among the elderly. Therefore, we analysed the relationship between ageing-related genes (AG) and DLBCL prognosis. Datasets related to DLBCL and human AGs were downloaded and screened from the Gene Expression Omnibus (GEO) database and HAGR website, respectively. LASSO and Cox regression were used to analyse AGs in the dataset and construct an AG predictive model related to DLBCL prognosis. Gene Ontology and the Kyoto Encyclopedia of Genes and Genomes enrichment were used to analyse the function of the AG predictive model. The immune microenvironment and immune cell infiltration in DLBCL and their relationship with the AG prediction model were also analysed. After the analysis, 118 AGs were identified as genes related to DLBCL prognosis. Using the LASSO and Cox regression analyses, 9 AGs (PLAU, IL7R, MYC, S100B, IGFBP3, NR3C1, PTK2, TBP, and CLOCK) were used to construct an AG prognostic model. In the training and verification sets, this model exhibited excellent predictive ability for the prognosis of patients with DLBCL who have different clinical characteristics. Further analysis revealed that the high- and low-risk groups of the AG prognostic model were significantly correlated with immune cell infiltration and tumour microenvironment in DLBCL. Functional enrichment analysis also showed that the genes in the AG model were associated with immune-related functions and pathways. In conclusion, we constructed an AG model with a strong predictive function in DLBCL, with the ability to predict the prognosis of patients with different clinical features. This model provides new ideas and potential therapeutic targets for the study of the pathogenesis of DLBCL.

1. Introduction

Diffuse large B-cell lymphoma (DLBCL) is the most common lymphoid neoplasm in adults, accounting for approximately 30% of non-Hodgkin's lymphomas (NHLs) diagnosed annually. DLBCL exhibits a striking heterogeneity at the clinical, genetic, and molecular levels [1]. The standard rituximab, cyclophosphamide, adriamycin, vincristine, and prednisone (R-CHOP) regimens are the first-line immunochemotherapy regimens for patients with DLBCL; however, 30%-40% of patients remain resistant to R-CHOP and are refractory or experience relapse [2, 3]. The prognosis of DLBCL has been developed from International Prognostic Index (IPI) scores, up to the genetic subtype classification [4]. Considering age, disease stage, serum lactate dehydrogenase (LDH) level, Eastern Cooperative Oncology Group (ECOG), performance status (PS), and the number of extranodal sites, patients with newly diagnosed DLBCL can be stratified into three different

risk groups. Furthermore, while recurrent genetic aberrations in individual genes have elucidated oncogenic mechanisms in DLBCL, the progress toward a genetic classification of DLBCL tumours is characterised by genomic aberrations in subtype-specific hallmark genes. The potential clinical utility of this genetic classification is evident from the association of the subtypes with outcomes following R-CHOP therapy [5].

Considering IPI and NCCN-IPI scores, age > 60 years is an adverse prognostic factor for DLBCL. Older patients with DLBCL (≥60 years) are associated with a worse outcome compared to younger patients (<60 years) [6]. Within 2 years after the diagnosis of DLBCL, the standard R-CHOP immunochemotherapy drugs can normalise the life expectancy of young patients, as exhibited by event-free survival rates; however, elderly patients will still experience high mortality [7]. Moreover, it should be noted that the main age group for DLBCL is among the elderly. The median age at the time of diagnosis is 66 years; furthermore, 20.1% of patients are diagnosed between 75 and 84 years of age, 25.0% between 65 and 74 years of age, and 21.2% between 55 and 64 years of age. At present, effective treatment among the elderly remains challenging owing to the adverse invasive biological characteristics of DLBCL, the baseline health status of this patient population, the late toxicity of chemotherapy, and the poor therapeutic effect of the current treatment scheme on elderly patients [8, 9]. Therefore, interest in the understanding of the molecular and genetic pathways dysregulated in ageing and DLBCL has tremendously increased, along with the interest in biomarkers as a quick and quantitative measure in all areas of biomedical research.

Ageing is a process wherein the adaptability and organ function of all organisms decline over time, eventually leading to death [10]. Ageing is often caused by changes in the genome and cells, including tissue degradation and disintegration caused by loss of stem cell renewal ability, genomic instability, telomere wear, metabolic changes, changes in cell communication, cell ageing, loss of protein homeostasis, and epigenetic changes [11]. Notably, B cell immune weakness is a sign of systemic weakness, and ageing may lead to a sharp decline in B cell diversity with age, which could have an important impact on the immune health of the elderly [12]. Because the incidence of DLBCL is mainly among the elderly and considering that the treatment effect for this patient population is poor, we speculate that DLBCL incidence is related to body ageing and cellular immunity. Therefore, because multiple molecular pathways are involved in the ageing process and can contribute to the various aspects of DLBCL, a panel of valid ageing genes (AGs) in DLBCL and its effect on immune function may allow both diagnosis and follow-up in preclinical and clinical settings.

2. Materials and Methods

2.1. Data Access, Acquisition of AGs, and Setting of Samples. We searched and screened the Gene Expression Omnibus (GEO) database (https://www.ncbi.nlm.nih.gov/geo/) and obtained the gene expression matrix and clinical data of three datasets: GSE10846 (which included tumour specimens and the clinical data of 414 patients with DLBCL from 10 institutions in North America and Europe) [13], GSE11318 (which included tumour specimens and the clinical data of 203 patients with DLBCL from the US National Institutes of Health and the University of Nebraska Medical Center, among others) [14], and GSE32918 (which included tumour specimens and the clinical data of 172 patients with DLBCL from the Yorkshire and Humberside Haematology Network) [15]. We used GSE10846 (included tumour specimens and the clinical data of 414 patients with DLBCL) in the screening of feature genes and as the training set during model construction, whereas GSE11318 and GSE32918 were used as the verification set (details on the original and clinical data of these datasets can be obtained in the cited references). A total of 307 AGs were obtained from HAGR (http://genomics.senescence.info/genes/) [16] (Supplementary Table 1). The expression matrix of the AGs in the training set was extracted and sorted out by using the limma package in R (version 4.0.2).

2.2. Screening and Modelling of Prognosis-Related Ageing Genes. Combined with the overall survival (OS) from the clinical information of the training set, prognosis-related AGs were screened using univariate Cox regression analysis. The "glmnet" package in R (version 4.0.2) was used to analyse the prognosis-related AGs through the least absolute shrinkage and selection operator (LASSO) Cox regression analysis, and a predictive model was constructed. The risk score of the model was determined according to the standardised expression level of each gene and the corresponding regression coefficient. The formula for calculating the risk score was as follows:

$$\text{Risk score} = \sum i = 1n\text{Coef}(i) \times x(i). \quad (1)$$

Patients were divided into high- and low-risk groups according to the risk values calculated by the model.

2.3. Verification of the Ageing Gene Prognostic Model. The risk score of the training set samples was scored according to the AG prognostic model. Then, principal component analysis (PCA) was performed according to the risk score. The "survminer" package was used to analyse survival in the training set samples scored by the model and to evaluate the prognosis prediction of the samples. The "timeROC" package was used to analyse the receiver-operating characteristic (ROC) curve of the training set to evaluate the model efficiency. Then, univariate and multivariate Cox analyses of the clinical characteristics of the model were performed according to the clinical characteristics. The AG prognostic model was used to score the risk in the two verification sets, and the survival and ROC curve analyses of the validation set were performed using the "survminer" and "timeROC" packages, respectively, to test the model reliability.

2.4. GO and KEGG Enrichment Analysis. The genes in the AG prognostic model were analysed using the Gene Ontology (GO) and Kyoto Encyclopedia of Genes and Genomes (KEGG) through the "clusterProfiler4.0" package [17].

2.5. Prediction of Clinical Features and Nomogram Construction Using the Ageing Gene Prognostic Model. The AG prognostic model was used to score and group the patients

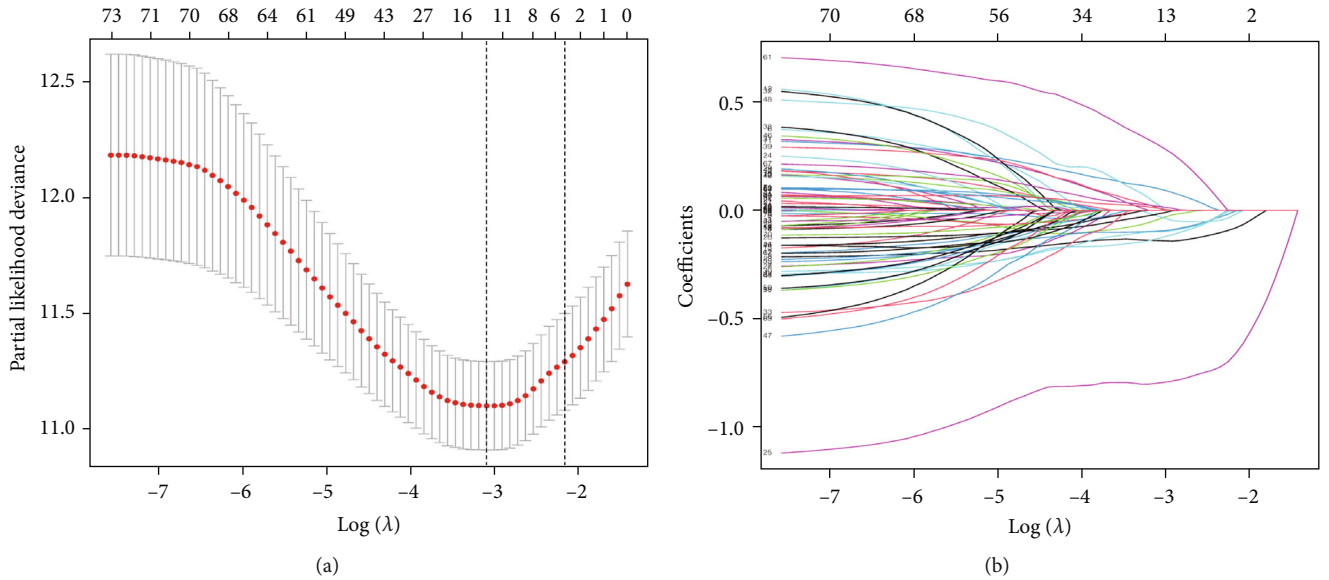

(a) (b)

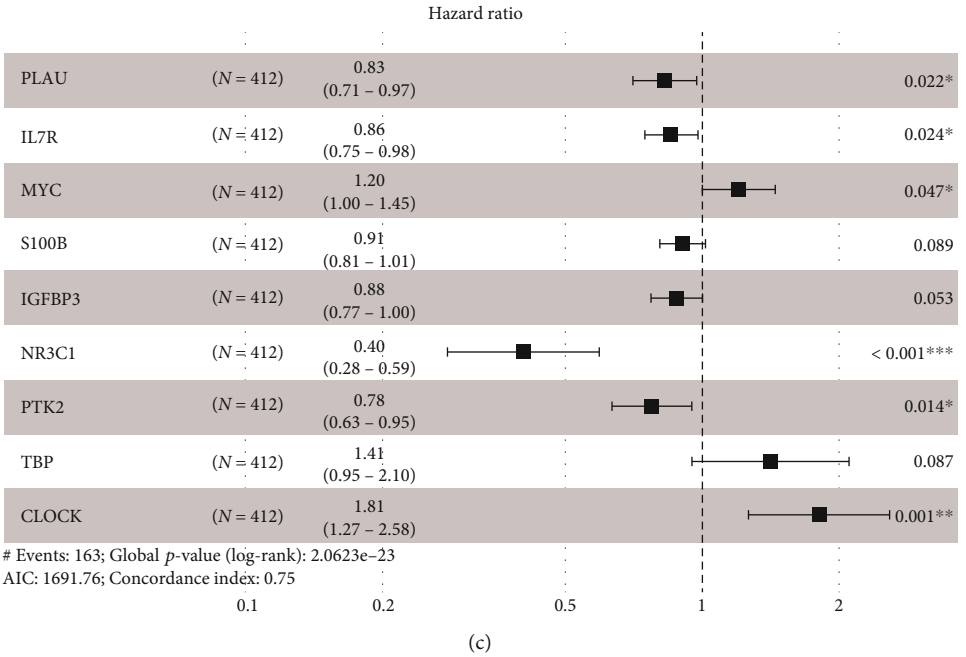

(c)

Figure 1: Continued.

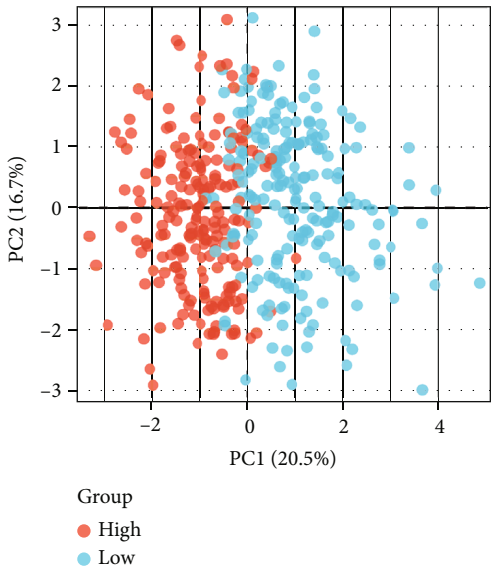

(d)

Figure 1: (a) Cross validation for adjusting parameters in the LASSO regression analysis. (b) LASSO regression analysis of the AG prognostic model (each curve represents each prognostic AG included in the construction of the prognostic model). (c) Gene forest map of the AG prediction model. (d) PCA cluster analysis of the training set samples.

Table 1: Risk score of the AGs prediction model.

ID	Coef	HR	HR.95L	HR.95H	*P* value
PLAU	-0.1877144	0.82885141	0.70623866	0.97275142	0.02155043
IL7R	-0.1559483	0.85560339	0.74739094	0.9794836	0.02379409
MYC	0.18640335	1.20490817	1.00234197	1.44841156	0.04715864
S100B	-0.0981711	0.90649381	0.80965196	1.01491883	0.08855595
IGFBP3	-0.127716	0.88010325	0.77334383	1.00160072	0.05290174
NR3C1	-0.9042901	0.40482918	0.27603495	0.59371708	3.69E-06
PTK2	-0.2531792	0.77632871	0.63465837	0.94962314	0.0137867
TBP	0.34647524	1.41407449	0.95060454	2.10351051	0.08727396
CLOCK	0.59230219	1.80814633	1.2671264	2.5801634	0.00109444

Table 2: Genes in prediction model.

Symbol	Name	Gene ID	Uniprot
PLAU	Plasminogen activator, urokinase	5328	UROK_HUMAN
IL7R	Interleukin 7 receptor	3575	IL7RA_HUMAN
MYC	v-myc avian myelocytomatosis viral oncogene homolog	4609	MYC_HUMAN
S100B	S100 calcium binding protein B	6285	S100B_HUMAN
IGFBP3	Insulin-like growth factor binding protein 3	3486	IBP3_HUMAN
NR3C1	Nuclear receptor subfamily 3, group C, member 1 (glucocorticoid receptor)	2908	GCR_HUMAN
PTK2B	Protein tyrosine kinase 2 beta	2185	FAK2_HUMAN
TAF1	TAF1 RNA polymerase II, TATA box-binding protein- (TBP-) associated factor, 250 kDa	6872	TAF1_HUMAN
CLOCK	Clock circadian regulator	9575	CLOCK_HUMAN

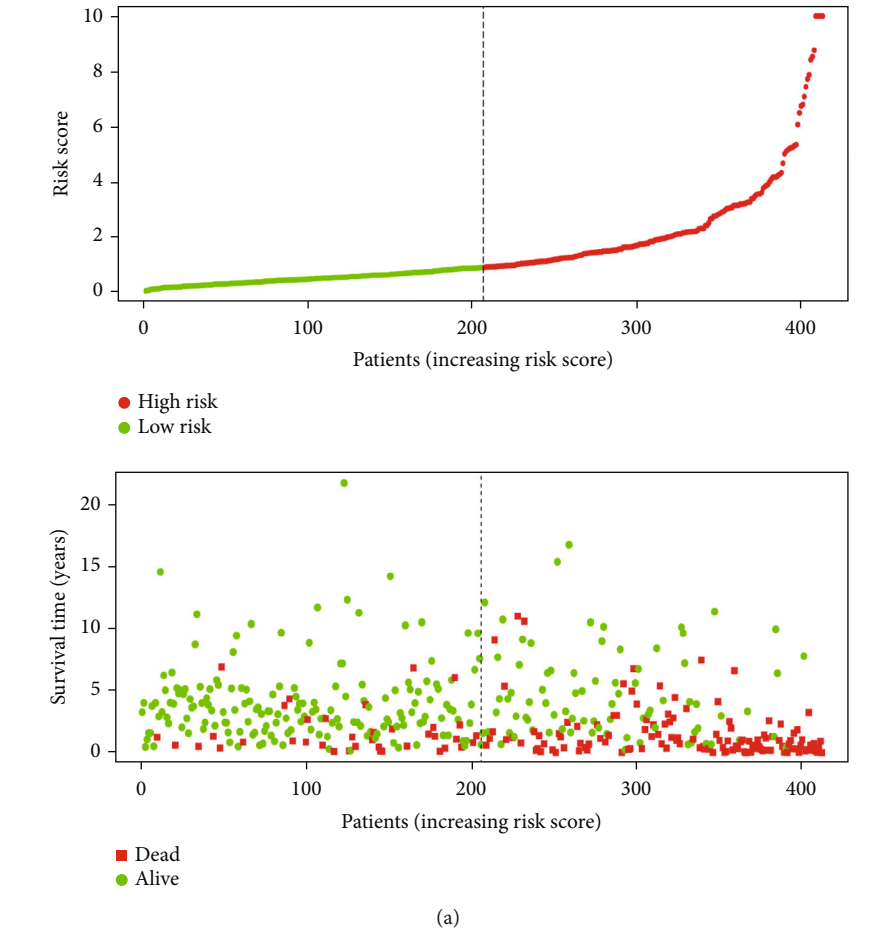

(a)

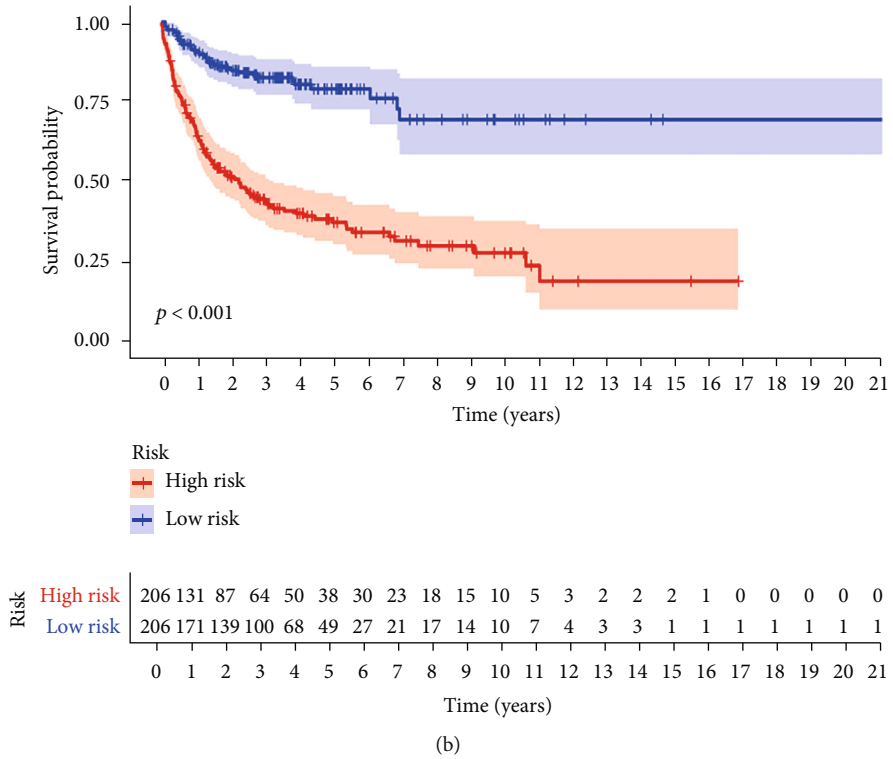

(b)

Figure 2: Continued.

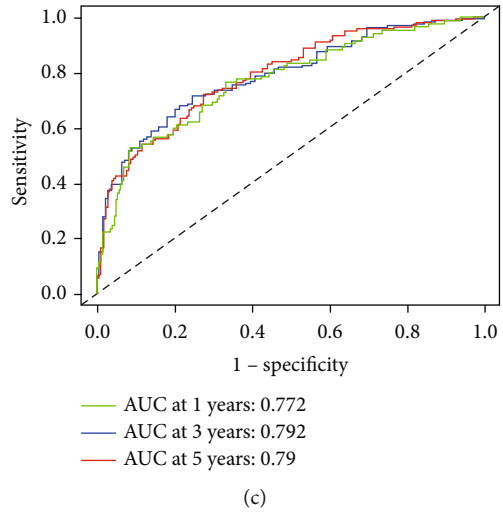

(c)

Figure 2: (a) The model divides patients in the training set into low-risk and high-risk groups, and the number of survival and deaths was compared between these two groups. (b) Kaplan-Meier curve between the high-risk and low-risk groups. (c) The subject working curve of the model in the training set.

with DLBCL who have different clinical characteristics (age, treatment, ECOG grade, subtype, gender, and stage) and to test the reliability of the grouping. A nomogram was constructed to predict the prognosis of these patients according to the various clinical characteristics.

2.6. Relationship between the Ageing Gene Prognostic Model and the Tumour Microenvironment. ESTIMATE [18] was used to score the tumour microenvironment (including tumour purity, immune score, stroma score, and ESTIMATE score) of the training set samples. Differences in the microenvironment between the high- and low-risk groups distinguished through the AG prognostic model were analysed, and survival analysis was performed using the survival time.

2.7. Relationship between the Ageing Gene Prognostic Model and the Immune Cell Infiltration and Immune Checkpoint. CIBERSORT [19] was used to score 22 types of immune cell infiltration in the training set samples. The difference in the high- and low-risk groups distinguished through the AG prognostic model was analysed, and survival analysis was performed using the survival time. We also analysed the relationship between the high- and low-risk groups and the 37 immune checkpoints as well as the relationship between immune checkpoints and prognosis.

2.8. Statistical Analysis. Survival analysis was performed using the "survminer" package. The ROC curve and ROC analysis were completed using the "timeROC" package. The Cox proportional hazard regression model was used for univariate and multivariate analyses. $P < 0.05$ was considered to have statistical significance, whereas $P < 0.01$ was significant.

3. Results

3.1. Screening and Modelling of Prognosis-Related Ageing Genes. Supplementary Figure 1 shows the flow chart of the work. We obtained the expression of 296 AGs using the "limma" package to extract the AGs from the training set GSE10847. Moreover, we obtained 118 AGs related to the prognosis of DLBCL (Supplementary Figure 2) using univariate Cox regression analysis combined with the total survival time in the training set. A model of the AGs related to prognosis was constructed using LASSO regression analysis (Figures 1(a) and 1(b)). A predictive model was also constructed using nine AGs: PLAU, IL7R, MYC, S100B, IGFBP3, NR3C1, PTK2, TBP, and CLOCK (Figure 1(c)). The risk score of the AG prediction model is shown in Table 1. The description of the nine model genes is shown in Table 2.

3.2. Verification of the Ageing Gene Prognostic Model. The AG prognostic model was used to score the training set and divide the patients into the high- and low-risk groups. Then, PCA was used to analyse the training set samples, with the results showing that the samples could be well distinguished (Figure 1(d)). The survival and ROC analyses of the high- and low-risk groups in the training set showed that the survival characteristics of the high-risk group were significantly lower than those of the low-risk group (Figures 2(a) and 2(b)). Moreover, the ROC analysis showed that the area under curve (AUC) value of the model for 1, 3, and 5 years was 0.772, 0.792, and 0.79 (Figure 2(c)), respectively, which indicates that the AG prognostic model had high prediction accuracy. The two other DLBCL datasets (GSE11318 and GSE32918) were used as independent validation datasets to verify the performance of the AG prognostic model. Consistent with the results of the training set, the survival characteristics of the high-risk group were significantly lower than those of the low-risk group in both verification sets (Supplementary Figures 3A, 3B, 3D, and 3E). Furthermore, the AUC value of the model in both verification sets was satisfactory (Supplementary Figures 3C and 3F). Univariate and multivariate regression analyses were also performed on

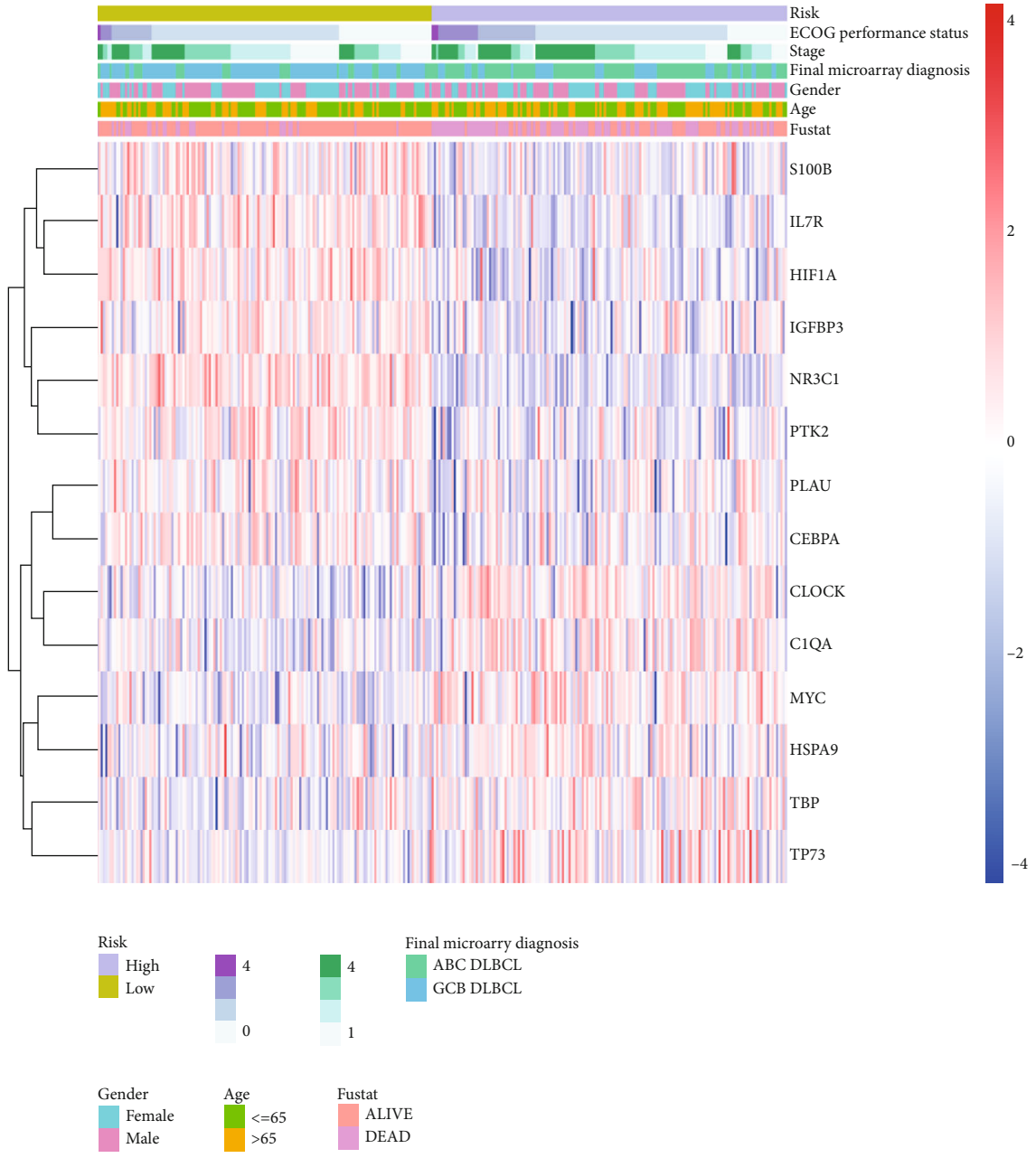

(a)

Figure 3: Continued.

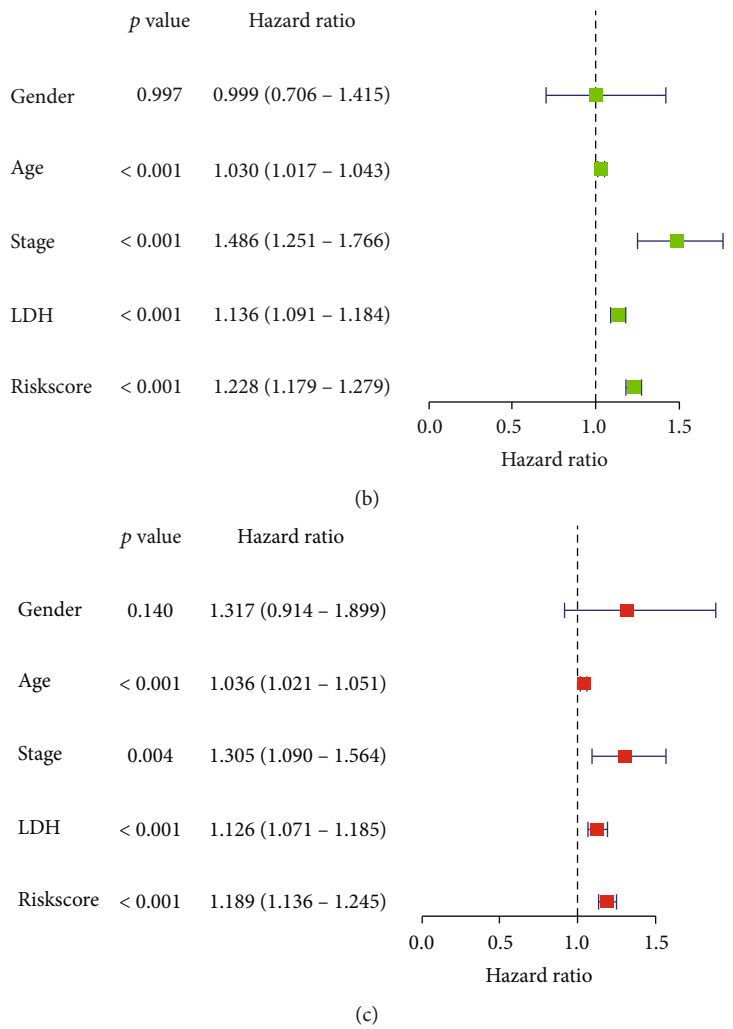

Figure 3: (a) The heatmap of clinical characteristics of the high- and low-risk group in the training focus. (b) Univariate analysis of the clinical characteristics of the training set (which shows whether these clinical features and prognostic models are related to the survival time of patients). (c) Multivariate analysis of the clinical characteristics of the training set (which shows whether these characteristics are still related to the survival time of patients, considering the mutual influence of these clinical features and the prognostic models).

the AG prognostic model combined with clinical characteristics. The clinical characteristics of the training set and the heatmaps of the 9 AG expression profiles are shown in Figure 3(a). The univariate and multivariate analyses shown in Figures 3(b) and 3(c) also demonstrate that the model could be used as independent prognostic factors in patients with DLBCL. The clinical features of the verification sets and the heatmaps of the nine AG expression profiles are shown in Supplementary Figures 4A and 4D. Similarly, the univariate and multivariate regression analyses demonstrated that the AG prognostic model could also be used as an independent prognostic factor for patients with DLBCL in both validation sets (Supplementary Figures 4B, 4C, 4E and 4F).

3.3. GO and KEGG Enrichment Analyses. The AG prognostic model genes were analysed through GO and KEGG enrichment analyses. Figures 4(a)–4(c) show that the model gene is related to the development of lymph nodes, the regulation of lymphocyte apoptosis, and the regulation of immune cells. Figures 4(d)–4(f) show that model genes are involved in transcriptional disorders, cell senescence, the PI3K-Akt signal pathway, and the JAK-STAT signal pathway in cancer.

3.4. Prediction of Clinical Features and Nomogram Construction Using the Ageing Gene Prognostic Model. We tested the stability of the AG prognostic model, and the results show that the model has high accuracy in distinguishing the prognosis of patients with different clinical characteristics, including age (>65 years, ≤65 years), treatment (CHOP, R-CHOP), ECOG grade (0-2 points, 3-4 points), subtype (ABC, GCB), sex (female, male), and grade (G1-2, G3-4) (Figures 5(a)–5(h) and 6(a)–6(d)). Notably, the IPI (International Prognostic Index) score is currently recognised as a prognostic indicator of lymphoma. It scores patients with DLBCL according to age, sites of involvement, clinical stage, ECOG grade, and LDH. The scores are divided into low (0-1), medium (2-3),

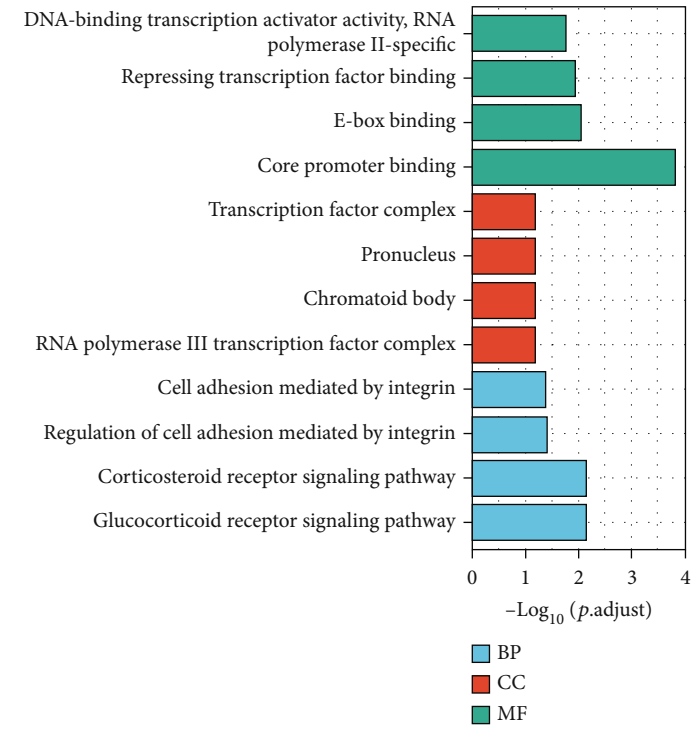

(a)

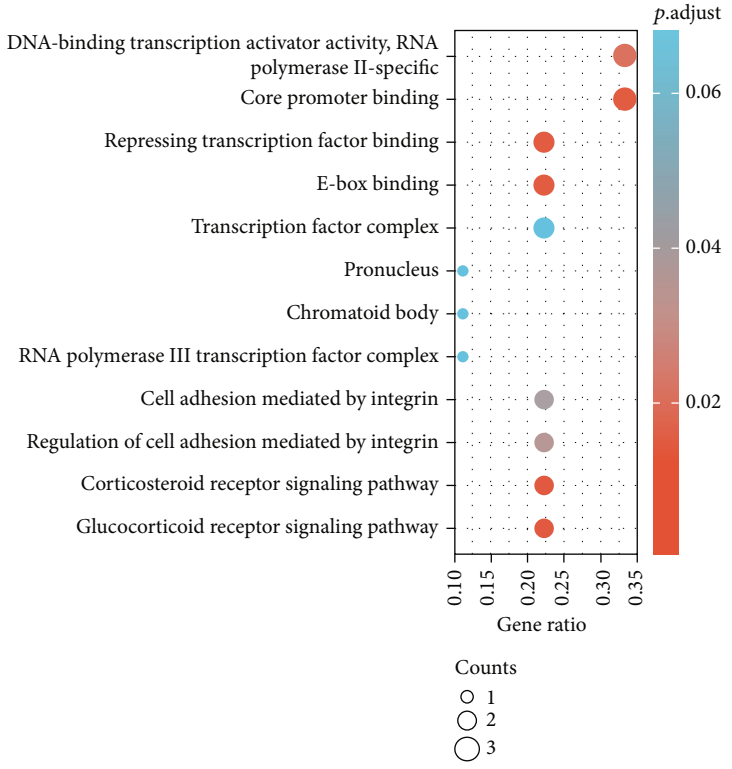

(b)

Figure 4: Continued.

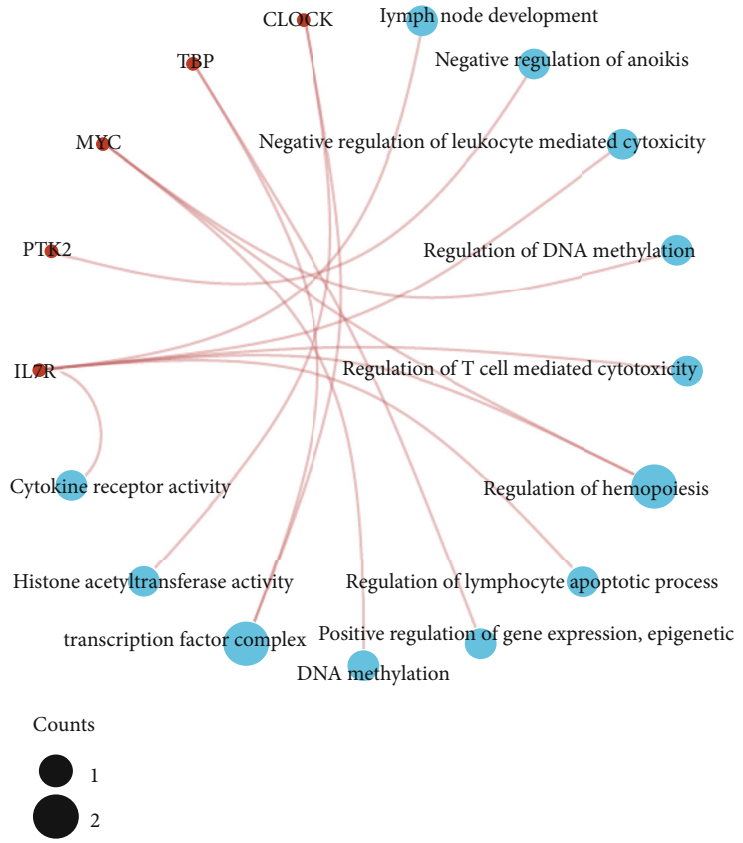

(c)

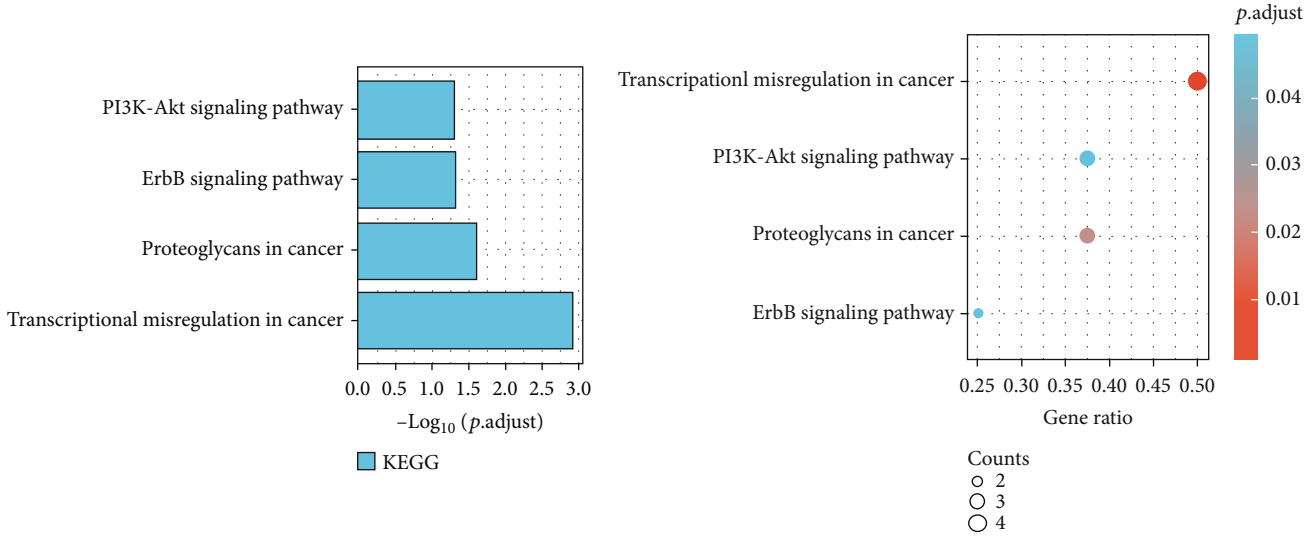

(d) (e)

Figure 4: Continued.

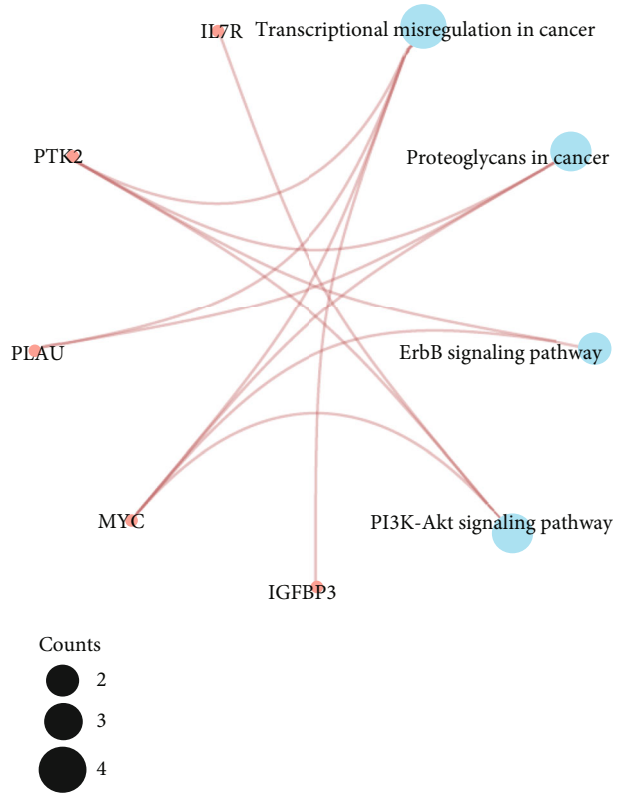

(f)

Figure 4: (a) Bubble map of the GO and KEGG enrichment analyses of prognostic model genes. (b) Scatter plot of the GO enrichment analysis of the prognostic model genes. (c) Scatter plot of the KEGG enrichment analysis of the prognostic model genes.

and high (4-5) risk. However, our model can further distinguish the prognosis of low-, medium-, and high-risk patients (Figures 6(e)–6(g)), suggesting that the AG prognostic model that we constructed has high reliability and accuracy for predicting the prognosis of patients with DLBCL who have different clinical characteristics, and can be combined with the IPI score for more accurate predictions. Combined with the survival analysis, we constructed a nomogram that includes the risk score and other clinicopathological information to predict the survival time of patients in the training set, as shown in Figures 6(h) and 6(i).

3.5. Relationship between the Ageing Gene Prognostic Model and the Tumour Microenvironment. Because the ageing of the body is usually accompanied by the decline of immune function and the GO and KEGG enrichment analyses showed that model genes are involved in immune-related functions and pathways, we used the ESTIMATE algorithm to determine stroma and immune scores and to explore the tumour microenvironment differences between the high- and low-risk groups. Figure 7(a) shows a heatmap of tumour purity, immune score, stroma score, and ESTIMATE score as well as the nine AG expression profiles. Consistent with our initial hypothesis, compared to the low-risk group, the high-risk group had significantly lower immunity, stroma, and ESTIMATE scores. Moreover, the survival analysis also showed that low scores in these three areas predicted a poor prognosis (Figures 7(b)–7(d)). Furthermore, the high-risk group had a high tumour purity score, which also predicted a poor prognosis (Figure 7(e)).

3.6. Relationship between the Ageing Gene Prognostic Model and Immune Cell Infiltration. We used the CIBERSORT algorithm to further analyse the difference in immune cell infiltration between the high- and low-risk groups. Figure 8(a) shows the infiltration of 22 immune cells in the high- and low-risk group. As demonstrated in Figure 8(b), there is a strong negative correlation between macrophage M1 and activated dendritic cells, immature B cells and memory B cells and macrophage M0 and macrophage M2. Figure 8(c) shows that there is an increased expression of immature B cells, resting NK cells, macrophage M2, eosinophils, and neutrophils in the high-risk group, whereas the expression of delta T cells, macrophages M0, dormant dendritic cells, and resting mast cells increased in the low-risk group. High M2 expression in eosinophils, monocytes, and macrophages was associated with poor prognosis (Figures 8(d)–8(f)), whereas high expression of macrophages M0, dormant dendritic cells, and delta T cells was related with good prognosis (Figures 8(g)–8(i)). This finding suggests that AGs affect the immune function of the body and ultimately affect the prognosis of patients with DLBCL by

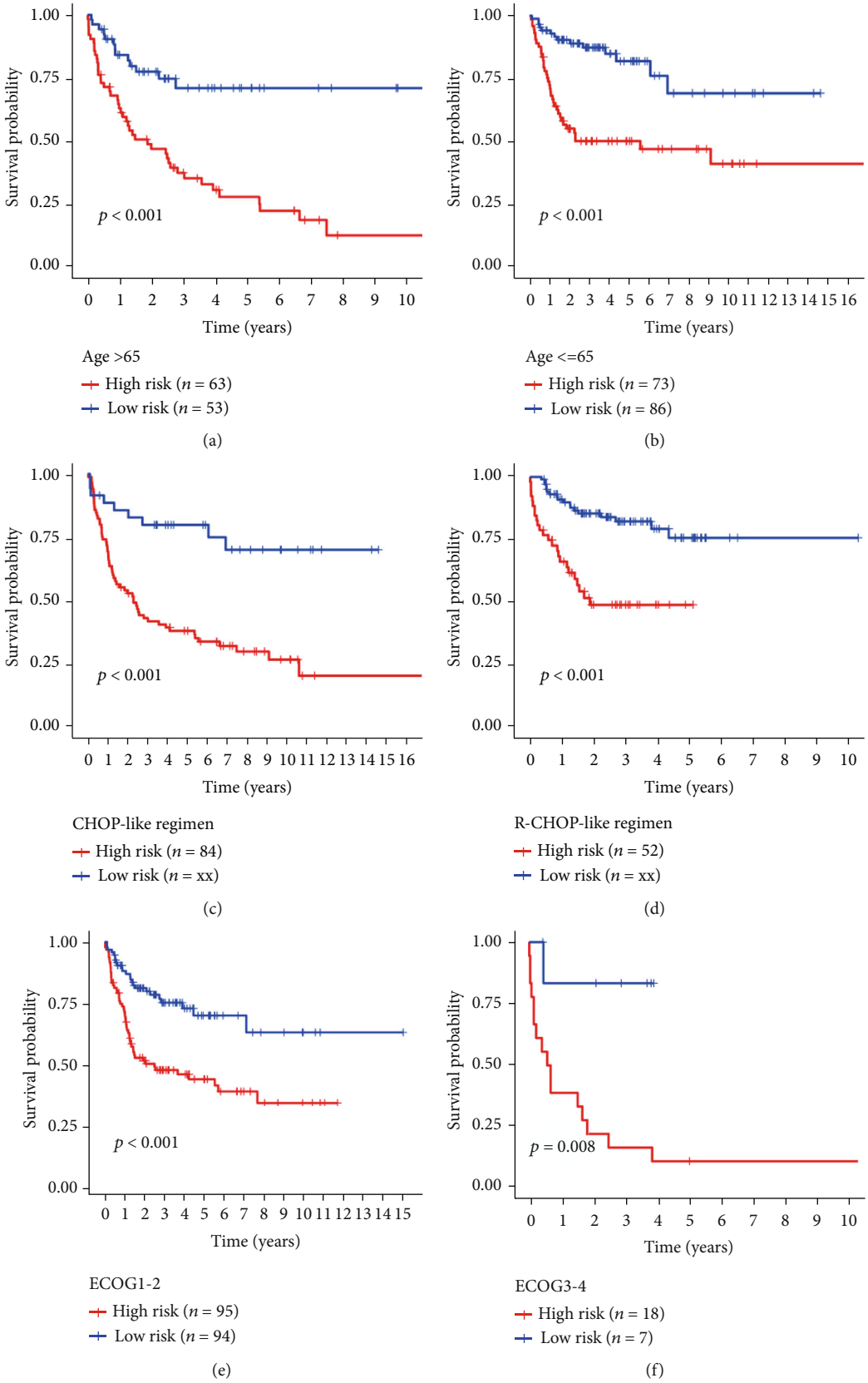

Figure 5: Continued.

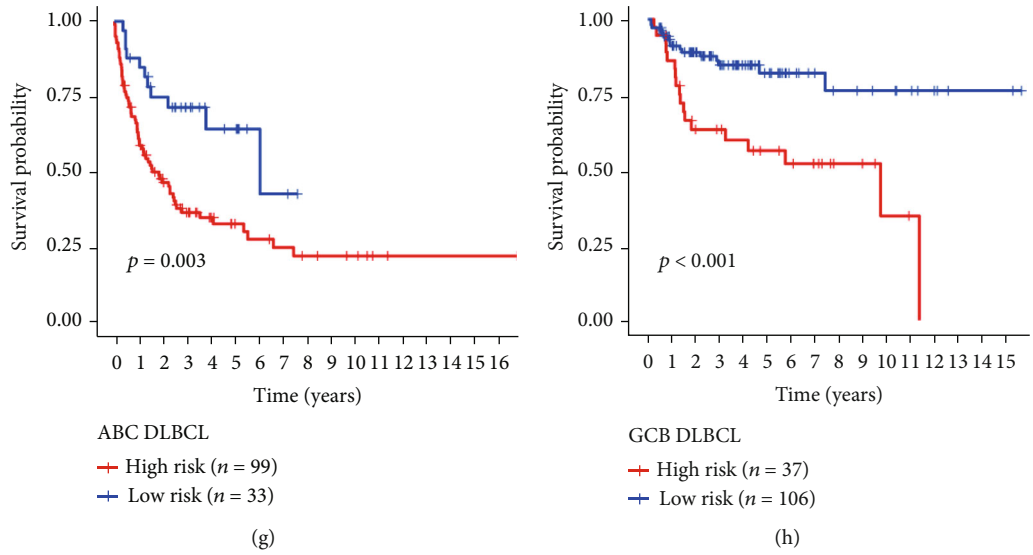

Figure 5: (a–h) Kaplan-Meier curves showing the relationship between age (>65 years, ≤65 years), treatment (CHOP, R-CHOP), ECOG grade (G1-2, G3-4), subtype (ABC, GCB), and survival time of patients with DLBCL in the high- and low-risk groups.

altering the infiltration of eosinophils, M2 macrophages, delta T cells, M0 macrophages, and dormant dendritic cells.

3.7. Relationship between the Ageing Gene Prognostic Model and Immune Checkpoint. Immune checkpoint blockers, which are at the forefront of immunotherapy, are effective in the treatment of many human cancers, especially malignant cancers and chemotherapy-tolerant cancers. Therefore, we analysed the differences in 37 immune checkpoints in DLBCL between the high- and low-risk groups. The results showed that the expression of TNFRSF9, SIGLEC15, PTPRC, PDCD1LG2, LDHA, JAK1, IL23A, ICOS, CD8A, CD86, CD40LG, CD28, and B2M was increased in the low-risk group (Figure 9(a)). The high expression of ICOS, IL23A, SIGLEC15, PTPRC, LDHA, B2M, TNFRSF9, and CD40LG was also associated with a good prognosis (Figures 9(b)–9(g) and 10(a) and 10(b)). Furthermore, the expression of YTHDF1, VTCN1, TNFSF9, TNFSF18, PVR, LGALS9, LDHC, LDHB, LAMA3, IL12A, FGL1, and CD274 was increased in the high-risk group (Figure 9(a)), and the high expression of YTHDF1, IL12A, LGALS9, TNFSF9, and PVR was associated with poor prognosis (Figures 10(c)–10(g)).

4. Discussion

The extreme genetic and phenotypic heterogeneity of DLBCL presents a challenge in terms of subtype classification, prognosis prediction, and precision treatment. Ageing is an unavoidable physiological process at present, and the accompanying high-risk disease probability remains an unchangeable fact. In this study, we constructed and verified a new AG prediction model that can well distinguish between the prognosis of patients with high- and low-risk DLBCL. To the best of our knowledge, this study is the first to predict the prognosis of patients with DLBCL characterised by AGs. In addition, we constructed a prognostic nomogram, which can be used to individually estimate the OS probability in patients with DLBCL, help to improve clinical monitoring, and guide the duration of adjuvant chemotherapy and treatment.

In the present study, we determined that the nine central AGs, namely, PLAU, IL7R, MYC, S100B, IGFBP3, NR3C1, PTK2, TBP, and CLOCK, were risk factors related to the prognosis of patients with DLBCL. These AGs were reportedly associated with the underlying mechanisms to facilitate DLBCL or lymphoblastic leukaemia formation and progression. Among them, only MYC is the star protein in DLBCL. Approximately 20%-30% of patients with DLBCL harbour the MYC rearrangement or translocation, which functions as an independent high-risk factor. MYC is also closely related to BCL2, and most patients with refractory DLBCL will exhibit double-hit lymphoma (MYC-BCL2 rearrangement) or double protein expression lymphoma (MYC-BCL2 high expression). The clinical manifestations of this kind of DLBCL are also more aggressive [20–22]. MYC binds to DHX33 and promotes PLAU transcription by directly binding to their promoters, thus promoting cancer cell migration [23]. IL-7R expression in non-GCB-type lymphoma is also significantly higher compared to that in GCB lymphoma [24]. S100B reportedly interacts with p53 involved in many tumours, and S100B (beta) sterically blocks sites of phosphorylation and acetylation on p53 that are important for transcription activation [25]. High S100B expression in antigen-presenting cells is associated with a good prognosis [26]. IGFBP-3 has been proven to play an important role in a variety of tumours. Zhou et al. reported that miR-196b/miR-1290 participates in the antitumour effect of resveratrol by regulating IGFBP3 expression in acute lymphoblastic leukaemia [27]. In in vitro experiments, IGFBP-3 enhancement can induce the apoptosis of breast cancer cells, and the low expression of IGFBP-3 indicates a poor prognosis [28]. In a previous study, high IGFBP-3 expression improved

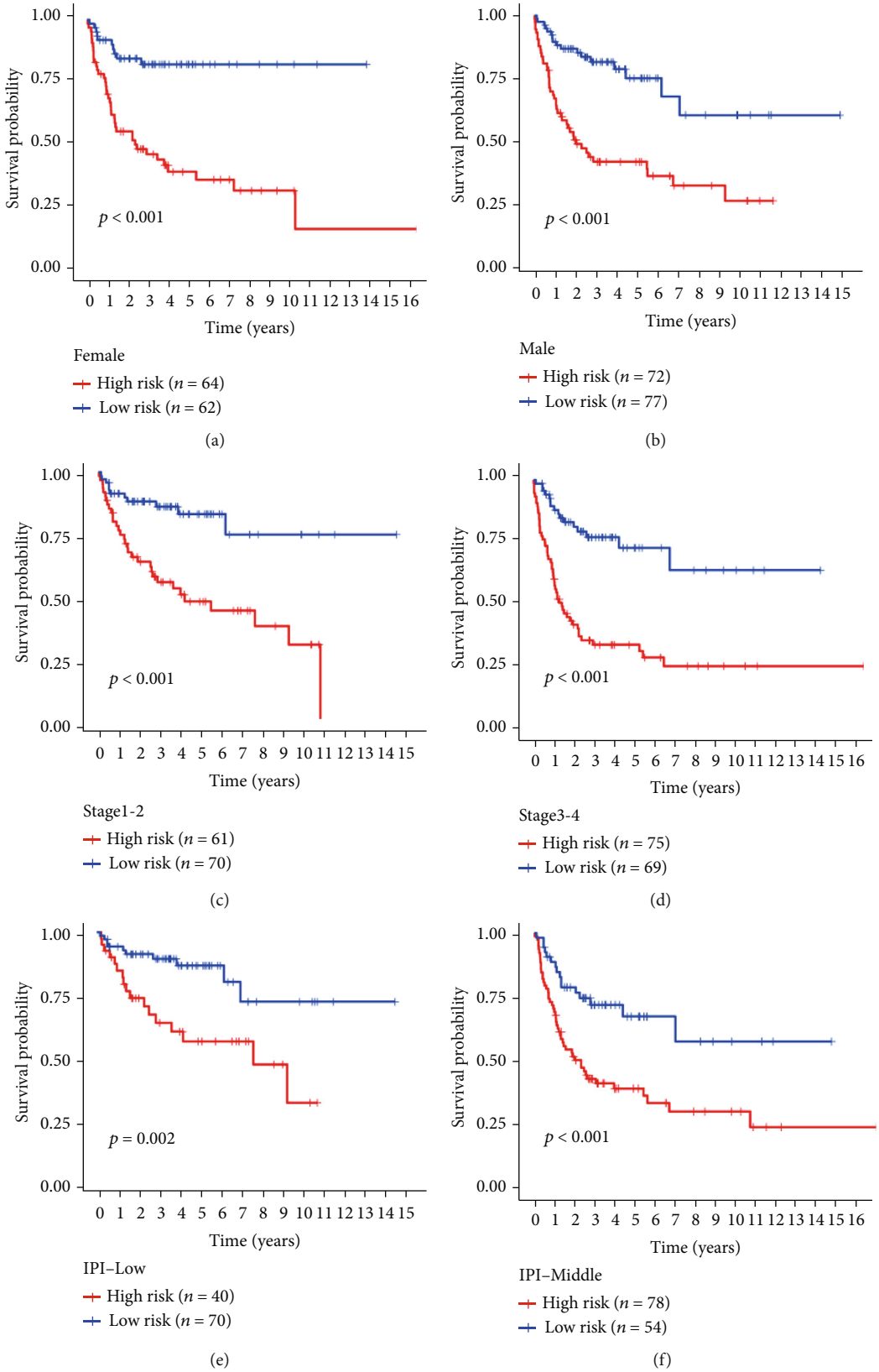

Figure 6: Continued.

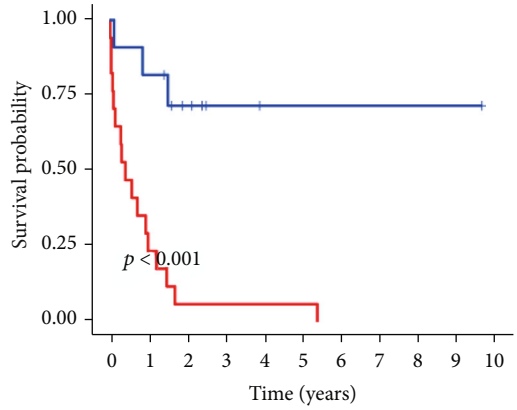

(g)

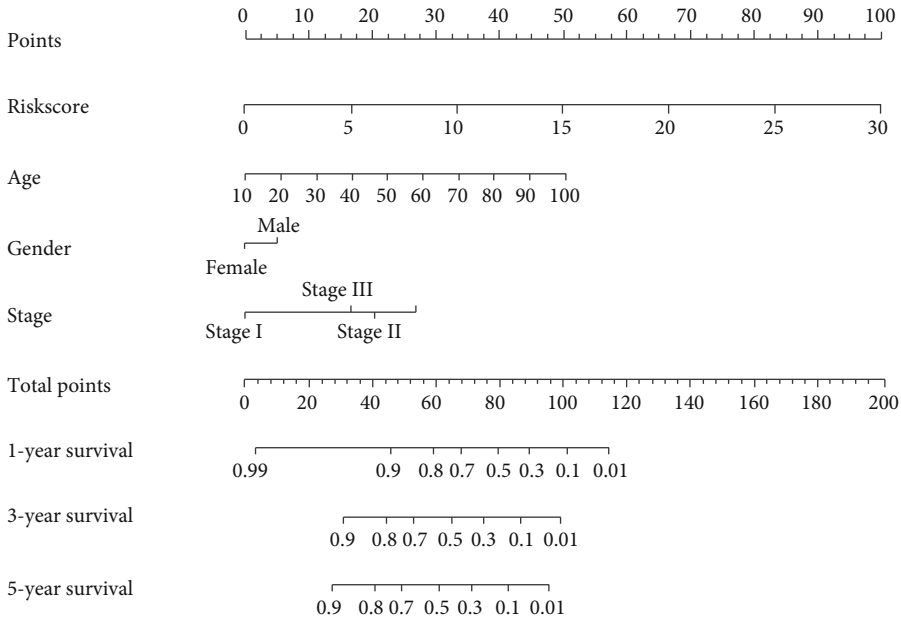

(h)

Figure 6: Continued.

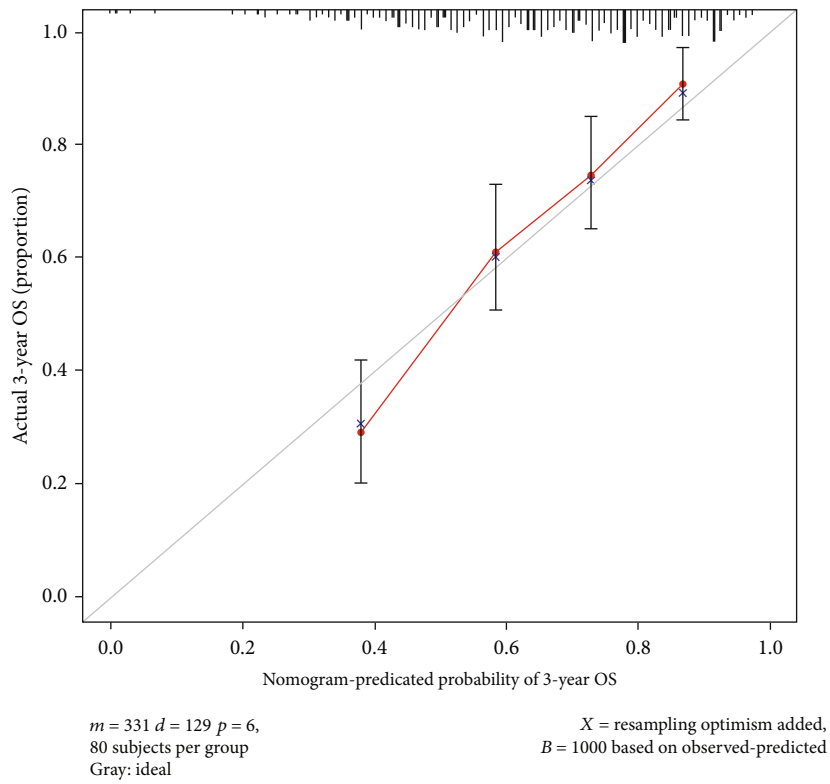

(i)

Figure 6: (a–g) Kaplan-Meier curves showing sex (female, male), stage (stage 1-2, stage 3-4), and IPI scores (low, middle, and high) in the high- and low-risk groups. (h) Nomogram constructed according to the prognostic model of patients with DLBCL. (i) The calibration curve used to predict the nomogram.

the survival rate of patients with oral squamous cell carcinoma, achieved through NF- κB/IL-6/ROS signalling to promote radiosensitivity [29]. Chan et al. identified the products of NR3C1 as one of the central effectors of the B-lymphoid restriction of glucose and the energy supply, functioning as metabolic gatekeepers by limiting the amount of cellular ATP to levels that are insufficient for malignant transformation [30]. NR3C1 also plays an important role in acute lymphoblastic leukaemia. Studies have confirmed that the deletion of NR3C1 is one of the reasons for the failure of acute lymphoblastic leukaemia induction. In addition, the mutation of NR3C1 may lead to glucocorticoid resistance and lead to treatment failure and recurrence of acute lymphoblastic leukaemia. TBP, a TATA binding protein, is closely related to metabolism. The increased expression of TBP-2 can lead to impaired insulin sensitivity and glucose-induced insulin secretion, as well as β-cell apoptosis, leading to diabetes. Furthermore, a transfection experiment showed that TBP-2 expression induces apoptosis in IL-2-independent ATL cells [31]. TBP can directly interact with MYC and regulate the transcriptional process [32–34]. The biological clock has always been thought to be associated with cancer, as in non-Hodgkin's lymphoma. Hoffman et al. have shown that the clock circadian regulator gene can affect the susceptibility to non-Hodgkin's lymphoma by affecting immune regulation, and the overexpression of MYC in U2OS cells (osteosarcoma cells) weakens the clock and in turn promotes cell proliferation [35]. Patients with DLBCL who have high CLOCK expression also show poor overall survival [36].

In our study, the relationship between AG and DLBCL prognosis was initially established, and nine AGs were then used to construct a risk score through the LASSO Cox regression model. This classification breaks DLBCL into two genetic subtypes that exhibit good performance in predicting prognosis both in the training and two validation sets. Compared with patients in the low-risk group, those in the high-risk group typically presented with more aggressive characteristics, advanced stages, and higher mortality (all $P < 0.05$). Furthermore, the ageing risk score exhibited better predictive capability in further distinguishing the low- and high-risk patients as having low, medium, and high risk when the IPI score was considered to predict the prognosis of patients with DLBCL more accurately. It is worth noting that this model was built from large sample datasets and was successfully verified in two small sample datasets, which shows that the performance of this model is very robust and effective.

Results of the GO and KEGG analyses showed that the nine AGs were related to the development of lymph nodes, the process of lymphocyte apoptosis, the regulation of immune cells, and the immune pathway. Ageing is often accompanied by a change in immune function. Therefore, we analysed the relationship between the AG model and

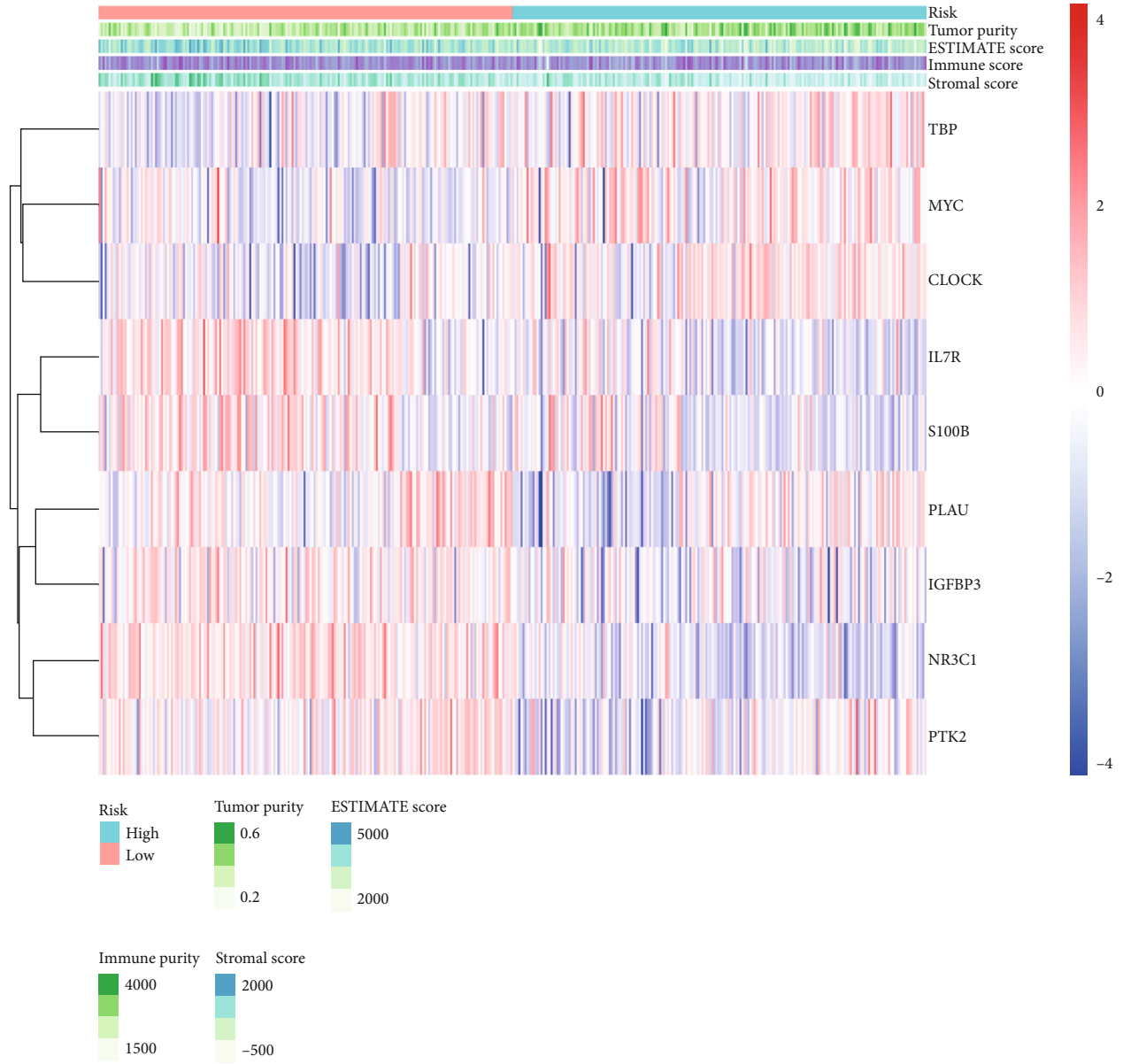

(a)

Figure 7: Continued.

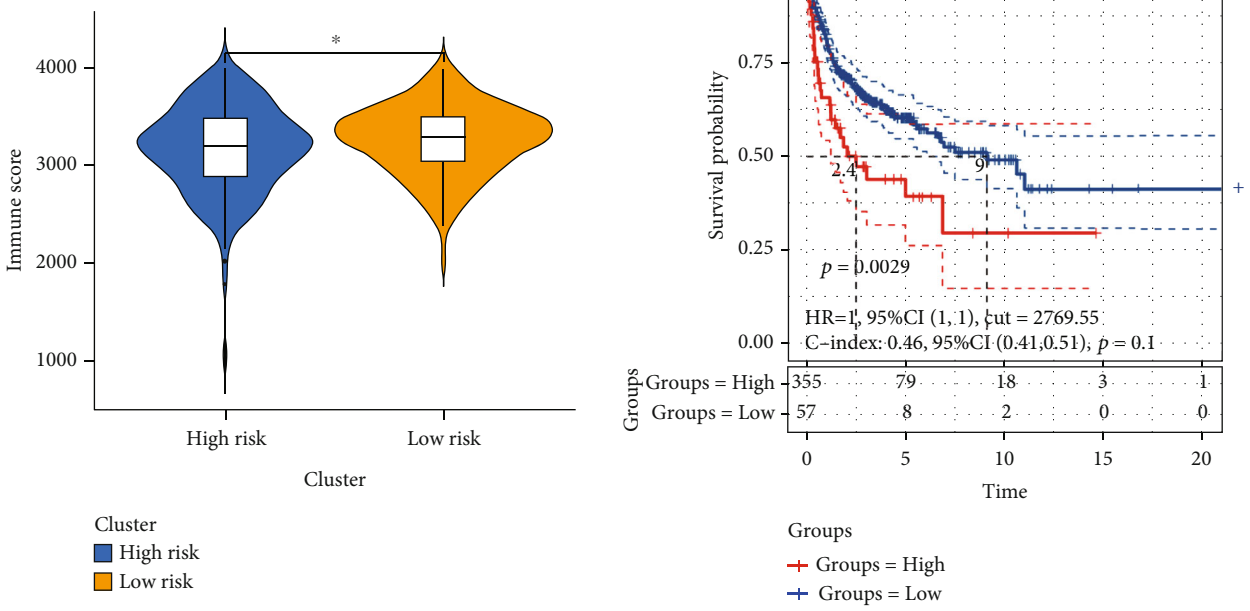

(b)

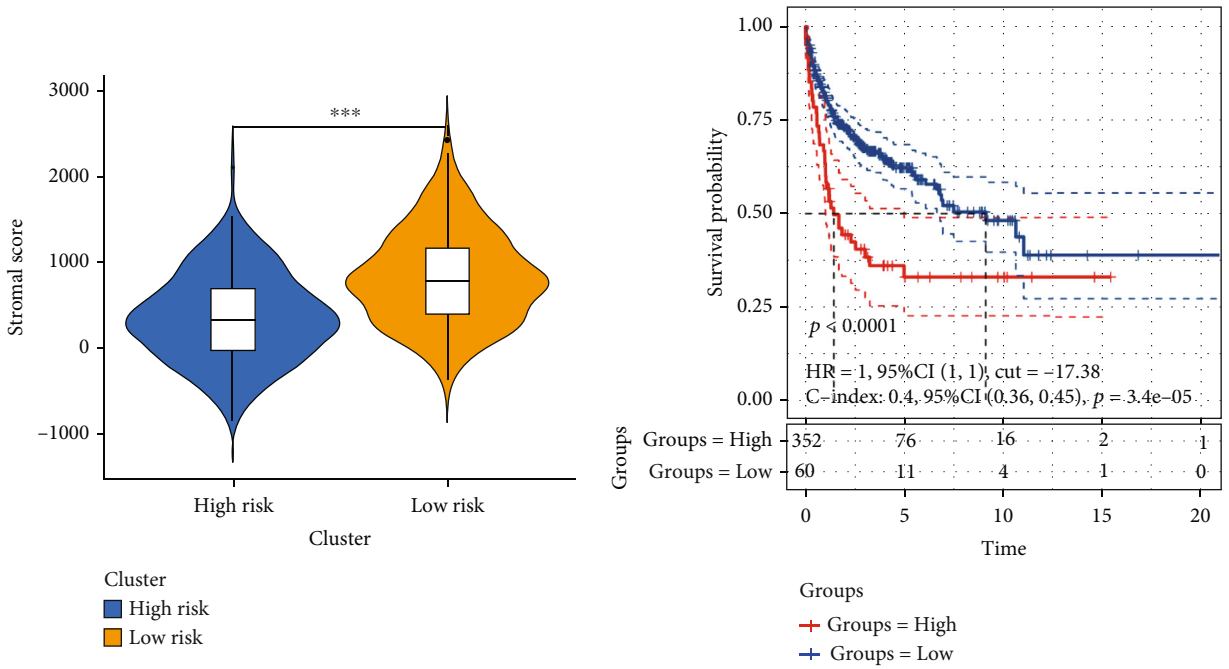

(c)

Figure 7: Continued.

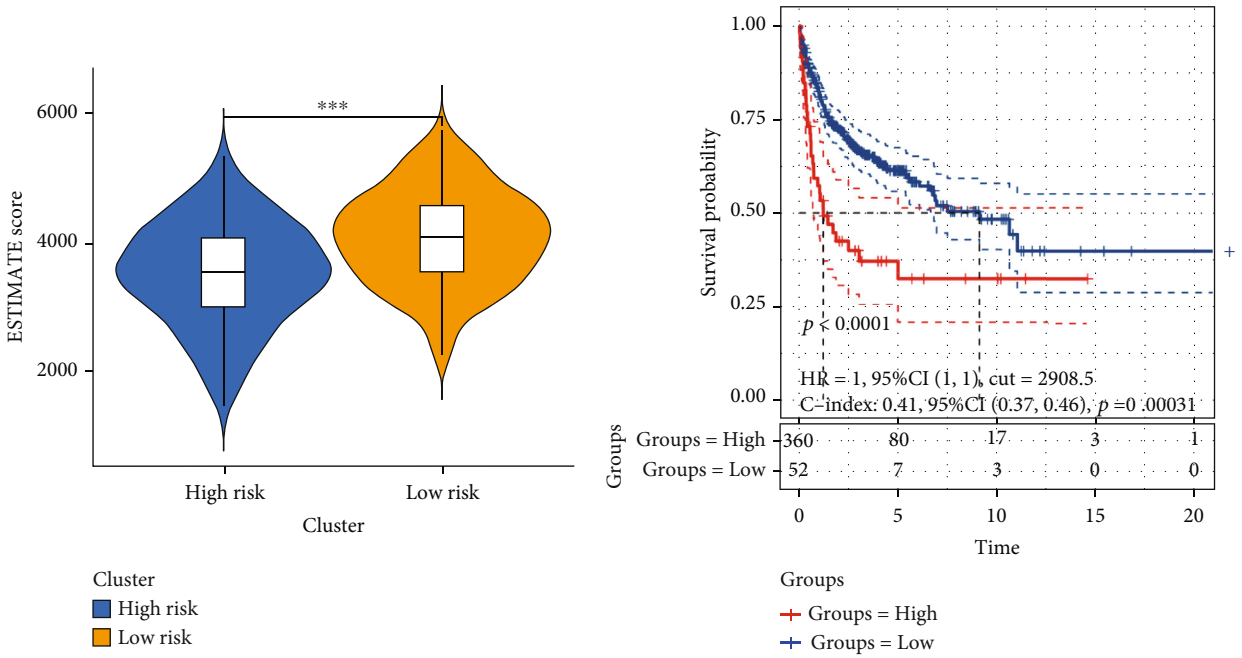

(d)

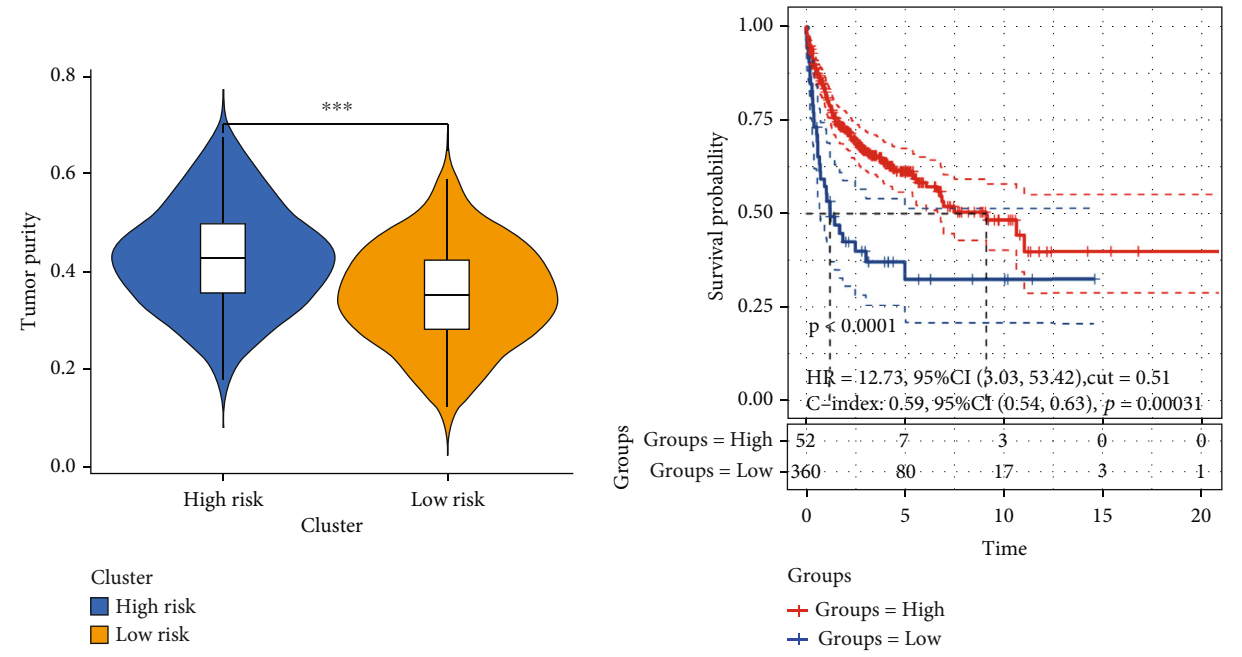

(e)

FIGURE 7: (a) Heatmap of the tumour microenvironment characteristics in the high- and low-risk groups. (b) Immune score map of the high- and low-risk groups and the Kaplan-Meier survival curve of the high- and low-immune score groups (blue represents the high-immune score group, whereas red represents the low-immune score group). (c) The matrix score map of the high- and low-risk groups and the Kaplan-Meier survival curve of the high- and low-matrix groups (blue represents the high matrix score, and red represents the low matrix score). (d) ESTIMATE score chart of the high- and low-risk groups and the Kaplan-Meier survival curve of high and low ESTIMATE scores (blue represents the high ESTIMATE score, and red represents the low ESTIMATE score). (e) Tumour purity score map of the high- and low-risk groups and the Kaplan-Meier survival curve of the high- and low-tumour purity score groups (blue represents the high tumour purity score, whereas red represents the low tumour purity immune score).

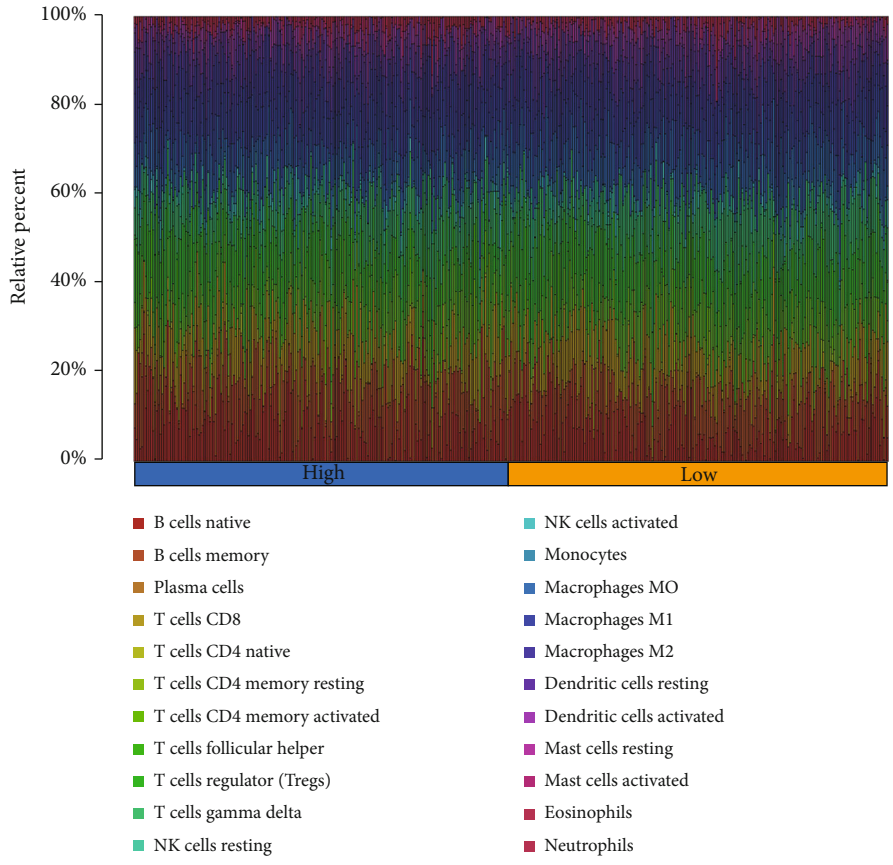

(a)

Figure 8: Continued.

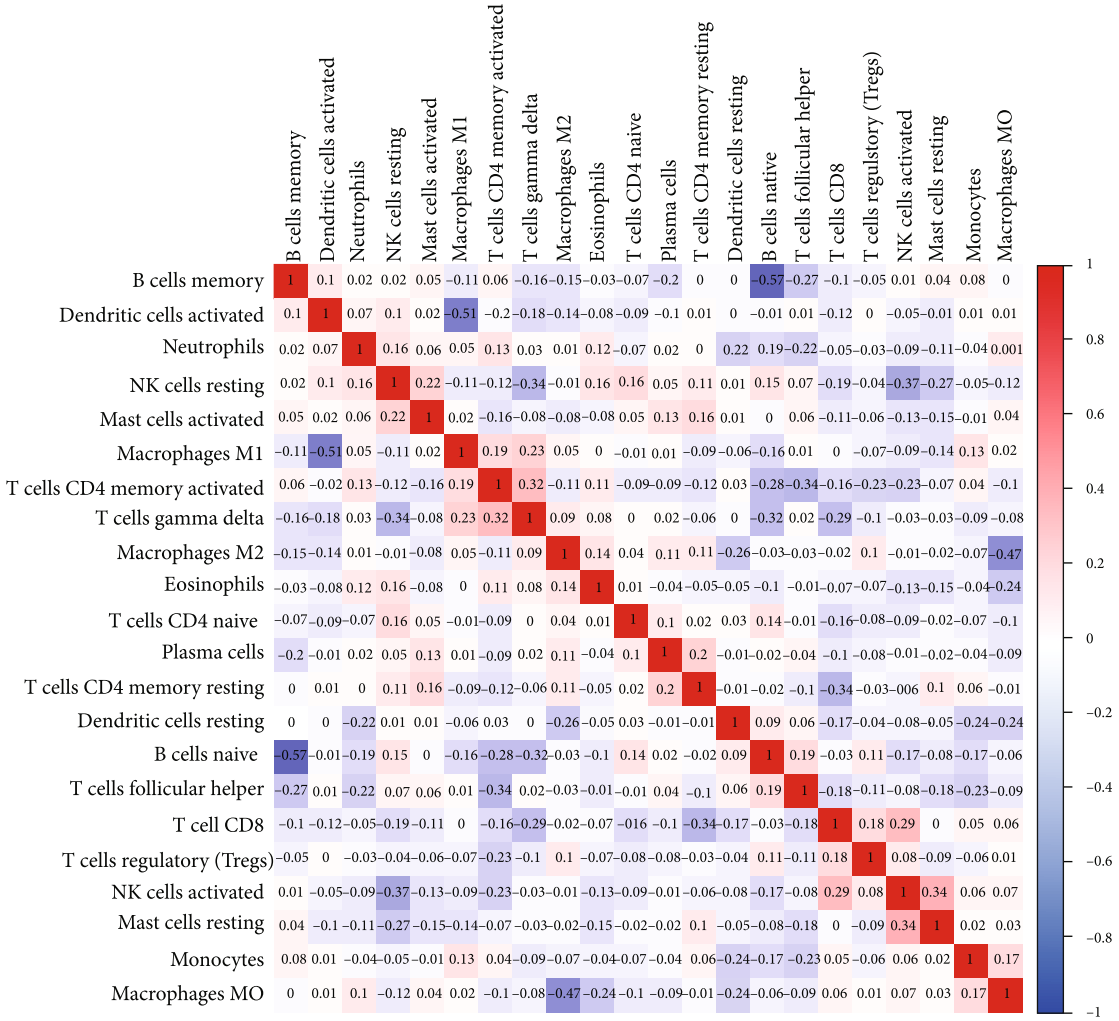

(b)

Figure 8: Continued.

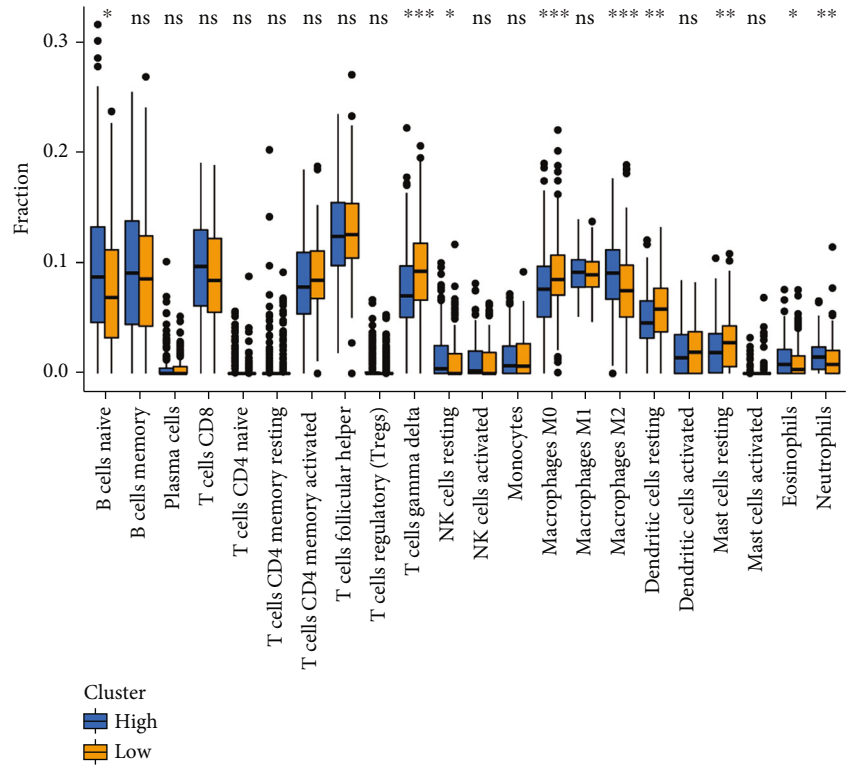

(c)

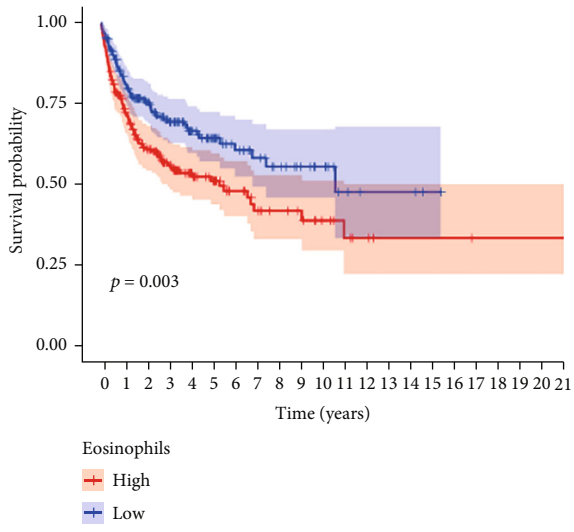

(d)

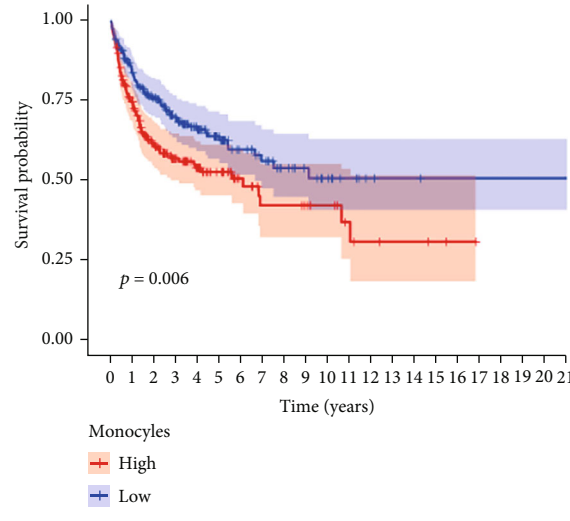

(e)

Figure 8: Continued.

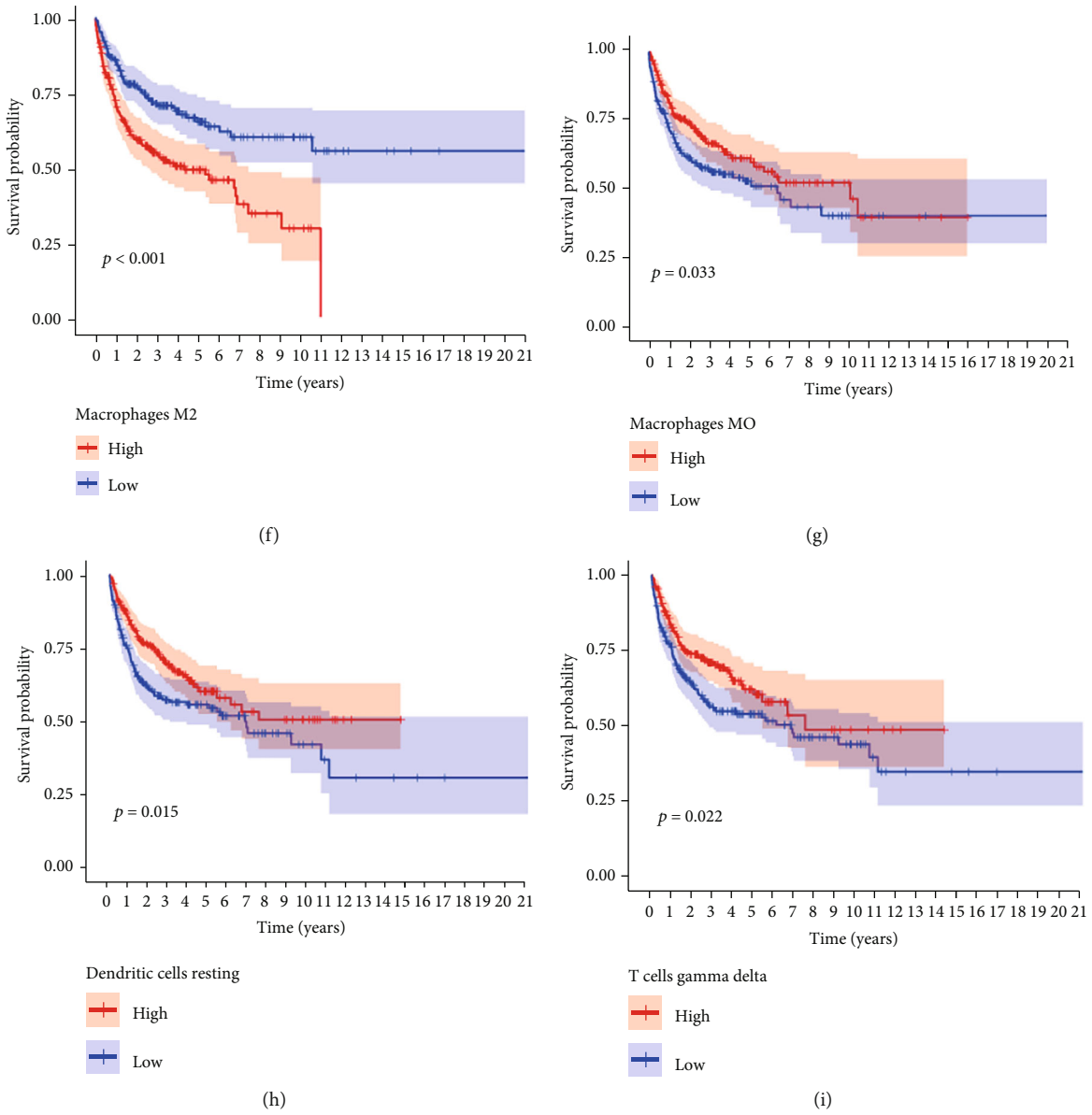

Figure 8: (a) The proportion of cell infiltration in 22 types of immune cells in the high- and low-risk groups. (b) The correlation diagram of the immune cells. (c) The scores of 22 types of immune cells in the high- and low-risk groups ($^{*}P < 0.05$, 0.01, $^{*}P < 0.001$). (d–i) Kaplan-Meier survival curves of eosinophils, monocytes, M2 macrophages, M0 macrophages, dormant dendritic cells, and delta T cells.

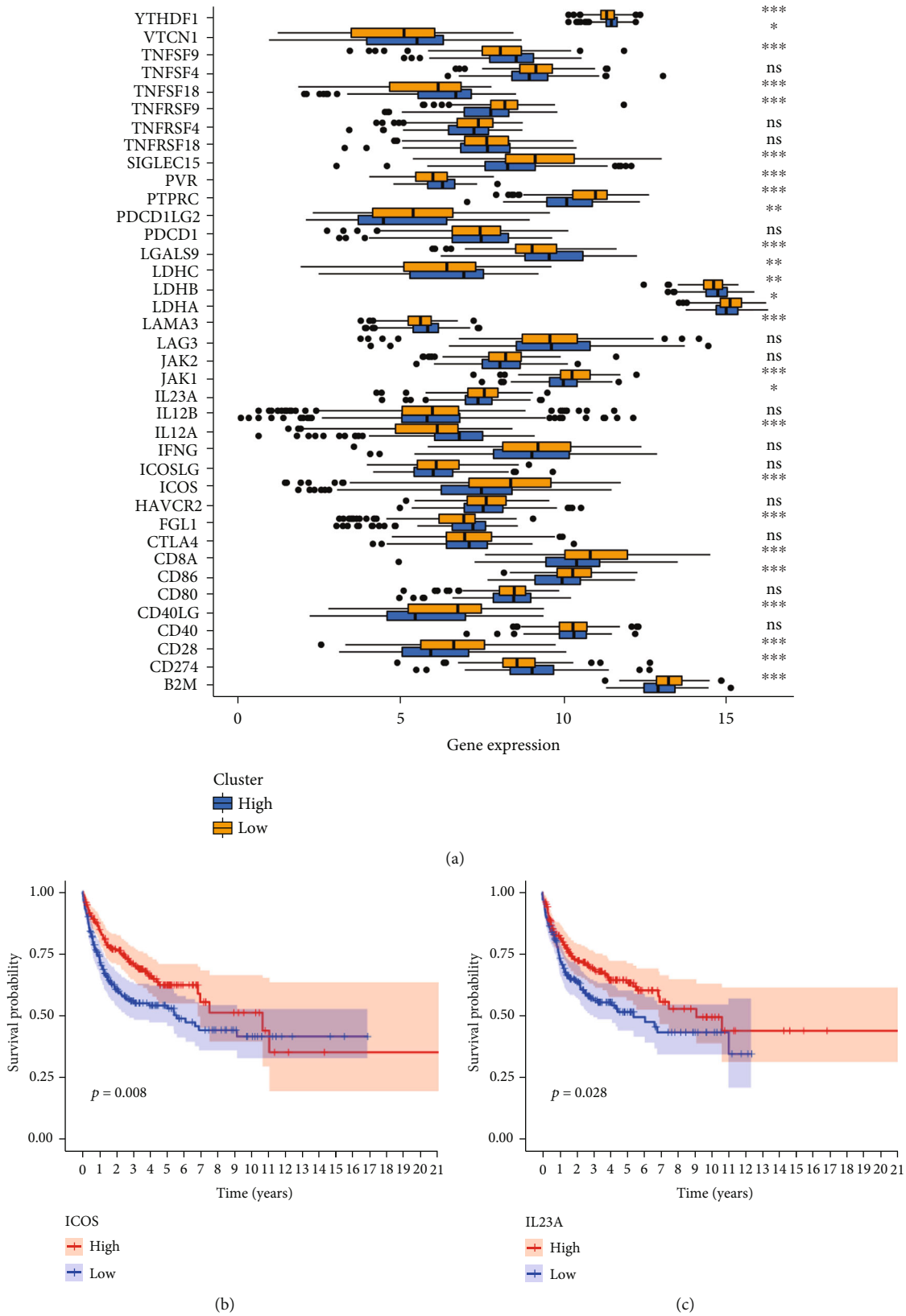

Figure 9: Continued.

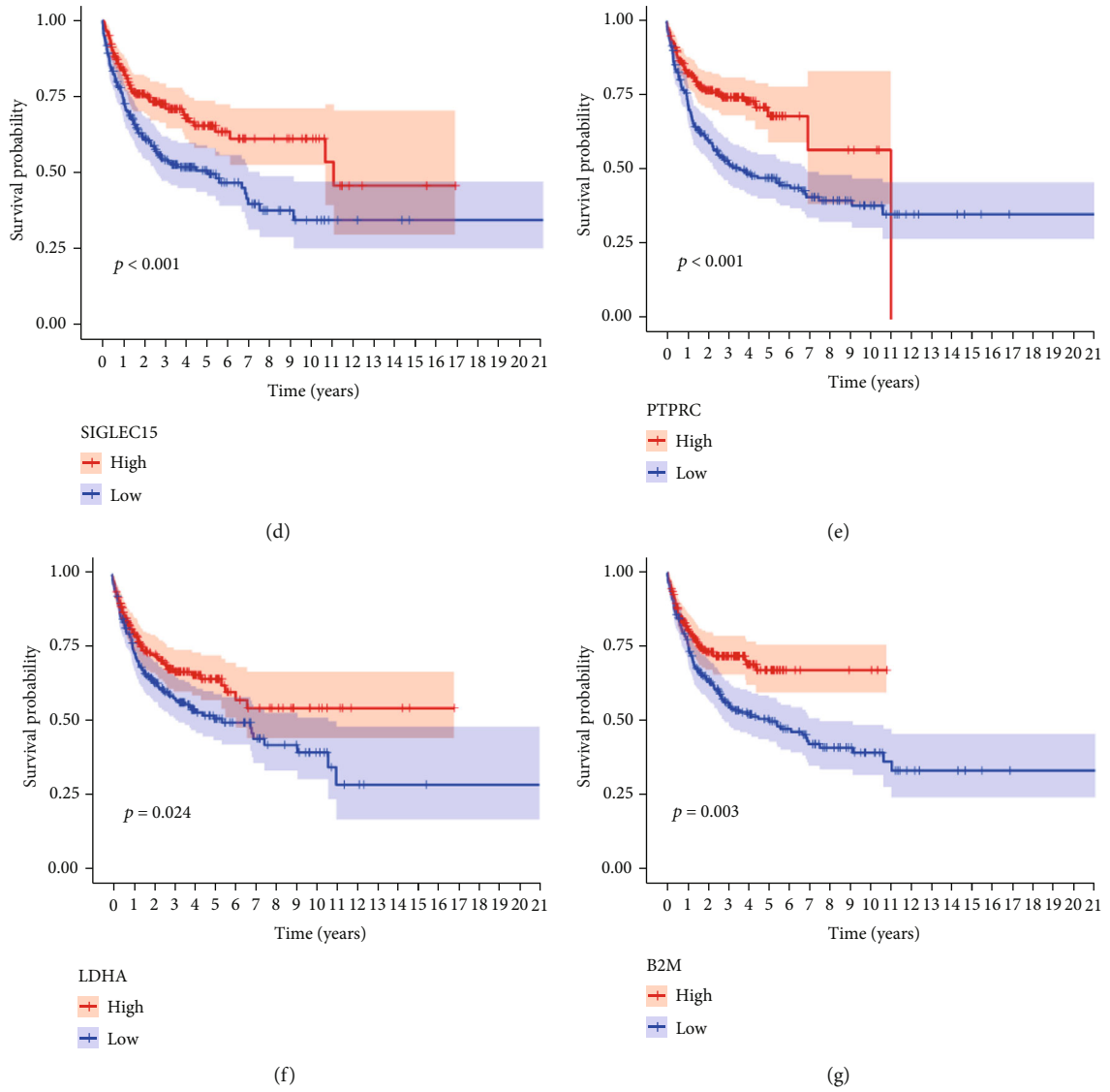

Figure 9: (a) Box chart of the difference distribution of immune checkpoints between the high- and low-risk groups ($^{*}P < 0.05$, $^{**}P < 0.01$, $^{***}P < 0.001$). (b–g) Kaplan-Meier survival curves of ICOS, IL23A, SIGLEC15, PTPRC, and LDHA.

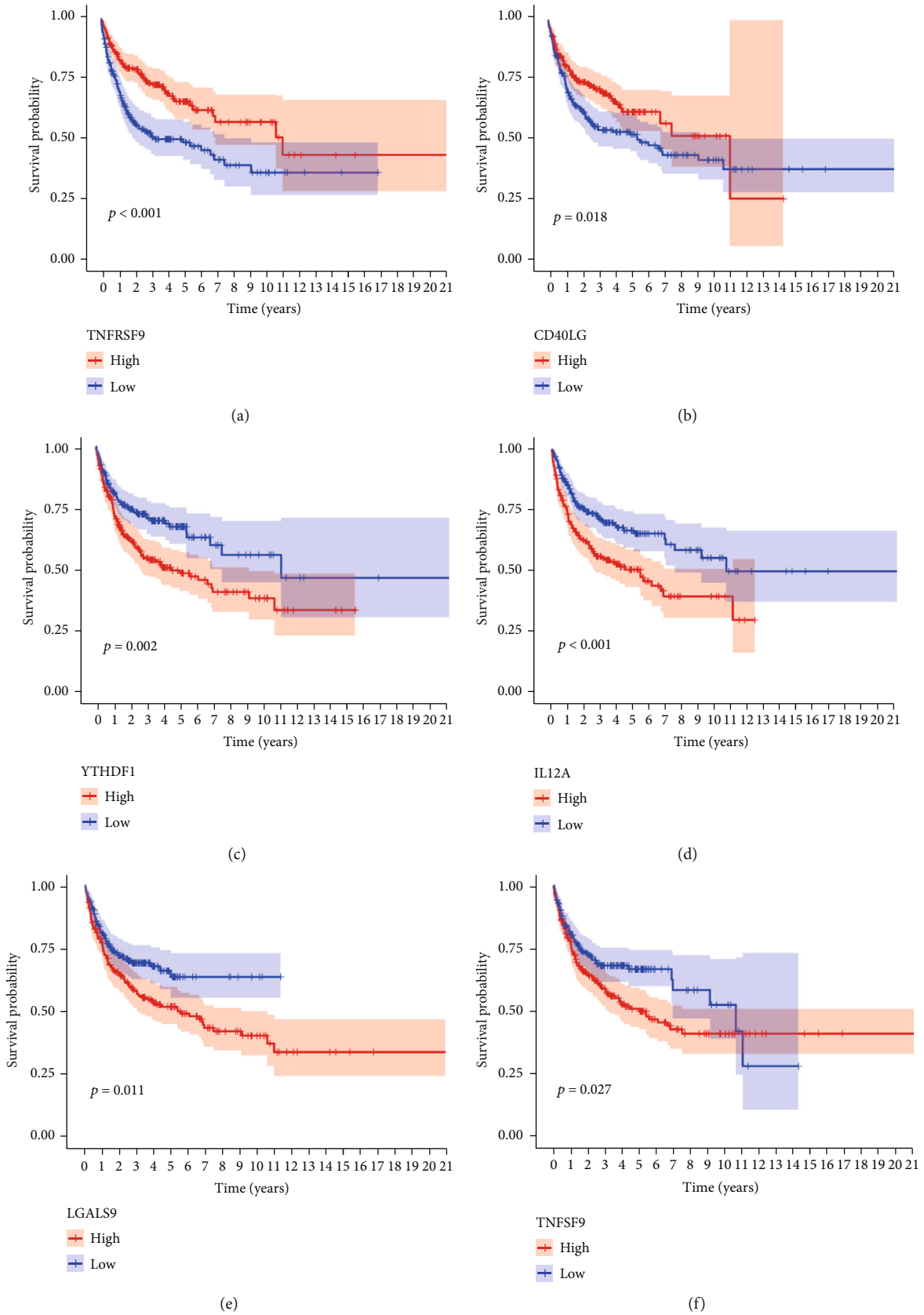

Figure 10: Continued.

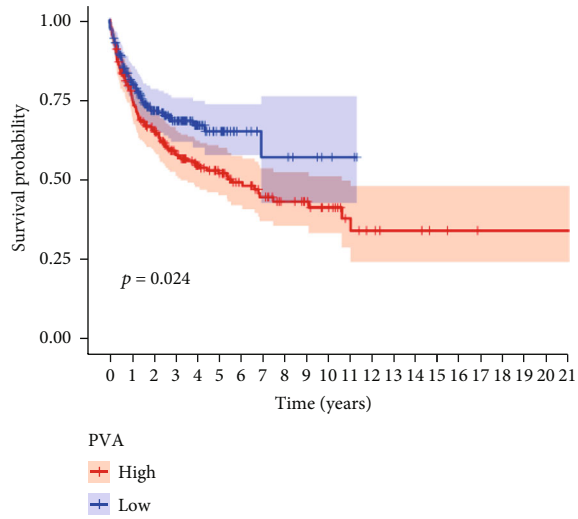

(g)

Figure 10: (a–g) Kaplan-Meier survival curves of B2M, TNFRSF9, CD40LG, YTHDF1, IL12A, LGALS9, TNFSF9, and PVR.

immune cell infiltration. The high-risk group had significantly lower immune and matrix scores and a significant increase in the number of dormant NK cells, M2 macrophages, and eosinophils, which represented a low survival rate. NK cells play a key role in preventing haematological malignancies; however, they may enter a state of dysfunction, thus limiting antitumour immunity. Studies have shown that NK cells participate in a large number of metabolic-related transcriptional reprogramming, whereas exposure to fatty acid lymphoma can effectively inhibit NK cell response and cell metabolism [37]. TBP is closely related to the metabolism of the body, and the two can interact with each other and affect DLBCL development. Marchesi et al. have confirmed that the M2 macrophage phenotype is associated with adverse outcomes in patients treated with R-CHOP. Eosinophils are more common in haematological tumours, such as non-Hodgkin's disease and some lymphomas, and may contribute to tumorigenesis and development by promoting angiogenesis and connective tissue formation in adjacent tumours [38–40], which is consistent with our immune cell survival analysis.

The ageing process is inevitably accompanied by changes in the immune system, such as changes in molecular subtypes or expression levels on the surface of immune cells and enhancement or suppression of immune cell function, and these changes may affect the immune monitoring process, including the immune checkpoint [41–43]. At present, immune checkpoint therapy has provided a huge breakthrough for the treatment of lymphomas. Finding reliable predictive biomarkers and potential targets can hence help reduce the side effects of immunosuppressive therapy and expand its applicability to patients with DLBCL. Therefore, we further investigated the relationship between the AG model and the immune checkpoint. The expression of TNFSF9, CD274, and PVR increased in the high-risk group of the AG model. Moreover, the blockers of CD274 (PD-L1) have been widely tested in patients with a variety of lymphomas, and the blockers of PD-L1, nivolumab, and pembrolizumab have been proven effective for the treatment of recurrent or refractory lymphomas [44]. Furthermore, repeated deletions of TNFSF9 have been detected in patients with DLBCL and Burkett's lymphoma [45]. PVR is a member of the laminin-like family, which not only promotes tumour progression and metastasis but also involves immunomodulation. It is also highly upregulated in the tumour cells of many cancer types and is associated with poor prognosis. In addition, the current PVR immune checkpoint inhibitors have been supported by a large number of experiments in preclinical cancer models, including colon cancer, liver cancer, and melanoma, with satisfactory results [46–50]. Our immune checkpoint survival analysis also showed that the high expression of TNFSF9 and PVR was associated with poor prognosis.

Although our study provides new ideas and potential therapeutic targets for the study of the pathogenesis of DLBCL. However, this study has some limitations. This is a retrospective study; therefore, designing a prospective study or obtaining clinical samples and evaluating them with Western blot or immunohistochemistry will be more convincing.

5. Conclusion

In conclusion, our study constructed an AG model that can predict the prognosis of patients with DLBCL who have different clinical features. We provide an ageing genetic framework from which to understand its pronounced genetic and clinical heterogeneity as well as the therapeutic responses in subsets of DLBCL tumours defined by shared pathogenesis. This classification breaks DLBCL into two genetic subtypes that differ with respect to gene expression phenotype, oncogenic pathway engagement, tumour microenvironment, and survival rates. In addition, we also explored the relationship between the AG and immune checkpoints in DLBCL and screened out potential immune checkpoints for treatment. This taxonomy provides a roadmap for the prediction and understanding of AGs involving the biological diversity encompassed within

the pathological mechanisms of the disease and will likely shed light on the heterogeneous responses of DLBCL to cytotoxic and molecular-targeted therapies.

Abbreviations

AG: Aging-related genes
GO: Gene Ontology enrichment
KEGG: Kyoto Encyclopedia of Gene and Genome
DLBCL: Diffuse large B cell lymphoma
NHLs: Non-Hodgkin's lymphomas
R-CHOP: Rituximab, cyclophosphamide, adriamycin, vincristine, prednisone
LDH: Lactate dehydrogenase
ECOG: Eastern Cooperative Oncology Group
IPI: International Prognostic Index
OS: Survival time
PCA: Principal component analysis
ROC: Receiver operating characteristic
AUC: Area under curve
TBP: TATA-binding protein.

Data Availability

The data used to support the findings of this study are available from the corresponding author upon request.

Ethical Approval

This article does not contain any studies with patients or animals performed by any of the authors.

Conflicts of Interest

There are no conflicts of interest in this study.

Authors' Contributions

Cancan Luo is responsible for the drafting the manuscript; Han Nie for the research design and helping to draft the manuscript; and Li Yu for the review and revision of the manuscript and writing guidance. Cancan Luo and HAN NIE are the co-first authors of this article; Cancan Luo is the 1st of the first authors; HAN NIE is the 2nd of the first authors.

Supplementary Materials

Supplementary 1. Supplementary Figure 1: the flow chart for analyzing AG prognostic model in DLBCL.

Supplementary 2. Supplementary Figure 2: univariate Cox analysis of AGs related to the survival time of patients with DLBCL.

Supplementary 3. Supplementary Figure 3: (a) the model divides the patients from the validation set (GSE11318) into the high- and low-risk groups, and the number of survivals and deaths were compared between these groups. (b) The Kaplan-Meier curve for the validation set (GSE11318) divided into the high- and low-risk groups. (c) The receiver operating curve of the model in the validation set (GSE11318). (d) The model divides the patients in the validation set (GSE32918) into the high and low-risk groups, and the number of survivals and deaths were compared between these groups. (e) The Kaplan-Meier curve of the validation set (GSE32918) divided between the high- and low-risk groups. (f) The receiver-operating curve of the model in the validation set (GSE32918).

Supplementary 4. Supplementary Figure 4: (a) heatmap of the clinical characteristics of the high- and low-risk groups in the validation set (GSE11318). (b) Univariate analysis of the clinical features in the validation set (GSE11318). (c) Multivariate analysis of the clinical features in the validation set (GSE11318). (d) Heatmap of clinical characteristics of the high- and low-risk groups in the validation set (GSE32918). (e) Univariate analysis of the clinical features in the validation set (GSE32918). (f) Multivariate analysis of the clinical features in the validation set (GSE32918).

Supplementary 5. Supplementary Table 1: three hundred nine genes related to aging.

References

[1] R. Lang and M. J. Gill, "Diffuse large B-cell lymphoma," *The New England Journal of Medicine*, vol. 384, no. 23, pp. 2261-2262, 2021.

[2] P. J. Lugtenburg, P. de Nully Brown, B. van der Holt et al., "Rituximab-CHOP with early rituximab intensification for diffuse large B-cell lymphoma: a randomized phase III trial of the HOVON and the Nordic Lymphoma Group (HOVON-84)," *Journal of Clinical Oncology*, vol. 38, no. 29, pp. 3377–3387, 2020.

[3] R. Vaidya and T. E. Witzig, "Prognostic factors for diffuse large B-cell lymphoma in the R(X) CHOP era," *Annals of Oncology*, vol. 25, no. 11, pp. 2124–2133, 2014.

[4] J. C. Wight, G. Chong, A. P. Grigg, and E. A. Hawkes, "Prognostication of diffuse large B-cell lymphoma in the molecular era: moving beyond the IPI," *Blood Reviews*, vol. 32, no. 5, pp. 400–415, 2018.

[5] J. L. Crombie and P. Armand, "Diffuse large B-cell lymphoma's new genomics: the bridge and the chasm," *Journal of Clinical Oncology*, vol. 38, no. 30, pp. 3565–3574, 2020.

[6] C. Thieblemont and B. Coiffier, "Lymphoma in older patients," *Journal of Clinical Oncology*, vol. 25, no. 14, pp. 1916–1923, 2007.

[7] L. H. Jakobsen, M. Bøgsted, P. . N. Brown et al., "Minimal loss of lifetime for patients with diffuse large B-cell lymphoma in remission and event free 24 months after treatment: a Danish population-based study," *Journal of Clinical Oncology*, vol. 35, no. 7, pp. 778–784, 2017.

[8] R. Cordoba, S. Luminari, and T. A. Eyre, "The use of frailty assessments in treating older adults with aggressive lymphomas," *British Journal of Haematology*, vol. 194, no. 4, pp. 677–685, 2021.

[9] M. Di, S. F. Huntington, and A. J. Olszewski, "Challenges and opportunities in the management of diffuse large B-cell lymphoma in older patients," *The Oncologist*, vol. 26, no. 2, pp. 120–132, 2021.

[10] B. K. Kennedy, S. L. Berger, A. Brunet et al., "Geroscience: Linking Aging to Chronic Disease," *Cell*, vol. 159, no. 4, pp. 709–713, 2014.

[11] C. López-Otín, M. A. Blasco, L. Partridge, M. Serrano, and G. Kroemer, "The Hallmarks of Aging," *Cell*, vol. 153, no. 6, pp. 1194–1217, 2013.

[12] K. L. Gibson, Y. C. Wu, Y. Barnett et al., "B-cell diversity decreases in old age and is correlated with poor health status," *Aging Cell*, vol. 8, no. 1, pp. 18–25, 2009.

[13] G. Lenz, G. Wright, S. S. Dave et al., "Stromal gene signatures in large-B-cell lymphomas," *The New England Journal of Medicine*, vol. 359, no. 22, pp. 2313–2323, 2008.

[14] G. Lenz, G. W. Wright, N. C. T. Emre et al., "Molecular subtypes of diffuse large B-cell lymphoma arise by distinct genetic pathways," *Proceedings of the National Academy of Sciences of the United States of America*, vol. 105, no. 36, pp. 13520–13525, 2008.

[15] S. L. Barrans, S. Crouch, M. A. Care et al., "Whole genome expression profiling based on paraffin embedded tissue can be used to classify diffuse large B-cell lymphoma and predict clinical outcome," *British Journal of Haematology*, vol. 159, no. 4, pp. 441–453, 2012.

[16] R. Tacutu, D. Thornton, E. Johnson et al., "Human ageing genomic resources: new and updated databases," *Nucleic Acids Research*, vol. 46, no. D1, pp. D1083–d1090, 2018.

[17] T. Wu, E. Hu, S. Xu et al., "Clusterprofiler 4.0: a universal enrichment tool for interpreting omics data," *The Innovations*, vol. 2, no. 3, p. 100141, 2021.

[18] K. Yoshihara, M. Shahmoradgoli, E. Martínez et al., "Inferring tumour purity and stromal and immune cell admixture from expression data," vol. 4, no. 1, p. 2612, 2013.

[19] A. M. Newman, C. L. Liu, M. R. Green et al., "Robust enumeration of cell subsets from tissue expression profiles," *Nature Methods*, vol. 12, no. 5, pp. 453–457, 2015.

[20] A. Rosenwald, S. Bens, R. Advani et al., "Prognostic significance ofMYCRearrangement and translocation partner in diffuse large B-cell lymphoma: a study by the Lunenburg lymphoma biomarker consortium," *Journal of Clinical Oncology*, vol. 37, no. 35, pp. 3359–3368, 2019.

[21] D. W. Scott, R. L. King, A. M. Staiger et al., "High-grade B-cell lymphoma with MYC and BCL2 and/or BCL6 rearrangements with diffuse large B-cell lymphoma morphology," *Blood*, vol. 131, no. 18, pp. 2060–2064, 2018.

[22] B. Coiffier and C. Sarkozy, "Diffuse large B-cell lymphoma: R-CHOP failure-what to do?," *Hematology. American Society of Hematology. Education Program*, vol. 2016, no. 1, pp. 366–378, 2016.

[23] J. Fu, Y. Liu, X. Wang, B. Yuan, and Y. Zhang, "Role of DHX33 in c-Myc-induced cancers," *Carcinogenesis*, vol. 38, no. 6, pp. 649–660, 2017.

[24] Y. Zhao, W. L. Cui, Z. Y. Feng, J. Xue, A. Gulinaer, and W. Zhang, "Expression of Foxp3 and interleukin-7 receptor and clinicopathological characteristics of patients with diffuse large B-cell lymphoma," *Oncology Letters*, vol. 19, no. 4, pp. 2755–2764, 2020.

[25] J. van Dieck, D. P. Teufel, A. M. Jaulent et al., "Posttranslational Modifications Affect the Interaction of S100 Proteins with Tumor Suppressor p53," *Journal of Molecular Biology*, vol. 394, no. 5, pp. 922–930, 2009.

[26] W. J. Chan, "Pathogenesis of diffuse large B cell lymphoma," *International Journal of Hematology*, vol. 92, no. 2, pp. 219–230, 2010.

[27] W. Zhou, S. Wang, Y. Ying, R. Zhou, and P. Mao, "miR-196b/miR-1290 participate in the antitumor effect of resveratrol via regulation of IGFBP3 expression in acute lymphoblastic leukemia," *Oncology Reports*, vol. 37, no. 2, pp. 1075–1083, 2017.

[28] H. A. Zielinska, C. S. Daly, A. Alghamdi et al., "Interaction between GRP78 and IGFBP-3 affects tumourigenesis and prognosis in breast cancer Patients," *Cancers (Basel)*, vol. 12, no. 12, p. 3821, 2020.

[29] S. H. Wang, Y. L. Chen, J. R. Hsiao et al., "Insulin-like growth factor binding protein 3 promotes radiosensitivity of oral squamous cell carcinoma cells via positive feedback on NF-κB/IL-6/ROS signaling," *Journal of Experimental & Clinical Cancer Research*, vol. 40, no. 1, p. 95, 2021.

[30] L. N. Chan, Z. Chen, D. Braas et al., "Metabolic gatekeeper function of B-lymphoid transcription factors," *Nature*, vol. 542, no. 7642, pp. 479–483, 2017.

[31] Z. Chen, D. A. Lopez-Ramos, E. Yoshihara et al., "Thioredoxin-binding protein-2 (TBP-2/VDUP1/TXNIP) regulates T-cell sensitivity to glucocorticoid during HTLV-I-induced transformation," *Leukemia*, vol. 25, no. 3, pp. 440–448, 2011.

[32] H. Masutani, E. Yoshihara, S. Masaki, Z. Chen, and J. Yodoi, "Thioredoxin binding protein (TBP)-2/Txnip and α-arrestin proteins in cancer and diabetes mellitus," *Journal of Clinical Biochemistry and Nutrition*, vol. 50, no. 1, pp. 23–34, 2012.

[33] J. R. Ribeiro, L. A. Lovasco, B. C. Vanderhyden, and R. N. Freiman, "Targeting TBP-associated factors in ovarian cancer," *Frontiers in Oncology*, vol. 4, p. 45, 2014.

[34] Y. Wei, D. Resetca, Z. Li et al., "Multiple direct interactions of TBP with the MYC oncoprotein," *Nature Structural & Molecular Biology*, vol. 26, no. 11, pp. 1035–1043, 2019.

[35] A. E. Hoffman, T. Zheng, R. G. Stevens et al., "Clock-cancer connection in non-Hodgkin's lymphoma: a genetic association study and pathway analysis of the circadian gene cryptochrome 2," *Cancer Research*, vol. 69, no. 8, pp. 3605–3613, 2009.

[36] X. Tan, F. Cao, F. Tang et al., "Suppression of DLBCL Progression by the E3 Ligase Trim35 Is Mediated by CLOCK Degradation and NK Cell Infiltration," *Journal of Immunology Research*, vol. 2021, Article ID 9995869, 13 pages, 2021.

[37] T. Kobayashi, P. Y. Lam, H. Jiang et al., "Increased lipid metabolism impairs NK cell function and mediates adaptation to the lymphoma environment," *Blood*, vol. 136, no. 26, pp. 3004–3017, 2020.

[38] F. Marchesi, M. Cirillo, A. Bianchi et al., "High density of CD68+/CD163+ tumour-associated macrophages (M2-TAM) at diagnosis is significantly correlated to unfavorable prognostic factors and to poor clinical outcomes in patients with diffuse large B-cell lymphoma," *Hematological Oncology*, vol. 33, no. 2, pp. 110–112, 2015.

[39] M. Samoszuk, "Eosinophils and human cancer," *Histology and Histopathology*, vol. 12, no. 3, pp. 807–812, 1997.

[40] S. Sakkal, S. Miller, V. Apostolopoulos, and K. Nurgali, "Eosinophils in cancer: favourable or Unfavourable?," *Current Medicinal Chemistry*, vol. 23, no. 7, pp. 650–666, 2016.

[41] J. Lian, Y. Yue, W. Yu, and Y. Zhang, "Immunosenescence: a key player in cancer development," *Journal of Hematology & Oncology*, vol. 13, no. 1, p. 151, 2020.

[42] R. Elias, T. Karantanos, E. Sira, and K. L. Hartshorn, "Immunotherapy comes of age: Immune aging & checkpoint inhibitors," *Journal of Geriatric Oncology*, vol. 8, no. 3, pp. 229–235, 2017.

[43] N. D. Johnson and K. N. Conneely, "The role of DNA methylation and hydroxymethylation in immunosenescence," *Ageing Research Reviews*, vol. 51, pp. 11–23, 2019.

[44] W. Xie, L. J. Medeiros, S. Li, C. C. Yin, J. D. Khoury, and J. Xu, "PD-1/PD-L1 pathway and its blockade in patients with classic Hodgkin lymphoma and non-Hodgkin large-cell lymphomas," *Current Hematologic Malignancy Reports*, vol. 15, no. 4, pp. 372–381, 2020.

[45] R. Scholtysik et al., "Recurrent deletions of the TNFSF7 and TNFSF9 genes in 19p13.3 in diffuse large B-cell and Burkitt lymphomas," *International Journal of Cancer*, vol. 131, no. 5, pp. E830–E835, 2012.

[46] J. S. O'Donnell, J. Madore, X. Y. Li, and M. J. Smyth, "Tumor intrinsic and extrinsic immune functions of CD155," *Seminars in Cancer Biology*, vol. 65, pp. 189–196, 2020.

[47] P. Kučan Brlić, T. Lenac Roviš, G. Cinamon, P. Tsukerman, O. Mandelboim, and S. Jonjić, "Targeting PVR (CD155) and its receptors in anti-tumor therapy," *Cellular & Molecular Immunology*, vol. 16, no. 1, pp. 40–52, 2019.

[48] D. K. Chiu, V. W. H. Yuen, J. W. S. Cheu et al., "Hepatocellular Carcinoma Cells Up-regulate PVRL1, Stabilizing PVR and Inhibiting the Cytotoxic T-Cell Response via TIGIT to Mediate Tumor Resistance to PD1 Inhibitors in Mice," *Gastroenterology*, vol. 159, no. 2, pp. 609–623, 2020.

[49] R. J. Johnston, L. Comps-Agrar, J. Hackney et al., "The Immunoreceptor TIGIT Regulates Antitumor and Antiviral $CD8^+$ T Cell Effector Function," *Cancer Cell*, vol. 26, no. 6, pp. 923–937, 2014.

[50] J. M. Chauvin, O. Pagliano, J. Fourcade et al., "TIGIT and PD-1 impair tumor antigen-specific $CD8^+$ T cells in melanoma patients," *The Journal of Clinical Investigation*, vol. 125, no. 5, pp. 2046–2058, 2015.